

Rec'd with letter dtd.
3/96/93



The Geology of North America
Volume K-2

QE
71
G48
1986
v. K-2

***Quaternary Nonglacial Geology:
Conterminous U.S.***

Edited by
Roger B. Morrison
Morrison and Associates
13150 West Ninth Avenue
Golden, Colorado 80401

#24009806



1991

102, 2

9304090035 930326
PDR WASTE PDR
WM-11

UNIVERSITY OF NEVADA, LAS VEGAS
LIBRARY

Acknowledgment

Publication of this volume, one of the synthesis volumes of *The Decade of North American Geology Project* series, has been made possible by members and friends of the Geological Society of America, corporations, and government agencies through contributions to the Decade of North American Geology fund of the Geological Society of America Foundation.

Following is a list of individuals, corporations, and government agencies giving and/or pledging more than \$50,000 in support of the DNAG Project:

Amoco Production Company
ARCO Exploration Company
Chevron Corporation
Cities Service Oil and Gas Company
Diamond Shamrock Exploration Corporation

Exxon Production Research Company
Getty Oil Company
Gulf Oil Exploration and Production Company
Paul V. Hoovler
Kennecott Minerals Company
Kerr McGee Corporation
Marathon Oil Company
Maxus Energy Corporation
McMoRan Oil and Gas Company
Mobil Oil Corporation
Occidental Petroleum Corporation

Pennzoil Exploration and Production Company
Phillips Petroleum Company
Shell Oil Company
Caswell Silver
Standard Oil Production Company
Oryx Energy Company (formerly Sun Exploration and Production Company)
Superior Oil Company
Tenneco Oil Company
Texaco, Inc.
Union Oil Company of California
Union Pacific Corporation and its operating companies:
Union Pacific Resources Company
Union Pacific Railroad Company
Upland Industries Corporation
U.S. Department of Energy

© 1991 by The Geological Society of America, Inc.
All rights reserved.

All materials subject to this copyright and included in this volume may be photocopied for the noncommercial purpose of scientific or educational advancement.

Copyright is not claimed on any material prepared by government employees within the scope of their employment.

Published by The Geological Society of America, Inc.
3300 Penrose Place, P.O. Box 9140, Boulder, Colorado 80301

Printed in U.S.A.

Cover Photo: East bluff of the Walker River viewed from middle of Weber Dam. At least two million years of Lake Lahontan lacustrine and subaerial history are shown here in about 42 m of strata in the Walker Lake basin, the southernmost of Lake Lahontan's subbasins. The top 6 m (light gray and light yellowish gray) are lacustrine gravel and sand of the middle member of the Seho Alloformation (about 13 ka) unconformably overlying eolian and slopewash sand bearing the Wyemaha Geosol (35–130 ka). Beneath another unconformity is 8 to 10 m of medium to pale gray lacustrine gravel, sand, and silt, equivalent to parts of

Library of Congress Cataloging-in-Publication Data

Quaternary nonglacial geology : conterminous U.S. / edited by Roger B. Morrison.

p. cm. — (The Geology of North America ; v. K-2)

Includes bibliographical references and index.

ISBN 0-8137-5215-9

1. Geology, Stratigraphic—Quaternary. 2. Geology—United States.

I. Morrison, Roger B. (Roger Barron), 1914– II. Series.

QE696.Q336 1991

551.79'0973—dc20

91-23046

CIP

the Eetza Alloformation (130–350 ka) in Lake Lahontan's northern subbasins. Below another unconformity is 6 to 10 m of darker gray, chiefly lacustrine gravel and sand (the upper pre-Eetza unit of Morrison and Davis, 1984b, p. 24, which contains the 1 Ma Glass Mountain G tephra layer). Beneath a marked erosional unconformity and extending to below the modern flood plain of the Walker River is 20+ m of tan-gray alluvial gravel and sand intercalated with many paleosols—a unit considerably older than the Lovelock Alloformation in the northern basins. Photo by R. B. Morrison.

<i>K-Ar dating of Quaternary volcanic rocks</i>	49
P. E. Damon	
<i>Fission-track dating</i>	53
C. W. Naeser and N. D. Naeser	
<i>Conventional uranium-series and uranium-trend dating</i>	55
B. J. Szabo and J. N. Rosholt	
<i>Paleomagnetic dating</i>	60
J. C. Liddicoat	
<i>Thermoluminescence dating</i>	61
S. L. Forman and M. N. Machette	
<i>Amino acid geochronology of fossil mollusks</i>	65
D. R. Muhs	
4. Quaternary volcanism in the western conterminous United States	75
R. G. Luedke and R. L. Smith	
5. Quaternary tephrochronology	93
A. M. Sarna-Wojcicki and J. O. Davis	
6. Tephrochronologic correlation of upper Neogene sediments along the Pacific margin, conterminous United States	117
A. M. Sarna-Wojcicki, K. R. Lajoie, C. E. Meyer, D. P. Adam, and H. J. Rieck	

REGIONAL CHAPTERS

7. Quaternary geology of the Pacific margin	141
W. R. Dupré, R. B. Morrison, H. E. Clifton, K. R. Lajoie, D. J. Ponti, C. L. Powell II, S. A. Mathieson, A. M. Sarna-Wojcicki, E. L. Leithold, W. R. Lettis, P. F. McDowell, T. K. Rockwell, J. R. Unruh, and R. S. Yeats	
<i>Introduction</i>	141
W. R. Dupré and H. E. Clifton	
<i>Quaternary coastal and shallow-marine facies sequences, Northern California and the Pacific Northwest</i>	143
H. E. Clifton and E. L. Leithold	
<i>Quaternary stratigraphy and geomorphic surfaces of the Willamette Valley, Oregon</i>	156
P. F. McDowell	
<i>Quaternary geology of the Great Valley, California</i>	164
W. R. Lettis and J. R. Unruh	
<i>Quaternary geology of the Southern California Coast Ranges</i>	176
W. R. Dupré	
<i>Quaternary geology of the Ventura and Los Angeles basins, California</i>	185
R. S. Yeats and T. K. Rockwell	

Chapter 3

Dating methods applicable to the Quaternary

John N. Rosholt*

U.S. Geological Survey, MS 963, Box 25046, Denver Federal Center, Denver, Colorado 80225

Steven M. Colman

U.S. Geological Survey, Woods Hole, Massachusetts 02543

Minze Stuiver

Department of Geological Sciences and Quaternary Research Center, University of Washington, Seattle, Washington 98195

Paul E. Damon

Department of Geosciences, University of Arizona, Tucson, Arizona 85721

Charles W. Naeser, Nancy D. Naeser, Barney J. Szabo, and Daniel R. Muhs

U.S. Geological Survey, MS 424, Box 25046, Denver Federal Center, Denver, Colorado 80225

Joseph C. Liddicoat

University of California, Santa Cruz, California 95064

Steven L. Forman

Institute of Arctic and Alpine Research and Department of Geological Sciences, University of Colorado, Boulder, Colorado 80309

Michael N. Machette and Kenneth L. Pierce

U.S. Geological Survey, MS 913, Box 25046, Denver Federal Center, Denver, Colorado 80225

SUMMARY OF QUATERNARY DATING METHODS

Steven M. Colman and Kenneth L. Pierce

INTRODUCTION AND COMPILATION OF QUATERNARY DATING METHODS

A wide variety of dating methods are used in Quaternary research, and each method has many applications and limitations. Because of this variety, we cannot discuss the applications and limitations of all methods here. The more versatile and widely used methods, including ^{14}C , K/Ar, fission-track, U-series, paleomagnetism, thermoluminescence, and amino acid dating are treated more comprehensively in this chapter than other methods that are shown on the summary chart. The summary chart is provided here to give an overview of dating work and research for the Quaternary.

This summary consists mainly of a table (Plate 2) that is modified and updated from Colman and Pierce (1977, Plate 1, ref. 66). The table is intended as an overview and concise guide to Quaternary dating methods. It contains many subjective judg-

ments and should not be considered definitive; the entries for applicability, age range, and optimum resolution are particularly interpretive. Details concerning assumptions, analytical techniques, uncertainties, and interpretations should be obtained from specialized references using the key references in Plate 2 as a guide. The dating methods described range from well-known and established techniques to experimental procedures whose results are subject to considerable interpretation.

Key references included on Plate 2 are intended as an entry into the vast literature on dating methods; space prohibits a more complete listing. We have emphasized recent review papers and notable examples of applications as sources of additional references and information. Dating methods discussed in other sections of this chapter are indicated by asterisks in the summary table. The first five references are reviews or edited volumes that discuss Quaternary dating methods in general; references 6-11 are edited volumes that focus on individual methods or closely related methods. In the interest of brevity and clarity, we have not cited individual papers in these edited volumes. Some dating methods are based on fundamental geological principles, such as stratigraphy, for which references are deemed unnecessary here.

For the purpose of our discussion and summary table, it is useful to classify dating methods, which can be done in a variety of ways. Perhaps the simplest classification is one that groups methods that share similar assumptions, procedures, or applica-

*Deceased.

Rosholt, J. N., Colman, S. M., Stuiver, M., Damon, P. E., Naeser, C. W., Naeser, N. D., Szabo, B. J., Muhs, D. R., Liddicoat, J. C., Forman, S. L., Machette, M. N., and Pierce, K. L., 1991. Dating methods applicable to the Quaternary, in Morrison, R. B., ed., Quaternary nonglacial geology: Conterminous U.S.: Boulder, Colorado, Geological Society of America, The Geology of North America, v. K-2.

TABLE 1. CLASSIFICATION OF QUATERNARY DATING METHODS*

----- Numerical-age -----					
----- Calibrated Age -----					
----- Relative-age -----					
----- Correlated-age -----					
Sidereal	Isotopic	Radiogenic	Chemical and Biochemical	Geomorphic	Correlation
Historical records	^{14}C	Uranium-trend	Amino acid racemization	Soil profile development	Stratigraphy
Dendrochronology	K-Ar and ^{39}Ar , ^{40}Ar	Thermoluminescence	Obsidian hydration	Rock and mineral weathering	Tephrochronology
Varve Chronology	Uranium-series -----?	Electron-spin resonance -----?	Tephra hydration	Rock varnish	Paleomagnetism
	Fission track	^{210}Pb	Lichenometry	Progressive land-form modification	Fossils and artifacts
		Other cosmogenic isotopes	Soil chemistry	Rate of deposition	Stable isotopes
				Rate of deformation	Astronomical correlation
				Geomorphic position	Tectites and microtectites

*Dashed line indicates the type of result most commonly produced by the methods below it; dotted line indicates the type of result less commonly produced by the methods below it.

*Methods above this line routinely produce numerical ages; methods below the line are more experimental and involve nonradioactive processes or processes whose effects on age estimates are not well established.

tions. Accordingly, we have grouped dating methods into six categories (Plate 2; Table 1, lower part of header): sidereal (annual), isotopic, radiogenic, chemical and biological, geomorphic, and correlation methods. Dating methods may also be classified by the type of result they produce (Plate 2; Table 1, upper header); numerical-age (quantitative estimate on a ratio scale), calibrated-rate (numerical-age based on the rate of a process rate that has been calibrated by another dating method), relative-age (chronologic order, in some cases including some measure of magnitudes of age differences), and correlated-age (correlated to independently dated deposits or to standard stratigraphic sections).

RADIOCARBON DATING

Minze Stuiver

INTRODUCTION

An early interest in radiocarbon dating of geological samples was expressed by Richard Foster Flint when attending a lecture given by W. F. Libby at the 1948 Viking Fund Supper Conference in New York. At the conclusion of Libby's remarks, the audience remained mute until Flint commented, "Well, if you people are not interested in this, I am. . . . If you don't want anything dated, I am for it, and would like to send some material"

(quote from Taylor [1987] which also contains other relevant references). The relatively large sample size (one pound of carbon) needed at that time may explain the reluctance of the archaeologists present at the meeting to commit themselves to the combustion of precious museum materials. The 40 years of progress in radiocarbon dating technology is best illustrated by comparing the above required sample size to the 0.05-mg C sample (Nelson and others, 1986) recently used for a radiocarbon age determination by accelerator mass spectrometry.

During the last decade, two major improvements were made. A major breakthrough has been the above-mentioned direct detection of ^{14}C in mg samples through accelerator mass spectrometry. In addition, the conventional decay counting technique can now deliver an enhanced level of exactness (Stuiver, 1978) that has resulted in a high precision radiocarbon age terminology. It is especially the latter improvement that is important for radiocarbon timescale calibration.

The cosmic ray-produced ^{14}C isotope is used for a wide array of scientific investigations. The technique is used in many disciplines, and requires of the radiocarbon "expert" a truly interdisciplinary mode of thinking. Applications can be found in cosmic ray and solar physics (paleochanges in cosmic ray flux and solar surface conditions [Stuiver and Quay, 1980]), oceanography (the mixing and circulation of water masses [Stuiver and

others, 1983b]), climatology (long-term changes in carbon reservoir properties related to the Holocene-Wisconsin climate change [Andree and others, 1986b]), environmental chemistry (fossil fuel dilution of atmospheric $^{14}\text{CO}_2$ [Stuiver and Quay, 1981] and particulate carbon and methane in the atmosphere [Currie and others, 1983; Levin, 1985]), glaciology (ice core stratigraphy [Andree and others, 1986a]), archeology (chronometry), geology (geochronometry as, for instance applied to earthquake frequency research [Sieh, 1984]), hydrology (groundwater dating [Mook, 1980]), and geophysics (earth geomagnetic field change deduced from long-term atmospheric ^{14}C change [Sternberg and Damon, 1983]).

The majority of geological applications is directed toward the determination of time. Because ^{14}C disappears fairly rapidly from the geological scene through radioactive decay, the applicable timespan is relatively short. With a half life of 5,570 yr, the amount of ^{14}C in a sample is reduced by a factor 2 every 5,570 yr. For 10 half lives, or 55,700 yr, the reduction is a factor $2^{10} = 1024$. For the maximum ages of about 75,000 yr determined so far, the amount of ^{14}C in a sample is only 1/10,000 of its original level. Clearly the timespan limitations of the radiocarbon method result from the obvious statistical truth that measurement error becomes infinitely large when the activity to be measured approaches zero.

As with all measuring devices, there are technical factors that limit the precision and accuracy with which an age can be determined. Major limitations are also imposed by the degree to which the basic assumptions of the ^{14}C dating method are correct. Whereas improvement of the technique can still lead to further progress, the limitations imposed by the basic assumptions provide much greater obstacles. For instance, with high-precision dating it is now possible to date a sample with a radiocarbon age error of ± 15 yr. After converting the radiocarbon age to a calendar year age, however, there can occasionally be an uncertainty of centuries in the calibrated age.

A conventional radiocarbon age can be calculated from the measured ^{14}C activity by using the conventional radiocarbon half life (5,568 yr) and by assuming constancy of atmospheric ^{14}C level in the past (Stuiver and Polach, 1977). The calculation also corrects for isotope fractionation by using the ^{13}C isotope as an indicator of possible enrichment or depletion of sample ^{14}C during its formation. The primary function of the laboratory is to measure the remaining ^{14}C activity of the sample and to determine the uncertainty (standard deviation) in the measurement. This information is then converted into a conventional radiocarbon age \pm a standard age error.

CONTAMINATION

Given the age supplied by the laboratory, the user has to decide whether the number given provides relevant information. A major concern will be adherence to another assumption: The remaining sample ^{14}C should be representative of its original activity, which implies a closed system with respect to carbon

exchange with its environment. In other words, samples should not receive, between the moment of formation and the moment of sampling, an admixture of carbonaceous material having a specific ^{14}C content different from that of the original sample.

The user can reduce the influence of contamination by selective sampling; for instance, collect samples far below the surface where root contamination is usually less. Remaining rootlets should be removed before drying the sample. Part of the laboratory procedure is oriented toward reducing the influence of contaminants. Organic materials are acidified to remove carbonates, and an alkali treatment is given to appropriate samples for the removal of humic materials.

In addition to the above in situ contamination, foreign materials can also be introduced during sampling and transport, or during storage and handling of the sample in the laboratory. These additions can usually be entirely avoided by following proper procedures. However, for in situ contamination, the best possible procedures, although minimizing the effects, do not necessarily remove all contaminants.

The influence of specific levels of modern contamination is largest for the older samples. As mentioned, a sample in the mid-50,000-yr range contains only 1/1,000 of its original activity. The addition of a similar minute amount of modern contamination will double its ^{14}C content, and reduce the sample age by one half life or 5,570 yr. For the 75,000-yr sample, contamination levels of only one part in 10,000 will have a similar impact. This should be a warning against attaching too much significance to very old dates. But even the forewarned user should realize that the existence of samples with 75,000-yr-old radiocarbon ages implies an upper limit of ^{14}C contamination of 1 part in 10,000. Thus it must be possible to collect "similar" samples (samples containing less than 1 part in 10,000 ^{14}C contamination) in the 50,000 to 60,000 yr range. These samples would then yield reliable ages because the low level of ^{14}C contamination would be negligible.

Contamination with older materials (e.g., graphite) is usually of lesser import than contamination with younger materials because the relative change in ^{14}C activity induced by the contaminants is often greater for the younger additions. For instance, a 10-mg-C-old (lacking ^{14}C) addition to a 1-g-C sample reduces the sample ^{14}C activity by 1 percent for all samples of any age. This one percent ^{14}C dilution results in an 80-yr-older radiocarbon age, because ^{14}C decays with a constant rate of approximately 1 percent per 80 yr. A 10-mg addition of younger material to a large sample also has relatively little influence when the sample is very young (after all, adding material of the same age would not change the age of the contaminated sample), but usually has drastic consequences for the age of an old sample. For instance, a 37,000-yr-old sample retains about 1 percent of its original ^{14}C activity. Doubling this activity by adding to a 1-g C sample another 10 mg C of modern material (defined as material of zero age or 100 percent ^{14}C activity) reduces the age of the contaminated material to 31,400 yr.

A detailed discussion of the contamination-induced change

in radiocarbon ages is given by Grootes (1983) and Bradley (1985).

Given the amount and activity of the contamination, the "new" radiocarbon age can be very precisely calculated. In actual practice, however, the influence of contamination can often only be evaluated in general terms such as, "the charcoal sample was very well preserved and a visual inspection indicated an absence of rootlets;" therefore, the chances of retaining contaminants after pretreatment are small.

The nonhomogenous dispersal of contaminating material has become important now that mg C samples are measured. For instance, consider a lake core with 5 percent graphite contamination. Combustion of a large sample would produce an age 400 yr too old. But a mg C sample selected randomly could well be a graphite particle and result in an infinite age. However, here the small-sample approach can also be used to eliminate the influence of graphite (or coal) contamination by selecting macrofossils (e.g., leaves) that were originally in ^{14}C equilibrium with the atmosphere.

RESERVOIR EFFECTS

A radiocarbon age is calculated with the aid of an equation in which the ratio of the measured sample ^{14}C activity to presumed initial ^{14}C activity is the important parameter. The initial activity used in the equation is that measured for the laboratory oxalic acid standard. The oxalic acid ^{14}C has been calibrated against the ^{14}C activity of a 19-century wood sample. Thus the initial activity used for the calculation of a conventional radiocarbon age is tied to atmospheric ^{14}C activity because, after correction for isotope fractionation, the wood reflects atmospheric ^{14}C level.

The ^{14}C content of nonatmospheric carbon reservoirs (e.g., oceans or lakes) may differ from the atmospheric value. Thus, a so-called reservoir correction has to be applied to account for the age differences between reservoirs. As these reservoirs usually have a lower specific ^{14}C activity (activity per gram C) than that of atmospheric carbon dioxide, the conventional radiocarbon ages have to be reduced.

The reservoir correction for the surface mixed layer of the midlatitude ocean is approximately 300 radiocarbon yr. A conventional radiocarbon age would therefore be 300 yr too old for samples properly corrected for isotope fractionation (for details, see Stuiver and Polach, 1977). For oceanic regions where upwelling of older waters reduces surface water ^{14}C activities even more, the reservoir correction is still larger. The largest correction is for Antarctic coastal regions, where shells of the last century may have conventional radiocarbon ages of 1,000 to 1,300 yr (Stuiver and others, 1983a).

The ages of the top of the sediment (or, to be more precise, a few cm below the top to avoid the influence of nuclear bomb ^{14}C) of lake cores reflect the reservoir deficiency of those lakes. These may range from a few hundred years for lakes approaching equi-

librium with the atmosphere to 2,500 yr for lakes with important groundwater bicarbonate contributions (Stuiver, 1975).

A weakness in the above approach is the assumption of a constant past reservoir deficiency. Variable lake levels and bicarbonate concentrations may well cause a variable reservoir deficiency. Here again, accelerator mass spectrometry provides a breakthrough because it is now possible to measure at various depths the age differences between plant macrofossils (in equilibrium with the atmosphere), lake carbonate, and gyttja. The first study of this kind has been made for the sediments of a small closed basin of the Lobsingensee, Switzerland (Andree and others, 1986c).

THE RADIOCARBON AGE ERROR

Most analytical facilities outside the radiocarbon community estimate an error (one standard deviation) in a measurement by assessing the data obtained for repeat analyses of identical samples. The histogram of repeat analyses gives the precision of measurement. Repeat analyses are only made for a limited number of samples because it is not cost effective to make multiple measurements of each sample. Thus the precision obtained for a limited number of analyses is used for an error estimate of all sample measurements.

The error in precision is not the only error in a measurement. A laboratory can be quite reproducible in its repeat measurements, yet be off in accuracy through a systematic deviation from the true value. Systematic errors are usually evaluated through interlaboratory comparisons of results obtained for the same sample.

Contributing to the radiocarbon age error is the statistical uncertainty in a radioactivity measurement. Radioactive disintegration varies randomly about a mean value, and measured count rates of the same sample form a Poisson probability curve. Even the laboratory with the most sophisticated instrumentation cannot escape the realities of Poisson counting statistics. Thus the Poisson error in the count rates, when converted into radiocarbon years, provides a minimum age error.

Unfortunately, the radiocarbon community has traditionally been satisfied with reporting age errors based on counting statistics alone. It is now clear that this was an unwise choice. Interlaboratory comparisons of results obtained for the same samples show substantial underreporting of the radiocarbon age errors (The International Study Group, 1982; Stuiver, 1982). In order to arrive at a realistic estimate of the precision error, as well as possible systematic errors, the recipient of a radiocarbon age should request from the supplier information on interlaboratory comparison and reproducibility measurements.

TIME-SCALE CALIBRATION

As previously mentioned, a radiocarbon age is derived from a comparison of present-day remaining ^{14}C activity to an atmospheric ^{14}C level which is assumed to have been constant during

the past. As atmospheric ^{14}C levels, however, did change, it is evident that a radiocarbon age is only an approximation of the actual age in calendar years. For a conversion of a radiocarbon age to a more realistic calendar date, a calibration curve is needed where radiocarbon ages of wood samples are plotted versus age in calendar years. Such calibration curves are obtained by determining the radiocarbon ages of wood samples dated independently by dendrochronological means.

The construction of a calibration curve from radiocarbon ages with limited precision is not a simple matter. Not only should the standard error in the determination be as small as possible, but the calculation of this error has to be realistic in that it should account for all variability encountered in the laboratory procedures. Proof of accuracy has to come from a comparison of results obtained in two or more laboratories.

High-precision calibration curves covering the last 4,500 yr are now available. The internationally recommended 4,500-yr curve (Stuiver and Kra, 1986) was obtained by combining the data of the Seattle and Belfast radiocarbon laboratories (Stuiver and Pearson, 1986; Pearson and Stuiver, 1986). The comparison of the Seattle and Belfast data demonstrate systematic differences of only a few radiocarbon years and age differences for contemporaneous samples that can be fully explained by the precisions quoted by the Belfast and Seattle laboratory. The above high-precision curve has, on average, a radiocarbon-age error of ± 12 yr (Stuiver and Pearson, 1986) for bi-decadal wood samples.

Additional calibration curves are given in the special 1986 issue of *Radiocarbon* on age calibration. Dendrochronologically dated wood currently available covers nearly the last 10,000 yr, and an extension by a few thousand years is possible using varve chronologies (Stuiver and others, 1986). Detailed age calibration further back in time is not yet possible.

Although the availability of a precise calibration curve reduces the margin of error in calibrated AD/BC dates, a substantial uncertainty remains, because a given radiocarbon age may correspond to several AD/BC dates. A continuous spectrum is even possible when ^{14}C levels in the atmosphere decline at the same rate as ^{14}C declines through radioactive decay. All samples formed during such an interval will have the same radiocarbon content at the end of the interval, and thus yield identical radiocarbon ages. Such a major disaster area for radiocarbon calibration occurs between 420 BC and 750 BC where radiocarbon ages are nearly all in a narrow 2,430 to 2,470-yr-BP band.

The wiggly nature of the calibration curve causes a radiocarbon date to be converted in a range (or ranges) of calibrated (cal) AD/BC (or cal BP where 0 BP equals 1950 AD ages), even if the radiocarbon-age determination could be made without error. Figure 1 is the graphic representation of these ranges encountered when converting ideal (zero error) radiocarbon ages into calibrated ages. The baseline ranges of up to a few decades are due to the uncertainty in the calibration curve, whereas the larger deviations are obtained when the conversion process is influenced by the wiggles. A large vertical Figure 1 spike represents a radiocarbon age that, after conversion, gives a wide range

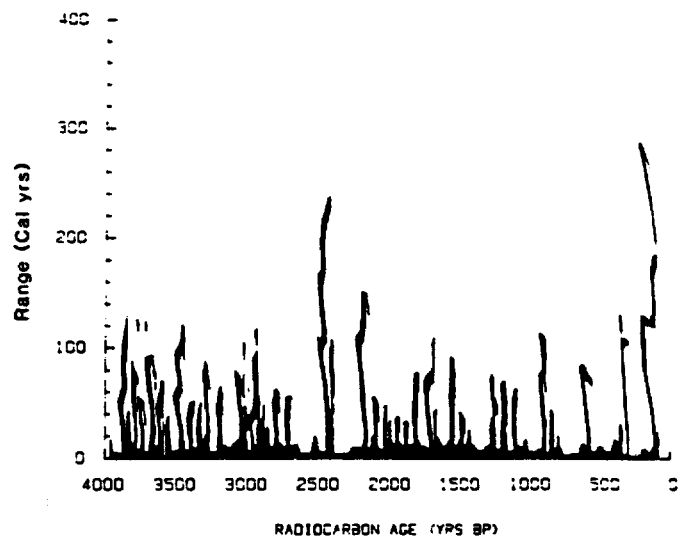


Figure 1. The ranges, in calendar years, obtained from the calibration of radiocarbon ages up to 4,000 yr B.P.

of cal years. Multiple intercepts are responsible for the wiggly nature of the individual cal age uncertainty.

For the above example (zero error in the sample ^{14}C determination), 50 percent of the ages show an age range larger than expected from the uncertainty in the calibration curve alone. This increases to 72 percent for an age determination with an 80-yr error (i.e., the oldest and youngest cal ages derived from a specific radiocarbon age differ by more than 160 yr in 72 percent of the cases). Unfortunately, the benefits of high-precision dating (with radiocarbon-age error circa 15 yr for 6-g C samples) appear to be partly, but not always, negated by the conversion process.

K-AR DATING OF QUATERNARY VOLCANIC ROCKS

Paul E. Damon

INTRODUCTION

There are two basic methods of isotopic dating that make use of the radioactive decay of ^{40}K to ^{40}Ar . These are the conventional K-Ar method and the $^{40}\text{Ar}/^{39}\text{Ar}$ method. In the conventional method, the K content of the sample is usually measured by flame photometry or atomic absorption spectrometry, and the radiogenic ^{40}Ar by mass spectrometric isotope dilution. In the $^{40}\text{Ar}/^{39}\text{Ar}$ method, ^{39}K is first converted to ^{39}Ar by an n, p reaction in a nuclear reactor, and the argon isotope ratios are determined by mass spectrometry. The $^{40}\text{Ar}/^{39}\text{Ar}$ method has the advantage of allowing both isotopes to be released from similar K sites in minerals by incremental heating. This yields a

TABLE 2. EFFECT OF CONTAMINATION BY 70 MICROGRAMS OF A PRECAMBRIAN FELDSPAR (1.5 Ga) CONTAINING 4.00×10^{-3} MOLES/GRAM RADIOGENIC ^{40}Ar ON A 30-ka FELDSPAR

	Weight (g)	K (%)	^{40}Ar Radiogenic - 12×10 mole	^{40}Ar Atmospheric - 12×10 mole	^{40}Ar Atmospheric (%)	K-Ar Date (ka)
Uncontaminated	12.600	9.48	6.36	20.6	76.4	30.7 ± 1.6
Contaminated	12.600	9.48	9.16	20.6	69.2	44.2 ± 1.8

spectrum of $^{40}\text{Ar}/^{39}\text{Ar}$ ratios as a function of the temperature of incremental release. Even though argon may have been lost from mineral sites in which argon was less tightly held, plateaus are frequently obtained at higher temperatures for tightly held argon, and the plateau data yields a better value of the time since the sample began retaining argon by correcting partial argon loss. The $^{40}\text{Ar}/^{39}\text{Ar}$ method is particularly useful for dating geologically old samples where there is a high probability of resetting of the K-Ar clock by argon loss during subsequent thermal events. Thermal resetting is much less probable and relatively easily recognized in Quaternary volcanic rocks, but other problems must be overcome. Several books and many papers have been written on the subject of K-Ar dating. A summary of both methods with many references is available in Faure (1986).

Three major problems are encountered in the dating of Quaternary volcanic rocks: (1) The correction for the atmospheric argon is very large and subject to error due to isotope fractionation resulting from incomplete equilibration (Krummenacher, 1970), (2) samples are more easily biased by extraneous older materials (e.g., see Fig. 8-7 of Dalrymple and Lanphere, 1969), (3) amounts of excess radiogenic argon that would be negligible for older samples may seriously affect the apparent age of Quaternary volcanic rocks (for review see Chapter 8 of Dalrymple and Lanphere, 1969).

Argon has three stable isotopes, which compose nearly 1 percent by volume of the Earth's atmosphere. The isotopic abundance of the three isotopes according to Nier (1950) is: ^{36}Ar (0.337%), ^{38}Ar (0.063%), and ^{40}Ar (99.60%). In the conventional method, measurement of ^{40}Ar and ^{36}Ar is made by isotope dilution in which the diluent is very pure ^{38}Ar . The concentration of ^{40}Ar and ^{36}Ar is measured relative to the known amount of ^{38}Ar diluent. Atmospheric ^{40}Ar must be subtracted from the measured sample ^{40}Ar to obtain radiogenic ^{40}Ar . ^{36}Ar is used as a measure of the atmospheric component. The atomic ratio of ^{40}Ar to ^{36}Ar in air is 295.5 but, as a result of instrumental fractionation, the ratio measured when pure air argon is introduced into a mass spectrometer may not be exactly 295.5. A fractionation correction must be determined by repeated, precise measurement of air argon samples. As an example, consider a Quaternary sample argon measurement comprising 95 percent air and 5 percent radiogenic ^{40}Ar . If the fractionation correction is 1 percent, a

failure to apply the correction would result in a 19 percent error in the radiogenic ^{40}Ar measurement.

There will be an error in the atmospheric air correction if the atmospheric Ar has been fractionated prior to measurement. For example, atmospheric Ar entering a rapidly cooling volcanic rock may not fully equilibrate. As a result of equipartition of energy, the average velocity of ^{36}Ar is 5.4 percent greater than ^{40}Ar and will equilibrate faster. The effect of nonequilibration would be a reduction in apparent age as a result of over correction for atmospheric Ar. It will be shown later that this effect can be minimized by using ground-mass crystallites rather than phenocrysts in the K-Ar dating of Quaternary volcanic rocks.

The effect of contamination by extraneous older materials can be very severe, as shown in Table 2. Large xenocrysts that may contain inherited radiogenic ^{40}Ar must be removed and extreme care taken to avoid contamination during sample preparation.

Radiogenic ^{40}Ar is released from rocks heated by magma, and argon is soluble in the magma and minerals. At the low Ar pressures likely to occur in magma chambers of volcanic flows, Henry's Law will hold (Damon, 1970):

$$^{40}\text{Ar}_E = Sp \quad (1)$$

where $^{40}\text{Ar}_E$ = moles/g of dissolved radiogenic ^{40}Ar , S = moles/g dissolved at 1 bar, and p = the partial pressure of argon. For example, S for albite at 1000°C is 3.9×10^{-9} moles/g. If the partial pressure of ^{40}Ar in the magma reached .001 bar, the albite would dissolve 3.9×10^{-12} m/g of ^{40}Ar . This amount would prohibit a meaningful date for a Quaternary volcanic rock. Fortunately, upon extrusion, the excess ^{40}Ar will tend to escape, but the mineral will also tend to equilibrate with atmospheric argon. Again, as will be shown, the smaller the mineral, the more rapid the equilibration.

EQUILIBRATION OF ARGON AT ELEVATED TEMPERATURES

A good approximation to diffusion in minerals can be obtained by use of the concept of an escape constant, λ_d (Damon, 1970):

TABLE 3. TIME FOR 99 PERCENT LOSS OF EXCESS $^{40}\text{Ar}_E$ AT 1,050° C*

r_c (cm)	0.142	0.071	0.027	0.006	0.001
t	1 month	1 week	1 day	1 hour	2 minutes

* $D_0 = 1.18 \times 10^{-4} \text{ cm}^2/\text{sec}$ and $E = 26 \text{ Kcal/mole}$.

 TABLE 4. TIME FOR 99 PERCENT LOSS OF EXCESS $^{40}\text{Ar}_E$ *

T	20° C	50° C	100° C	200° C	300° C	400° C
t (yr)	1.22×10^{11}	1.93×10^9	8.44×10^6	5.08×10^3	41	1.4

T	515° C	590° C	715° C	1,030° C	1,100° C
t	1 month	1 week	1 day	1 hour	35 minutes

* $r_c = 0.005 \text{ cm}$; diffusion parameters are those of Table 2.

$$\lambda_d = \frac{gD}{X^2} \quad (2)$$

where g is a geometry factor, D is the diffusion coefficient, and X is the pertinent diffusion dimension, e.g., the radius of a sphere or the thickness of thin slab of large area. D is related to temperature by the Arrhenius equation:

$$D = D_0 \exp(-E/RT) \quad (3)$$

where E is the activation energy for diffusion, R is the Boltzmann constant, and T is the temperature in degrees Kelvin.

At magmatic temperatures in the magma chamber before eruption, argon will rapidly equilibrate, and the argon content of the mineral will be the excess ^{40}Ar supported by the partial pressure of ^{40}Ar in the magma chamber (Equation 1).

Upon extrusion, the lava with its contained minerals will tend to approach equilibrium with the atmosphere. The excess ^{40}Ar will escape and atmospheric Ar will enter. For the dating of Quaternary rocks, we require a close approximation to equilibrium, i.e., a $^{40}\text{Ar}/^{36}\text{Ar}$ ratio of 295.5. For example, consider a small plagioclase crystal in the melt with $D_0 = 1.18 \times 10^{-4} \text{ cm}^2/\text{sec}$ and $E = 26 \text{ Kcal/mole}$ (Laughlin, 1969), and approximate its geometry as that of a cylinder whose length is great compared to its radius r_c . According to Jost (1960), the escape of excess ^{40}Ar for losses greater than 30 percent closely approximates an exponential relationship.

$$^{40}\text{Ar}(t) = \frac{^{40}\text{Ar}_E(0)}{(2.405)^2} \exp(-\lambda_d t) \quad (4)$$

where $^{40}\text{Ar}_E(t)$ is the average concentration of $^{40}\text{Ar}_E$ after a time

t , $^{40}\text{Ar}_E(0)$ is the initial concentration before eruption, t is the time after eruption, and g in Equation 2 is $(2.405)^2$. Because the square of the radius (r_c^2) and temperature (T) enter into the exponential of Equation 4, the rate of loss is critically dependent upon crystal size (Table 3) and temperature (Table 4). At magmatic temperatures, ground mass plagioclase microlites would lose 99 percent of excess radiogenic argon within minutes, whereas phenocrysts would retain much of their excess radiogenic argon during the cooling process. This effect would tend to yield anomalously old ages. On the other hand, the phenocrysts will also not equilibrate completely, resulting in fractionation of atmospheric argon. The excess ^{36}Ar , when multiplied by the air ratio, will tend to produce anomalously young ages. Thus, ages which are too young or too old may result, depending on which effect is dominant in each particular case.

Groundmass plagioclase microlites lose their excess argon rapidly and equilibrate rapidly with air. Consequently, they tend to yield consistent ages if not reset by subsequent thermal events. It should be emphasized that a temperature of 100°C sustained for a sufficiently long time could cause a significant error in the age of plagioclase microlites. From Table 5, it can be seen that a temperature of 100°C sustained for 60,000 yr would result in a 15 percent loss of argon from the microlites.

COMPARISON OF THEORY WITH PRACTICE

Theory then suggests that for young samples that have not been deeply buried or otherwise thermally reset, plagioclase microlites are better K-Ar clocks than phenocrysts that may not have completely lost excess argon or equilibrated with air. Our

TABLE 5. PERCENT ^{40}Ar LOSS AT 100° C*

Percent loss	15	30	45	60	75	90
t (yr)	6.0×10^4	1.7×10^5	4.5×10^5	1.1×10^6	2×10^6	3.9×10^6

*Diffusion parameters of Table 2, $r_c = 0.005$ cm.

TABLE 6. WORST CASE EXAMPLES FOR K-Ar DISCORDANCY BETWEEN
PLAGIOCLASE MICROLITE CONCENTRATES AND PHENOCRYSTS

Sample No.	Type	K (%)	$^{40}\text{Ar}_{\text{rad}}$ (10^{-12} m/g)	$^{40}\text{Ar}_{\text{air}}$ (%)	K-Ar Date (Ma)
UAKA-6-65	Microlite	0.852	3.59	88.4	2.43 ± 0.32
UAKA-6-65	Phenocryst	0.190	3.14	39.2	9.52 ± 0.81
UAKA-85-365	Microlite	0.992	10.82	37.2	6.28 ± 0.15
UAKA-85-365	Phenocryst	0.318	1.88	89.3	3.41 ± 0.24
UAKA-85-367	Microlite	0.762	8.301	40.6	6.27 ± 0.16
UAKA-85-367	Phenocryst	0.135	0.962	79.6	4.10 ± 0.24
UAKA-85-378	Microlite	1.202	1.032	83.1	0.49 ± 0.035
UAKA-85-378	Phenocryst	0.162	0.271	95.6	0.967 ± 0.158

experience has confirmed theoretical expectations. Dates on microlite concentrates yield reasonable results consistent with stratigraphy, whereas K-Ar dates on phenocrysts are often discordant. This is true not only for plagioclase; biotite and hornblende phenocrysts also frequently yield discordant ages for Quaternary rocks. However, sanidine phenocrysts usually give concordant dates.

Table 6 shows the worst cases that we have observed during years of dating young rocks. Sample UAKA-6-65 was one of the earliest and the most extreme examples of the not infrequent discordance between K-Ar dates on plagioclase microlites and phenocrysts from the same rock and, fortunately, alerted us to the problem. Phenocrysts from this sample are very large, up to 2 cm, translucent and semiperfect. This sample had not completely equilibrated with air nor lost all of its excess ^{40}Ar . However, the dominant effect was the large amount of excess ^{40}Ar . This also occurred for sample UAKA-85-378. The dominant effect in samples UAKA-85-365 and UAKA-85-367 seems to be incomplete equilibration with air, leading to over correction.

An added factor in favor of dating the microlites is the much higher K content of the more sodic microlites compared to the more calcic phenocrysts. This results in a higher radiogenic ^{40}Ar content and, typically, a lower air correction. Sample UAKA-6-65 is atypical because of its extremely high excess ^{40}Ar content that results in a relatively low percent air correction.

It is important to sample the Quaternary rock to be dated in such a way as to minimize error. The quickly quenched parts of a flow may not have been purged of excess argon or equilibrated with air. The rubbly bottom of a flow may contain extraneous older material, and vuggy samples may contain exorbitant amounts of air. We prefer to sample the massive interior of the flow; it has few vesicles and has cooled relatively slowly, allowing time to purge excess ^{40}Ar . Typically, air corrections are usually also much lower for samples from the interior of the flow.

In preparing the Quaternary volcanic rock sample, phenocrysts, xenocrysts, and xenoliths should be removed before preparing the microlite concentrate. Glass, clay, and ferromagnesians should be removed from the sieve-classified fraction (e.g., <100>150) by the usual heavy-liquid and magnetic-separation methods. Carbonate, if present, and residual glass should be removed by washing in dilute acids.

CONCLUSIONS

The fundamental limitation in K-Ar dating of Quaternary volcanic rocks is not our inability to measure argon precisely. Rather, it is intrinsic to several basic assumptions of the method which are not always met. Specifically, the sample to be dated must have no excess ^{40}Ar or extraneous ^{40}Ar from contamination and it must have equilibrated with atmospheric argon. In addi-

tion, the atmospheric correction should not be prohibitively high. These limitations can be minimized by careful sampling, careful sample preparation, and by dating groundmass feldspar concentrates rather than phenocrysts. Because of their small size, micro-lites lose excess ^{40}Ar and equilibrate with atmospheric argon much more rapidly than phenocrysts. Guided by this strategy, we have had gratifying success in dating volcanic rocks even as young as Wisconsin. But, in the words of Bobby Burns, the Scottish bard, "The best laid plans of mice and men gang oft aglae."

FISSION-TRACK DATING

Charles W. Naeser and Nancy D. Naeser

INTRODUCTION

Fission-track dating has been applied to many problems in Quaternary geology. Most studies involve dating of volcanic ash layers or determining rates of landform development. Examples of such studies are given below. To a more limited extent, the method has been used in archaeological studies (for example, Fleischer and others, 1965b; Bigazzi and Bonadonna, 1973; Wagner, 1978; Gleadow, 1980).

THEORY AND METHODS

A fission track is a zone of intense damage formed when a fission fragment passes through a solid. When an atom of ^{238}U fissions, the nucleus breaks up into two lighter nuclei, one averaging about 90 atomic mass units and the other about 135 atomic mass units, with the liberation of about 200 MeV of energy. The two highly charged nuclei recoil in opposite directions and disrupt the electron balance of the atoms in the host mineral or glass along their path. This disruption of electron charge in turn causes the mutual repulsion of positively charged ions and the displacement of the ions from their normal crystallographic positions in the host. The result is a zone of damage defining the fission track (Fleischer and others, 1975). The new track is tens of angstroms in diameter and about 10 to 20 μm in length.

A track in its natural state can only be observed with a transmission electron microscope, but a suitable chemical etchant can enlarge the damage zone so that it can be observed with an optical microscope at intermediate magnifications ($\times 200$ – 500). Common etchants used to develop tracks include nitric acid (for apatite), hydrofluoric acid (mica and glass), concentrated basic solutions (sphene), and alkali fluxes (zircon) (Fleischer and others, 1975; Gleadow and others, 1976).

Because ^{238}U fissions spontaneously at a constant rate, the age of a mineral or glass can be calculated from the number of spontaneous fission tracks and the amount of uranium that it contains. The relative abundance of ^{238}U and ^{235}U is constant in nature, and thus the easiest and most accurate way to determine the amount of uranium is to create a new set of fission tracks by

irradiating the sample in a nuclear reactor to induce fission of ^{235}U with a known dose of thermal neutrons. Early development of the fission-track method is reviewed by Fleischer and others (1975) and Naeser (1979).

Two major factors determine whether or not a sample can be dated by the fission-track method. First, the sample must contain a mineral or glass of appropriate uranium content. In Quaternary samples, there must be enough uranium that a statistically significant number of tracks can be counted in a reasonable time. Second, tracks must completely retained once they are formed, or the calculated age will be anomalously young. Heating can cause partial to complete fading (annealing) of the spontaneous tracks. The fission track is stable in most non-opaque minerals at temperatures of 50°C or less, but fission tracks in natural glasses can be affected at much lower temperatures (Seward, 1979; Naeser and others, 1980). Several Quaternary studies have made use of track fading, for example, to determine rates of landform development (e.g., Zeitler and others, 1982; Naeser and others, 1983; Coates and Naeser, 1984).

In the Quaternary studies, only zircon and glass are routinely used for fission-track dating, and they require two different laboratory procedures. The external detector method (Naeser, 1976, 1979) is used to date single crystals of zircon because the uranium distribution is inhomogeneous in individual zircon grains. In contrast, glass is usually dated by the population method (Naeser, 1976, 1979); because all of the glass from a single source has a similar uranium concentration, it is possible to determine the spontaneous and induced track densities from different splits of the same sample. (The reader is referred to Naeser and Naeser [1984] for a more detailed discussion of the theory and methodology of fission-track dating.)

ADVANTAGES AND LIMITATIONS

One advantage that fission-track dating has over most other methods is that sample contamination often can be readily recognized and, therefore, minimized. In conventional radiocarbon and K-Ar dating, bulk samples must be analyzed. Contamination of a sample with older or younger carbon can result in an erroneous radiocarbon age, and a few older detrital grains can have a significant effect on a K-Ar age (Damon, this chapter; Naeser and others, 1981). Fission-track dating is a grain-specific method in which individual grains are scanned and counted. In the case of zircon dating, an age is obtained on each grain that is counted. Therefore, older detrital grains often can be recognized and discarded from the age calculation.

A major limitation of fission-track dating of Quaternary samples is that very young samples ($< 100,000$ yr) usually have a very low spontaneous track density. This requires tedious examination of large numbers of mineral grains or glass shards and produces ages with large analytical uncertainties. Naeser and others (1982) noted one glass sample in which they did not see any spontaneous tracks after scanning thousands of shards. However, even though the analytical uncertainty is large for very young

samples, some such results can solve significant geological problems.

Zircons, although preferable to glass, are not present in all samples. In tephra, their presence depends on the chemistry of the parent magma. Acidic tephra are more likely to yield usable zircons than basic tephra. Zircons that are extremely fine grained ($<75 \mu\text{m}$) cannot be dated by the fission-track method, and this is often the case in tephra sampled a long distance from the vent.

Natural glasses have been extensively dated because of the widespread occurrences of tephra and obsidian in Quaternary rocks. The dating of natural glasses presents special problems. The greatest of these is the ease with which glass can lose spontaneous tracks by annealing (Fleischer and others, 1965a; Storzer and Wagner, 1969; MacDougall, 1976; and Seward, 1979). Hydrated glass shards, which are found in most tephra beds, are particularly susceptible to annealing (Lakatos and Miller, 1972). Work by Naeser and others (1980) has shown that both hydrated and nonhydrated glass can lose tracks at ambient surface temperatures over periods of geologic time. In a study of 14 tephra from upper Cenozoic ($<30 \text{ Ma}$) deposits of the western United States, only one glass had a fission-track age that was concordant with the fission-track age of coexisting zircon. All other samples had ages that were significantly younger than the zircon ages. Seward (1979) showed that 60 percent of the glass fission-track ages of Quaternary tephra studied in New Zealand were significantly younger than the fission-track ages of the coexisting zircons.

APPLICATIONS

Tephrochronology

The major contribution of fission-track dating to Quaternary studies has been in the field of tephrochronology. Fission tracks have proved to be the most suitable method for dating tephra, particularly those older than the maximum limit of radiocarbon dating, which for most analyses is 40 to 50 ka.

The following two studies illustrate the use of fission-track dating in tephrochronology. Volcanic ash beds of the Pearlette family occur in Pleistocene deposits of western North America (Izett and others, 1970, 1972). Before 1970, the Pearlette ash was considered to be the product of a single eruption, and it was used as an isochronous time marker for many midcontinent Quaternary deposits. Izett and others (1970, 1972) reported consistent chemical differences among three subsets of the Pearlette ash samples. They suggested that the three subsets could be correlated geochemically with three major ash-flow deposits originating in the region of Yellowstone National Park, Wyoming. The three ash-flow deposits were dated at $2.02 \pm 0.08 \text{ Ma}$ (Huckleberry Ridge Tuff), $1.27 \pm 0.10 \text{ Ma}$ (Mesa Falls Tuff), and $0.616 \pm 0.008 \text{ Ma}$ (Lava Creek Tuff) by the K-Ar method (J. D. Obradovich, personal communication, 1973). Naeser and others (1973) dated zircons from two of the three subsets of Pearlette tephra and obtained ages of $1.9 \pm 0.1 \text{ Ma}$ for ash correlated with the Huckleberry Ridge Tuff and $0.6 \pm 0.1 \text{ Ma}$ for ash correlated

with the Lava Creek Tuff. These ages matched the ages in the source region and confirmed the geochemical evidence of Izett and others (1970, 1972) that there were three Pearlette ashes rather than just one.

In another study, fission-track dating has demonstrated that a tephra is considerably older than had been inferred from radiocarbon dating of associated organic matter. The Salmon Springs Drift at its type locality, at Salmon Springs, Washington, consists of two drift sheets separated by about 1.5 m of peat, silt, and volcanic ash (Lake Tapps tephra) (Crandell and others, 1958; Easterbrook and others, 1981). The peat grades downward with decreasing organic content into about one meter of silt, which in turn grades into the volcanic ash (D. J. Easterbrook, personal communication, 1980). The peat was radiocarbon dated at $71,500^{+1700}_{-1400} \text{ yr BP}$ by the enrichment method (Stuiver and others, 1978), and the drift sheets were thus considered early Wisconsin in age. Fission-track dating of this ash and a correlative ash at Auburn, Washington, along with paleomagnetic and tephrochronological evidence, shows that the Lake Tapps tephra is ca. 860,000 yr old, and thus the Salmon Springs Drift is an order of magnitude older than indicated by the radiocarbon date (Easterbrook and others, 1981).

Landscape evolution

Several studies have used fission-track dating to determine rates of landform development. An example is a study in the Powder River Basin, Wyoming, that involved dating of clinker formed by natural burning of coal beds.

The burning of the coal occurs when the coal beds are exposed to atmospheric oxygen. In the Rochelle Hills, coal beds are exposed as east-flowing streams cut headward through the west-dipping coal. This headward erosion lowers the water table in the coal, allowing it to burn. If the heat from the burning coal anneals the spontaneous tracks in the detrital zircons, then the zircons record the time when the clinker cooled after the burn.

Coates and Naeser (1984) dated zircons separated from the clinker capping the mesa north of Little Thunder Creek, Wyoming. This study showed that the ages of zircons in the clinker become progressively younger from east to west. Zircons from eastern end of the mesa give ages of ca. 700,000 yr, while zircons at the western edge of clinker development do not contain any spontaneous fission tracks, indicating an age of $<80,000 \text{ yr}$ for that burn. The results of this study show that during the last 700,000 yr, the burn front at Little Thunder Creek has migrated westward about 8 km, and that there has been about 200 m of downcutting of the eastern edge of the escarpment.

Another example of using fission-track dating to study landscape evolution is the use of apatite ages to determine the uplift and erosion (cooling) history of a mountain block. Apatite will not retain fission tracks if it is held at temperatures in excess of 105°C (for heating of 10^8 yr duration) to 150°C (10^5 yr). When a rock containing apatite cools during an uplift/erosion cycle, the apatite in that rock will begin to record fission tracks.

Therefore, apatite fission-track ages provide information on the uplift history of a mountain block.

Naeser and others (1983) used apatite ages to determine an uplift/erosion rate of the Wasatch Mountains northeast of Salt Lake City, Utah. They separated and dated apatite from the Precambrian rocks of the Farmington Canyon Complex. Apatite fission-track ages as young as 5 Ma were found at the base of the mountains near the Wasatch Fault, indicating that these rocks had been at a temperature in excess of $\sim 120^{\circ}\text{C}$ prior to 5 Ma. The data indicate further that the latest episode of uplift in this segment of the Wasatch Mountains began about 10 Ma and has continued to the present with an average uplift rate of 0.4 mm/yr, and that these rocks have been cooling at a rate of about $12^{\circ}\text{C}/\text{m.y.}$

SUMMARY

Fission-track dating has widespread application in Quaternary studies. The major contribution has been in the field of tephrochronology, where fission-track dating has been used to date tephra horizons in Quaternary deposits and thereby date Quaternary events. The method has also been used to study the rates of landform development and to determine rates of tectonic processes and how those rates relate to the overall development of the landscape.

CONVENTIONAL URANIUM-SERIES AND URANIUM-TREND DATING

B. J. Szabo and J. N. Rosholt

INTRODUCTION

Climatic fluctuation was the dominating condition during the Quaternary. It resulted in expansion and recession of pluvial lakes, glaciation and deglaciation, large glacio-eustatic sea-level changes affecting both stable and uplifting coastlines, and landscape evolution. The alternating periods of higher versus lower precipitation and temperature influenced rock weathering, alluviation, and soil evolution; also, climatic changes enhanced the mobility of elements in soil profiles and formation of associated secondary minerals. Many of these secondary deposits and some young volcanic rocks are potentially datable by conventional U-series dating, and the time of deposition of some Quaternary sediments can be estimated by uranium-trend dating; both techniques of dating provide the opportunity for deciphering the timing of some of the complex Quaternary events.

The natural radioactive series of ^{238}U , ^{235}U , and ^{232}Th produce numerous daughter products of varying chemical properties and half lives (Fig. 2). Both the parents and their daughter elements are common trace constituents in nearly all geologic materials. If any of these materials containing the parent isotopes remain undisturbed for a period of about 2 m.y., a state of secular equilibrium between parents and all of their respective radioac-

tive daughter nuclides will become established—that is, all measured parent-to-daughter activity ratios are unity. However, several geochemical processes can cause isotopic and elemental fractionation resulting in states of disequilibrium. Conventional uranium-series dating is based on the measurement of the extent to which the state of secular equilibrium is approached in a closed system after the initial disturbance. In contrast, uranium-trend dating is based on the measurement and modeling required to determine the extent and maintenance of disequilibrium in an open system after sedimentation.

CONVENTIONAL URANIUM-SERIES DATING

The conditions for reliable conventional U-series dating are that the material remained a closed system through geologic time with respect to the nuclides of interest, and that the material is pure, reasonably uniform, and was not subject to recrystallization or other processes that could produce subsequent mobilization of daughter products.

The most commonly utilized methods for Quaternary deposits rely on the measurements of disequilibrium between ^{230}Th and ^{234}U (^{230}Th deficiency method), between ^{231}Pa and ^{235}U (^{231}Pa deficiency method), and ^{234}U and ^{238}U (^{234}U excess method). Deficiencies of ^{230}Th and ^{231}Pa in secondary minerals are due to the marked difference between the aqueous mobility of uranium relative to thorium and protactinium. Uranium is readily leached from weathered source rocks, then transported and re-deposited, whereas ^{230}Th and ^{231}Pa are extremely insoluble, and trace amounts dissolved from source rocks are effectively removed from solution by adsorption during transport. Materials datable by the ^{230}Th and ^{231}Pa deficiency methods are either (1) geologically derived, such as various forms of carbonates, sulfates, phosphates, opal, and young volcanic rocks, or (2) biogenic in origin, such as corals, mollusks, bones, and peat deposits. The upper (oldest) limit of ^{230}Th deficiency dating is about 360 ka; the upper limit of ^{231}Pa deficiency dating (used mainly as a complementary method to ^{230}Th dating) is about 180 ka.

Natural waters and secondary minerals generally contain excess ^{234}U relative to ^{238}U because the alpha recoil (Fleischer, 1980) associated with the process of ^{238}U radioactive decay to ^{234}U (Fig. 1) displaces the ^{234}U atoms to more leachable sites than those of ^{238}U atoms, which occupy the original crystal lattice positions. The excess ^{234}U is then the measure of the age of the material, provided that the initial $^{234}\text{U}/^{238}\text{U}$ activity ratio can be ascertained. The ^{234}U excess method has been used for dating corals, speleothems, and calcitic veins. The range for practical dating by this method is between about 100,000 and 1.5 m.y. Equations used for the age calculations and general chemical procedures are described by Ivanovich (1982) and Lally (1982).

Secondary carbonates

Inorganic (predominantly calcite) and organic (aragonite or calcite) carbonate deposits are common components in most

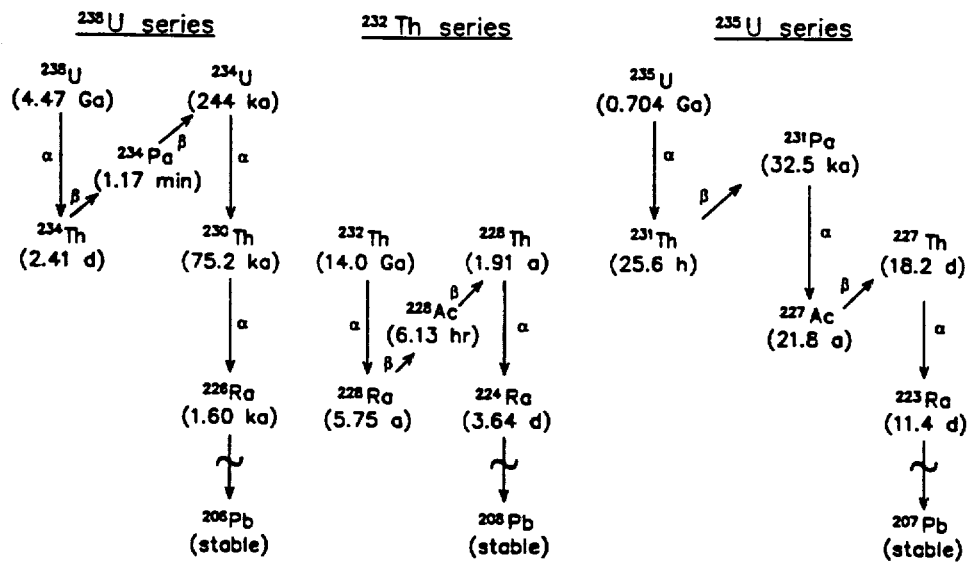


Figure 2. Decay series of naturally occurring uranium and thorium nuclides.

depositional environments, and they display a variety of textures and structures. Most of the dense, pure carbonates are suitable for reliable U-series dating.

Speleothems (carbonates precipitated in caves) are usually good material for U-series dating. Results are utilized in various ways. Ages can establish the local cave chronology and rates of deposition (Thompson and others, 1975). Speleothem growth in an arid climate may indicate pluvial periods, and lack of growth may indicate dry climatic conditions (Harmon and Curl, 1978). The absence of speleothem growth in alpine caves indicates periods of prolonged cold, preventing the movement of ground water (Harmon and others, 1977 and Lively, 1983). Combinations of speleothem dating with stable isotopic analyses are used in paleoclimatic studies in both temperate and glacial zones (Mills, this volume; Schwartz and others, 1976; Thompson and others, 1976; Harmon and others, 1978a; and Harmon and others, 1978b).

Calclitic veins are dense, low-temperature precipitates from calcium carbonate-saturated ground water that fill or line fractures. Some of these veins provide a continuous record for the past 2 m.y., and they can be dated reliably by the ^{230}Th deficiency and ^{234}U excess methods (Winograd and Doty, 1980). Reduced deuterium contents in fluid inclusions of U-series-dated calclitic veins from the southern Great Basin indicate major uplift of the Sierra Nevada during the Quaternary (Winograd and others, 1985). Dates on calclitic veins in the Amargosa Desert, Nevada, indicate a lowering of the paleo-ground-water table at that area by about 0.04 m/1000 yr, probably due to an increase in aridity during the Pleistocene (Winograd and Szabo, 1985), and these dates provide other implications for the climatic record (Winograd and others, 1988). Uranium-series dating of calclitic

veins occurring in ash-flow tuffs at Yucca Mountain, Nevada, suggests episodic fluid movements and fracture filling during the past 400,000 yr (Szabo and Kyser, 1985).

Travertines (dense and clean varieties of spring-deposited carbonates) are also suitable for U-series dating. They often occur as extensive horizontal or sloping layers, mounds, or steep drapings. Travertines may cap fluvial terrace deposits, thus providing limiting ages for periods of deposition and terrace cutting (Schwartz and Gascoyne, 1984). Extensive erosion during the Pleistocene developed pediments in central Montana. Dating travertines associated with one pediment surface indicates that the surface is older than about 320,000 yr (Szabo and Lindsey, 1986). Evidence for paleospring activities is represented by travertine deposits in Grand Canyon National Park, Arizona dated at about 170, 110, and 80 ka (Szabo and others, 1986).

The porous variety of spring-deposited calcium carbonate (calcareous tufa), usually contains detrital materials, and their open structure permits secondary mobilization or addition of the U-series nuclides. Separation and analysis of both the acid-soluble carbonates and acid-insoluble residues of carefully selected samples may yield useful limiting dates for various Quaternary processes (Szabo and others, 1981a).

Clean and dense parts of lacustrine carbonates may yield reasonable dates by U-series analysis (Kaufman and Broecker, 1965). Lacustrine carbonates, however, usually contain various amounts of detrital materials, thus requiring large age corrections due to initial ^{230}Th contamination (Kaufman, 1971).

Secondary carbonate, concretions, rinds, and components that may be either pedogenic or nonpedogenic and are referred to as caliches or calcretes are potentially datable by U-series meth-

ods. These deposits usually contain large amounts of detrital residues, therefore, extensive age corrections are required for the uranium and thorium derived from the noncarbonate fraction. Selected dense calcretes from the Nevada Test Site region yielded useful limiting ages for recent faulting (Knauss, 1981; Szabo and others, 1981a). By multiple analysis of both the carbonate and the detrital fractions of caliche cement samples, Ku and others (1979) determined periods of carbonate cementation in alluvial deposits of the Mohave Desert, California.

Carbonate-rinds, nodules, and rhizocretions are pedogenic or ground-water-precipitated carbonates that coat rock surfaces, form in sediments, or form root-like structures. If dense and relatively clean, these materials can be successfully dated by U-series methods. Carbonate-rinds on boulders from fan deposits near Arco, Idaho, have been dated. Rind carbonates accumulated between about 10,000 and 100,000 yr ago, and apparently remained a closed system with respect to uranium and thorium migration (Szabo and Rosholt, 1982). Carbonate-rind dates indicate an age of about 200,000 yr for the Yermo fan deposit at Calico, California (Bischoff and others, 1981).

Corals have consistently yielded reliable age results, provided they are composed of unrecrystallized aragonite and are free of void-filling contaminants. Coral flourishes in the tropics, but certain solitary species occur even in temperate regions. Up to the present, only four California and one Oregon Pacific coast localities yielded enough coral material for U-series dating. The California localities are: Nestor Terrace, San Diego (Ku and Kern, 1974); Cayucos, San Luis Obispo County; San Nicolas Island (listed in Ku and Kern, 1974); and San Clemente Island (Muhs and Szabo, 1982). The Oregon coral is from the Whiskey Run Terrace, Bandon (Kennedy and others, 1982). The dating results of corals have been applied for calculating local uplift rates and for calibrating amino-acid ratios from mollusks, which in turn were used for regional correlations and relative dating (Wehmiller and others, 1977; Kennedy and others, 1982; and Muhs, 1985).

Over 55 fossil corals have been dated from marine deposits (some in place) along the southeastern U.S. Atlantic Coastal Plain (Szabo, 1985). Ages of these corals have been used for paleoclimatic reconstruction (Cronin and others, 1981) and for lithostratigraphic and biostratigraphic differentiation (Colquhoun, this volume; Mixon and others, 1982; and McCartan and others, 1982). Fossiliferous deposits along the northern part of the Atlantic Coastal Plain contain scarce corals; dated fragments from the Pleistocene Sankasty Sand, southeastern Massachusetts, indicate a last interglacial age (about 130,000 yr) for the deposition of this marine unit (Oldale and others, 1982). Of the conterminous United States, reef-building corals occur only in southern Florida. Dates from fossil corals from the Pleistocene Key Largo Limestone and reef deposits of the Bahamas indicate that reef formation occurred about 135 ka in the southern Florida area, while sea level was several meters above its present level (Osmond and others, 1965; Neumann and Moore, 1975; and Harmon and others, 1978b).

Mollusks, abundant in many marine, fluvial and lacustrine sediments, are potentially datable by U-series methods. Unlike corals, however, major amounts of uranium enter the molluscan shells after the death of the animals, and they often remain susceptible to gradual or episodic post-depositional assimilation of uranium so that some pre-Pleistocene samples give erroneous finite dates (Kaufman and others, 1971). Furthermore, shells may be subject to recoil gain of ^{231}Pa , ^{230}Th , and ^{234}U (Szabo and Rosholt, 1969); to partial loss of ^{230}Th and/or ^{231}Pa (Szabo and Gard, 1975; and Szabo and others, 1981b); and to initial ^{230}Th contamination, as determined by measured ^{232}Th (Osmond and others, 1970). In the absence of other U-series datable materials, and in conjunction with other correlative techniques, mollusk dates generally are only approximate, usually minimum, ages for depositional events (Szabo and Rosholt, 1969; Szabo and Vedder, 1971; Bradley and Addicott, 1968—redated by Szabo, 1980a; Wehmiller and others, 1977; and Mixon and others, 1982). Fossil echinoids from California also show open-system conditions similar to mollusks (Muhs and Kennedy, 1985).

Secondary deposits other than carbonates

Detritus-free evaporites may yield useful U-series dates for the time of sedimentation. Dates on bulk salt samples (mostly halite, trona, and gaylussite) in Searles Lake, California, have been reported recently (Peng and others, 1978; and Bischoff and others, 1985), where the lake sediment consists of sequences of mud (pluvial) and salt (arid) layers. Results indicate semidry and intermediate climate with moderate salinities during the period from about 200 to 300 ka, followed by a generally wet climate and greater water depth with low salinities during about the last 100,000 yr.

Under favorable conditions, other evaporites such as sulfates are also datable. Anhydrite samples from Stanton's Cave, Grand Canyon National Park, Arizona, yielded apparently reliable U-series dates between 16 and 59 ka (Rosholt and others, 1987a). Dating of gypsum spring deposits near Carlsbad, New Mexico, was attempted (Szabo and others, 1980), but the results show that these surface-exposed samples contain detrital contaminants, and did not remain an ideal closed system with respect to uranium and daughter elements.

Knauss (1981) reported that some pure secondary silica, opal deposits, contain uranium, but negligible amounts of thorium, and that the samples appear to constitute a closed system with respect to uranium isotopes and their respective radioactive daughters. Laminated opal from the Yucca Mountain region, Nevada (Szabo and O'Malley, 1985), and opal-filling fractures in ash-flow tuffs of Yucca Mountain, Nevada (Szabo and Kyser, 1985), have been dated but there is at present no independent age control to test the reliability of the results. In theory, clean secondary accumulations of iron and manganese hydroxides and oxides can be dated by U-series. Desert varnishes, dark coatings of ferromanganese oxides on exposed rock surfaces in arid climate regions, have been proposed as suitable materials for dating

(Knauss and Ku, 1980), but again, no independent age control is as yet available.

Fossil bones take up uranium after the death of the animal, and do so presumably until all active organic matter within the bone has decomposed. Comparison of U-series and ^{14}C dates of bones younger than 30,000 yr indicates that most secondary uranium assimilation occurs within a few thousand years after burial, but in some cases the progressive uranium uptake by these fossils can be considerably longer (Szabo, 1980b). Some of the older U-series-dated bone samples from alluvial deposits of Colorado (Szabo, 1980b), from the middle unit of the Riverbank alluvium near Sacramento, California (Hansen and Begg, 1970), and from gypsum deposits, Carlsbad, New Mexico (Szabo and others, 1980), have provided useful, although probably minimum-age estimates for the deposition of sediments containing the fossils. Severe weathering can cause uranium loss, resulting in U-series ages that are older than the actual burial age of the bone (Bada and others, 1984). Other materials, such as wood (Szabo, 1972), peat (Vogel and Kronfeld, 1980; Zielinski and others, 1986), and organic matter adhering to sand (Szabo, 1982) have been attempted for U-series dating, but most of these studies resulted in minimum-age estimates only, due to the open-system behavior of uranium.

Volcanic rocks

Young volcanic rocks can be dated by U-series methods in certain favorable circumstances. The requirements are: (1) that secular equilibrium was maintained between ^{238}U , ^{234}U , and ^{230}Th during the process of partial melting and during uprising and eruption of the magma, (2) that no contamination occurred by remelting of the older crust, and (3) that the volcanic rock remained a chemically closed system after solidification. During crystallization of the volcanic rocks, all individual mineral phases are assumed to have the same $^{230}\text{Th}/^{232}\text{Th}$ activity ratios, but their $^{238}\text{U}/^{232}\text{Th}$ would differ according to the relative partition coefficients of uranium and thorium in the different mineral phases. In all mineral phases, the ^{230}Th then approaches reestablishment of radioactive equilibrium relative to the amount of uranium in that particular phase. In an ideal case, a plot of $^{230}\text{Th}/^{232}\text{Th}$ against $^{238}\text{U}/^{232}\text{Th}$ defines a line, the slope of which will vary as a function of time (Harmon and Rosholt, 1982). This method has been utilized to date rhyolites from Mono Crater, California (Taddeucci and others, 1967), and Long Valley, California (Baranowski and Harmon, 1978).

URANIUM-TREND DATING

For successful conventional uranium-series dating, a closed system is required to exist throughout the history of a sample, meaning that there has been no postdepositional migration of ^{238}U or of its daughter products, ^{234}U and ^{230}Th . In contrast, open-system dating techniques require no such restrictions on postdepositional migration of these radioisotopes within and be-

tween deposits. Results of many studies of U-series disequilibria indicate that uranium commonly exhibits open-system behavior in many near-surface deposits (Ivanovich and Harmon, 1982). Because materials suitable for closed-system dating often are lacking in Quaternary deposits, an open-system dating method is needed. The model for uranium-trend dating was developed by Rosholt (1985) and applied to a variety of Quaternary deposits, including alluvium, eolian sediments, glacial deposits, zeolitized volcanic ash, and marine terrace deposits (Muhs and others, 1989). This open-system, empirical model requires a calibration based on deposits of known age; results of such calibrations are included in Rosholt and others (1985b).

For U-trend dating of sediments, the distribution of uranium-series members during and after sedimentation must have been controlled by their open-system behavior. Sediments and soils are penetrated continuously or episodically with ground water or soil water that contains at least small amounts of dissolved uranium, some of which may include exchange of locally leached and/or adsorbed uranium. As this waterborne uranium decays, it produces a trail of radioactive daughter products that are readily adsorbed in solid matrix materials such as clay and silt. If the trail of daughter products, ^{234}U and ^{230}Th , is distributed through the deposit in a consistent pattern, then uranium-trend dating is possible. The large number of geochemical variables in an open system precludes the definition of a rigorous mathematical model for uranium migration. Instead, an empirical model is used to define the parameters that can reasonably explain the patterns of isotopic distribution. This model requires independent time calibration with known-age deposits and careful evaluation of the stratigraphic relationships of the deposits to be dated; however, they do not have to occur in the same geographic area as the calibration deposits (Rosholt and others, 1985b).

Analyses of the abundances of ^{238}U , ^{234}U , ^{230}Th , and ^{232}Th in a single sample do not establish a meaningful time-related relationship of isotopic distribution in an open-system environment. However, analyses of several samples, each of which has only slightly different physical properties and only slightly different chemical compositions within a unit, may provide a consistent pattern in the distribution of these isotopes (Rosholt, 1985). Analyses of 5 to 8 samples per unit from several alluvial, colluvial, glacial, and eolian deposits have shown that these types of deposits, ranging from clay-silt to gravel units, have isotopic distributions that appear to fit an open-system model (Rosholt and others, 1985a and 1985b). To obtain a U-trend date, several samples are collected from a vertical section of each separate stratigraphic unit. The number of samples required to establish a reliable linear trend in the data depends on the variation in ratios of uranium and thorium that define the trend line.

It is preferable to collect samples from a channel cut through deposits exposed in a trench wall or a relatively fresh, well-exposed outcrop; existence of soil development is not a necessary requirement, nor is sampling of the entire stratigraphic unit always necessary. Pebbles and other larger fragments are removed

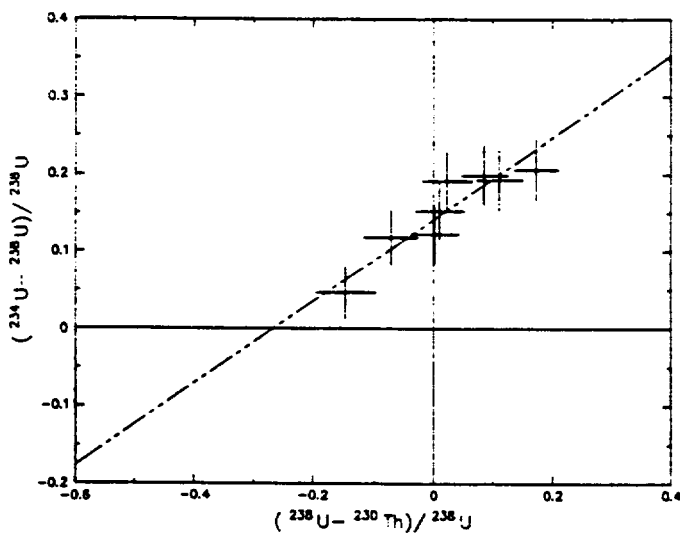


Figure 3. Uranium-trend plot of alluvium (160 ka) at Charlie Brown Quarry, Shoshone, California. All samples are plotted in terms of activity ratios; zero coordinates represent radioactive equilibrium in isotopic ratios (reproduced from Rosholt and others, 1985a).

by sieving and the remaining less-than-2-mm size fraction is pulverized to less-than-0.2-mm size, homogenized, and retained for analysis. Chemical procedures used for separating uranium and thorium for alpha spectrometry measurements are those described by Rosholt (1984 and 1985). For defining uranium-trend slopes, the results of these analyses are plotted in the form of $(^{234}\text{U} - ^{238}\text{U})/^{238}\text{U}$ against $(^{238}\text{U} - ^{230}\text{Th})/^{238}\text{U}$. Ideally, this yields a linear relationship, as shown in Figure 3, in which the slope is a function of the age of the deposit based on the calibration.

Applications for dating Quaternary deposits

In a report for the Nevada Test Site (Rosholt and others, 1985a), 31 of 37 depositional units analyzed were datable by the U-trend method. These results have median age estimates that indicate four separate time frames of deposition during the late and middle Pleistocene in this geographic area: 40 ± 15 ka, 170 ± 40 ka, 270 ± 50 ka, and 440 ± 60 ka. The results are reasonably consistent with other dates (Swadley and others, 1984) and with estimates based on geomorphic evidence. Analyses of deposits from a trench near Beatty, Nevada, suggest that a sequence of several fluvial deposits was laid down by the Amargosa River at the base of the Beatty scarp during the last 500,000 yr (Rosholt and others, 1988). Deposition of silts, sands, and gravel were dated at 75 ± 10 ka, 155 ± 30 ka, and 500 ± 100 ka.

Nine units from deposits in New Mexico have yielded ages ranging from about 20 ka to about 700 ka (Rosholt and others,

unpublished data). The deposits include alluvium, colluvium, eolian sand, and gypsum; some of the alluvial deposits now have well-developed carbonate horizons. The U-trend dates for two of these middle Pleistocene calcretes appear to be too young, based on geologic considerations, because of the effect of late stages of carbonate accumulation. The remaining deposits give reasonable ages based on stratigraphic relationships. Uranium-trend systematics of deposits in New Mexico and in Nevada indicate that resolution of chronology is better for calcareous deposits than for noncalcareous deposits such as glacial till and loess. However, very strong calcium carbonate development, such as in calcretes, tends to yield ages closer to the mean age of carbonate enrichment rather than the ages of deposition of the host sediments. Alluvial deposits, which tend to be more poorly sorted and of mixed mineralogy, usually yield a better spread of the data on the uranium-trend plot than do eolian, quartz-rich sand deposits.

Studies of unconsolidated Quaternary deposits in Grand Canyon National Park along the Colorado River near Nankoweep Creek and in the vicinity of Basalt Canyon and Tanner Creek reveal a history of relatively young downcutting and deposition in the lowest 100 m of the canyon (Patton this volume; Machette and others, 1986). This interpretation is based on U-trend ages of the deposits and on the stratigraphic relations between deposits. Ages were obtained on Pleistocene deposits that form prominent terraces from 20 m to 50 m above the present river level; four ages were determined, ranging from 40 ± 24 ka to 150 ± 30 ka, with increasing age for higher level terraces. A rockfall debris 60 m above the river on the Nankoweep delta was dated at 210 ± 25 ka. Farther from the river, alluvial deposits in high valleys (400 to 500 m above the river) at Chuar Valley and Surprise Valley were dated at 300 ± 100 ka and 250 ± 30 ka, respectively (Rosholt and others, 1986).

In Fisher Valley, Utah (Colman and others, 1986), U-trend ages were reported on basin-fill sediments. A Lava Creek Ash horizon was dated at 530 ± 70 ka; ages of 240 ± 35 ka and 210 ± 40 ka were obtained for the top of the basin-fill sediments; and 9 ± 11 ka was obtained for Holocene eolian sand. These results for the oldest and youngest units are in fair agreement with ages determined by tephrochronology (610 ka) and radiocarbon (8 and 9 ka) methods, respectively (Patton and others, this volume).

In the San Joaquin Valley, the U-trend method was used to determine ages on sediments ranging from about 30 to 600 ka (J. N. Rosholt, unpublished data); these included Pleistocene deposits of the upper and lower members of the Modesto Formation, the upper and middle units of the Riverbank Formation, and the upper unit of the Turlock Lake Formation. Of 13 depositional units analyzed, 5 were not datable because the U-trend method does not appear to work for soils with missing horizons or for soils that have developed in parent materials of more than one age. On the California coast, marine terrace deposits near San Pedro were dated by U-trend method at 150 ± 50 ka, 230 ± 60 ka, and >700 ka (Muhs and others, 1989). These dates are in agreement with conventional U-series and amino acid age determinations.

DISCUSSION

A variety of middle and late Pleistocene depositional, erosional, climatic, and volcanic events can be dated, and rates of change can be determined, by applying U-series methods. To obtain reliable results, however, one needs to find the high-quality, homogenous samples that have formed in a short period in relation to their age and represent a discrete geologic event. Unfortunately, nature rarely provides such ideal samples; therefore, investigators have devised different correction techniques to account for the presence of impurities. The closed-system condition (no migration or addition of nuclides) is always required in conventional U-series dating, but it is seldom ascertained. Because of uranium mobility, often the uptake of uranium is dated, not the deposit itself, and in these cases dates should be interpreted as minimum-age estimates.

Uranium-trend dating results show that it is a suitable method of estimating the age of some Quaternary deposits. The most reliable ages appear to be in the time range of 60,000 to 600,000 yr, which, at best, may be accurate within ± 10 percent for a deposit whose samples provide a linear pattern of isotopic variation. The U-trend ages have large relative errors near the lower (10 ka) and upper (800 ka) limits of the method: deposits younger than 20 ka have errors near or greater than ± 100 percent, and deposits older than 600 ka have errors greater than ± 20 percent.

Conventional U-series and U-trend dating have yielded useful results for various Quaternary dating problems. Due to the imperfections, the reliability and accuracy of the dates are not uniform, however. Therefore it is a good practice to test the dating results against the stratigraphic constraints of the particular geologic application.

PALEOMAGNETIC DATING

Joseph C. Liddicoat

Two characteristics of the Earth's magnetic field have application for dating stratigraphy—reversals of polarity and systematic changes in the paleomagnetic vector. The benefits and limitations of each are controlled by several factors, and among them is the time interval. Whereas the reversal time scale (Harland and others, 1982) covers all of the Quaternary (and beyond), records of short- and long-term behavior (called secular variation) of the field apply only to the post-Wisconsin and Holocene. Also restricting are the location and areal extent of the study; there are no bounds on magnetostratigraphic studies, but secular variation is confined mainly to regions several thousand kilometers across. In this discussion, we will not deal with the specifics of paleomagnetism or the Earth's magnetic field, which are in McElhinny (1973) and Merrill and McElhinny (1983), but will highlight those elements that bear on stratigraphic correlation and dating.

A reversal of polarity is easy to conceptualize as a stratigraphic marker because it occurs simultaneously around the world. Four boundaries are well known for the Quaternary, and their age is established primarily by K/Ar dating of volcanic rocks: termination of the Olduvai Normal Subchron (1.67 Ma), limits of the Jaramillo Normal Subchron (0.97 Ma and 0.90 Ma), and onset of the Brunhes Normal Chron (0.73 Ma; Mankinen and Dalrymple, 1979). Additional reversals have been encountered and dated in Quaternary volcanic rocks, and they likewise serve as distinct horizons wherever identified. The best data are for the Cobb Mountain Normal Subchron in California (1.19 ± 0.2 Ma; Mankinen and others, 1978), the Emperor Reversed Subchron in Idaho (0.46 ± 0.05 Ma; Ryan, 1972; Champion and others, 1981), and the Laschamp Reversed Subchron in France (Bonhommet and Zähringer, 1969) that is assigned the age of about 0.04 Ma (Heller and Peterson, 1982). Another brief reversal is the Blake Reversed Subchron at about 0.12 Ma (Denham and others, 1977) that was discovered in cored sediment from the Blake Plateau in the western North Atlantic (Smith and Foster, 1969), but is not found in all sections believed to span that interval. The same applies to several other short episodes of reversed polarity in the Brunhes Normal Chron that are not universally recognized for a variety of reasons; examples are the Gothenburg in Sweden (Mörner and others, 1971) and Biwa in Japan (Kawai and others, 1972). As a result, they are not in all compilations of the reversal time scale, including the one adapted for the Decade of North American Geology (Palmer, 1983).

If the magnetostratigraphy is complete to the base of the Quaternary (as in a core of lacustrine or deep-sea sediment), dating the stratigraphy using only the reversal time scale can be done with a high level of confidence. However, where there are hiatuses in the section, a safe assumption is that rocks possessing reversed polarity acquired that magnetization before 0.73 Ma. A similar rationale cannot be used for rocks of normal polarity because they might be remagnetized by the present (normal) field. Fortunately, field and laboratory (demagnetization) experiments can usually establish whether the magnetization is primary or secondary in origin. In a section where the polarity is normal exclusively, improvement of the dating beyond assignment to the Brunhes Normal Chron is left to correlating secular variation of the paleomagnetic field. It is a subject that has received considerable attention in recent years both in stratigraphic studies and in investigations of the dynamics of the Earth's core.

Because secular variation is the result of a complex interaction between the dipole and non-dipole fields, it is highly variable when considered worldwide. Still, where systematic changes in declination, inclination, and intensity are calibrated by radiometric dates, the curves are potentially useful for correlating and dating stratigraphy on a regional scale. Among the places where successful application has been made using wet lake sediments are the midwestern United States, Canada, Great Britain, Europe, and Australia. The curves for those and additional regions are in Creer and others (1983).

Changes in the paleomagnetic vector and field strength are also preserved as thermal remanent magnetization in baked clay at archeological sites. Because of the very good age control on samples (usually by radiocarbon) and stringent requirements on archeomagnetic data, reliable curves for much of the Holocene are available for the southwestern United States, Britain, Europe, the Middle East, and Australia (Wolfman, 1983). The curves not only have utility in stratigraphic studies, but help to confirm the secular variation measured in lake sediments as recorded by the process of detrital remanent magnetization.

The value of detailed curves of secular variation would be enhanced if there is a large departure from typical field behavior that does not constitute a reversal; such directions are called an excursion (Cox and others, 1975). In practice, excursions are difficult to locate in the stratigraphic record because they have a duration of only a few thousand years at most. A case in point is the Moho Lake Excursion (Denham and Cox, 1971; Liddicoat and Coe, 1979) that occurred about 26 ka (Liddicoat and others, 1982) in exposed dry lake sediments in east-central California. Within the structural basin containing pluvial Lake Russell (of which Moho Lake is the remnant), the excursion can be positively traced over a distance of 20 km using a distinctive tephra layer as a marker (Denham, 1974). Only recently, and after several unsuccessful attempts at other localities (Verosub, 1982), was the excursion discovered in sediment from another pluvial lake. The closest one, Lake Lahontan in southwestern Nevada, is 200 km away (Liddicoat and others, 1982), and the other, Summer Lake, is 300 km farther to the north in southern Oregon (Negrini and others, 1984). In each instance, it was not the excursion that was first identified, but the associated tephra layer or another one close in age (Davis, 1985). Thus, the utility of an excursion alone as a method for placing an age on stratigraphy in a large geographical area (such as the Great Basin of the western United States) remains to be demonstrated. Other excursions in the Pleistocene have been reported, but they have not been verified at multiple sites (Banerjee and others, 1979; Verosub, 1982) and as yet do not warrant serious consideration as stratigraphic markers.

Rock-magnetic information, such as susceptibility, and other laboratory experiments designed to identify the physical properties and composition of the carrier of magnetization are akin to records of secular variation in wet lake sediment. The approach is relatively quick and circumvents the problems associated with paleomagnetic studies of cores in which there might be errors in orientation or there has been disturbance to the sediment during recovery and subsequent sampling. The early work in North America began in the Midwest (Banerjee, 1981) and followed a successful application of the technique in Great Britain (Blomendal and others, 1979). Rock-magnetic studies are thus becoming an important part of detailed investigations of wet lake sediments, and complement the other methods for dating and correlating stratigraphy within late Pleistocene and Holocene lakes or in a drainage basin (Thompson and others, 1975; 1980).

THERMOLUMINESCENCE DATING

Steven L. Forman and Michael N. Machette

INTRODUCTION

The development of thermoluminescence (TL) dating techniques during the past two decades came about through TL studies of pottery from archaeological sites (Flemming, 1979; Aitken, 1974, 1985). During the past ten years these techniques have been applied successfully to dating of Quaternary sediments (see review articles by Dreimanis and others, 1978; Wintle and Huntley, 1982; Singhvi and Mejdahl, 1985). The basic principles of the technique for dating Quaternary sediment are similar to those used in dating archaeological materials. However, heating of pottery removes any TL signal that may have accumulated in the minerals, whereas in sediments the inherited TL in minerals is assumed to be zeroed by exposure to sunlight (light bleaching) prior to deposition. This important difference in zeroing mechanisms prompted development of new laboratory procedures for dating sediments (i.e., see Wintle and Huntley, 1980). For TL dating of sediments, environments of deposition are evaluated in terms of their effectiveness in removing previously acquired TL from minerals. Samples are taken from sediment that has not been exposed to sunlight since it was deposited.

As a dating technique, TL does not depend on presence of organic or volcanic materials, and it has the distinct advantage of directly dating many kinds of sediment. More importantly, it can provide age determinations at close intervals and at significant positions in a stratigraphic section. The TL method can be applied to sediments ranging from younger than 100 ka to possibly as old as 500 ka. Because of its wide applicability, TL is an extremely important new dating technique for Quaternary deposits. This brief review explains the method, discusses the types of materials that can be dated, and discusses some of the problems involved in different applications of the method. Extensive literature on TL dating is reviewed in Aitken (1985), PACT volumes 3, 6, and 9 (Journal of the European Study Group on Physical, Chemical, and Mathematical Techniques Applies to Archaeology and in Nuclear Tracks and Radiation Measurements (1985, v. 10, nos. 1, 2, 4-6). These sources give more complete reference listings dedicated to this subject.

THERMOLUMINESCENCE DATING OF GEOLOGIC MATERIAL

Thermoluminescence dating of minerals was first attempted by Daniels and others (1953). They measured TL signals from some common minerals, but production of reliable age determinations was difficult. McDougall (1968) summarized much of the early research on thermoluminescence of geologic materials. The potential of dating unheated sediment by TL was first recognized by Morozov (1968) and later described by Shelkopyas (1971),

who obtained ages for sediments in the Soviet Union. In assessing the early Soviet TL dating, Wintle and Huntley (1982) concluded that the obtained TL dates may be in correct chronologic sequence but that they may be in error by a factor of 2 to 10. Bothner and Johnson (1969) reported TL studies from four deep-sea cores rich in nanofossils. They found that the naturally induced TL, thought to be characteristic of foraminiferal calcite (Johnson and Blanchard, 1967), increased down-core to a plateau (saturation) value. Huntley and Johnson (1976) reported a similar increase in equivalent dose with depth in a core of radiolarian-rich sediment. These studies led to Wintle and Huntley's (1979) recognition that the TL in these marine sediments was from detrital grains that adhere to the nanofossils, rather than the nanofossils themselves. Following this fundamental discovery there has been increased interest in and application of thermoluminescence to dating of mineral sediments.

Two new dating techniques related to thermoluminescence are electron-spin resonance (ESR) (Hennig and Grün, 1983) and optical dating (Huntley and others, 1985). ESR dating is based on direct measurement of radiation-induced paramagnetic electrons that have been trapped in crystal defects through geologic time. The technique has been applied to apatite and to organic and inorganic carbonate, and research is underway using silicate minerals. Optical dating involves photo-stimulated luminescence, rather than heat stimulation (thermoluminescence). Electrons accumulated in traps through geological time are freed by laser light, thus transferring electrons to luminescence centers, which transmit visible light.

FUNDAMENTALS OF THERMOLUMINESCENCE DATING

The TL signal emitted by mineral grains is acquired by exposure to ionizing radiation. The radiation causes electrons to be displaced from outer electron shells and trapped in crystal defects. In most environments, the contribution from cosmic rays is small, especially at depths of more than 10 cm in sediment. Therefore the causative radiation in sediment is almost entirely alpha, beta, and gamma particles that are released during the decay of radioactive nuclei of ^{40}K , ^{238}U , and ^{232}Th contained in the sediment. In order to obtain a reliable date from a given sample of mineral sediment, its electron traps initially must have been emptied by exposure to light, and these traps subsequently must have accumulated and retained a post-deposition TL signal. The TL signal is quantified by measuring the light emitted as a sample is heated continuously from about 25° to 500°C at a rate of about 5°C/sec in an oxygen-free atmosphere (see Fig. 4). Minerals such as feldspar, quartz, and calcium carbonate have diagnostic TL-response (glow) curves at different temperature ranges.

To evaluate the amount of radiation received by the sample in its geologic environment, the sample's sensitivity to radiation must be determined. This sensitivity is assessed in the laboratory by measurement of the TL response to irradiation from a cali-

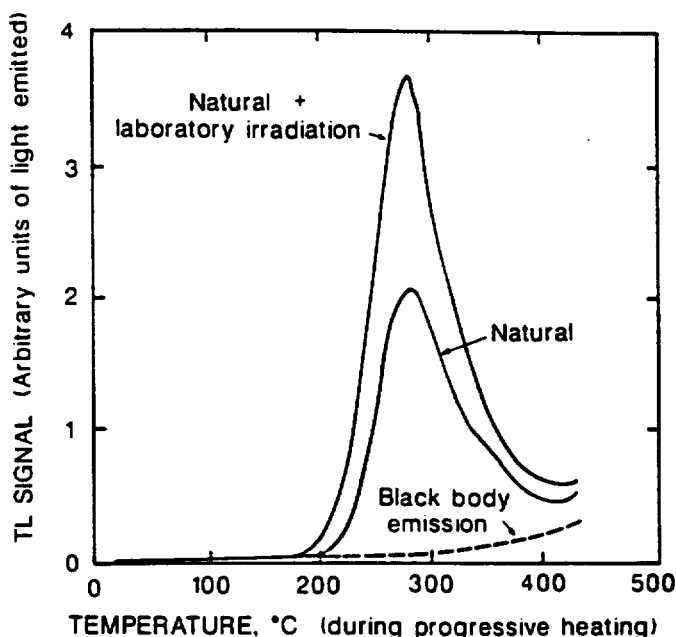


Figure 4. Natural TL glow curve and laboratory TL glow curve caused by an additional 360 gray of radiation. Material is a fine-grained poly-mineralic sediment. Samples were preheated at 150°C for 16 hours prior to glowing to enhance the TL signal above 200°C.

brated source of beta or gamma rays. Assuming that the laboratory irradiation simulates natural conditions and that TL does not decay more in nature (under long-term conditions) than in the laboratory (short-term conditions), the equivalent dose (ED) can be determined. Equivalent dose is the amount of laboratory radiation that produces a TL response "equivalent" to that of the natural sediment.

Three methods have been developed to assess ED (Fig. 5).

1. Regeneration method (Wintle and Prószyńska, 1983). The natural TL in sediment is measured and then aliquots of the sediment are bleached in the laboratory to their experimentally determined pre-depositional TL level. These aliquots then are re-exposed to increasing doses of radiation, and the level of natural TL is matched to the regenerated TL curve. ED is determined as shown on Figure 5A. This method is used predominantly on sediments that have been zeroed (light bleached) of TL prior to their deposition. These sediments are mainly wind-transported materials, such as loess and eolian sand.

2. Total bleach method (Singhvi and others, 1982). Without prior laboratory bleaching, the natural sediment is irradiated at progressive levels, and the rate of TL acquisition is defined by a sloping line shown in Figure 5B. ED is the intercept of this sloping line with the TL level induced by total light bleaching (horizontal dashed line). This method commonly is applied to eolian sediments to check for sensitivity changes relative to the

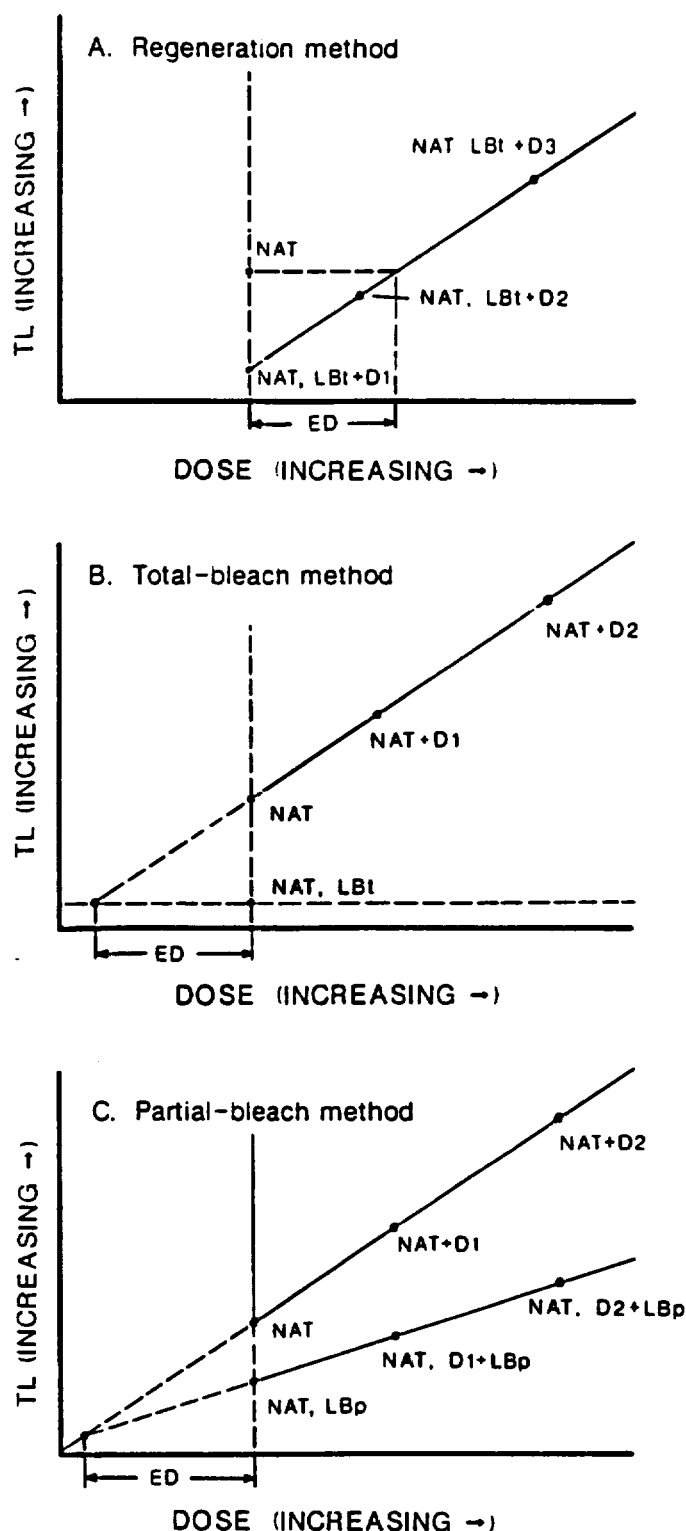


Figure 5. Three methods used to determine equivalent dose (ED) in TL dating of sediment: A) regeneration method, B) total bleach method, and C) partial bleach method. Abbreviations indicate the following: NAT, natural TL of sediment; LB, light-bleach procedure performed on sediment (LBp, partial bleach; LBt, total bleach) and D, additional incremental doses of radiation to sediment (D_1 , D_2 , D_{12}). Modified from Singhvi and Mejdahl (1985).

regeneration method and to ascertain if the growth in the TL signal is linear with increasing radiation.

3. *Partial bleach method* (Wintle and Huntley, 1980). ED is defined by the intersection of two sloping lines, as shown in Figure 5C: (1) the regression line defined by TL resulting from progressive doses of laboratory radiation on natural sediment, and (2) the regression line determined from partially light-bleached sediment that previously has been exposed to progressive doses of laboratory radiation. A level of partial bleaching that has been determined experimentally on the basis of the sediment's environment of deposition is applied. This technique commonly is used for water-lain sediments (alluvial, lacustrine, and debris-flow deposits) that may not have been fully light bleached prior to deposition (i.e., the inherited TL signal is only partially zeroed).

Depending on the type of material being analyzed, TL is measured on specific grain sizes and (or) mineral fractions. Most workers prefer the 3 to 11 μm micrometer fraction of polymineralic materials or the 100 to 300 μm fraction of quartz or feldspar grains. The radiation contributed by alpha, beta, and gamma particles is assessed most easily for these minerals and grain sizes. The 3 to 11 μm grains are exposed to the full effect of alpha, beta, and gamma radiation, whereas the 100 to 300 μm grains are incompletely penetrated by alpha and beta particles. However, there will be no apparent effect from alpha particles and there will be a reduced contribution of TL from beta particles if the outer surface of the grains are removed by acid etching. The effect of beta radiation in large mineral grains is not well understood, but it does depend on grain size (Mejdahl, 1979). Additionally, radiation generated internally may be an important contribution in the larger grains.

Wintle (1973) showed that sediments that were stored after irradiation had lost TL compared with those samples measured shortly after irradiation. This loss of TL was termed "anomalous fading" because the observed stability of the TL signal is much less than that predicted from kinetic considerations. The phenomenon is not present in all minerals, although feldspars—especially those of volcanic origin—seem to be particularly susceptible to fading (Wintle, 1973; 1977). If corrections are not made for anomalous fading, then both the ED and the TL age will be underestimated. Lamothe (1984), Berger (1984, 1985a), and Templer (1985) developed procedures to circumvent the effects of anomalous fading.

Once an acceptable value of ED has been determined, the sample's age is calculated from the following relation:

$$\text{TL Age} = \frac{\text{Equivalent Dose (ED)}}{\text{Dose Rate (DR)}}$$

where DR is the annual dose rate (grays/yr) in the material's natural environment. DR is calculated from the types and amounts of radioactive elements in the sample and their rates of production of gamma, beta, and alpha particles. The gamma component can be measured directly by placing field dosimeters

in the sediment (for as much as a year), by using a gamma spectrometer, or by elemental analysis of the sediment. The alpha and beta contributions usually are determined by measuring the alpha activity of the uranium and thorium decay chains and the total potassium content of the sample. Alpha particles are 5 to 20 percent as effective as beta and gamma particles in producing TL because of localized saturation in the alpha track (Zimmerman, 1972). The calculated dose rate (DR) commonly is corrected for absorption of alpha, beta, and gamma radiation by water in the sediment. This correction factor is the greatest potential source of error in a TL age determination for sediment because of possible variations in pore-water content during and after burial (i.e., as a result of periodic drying and wetting). An additional problem may be caused by disequilibrium of the uranium-decay chain, especially if a significant amount of radon has diffused through the sediment. For example, uranium-series disequilibrium occurs during deposition of deep-sea sediments and cave speleothems, and analysis of these materials requires using a model of time-dependent dose rates (Wintle, 1978; Wintle and Huntley, 1980). Post-depositional weathering, accumulations of secondary minerals in soils (silica, calcium carbonate, and clay), and ground-water movement also can change the amounts and types of radioactive elements in the sampled material.

APPLICATION OF THERMOLUMINESCENCE TO DATING

Only recently has TL been used as in Quaternary studies in North America. Much of the pioneering work on TL dating of sediment was on the loesses of Europe (i.e., Wintle and others, 1984). Loesses and loess-like deposits are widespread, they have paleoclimatic significance, and they have been difficult to date by methods other than radiocarbon. Eolian sediments are ideal for TL dating because they satisfy the basic criterion of exposure to sunlight during deposition.

In the United States, the preliminary studies by Johnson and others (1984) on loess from southern Mississippi indicate that the TL signal may have been accumulated linearly during the past 130,000 yr. TL ages from the Peoria Loess (late Wisconsin, latest Pleistocene) are in agreement with radiocarbon ages from the same deposits. Similar results (but having considerable scatter and showing chronologic reversals) were obtained from the Peoria Loess in Iowa (Norton and Bradford, 1985). However, three of their TL ages, from the older Farmdale Loess and Loveland Loess, are in conflict with ages inferred from stratigraphic and climatic relations. The significance of the TL dates from the older loesses is difficult to evaluate because there are only a few analyses and the basic laboratory data were not presented.

Wintle and Westgate (1986) made a detailed study of the mineralogy and thermoluminescence properties of loess interbedded with the Old Crow tephra (volcanic ash) near Fairbanks, Alaska. The TL signal in the fine fraction of the loess was prima-

rily from feldspar, which did not exhibit anomalous fading. Four determinations on loess yielded an average TL age of 86 ± 8 ka, which is consistent with geologic constraints on the tephra's age.

Significant advances have been made on TL dating of water-laid sediments. Mineral grains transported by and deposited in water are exposed to a less intense and more restricted spectrum of light than are mineral grains deposited in eolian sediments. Huntley (1985) summarized methods for dating incompletely light-bleached sediments of marine, fluvial, and lacustrine sediments. Berger's (1984, 1985a) TL studies of glacial-lacustrine silt units showed that those sediments were incompletely bleached prior to deposition. He also showed that in rapidly deposited water-lain sediments from British Columbia, Canada, feldspars were bleached preferentially over quartz. Also, the pre-depositional (inherited) TL signal of glacial silt was not significantly reset before deposition in lakes, but mudflow silts were sufficiently bleached to be dated. By using an artificial light spectrum that simulated attenuated light bleaching in the lacustrine environment, Berger (1984) obtained TL ages of 36 and 66 ka for the glacial-lacustrine silt units, in agreement with age controls based on regional stratigraphic correlations.

A similar procedure of partial light bleaching was used to date sediments of the St. Pierre interstade in southern Quebec (Lamothe, 1984). Sediments of the interstade exhibited significant anomalous fading, but delayed measurement of the post-irradiation TL signal minimized the fading; the determined TL age of 61.1 ± 9.2 ka is consistent with the enrichment radiocarbon age for the unit. TL dates for lacustrine silt units related to the past three major lake cycles in the Bonneville Basin in Utah were used to establish a local history of faulting (McCalpin, 1986). In this study, the moisture history of the sediment was reconstructed and its effects on dose rate (DR) were considered in the age determinations. The TL ages of 13 to 138 ka are compatible with accepted ages of the lacustrine units that are based on amino acid racemization ratios from shells, soil development, and the regional history of the Bonneville basin.

The TL technique also has proven useful in dating soils. Huntley and others (1983) reported TL ages for buried soils from two late Holocene archaeological sites in British Columbia. The A horizons yielded ages that agreed with radiocarbon dates from the soil parent material. Wintle and Catt (1985) studied a surface soil and two buried soils developed in Holocene deposits; they determined that the degree of light bleaching in a soil is related chiefly to the depth and degree of pedoturbation (mixing). In these soils, surface A horizons commonly are zeroed, and TL in the upper part of B horizons may be partly zeroed, depending on the extent and depth of mixing. The upper horizons of a buried soil in loess yielded apparent TL ages of 4.6 ± 0.4 ka and 7.4 ± 0.7 ka, in general agreement with a radiocarbon age from the same material. However, the lower part of the soil yielded TL ages that were younger than expected, indicating that weathering may affect TL acquisition in the loess.

TL has been applied to the dating of soluble minerals that

accumulate in sediments. The precipitation and crystallization of soluble minerals, such as calcium carbonate, gypsum, and halite, sets the TL clock of each individual crystal into motion (Zeller and others, 1955). TL has been applied with limited success to the dating of calcite stalagmites (Wintle, 1978; Hennig and others, 1980; Debenham and Aitken, 1984). Recently, the TL properties of pedogenic calcium carbonate were studied from calcic soils of known age in the Rio Grande Valley of New Mexico (May and Machette, 1984). The TL signal increased systematically in soils ranging in age from about 15 ka to at least 400 ka, but the processes of TL acquisition and dose rate history of these soils are complex and still poorly understood. Nonetheless, the method is potentially useful for dating secondary precipitates in soils and sediments.

Significant advances in the analytical techniques of TL now permit the dating of volcanic ashes (Berger and Huntley, 1983; Berger, 1985b). Due to the high temperatures involved in the eruption and deposition of volcanic ash, the ash is emplaced without inherited TL. The glass fraction from ash exhibits negligible anomalous fading and it may retain a stable TL signal for as much as 500 ka.

SUMMARY

In North America, the application of TL dating to geologic materials has gained popularity since Wintle and Huntley's (1979) study of deep marine sediments. TL has been applied to a variety of terrestrial deposits; during the past five years, intensive research on TL dating of eolian and water-laid sediments has produced new techniques that provide near-routine dating capabilities. Recently, research has expanded to chemical precipitates, volcanic ashes, and buried soils; preliminary results from these studies are promising. However, since the TL technique is still in its infancy, it should be considered experimental and should be applied judiciously. The measurement of TL and the processes of TL acquisition by natural materials are complex and not fully understood at present. Additionally, the mechanisms of bleaching by sunlight are not understood, including the physical mechanisms for different levels of bleaching. Significant problems remain in determining past dose rates, particularly where diagenetic processes have changed initial concentrations of radioactive elements.

Although the TL technique has restrictions and limitations (as do most dating techniques), the greatest asset of thermoluminescence is that it directly dates a wide variety of types and ages of sediment. Thus, the method can provide detailed chronologic information about past geologic events that cannot be dated by other methods. Study of deposits with independent dating control and clear stratigraphic relations may result in refinement of the method and may provide important information related to the effect of light bleaching in different sedimentary environments, the mobility of radioactive elements, and the moisture history of sediments.

AMINO ACID GEOCHRONOLOGY OF FOSSIL MOLLUSKS

D. R. Muhs

INTRODUCTION

In the last two decades, considerable progress has been made in using ratios of the protein amino acids in fossils, such as shell and bone, to estimate the fossil's relative or numerical age. The basis of amino acid geochronology is the observation that the protein of living organisms contains only amino acids of the L configuration. Upon the death of an organism, amino acids of the L configuration convert to amino acids with D configuration, a process referred to as racemization. Racemization is a reversible reaction that results in increased D/L ratios in a fossil through time until a D/L equilibrium ratio (1.00 to 1.30, depending on the amino acid) is reached. Thus, in a simplified view, a higher D/L ratio in a fossil indicates a relatively greater age.

Several lines of evidence suggest that amino acid ratios do not increase linearly over time; in other words, they do not follow simple, first-order reversible kinetics. Analyses of reasonably well-dated deep-sea sediments (Wehmiller and Hare, 1971; King and Neville, 1977) indicate that foraminifera experience a rapid linear change at first, followed by a much slower linear rate of change, with an uncertain area in between (Fig. 6). Fossil mollusks have been thought to follow similar, nonlinear kinetic pathways, but sufficient data to prove this are still lacking (Wehmiller, 1982). Pyrolysis experiments at elevated temperatures on modern mollusks clearly indicate that nonlinear kinetics are followed in the racemization reaction. However, some pyrolysis experiments indicate that the break in slope may occur at higher D/L ratios than is indicated by analyses of deep-sea foraminifera (Masters and Bada, 1977; Kriaušakul and Mitterer, 1978). In any case, it is generally agreed that the causes of the change in rate of racemization are related to two factors: (1) racemization occurs at strikingly different rates depending on the position of the amino acid in the peptide chain (internal, terminal, or free) and (2) the changing abundances of different molecular weight components in the fossils (Wehmiller, 1984a).

Amino acid geochronology has been used in the U.S. in a wide variety of contexts in Quaternary stratigraphy, tectonics, paleoclimate, sea-level history, and archaeology. This section will only highlight some recent results on mollusks in the conterminous U.S. More detailed reviews are found in Williams and Smith (1977), Hare and others (1980), Wehmiller (1982, 1984a), Miller (1985), and Bada (1985).

FACTORS AFFECTING AMINO ACID RATIOS

Several variables are known to affect amino acid racemization rates and/or observed ratios in fossils including temperature (both the mean annual temperature and the amplitude of the

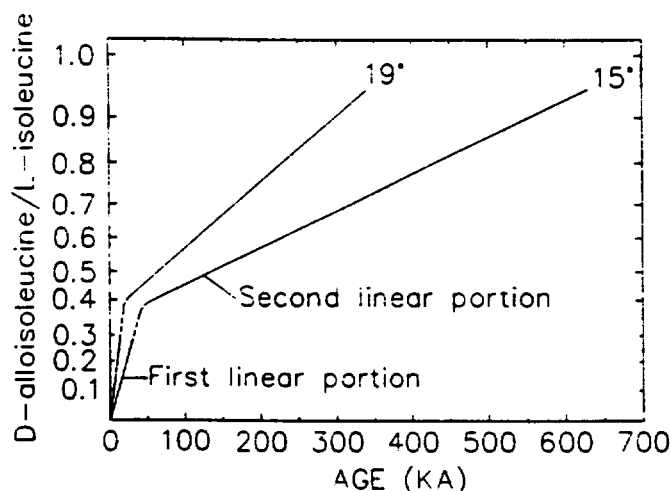


Figure 6: Possible pathways of racemization based on extrapolation of deep-sea foraminifera kinetics to higher temperatures, derived from data in Wehmiller and Belknap (1978). Particularly uncertain areas are indicated by dashed lines.

annual temperature cycle), genus, type of amino acid, and diagenetic processes (Wehmiller, 1982). Temperature history is one of the most critical factors, because higher temperatures greatly increase racemization rates. However, because of repeated climatic changes, it generally is difficult to estimate diagenetic temperature histories. Wehmiller (1982) gives a method for estimating what he calls the Effective Quaternary Temperature (EQT) of a sample from paleoclimatic data. The EQT is defined as the integrated kinetic effect of all temperatures to which a sample has been exposed during its burial history. Refinement of EQTs for various localities by Wehmiller's method will be an important advancement in amino acid studies.

An important and often overlooked factor is the effect of burial depth on temperature. Wehmiller (1977) found that average racemization rate constants varied by more than four times within a depth interval of 1.5 m in a Holocene shell midden in California, due to differences in the amplitude of the annual temperature cycle. Similar results have been reported by McCoy (1987) in the Great Basin. Often, information about depth of sampling is not given in amino acid studies, but it is clear from Wehmiller and McCoy's data that depth of burial has a considerable effect on amino acid ratios in shells from the same deposit.

The rate of racemization is not constant among different genera or among different amino acids in the same molluscan genus. Lajoie and others (1980) have reported a large number of amino acid ratios for different, co-existing genera of west coast marine mollusks from the same stratigraphic unit. Their data indicate that some genera racemize much more quickly than others (as much as 40 to 50 percent), but there is no significant

difference in rates of racemization between species of the same genus. Miller and Hare (1980) also report significant differences in amino acid ratios between different genera of nonmarine mollusks. Apparently, however, there are also reversals of this generalization in the later stages of diagenesis: in some older deposits, amino acid ratios of a given genus are greater than those of another genus, whereas the opposite relationship holds for the same two genera in younger deposits (Lajoie and others, 1980). These investigators also found that there are differences in rates of racemization among different amino acids in the same genus, with proline being most rapid and valine the slowest. Brigham (1983) conducted experiments with valves of a single species from a single deposit in order to investigate intrashell variability. Her results indicate that amino acid ratios did not vary significantly between five anatomically different shell parts; however, results from the central or hinge parts of valves had less variability about their mean values. She also found that the absolute concentrations of various amino acids did vary significantly between shell parts.

In addition to natural sources of variability in amino acid ratios, there are also differences in reported amino acid ratios due to the type of laboratory analysis used. At present, there are four analytical methods in routine use, three using gas chromatographic (GC) techniques (Kvenvolden and others, 1972; Frank and others, 1977; Hoopes and others, 1978) and one using ion-exchange liquid chromatography (LC) (Hare, 1975). The LC method is most commonly used, but the only amino acid ratio obtained is D-alloisoleucine/L-isoleucine. The GC methods are more expensive and are less commonly used, but yield D/L ratios for several amino acids, including alanine, valine, leucine, proline, aspartic acid, glutamic acid, and phenylalanine. Unfortunately, alloisoleucine and isoleucine are usually not well resolved on GC systems, so it is often not possible to compare results from GC and LC systems. Most investigators report amino acid ratios of total extractions, i.e., those including both protein-bound amino acids and those freed by natural hydrolysis. However, the pool of free amino acids contains amino acids from terminal positions where the rate of racemization is high (Kriaušakul and Mitterer, 1978), so some investigators analyze separate extractions of free amino acids as well as total extractions. In cold regions such as arctic North America, amino acid ratios in the free fraction are useful because the overall rate of racemization is low (Nelson, 1982; Miller, 1985). Interlaboratory comparisons indicate that there are differences in results on control samples (Wehmiller, 1984b). Coefficients of variation range from 3 to 18 percent, depending on the amino acid and are best for alanine, glutamic acid, and aspartic acid and worst for isoleucine, proline, and valine. Instrumental rather than wet-chemical preparation procedures are apparently responsible for most of the variability.

AMINOSTRATIGRAPHY AND RELATIVE AGES

The simplest application of amino acid ratios in geochronological studies is relative age determination and lateral correla-

tion, or aminostratigraphy (Miller and Hare, 1980). The main assumption in this approach is that the localities studied have had similar temperature histories. Stratigraphic units that have mollusks with amino acid ratios that cluster around a certain value can be identified as aminozones (Nelson, 1982).

The aminostratigraphic approach has been used with considerable success on the west coast of the U.S. by Wehmiller and others (1977), Lajoie and others (1979), and Kennedy and others (1982). Similarity of D/L leucine ratios in fossil bivalves allows correlation of discontinuous exposures of the lowest emergent marine terrace in southern California. At other localities on the west coast, small but significant differences in D/L ratios between the lowest terraces and terraces 10 to 30 m higher indicate two distinct high stands of sea that are closely spaced in time, such as high stands of ~120 ka versus high stands of ~105 ka or ~80 ka. Such results were obtained for terrace pairs in California near San Diego, Santa Barbara, and Point Año Nuevo, and on Whidbey Island, Washington. Similar results were obtained for low-elevation terrace pairs on the southern California Channel Islands by Muhs (1983, 1985). Wehmiller and others (1977) and Lajoie and others (1979) found unusually low D/L ratios in fossils collected from low terraces near Goleta and Ventura, California, and Cape Blanco, Oregon. These terraces are estimated to be on the order of 30,000 to 50,000 yr old rather than 80,000 to 120,000 yr old as is the case with low terraces found elsewhere on the Pacific coast of North America. The significance of these results is two fold: (1) the time-honored concept that the lowest emergent terrace along the Pacific coast is everywhere equivalent in age is clearly in error, and (2) significantly higher uplift rates are implied for localities where young terraces are found.

The major aminostratigraphic studies in the U.S. using freshwater mollusks have been conducted by W. D. McCoy and co-workers in the Great Basin. In the Lake Bonneville Basin, McCoy (1987) and Scott and others (1983) recognize four major aminozones related to major lake cycles. The oldest deposit is >600 ka, and the youngest is ~11 to 30 ka. In the Lahontan Basin, McCoy (1981) recognizes five major lake cycles and has distinguished three of them with amino acid ratios. Comparing amino acid ratios in shells from the last two major lake cycles in the Bonneville and Lahontan basins, McCoy (1981) suggests the cycles can be correlated.

In the midcontinent of the U.S., terrestrial gastropods in glacial tills or sediment associated with till appear to be suitable for aminostratigraphic correlation. Miller and others (1987) analyzed terrestrial gastropods from glaciated parts of Indiana and found four distinct aminozones ranging in age from late Wisconsin (~20 ka) to >730 ka. Midcontinent tills, loesses, and other sediments have considerable potential for aminostratigraphy because terrestrial gastropods are common there.

AMINOSTRATIGRAPHY USING LATITUDINAL TEMPERATURE GRADIENTS

A refinement to the aminostratigraphic approach used above was presented by Kennedy and others (1982), Wehmiller

and Belknap (1982), Wehmiller (1982), and Hearty and others (1986), who combined local aminostratigraphic data with regional temperature gradients to develop regional amino acid isochrons. The idea is based on the assumption that, while paleotemperatures along a north-south trending coastline may have differed from those of the present, regional temperature gradients have always been in the same direction. Thus, in deposits of similar age, one should expect to find systematically lower D/L ratios in fossils as one moves north into cooler latitudes. Kennedy and others (1982) used this approach for lateral terrace correlation on the Pacific coast of the U.S. (Fig. 7). They plotted D/L ratios in fossil *Saxidomus* as a function of latitude and connected geographically proximal points into isochrons. Age control for Pleistocene deposits was provided by U-series ages of coral at a few localities. Their correlations are supported by faunal aspects: terraces thought to be 80 to 105 kyr old are characterized by cool-water faunas, whereas terraces thought to be ~120 kyr old are characterized by warm-water faunas.

A similar latitudinal gradient approach to aminostratigraphy was developed for U.S. Atlantic coast marine deposits by Wehmiller and Belknap (1982). They generated latitudinal isochron plots of D/L leucine ratios in fossil *Mercenaria* and their results indicate at least six major periods of marine sedimentation. Thus, their data suggest more depositional episodes than the biostratigraphic criteria of Cronin (1980) and the multiple criteria of McCartan and others (1982). One interpretation of these conflicting results is that amino acid ratios may be more sensitive age-indicators than biostratigraphic or other criteria. For some localities, however, uranium-series age estimates conflict with amino acid results (Wehmiller and Belknap, 1982; Szabo, 1985). Wehmiller and Belknap (1982) suggest that the problem may be related to uranium-series-dated samples that have relatively low $^{230}\text{Th}/^{232}\text{Th}$ ratios. Correction for the samples with low $^{230}\text{Th}/^{232}\text{Th}$ ratios does not eliminate the conflict, however (Szabo, 1985). Also, Wehmiller and Belknap (1982) used different uranium-series age estimates of corals to calibrate their isochrons; thus the issue of agreement versus disagreement of uranium-series and amino acid age estimates depends on which deposits are selected for age comparison and which dated deposits are used for calibration.

NUMERICAL AGES FROM KINETIC MODELS

An important goal of amino acid geochronology is the development of numerical ages from amino acid ratios. Such age estimates require not only knowledge of sample temperature history but also an understanding of racemization kinetics. Some studies have assumed that racemization follows simple linear kinetics and numerical ages have been generated using independent age control on one or more deposits for calibration. For example, Mitterer (1975) assumed an age of ~124 ka for the Coffee Mill Hammock Formation in Florida and used this age estimate and some radiocarbon-dated Holocene deposits as calibration points to generate linear kinetic model ages for four older units. Al-

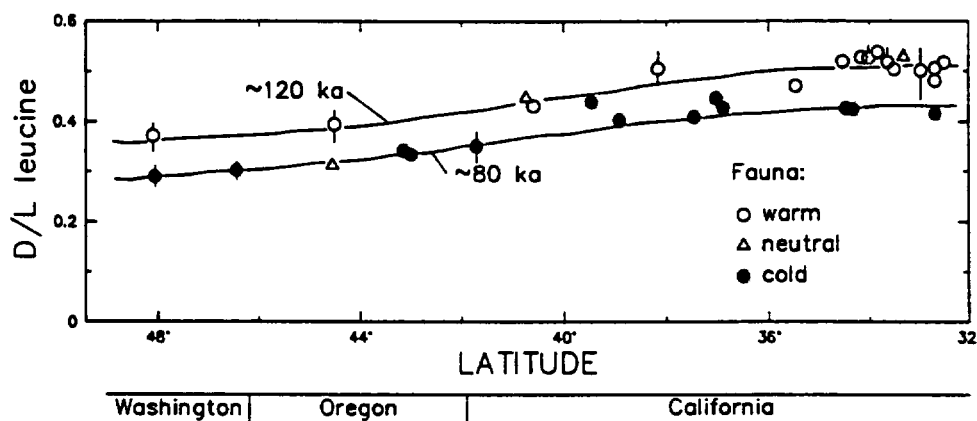


Figure 7. Latitudinal isochron plots of D/L ratios (leucine) in *Saxidomus* from the Pacific coast of the U.S. from marine terraces of the last interglacial complex. Modified from Kennedy and others (1982).

though his age estimates seemed to be reasonable based on similar dates derived from other coastlines and the deep-sea record, his results were criticized by Wehmiller and Belknap (1978), who showed that Mitterer's age estimates would require temperature histories that were incompatible with available paleoclimatic data. They showed that a nonlinear kinetic model made more reasonable assumptions about temperature history for the area, and recalculated ages for the Florida units based on Mitterer's amino acid ratios and their nonlinear model. The new age estimates are significantly older than Mitterer's original determinations.

In colder regions where the rate of racemization is low, even old deposits may have D/L ratios that fall on the first linear portion of the racemization pathway of Figure 6. In such situations, it is probably reasonable to calculate numerical ages assuming linear kinetics, and the main uncertainty remaining is temperature history; where this is the case, alternative numerical ages can be calculated using a variety of temperature history models. Nelson and Van Arsdale (1986) used such an approach for fossil gastropods found in alluvium in central Utah and used the derived ages to determine fault slip rates. A similar approach was used by Miller (1985) to develop a chronology for marine deposition in Arctic Canada.

Nonlinear kinetic models for amino acid racemization have been developed by a number of investigators. Using the assumption that foraminifera provide a reasonable analog to mollusks and extrapolating foraminifera racemization pathways to higher temperatures, nonlinear kinetic models have been used to generate numerical age estimates for marine mollusks on both the east and west coasts of the U.S. by Wehmiller and others (1977), Wehmiller and Belknap (1978, 1982), Lajoie and others (1979), Belknap and Wehmiller (1980), Wehmiller (1981), Muhs and Rosholt (1984), and Muhs (1983, 1985). Calibration for most of these studies was from deposits with coral that have U-series ages of ~120 ka. In all studies, an assumption was made that marine fossils older than ~120 ka have experienced temperature

histories similar to ~120 ka samples. On San Nicolas Island, California, nonlinear kinetic model age estimates calculated for the same terraces by Wehmiller and Belknap (1978) and Muhs (1985) disagree significantly. The problem may be related to the fact that different genera, differing numbers of samples, and different amino acids were analyzed in the two studies, but the results imply that nonlinear kinetic modeling as presented by Wehmiller and others (1977) is perhaps not universally applicable. An alternative approach that has been used by some workers is to calculate numerical ages based on linear kinetics, but to treat these as minimum-age estimates (Masters and Bada, 1977; Karrow and Bada, 1980; Muhs, 1985). Whereas the analysis presented by Wehmiller and Belknap (1978) argues convincingly against linear kinetics applied to numerical age estimates, probably there are still too few calibration points to define accurately a racemization pathway for mollusks.

ADVANTAGES OF AMINO ACID GEOCHRONOLOGY

Several factors make amino acid geochronology a particularly useful technique in Quaternary studies. One advantage is that mollusks suitable for such work are common in Quaternary deposits. A second advantage is that very small sample sizes are required, normally only 100 to 400 mg (Miller and Hare, 1980), but sometimes as little as 5 mg (Wehmiller, 1984a). This gives the investigator the possibility of analyzing the same shell for both amino acid ratios and accelerator ^{14}C dating. In addition, because individual shells can be analyzed, amino acid ratios can identify mixed populations, or deposits that contain shells of more than one age. Evidence for reworking of shells into younger deposits based on amino acid ratios has been documented by Nelson (1982). Finally, in most environments, racemization rates are low enough that amino acid ratios can be used for relative age determinations of shells that are well beyond the range of radiocarbon dating.

REFERENCES CITED

- Aitken, M. J., 1974, *Physics and archaeology*, 2nd edition: Oxford, Oxford University Press, 291 p.
- , 1985, *Thermoluminescence dating*: New York, Academic Press, 351 p.
- Andree, M., Beer, J., Loetscher, H. P., Moor, E., Oeschger, H., Bonani, G., Hofmann, H. J., Morinzoni, E., Nessi, M., Suter, M., and Woelfli, W., 1986a, Dating polar ice by ^{14}C accelerator mass spectrometry: *Radiocarbon*, v. 28, p. 417–423.
- Andree, M., Oeschger, H., Broecker, W., Beavean, N., Klas, M., Mix, A., Bonani, G., Hofmann, H. J., Suter, M., Woelfli, W., and Peng, T. H., 1986b, Limits on the ventilation rate for the deep ocean over the last 12,000 years: *Climate Dynamics*, v. 1, p. 53–62.
- Andree, M., Oeschger, H., Siegenthaler, U., Riesen, T., Moell, M., Amman, B., and Tobolski, K., 1986c, ^{14}C dating by AMS of plant macrofossils in lake sediment: *Radiocarbon*, v. 28, p. 411–416.
- Bada, J. L., 1985, Amino acid racemization dating of fossil bones: *Annual Reviews of Earth and Planetary Sciences*, v. 13, p. 241–268.
- Bada, J. L., Gillespie, R., Gowlett, J. A. J., and Hedges, R. E. M., 1984, Accelerator mass spectrometry radiocarbon ages of amino acid extracts from California paleoindian skeletons: *Nature*, v. 312, p. 442–444.
- Banerjee, S. K., 1981, Experimental techniques in rock magnetism and paleomagnetism: *Advances in Geophysics*, v. 23, p. 25–99.
- Banerjee, S. K., Levi, S., and Lund, S. P., 1979, Geomagnetic record in Minnesota lake sediments: Absence of the Gothenberg and Erieau excursions: *Geology*, v. 7, p. 588–591.
- Baranowski, J., and Harmon, R. S., 1978, U-series chronology of two rhyolites of late Pleistocene age from Long Valley, California, in Zartman, R. E., ed., *Short papers of the Fourth International Conference on Geochronology, Cosmochronology and Isotope Geology*: U.S. Geological Survey Open-File Report 78-0701, p. 22–24.
- Belknap, D. F., and Wehmiller, J. F., 1980, Amino acid racemization in Quaternary mollusks: Examples from Delaware, Maryland, and Virginia, in Hare, P. E., Hoering, T. C., and King, K., Jr., eds., *Biogeochemistry of amino acids*: New York, John Wiley and Sons, p. 401–414.
- Berger, G. W., 1984, Thermoluminescence dating studies on glacial silts from Ontario: *Canadian Journal of Earth Sciences*, v. 21, p. 1393–1399.
- , 1985a, Thermoluminescence dating studies of rapidly deposited silts from south-central British Columbia: *Canadian Journal of Earth Sciences*, v. 22, p. 704–710.
- , 1985b, Thermoluminescence dating of volcanic ash: *Journal of Volcanology and Geothermal Research*, v. 25, p. 333–347.
- Berger, G. W., and Huntley, D. J., 1983, Dating of ash by thermoluminescence: *PACT*, v. 9, p. 581–592.
- Bigazzi, G., and Bonadonna, F., 1973, Fission track dating of the obsidian of Lipari Island (Italy): *Nature*, v. 242, p. 322–323.
- Bischoff, J. L., Schlemon, R. J., Ku, T.-L., Simpson, R. D., Rosenbauer, R. J., and Budinger, F. E., Jr., 1981, Uranium-series and soil-geomorphic dating of the Calico archeological site, California: *Geology*, v. 9, p. 576–582.
- Bischoff, J. L., Rosenbauer, R. J., and Smith, G. L., 1985, Uranium-series ages of sediments from Searles Lake: Differences between continental and marine climatic records: *Science*, v. 227, p. 1222–1224.
- Blomendal, J., Oldfield, F., and Thompson, R., 1979, Magnetic measurements used to assess sediment influx at Llyn Goddionduon: *Nature*, v. 280, p. 50–53.
- Bonhommet, N., and Zähringer, J., 1969, Paleomagnetism and potassium argon age determinations of the Laschamp geomagnetic polarity event: *Earth and Planetary Science Letters*, v. 6, p. 43–46.
- Bothner, M. H., and Johnson, N. M., 1969, Natural thermoluminescent dosimetry in late Pleistocene pelagic sediments: *Journal of Geophysical Research*, v. 74, p. 5331–5338.
- Bradley, R. S., 1985, *Quaternary paleoclimatology*: Boston, Allen and Unwin, 472 p.
- Bradley, W. C., and Addicot, W. O., 1968, Age of first marine terrace near Santa Cruz, California: *Geological Society of America Bulletin*, v. 79, p. 1203–1210.
- Brigham, J. K., 1983, Intrashell variations in amino acid concentrations and isoleucine epimerization ratios in fossil *Hiatella arctica*: *Geology*, v. 11, p. 509–513.
- Champion, D. E., Dalrymple, G. B., and Kuntz, M. A., 1981, Radiometric and paleomagnetic evidence for the Emperor reversed polarity event at 0.46 ± 0.05 m.y. in basalt flows from the eastern Snake River Plain, Idaho: *Geophysical Research Letters*, v. 8, p. 1055–1058.
- Coates, D. A., and Naeser, C. W., 1984, Map showing fission-track ages of clinker in the Rochelle Hills, southern Campbell and Weston counties, Wyoming: U.S. Geological Survey Miscellaneous Investigation Series Map I-1462, scale 1:50,000.
- Colman, S. M., and Pierce, K. L., 1977, Summary table of Quaternary dating techniques: U.S. Geological Survey Miscellaneous Field Studies Map MF-904.
- Colman, S. M., Choquette, A. F., Rosholt, J. N., Miller, G. H., and Huntley, D. J., 1986, Dating the upper Cenozoic sediments in Fisher Valley, southeastern Utah: *Geological Society of America Bulletin*, v. 97, p. 1422–1431.
- Cox, A., Hillhouse, J., and Fuller, M., 1975, Paleomagnetic records of polarity transitions, excursions, and secular variation: *Reviews of Geophysics and Space Physics*, v. 13, p. 185–226.
- Crandell, D. R., Mullineaux, D. R., and Waldron, H. H., 1958, Pleistocene sequence in the southeastern part of the Puget Sound lowland, Washington: *American Journal of Science*, v. 256, p. 384–398.
- Creer, K. M., Tucholka, P., and Barton, C. E., 1983, Paleomagnetism of unconsolidated sediments, in Creer, K. M., Tucholka, P., and Barton, C. E., eds., *Geomagnetism of baked clays and recent sediments*: Amsterdam, Elsevier, p. 197–272.
- Cronin, T. M., 1980, Biostratigraphic correlation of Pleistocene marine deposits and sea levels, Atlantic Coastal Plain of the southeastern United States: *Quaternary Research*, v. 13, p. 213–229.
- Cronin, T. M., Szabo, B. J., Ager, T. A., Hazel, J. E., and Owens, J. P., 1981, Quaternary climates and sea levels of the U.S. Atlantic Coastal Plain: *Science*, v. 211, p. 233–240.
- Currie, L. A., Klouda, G. A., Continetti, R. E., Kaplan, I. R., Wong, W. W., Dzubay, T. G., and Stevens, R. K., 1983, On the origin of carbonaceous particles in American cities: Results of radiocarbon dating and chemical characterization: *Radiocarbon*, v. 25, p. 603–614.
- Dalrymple, G. B., and Lanphere, M. A., 1969, Potassium-argon dating: San Francisco, W. H. Freeman and Co., 258 p.
- Damon, P. E., 1970, A theory of "real" K-Ar clocks: *Eclogae Geologicae Helveticae*, v. 63, p. 69–76.
- Daniels, F., Boyd, C. A., and Saunders, D. F., 1953, Thermoluminescence as a research tool: *Science*, v. 117, p. 343–349.
- Davis, J. O., 1985, Correlation of late Quaternary tephra layers in a long pluvial sequence near Summer Lake, Oregon: *Quaternary Research*, v. 23, p. 38–53.
- Debenham, N. C., and Aitken, M. J., 1984, Thermoluminescence dating of stalagmitic calcite: *Archaeometry*, v. 26, p. 155–170.
- Denham, C. R., 1974, Counter-clockwise motion of paleomagnetic directions 24,000 years ago at Mono Lake, California: *Journal of Geomagnetism and Geoelectricity*, v. 26, p. 487–498.
- Denham, C. R., and Cox, A., 1971, Evidence that the Laschamp polarity event did not occur 13,300–30,400 years ago: *Earth and Planetary Science Letters*, v. 13, p. 181–190.
- Denham, C. R., Anderson, R. F., and Bacon, M. P., 1977, Paleomagnetism and radiochemical age estimates for late Brunhes polarity episodes: *Earth and Planetary Science Letters*, v. 35, p. 384–397.
- Dreimanis, A., Hutt, G., Raukas, A., and Whippiey, P. W., 1978, Dating methods of Pleistocene deposits and their problems: *Thermoluminescence-dating*: *Geoscience Canada*, v. 5, p. 55–60.

- Easterbrook, D. J., Briggs, N. D., Westgate, J. A., and Gorton, M. P., 1981, Age of the Salmon Springs glaciation in Washington: *Geology*, v. 9, p. 87-93.
- Faure, G., 1986, *Principles of isotope geology*: New York, John Wiley, 589 p.
- Fleischer, R. L., 1980, Isotopic disequilibrium of uranium: Alpha-recoil damage and preferential solution effects: *Science*, v. 207, p. 979-981.
- Fleischer, R. L., Price, P. B., and Walker, R. M., 1965a, Effects of temperature, pressure, and ionization on the formation and stability of fission tracks in minerals and glasses: *Journal of Geophysical Research*, v. 70, p. 1497-1502.
- Fleischer, R. L., Price, P. B., Walker, R. M., and Leakey, L.S.B., 1965b, Fission-track dating of a Mesolithic knife: *Nature*, v. 205, p. 1138.
- Fleischer, R. L., Price, P. B., and Walker, R. M., 1975, *Nuclear tracks in solids: Principles and applications*: Berkeley, University of California Press, 605 p.
- Flemming, S. J., 1979, *Thermoluminescence techniques in archaeology*: Oxford, Clarendon Press, 266 p.
- Frank, H., Nicholson, G. J., and Bayer, E., 1977, Rapid gas chromatographic separation of amino acid enantiomers with a novel chiral stationary phase: *Journal of Chromatographic Science*, v. 15, p. 174-176.
- Gleadow, A.J.W., 1980, Fission-track age of the KBS Tuff and associated hominid remains in northern Kenya: *Nature*, v. 284, p. 225-230.
- Gleadow, A.J.W., Hurford, A. J., and Quaife, R. D., 1976, Fission-track dating of zircon: Improved etching techniques: *Earth and Planetary Science Letters*, v. 33, p. 273-276.
- Grootes, P. M., 1983, Radioactive isotopes in the Holocene, in Wright, H. E., ed., *Late-Quaternary environments of the United States*: Minneapolis, University of Minnesota Press, p. 86-108.
- Hansen, R. O., and Begg, E. L., 1970, Age of Quaternary sediments and soils in the Sacramento area, California, by uranium and actinium series dating of vertebrate fossils: *Earth and Planetary Science Letters*, v. 8, p. 411-419.
- Hare, P. E., 1975, Amino acid composition by column chromatography, in Needleman, S. B., ed., *Molecular biology, biochemistry, and biophysics*, v. 8: New York, Springer-Verlag, p. 205-231.
- Hare, P. E., Hoering, T. C., and King, K., Jr., 1980, *Biogeochemistry of amino acids*: New York, John Wiley, 558 p.
- Harland, W. B., Cox, A. V., Llewellyn, P. G., Pickton, C.A.G., Smith, A. G., and Walters, R., 1982, *A geologic time scale*: Cambridge, Cambridge University Press, 131 p.
- Harmon, R. S., and Curl, R. L., 1978, Preliminary results on growth rate and paleoclimatic studies of stalagmite from Ogle Cave, New Mexico: *National Speleological Society Bulletin*, v. 40, p. 25-26.
- Harmon, R. S., and Rosholt, J. N., 1982, Igneous rocks, in Ivanovich, M., and Harmon, R. S., eds., *Uranium series disequilibrium: Applications to environmental problems*: Oxford, Clarendon Press, p. 145-166.
- Harmon, R. S., Ford, D. C., and Schwarcz, H. P., 1977, Interglacial chronology of the Rocky and MacKenzie mountains based upon ^{230}Th - ^{234}U dating of calcite speleothems: *Canadian Journal of Earth Sciences*, v. 14, p. 2543-2552.
- Harmon, R. S., Schwarcz, H. P., and Ford, D. C., 1978a, Stable isotope geochemistry of speleothems and cave waters from the Flint Ridge-Mammoth Cave system, Kentucky: Implications for terrestrial climate change during the period 230,000 to 100,000 years B.P.: *Journal of Geology*, v. 86, p. 373-384.
- Harmon, R. S., Thompson, P., Schwarcz, H. P., and Ford, D. C., 1978b, Late Pleistocene paleoclimates of North America as inferred from stable isotope studies of speleothems: *Quaternary Research*, v. 9, p. 54-70.
- Hearty, P. J., Miller, G. H., Stearns, C. E., and Szabo, B. J., 1986, Aminostratigraphy of Quaternary shorelines in the Mediterranean Basin: *Geological Society of America Bulletin*, v. 97, p. 850-858.
- Heller, F., and Peterson, N., 1982, The Laschamp excursion: *Royal Society of London Philosophical Transactions. Ser. A*, v. 306, p. 169-177.
- Hennig, G. J., and Grün, R., 1984, ESR dating in Quaternary geology: *Quaternary Science Reviews*, v. 2, p. 157-238.
- Hennig, G. J., Bangert, U., Herr, W., and Poulanos, A., 1980, Uranium series dating and thermoluminescence ages of speleothem from Petralona Cave: *Anthropos*, v. 7, p. 174-214.
- Hoopes, E. A., Peltzer, E. T., and Bada, J. L., 1978, Determination of amino acid enantiomeric ratios by gas liquid chromatography of the N-trifluoroacetyl-L-prolyl-peptide methyl esters: *Journal of Chromatographic Sciences*, v. 16, p. 556-560.
- Huntley, D. J., 1985, On the zeroing of the thermoluminescence of sediments: *Physics and Chemistry of Minerals*, v. 12, p. 122-127.
- Huntley, D. J., and Johnson, H. P., 1976, Thermoluminescence as a potential means of dating siliceous ocean sediments: *Canadian Journal of Earth Sciences*, v. 13, p. 593-596.
- Huntley, D. J., Berger, G. W., Divigalpitiya, W.M.R., and Brown, T. A., 1983, Thermoluminescence dating of sediments: *PACT*, v. 9, p. 607-618.
- Huntley, D. J., Godfrey-Smith, D. I., and Thewalt, M.L.W., 1985, Optical dating of sediments: *Nature*, v. 313, p. 105-107.
- International Study Group, 1982, An inter-laboratory comparison of radiocarbon measurements in tree rings: *Nature*, v. 298, p. 619-623.
- Ivanovich, M., 1982, Uranium series disequilibria applications in geochronology, in Ivanovich, M., and Harmon, R. S., eds., *Uranium series disequilibrium: Applications to environmental problems*: Oxford, Clarendon Press, p. 56-78.
- Ivanovich, M., and Harmon, R. S., 1982, *Uranium series disequilibrium: Applications to environmental problems*: Oxford, Clarendon Press, 571 p.
- Izett, G. A., Wilcox, R. E., Powers, H. A., and Desborough, G. A., 1970, The Bishop ash bed, a Pleistocene marker bed in the western United States: *Quaternary Research*, v. 1, p. 121-132.
- Izett, G. A., Wilcox, R. E., and Borchardt, G. A., 1972, Correlation of a volcanic ash bed in the Pleistocene deposits near Mount Blanco, Texas, with the Guaje pumice bed of the Jemez Mountains, New Mexico: *Quaternary Research*, v. 2, p. 554-578.
- Johnson, N. M., and Blanchard, R. L., 1967, Radiation dosimetry from the natural thermoluminescence of fossil shell: *American Mineralogy*, v. 52, p. 1297-1310.
- Johnson, R. A., Pye, K., and Stipp, J. J., 1984, Thermoluminescence dating of southern Mississippi loess: *American Quaternary Association, Eighth Biennial Meeting, Boulder, Colorado, Abstracts*, p. 64.
- Jost, W., 1960, *Diffusion in solids, liquids, gases*: New York, Academic Press, 558 p.
- Karrow, P. F., and Bada, J. L., 1980, Amino acid racemization dating of Quaternary raised marine terraces in San Diego County, California: *Geology*, v. 8, p. 200-204.
- Kaufman, A., 1971, U-series dating of Dead Sea Basin carbonates: *Geochimica et Cosmochimica Acta*, v. 35, p. 1269-1281.
- Kaufman, A., and Broecker, W. S., 1965, Comparison of Th^{230} and C^{14} ages for carbonate materials from Lakes Lahontan and Bonneville: *Journal of Geophysical Research*, v. 70, p. 4039-4054.
- Kaufman, A., Broecker, W. S., Ku, T.-L., and Thurber, D. L., 1971, The status of U-series methods of mollusk dating: *Geochimica et Cosmochimica Acta*, v. 35, p. 1155-1181.
- Kawai, N., Yaskawa, K., Nakajima, M., Torii, M., and Horie, S., 1972, Oscillating geomagnetic field with a recurring reversal discovered from Lake Biwa: *Proceedings of Japanese Academy*, v. 48, p. 186-190.
- Kennedy, G. L., Lajoie, K. R., and Wehmiller, J. F., 1982, Aminostratigraphy and faunal correlations of late Quaternary marine terraces, Pacific Coast, USA: *Nature*, v. 299, p. 545-547.
- King, K., Jr., and Neville, G., 1977, Isoleucine epimerization for dating marine sediments: Importance of analyzing monospecific foraminiferal samples: *Science*, v. 195, p. 1333-1335.
- Knauss, K. G., 1981, Dating fault associated Quaternary material from the Nevada Test Site using uranium-series methods: *Lawrence Livermore Laboratory Report UCRL-53231*, 51 p.
- Knauss, K. G., and Ku, T.-L., 1980, Desert varnish: Potential for age dating via uranium-series isotopes: *Journal of Geology*, v. 88, p. 95-100.
- Kriausakul, N., and Mitterer, R. M., 1978, Isoleucine epimerization in peptides and proteins: Kinetic factors and application to fossil proteins: *Science*, v. 201, p. 1011-1014.

- Krummenacher, D., 1970. Isotopic composition of argon in modern surface volcanic rocks: *Earth and Planetary Science Letters*, v. 8, p. 109-117.
- Ku, T.-L., and Kern, J. P., 1974. Uranium-series age of the upper Pleistocene Nestor Terrace, San Diego, California: *Geological Society of America Bulletin*, v. 85, p. 1713-1716.
- Ku, T.-L., Bull, W. B., Freeman, S. T., and Knauss, K. G., 1979, Th²³⁰-U²³⁴ dating of pedogenic carbonates in gravelly desert soils of Vidal Valley, south-eastern California: *Geological Society of America Bulletin*, Part 1, v. 90, p. 1063-1073.
- Kvenvolden, K. A., Peterson, E., and Pollock, G. E., 1972. Geochemistry of amino acid enantiomers: Gas chromatography of their diastereoisomeric derivatives, in von Gaertner, H. R., and Wehner, H., eds., *Advances in organic geochemistry 1971*: Braunschweig, Pergamon, p. 387-401.
- Lajoie, K. R., Kern, J. P., Wehmiller, J. F., Kennedy, G. L., Mathieson, S. A., Sama-Wojcicki, A. M., Yerkes, R. F., and McCrory, P. F., 1979, Quaternary marine shorelines and crustal deformation, San Diego to Santa Barbara, California, in Abbott, P. L., ed., *Geological excursions in the southern California area: San Diego, California*. San Diego State University Department of Geological Sciences, p. 3-15.
- Lajoie, K. R., Wehmiller, J. F., and Kennedy, G. L., 1980. Inter- and intrageneric trends in apparent racemization kinetics of amino acids in Quaternary Mollusks, in Hare, P. E., Hoering, T. C., and King, K., Jr., eds., *Biogeochemistry of amino acids*: New York, John Wiley and Sons, p. 305-340.
- Lakatos, S., and Miller, D. S., 1972, Evidence for the effect of water content of fission-track annealing in volcanic glass: *Earth and Planetary Science Letters*, v. 14, p. 128-130.
- Lally, A. E., 1982. Chemical procedures, in Ivanovich, M., and Harmon, R. S., eds., *Uranium series disequilibrium: Applications to environmental problems*: Oxford, Clarendon Press, p. 79-106.
- Lamothe, M., 1984. Apparent thermoluminescence ages of St. Pierre sediments at Pierreville, Quebec, and the problem of anomalous fading: *Canadian Journal of Earth Sciences*, v. 21, p. 1406-1409.
- Laughlin, A. W., 1969, Excess radiogenic argon in pegmatite minerals [Ph.D. thesis]: Tucson, University of Arizona, 187 p.
- Levin, I., 1985. Isotopic composition of atmospheric methane, in *The 12th International Radiocarbon Conference Abstracts*, Trondheim, Norway, June 24-28, 1985: Trondheim Norway, University of Trondheim, p. 89.
- Liddicoat, J. C., and Coe, R. S., 1979, Mono Lake geomagnetic excursion: *Journal of Geophysical Research*, v. 84, p. 261-271.
- Liddicoat, J. C., Lajoie, K. R., and Sama-Wojcicki, A. M., 1982, Detection and dating of the Mono Lake excursion in the Lake Lahontan Schoo Formation, Carson Sink, Nevada [abs.]: *EOS American Geophysical Union Transactions*, v. 63, p. 920.
- Lively, R. S., 1983, Late Quaternary U-series speleothem growth record from southeastern Minnesota: *Geology*, v. 11, p. 259-262.
- MacDougall, J. D., 1976, Fission-track annealing and correction procedures for oceanic basalt glasses: *Earth and Planetary Science Letters*, v. 30, p. 19-26.
- Machette, M. N., Rosholt, J. N., and Bush, C. A., 1986, Uranium-trend ages of Quaternary deposits along the Colorado River, Grand Canyon National Park, Arizona: *Geological Society of America Abstracts with Programs*, v. 18, p. 393.
- Mankinen, E. A., and Dalrymple, G. B., 1979, Revised geomagnetic polarity time scale for the interval 0-5 m.y. BP: *Journal of Geophysical Research*, v. 84, p. 615-626.
- Mankinen, E. A., Donnelly, J. M., and Grommé, C. S., 1978, Geomagnetic polarity event recorded at 1.1 m.y. BP on Cobb Mountain, Clear Lake Volcanic field, California: *Geology*, v. 6, p. 653-656.
- Masters, P. M., and Bada, J. L., 1977, Racemization of isoleucine in fossil mollusks from Indian middens and interglacial terraces in southern California: *Earth and Planetary Science Letters*, v. 37, p. 173-183.
- May, R. J., and Machette, M. N., 1984, Thermoluminescence dating of soil carbonate: *U.S. Geological Survey Open-File Report 84-083*, 23 p.
- McCalpin, J., 1986, Thermoluminescence (TL) dating in seismic hazard evaluations: An example from the Bonneville Basin, Utah, in *Proceedings of the 22nd Biannual Symposium on Engineering Geology and Soils Engineering*, 1986: Boise, Idaho, Idaho Department of Transportation, p. 156-176.
- McCartan, L., Owens, J. P., Blackwelder, B. W., Szabo, B. J., Belknap, D. F., Kriausa-kul, N., Mitterer, R. M., and Wehmiller, J. F., 1982, Comparison of amino acid racemization geochronometry with lithostratigraphy, biostratigraphy, uranium-series coral dating, and magnetostratigraphy in the Atlantic Coastal Plain of the southeastern United States: *Quaternary Research*, v. 18, p. 337-359.
- McCoy, W. D., 1981, Quaternary aminostratigraphy of the Bonneville and Lahontan basins, western U.S., with paleoclimatic implications [Ph.D. thesis]: Boulder, University of Colorado, 603 p.
- McCoy, W. D., 1987, Quaternary aminostratigraphy of the Bonneville Basin, western United States: *Geological Society of America Bulletin*, v. 98, p. 99-112.
- McDougall, D. J., ed., 1968, *Thermoluminescence of geological materials*: New York, Academic Press, 527 p.
- McElhinny, M. W., 1973, *Palaeomagnetism and plate tectonics*: Cambridge, Cambridge University Press, 358 p.
- Mejdahl, V., 1979, Thermoluminescence dating: Beta-dose in quartz grains: *Archaeometry*, v. 21, p. 61-73.
- Merrill, R. T., and McElhinny, M. W., 1983, *The earth's magnetic field: Its history, origin, and planetary perspective*: New York, Academic Press, 401 p.
- Miller, B. B., McCoy, W. D., and Blever, N. K., 1987, Stratigraphic potential of amino acid ratios in Pleistocene terrestrial gastropods: An example from west-central Indiana, U.S.A.: *Boreas*, v. 16, p. 133-138.
- Miller, G. H., 1985, Aminostratigraphy of Baffin Island shell-bearing deposits, in Andrews, J. T., ed., *Quaternary studies on Baffin Island, West Greenland and in Baffin Bay*: London, George Allen and Unwin, p. 394-427.
- Miller, G. H., and Hare, P. E., 1980, Amino acid geochronology: Integrity of the carbonate matrix and potential of molluscan fossils, in Hare, P. E., Hoering, T. C., and King, K., Jr., eds., *Biogeochemistry of amino acids*: New York, John Wiley and Sons, p. 415-443.
- Mitterer, R. M., 1975, Ages and diagenetic temperatures of Pleistocene deposits of Florida based on isoleucine epimerization: *Earth and Planetary Science Letters*, v. 28, p. 275-282.
- Mixon, R. B., Szabo, B. J., and Owens, J. P., 1982, Uranium-series dating of mollusks and corals, and age of Pleistocene deposits, Chesapeake Bay area, Virginia and Maryland: *U.S. Geological Survey Professional Paper 1067-E*, 18 p.
- Mook, W. G., 1980, Carbon-14 in hydrogeological studies, in Fritz, P., and Fontes, J. Ch., eds., *Handbook of environmental isotopic geochemistry*: Amsterdam, Elsevier, p. 49-74.
- Mörner, N.-A., Lanser, J. P., and Hospers, J., 1971, Late Weichselian palaeomagnetic reversal: *Nature, Physical Science*, v. 234, p. 173-174.
- Morozov, G. V., 1968, The relative dating of Quaternary Ukrainian sediments by the thermoluminescence method: *VIIth International Quaternary Association Congress Abstracts*, Paris, France (1969), p. 167.
- Muhs, D. R., 1983, Quaternary sea level events on northern San Clemente Island, California: *Quaternary Research*, v. 20, p. 322-341.
- , 1985, Amino acid age estimates of marine terraces and sea levels on San Nicolas Island, California: *Geology*, v. 13, p. 58-61.
- Muhs, D. R., and Kennedy, G. L., 1985, An evaluation of uranium-series dating of fossil echinoids from southern California Pleistocene marine terraces: *Marine Geology*, v. 69, p. 187-193.
- Muhs, D. R., and Rosholt, J. N., 1984, Ages of marine terraces on the Palos Verdes Hills, California, by amino acid and uranium-trend dating: *Geological Society of America Abstracts with Programs*, v. 16, p. 603.
- Muhs, D. R. and Szabo, B. J., 1982, Uranium-series age of the Eel Point terrace, San Clemente Island, California: *Geology*, v. 10, p. 23-26.
- Muhs, D. R., Rosholt, J. N., and Bush, C. A., 1989, The uranium-trend dating method: principles and application for southern California marine terrace deposits: *Quaternary International*, v. 1, p. 19-34.
- Naeser, C. W., 1976, Fission-track dating: *U.S. Geological Survey Open-File*

- Report 76-190, 65 p.
- , 1979, Fission-track dating and geologic annealing of fission tracks, in Jager, E., and Hunziker, J. C., eds., *Lectures in isotope geology*: New York, Springer-Verlag, p. 154-169.
- Naeser, N. D., and Naeser, C. W., 1984, Fission-track dating, in Mahaney, W. C., ed., *Quaternary dating methods*: Amsterdam, Elsevier, p. 87-100.
- Naeser, C. W., Izett, G. A., and Wilcox, R. E., 1973, Zircon fission-track ages of Pearllette family ash beds in Mead County, Kansas: *Geology*, v. 1, p. 187-189.
- Naeser, C. W., Izett, G. A., and Obradovich, J. D., 1980, Fission-track and K-Ar ages of natural glasses: U.S. Geological Survey Bulletin 1489, 31 p.
- Naeser, C. W., Briggs, N. D., Obradovich, J. D., and Izett, G. A., 1981, Geochronology of Quaternary tephra deposits, in Self, S., and Sparks, R.S.J., eds., *Tephra studies: North Atlantic Treaty Organization Advanced Studies Institute, Series C*, Dordrecht, Netherlands, Reidel Publishing Company, p. 13-47.
- Naeser, N. D., Westgate, J. A., Hughes, O. L., and Péwé, T. L., 1982, Fission-track ages of late Cenozoic distal tephra beds in the Yukon Territory and Alaska: *Canadian Journal of Earth Sciences*, v. 19, p. 2167-2178.
- Naeser, C. W., Bryant, B., Crittenden, M. D., and Sorensen, M. L., 1983, Fission-track ages of apatite in the Wasatch Mountains, Utah: An uplift study: *Geological Society of America Memoir* 157, p. 29-36.
- Negrini, R. M., Davis, J. O., and Verosub, K. L., 1984, Mono Lake geomagnetic excursion found at Summer Lake, Oregon: *Geology*, v. 12, p. 643-646.
- Nelson, A. R., 1982, Aminostratigraphy of Quaternary marine and glaciomarine sediments, Quivira Peninsula, Baffin Island: *Canadian Journal of Earth Sciences*, v. 19, p. 945-961.
- Nelson, A. R., and Van Arsdale, R. B., 1986, Recurrent late Quaternary movement on the Strawberry normal fault, Basin and Range-Colorado Plateau transition zone, Utah: *Neotectonics*, v. 1, p. 7-37.
- Nelson, D. E., Loy, T. H., Vogel, J. S., and Southan, J. R., 1986, Radiocarbon dating blood residues on prehistoric stone tools: *Radiocarbon*, v. 28, p. 170-174.
- Newmann, A. C., and Moore, W. S., 1975, Sea level events and Pleistocene coral ages in the northern Bahamas: *Quaternary Research*, v. 5, p. 215-224.
- Nier, A. O., 1950, A redetermination of the relative abundances of the isotopes of carbon, nitrogen, oxygen, argon, and potassium: *Physical Review*, v. 77, p. 789-793.
- Norton, D. L., and Bradford, J. M., 1985, Thermoluminescence dating of loess from western Iowa: *Soil Science Society of America Journal*, v. 49, p. 708-712.
- Oldale, R. N., Valentine, P. C., Cronin, T. M., Spiker, E. C., Blackwelder, B. W., Belknap, D. F., Wehmiller, J. F., and Szabo, B. J., 1982, Stratigraphic, structure, absolute age, and paleontology of the upper Pleistocene deposits at Sankaty Head, Nantucket Island, Massachusetts: *Geology*, v. 10, p. 246-252.
- Osmond, J. K., Carpenter, J. R., and Windom, H. L., 1965, $\text{Th}^{230}/\text{U}^{234}$ age of Pleistocene corals and oolites of Florida: *Journal of Geophysical Research*, v. 70, p. 1843-1847.
- Osmond, J. K., May, J. P., and Tanner, W. F., 1970, Age of the Cape Kennedy Barrier-and-lagoon complex: *Journal of Geophysical Research*, v. 75, p. 469-479.
- Palmer, A. R., 1983, The Decade of North American Geology 1983 geologic time scale: *Geology*, v. 11, p. 503-504.
- Pearson, G. W., and Stuiver, M., 1986, High-precision calibration of the radiocarbon time scale 500 B.C.-2,500 B.C.: *Radiocarbon*, v. 28, p. 839-862.
- Peng, T.-H., Goddard, J. G., and Broecker, W. S., 1978, A direct comparison of ^{14}C and ^{230}Th ages at Searles Lake, California: *Quaternary Research*, v. 9, p. 319-329.
- Rosholt, J. N., 1984, Radioisotope dilution analyses of geological samples using ^{236}U and ^{229}Th : *Nuclear Instruments and Methods in Physics Research*, v. 223, p. 572-576.
- , 1985, Uranium-trend systematics for dating Quaternary sediments: U.S. Geological Survey Open-File Report 85-298, 48 p.
- Rosholt, J. N., Bush, C. A., Carr, W. J., Hoover, D. L., Swadley, W. C., and Dooley, J. R., Jr., 1985a, Uranium-trend dating of Quaternary deposits in the Nevada Test Site area, Nevada and California: U.S. Geological Survey Open-File Report 85-540, 72 p.
- Rosholt, J. N., Bush, C. A., Shroba, R. R., Pierce, K. L., and Richmond, G. L., 1985b, Uranium-trend dating and calibrations for Quaternary sediments: U.S. Geological Survey Open-File Report 85-299, 48 p.
- Rosholt, J. N., Downs, W. R., and O'Malley, P. A., 1986, Uranium-trend ages of surficial deposits in the central Grand Canyon National Park, Arizona: *Geological Society of America Abstracts with Programs*, v. 18, p. 408.
- Rosholt, J. N., Emslie, S., and Stevens, L., 1987a, Paleoclimatic and paleohydrologic significance of uranium-series ages of anhydrite and gypsum in caves, Grand Canyon National Park, Arizona: *Geological Society of America Abstracts with Programs*, v. 19, p. 330.
- Rosholt, J. N., Swadley, W. C., and Bush, C. A., 1988, Uranium-trend dating of fluvial and fan deposits in the Beatty area, Nevada, in Carr, M. D. and Yount, J. C., eds., *Geologic and hydrologic investigations of a potential nuclear waste disposal site at Yucca Mountain, southern Nevada*: U.S. Geological Survey Bulletin 1790, p. 124-137.
- Ryan, W.B.F., 1972, Stratigraphy of late Quaternary sediments in the eastern Mediterranean, in Stanley, D. J., ed., *The Mediterranean Sea*: Stroudsburg, Pennsylvania, Dowden Hutchinson and Ross, p. 149-169.
- Schwarz, H. P., and Gascoyne, M., 1984, Uranium-series dating of Quaternary deposits, in Mahaney, W. C., ed., *Quaternary dating methods*: Amsterdam, Elsevier, p. 33-51.
- Schwarcz, H. P., Harmon, R. S., Thompson, P., and Ford, D. C., 1976, Stable isotope studies of fluid inclusions in speleothems and their paleoclimatic significance: *Geochimica et Cosmochimica Acta*, v. 40, p. 657-665.
- Scott, W. E., McCoy, W. D., Shroba, R. R., and Rubin, M., 1983, Reinterpretation of the exposed record of the last two cycles of Lake Bonneville, western United States: *Quaternary Research*, v. 20, p. 261-285.
- Seward, D., 1979, Comparison of zircon and glass fission-track ages from tephra horizons: *Geology*, v. 7, p. 479-482.
- Shelkopyas, V. N., 1971, Dating of the Quaternary deposits by means of thermoluminescence, in *Chronology of the Glacial Age*: Leningrad, Geographic Society of the USSR, Pleistocene Commission, p. 155-160.
- Sieh, K. E., 1984, Lateral offsets and revised dates of large prehistoric earthquakes at Palmett Creek, Southern California: *Journal of Geophysical Research*, v. 89, p. 7641-7670.
- Singhvi, A. K., and Mejdahl, V., 1985, Thermoluminescence dating of sediments: *Nuclear Tracks*, v. 10, p. 137-162.
- Singhvi, A. K., Sharma, Y. P., and Agrawal, D. P., 1982, Thermoluminescence dating of sand dunes in Rajasthan, India: *Nature*, v. 295, p. 313-315.
- Smith, J. D., and Foster, J. H., 1969, Geomagnetic reversal in Brunhes normal polarity epoch: *Science*, v. 163, p. 365-367.
- Sternberg, R. S., and Damon, P. E., 1983, Atmospheric radiocarbon: Implications for the geomagnetic dipole moment: *Radiocarbon*, v. 25, p. 239-248.
- Storzer, D., and Wagner, G. A., 1969, Correction of thermally lowered fission-track ages of tektites: *Earth and Planetary Science Letters*, v. 5, p. 463-468.
- Stuiver, M., 1975, Climate versus ^{13}C content of the organic component of lake sediments during the late Quaternary: *Quaternary Research*, v. 5, p. 251-262.
- , 1978, Radiocarbon timescale tested against magnetic and other dating methods: *Nature*, v. 273, p. 271-274.
- , 1982, A high-precision calibration of the AD Radiocarbon time scale: *Radiocarbon*, v. 24, p. 1-26.
- Stuiver, M. and Kra, R., eds., 1986, *Proceedings of the 12th International Radiocarbon Conference*, June 24-28, 1985: *Radiocarbon*, v. 28, p. 175-1030.
- Stuiver, M., and Pearson, G. W., 1986, High-precision calibration of the radiocarbon time scale 1950 A.D.-500 B.C.: *Radiocarbon*, v. 28, p. 805-838.
- Stuiver, M., and Polach, H. S., 1977, Discussion: Reporting of ^{14}C data: *Radiocarbon*, v. 19, p. 355-363.
- Stuiver, M., and Quay, P. D., 1980, Changes in atmospheric carbon-14 attributed to a variable sun: *Science*, v. 207, p. 11-19.

- Stuiver, M., and Quay, P. D., 1981, Atmospheric ^{14}C changes resulting from fossil fuel CO_2 release and cosmic ray flux variability: *Earth and Planetary Science Letters*, v. 53, p. 349-362.
- Stuiver, M., Heusser, C. J., and Yang, I. C., 1978, North American glacial history extended to 75,000 years ago: *Science*, v. 200, p. 16-21.
- Stuiver, M., Denton, G. H., Hughes, T. J., and Fastook, J. L., 1983a, History of the marine ice sheet West Antarctica during the last glaciation: A working hypothesis, in Denton, G. H., and Hughes, T. J., eds., *The last great ice sheets*: New York, Wiley Interscience, p. 319-439.
- Stuiver, M., Quay, P. D., and Ostlund, H. G., 1983b, Abyssal water carbon-14 distribution and the age of the world oceans: *Science*, v. 219, p. 849-851.
- Stuiver, M., Kromer, B., Becker, H., and Ferguson, C. W., 1986, Radiocarbon age calibration back to 13,300 yr BP and the ^{14}C age matching of the German oak and U.S. bristlecone pine chronologies: *Radiocarbon*, v. 28, p. 969-979.
- Swadley, W. C., Hoover, D. L., and Rosholt, J. N., 1984, Preliminary report on late Cenozoic faulting and stratigraphy in the vicinity of Yucca Mountain, Nye County, Nevada: U.S. Geological Survey Open-File Report 84-788, 42 p.
- Szabo, B. J., 1972, Uranium-series systematics in natural materials from the Newport area, Oregon: U.S. Geological Survey Professional Paper 800-C, p. C199-C201.
- , 1980a, ^{230}Th and ^{231}Pa dating of unrecrystallized fossil mollusks from marine terrace deposits in west-central California: *Isochron/West*, no. 27, p. 3-4.
- , 1980b, Results and assessment of uranium-series dating of vertebrate fossils from Quaternary alluviums in Colorado: *Arctic and Alpine Research*, v. 12, p. 95-100.
- , 1982, Extreme fractionation of $^{234}\text{U}/^{238}\text{U}$ and $^{230}\text{Th}/^{234}\text{U}$ in spring waters, sediments, and fossils at the Pomme de Terre Valley, southwestern Missouri: *Geochimica et Cosmochimica Acta*, v. 46, p. 1675-1679.
- , 1985, Uranium-series dating of fossil corals from marine sediments of southeastern United States, Atlantic Coastal Plain: *Geological Society of America Bulletin*, v. 96, p. 398-406.
- Szabo, B. J., and Gard, L. M., 1975, Age of the South Bight II marine transgression at Amchitka Island, Aleutians: *Geology*, v. 2, p. 457-460.
- Szabo, B. J., and Kyser, T. K., 1985, Uranium, thorium isotopic analyses and uranium-series ages of calcite and opal, and stable isotopic compositions of calcite from drill cores UE25a#1, USW G-2, and USW G-3/GU-3, Yucca Mountain, Nevada: U.S. Geological Survey Open-File Report 85-224, 25 p.
- Szabo, B. J., and Lindsey, D. H., 1986, Estimating limiting age for Pleistocene erosional surfaces in central Montana by uranium-series dating of associated travertines: *Earth Surface Processes and Landforms*, v. 11, p. 223-228.
- Szabo, B. J., and O'Malley, P. A., 1985, Uranium-series dating of secondary carbonate and silica precipitates relating to fault movements in the Nevada Test Site region and of caliche and travertine samples from the Amorgasa Desert: U.S. Geological Survey Open-File Report 85-471, 12 p.
- Szabo, B. J., and Rosholt, J. N., 1969, Uranium-series dating of Pleistocene molluscan shells from southern California: An open system model: *Journal of Geophysical Research*, v. 74, p. 3253-3260.
- , 1982, Surficial continental sediments, in Ivanovich, M., and Harmon, R. S., eds., *Uranium series disequilibrium: Applications to environmental problems*: Oxford, Clarendon Press, p. 246-267.
- Szabo, B. J., and Vedder, J. B., 1971, Uranium-series dating of some Pleistocene marine deposits in southern California: *Earth and Planetary Science Letters*, v. 11, p. 283-290.
- Szabo, B. J., Gottschall, W. C., Rosholt, J. N., and McKinney, C. R., 1980, Uranium-series disequilibrium investigations related to the WIPP Site, New Mexico: Part I, A preliminary study of uranium-thorium systematics in dissolution residues at the top of evaporites of the Salado Formation; Implications to process and time; Part II, Uranium-trend dating of surficial deposits and Gypsum Spring deposits near WIPP Site, New Mexico: U.S. Geological Survey Open-File Report 80-879, 21 p.
- Szabo, B. J., Carr, W. J., and Gottschall, W. C., 1981a, Uranium-thorium dating of Quaternary carbonate accumulations in the Nevada Test Site region, southern Nevada: U.S. Geological Survey Open-File Report 81-110, 35 p.
- Szabo, B. J., Miller, G. H., Andrews, J. T., and Stuiver, M., 1981b, Comparison of uranium-series, radiocarbon, and amino acid data from marine molluscs, Baffin Island, Arctic Canada: *Geology*, v. 9, p. 451-457.
- Szabo, B. J., O'Malley, P. A., and Schafer, J. P., 1986, Uranium-series dating of travertine deposits in Grand Canyon National Park, Arizona: *Geological Society of America Abstracts with Programs*, v. 18, p. 417.
- Taddeucci, A., Broecker, W. S., and Thurber, D. L., 1967, ^{230}Th dating of volcanic rocks: *Earth and Planetary Science Letters*, v. 3, p. 338-342.
- Taylor, R. E., 1987, Radiocarbon dating: An archaeological perspective: New York, Academic Press, 212 p.
- Templer, R. H., 1985, The removal of anomalous fading in zircon: *Nuclear Tracks*, v. 10, p. 531-538.
- Thompson, P., Ford, D. C., and Schwarcz, H. P., 1975, $\text{U}^{234}/\text{U}^{238}$ ratios in limestone cave seepage waters and speleothem from West Virginia: *Geochimica et Cosmochimica Acta*, v. 39, p. 661-669.
- Thompson, P., Schwarcz, H. P., and Ford, D. C., 1976, Stable isotope geochemistry, geothermometry, and geochronology of speleothems from West Virginia: *Geological Society of America Bulletin*, v. 87, p. 1730-1738.
- Thompson, R., Battarbee, R. W., O'Sullivan, P. E., and Oldfield, F., 1975, Magnetic susceptibility of lake sediments: *Limnology and Oceanography*, v. 20, p. 687-698.
- Thompson, R., Blomendal, J., Dearing, J. A., Oldfield, R., Rummery, T. A., Stober, J. C., and Turner, G. M., 1980, Environmental applications of magnetic measurements: *Science*, v. 207, p. 481-486.
- Verosub, K. L., 1982, Geomagnetic excursions: A critical assessment of the evidence as recorded in sediments of the Brunhes Epoch: *Royal Society of London Philosophical Transactions, Ser. A*, v. 306, p. 161-168.
- Vogel, J. C., and Kronfeld, J., 1980, A new method for dating peat: *South African Journal of Science*, v. 76, p. 557-558.
- Wagner, G. A., 1978, Archaeological applications of fission-track dating: *Nuclear Track Detection*, v. 2, p. 51-64.
- Wehmiller, J. F., 1977, Amino acid studies of the Del Mar, California, midden site: Apparent rate constants, ground temperature models, and chronologic implications: *Earth and Planetary Science Letters*, v. 37, p. 184-196.
- , 1981, Kinetic model options for interpretation of amino acid enantiomeric ratios in Quaternary mollusks; Comments on a paper by Kvenvolden et al. (1979): *Geochimica et Cosmochimica Acta*, v. 45, p. 261-264.
- , 1982, A review of amino acid racemization studies in Quaternary mollusks; Stratigraphic and chronologic applications in coastal and interglacial sites, Pacific and Atlantic coasts, United States, United Kingdom, Baffin Island, and Tropical Islands: *Quaternary Science Reviews*, v. 1, p. 83-120.
- , 1984a, Relative and absolute dating of Quaternary mollusks with amino acid racemization; Evaluation, applications, and questions, in Mahaney, W. C., ed., *Quaternary dating methods*: Amsterdam, Elsevier, p. 171-194.
- , 1984b, Interlaboratory comparison of amino acid enantiomeric ratios in fossil Pleistocene mollusks: *Quaternary Research*, v. 22, p. 109-120.
- Wehmiller, J. F., and Belknap, D. F., 1978, Alternative models for the interpretation of amino acid enantiomeric ratios of Pleistocene mollusks; Examples from California, Washington, and Florida: *Quaternary Research*, v. 9, p. 330-348.
- , 1982, Amino acid age estimates, Quaternary Atlantic Coast Plain: Comparison with U-series dates, biostratigraphy, and paleomagnetic control: *Quaternary Research*, v. 18, p. 311-336.
- Wehmiller, J. F., and Hare, P. E., 1971, Racemization of amino acids in marine sediments: *Science*, v. 173, p. 907-911.
- Wehmiller, J. F., Lajoie, K. R., Kvenvolden, K. A., Peterson, E., Belknap, D. F., Kennedy, G. L., Addicott, W. O., Vedder, J. G., and Wright, R. W., 1977, Correlation and chronology of Pacific Coast marine terrace deposits of continental United States by fossil amino acid stereochemistry: Technique evaluation, relative ages, kinetic model ages, and geologic implications: U.S. Geological Survey Open-File Report 77-680, 196 p.
- Williams, K. M., and Smith, G. G., 1977, A critical evaluation of the application

- of amino acid racemization to geochronology and geothermometry: *Origins of Life*, v. 8, p. 91-144.
- Winograd, I. J., and Doty, G. C., 1980, Paleohydrology of the southern Great Basin with special reference to water table fluctuations beneath the Nevada Test Site during the late(?) Pleistocene: U.S. Geological Survey Open-File Report 80-569, 91 p.
- Winograd, I. J., and Szabo, B. J., 1985, Water-table decline in the south-central Great Basin during the Quaternary period; Implications for toxic-waste disposal: U.S. Geological Survey Open-File Report 85-697, 18 p.
- Winograd, I. J., Szabo, B. J., Coplen, T. B., Riggs, A. C., and Kolesar, P. T., 1985, Two-million-year record of deuterium depletion in Great Basin ground waters: *Science*, v. 227, p. 519-522.
- Winograd, I. J., Szabo, B. J., Coplen, T. B. and Riggs, A. C., 1988, A 250,000-year climatic record from Great Basin vein calcite: implications for Milankovitch theory: *Science*, v. 242, p. 1275-1280.
- Wintle, A. G., 1973, Anomalous fading of thermoluminescence in mineral samples: *Nature*, v. 245, p. 143-144.
- , 1977, Detailed study of a thermoluminescence mineral exhibiting anomalous fading: *Journal of Luminescence*, v. 15, p. 385-393.
- , 1978, A thermoluminescence study of some Quaternary calcite: Potential and problems: *Canadian Journal of Earth Sciences*, v. 15, p. 1977-1986.
- Wintle, A. G., and Catt, J., 1985, Thermoluminescence dating of soils developed in late Devensian loess at Pegwell Bay, Kent: *Journal of Soil Science*, v. 36, p. 293-298.
- Wintle, A. G., and Huntley, D. H., 1979, Thermoluminescence dating of deep sea ocean core: *Nature*, v. 279, p. 710-712.
- , 1980, Thermoluminescence dating of ocean sediment: *Canadian Journal of Earth Sciences*, v. 17, p. 348-360.
- , 1982, Thermoluminescence dating of sediments: *Quaternary Science Reviews*, v. 1, p. 31-53.
- Wintle, A. G., and Prószyńska, H., 1983, TL-dating of loess in Germany and Poland: *PACT*, v. 9, p. 547-554.
- Wintle, A. G., and Westgate, J. A., 1986, Thermoluminescence properties of loess in relation to the age of Old Crow Tephra in Alaska: *Geology*, v. 14, p. 594-597.
- Wintle, A. G., Shackleton, N. J., and Lantieri, J. P., 1984, Thermoluminescence dating of periods of loess deposition and soil formation in Normandy: *Nature*, v. 310, p. 491-493.
- Wolfman, D., 1983, Archaeomagnetism of baked clays, in Creer, K. M., Tucholka, P., and Barton, C. E., eds., *Geomagnetism of baked clays and recent sediments*: Amsterdam, Elsevier, p. 76-196.
- Zeitler, P. K., Johnson, N. M., Naeser, C. W., and Tahirkheli, R.A.K., 1982, Fission-track evidence for Quaternary uplift of the Nanga Parbat region, Pakistan: *Nature*, v. 298, p. 255-257.
- Zeller, E. J., Wray, J. L., and Daniels, F., 1955, Thermoluminescence induced by pressure and by crystallization: *Journal of Chemical Physics*, v. 23, p. 2187-2189.
- Zielinski, R. A., Bush, C. A., and Rosholt, J. N., 1986, Uranium-series disequilibrium in a young surficial uranium deposit, northeastern Washington: *Applied Geochemistry*, v. 1, p. 503-511.
- Zimmerman, D. W., 1972, Relative thermoluminescence effects of alpha- and beta-radiation: *Radiation Effects*, v. 14, p. 81-92.

MANUSCRIPT ACCEPTED BY THE SOCIETY JUNE 10, 1987

ACKNOWLEDGMENTS

Radiocarbon research at Stuiver's Quaternary Isotope Laboratory is supported through National Science Foundation (NSF) Grants ATM-8318665 and EAR-8115994.

The K-Ar dating research of Damon was supported by NSF Grant EAR-7811535 and the State of Arizona during development of the described methodology and its theoretical rationale. Dr. Muhammad Shafiqullah has been a diligent and effective collaborator in this research.

Forman's research on thermoluminescence was supported by NSF Grant DPP-8303425. Forman and Machette thank A. G. Wintle for sharing her extensive knowledge of thermoluminescence dating, and G. H. Miller, J. T. Andrews, D. S. Fullerton, and K. L. Pierce for comments on early versions of the thermoluminescence section of this chapter.

Muhs thanks G. H. Miller, A. R. Nelson, and B. J. Szabo for helpful comments on early versions of the amino acid geochronology section of this section.

NOTES ADDED IN PROOF

Addition to section by S. M. Colman and K. L. Pierce

A derivative paper concerning classification and terminology for dating methods was published in 1987 (Colman and others, 1987). Major advances in research into dating methods have occurred between 1986 and the time of publication of this volume. Some of the recent advances in dating methods have been published in recent collections of papers by Easterbrook (1989), Rutter and others (1989), and Townsend and others (1988).

Addition to section by C. W. Naeser and N. D. Naeser

An important recent advancement in application of fission track dating to Quaternary tephra is development of the isothermal plateau method for correcting thermally lowered fission-track ages on hydrated glass shards (Westgate, 1988, 1989). This method has produced glass ages that are concordant with zircon fission-track, K-Ar, $^{40}\text{Ar}/^{39}\text{Ar}$, and thermoluminescence ages on coexisting minerals from rocks ranging from Quaternary to Cretaceous (Westgate, 1988, 1989).

Addition to section by S. L. Forman and M. N. Machette

Since 1986 when this chapter was completed there have been some significant advances in luminescence dating. Thermoluminescence dating of buried soils, loess and eolian sand has yielded ages in agreement with a radiocarbon chronology (Berger, 1988; Forman, 1989). The temporal limitations of the method remain uncertain but apparently accurate ages of ca. 100 ka have been reported (Forman, 1989). The more energy sensitive analysis provided by optical stimulated luminescence may be a better geochronometer (Huntley and others, 1985).

ADDITIONAL REFERENCES

- Berger, G. W., 1988, Dating Quaternary events by luminescence, in Easterbrook, D. J., ed., *Dating Quaternary sediments*: Geological Society of America Special Paper 227, p. 13-50.
- Colman, S. M., Pierce, K. L., and Birkeland, P. W., 1987, Suggested terminology for Quaternary dating methods: *Quaternary Research*, v. 28, p. 314-319.
- Easterbrook, D. L. (ed.), 1989, *Dating Quaternary Sediments*: Geological Society of America Special Paper 227, 165 p.
- Forman, S. L., 1989, Applications and limitations of thermoluminescence to date Quaternary sediments: *Quaternary International*, v. 1, p. 47-59.
- Huntley, D. W., Godfrey-Smith, D. L., and Thewalt, M.L.W., 1985, Optical dating of sediments: *Nature*, v. 313, p. 105-107.
- Rendell, H., and Townsend, P. D., 1988, Thermoluminescence dating of a 10 m loess profile in Pakistan: *Quaternary Science Reviews*, v. 7, p. 251-255.
- Rutter, N., Brigham-Grette, J., and Catto, N. (eds.), 1989, *Applied Quaternary Geology*: Quaternary International, v. 1, 166 p.
- Townsend, P. D., and 9 others (eds.), 1988, *Thermoluminescence and Electron-Spin-Resonance Dating*: Quaternary Science Reviews, v. 7, p. 245-536.
- Westgate, J. A., 1988, Isothermal plateau fission-track age of the late Pleistocene Old Crow tephra, Alaska: *Geophysical Research Letters*, v. 15, p. 376-379.
- , 1989, Isothermal plateau fission-track ages of hydrated glass shards from silicic tephra beds: *Earth and Planetary Science Letters*, v. 95, p. 226-234.

- of amino acid racemization to geochronology and geothermometry: *Origins of Life*, v. 8, p. 91-144.
- Winograd, I. J., and Doty, G. C., 1980, Paleohydrology of the southern Great Basin with special reference to water table fluctuations beneath the Nevada Test Site during the late(?) Pleistocene: U.S. Geological Survey Open-File Report 80-569, 91 p.
- Winograd, I. J., and Szabo, B. J., 1985, Water-table decline in the south-central Great Basin during the Quaternary period; Implications for toxic-waste disposal: U.S. Geological Survey Open-File Report 85-697, 18 p.
- Winograd, I. J., Szabo, B. J., Coplen, T. B., Riggs, A. C., and Kolesar, P. T., 1985, Two-million-year record of deuterium depletion in Great Basin ground waters: *Science*, v. 227, p. 519-522.
- Winograd, I. J., Szabo, B. J., Coplen, T. B. and Riggs, A. C., 1988, A 250,000-year climatic record from Great Basin vein calcite: implications for Milankovitch theory: *Science*, v. 242, p. 1275-1280.
- Wintle, A. G., 1973, Anomalous fading of thermoluminescence in mineral samples: *Nature*, v. 245, p. 143-144.
- , 1977, Detailed study of a thermoluminescence mineral exhibiting anomalous fading: *Journal of Luminescence*, v. 15, p. 385-393.
- , 1978, A thermoluminescence study of some Quaternary calcite: Potential and problems: *Canadian Journal of Earth Sciences*, v. 15, p. 1977-1986.
- Wintle, A. G., and Catt, J., 1985, Thermoluminescence dating of soils developed in late Devensian loess at Pegwell Bay, Kent: *Journal of Soil Science*, v. 36, p. 293-298.
- Wintle, A. G., and Huntley, D. H., 1979, Thermoluminescence dating of deep sea ocean core: *Nature*, v. 279, p. 710-712.
- , 1980, Thermoluminescence dating of ocean sediment: *Canadian Journal of Earth Sciences*, v. 17, p. 348-360.
- , 1982, Thermoluminescence dating of sediments: *Quaternary Science Reviews*, v. 1, p. 31-53.
- Wintle, A. G., and Prószyńska, H., 1983, TL-dating of loess in Germany and Poland: *PACT*, v. 9, p. 547-554.
- Wintle, A. G., and Westgate, J. A., 1986, Thermoluminescence properties of loess in relation to the age of Old Crow Tephra in Alaska: *Geology*, v. 14, p. 594-597.
- Wintle, A. G., Shackleton, N. J., and Lautridou, J. P., 1984, Thermoluminescence dating of periods of loess deposition and soil formation in Normandy: *Nature*, v. 310, p. 491-493.
- Wolfman, D., 1983, Archaeomagnetism of baked clays, in Creer, K. M., Turcholka, P., and Barton, C. E., eds., *Geomagnetism of baked clays and recent sediments*: Amsterdam, Elsevier, p. 76-196.
- Zeitler, P. K., Johnson, N. M., Naeser, C. W., and Tahirkheli, R.A.K., 1982, Fission-track evidence for Quaternary uplift of the Nanga Parbat region, Pakistan: *Nature*, v. 298, p. 255-257.
- Zeller, E. J., Wray, J. L., and Daniels, F., 1955, Thermoluminescence induced by pressure and by crystallization: *Journal of Chemical Physics*, v. 23, p. 2187-2189.
- Zielinski, R. A., Bush, C. A., and Rosholt, J. N., 1986, Uranium-series disequilibrium in a young surficial uranium deposit, northeastern Washington: *Applied Geochemistry*, v. 1, p. 503-511.
- Zimmerman, D. W., 1972, Relative thermoluminescence effects of alpha- and beta-radiation: *Radiation Effects*, v. 14, p. 81-92.

MANUSCRIPT ACCEPTED BY THE SOCIETY JUNE 10, 1987

ACKNOWLEDGMENTS

Radiocarbon research at Stuiver's Quaternary Isotope Laboratory is supported through National Science Foundation (NSF) Grants ATM-8318665 and EAR-8115994.

The K-Ar dating research of Damon was supported by NSF Grant EAR-7811535 and the State of Arizona during development of the described methodology and its theoretical rationale. Dr. Muhammad Shafiqullah has been a diligent and effective collaborator in this research.

Forman's research on thermoluminescence was supported by NSF Grant DPP-8303425. Forman and Machette thank A. G. Wintle for sharing her extensive knowledge of thermoluminescence dating, and G. H. Miller, J. T. Andrews, D. S. Fullerton, and K. L. Pierce for comments on early versions of the thermoluminescence section of this chapter.

Muhs thanks G. H. Miller, A. R. Nelson, and B. J. Szabo for helpful comments on early versions of the amino acid geochronology section of this section.

NOTES ADDED IN PROOF

Addition to section by S. M. Colman and K. L. Pierce

A derivative paper concerning classification and terminology for dating methods was published in 1987 (Colman and others, 1987). Major advances in research into dating methods have occurred between 1986 and the time of publication of this volume. Some of the recent advances in dating methods have been published in recent collections of papers by Easterbrook (1989), Rutter and others (1989), and Townsend and others (1988).

Addition to section by C. W. Naeser and N. D. Naeser

An important recent advancement in application of fission track dating to Quaternary tephra is development of the isothermal plateau method for correcting thermally lowered fission-track ages on hydrated glass shards (Westgate, 1988, 1989). This method has produced glass ages that are concordant with zircon fission-track, K-Ar, $^{40}\text{Ar}/^{39}\text{Ar}$, and thermoluminescence ages on coexisting minerals from rocks ranging from Quaternary to Cretaceous (Westgate, 1988, 1989).

Addition to section by S. L. Forman and M. N. Machette

Since 1986 when this chapter was completed there have been some significant advances in luminescence dating. Thermoluminescence dating of buried soils, loess and eolian sand has yielded ages in agreement with a radiocarbon chronology (Berger, 1988; Forman, 1989). The temporal limitations of the method remain uncertain but apparently accurate ages of ca. 100 ka have been reported (Forman, 1989). The more energy sensitive analysis provided by optical stimulated luminescence may be a better geochronometer (Huntley and others, 1985).

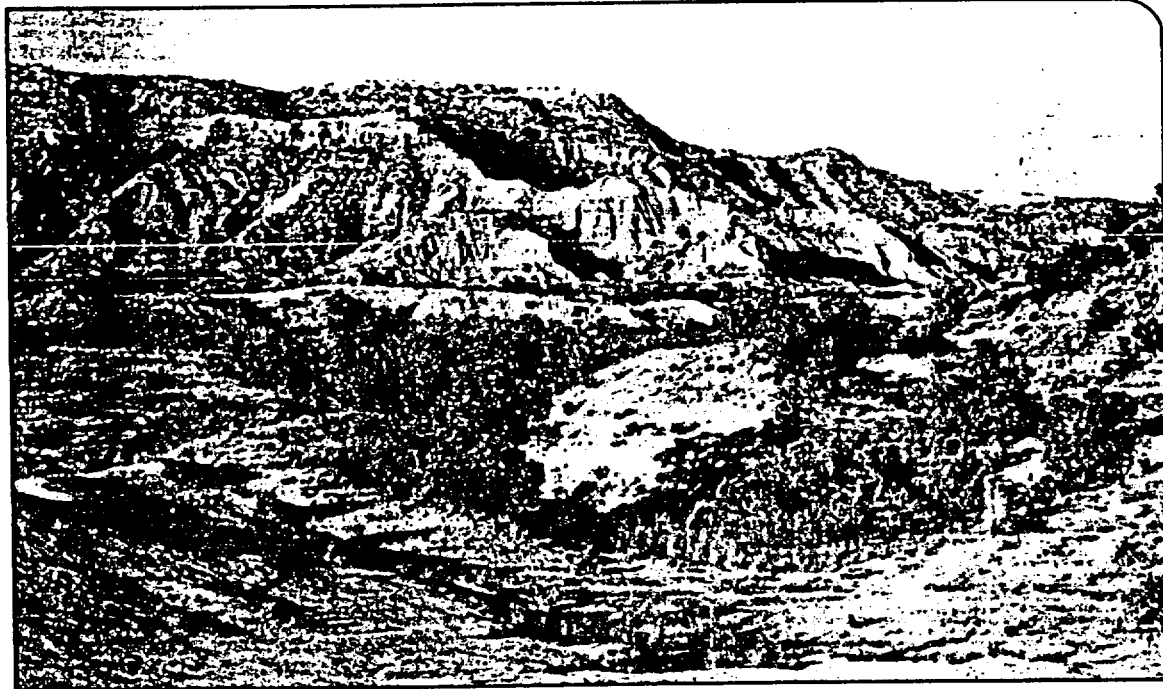
ADDITIONAL REFERENCES

- Berger, G. W., 1988, Dating Quaternary events by luminescence, in Easterbrook, D. J., ed., *Dating Quaternary sediments*: Geological Society of America Special Paper 227, p. 13-50.
- Colman, S. M., Pierce, K. L., and Birkeland, P. W., 1987, Suggested terminology for Quaternary dating methods: *Quaternary Research*, v. 28, p. 314-319.
- Easterbrook, D. L. (ed.), 1989, *Dating Quaternary Sediments*: Geological Society of America Special Paper 227, 165 p.
- Forman, S. L., 1989, Applications and limitations of thermoluminescence to date Quaternary sediments: *Quaternary International*, v. 1, p. 47-59.
- Huntley, D. W., Godfrey-Smith, D. I., and Thewalt, M.L.W., 1985, Optical dating of sediments: *Nature*, v. 313, p. 105-107.
- Rendell, H., and Townsend, P. D., 1988, Thermoluminescence dating of a 10 m loess profile in Pakistan: *Quaternary Science Reviews*, v. 7, p. 251-255.
- Rutter, N., Brigham-Grette, J., and Catto, N. (eds.), 1989, *Applied Quaternary Geology*: Quaternary International, v. 1, 166 p.
- Townsend, P. D., and 9 others (eds.), 1988, *Thermoluminescence and Electron-Spin-Resonance Dating*: Quaternary Science Reviews, v. 7, p. 245-536.
- Westgate, J. A., 1988, Isothermal plateau fission-track age of the late Pleistocene Old Crow tephra, Alaska: *Geophysical Research Letters*, v. 15, p. 376-379.
- , 1989, Isothermal plateau fission-track ages of hydrated glass shards from silicic tephra beds: *Earth and Planetary Science Letters*, v. 95, p. 226-234.

Report of Investigations No. 180

Geomorphic Processes and Rates of Retreat Affecting the Caprock Escarpment, Texas Panhandle

Thomas C. Gustavson
and
William W. Simpkins



1989



Bureau of Economic Geology

W. L. Fisher, Director

The University of Texas at Austin

Austin, Texas 78713

9303110376

Report of Investigations No. 180

Geomorphic Processes and Rates of Retreat Affecting the Caprock Escarpment, Texas Panhandle

Thomas C. Gustavson
and
William W. Simpkins*



1989



Bureau of Economic Geology
W. L. Fisher, Director
The University of Texas at Austin
Austin, Texas 78713

*Department of Geology and Geophysics
University of Wisconsin
Madison, Wisconsin 53705

CONTENTS

Abstract	1
Introduction	2
Geologic Setting	3
Structural Development	3
Stratigraphy	4
Regional Hydrology	5
Geomorphology and Physiography	5
Climate	5
Runoff	8
Relation of Dissolution-Induced Subsidence to the Caprock Escarpment	10
Stratigraphy beneath the High Plains, Caprock Escarpment, and Rolling Plains	10
Structure on the Tubb Interval	10
Salt Thickness	13
Structure on the Alibates Formation	13
Middle Tertiary Erosional Surface	13
Relation of Post-Ogallala Lake Basins to the Caprock Escarpment	18
Fracture Systems and Landform Development	18
Systematic and Nonsystematic Fractures	18
Clastic Dikes	19
Ground-Water Flow beneath the Caprock Escarpment	20
Conceptual Model of Ground-Water Flow beneath the Caprock Escarpment	22
Numerical Model of Ground-Water Flow beneath the Caprock Escarpment	24
Modeling Results	25
Surface Processes Causing Scarp Retreat	27
Surface Runoff	27
Drainage Development	27
Thresholds for Sediment Movement	28
Spring Sapping and Seepage Erosion	29
Rockfalls	31
Rotational Slumping	31
Piping	34
Stages in the Physiographic Development of the Eastern Caprock Escarpment	35
Rates of Retreat of the Caprock Escarpment	38
Rates of Interstratal Salt Dissolution along the Caprock Escarpment	38
Procedure for Calculating Salt Dissolution Rates	38
Salt Dissolution Rates	39
Surface Erosion Rates	41
Effect of Diminished Spring Discharge on Geomorphic Processes	42
Summary and Conclusions	44
Acknowledgments	45
References	45

Figures

1. Location of the study area in the eastern Texas Panhandle	2
2. Major structural elements, Texas Panhandle and surrounding area	3
3. Stratigraphic nomenclature of Permian and younger strata, Texas Panhandle	4
4. Topography along the Caprock Escarpment	6
5. Views of the Eastern Caprock Escarpment in Palo Duro Canyon State Park	7
6. Three-day total rainfall distribution, June 24-26, 1965, along the Eastern Caprock Escarpment	8
7. Intensity-duration profiles of four storms along the Caprock Escarpment	9
8. Regional stratigraphic cross section illustrating zones of section lost owing to dissolution of salt and collapse of overlying strata beneath the Southern High Plains, Caprock Escarpment, and Rolling Plains	11
9. Structure-contour map of the top of the middle Permian Tubb interval	12
10. Net-thickness map of salt in the Permian upper Clear Fork Group and San Andres, Seven Rivers, and Salado Formations	14
11. Net-thickness map of salt in the Salado and Seven Rivers Formations	15
12. Structure-contour map of the top of the Upper Permian Alibates Formation	16
13. Structure-contour map of the base of the High Plains aquifer (Ogallala Formation)	17
14. Head map of the unconfined aquifers in the Palo Duro Basin	20
15. Potentiometric-surface map of lower Dockum Group ground water	21
16. Map of physiographic units, major streams, and brine emission areas in the study area	22
17. Conceptual model of ground-water flow and its impact on Permian bedded salt beneath the High Plains Caprock Escarpment and Rolling Plains	23
18. Finite-element mesh design based on cross section shown in figure 8	24
19. Steady-state hydraulic heads and recharge/discharge rates computed by ground-water flow model	26
20. Plot of maximum rainfall intensity versus percent of erosion pins showing erosion at the Buffalo Lake National Wildlife Refuge station	29
21. Area of spring sapping at the head of Red Canyon, Palo Duro Canyon State Park	30
22. Detail of the spring discharge area illustrated in figure 21	30
23. Rockfall consisting of blocks of massive channel sandstones, Upper Triassic Dockum Group at the head of Tub Springs Draw, Palo Duro Canyon State Park	31
24. a. Fracture in caprock caliche of the Miocene-Pliocene Ogallala Formation at Fortress Cliff, Palo Duro Canyon State Park	32
b. Fracture in sandstone of the Upper Triassic Dockum Group in Tub Springs Draw	32
25. Distribution of rotational slumps and landslides in Palo Duro Canyon, Palo Duro Canyon State Park	33
26. Three segments of rotational slumps exposed along the northeastern side of Palo Duro Canyon	34
27. Entrance to a large pipe in Caprock Canyons State Park	35
28. Outlet for a large pipe in Palo Duro Canyon State Park	35
29. Stages in development of drainage at the Caprock Escarpment	36
30. Drainage basins and gauging stations in the Rolling Plains	40

Tables

1. Rainfall intensity-duration-frequency relationships, Amarillo, Texas, 1904-1951	9
2. Hydrostratigraphic units and hydraulic conductivities used in the ground-water flow model	25
3. Erosion-pin measurements made on eroded canyon slopes following storm on May 26, 1978	28
4. Record of intense storms at Buffalo Lake National Wildlife Refuge	28
5. Dissolved chloride loads for streams, calculated salt volumes, and salt dissolution rates for selected drainage basins, Texas Panhandle	39
6. Spring discharge rates, Eastern Caprock Escarpment, Texas Panhandle	43

Abstract

The interaction of geomorphic and ground-water processes has produced the Caprock Escarpment that bounds the eastern margin of the Southern High Plains in the Texas Panhandle. Spring sapping, slumping, and piping at the surface and salt dissolution in the subsurface are some of the many erosional processes affecting the escarpment.

Substantial thicknesses of bedded Permian salt (halite) have been dissolved from the Salado, Seven Rivers, San Andres, and Glorieta Formations beneath the Caprock Escarpment and the Rolling Plains, east of the escarpment. Dissolution of salt from the Salado and Seven Rivers Formations beneath the Caprock Escarpment has resulted in subsidence and development of a regional dip reversal in the overlying Alibates Formation. Although most dissolution has taken place beneath the Caprock Escarpment and Rolling Plains, dissolution and subsidence extend westward beyond the escarpment to beneath the Southern High Plains. Dissolution-induced subsidence apparently accounts for as much as 75 m (250 ft) of Caprock Escarpment relief.

Complex fracture systems along the escarpment have developed in part because of subsidence. Permian and Triassic strata contain systematic and nonsystematic fractures, extension fractures, and, locally, clastic dikes. The Ogallala Formation contains systematic fractures in basal calcretes and silcretes and, locally, clastic dikes. Of these, the nonsystematic fractures, extension fractures, and clastic dikes probably result from salt dissolution and subsidence. Ground-water leakage downward toward the salt-bearing zones is most likely enhanced by fractures.

Conceptual and numerical models of ground-water flow beneath the Caprock Escarpment suggest that low-salinity ground water flows downward from the Ogallala and Dockum aquifers to dissolve Permian salt. Brines flow eastward through permeable anhydrites, dolomites, and dissolution breccias beneath the Rolling Plains to discharge as springs in topographic lows.

Dissolution is active along the Caprock Escarpment; during a 15-yr period it resulted in the loss of over 15 million m³ (525 million ft³) of salt from the study area. Westward expansion of the active dissolution zone along the Caprock Escarpment and beneath the Rolling Plains occurs at a mean rate of 0.02 km/1,000 yr (0.013 mi/1,000 yr).

Surface erosion on the hillslopes of the Caprock Escarpment occurs by sheetflooding, slope wash, rill wash, rockfalls, spring sapping, piping, and rotational slumping. Fluvial erosion dominates in canyon bottoms. Sheetflooding, slope wash, and rill wash resulting from runoff from episodic, high-intensity rainfall events have modified the upper margin of the escarpment. Runoff from these same events scours canyons and their tributaries. Sapping below areas of spring discharge in strata of the Dockum Group and Ogallala Formation helps to remove sediment and contributes to the development of rockfalls. Numerous rotational slumps and landslides have substantially accelerated slope degradation in Palo Duro Canyon. Large pipes commonly develop along the slip planes of these slumps.

Scarp retreat rates based on surface erosion rates were examined and compared with the subsurface salt dissolution rates. Scarp retreat rates based on projected former positions of the Caprock Escarpment are probably maximum rates that range from 0.06 km/1,000 yr (0.038 mi/1,000 yr) to 0.19 km/1,000 yr (0.119 mi/1,000 yr). Short-term erosion rates based on semiannual measurement of erosion pins and stream headcuts range from 0.01 to 0.03 km/1,000 yr (0.006 to 0.019 mi/1,000 yr). The mean horizontal dissolution rate for salt in the study region is 0.02 km/yr (0.013 mi/yr). Because the Caprock Escarpment parallels and overlies the zone of salt dissolution, the retreat rates of these two features are comparable and appear to converge in the range of 0.01 to 0.20 km/1,000 yr (0.006 to 0.12 mi/1,000 yr).

Discharge from many springs along the Caprock Escarpment has decreased as much as an order of magnitude over the last 50 yr as a result of widespread exploitation of the Ogallala aquifer for irrigation. Because of this trend, associated erosional processes such as spring sapping, slumping, rockfalls, and stream discharge have most likely decreased as well, thus slowing the westward retreat of the Caprock Escarpment.

Keywords: Caprock Escarpment, fractures, geomorphic processes, ground-water flow systems, Rolling Plains, salt dissolution, scarp retreat rates, Southern High Plains, Texas Panhandle

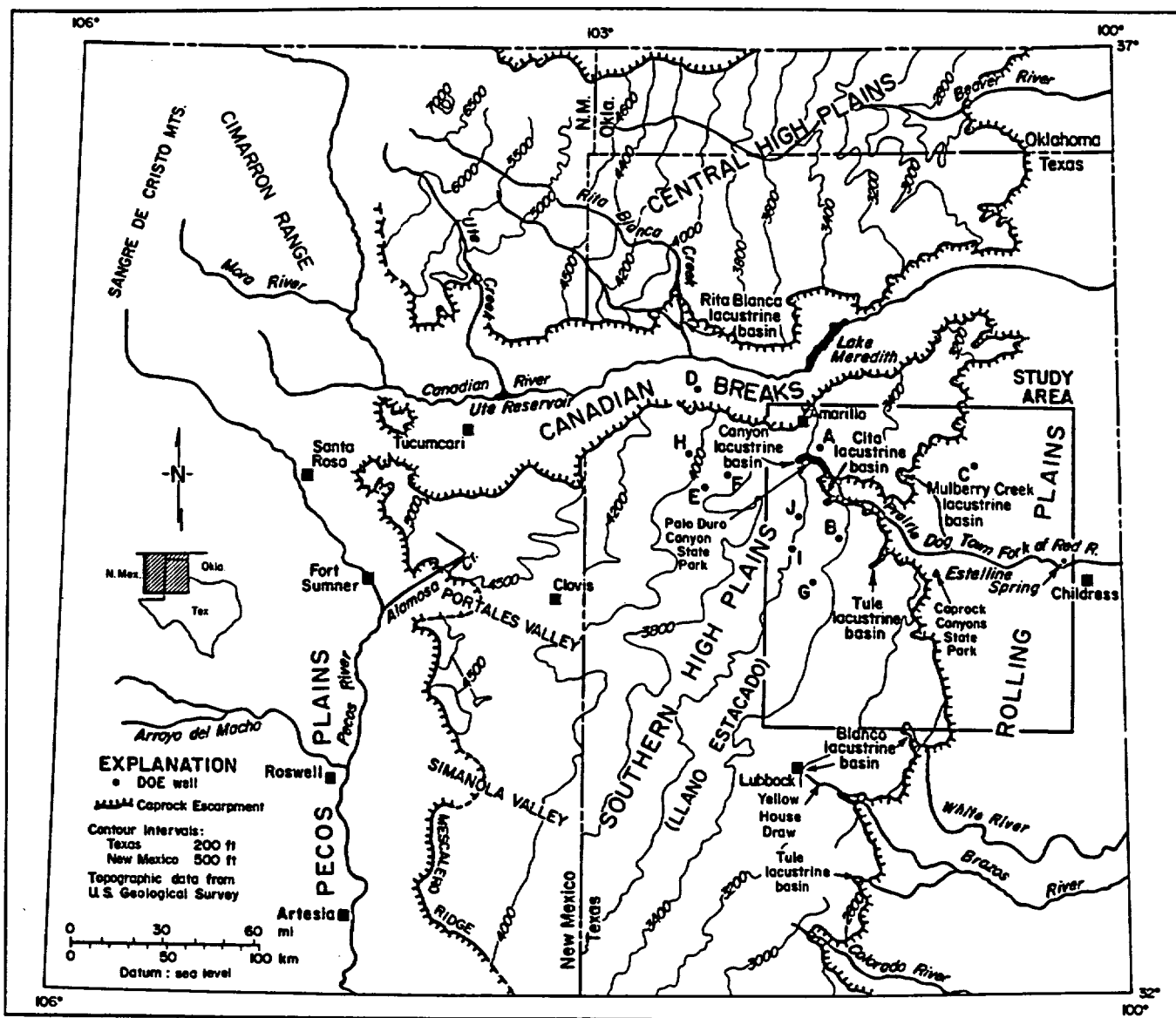


FIGURE 1. Location of the study area in the eastern Texas Panhandle. Major physiographic divisions of eastern New Mexico, the Texas Panhandle, and the Oklahoma panhandle are shown. Letters A through J locate Department of Energy stratigraphic and hydrologic test wells: (A) DOE-Gruy Federal Rex White No. 1; (B) DOE-Gruy Federal Grabbe No. 1; (C) Stone and Webster Engineering Corporation (SWEC) Sawyer No. 1; (D) SWEC Mansfield No. 1; (E) SWEC Dettan No. 1; (F) SWEC G. Freimel No. 1; (G) SWEC Zeeck No. 1; (H) SWEC J. Freimel No. 1; (I) SWEC Harman No. 1; (J) SWEC Holtzclaw No. 1.

Introduction

The Southern High Plains of eastern New Mexico and northwestern Texas is bounded by a high escarpment on its western, northern, and eastern sides (fig. 1) and merges to the south with the Edwards Plateau. Field observations from 1978 to 1986 indicate that erosion and retreat of the escarpment were most active along the eastern margin of the Southern High Plains, the Eastern Caprock Escarpment. Previous studies suggest that several geomorphic processes affect scarp retreat (for example, salt dissolution, subsidence,

spring sapping, seepage erosion, and slumping) and that both the position of the escarpment and the processes that cause retreat are affected by interaction with ground-water systems. On the basis of literature review, Gustavson (1983) and Osterkamp and others (1987) concluded that geomorphic processes related to ground-water discharge, such as springs and seeps, dominate landform development on the southern Great Plains. Zones of active salt (primarily halite) dissolution lie beneath the escarpment (Gustavson and

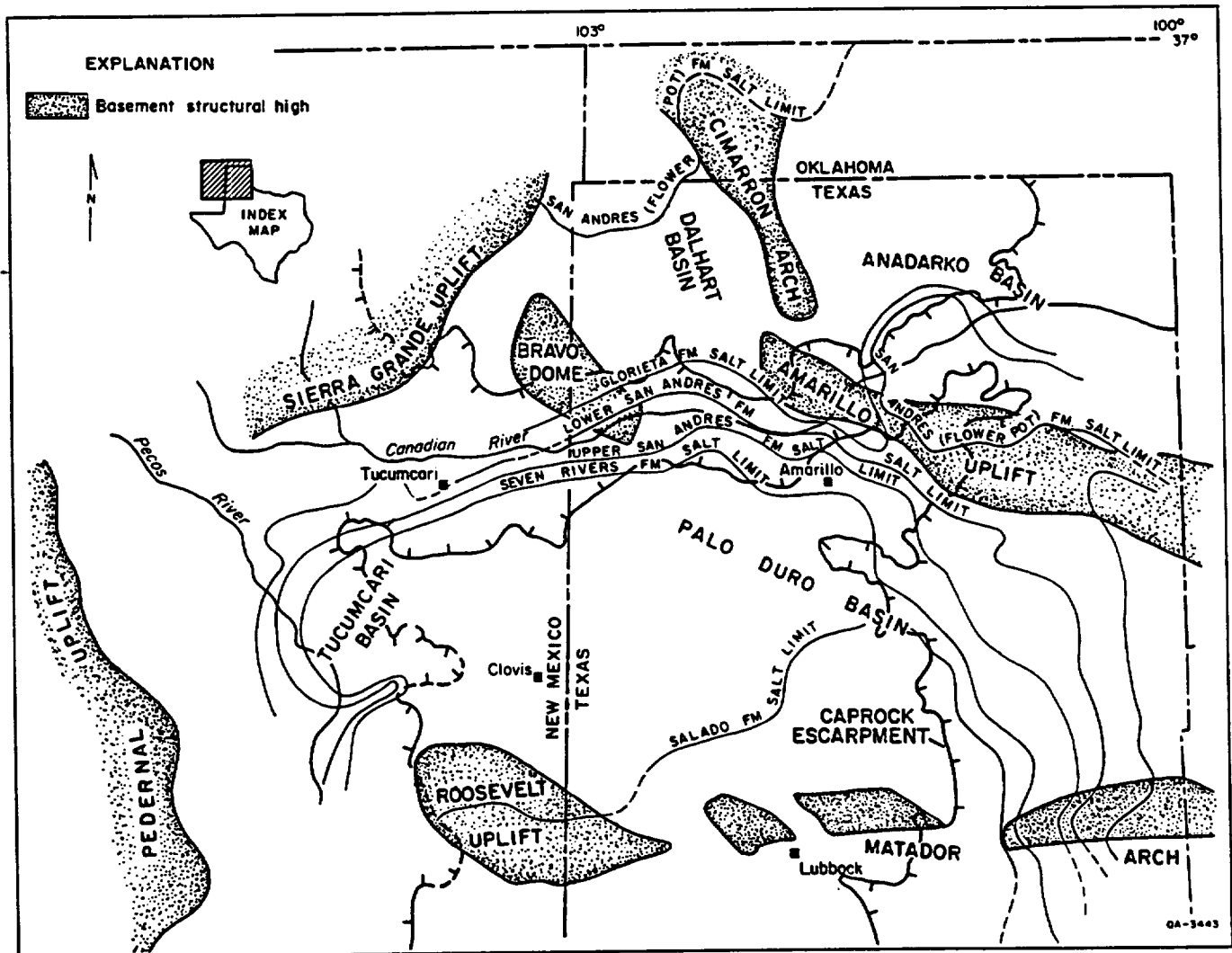


FIGURE 2. Major structural elements, Texas Panhandle and surrounding area (modified from Nicholson, 1960). Limits of Permian bedded salts are closely associated with the structural margins of the Palo Duro Basin. Structurally high areas are most likely to be affected by salt dissolution.

others, 1980; Simpkins and Fogg, 1982; Gustavson and Finley, 1985; Gustavson, 1986a), and exposed strata are fractured and deformed as a result of dissolution-induced subsidence (Gustavson and others, 1980; Collins, 1983, 1984; and Goldstein and Collins, 1984).

To understand the development of a major physiographic feature such as the Caprock Escarpment, it is necessary to analyze both surface and subsurface geomorphic processes as well as the stratigraphic, hydrologic, and structural framework of the region. The study area, which includes approximately 210 km (131 mi) of the Caprock Escarpment in the Texas Panhandle (fig. 1), was chosen because the escarpment in this region overlies a zone of interstratal dissolution of bedded Upper Permian salt and because spring sapping is active in many valleys in this region.

In this report, we describe the major geomorphic processes affecting development of the Caprock Escarpment, their interaction, and the rates at which they

occur. Integrating the results of previous work by Finley and Gustavson (1980, 1981, 1983), Gustavson and others (1980, 1981, 1982), Simpkins and Fogg (1982), Gustavson and Finley (1985), and Simpkins and Gustavson (1987), we have concluded that groundwater processes play a significant role in scarp retreat and that rates of westward scarp retreat are similar to the rate of westward advancement of the salt dissolution zone.

Geologic Setting

Structural Development

The Caprock Escarpment roughly parallels the flanks of the Palo Duro Basin. The Palo Duro Basin is bounded by the Amarillo Uplift trend on the northeast and by the Matador Arch-Roosevelt Uplift on the south (fig. 2). To the west the Palo Duro Basin is bounded by the Pedernal and Sierra Grande Uplifts. These positive

structural elements resulted from faulting and uplift initiated during the Paleozoic, perhaps as early as the late Cambrian.

During the Pennsylvanian and early Permian, tectonic movement along the Amarillo Uplift and the Matador Arch controlled sedimentation and facies distribution in the Palo Duro Basin (Dutton and others, 1979). Epeirogenic uplift during the Triassic formed the terrestrial basin that contains the Dockum Group (fig. 3) (McGowen and others, 1979). By Cretaceous time the region had subsided to below sea level. Epeirogenic movements continued into the Tertiary and elevated Cretaceous marine strata in the study area to more than 940 m (3,100 ft) above sea level (Eifler, 1968; Gable and Hatton, 1983; Budnik, 1984).

Nontectonic deformation, expressed as regional subsidence induced by extensive dissolution of Permian bedded salt, has occurred beneath the entire study area (Gustavson and others, 1980, 1982; Johnson, 1981; Boyd and Murphy, 1984; Gustavson and Budnik, 1985; Gustavson and Finley, 1985; Reeves, 1985; DeConto and Murphy, 1986; Gustavson, 1986a, 1986b; Reeves and Temple, 1986). Several of the lacustrine basins on the High Plains may have formed in part from dissolution-induced subsidence during the late Tertiary or Quaternary (Baker, 1915; Gustavson and Budnik, 1985; Gustavson and Finley, 1985; Reeves, 1985; Reeves and Temple, 1986). Other interpretations suggest that dissolution beneath the High Plains occurred during the Triassic and could not have affected Tertiary or Quaternary lacustrine basins (DeConto and Murphy, 1986).

In addition to causing surface subsidence, dissolution has resulted in the widespread development of extension fractures in strata above zones of salt dissolution. These fractures commonly occur in Permian mudstones and locally in mudstones of the Triassic Dockum Group. Extension fractures are recognized by their filling of fibrous gypsum (var. satin spar), in which the elongate crystals are oriented primarily vertically (Gustavson and others, 1981; Goldstein and Collins, 1984; Machel, 1985).

Stratigraphy

In the eastern Texas Panhandle, episodes of deposition on shallow marine shelves alternated with periods of erosion during the early Paleozoic. Terrigenous clastics, informally called granite wash, were derived from the Matador Arch and Amarillo Uplift during the Pennsylvanian and Early Permian and deposited as fan deltas (Handford and Dutton, 1980). Marine sedimentation during the Late Pennsylvanian and Early Permian was dominated by shelf-margin carbonates, while the deeper parts of the basin were being filled by fine-grained terrigenous clastic sediments. During the middle and Late Permian, a wide, low-relief marine shelf developed, and salt, anhydrite, dolomite, limestone, and red beds were deposited (Presley, 1979a, 1979b, 1980a, 1980b; McGillis and Presley, 1981; Hovorka and others, 1985; Fracasso and Hovorka, 1987).

AGE	PALO DURO BASIN		
	West and central		
QUATERNARY	Blackwater Draw Formation	Tahoka Formation Double Lakes Formation Tule Formation	
	Blanco Formation	Cita Canyon lake beds	
TERTIARY	Ogallala Formation		
CRETACEOUS	Edwards Limestone		
TRIASSIC	Dockum Group		
?			
UPPER PERMIAN	Guadalupian and Ochoan Series	Dewey Lake Formation	
		Alibates Formation	
		Salado Formation	
		Tansill Formation	
		Yates Formation	
		Seven Rivers Formation	
		Queen and Grayburg Formations	
		ARTESIA GROUP	
LOWER PERMIAN	Leonardian Series	Glorieta Sandstone	
		?	
		upper Clear Fork salt	
		Cimarron anhydrite	
		Tubb interval	
		lower Clear Fork salt	
		Red Cave Formation	
		CLEAR FORK GROUP	

Salt-bearing units

QA 6507

QA 6607

FIGURE 3. Stratigraphic nomenclature of Permian and younger strata, Texas Panhandle. Principal salt units are shaded (modified from Johnson, 1976).

Post-Permian stratigraphic units are well represented in the study area. Fluvial, deltaic, and lacustrine sandstones and mudstones of the Triassic Dockum Group unconformably overlie Permian strata (McGowen and others, 1979). Although Jurassic rocks are not preserved in the study area, the Lower Cretaceous Edwards Limestone unconformably overlies the Dockum Group. During the Late Cretaceous and early Tertiary, extensive erosion exposed both Triassic and Lower Cretaceous strata. Fluvial and eolian sediments of the Neogene Ogallala Formation overlie the Tertiary erosional surface (Seni, 1980; Winkler, 1984, 1985; Gustavson and Holliday, 1985; Gustavson and Winkler, 1988). Locally, Pliocene lacustrine sediments of the Blanco Formation and Cita Canyon lake beds overlie the Ogallala Formation. The Quaternary Blackwater Draw Formation, which is composed primarily of eolian sediments, overlies the Ogallala Formation and Pliocene lacustrine formations (Gustavson and Holliday, 1985; Machenberg and others, 1985). Lacustrine sediments of the Tule Formation are interbedded with the Blackwater Draw Formation. Thick, widespread Quaternary eolian, fluvial, and lacustrine deposits, composed of sediments eroded from the Caprock Escarpment, overlie Triassic and Permian strata on the Rolling Plains at the foot of the Caprock Escarpment (Caran and others, 1985).

Regional Hydrology

Studies of the hydrology of the Palo Duro Basin indicate that the lower (Wolfcampian) brine aquifer is separated from aquifers in the overlying Ogallala Formation and Dockum Group by an aquitard composed of upper Permian evaporites and salt-cemented terrigenous clastics. Regional flow of the Wolfcampian aquifer is toward the northeast (Smith and others, 1983). Ground-water movement through the evaporite aquitard is minimal; flow is to the east and southeast (Dutton, 1983; Orr, 1983; Kreitler and others, 1985). Ground-water flow in the unconfined Ogallala aquifer and in the Dockum aquifer is also toward the east and southeast (Dutton and Simpkins, 1986; Nativ, 1988). A model of ground-water flow along a west-to-east cross section across the Caprock Escarpment suggests that leakage of fresh water from the Ogallala Formation is downward into the salt dissolution zone and eastward beneath the Rolling Plains (Simpkins and Fogg, 1982). Sodium chloride ground waters from the salt dissolution zone beneath the Southern High Plains have ^{14}C ages of less than $16,200 \pm 3,500$ yr and $23,500 \pm 1,000$ yr and salinities of 95,000 to 68,000 ppm (Dutton, 1987). Numerous fresh-water springs, which mark discharge points of the Ogallala and Dockum aquifers, are present along the Caprock Escarpment at the base of the Ogallala Formation and to a lesser extent at the base of Dockum Group sandstones (fig. 4) (Brune, 1981). Springs discharging brines derived from halite dissolution occur in several areas east of the escarpment (U.S. Army Corps of Engineers, 1975; Richter and Kreitler, 1986).

Geomorphology and Physiography

The study area includes parts of two major physiographic regions—the Southern High Plains to the west and the Rolling Plains to the east—and the Caprock Escarpment, which separates the two regions (fig. 1). The Southern High Plains is characterized by a flat, low-relief surface partly covered with small playa lake basins. Drainage of the High Plains is mostly internal into these lake basins. Widely separated draws with very narrow drainage basins slope to the east and southeast. Adjacent draws do not share common drainage divides but rather are separated by broad interfluvies containing numerous playa lake basins.

Relief along the Caprock Escarpment locally exceeds 305 m (1,000 ft) near the mouth of Palo Duro Canyon. The western, or upper, topographic limit of the Caprock Escarpment is clearly defined as a sharp eastward-facing break in slope (fig. 4). The eastern limit of the escarpment occurs where the eastward slope is diminished at the western edge of the Rolling Plains. Locally, however, the Caprock Escarpment extends downward without interruption to the floor of the Palo Duro Canyon. In Randall, Armstrong, and northern Briscoe Counties the escarpment is steep and relatively narrow. Escarpment width in these areas is approximately 5 km (3.1 mi). In Motley, Floyd, and southern Briscoe Counties the escarpment is less steep but is as much as 16 km (10 mi) wide. In all areas the terrain of the escarpment is highly dissected and characterized by numerous short, steep canyons; tributaries in the headwaters of the canyons near the top of the escarpment are arranged in a partly centripetal pattern (pectinate drainage of Higgins, 1982). Relief of the escarpment is supported by resistant calcretes and silicified zones of the Ogallala Formation and resistant sandstones of the Dockum Group and Permian Quartermaster Formation (fig. 5). The escarpment parallels and overlies the western margin of the zone of active salt dissolution (Gustavson and others, 1981; Gustavson and Finley, 1985).

The Rolling Plains, which were developed primarily on easily eroded Permian strata of the Quartermaster and Whitehorse Formations (Bath, 1980; Gustavson and others, 1981; Simpkins and Gustavson, 1987), are locally highly dissected. In most upland areas, however, topography is rolling, hence the name Rolling Plains. Drainage in the Rolling Plains tends to parallel the margins of subsurface salt units undergoing dissolution, and karst features resulting from dissolution-induced subsidence are common (Simpkins and others, 1981; Gustavson and others, 1982; Gustavson and Finley, 1985).

Climate

Climate in the study area is continental semiarid to subhumid (45 to 55 cm [18 to 22 inches] mean annual precipitation), although annual precipitation varies widely (Orton, 1964; U.S. Department of Commerce, 1978a, 1978b). Approximately 75 percent of the annual precipitation occurs between the end of March and the

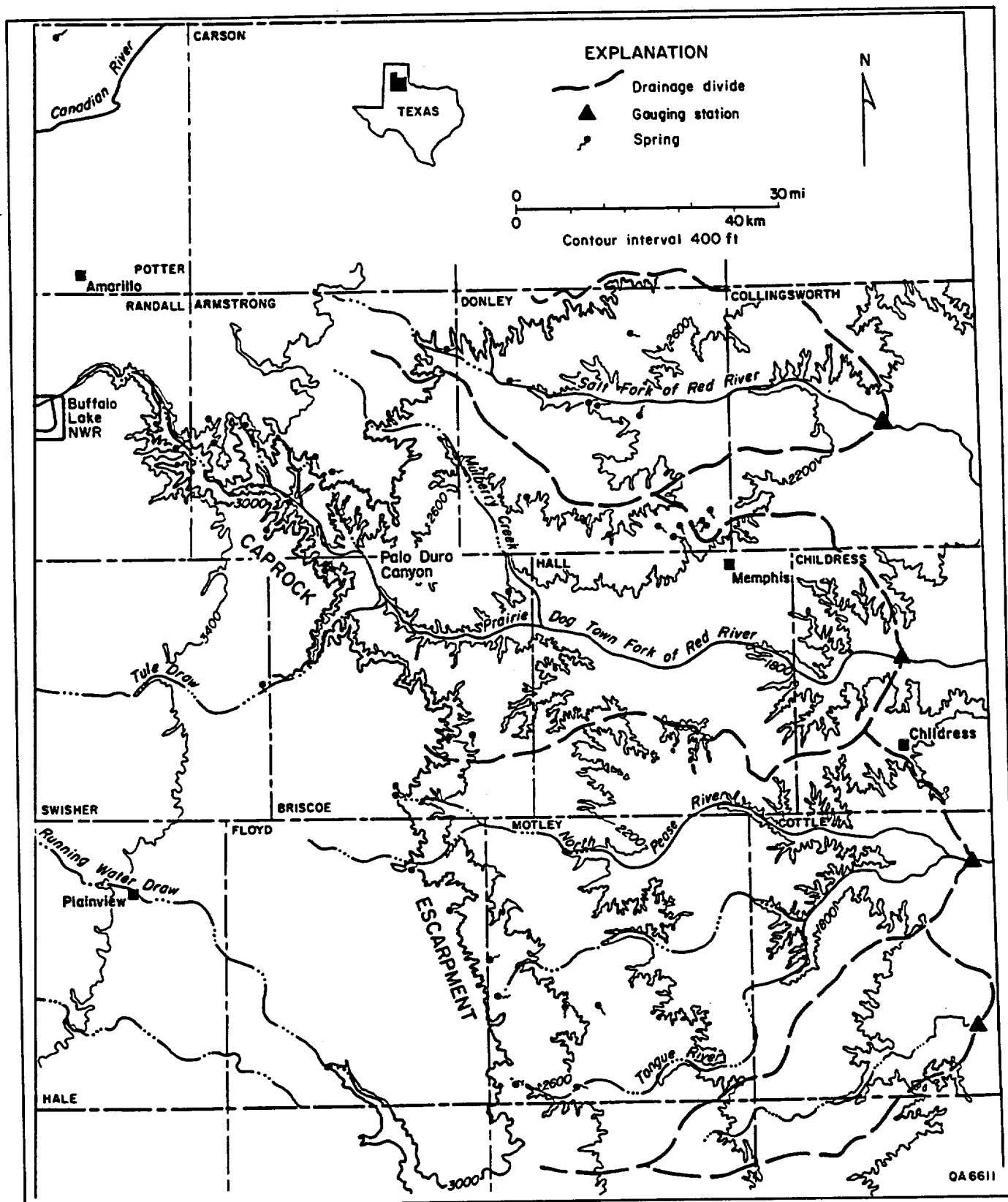


FIGURE 4. Topography along the Caprock Escarpment. The escarpment is approximately defined by the area between the 2,600- and 3,000-ft contours; the Southern High Plains and the Rolling Plains occur to the west and east, respectively. Locations of springs are from Brune (1981). The drainage divide marked by the Caprock Escarpment separates areas that contribute runoff to the escarpment and Rolling Plains from areas that contribute runoff mostly to playa lake basins of the Southern High Plains.

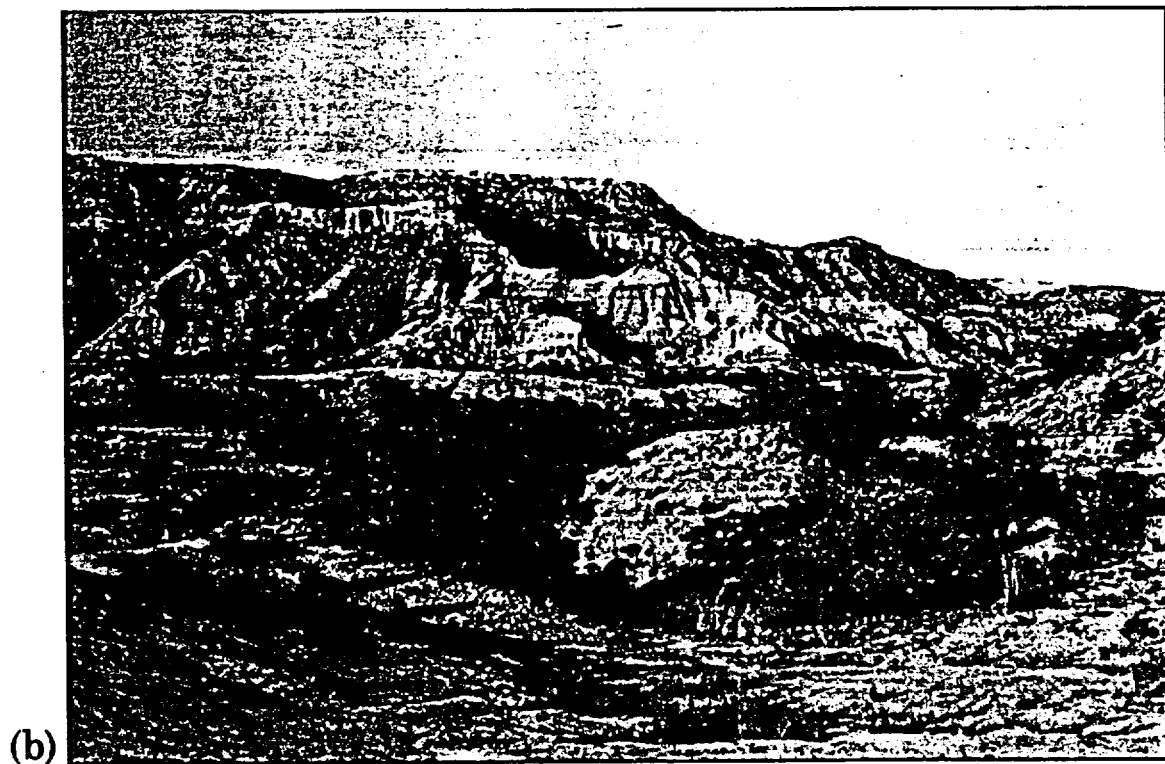
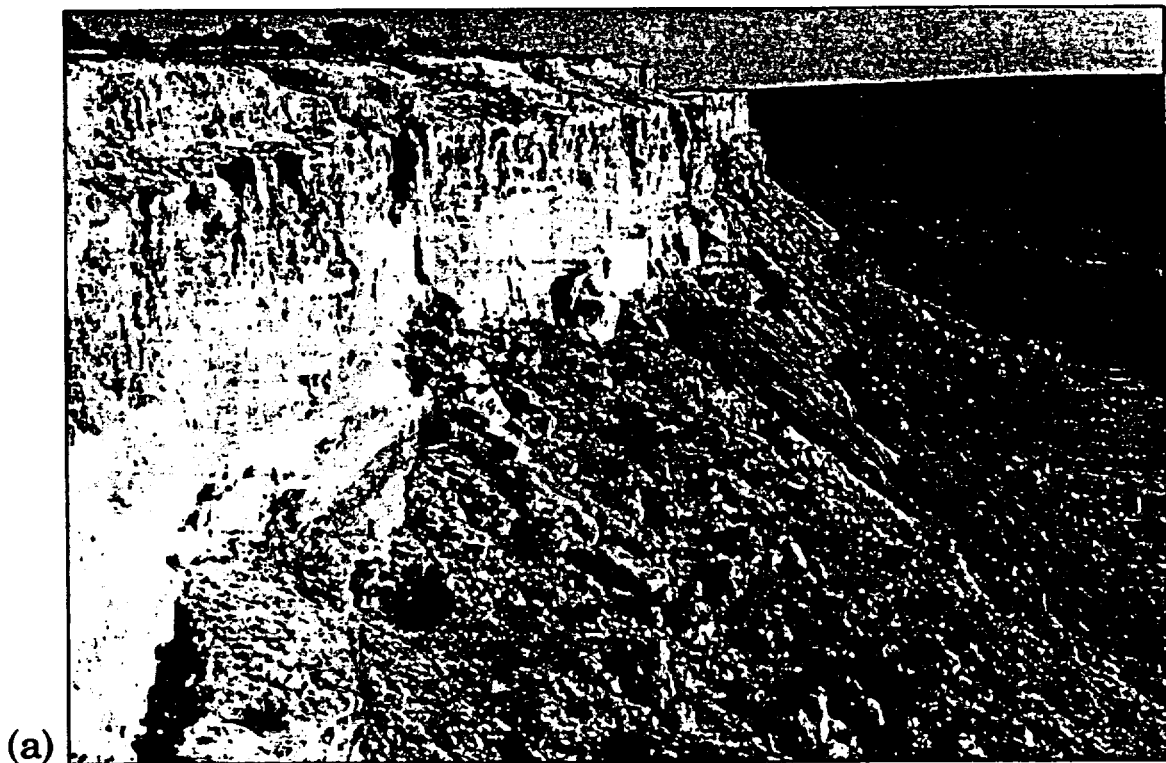


FIGURE 5. Views of the Eastern Caprock Escarpment in Palo Duro Canyon State Park (fig. 25). Topography of the escarpment varies from (a) steep cliffs at Fortress Cliff to (b) deeply dissected slopes. Relief at Fortress Cliff, including the vertical cliff and the steep talus apron, is approximately 100 m. The vertical cliff (a) is supported by the upper Tertiary Ogallala Formation, and Triassic Dockum Group strata underlie the toe of the talus apron. Relief along the dissected slope in (b) is approximately 200 m from the floor of the canyon to the skyline; the Upper Permian Quartermaster Formation is exposed in the foreground, and Ogallala and Dockum strata are exposed in deeply dissected terrain of the middle ground.

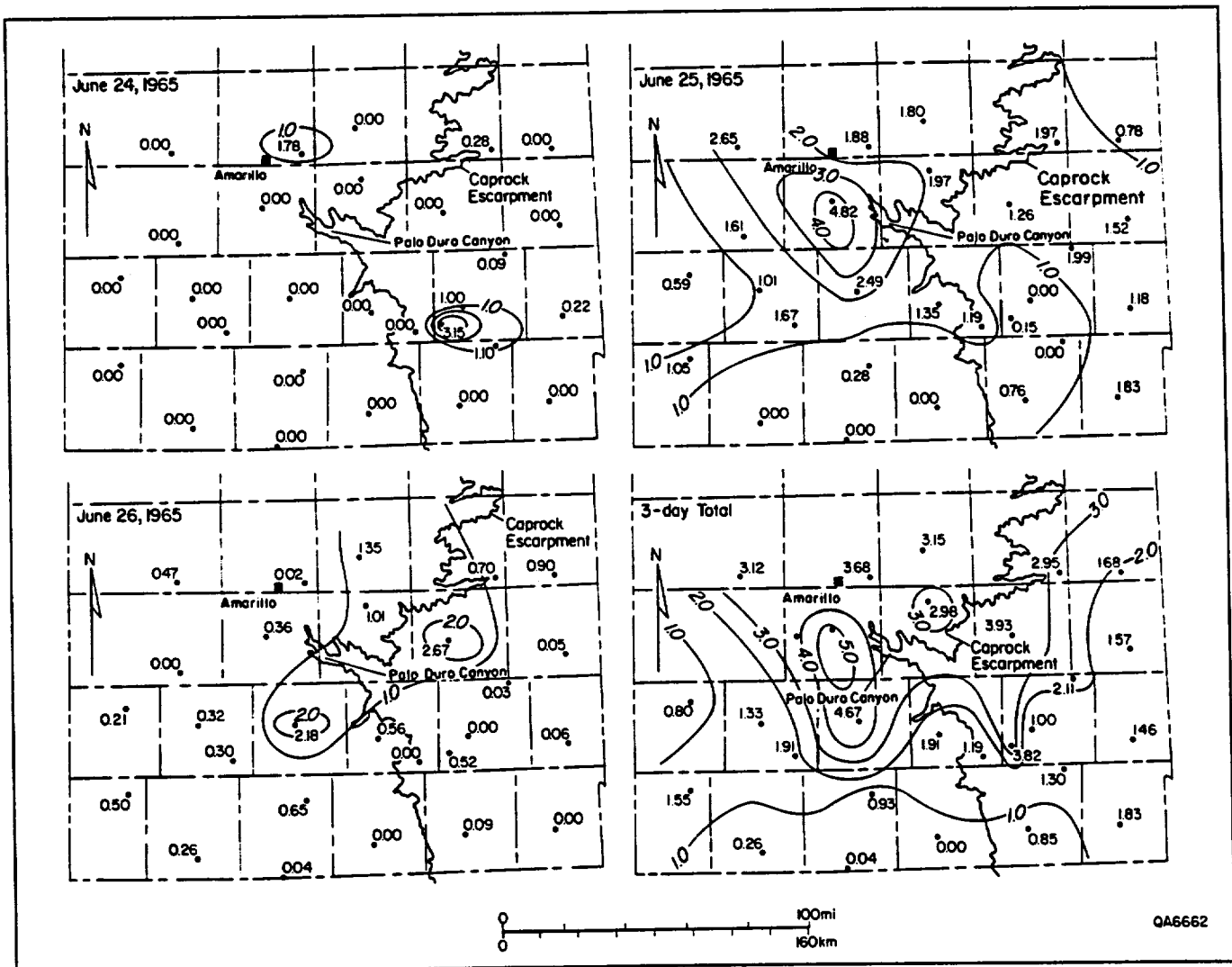


FIGURE 6. Three-day total rainfall distribution, June 24-26, 1965, along the Eastern Caprock Escarpment. Daily station totals are not for the same time periods. Contours are in inches (modified from Finley and Gustavson, 1980).

beginning of October. Annual pan evaporation is approximately 158 cm (62 inches) (Kier and others, 1977). Rapid temperature changes and large ranges in daily and annual temperature are characteristic (Orton, 1964).

Erosional processes on the Caprock Escarpment are dominated by high-intensity, short-duration rainfall from convective storms during the spring and summer (Finley and Gustavson, 1980). Thunderstorms in the Texas Panhandle commonly yield heavy rainfalls that result in flash floods, especially in the canyons that cut into the Caprock Escarpment. Figure 6 illustrates a series of intense rainfall events resulting in local precipitation depths of 12.5 to 22 cm (5 to 8.7 inches) along the Caprock Escarpment. These and other data suggest that the Caprock Escarpment may cause orographic uplift of moisture-laden tropical maritime air flowing from the southeast sufficient to encourage thunderstorm development along the escarpment.

Runoff

Runoff from precipitation occurs when the infiltration capacity of surface soils is exceeded (Young, 1972). Infiltration capacity is largely a function of antecedent moisture and textural composition of the soil. In the High Plains along the Eastern Caprock Escarpment, soils are primarily sandy and clayey loams of the Acuff, Amarillo, Mansker, and Pullman series. These soils are moderately to poorly permeable, and infiltration rates range from 0.5 to 5 cm/hr (0.2 to 2 inches/hr) (U.S. Department of Agriculture, Soil Conservation Service, 1972, 1977a, 1977b, 1977c). Surface soils on the escarpment belong to the Quinlan-Burson-Obaro association and are shallow, permeable, and subject to moderate to very rapid runoff. Triassic and Permian bedrock, primarily sandstone and mudstone, is exposed over much of the Caprock Escarpment; infiltration rates of these rocks are low except

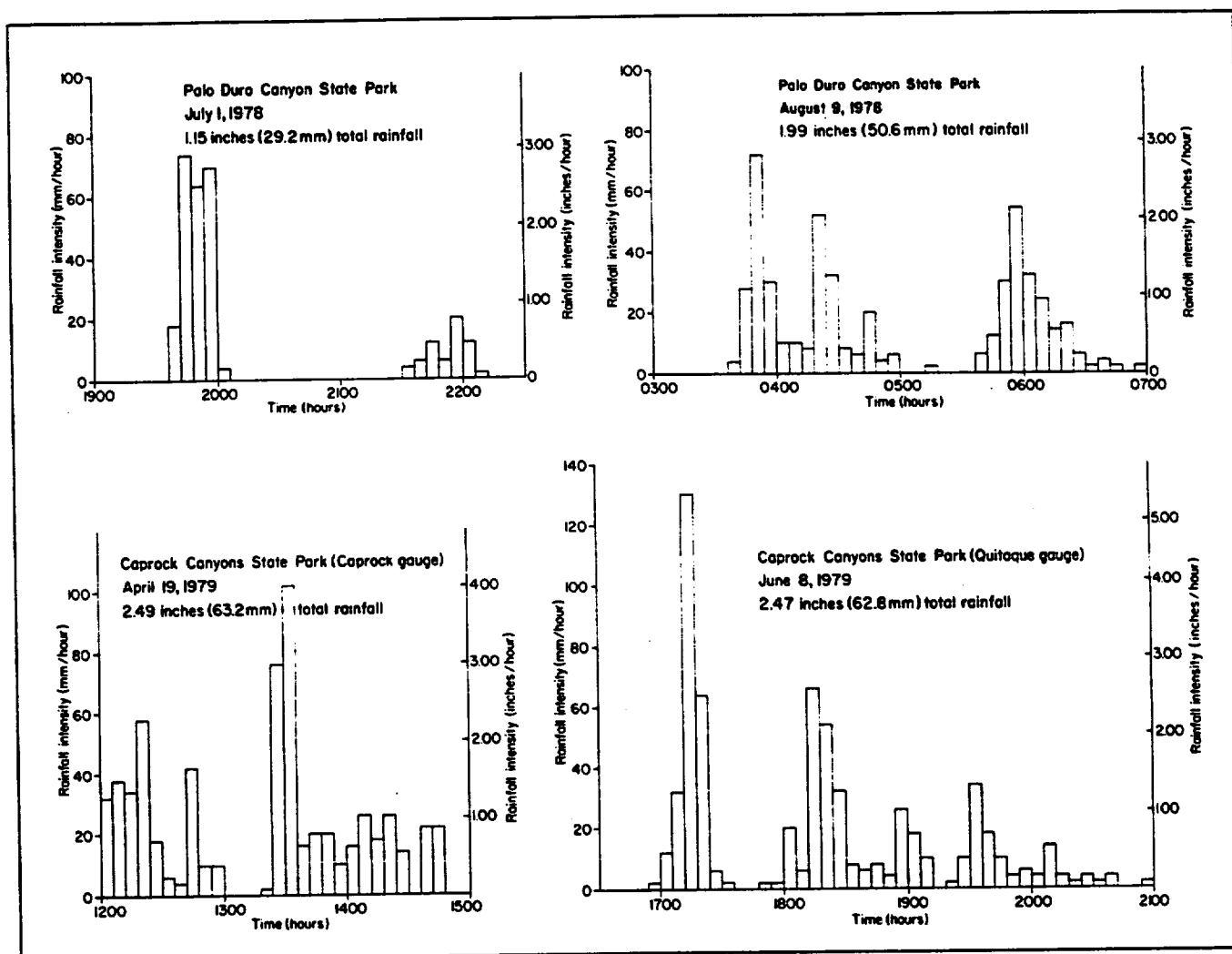


FIGURE 7. Intensity-duration profiles of four storms along the Caprock Escarpment (modified from Finley and Gustavson, 1980).

along fractures. Along the upper part of the escarpment, sediments of the Ogallala Formation are exposed, and infiltration rates of this material probably vary from low in well-cemented sections to high in sections of poorly cemented sand or gravel.

Rainfall intensity can also affect runoff. In very intense storms, runoff may occur before the moisture capacity of the lower part of the soil profile has been reached by infiltration (Linsley and others, 1949). The combination of soils and bedrock with moderate to low infiltration rates and intense rainfall yields high runoff rates on the High Plains and along the Caprock Escarpment. Rainfall intensity-duration-frequency data from Amarillo, Texas (table 1), illustrate that high-intensity rainfall events occur often on the High Plains. High-intensity precipitation events are also common along the Caprock Escarpment (fig. 7), where peak intensities have exceeded 12.5 cm/hr (5 inches/hr) and intensities of 2.5 cm/hr (1 inch/hr) are typical (Finley and Gustavson, 1980).

TABLE 1. Rainfall intensity-duration-frequency relationships, Amarillo, Texas, 1904-1951 (modified from U.S. Department of Commerce, 1955, and Finley and Gustavson, 1980).

Return period (yr)	2	5	10	25	50	100
Duration	Rainfall intensity*					
5 min	4.50	6.00	6.90	8.00	9.00	9.60
15 min	3.00	4.10	4.90	5.50	6.10	6.90
30 min	2.10	2.90	3.50	4.00	4.50	5.00
60 min	1.30	1.80	2.20	2.50	2.90	3.40
2 hr	0.78	1.10	1.33	1.50	1.75	2.00
6 hr	0.33	0.47	0.56	0.68	0.76	0.85
12 hr	0.19	0.27	0.32	0.39	0.44	0.48
24 hr	0.11	0.15	0.18	0.23	0.25	0.27

*Intensity expressed in inches/hr (1 inch/hr = 25.4 mm/hr).

Relation of Dissolution-Induced Subsidence to the Caprock Escarpment

To test the hypothesis that dissolution of Permian salt and subsidence of overlying strata have affected the position and rate of retreat of the Caprock Escarpment, we must establish the likelihood that salt was once present where it is now absent beneath and to the east of the escarpment. In addition, structures attributed to dissolution-induced subsidence must be differentiated from tectonic structures. Several lines of evidence suggest that dissolution has truncated or thinned salt beds that currently underlie the Southern High Plains, the Caprock Escarpment, and the Rolling Plains.

(1) Interpretation of geophysical logs indicates that where structural collapse of overlying beds has occurred, abrupt loss of subjacent salt sequences between wells probably resulted from salt dissolution rather than from facies change (Johnson, 1976; Gustavson and others, 1980, 1982; Gustavson and Finley, 1985; Gustavson, 1986a, 1986b; McGookey and others, 1988).

(2) Brecciated zones, fractures with slickensides, extension fractures, and insoluble residues composed of mudstone, anhydrite, and dolomite overlie the uppermost salts in core from wells A through I (fig. 1), indicating that dissolution has occurred beneath both the Southern High Plains and the Rolling Plains.

(3) Permian outcrops throughout most of the Rolling Plains and the Palo Duro Canyon contain folds, systems of extension fractures, and, locally, breccia beds interpreted to have resulted from dissolution of salt and collapse of overlying beds (Gustavson and others, 1980; Goldstein, 1982; Collins, 1984; Goldstein and Collins, 1984; Machel, 1985; and Gustavson, 1986b).

(4) High chloride concentrations in many streams draining the Rolling Plains indicate that salt dissolution is active beneath most of the Rolling Plains and along most of the Eastern Caprock Escarpment (U.S. Geological Survey, 1969-1983).

Stratigraphy beneath the High Plains, Caprock Escarpment, and Rolling Plains

Regional stratigraphic relations along the eastern margin of the Palo Duro Basin are shown in figure 8. Permian salt thins along the eastern margin of the Palo Duro Basin primarily as a result of salt dissolution and, to a lesser extent, facies change or depositional thinning toward the basin margin. Nonsalt units such as the Alibates Formation, anhydrite/gypsum and dolomite strata within the San Andres/Blaine Formation, and anhydrite within the upper Clear Fork Formation thin only slightly to the east (fig. 8). Clastic strata of the Tubb interval maintain the same thick-

ness across the section. These relations indicate that Permian strata beneath the Rolling Plains were not substantially affected by differential basin subsidence and that within the study area these strata do not thin much toward the eastern margin of the Palo Duro Basin. Salt beds of the upper San Andres Formation, however, thin considerably between wells 6 and 7 (fig. 8), but nonsalt units do not. The significant decrease in the westward dip of strata above the remaining San Andres salt beds is interpreted as evidence of removal of section through dissolution and subsidence of overlying strata. Similarly, changes in thicknesses of salt beds of the San Andres, Seven Rivers, and Salado Formations are accompanied by radical changes in the dip of overlying units between wells 8 and 9, wells 4 and 5, and wells 3 and 4, respectively (fig. 8). These relations also indicate dissolution of Salado, Seven Rivers, and San Andres salts and subsidence of overlying strata. Furthermore, figure 8 illustrates a stepwise pattern of dissolution in which stratigraphically higher salts are first dissolved in areas closer to the escarpment. This pattern, in conjunction with structural changes, suggests dissolution by ground water; it is not a relict facies pattern. A facies change in the upper Clear Fork Group from salt and anhydrite to clastic sediments, however, occurs between wells 10 and 11 (fig. 8). Consequently, only minor salt thinning is due to dissolution there.

In the study area approximately 30 m (100 ft) of salt has been dissolved from the Salado Formation beneath the Southern High Plains and approximately 45 m (150 ft) from the Seven Rivers Formation beneath the Caprock Escarpment. Consequently, as much as 75 m (250 ft) of the relief of the Caprock Escarpment can be attributed to dissolution and subsidence. Approximately 130 m (425 ft) of salt has been dissolved from the San Andres Formation beneath the western Rolling Plains and approximately 35 m (115 ft) from the Clear Fork Group beneath the central Rolling Plains. If the entire salt section was originally present as far east as Childress County, as is suggested by the continuity in thickness of nonsalt strata, then as much as 240 m (790 ft) of salt has been dissolved in that area.

Structure on the Tubb Interval

The Tubb interval, an informal subsurface stratigraphic unit of the Clear Fork Group, underlies all the salt-bearing formations that have been affected by dissolution. Therefore, we conclude that structure on the Tubb interval (fig. 9) has not been influenced by dissolution and subsidence but is rather the result of tectonic movement. The map in figure 9 illustrates a nearly uniform dip of approximately 7 m/km (35 ft/mi)

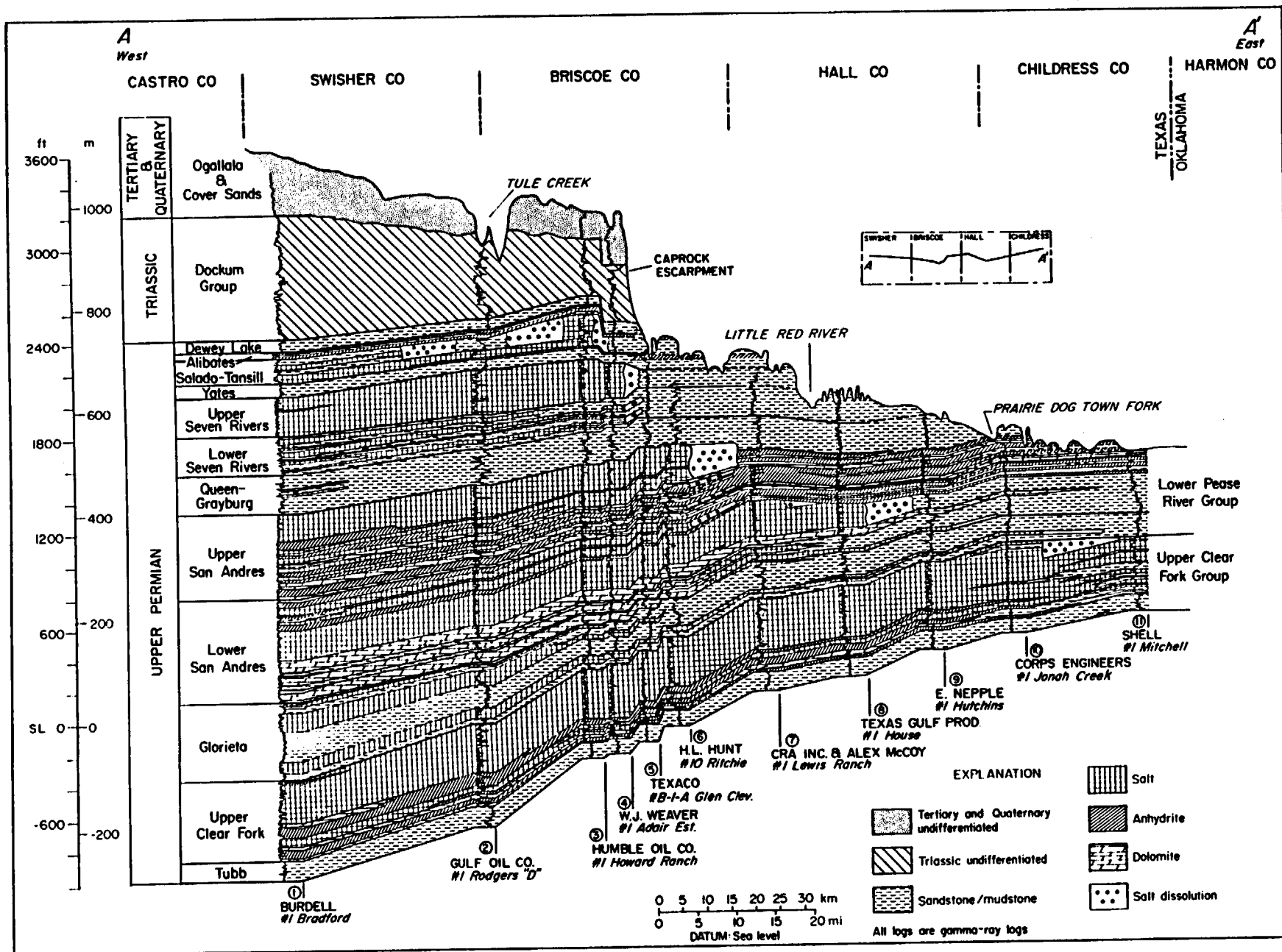


FIGURE 8. Regional stratigraphic cross section illustrating zones of section lost owing to dissolution of salt and collapse of overlying strata beneath the Southern High Plains, Caprock Escarpment, and Rolling Plains. Section A-A' is located in figures 9 through 13 and 16.

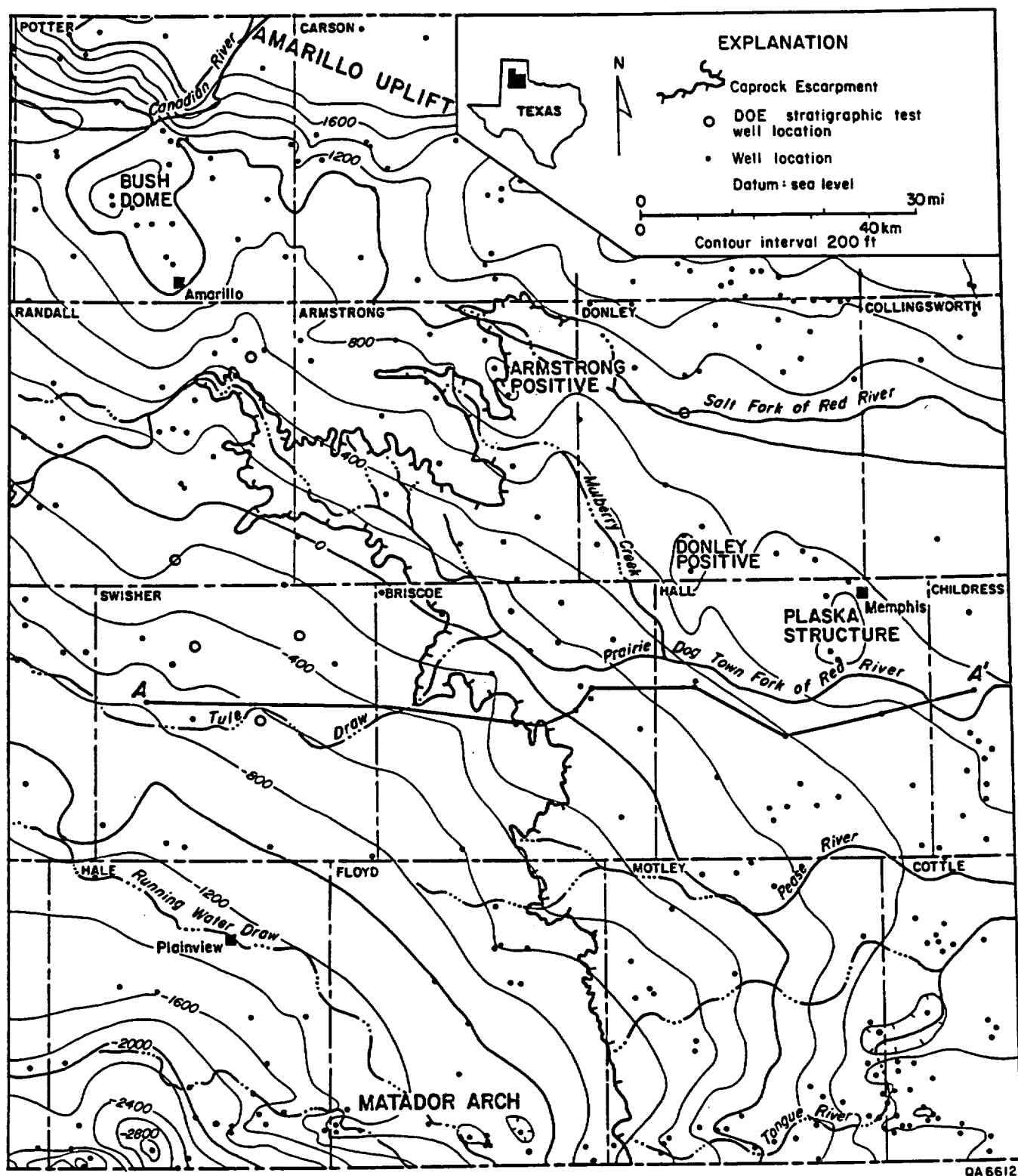


FIGURE 9. Structure-contour map of the top of the middle Permian Tubb interval shows that major structural elements of the study area are unaffected by salt dissolution (modified from Budnik, 1984). A-A' locates cross section shown in figure 8.

to the southwest over the northeastern flank of the Palo Duro Basin. Major structural elements are the Bush Dome and Amarillo Uplift, north of Amarillo, the Donley County and Armstrong County positives, the Plaska structure in Hall County, and the Matador Arch, near the southern limit of the study area. In the southwestern corner of Carson County the Tubb interval differs only slightly in elevation from the Bush Dome and dips to the southwest. Comparison of the outline of the upper physiographic, or western, limit of the Caprock Escarpment with structure contours on the Tubb surface fails to reveal any relation between regional structure resulting from tectonic movement and position of the Caprock Escarpment in the study area.

Salt Thickness

Cumulative thickness of salt units of the Salado, Seven Rivers, San Andres, and Clear Fork Formations decreases from west to east, but the most abrupt thickness changes occur beneath the Caprock Escarpment and the western part of the Rolling Plains (fig. 10). Salt thinning is attributed primarily to dissolution. The zone of abrupt thinning of the Salado and Seven Rivers Formations also closely coincides with the Caprock Escarpment and the western margin of the Rolling Plains, indicating that interstratal salt dissolution has strongly affected and perhaps continues to affect the retreat of the escarpment (fig. 11) (for additional discussion of dissolution of the Salado and Seven Rivers salts, see Boyd and Murphy, 1984, and DeConto and Murphy, 1986).

Salt dissolution also appears to have occurred west of the escarpment. For example, Salado salts thin beneath the eastern margin of the Southern High Plains near the Tule Draw and west of the headwaters of Pease River tributaries. This relationship suggests that, at least locally, dissolution precedes the southward backwasting of the escarpment. Additional evidence of dissolution beneath the Southern High Plains comes from core from the DOE-Gruy Federal Rex White No. 1 and the Stone and Webster Engineering Corporation (SWEC) Harman No. 1 wells in Randall and Swisher Counties, respectively (fig. 1), which contain insoluble residues and extension fractures related to dissolution of both Salado and Seven Rivers salts. Cores from the DOE-Gruy Federal Grabbe No. 1 and the SWEC Zeeck No. 1 wells in Swisher County (fig. 1) also contain insoluble residues and extension fractures related to dissolution of Salado Formation salts.

Structure on the Alibates Formation

Structure on the Permian Alibates Formation (fig. 12), which overlies the salt-bearing interval, is markedly different from the structure on the Tubb interval (fig. 9) near the Caprock Escarpment and the

western margin of the Rolling Plains. West of the escarpment and beneath the Southern High Plains, the Alibates Formation dips regionally to the southwest at 2 to 3 m/km (10 to 15 ft/mi). Regional dip reversal occurs along the trend of the Caprock Escarpment and overlies the zone where, owing to dissolution, salts of the Salado, Seven Rivers, and San Andres Formations rapidly thin (figs. 10 and 11). The floor of a large closed structural basin in southwestern Carson County lies as much as 300 m (1,000 ft) below the crest of the adjacent Bush Dome (compare figs. 9 and 12). Thus, the change in dip from southwestward to northeastward to form a broad anticline beneath the Caprock Escarpment has resulted from dissolution of salts of the Salado and Seven Rivers Formations and subsidence of overlying strata.

The axial trace of the broad anticline on the Alibates Formation crosses the western limit of the Caprock Escarpment in several areas and locally underlies the Southern High Plains and the western margin of the Rolling Plains (fig. 12). In conjunction with the aforementioned thinning of salt beds of the Salado and Seven Rivers Formations west of the Caprock Escarpment, this relationship provides further evidence that dissolution of Permian bedded salts locally precedes the westward retreat of the Caprock Escarpment.

Middle Tertiary Erosional Surface

An extensive unconformity separates Triassic strata from the overlying Miocene-Pliocene Ogallala Formation (figs. 3 and 8). Although much of this surface (fig. 13) in other parts of the Texas Panhandle has been extensively deformed because of dissolution-induced subsidence (Gustavson and others, 1980; Gustavson and Budnik, 1985; Gustavson and Finley, 1985), the middle Tertiary erosional surface in the study area appears to be only locally modified by subsidence.

The regional paleoslope of the erosional surface is to the southeast. Aligned groups of V-shaped contours point upslope and probably mark broad paleovalleys that contained streams that drained the erosion surface before Ogallala deposition. Although the regional paleoslope of this surface is to the southeast, beneath the Caprock Escarpment and in southwestern Carson County, slope is locally to the northeast. Such slope changes occur along Palo Duro Canyon, in the canyon of Mulberry Creek, in central and northwestern parts of Briscoe County, and in southwestern Motley County. These areas overlie areas where salt thins abruptly, and where the Alibates Formation maintains a northeasterly dip beneath the Southern High Plains. Such changes in slope direction support our interpretation that dissolution and subsidence locally preceded Caprock Escarpment retreat.

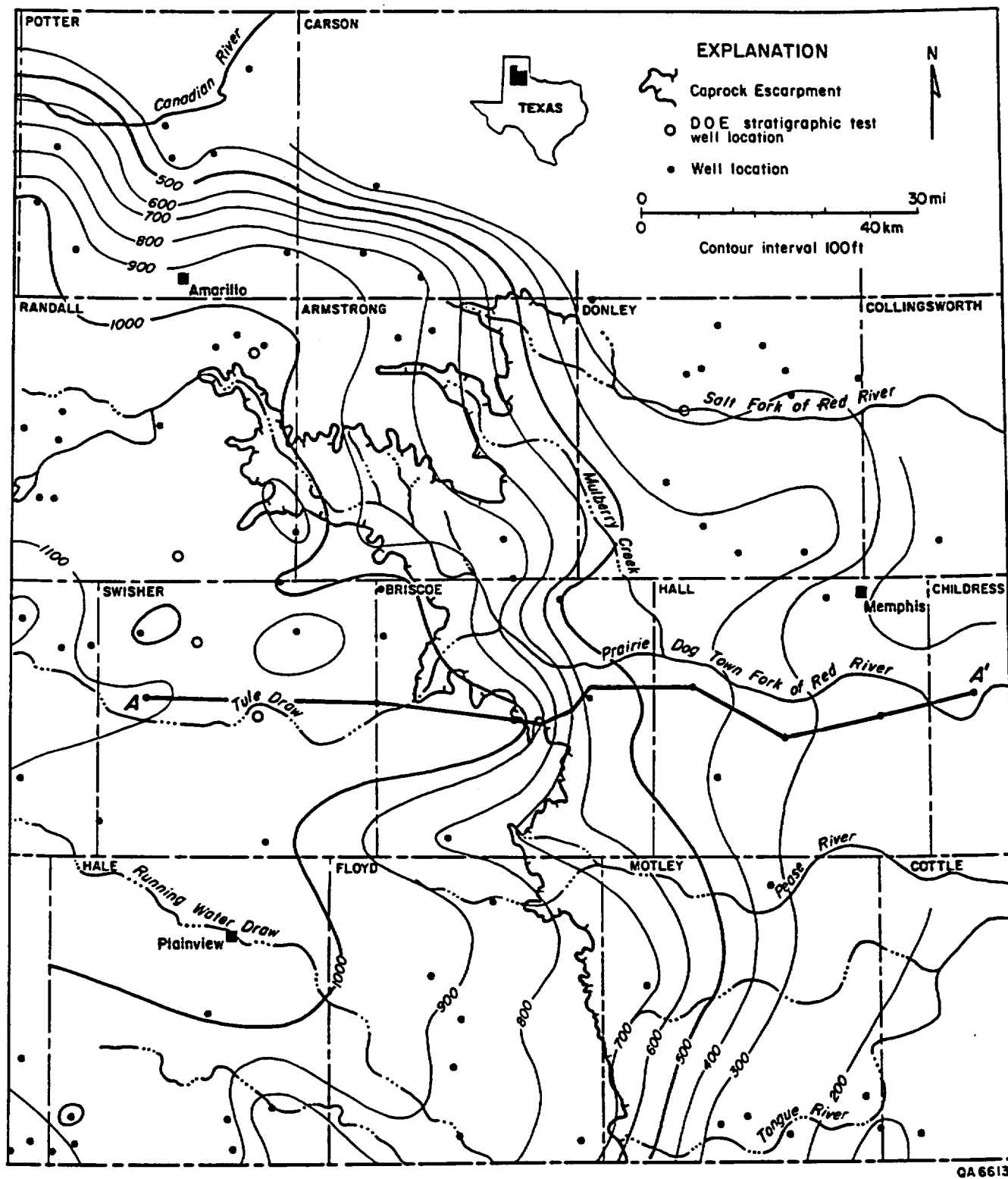


FIGURE 10. Net-thickness map of salt in the Permian upper Clear Fork Group and San Andres, Seven Rivers, and Salado Formations. A-A' locates cross section shown in figure 8.

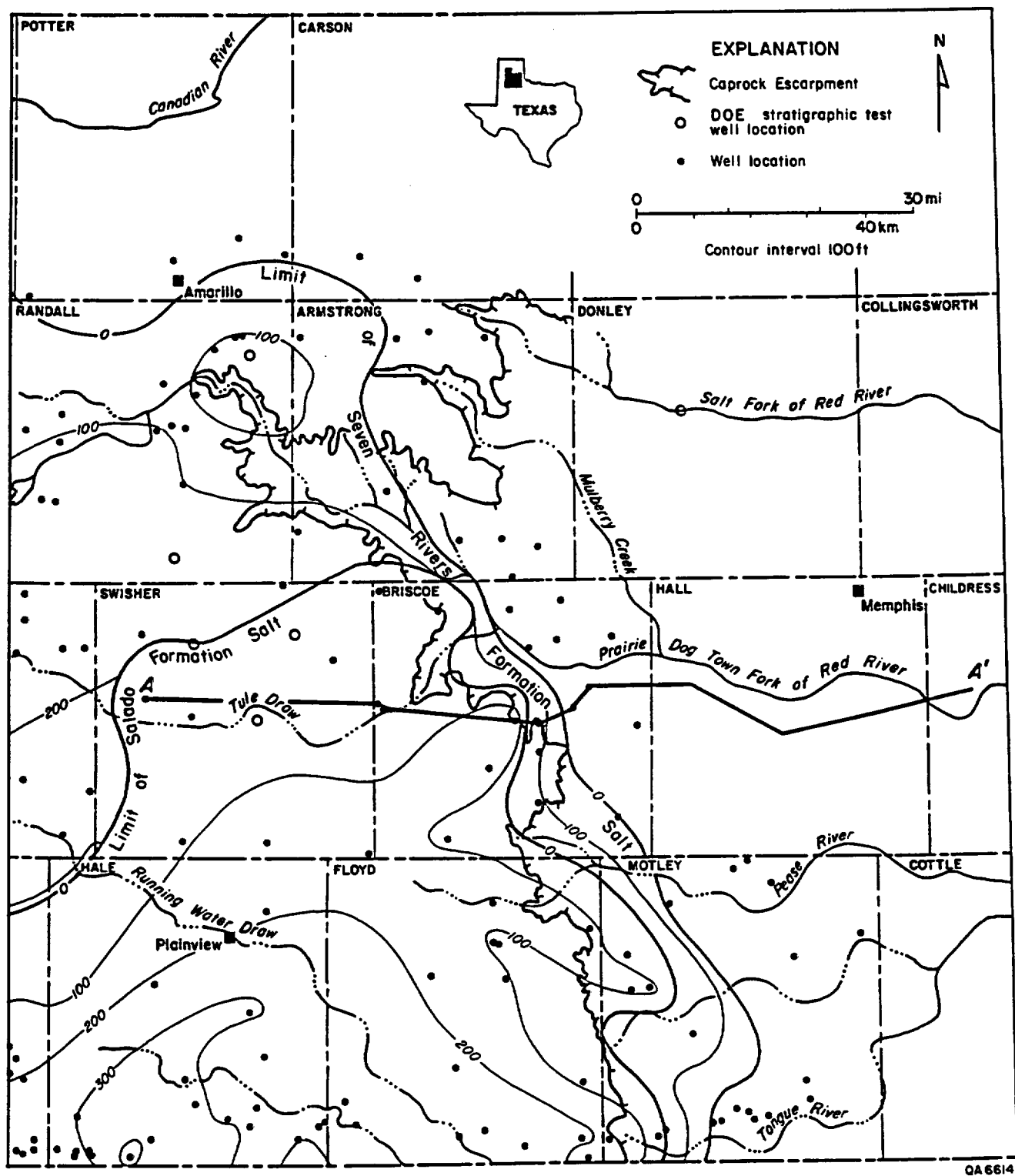


FIGURE 11. Net-thickness map of salt in the Salado and Seven Rivers Formations. Salt thickness of the Seven Rivers Formation is shown where no overlying Salado salt exists. A-A' locates cross section shown in figure 8.

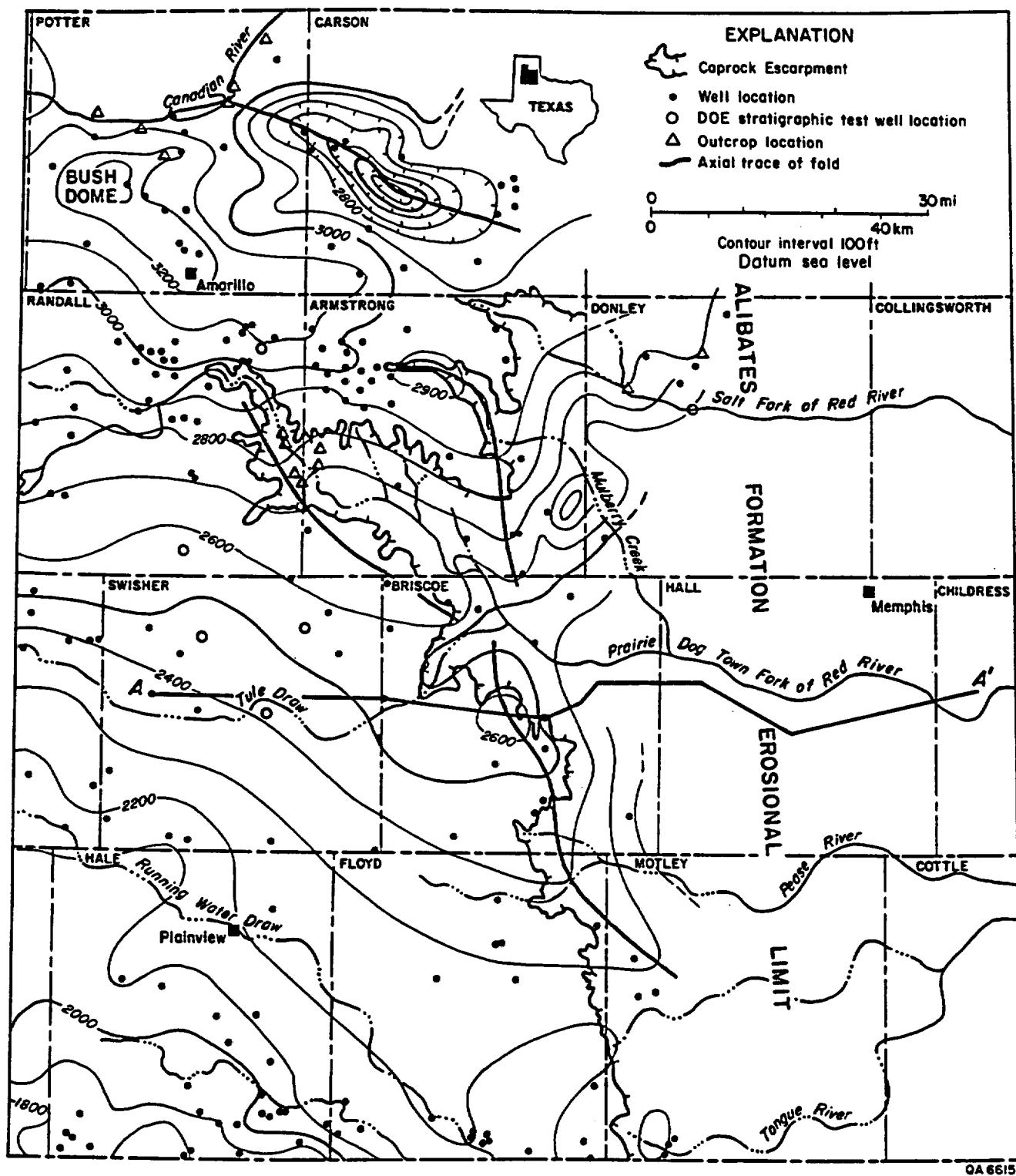


FIGURE 12. Structure-contour map of the top of the Upper Permian Alibates Formation. A-A' locates cross section shown in figure 8.

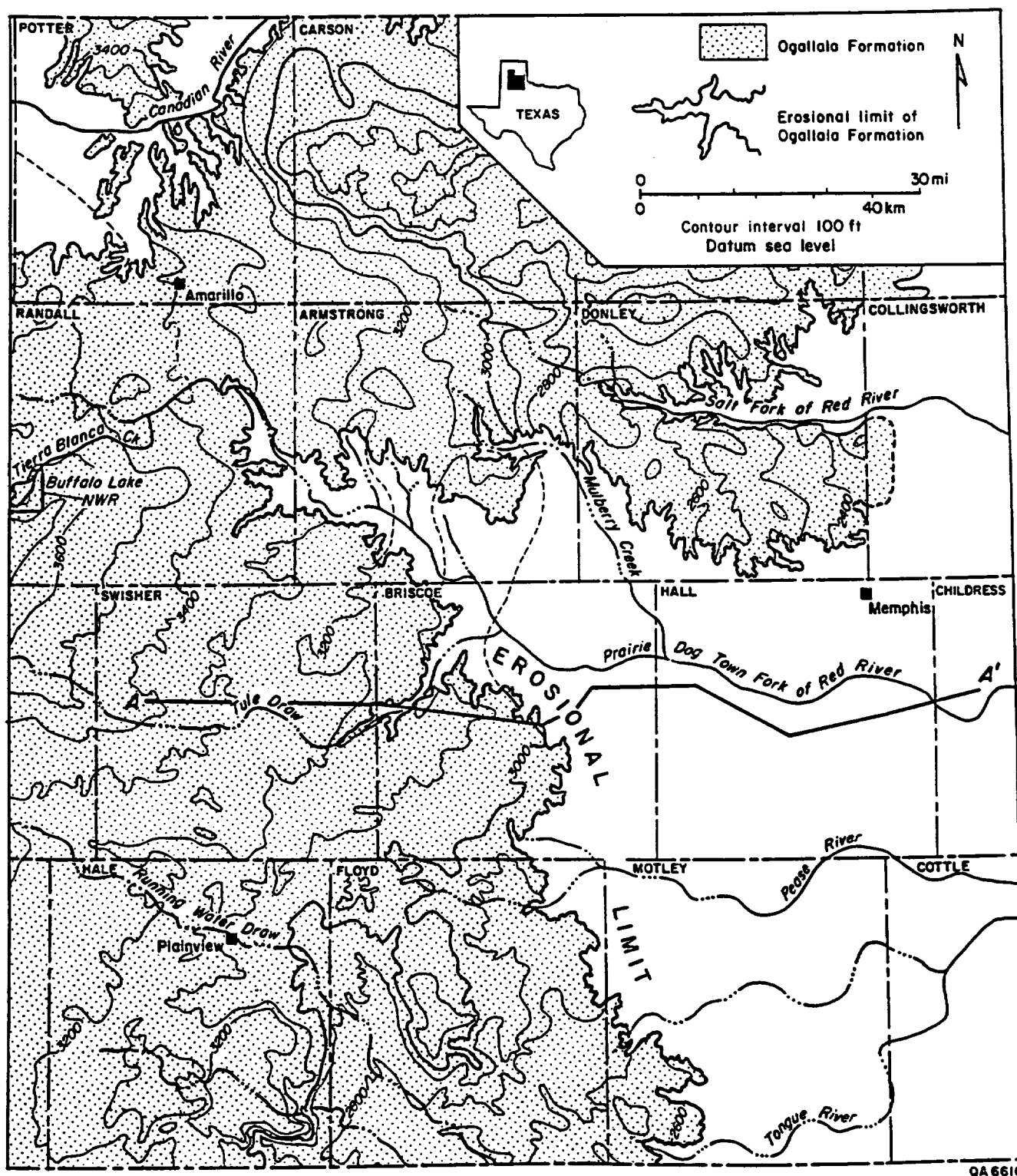


FIGURE 13. Structure-contour map of the base of the High Plains aquifer (Ogallala Formation) (modified from Knowles and others, 1982). The Miocene-Pliocene Ogallala Formation was deposited on the middle Tertiary erosional surface; therefore, this figure also represents a paleotopographic map of the unconformity between the base of the Ogallala and underlying Permian, Triassic, and Cretaceous Systems. A-A' locates cross section shown in figure 8.

Relation of Post-Ogallala Lake Basins to the Caprock Escarpment

Several large breached lake basins can be recognized along the Caprock Escarpment, including basins containing (1) the Quaternary Tule Formation in the headwaters of the Double Mountain Fork of the Brazos River and along Tule Draw, (2) the Pliocene Blanco Formation along Yellowhouse Draw and along the White River, (3) the Pliocene Cita beds in Palo Duro Canyon (Prairie Dog Town Fork of the Red River), and (4) unnamed lacustrine sediments in Mulberry Creek and Tierra Blanca Creek at Canyon, Texas (Evans and Meade, 1944; Eifler, 1967, 1968; Schultz, 1977, 1986). All of these former lake basins, except the basins along the Brazos and White Rivers, occur in the study area (fig. 1).

Breached lake basins along the escarpment determine where major streams intersect the escarpment and, therefore, the morphology of the scarp. All major reentrants along the escarpment (the valleys of Mulberry Creek, the Prairie Dog Town Fork of the Red River, Tule Creek, White River, Yellowhouse Draw, and the Double Mountain Fork of the Brazos River) contain remnants of former lake basins at or near the Caprock Escarpment.

Many of the larger lake basins on the surface of the Southern High Plains and the breached lake basins along the margin of the High Plains have been attributed wholly or partly to subsidence over areas of salt dissolution during Pliocene and Quaternary time. For example, because Triassic strata are deformed, the Tule lacustrine basin in Swisher and Briscoe Counties and the remnants of the lake basin in Mulberry Creek valley were thought to have resulted from subsidence following dissolution of Permian salts (Evans and Meade, 1944). On the basis of subsurface stratigraphic and structural data, the following basins are thought to have developed partly from dissolution and subsidence: (1) the Rita Blanca Formation near Channing, Texas;

(2) lacustrine sediments near Canyon, Texas; (3) the Cita beds in Palo Duro Canyon; (4) the Tule Formation in Swisher and Briscoe Counties; and (5) the Blanco Formation in the White River-Running Water Draw valley (Gustavson and Budnik, 1985; Gustavson and Finley, 1985; Gustavson, 1986a, 1988). Most of the large alkaline lake basins south of Lubbock that contain Quaternary strata are underlain by areas of thin salt and structural lows on horizons above the salt; these basins probably formed at least in part by dissolution and subsidence (Reeves and Temple, 1986). Contrary to these studies, DeConto and Murphy (1986) suggested that dissolution beneath the High Plains occurred during the Triassic and therefore development of surface geomorphic features is unrelated to Cenozoic dissolution and subsidence. Although most of the aforementioned studies demonstrate that areas of thin salt and structural lows in units overlying the salts occur beneath these lake basins, the full extent of most basins cannot be attributed to dissolution and subsidence. Eolian deflation most likely contributed to their formation (Evans and Meade, 1944), as is suggested by the presence of dunes along the eastern, or lee, side of most of the larger lakes on the High Plains surface. Dissolution of soil carbonate, including the Caprock caliche, also may have played a role in lake basin development (Osterkamp and Wood, 1987; Wood and Osterkamp, 1987).

The relation between reentrants in the escarpment and lacustrine basins that formed partly because of salt dissolution suggests that the position of the reentrants is, in part, structurally controlled. Clearly, retreat of the escarpment by backwasting and headward extension of streams was also accelerated where the escarpment extends into the preserved catchment areas of Cenozoic lake basins because of an increased source of runoff.

Fracture Systems and Landform Development

Several types of fractures have influenced landform development along the Caprock Escarpment. These include both tectonically induced systematic fractures and nonsystematic fractures that apparently resulted from vertical extension over zones of salt dissolution. Clastic dikes also commonly occur in lower Ogallala Formation, Dockum Group, and Dewey Lake Formation strata.

Systematic and Nonsystematic Fractures

Development of linear segments of streams and other landforms in the Rolling Plains may be related to adjustment to fractures. Linear segments of the valleys

of the Salt Fork and Double Mountain Fork of the Brazos River have north-south, northwest-southeast, and northeast-southwest orientations. Although he did not describe regional fracture orientations, Reeves (1971) inferred that these streams may have responded to the "Earth's regmatic fracture pattern." Linear valley segments of the Middle and North Pease Rivers and the Prairie Dog Town Fork of the Red River have been attributed to the influence of fractures formed by the dissolution of salt, gypsum, and possibly dolomite and the subsequent collapse of overlying strata (U.S. Army Corps of Engineers, 1975). Lineament trends recognized from Landsat images, including linear segments of streams, topographic elements, and tonal anomalies, are similar to orientations of joints exposed

in the Caprock Escarpment and to subsurface structural trends (Finley and Gustavson, 1981). On the basis of these observations, linear physiographic features were interpreted to be structurally controlled.

Karst landforms, primarily dolines and open fissures, developed on the Rolling Plains as a result of salt dissolution and associated collapse (Gustavson and others, 1982). Orientations of fissures and the long axes of dolines are similar to trends of regional joint systems. Zones or concentrations of systematic vertical joints, which result from horizontal extension, intersect Permian and Triassic strata in the Caprock Escarpment, having an average concentration of 5 joints per meter for sandstone beds 3 m (10 ft) thick (Goldstein, 1982; Collins, 1983, 1984; Goldstein and Collins, 1984; Collins and Luneau, 1986). Synclinal depressions, minor faults, and extension fractures filled with gypsum (var. satin spar) are common in upper Permian strata exposed near the base of the escarpment; these structures probably resulted from subsidence over dissolution zones. The synclinal depressions trend parallel to systematic joints. Similarity in orientation among synclinal depressions, dolines, fissures, and joint systems suggests that ground-water flow and dissolution were more pronounced along zones of systematic fractures, and, as result, systematic fractures strongly influence the distribution and morphology of subsidence structures.

Along the Caprock Escarpment, nonsystematic vertical joints are typically curved, have no preferred orientation, and are commonly truncated against systematic joints. Nonsystematic joints therefore postdate systematic joints (Goldstein, 1982). Nonsystematic joints, which locally display convex-upward Wallner lines indicating upward propagation of the fracture, were attributed to subsidence induced by salt dissolution (Goldstein and Collins, 1984). Horizontal or bedding-plane extensional fractures filled with fibrous gypsum occur in Permian strata throughout the region and have also been attributed to subsidence over areas of salt dissolution (Goldstein and Collins, 1984). The highly fractured strata exposed in the Caprock Escarpment probably enhance downward leakage of ground water as well as chemical and mechanical weathering of these rocks.

Clastic Dikes

Along the northern flank of Mulberry Creek valley (fig. 4) numerous clastic dikes occur locally in the Ogallala Formation and in the underlying Permian Dewey Lake Formation. Their orientations range from N 80° W to S 40° W. Clastic dikes in the Ogallala Formation are filled with sediment that appears to have washed down from the overlying Quaternary Blackwater Draw Formation. Although they pinch,

swell, and sometimes form a network of veins, overall the clastic dikes are wedge shaped, being widest near their upper ends and narrowing with depth. They may extend vertically for as much as 30 m (100 ft). In the Mulberry Creek valley, the Ogallala and overlying lacustrine sediments are deformed so that the lacustrine sediments strike N 80° W and dip 32° S, an orientation that coincides with that of most of the clastic dikes. Deformation of strata exposed in this valley was attributed by Evans and Meade (1944) to subsidence due to salt dissolution. Our regional subsurface maps (figs. 9 through 13) also indicate that the zone of active salt dissolution extends beneath the Mulberry Creek valley and that the deformation exposed there is most likely due to dissolution-induced subsidence. The attenuated wedge shape of these clastic dikes suggests that they formed from horizontal extension, their principal stress directions being perpendicular to the axis of the subsidence basin (fig. 12). The postulated genetic relation between locally occurring tensional fractures (clastic dikes) and folding from dissolution-induced subsidence is consistent with our interpretation of regional deformation due to dissolution along the Caprock Escarpment.

Several open fractures, partly filled with sediments washed in from the surface of the Rolling Plains, were described by Gustavson and others (1982) and Gustavson (1986b). The fractures occur on the flanks of large dolines that formed in Hall County above an area of extensive salt dissolution. In 8 yr (between 1978 and 1986) these features opened several times, only to be filled each time by loose surface sediment washed in during subsequent rainfalls or when farmers cultivated fields crossed by the fractures.

The presence of clastic dikes deep in the Ogallala and Dewey Lake Formations in the Mulberry Creek valley indicates that ground water has been important in moving near-surface sediments downward into the Ogallala Formation and as deep as the Permian Dewey Lake Formation. If dissolution-induced subsidence resulted in open fractures that were later filled with near-surface sediment, then the same fractures were probably open conduits for enhanced leakage to strata as deep as the salt-bearing Permian System.

Fractures and clastic dikes probably have enhanced the leakage of low-salinity ground water downward toward Permian strata and the dissolution zone. Furthermore, both nonsystematic fractures and clastic dikes appear to result from dissolution-induced subsidence. Thus, a feedback system is created by which ground-water flow through sediments and along fractures leads to interstratal salt dissolution. Resulting subsidence causes additional fracturing or the opening of existing fractures, which in turn allows the flow of more water toward the dissolution zone.

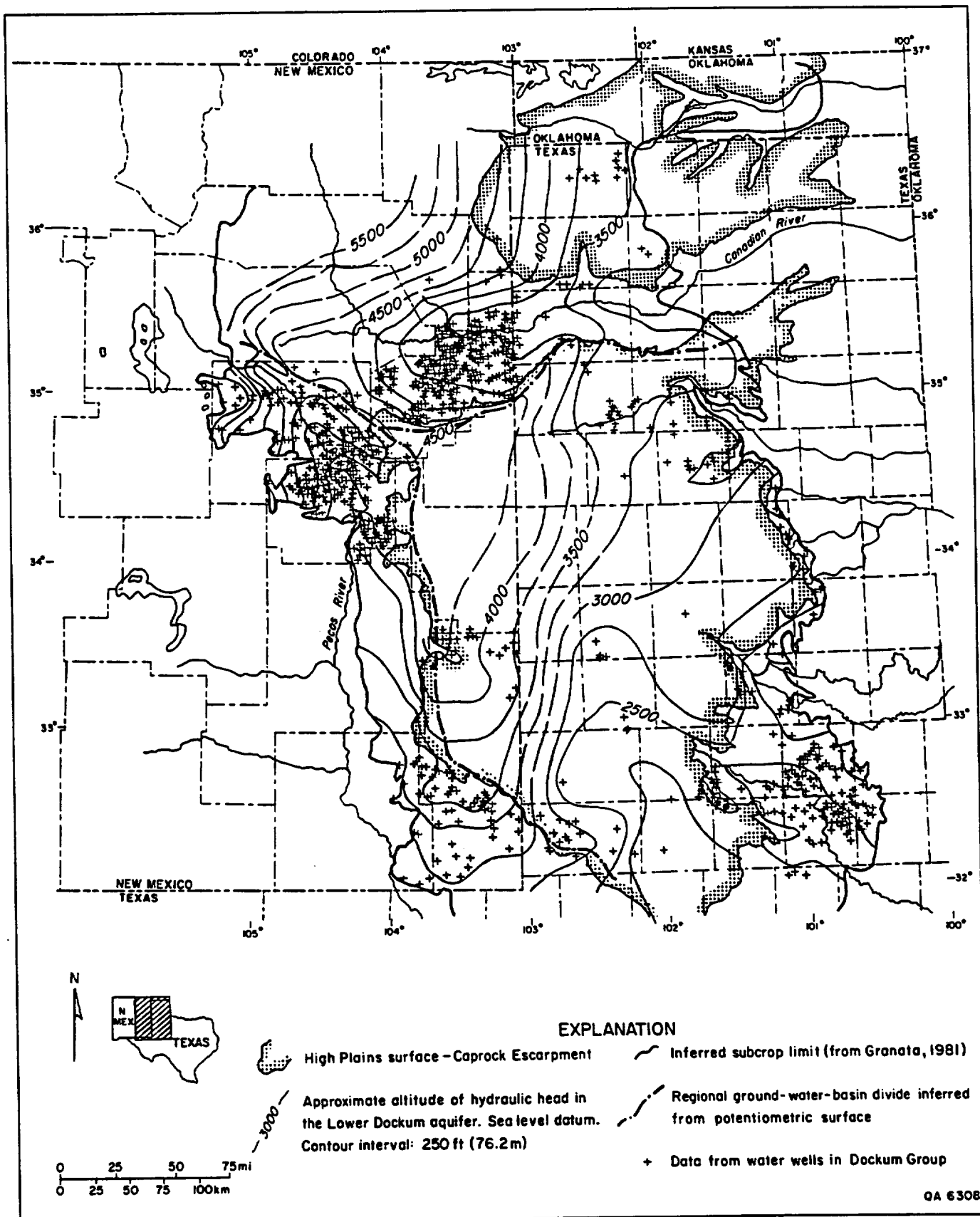


FIGURE 15. Potentiometric-surface map of lower Dockum Group ground water (modified from Dutton and Simpkins, 1986). Potentiometric gradient steepens at the Eastern Caprock Escarpment.

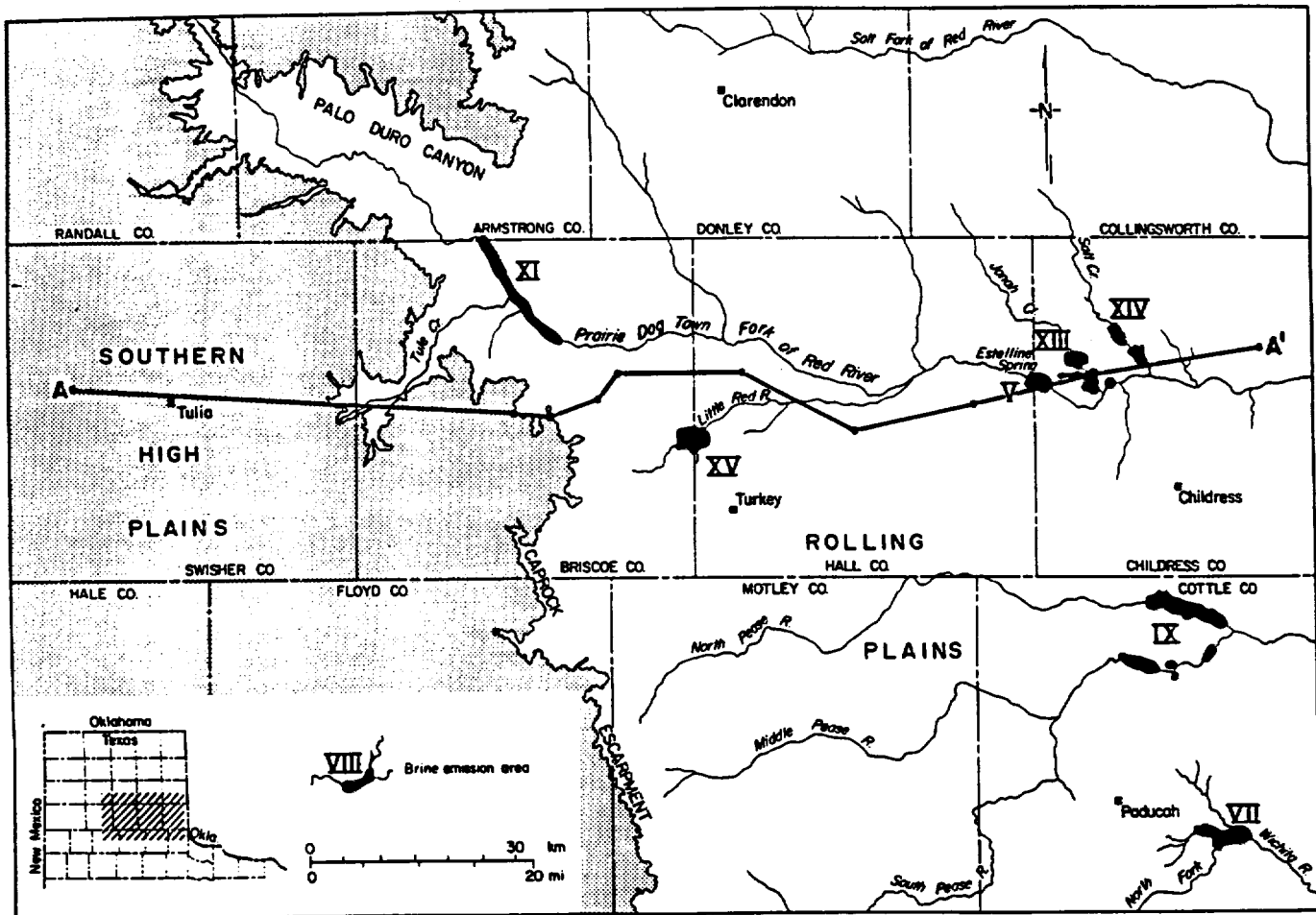


FIGURE 16. Map of physiographic units, major streams, and brine emission areas (U.S. Army Corps of Engineers, 1975) in the study area. Brine emission areas XI and XV occur in outcrops of strata equivalent to the Seven Rivers Formation. Brine emission areas V, VII, IX, XIII, and XIV occur in outcrops of strata equivalent to the San Andres Formation. A-A' locates figures 8 and 17 (Simpkins and Fogg, 1982, their fig. 91).

layers of low hydraulic conductivity and the path of least resistance is to discharge at the boundary. Numerous springs are, in fact, present along the Caprock Escarpment above strata of low hydraulic conductivity, such as Dockum mudstones. This in turn suggests that spring sapping and seepage erosion contribute to backwasting of the Caprock Escarpment. Sapping and seepage erosion are discussed on p. 29.

Discharge from this flow system occurs to the east, where saline springs in the Rolling Plains discharge a mixture of both locally derived and deeper ground waters, as evidenced by geochemical and isotopic data (Richter and Kreitler, 1986). Large areas of saline discharge have developed in topographically low parts of outcrop belts of the Salado, Seven Rivers, and San Andres Formations (compare figs. 8 and 16).

Conceptual Model of Ground-Water Flow beneath the Caprock Escarpment

Hypothetical flow paths of low-salinity ground water through the dissolution zones in Permian bedded salt are shown in the conceptual model in figure 17. The model illustrates how the hydraulic-head distribution imposed by the escarpment boundary could be the major force behind ground-water flow to salts in the subsurface and to springs along the escarpment, where zones of low hydraulic conductivity exist. Low-salinity ground water moves downward to discharge as springs along the escarpment and laterally to the relatively shallow updip elements of Permian bedded salt. Per-

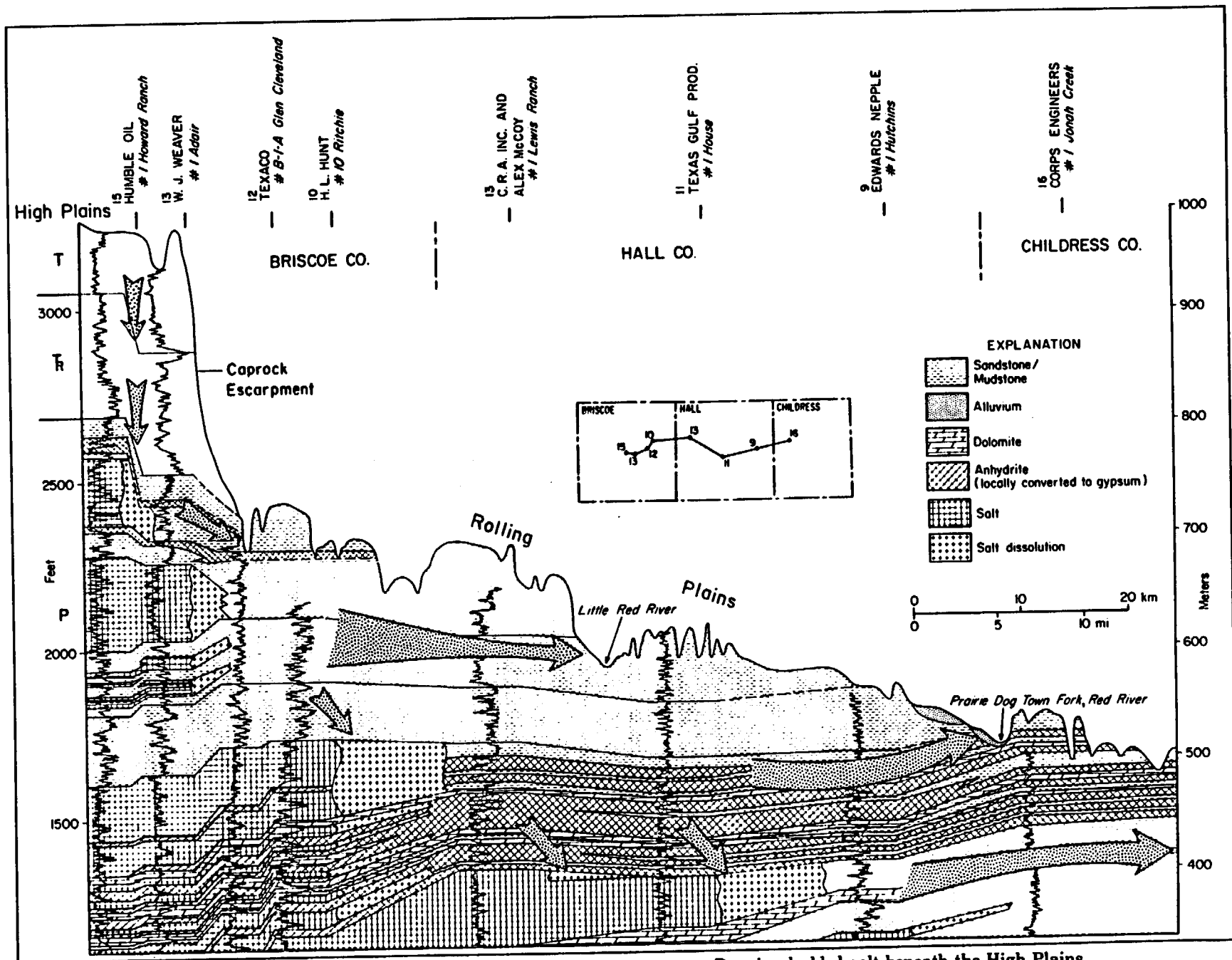


FIGURE 17. Conceptual model of ground-water flow and its impact on Permian bedded salt beneath the High Plains, Caprock Escarpment, and Rolling Plains (from Gustavson and others, 1980). Inferred flow paths are indicated by arrows. Stratigraphic units are identified in figure 8. Datum sea level.

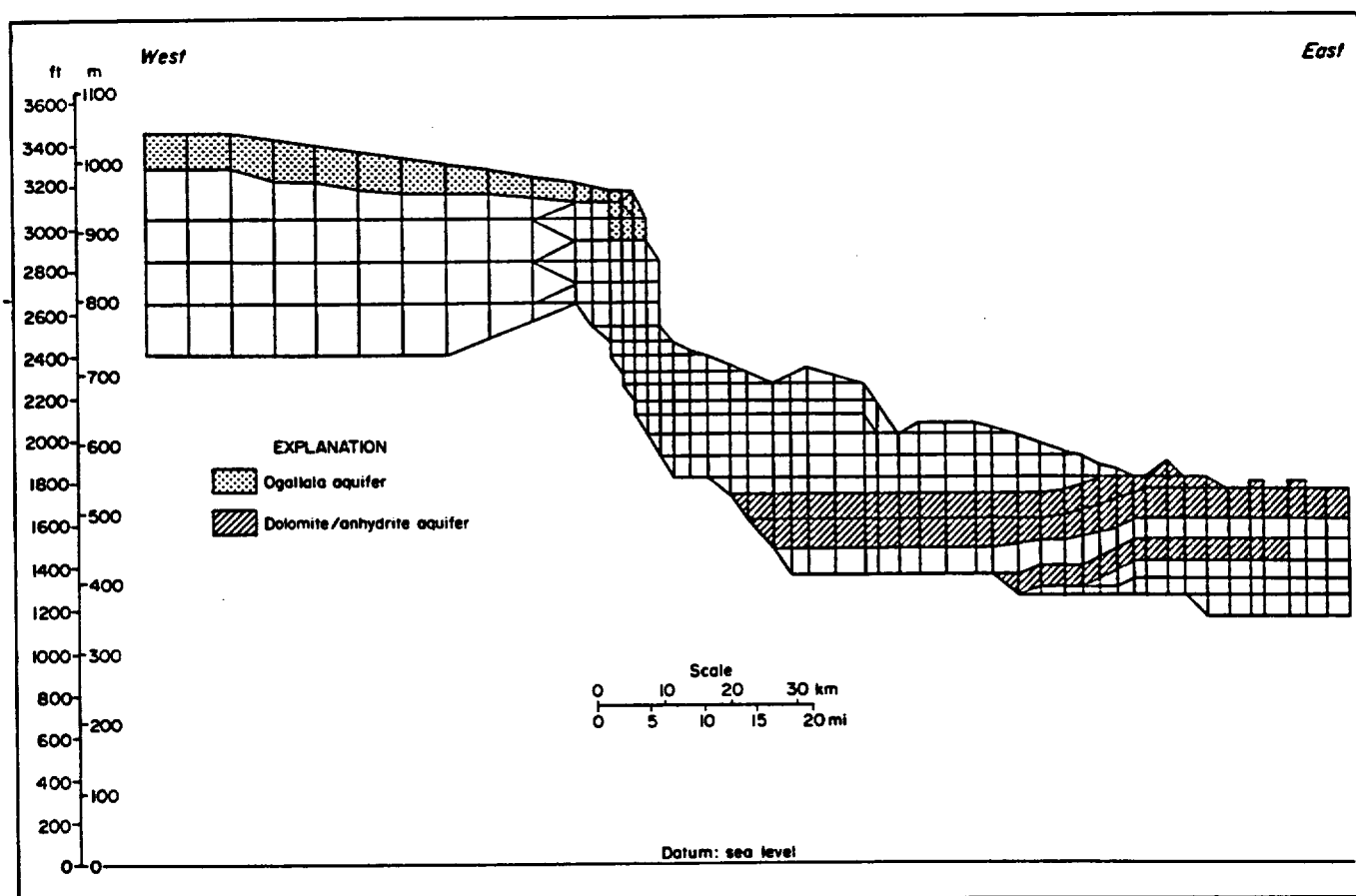


FIGURE 18. Finite-element mesh design based on cross section shown in figure 8. Upper surface is the water table. Lower surface is drawn at upper stratigraphic limit of salt-bearing units (from Simpkins and Fogg, 1982, their fig. 93).

mian salt is readily dissolved as it comes into contact with low-salinity ground water, and the resulting brines flow eastward through highly transmissive dolomite and anhydrite/gypsum beds to discharge into topographically low areas.

Numerical Model of Ground-Water Flow beneath the Caprock Escarpment

Numerical simulations were conducted by Simpkins and Fogg (1982) to evaluate the importance of topography, hydraulic head, permeability, and boundary conditions in the hydrologic system. Their model, which is summarized here, simulated ground-water flow in two dimensions and was based on the same stratigraphic cross section as that used in the conceptual ground-water flow model (fig. 17) in this report. Their numerical model was oriented vertically to take advantage of the detailed stratigraphic framework provided by well data and to enable examination of vertical hydraulic-head gradients. Vertical gradients

are particularly important because they provide the drive by which low-salinity ground water reaches Permian salt-bearing units and by which brines from salt dissolution zones are discharged to the surface at saline springs in the Rolling Plains region (fig. 16).

In the numerical model, the prescribed hydraulic-head boundary conditions are imposed on the upper, left, and right boundaries. The upper boundary is the water table (Knowles and others, 1982). The lower boundary is a no-flow boundary (upper stratigraphic limit of salt beds), and thus it is assumed that any upward leakage from the deeper units occurs at a negligible rate compared with the flow rate in the modeled area.

Ground-water flow was simulated using the computer program FLUMP, which employs a finite-element, mixed explicit-implicit numerical scheme for solving linear and nonlinear subsurface-water-flow problems (Neuman and Narasimhan, 1977). The finite-element mesh (fig. 18) was designed to accommodate the heterogeneities of the local stratigraphic system and to provide greater accuracy near the Caprock Escarpment, where hydraulic gradients are steepest.

TABLE 2. Hydrostratigraphic units and hydraulic conductivities used in the ground-water flow model (from Simpkins and Fogg, 1982) (1 ft/day = 0.3 m/day).

Hydrostratigraphic unit	Hydraulic conductivity (ft/day)		Source
	Kh	Kv	
Ogallala (sand and gravel)	26.7	26.7	Both values from Myers, 1969
Dockum (sand, silt, clay)	2.7	2.7	Both values from Myers, 1969
Quartermaster/Cloud Chief (mudstone)	0.27	0.00027*	Kh value from P. R. Stevens, personal communication, 1980
Whitehorse (sandstone)	3.0	3.0	Both values from Freeze and Cherry, 1979
Blaine and San Andres cycle 4 in shallow sub- crops (dolomite/ anhydrite)	10.0	10.0	Both values from U.S. Army Corps of Engineers, personal communication, 1980
Flowerpot (mudstone)	0.27	0.00027*	Kh value from P. R. Stevens, personal communication, 1980

*Values were not estimated from field or laboratory tests but are based on the fact that these units are horizontally stratified mudstones containing small amounts of sand, thus indicating large Kh/Kv (horizontal and vertical conductivity) values.

Hydraulic conductivities (K) of the various stratigraphic units were compiled from several sources (table 2). Most values are estimates of a range of K data from pumping tests. Where data were unavailable, K was estimated either by extrapolation from other data for units of similar lithology or by selection of a "typical value" from the literature (such as from Freeze and Cherry, 1979). Vertical K values (Kv) of the Upper Permian mudstones (table 2) are not from field or laboratory tests; rather, their calculation is based on the observation that these units are horizontally stratified mudstones containing small amounts of sand.

Key uncertainties that may be important in interpreting the results of the model are (1) Kv values in the vicinity of the Caprock Escarpment that control the rate and amount of low-salinity water introduced to Permian salt beds in the subsurface and (2) Kv and Kh (horizontal hydraulic conductivity) values for the dolomite/anhydrite units and Kv values for other units east of the Caprock Escarpment that govern where the high-salinity waters discharge and to what extent topography affects the ground-water flow system.

Modeling Results

Several simulations were made by Simpkins and Fogg (1982) to calibrate the model and to determine its sensitivity to hydraulic conductivity (K) variations. Hydraulic heads and recharge/discharge rates com-

puted by the numerical model using the values of K listed in table 2 are shown in figure 19. Unfortunately, ground-water flow lines cannot be drawn perpendicular to the hydraulic-head contours in figure 19 because of anisotropy and the extreme vertical exaggeration of the cross section. The effects of vertical exaggeration are greatest at the escarpment, where the vertical (downward) gradient computed by the model is substantial; however, in figure 19, head contours seem to indicate only horizontal flow. Our interpretation of the results is therefore based on node-to-node hydraulic heads and ground-water fluxes printed in the model output listing.

According to Simpkins and Fogg (1982) the numerical model supports the conceptual model of salt dissolution by indicating (1) downward flow of fresh ground water from the Ogallala aquifer into the salt-bearing strata beneath the Caprock Escarpment; (2) eastward movement of the resultant brine through transmissive dolomite/anhydrite beds of the San Andres Formation; and (3) discharge of the brine into saline springs in topographically low areas of the Rolling Plains. The numerical model also suggests that nearly all ground-water discharge from the system can be accounted for by horizontal flow along bedding and by vertical (upward) discharge through saline springs. Discharge along the right-hand prescribed head boundary is negligible (fig. 19).

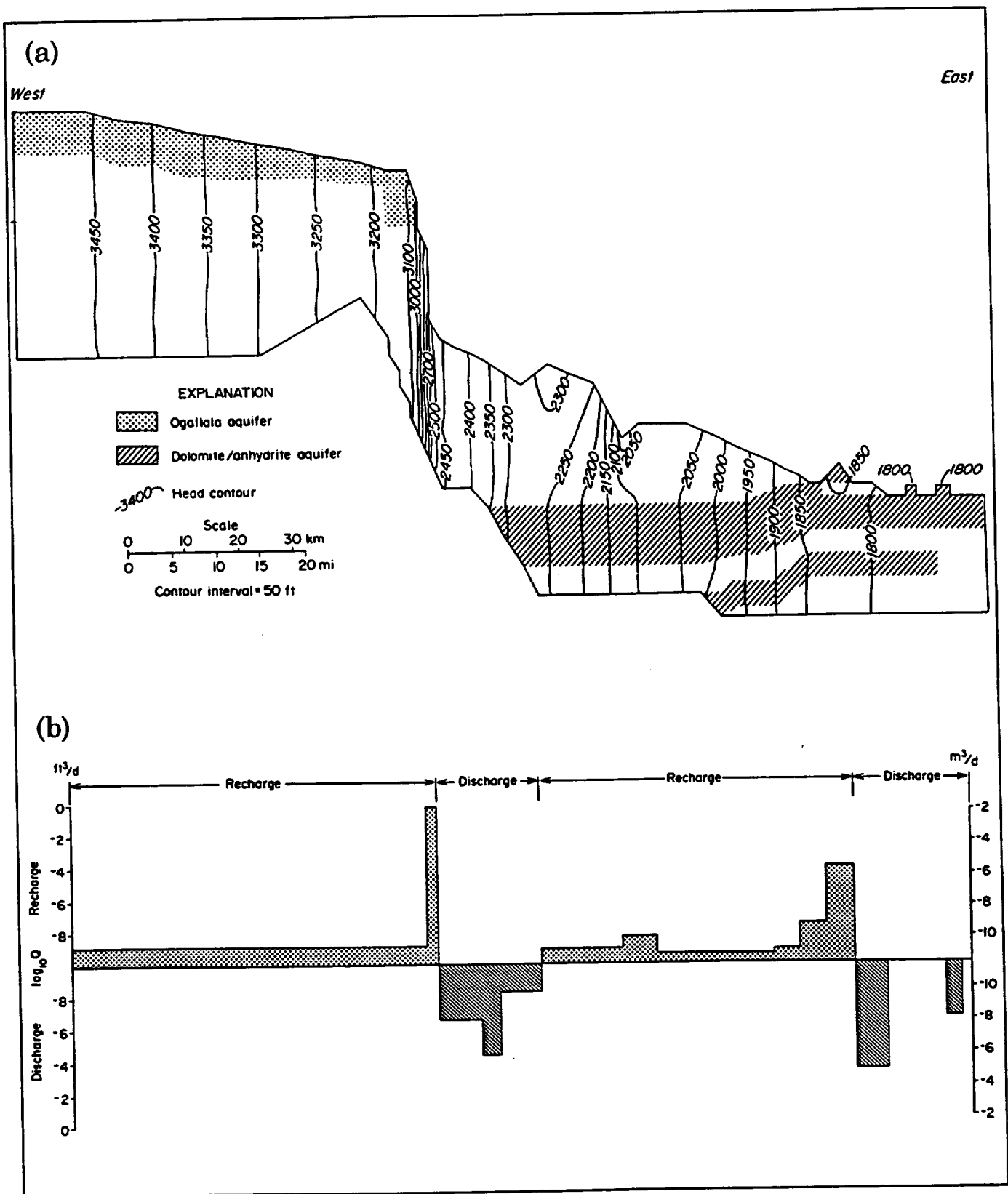


FIGURE 19. Steady-state hydraulic heads and recharge/discharge rates computed by ground-water flow model (from Simpkins and Fogg, 1982). (a) Flow lines cannot be assumed to be orthogonal to the head contours because of anisotropic K values and because the vertical scale exaggeration is approximately 104 to 1. (b) The recharge/discharge rates shown are regional averages of rates computed at groups of nodes and thus reflect only major recharge and discharge areas. Flow rates through the sides of the model are on the order of $10^{-11} \text{ m}^3/\text{day}$, which are minute compared with the rates illustrated.

Surface Processes Causing Scarp Retreat

Fluvial erosion, spring sapping, seepage erosion, and mass wasting are important erosional processes all along the escarpment. However, in Palo Duro Canyon, and especially in the northern part of the canyon in Palo Duro Canyon State Park, rotational slumping plays a major role in scarp retreat.

Surface Runoff

Rainfall near the Caprock Escarpment results predominantly from convective storms. Single storms with precipitation in excess of 6 cm (2.4 inches) generally occur at least once every 24 months in the Amarillo area, and rainfall intensities of 2.5 cm/hr (1 inch/hr) or more account for more than 8 percent of the hourly rainfall for the region (Finley and Gustavson, 1980). A 24-hour rainfall of approximately 25 cm (10 inches) occurs about once every 19 yr. During especially heavy rainfalls the infiltration capacity of the soil, as well as the capacity of certain playa lake basins, is exceeded, and overland discharge from the playas occurs locally.

During field studies we observed the effects of several sheetfloods on the High Plains. Rainwater that falls on the Southern High Plains moves to the rim of the Caprock Escarpment as sheetfloods. Sheet wash and rill wash occur when waters from heavy rains and sheetfloods flow down the walls of the canyons (Bath, 1980; Simpkins and Gustavson, 1985, 1987). Runoff, concentrated in the floors of canyons, removes stored sediment, erodes the channel floor, and, as discharge wanes, deposits sediment eroded from the canyon floor and walls.

The area of the High Plains surface that contributes runoff to the Caprock Escarpment is small. A drainage divide exists between the Caprock Escarpment and the first playa lake basins west of the escarpment because of the distribution of internally drained playa lake basins on the High Plains surface. The surface that normally contributes runoff, therefore, is a narrow band of terrain containing silty and clayey Pullman and Amarillo series soils that lies just west of the top of the escarpment. Along many segments of the escarpment this band is usually less than 1 km (0.6 mi) wide and rarely more than 2 to 3 km (1.3 to 1.9 mi) wide. Although the area potentially contributing runoff to the escarpment is small, sheetflood and slope erosion are important to canyon and slope degradation. Surface runoff, however, occurs only when the infiltration capacity of the soil is exceeded.

Drainage Development

Finley and Gustavson (1983) and Simpkins and Gustavson (1985) described the geomorphic effects of two 10-year return interval storms (May 26, 1978, and June 10, 1984) on a small, instrumentally monitored drainage basin that is a tributary of Tierra Blanca

Creek within the Buffalo Lake National Wildlife Refuge, Randall County (fig. 13). This drainage basin is morphologically similar to drainage basins on the Caprock Escarpment, and it is developed in the Ogallala and Blackwater Draw Formations, the same strata underlying small drainage basins along the crest of the escarpment. The Buffalo Lake National Wildlife Refuge study basin, located 48 km (30 mi) west of the escarpment, and drainage basins within the Caprock Escarpment are subject to the same weather conditions. For these reasons we believe that geomorphic processes at the Buffalo Lake site are comparable to processes that are shaping drainage basins of the upper part of the Caprock Escarpment.

Instrumentation for data collection at the Buffalo Lake site included a recording rain gauge, air- and ground-temperature-recording probes, soil-moisture probes, several groups of erosion pins, lines of marked gravel clasts, and markers set into headcuts within the channel at the floor of the canyon. Weather data at Buffalo Lake were collected continuously from January 1977 to November 1987. Erosion pins and headcut markers were measured biannually or after severe storms. Before the first storm (in 1978), the long profile of the canyon, topographic cross sections, and detailed topography of headcut areas were surveyed.

The drainage basin at the Buffalo Lake site received 7.1 cm (2.8 inches) of rain during a 3.2-hr storm on May 26, 1978; maximum intensity of rainfall was 6.4 cm/hr (2.5 inches/hr) over a 30-min period. Intense rainfall during the storm rapidly exceeded the infiltration capacity of soils on the High Plains surface, and large volumes of water were directed into the headwaters of the canyon and over the canyon rim. Sheetflooding on the High Plains surface was indicated by drift lines of plant debris 6 to 8 cm (2.4 to 3 inches) high on cacti and fenceposts. Erosion pins on the low-sloping (2 to 3°) High Plains surface showed either no change or 1 to 2 mm (0.04 to 0.08 inch) of net deposition. Gullied slopes (34° and 27°) in very fine sand of the Quaternary Blackwater Draw Formation at the top of the canyon were eroded as much as 6.2 cm (2.4 inches) by rill wash and sheet wash (table 3). Gully floors in the Ogallala Formation were scoured to bedrock in some cases, and small fans of pebble- to cobble-sized gravel were deposited on the canyon floor. Sheet wash and rill wash on the canyon slopes resulted in an average erosion of 2.2 cm (0.9 inch) in all slope classes; a maximum of 6.2 cm (2.4 inches) was recorded. In addition, an average of 41 percent of pebble- to cobble-sized clasts were moved by sheet wash from lines of painted clasts. Large volumes of pebble- to boulder-sized sediment were deposited on the canyon floor, and large volumes of mostly sand- and pebble-sized sediment were carried out of the canyon and deposited on the valley floor of Tierra Blanca Creek.

As a result of the 1978 storm, bedrock surfaces in the canyon were scoured of loose sediment. Between 1978

TABLE 3. Erosion-pin measurements made on eroded canyon slopes following storm on May 26, 1978 (modified from Finley and Gustavson, 1980). Storm duration was 3.1 hr (25.4 mm = 1 inch).

Slope class	Average vegetative cover (%)	Number of pins	Net erosion (mm)		
			Average	Max.	Min.
0-9°	22	8	24	59	6
10-19°	11	6	27	54	9
20-29°	15	21	19	62	3
30-39°	14	9	17	60	6
42°	10	1	-	51	-
52°	5	1	-	19	-

and 1984, more loose sediment accumulated, and these bedrock surfaces assumed their pre-1978 appearance. Alluvium and colluvium accumulated on canyon slopes and on the canyon floor as a result of small rainfalls.

On June 10, 1984, intense rainfall (9.3 cm [3.7 inches]) during a 4-hr period again caused significant scour and deposition of sediment in the tributary canyon of Tierra Blanca Creek. A maximum 30-min precipitation intensity of 6.9 cm/hr (2.7 inches/hr) was attained during that storm. The Canyon, Texas, Fire Station recorded 11.7 cm (4.6 inches), and the Amarillo National Weather Service office recorded 12.5 cm (4.9 inches) of precipitation on June 10, 1984. Effects of the 1984 storm were similar to those of the May 26, 1978, storm discussed by Finley and Gustavson (1983). The 1978 and 1984 storms were both preceded by relatively dry periods in the short-term climatic record, although, overall, 1984 was wetter than 1978. Rainfall of similar magnitude (total amount and intensity) occurred between these two events (table 4), yet these

two storms caused the most erosion in the canyon, according to field observations and erosion-pin readings.

Inclusion of data from the June 10, 1984, storm in the climate data base helped us to identify the effect of intense rainfall on erosion. Figure 20 is a plot of the maximum 30-min rainfall intensity (most intense storm per measurement period) versus the percent of erosion pins showing erosion (Simpkins and Gustavson, 1987). All rainfall event intensities lasted for at least 30 min, a few slightly longer. An exponential relationship is indicated, and field evidence suggests that a critical geomorphic threshold is crossed during storms with rainfall amounts of approximately 6.0 cm (2.4 inches) and intensities greater than 6.0 cm/hr (2.4 inches/hr). Scatter in the data is related to variation in rainfall frequency during a period and to availability of erodible sediment. The somewhat anomalous value for the 1978 storm may be partly due to the location of erosion pins that were set high on the drainage divides in the erodible Pleistocene loess (Blackwater Draw Formation) instead of down in the tributary canyon. The large volume of sediment moved during this event strongly suggests that the availability of loose sediment affected the amount of erosion.

Thresholds for Sediment Movement

Study of sediment movement in the tributary canyon at Buffalo Lake National Wildlife Refuge after episodes of intense rainfall suggests that sediment is transported and stored in a stepwise manner. Three incremental steps are related to attainment of critical thresholds in rainfall intensity. Minor rainfall events (less than 6.0 cm/hr [2.4 inches/hr]) (step 1) move sediments down hillslopes and lower alluvial surfaces; most of that sediment is stored there until an intense rainfall event occurs. Intense rainfalls (greater than 6.0 cm/hr [2.4 inches/hr]) (step 2) generally cause ero-

TABLE 4. Record of intense storms at Buffalo Lake National Wildlife Refuge during the course of this study. These data were used to construct the plot in figure 20 (25.4 mm = 1 inch).

Date	Total precipitation (mm)	Period (hr)	30-min maximum intensity (mm/hr)	Percentage of pins showing erosion
05/26/78	71.0	3.1	64.0	91.0
10/29/79	12.8	3.5	20.0	30.8
06/21/80	26.0	1.95	47.6	42.3
08/05/80	20.2	2.1	36.0	32.7
08/16-17/81	82.0	4.5	76.8	53.8
10/15/81	27.2	5.3	18.0	30.8
07/20/82	52.0	1.5	52.0	42.3
09/07/82	15.0	2.7	24.8	17.3
10/07/82	18.6	1.2	35.6	28.0
09/10/83	20.8	0.5	38.4	37.0
06/10/84	93.4	4.0	69.0	66.0

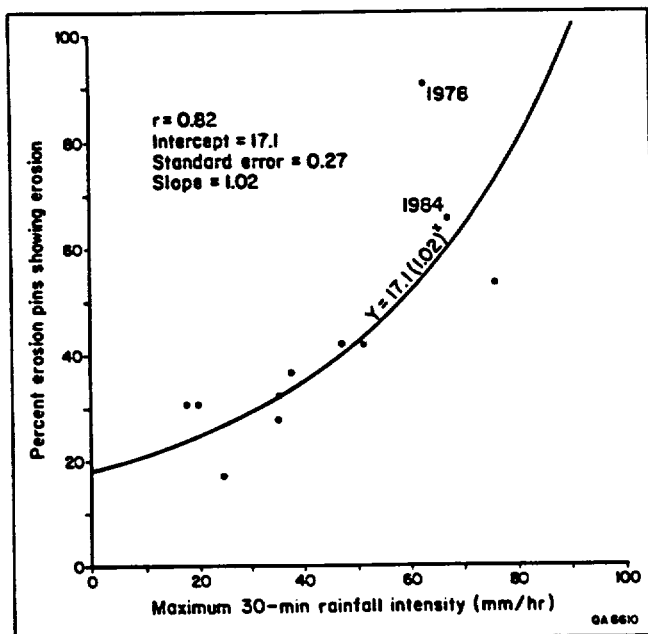


FIGURE 20. Plot of maximum rainfall intensity versus percent of erosion pins showing erosion at the Buffalo Lake National Wildlife Refuge station (modified from Simpkins and Gustavson, 1987, their fig. 37). Correlation coefficient is 0.82. Although based on only two data points (1978, 1984) a critical geomorphic threshold seems to occur when rainfall intensity values exceed 60 mm/hr, depending on sediment availability. Plotted values are provided in table 4.

sion on hillslopes, erosion and deposition on the canyon bottom, and deposition in Tierra Blanca Creek. Large boulders carried to the canyon floor by smaller tributary canyons act as sediment traps for finer grained material moving down the thalweg or tributaries. Step 3 represents a storm capable of removing sediment along Tierra Blanca Creek and its tributary canyons. No storm of this magnitude, however, was recorded during the study period. In this model of sediment transport, sediment is constantly created by weathering and disaggregation and is transported down canyon walls by small rainfall events. Intense rainfall events have a significant erosional impact only when they occur periodically, thereby allowing enough time for loose sediment to be created, stored, and ultimately eroded. High-intensity rainfalls may not transport sediment, as this model predicts, if most stored sediment was removed by an earlier storm (Simpkins and Gustavson, 1987).

Because of the similarities in soils, bedrock, and scarp morphology, the processes and rates of erosion affecting the upper part of the Caprock Escarpment, which is developed in the Ogallala and Blackwater Draw Formations, are probably similar to the processes and rates that Finley and Gustavson (1983) and Simpkins and Gustavson (1985) observed at Buffalo Lake canyon.

Spring Sapping and Seepage Erosion

In addition to the interstratal dissolution of bedded salt, spring sapping and seepage erosion are groundwater-related geomorphic processes active along bases of cliff faces and in the headwaters of streams draining the Caprock Escarpment. Sapping and seepage erosion in these areas have apparently had a marked effect on headward erosion of stream valleys.

Higgins (1982, 1983) recently described spring sapping as a process by which larger drainage systems are developed. Although spring sapping is commonly understood to influence development of gullies and smaller streams, especially in semiarid climates, its contribution to larger drainage systems has been reported only rarely (Higgins, 1982). Active sapping in large drainage systems or valleys has not been observed, except in Nebraska (Gerster, 1976) and some southwestern states (Gregory, 1917), but it has been inferred from ground observations in Egypt (Peel, 1941) and from spacecraft images of Mars (Higgins, 1982).

Spring sapping and seepage erosion are extending the stream network that drains the approximately 210-km (130-mi) length of the Eastern Caprock Escarpment in the study area. Field observations in Luttrell Canyon, Tub Springs Canyon, Capitol Peak Canyon, Red Canyon, and Timber Canyon (all tributaries of Palo Duro Canyon) and interpretation of aerial photographs of other areas along the escarpment indicate that sapping and seepage erosion are active beneath thick (3 m to 7 m [10 ft to 23 ft]), coarse fluvial sandstone beds of the Triassic Dockum Group and beneath basal sand and gravel of the Ogallala Formation (fig. 21). Seepage discharge from the base of these sandstones carries away particles of underlying mudstones, which are continually wet, and promotes weathering and erosion (fig. 22). Even on vertical faces, a continuous supply of water encourages the growth of plants, and root growth probably aids in the mechanical breakdown of the mudstones. On some exposures, crusts of gypsum and calcite are deposited as mineralized ground water evaporates. Formation of crusts may also encourage the disintegration of Dockum strata by interstitial growth and bedrock displacement by evaporite precipitation.

Discharge records from springs and seeps in these canyons are unavailable. Discharge, however, is probably perennial, at least near the headwaters of the canyons, because the water source is the High Plains aquifer, not local recharge. A few seeps are ephemeral and apparently related to local recharge. Cottonwood, horsetail rush, and leopard frogs can be found at the spring sites, all of which require a nearly continuous supply of water. Nonetheless, these streams become ephemeral in their lower reaches because discharge is absorbed into alluvium.

The resistant sandstone beds of the Dockum Group and carbonate-cemented or silicified sands and gravels of the basal Ogallala Formation also support pour-offs (waterfalls). Plunge pools are commonly present

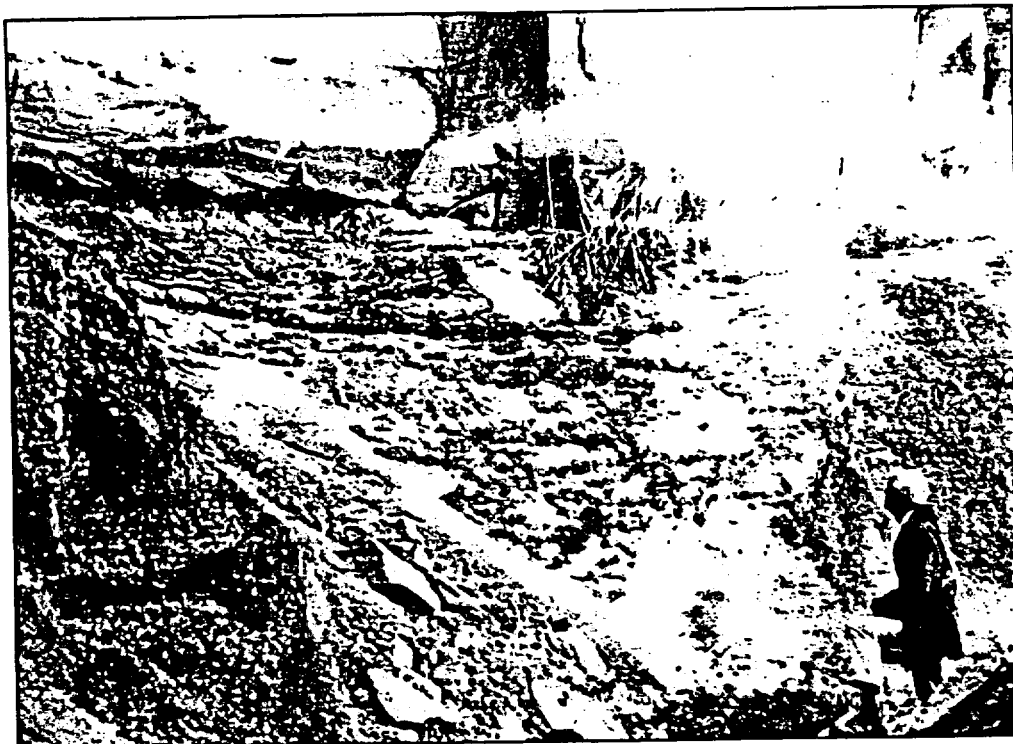


FIGURE 21. Area of spring sapping at the head of Red Canyon, Palo Duro Canyon State Park. Efflorescence is primarily gypsum. Discharge is through a Lower Triassic Dockum Group sandstone in contact with an underlying mudstone. Figure stands on blocks of sandstone that are part of a rockfall. Erosion of mudstone is beginning to undercut the overlying sandstone block. See figure 25 for location.



FIGURE 22. Detail of the spring discharge area illustrated in figure 21. Plants have rooted in the discharge zone, and roots probably help to disaggregate rocks at the contact between Dockum sandstone and mudstone.

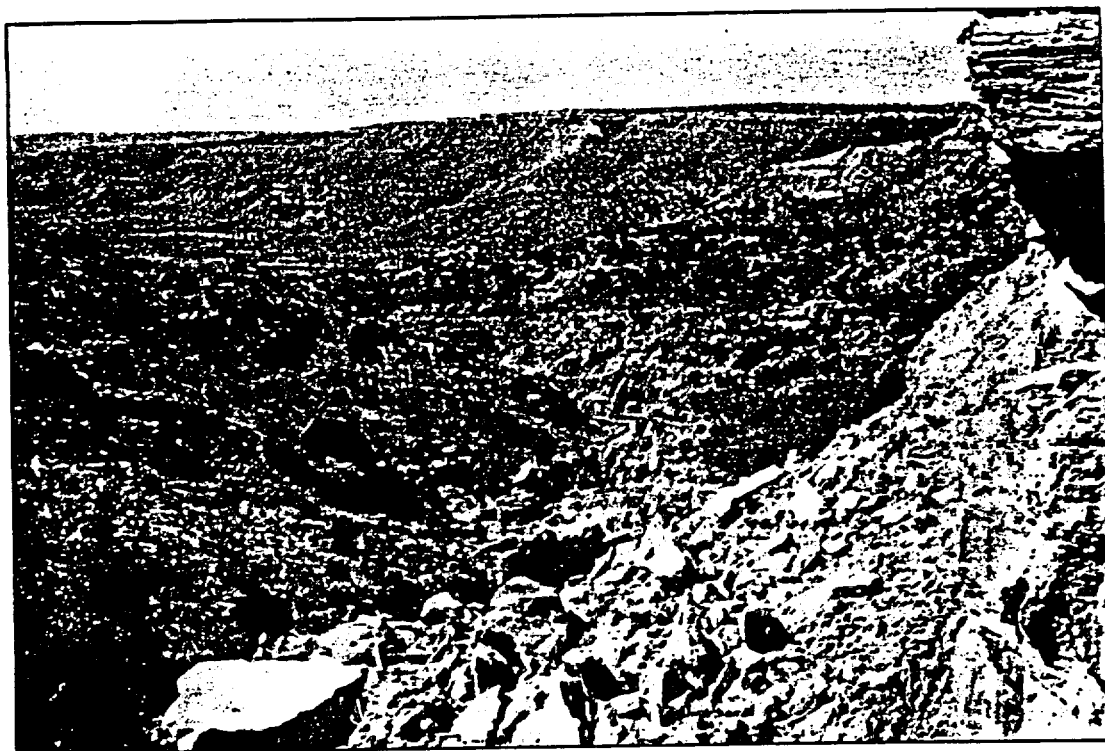


FIGURE 23. Rockfall consisting of blocks of massive channel sandstones, Upper Triassic Dockum Group at the head of Tub Springs Draw, Palo Duro Canyon State Park. Spring sapping at the contact between lower Dockum Group sandstone and underlying mudstone (obscured by rockfall) probably caused this rockfall. Spring discharge is active here and continues to undercut Dockum sandstones. See figure 25 for location.

beneath the pouroffs. Stream discharge from canyon segments above the elevation of spring sapping appears to be important in preventing the area of sapping from being blocked or covered by rockfall debris. Stream discharge over the pouroffs moves alluvium downstream in the process of creating the plunge pool, thereby removing material that might otherwise eventually cover the rock face undergoing sapping.

Rockfalls

Sapping observed in tributaries of Palo Duro Canyon has undercut one or more of the thick Dockum sandstones or basal Ogallala calcretes, causing rockfalls of the sandstone beds. In Luttrell Springs Canyon and Red Canyon the appearance of fresh rockfall scars and the jumble of large and small fragments suggest that rockfalls have occurred recently (fig. 23). A large block of Dockum sandstone (approximately 3 m × 7 m × 15 m [10 ft × 23 ft × 50 ft]) separated from the main body of a Dockum sandstone bed in 1977 and fell into Tub Springs Canyon. Processes leading to rockfalls continue in Palo Duro Canyon and its tributary canyons, as evidenced by tension cracks that developed in Dockum sandstones due to removal of underlying support, commonly by spring sapping (fig. 24).

Rotational Slumping

Substantial parts of the Eastern Caprock Escarpment have been affected by rotational slumping. Slumping (Varnes, 1958) is particularly evident in Palo Duro Canyon State Park, where more than 100 slumps are preserved (fig. 25), and is common throughout the northern half of Palo Duro Canyon (fig. 1). The largest area of slumping occurs at the foot of Fortress Cliff, along the eastern slope of Palo Duro Canyon. Here, at least 40 separate slumps can be recognized. Individual rotational slumps vary markedly in size, but the largest apparently continuous slump blocks in Palo Duro Canyon exceed 550 m (1,800 ft) in width.

Much of the terrain along the escarpment that is underlain by lacustrine mudstones of the Triassic Dockum Group has been subjected to slumping. Coherent rotated blocks, composed of Dockum sandstone and lithified units of the Ogallala Formation, commonly dip steeply toward the canyon walls (fig. 26). The best preserved blocks, however, occur high up on the canyon slopes. Slump blocks in these areas have moved relatively short distances and are not severely broken up. These are apparently the most recent slumps because they occur nearest undisturbed Dockum and Ogallala strata. Disruption and deformation of slump blocks

(a)



FIGURE 24a. Fracture in caprock caliche of the Miocene-Pliocene Ogallala Formation at Fortress Cliff, Palo Duro Canyon State Park—an incipient rockfall.

(b)

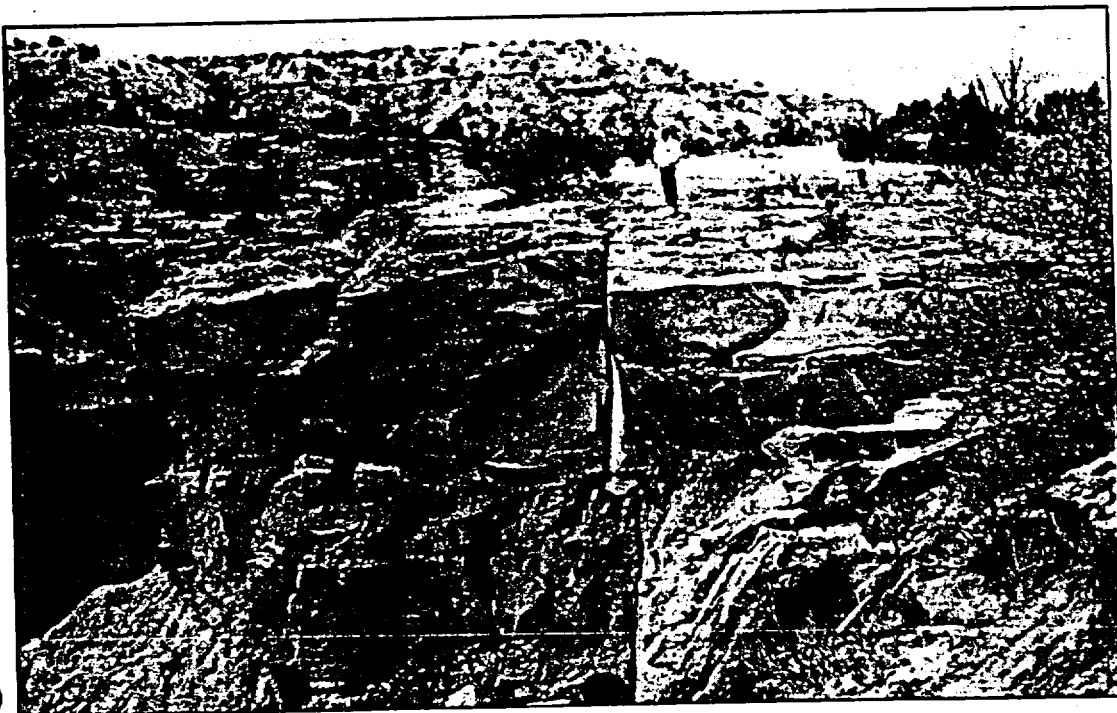


FIGURE 24b. Fracture in sandstone of the Upper Triassic Dockum Group in Tub Springs Draw. Fracture is 5 to 10 cm (2 to 4 inches) wide and apparently has formed as the underlying mudstone erodes and undercuts the sandstone by means of spring sapping. See figure 25 for location.

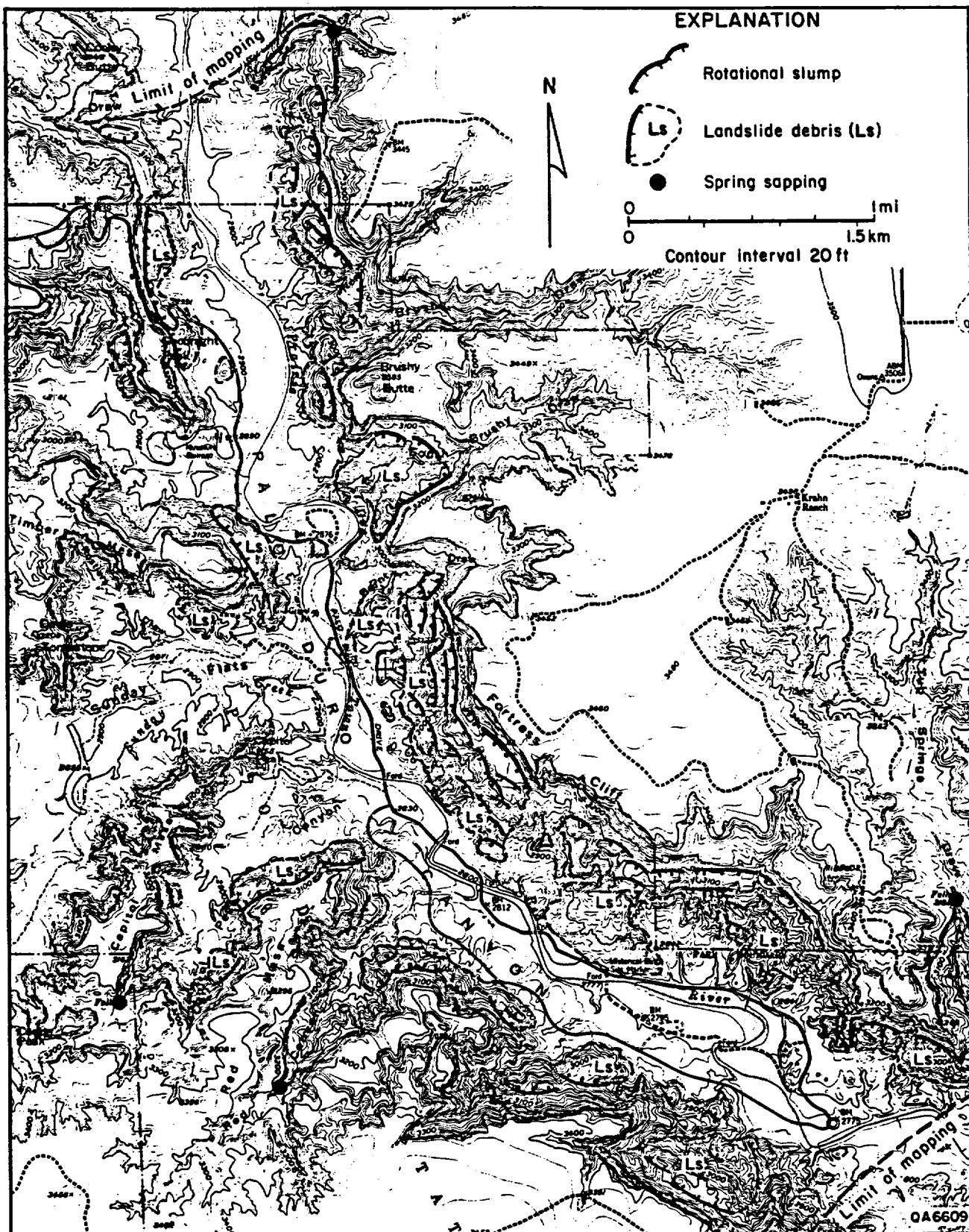


FIGURE 25. Distribution of rotational slumps and landslides in Palo Duro Canyon, Palo Duro Canyon State Park. Areas of spring sapping occur where springs discharge from the base of the Ogallala Formation or from the base of permeable sandstones in the Dockum Group. Base from U.S. Geological Survey 7.5-minute (topographic) series, Fortress Cliff Quadrangle.

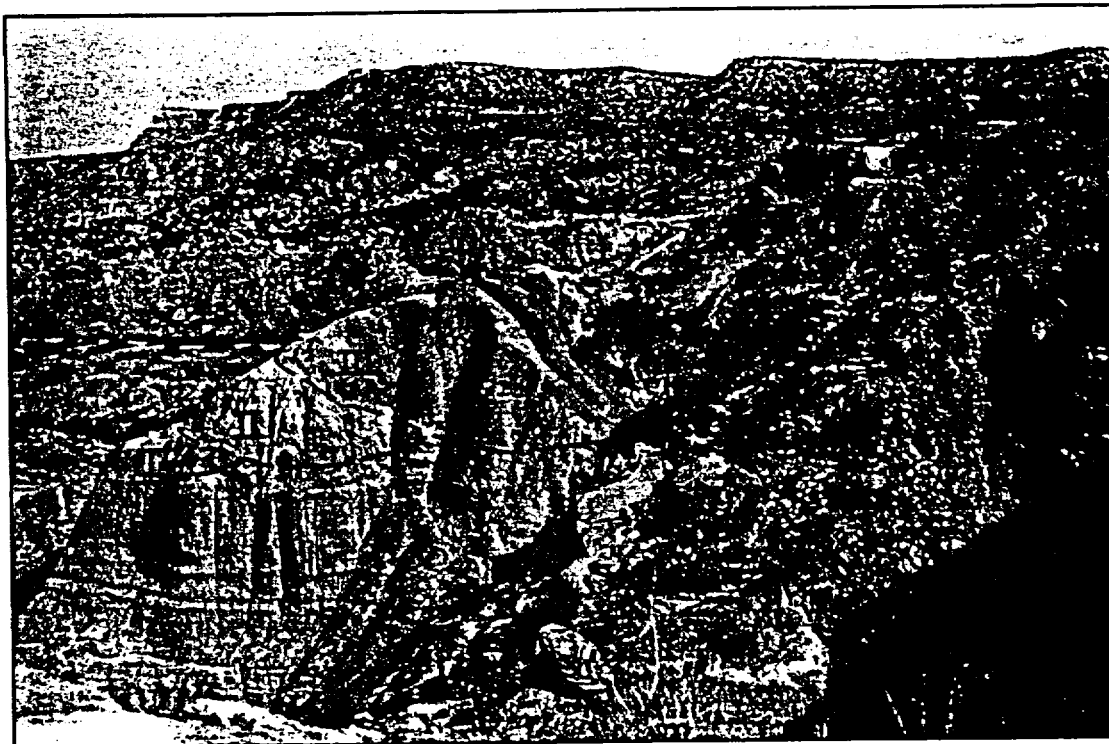


FIGURE 26. Three segments of rotational slumps (I-III) are exposed along the northeastern side of Palo Duro Canyon (viewer facing north). The three planes of rotation exposed here are in lower Dockum Group smectitic mudstones. Relief on the slumped mass is approximately 12 m. See figure 25 for location. Dashed lines mark bases of slump blocks.

Piping

increase downslope. Near the canyon floor, blocks of resistant Dockum sandstones and, to a lesser extent, calcretes of the Ogallala Formation are widely dispersed, and slumped Dockum mudstones are severely disturbed. In some areas only chaotically arranged resistant blocks of Ogallala and Dockum strata remain, capping hills of relatively undisturbed Permian red beds. These are apparently the eroded remnants of substantially older mass movements.

The lower part of the rotational plane of most slumps appears to have been either partly within or at the upper contact of the relatively impermeable and incompetent lacustrine mudstones of the Dockum Group. The Dockum mudstones contain expansive smectitic clays (Bath, 1980), which probably also provide lubrication along the lower part of the slip surface. The mudstones, which are effective aquitards, also cause ground waters to saturate overlying Dockum sandstones; as saturation increases, pore pressure increases and the strength of the rock mass is reduced. In this sense, ground water has affected the retreat of the escarpment by facilitating slumping. Where Dockum lacustrine mudstones are absent, slumping is only a minor process.

Piping is the process whereby water percolating through the subsoil erodes narrow tunnels or pipes by removing soluble or granular soil material. Examples of both large- and small-scale piping occur in many areas along the Caprock Escarpment. Large pipes commonly occur at the contact between rotational slump blocks and undisturbed strata. Large slump blocks typically have a back-tilted upper surface where precipitation and sediment are ponded. Precipitation and runoff ponded behind slump blocks partly drain along surfaces of rotation, and water movement along these surfaces erodes numerous large pipes. The pipes, sometimes called pseudokarst features, begin as sinks or closed depressions as much as 10 m (30 ft) in diameter that drain downward into single or complex passageways as much as a meter or more in diameter (fig. 27). The exits of these pipes are large caverns at the eroded bases of slump blocks and may be as much as 4 m (13 ft) high (fig. 28). Small-scale piping occurs to a lesser extent in Ogallala sediments within a few meters of the edge of the canyon. These pipes are narrow and short, rarely exceeding a few meters in length. They are usually related to erosion and transport of surface sediment through fractures in well-cemented calcrete.



FIGURE 27. Entrance to a large pipe in Caprock Canyons State Park. The pipe developed in thin-bedded Permian mudstones and sandstones that were subjected to 50 to 100 m (165 to 330 ft) of subsidence induced by dissolution of Permian salt. Most of the pipe has collapsed, leaving a 15-m- (50-ft-) long segment as a natural bridge on which the figure is standing.



FIGURE 28. Outlet for a large pipe in Palo Duro Canyon State Park. Approximately 3 × 5 m (10 × 17 ft), this pipe is located on the southwestern side of Palo Duro Canyon at the contact between Permian mudstone of the Quartermaster Group and a large mass of debris from a rotational slump. Several sinks exposed along the skyline are apparent entrances to the pipe.

Stages in the Physiographic Development of the Eastern Caprock Escarpment

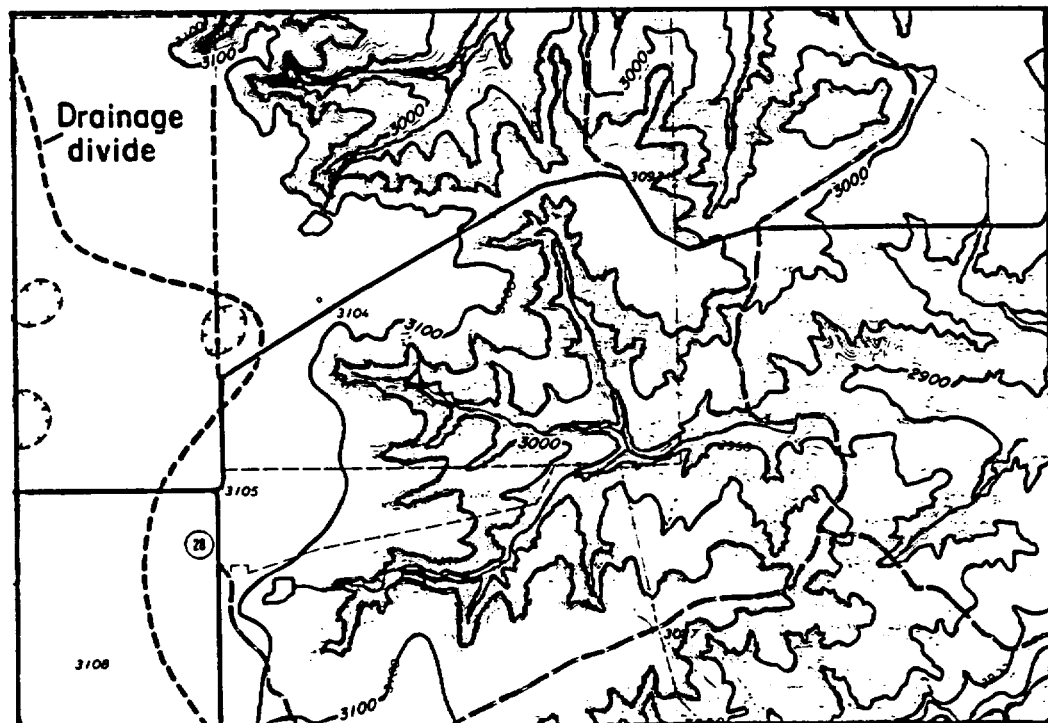
Drainage developing on most of the Eastern Caprock Escarpment is characterized by short, steep canyons with headwater tributaries arranged in a centripetal pattern (fig. 29). Higgins (1982) considered the centripetal pattern to be indicative of spring sapping. These canyons are developed in the same stratigraphic units as Luttrell Springs, Tub Springs, and Red and Capitol Peak Canyons and are morphologically similar (fig. 25). We can infer, therefore, that areas of spring sapping and pouroffs observed in the field are also present near the heads of canyons in many places along the scarp. The presence of pouroffs and springs along the scarp was confirmed by interpretation of aerial photographs. Furthermore, the headwaters of these canyons are developed in the same strata and exposed to the same climatic conditions as

the instrumentally monitored tributary canyon of Tierra Blanca Creek. Therefore, the processes that created the drainages shown in figure 29 are probably similar to those operating at the monitored canyon.

Processes of erosion by surface runoff and spring sapping that are active at the Caprock Escarpment appear to have resulted in a characteristic morphology that evolves through time. Segments of the Caprock Escarpment shown in figure 29 illustrate postulated successive stages in the development of landforms that characterize a substantial part of the Caprock Escarpment. In the initial stages (fig. 29a), drainage segments are predominantly subparallel, and areas of converging or partly centripetal drainage along the western margin of the scarp are poorly developed. Divides between areas of incipient centripetal drainage in the heads of

(c)

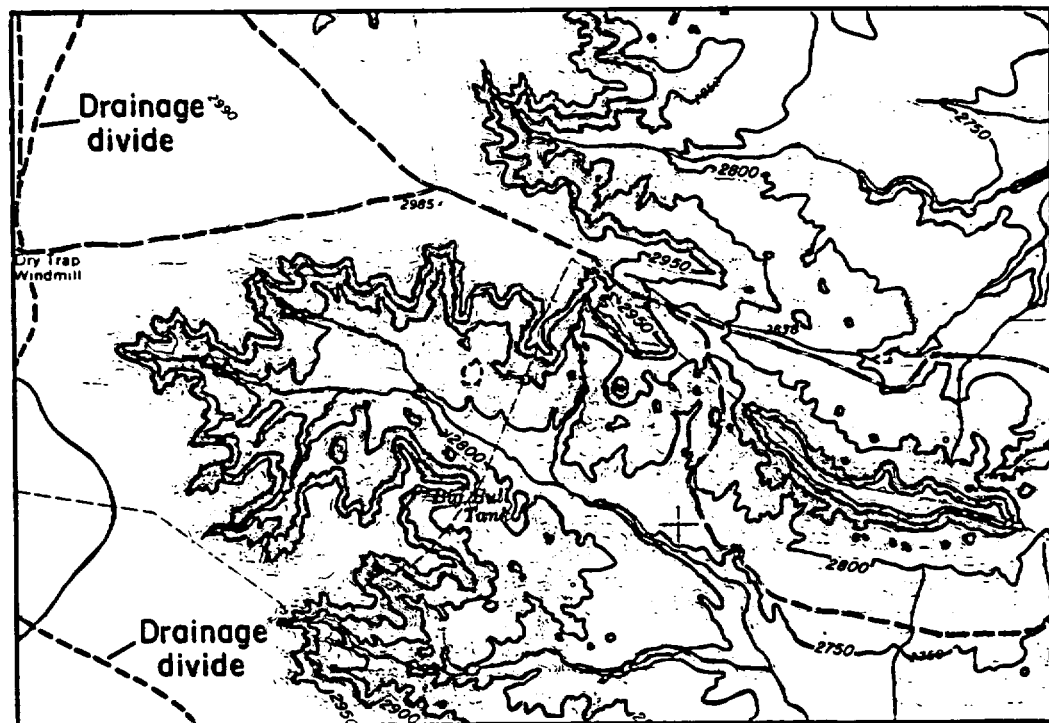
DICK MOORE CANYON QUADRANGLE



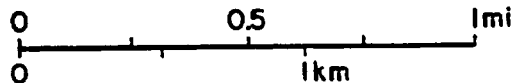
Index contour interval 100 ft

COLLETT SPRINGS QUADRANGLE

(d)



Index contour interval 50 ft



QA6608B

stages in drainage development. (d) A late stage in drainage development, where divides between areas of centripetal drainage are well established and in some instances have been separated from the Caprock Escarpment.

canyons are absent. The upper margin of the escarpment is cut by a profusion of small stream heads; on topographic maps the scarp appears to be crenulated, but regionally it is straight. Progressive drainage development leads to well-defined areas of radial drainage at the heads of steep, relatively straight canyons (fig. 29b). Ground-water flow converges at areas of radial drainage at heads of canyons, and the resulting increase in spring and seep discharge accelerates headward erosion of the canyon. The margin of the escarpment is highly crenulated, and divides between areas of radial drainage are forming. Continued headward erosion extends the area of radial drainage westward, and large divides (upland areas) consisting of remnants of

the Southern High Plains are preserved here (fig. 29c). Erosion rates on divides are lower than those in the headwaters of canyons because ground-water flow converges at the heads of the canyons, thus reducing ground-water flow to divides and also reducing the effects of spring sapping and seepage erosion along divides. Divides become elongate and, with further erosion, are reduced in width to the point of detachment from the High Plains. The last stage of development occurs when segments of divides are separated from the High Plains surface (fig. 29d). As divides between canyons are separated from the escarpment, the sequence of evolving landforms is reestablished.

Rates of Retreat of the Caprock Escarpment

Estimating the rates at which a major physiographic feature such as the Eastern Caprock Escarpment of the Southern High Plains has retreated during geologic time is at best difficult. Nevertheless, the following discussion of erosion rates reviews published surface erosion rates and offers new information on scarp-retreat rates based on rates of salt dissolution. Both surface and subsurface processes have affected escarpment retreat. Because the Caprock Escarpment closely parallels the western edge of the zone of active dissolution, both features may be retreating westward at comparable rates. If this parallelism is not merely coincidental, then the rates of westward interstratal salt dissolution reflect rates of scarp retreat.

Rates of Interstratal Salt Dissolution along the Caprock Escarpment

The average annual solute discharge of streams draining the study area was 1,376,304 t (1,513,934 tons) between 1969 and 1983, including approximately 919,455 t (1,011,400 tons) of dissolved halite and 456,818 t (502,500 tons) of dissolved gypsum (U.S. Geological Survey, 1969-1983). Dissolution of gypsum appears to be primarily a surface or near-surface phenomenon occurring on outcrop faces and along joint planes (Gustavson and others, 1982), whereas dissolution of salt is an interstratal process occurring beneath the Caprock Escarpment and Rolling Plains at depths as great as 300 m (1,000 ft) (fig. 8).

Discussions of salt dissolution rates are presented by Swenson (1974) for a part of the headwaters of the Salt Fork of the Brazos River and by Gustavson and others (1980) for all the gauged streams draining the eastern Texas Panhandle from the Canadian River on the north to the Brazos River on the south. Previous estimates of dissolution rates were based on only 3 to 9 yr of discharge data, including, in the study area,

9 yr of data for the Salt Fork of the Red River, 5 yr of data for the Prairie Dog Town Fork of the Red River, 5 yr of data for the Pease River, and 6 yr of data for the North Fork of the Wichita River. Horizontal dissolution rates for the 15 drainage basins in the eastern Texas Panhandle calculated by Gustavson and others (1980) varied by more than three orders of magnitude. To avoid some of the variability seen in earlier calculations, we analyzed solute discharge only from downstream gauging stations near the Oklahoma-Texas border, using 8 to 14 yr of water quality data (fig. 4).

Procedure for Calculating Salt Dissolution Rates

Data used to calculate horizontal rates of salt dissolution (table 5) were taken from *Water Resources for Texas* (U.S. Geological Survey, 1969-1983). Mean chloride solute load, expressed in tons, was obtained by dividing the total chloride load by the number of years of record. Richter and Kreitler (1986) have shown that in the study area brines encountered in springs and test holes were mostly derived from salt dissolution. They recognized that salt dissolution brines typically have molar Na/Cl ratios near 1 and Br/Cl and I/Cl weight ratios less than 4×10^{-4} and 1×10^{-5} , respectively. These values are significantly different from Na/Cl, Br/Cl, and I/Cl ratios of deep-basin brines. Therefore, we assume that all chloride came from dissolved bedded Permian salt, although we recognize that ground water contains approximately 30 ppm of chloride in the Ogallala aquifer and locally as much as 25,000 ppm of chloride in the Dockum aquifer. Since NaCl is 60.66 percent by weight chloride, tons of chloride were divided by 0.6066 to obtain tons of NaCl. Tons of NaCl were converted to kilograms by multiplying by 900 kg/ton. The mean volume of salt undergoing dissolution annually was obtained by dividing the mass in kilograms of salt being transported from the eastern Texas Panhandle by the density of the salt (0.002 kg/cm^3).

TABLE 5. Dissolved chloride loads for streams, calculated salt volumes, and salt dissolution rates for selected drainage basins, Texas Panhandle.

Drainage basin	Years of data	Total dissolved chloride (tons)*	Mean dissolved chloride (tons/yr)	NaCl (tons/yr)	Volume of NaCl (cm ³ /yr)	Cross-sectional area of salt (cm ²)
Salt Fork of Red River	15	129,500	8,633	14,232	5.8222×10^9	7.0371×10^9
Prairie Dog Fork of Red River	14	6,595,000	471,071	776,576	317.69×10^9	137.56×10^9
Pease River	14	1,755,700	125,400	206,726	85.57×10^9	130.73×10^9
North Fork of Wichita River	8	649,200	81,213	133,882	54.77×10^9	0.7273×10^9
Combined drainage basins	8-15	9,129,300	687,317	1,131,416	463.85×10^9	276.47×10^9
		Mean horizontal rate of dissolution (cm/yr)	Maximum annual rate of dissolution (cm/yr)	Minimum annual rate of dissolution (cm/yr)		
Salt Fork of Red River		0.82	1.69	0.21		
Prairie Dog Town Fork of Red River		2.33	3.97	1.35		
Pease River		0.65	1.06	0.37		
North Fork of Wichita River		75.31	90.60	60.12		
Combined drainage basins		1.68	—	—		

* U.S. Geological Survey (1969-1983); values in English units.

The area of the salt surface undergoing dissolution was estimated from salt-thickness maps of all four salt-bearing formations (Salado, Seven Rivers, San Andres, and Glorieta Formations) (fig. 30). Each line was segmented in lengths of equal thickness of salt, and, using a map wheel, the length of each thickness segment was measured and multiplied by the average thickness of salt along the line to obtain the cross-sectional area of salt. Salt thicknesses along the line were interpreted from geophysical logs. The total cross-sectional area of salt in the study area is the sum of the area along each of the contours crossing a given drainage basin.

The horizontal rate of dissolution is the mean volume of salt discharged per year divided by the total cross-sectional area of salt in the drainage basin (table 5). Maximum and minimum rates were determined by taking the highest and lowest annual chloride loads for the years of data available and performing the same calculations (table 5).

Salt Dissolution Rates

Dissolution rates determined for this report differ only slightly from dissolution rates for the same drainage basins determined by Gustavson and others (1980). For example, Gustavson and others (1980) calculated a dissolution rate of 2.59 cm/yr (1.02 inches/yr) for the drainage basin of the Prairie Dog Town Fork of the Red River for the years 1969 to 1977, whereas the dissolution rate that we calculated for the same area for 1969 to 1982 is 2.33 cm/yr (0.92 inch/yr). Current dissolution rates range from 0.82 cm/yr (0.32 inch/yr) for the Salt Fork of the Red River to 75.31 cm/yr (29.6 inches/yr) for the North Wichita River. The mean interstratal dissolution rate for salts in the study area is 1.68 cm/yr (0.66 inch/yr), close to the 2.33-cm/yr (0.92-inch/yr) dissolution rate for the drainage basin of the Prairie Dog Town Fork of the Red River, the largest drainage basin in the study area.

These dissolution rates are conservative estimates because they are based only on solute loads carried by

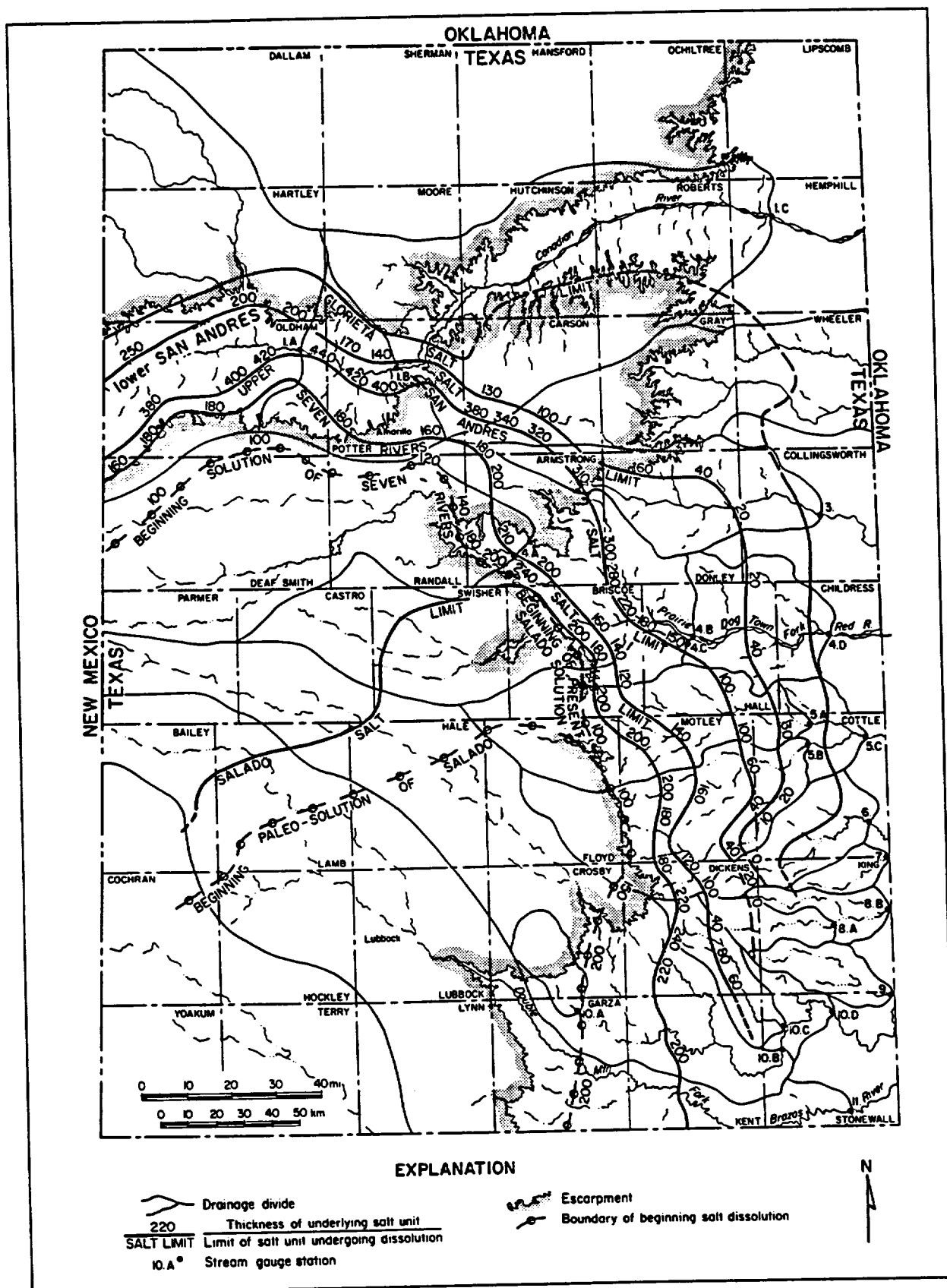


FIGURE 30. Drainage basins and gauging stations in the Rolling Plains. Salt thicknesses are shown for the Salado, Seven Rivers, upper and lower San Andres, and Glorieta Formations at the eastern and northern limits of the next stratigraphically higher salt unit (from Gustavson and others, 1980, their fig. 29).

surface waters. No data on solute load or discharge are available for ground water discharging out of this region, although numerical simulations suggest that ground-water discharge on the Rolling Plains could account for all flow out of the system. Furthermore, these dissolution rates are determined for a climate that was probably both warmer and drier than the Quaternary glacial episodes (Caran, 1984); both discharge and solute load were presumably higher during glacial periods. Although spring discharge has decreased substantially since the onset of irrigation on the High Plains, no corresponding decrease in stream discharge is evident. This probably results from the fact that most gauging stations on streams draining the escarpment lie approximately 60 to 100 km (40 to 60 mi) east of the escarpment, and any change in spring discharge along the escarpment is likely to be masked by surface runoff.

If the alignment between the Caprock Escarpment and zones of salt dissolution and subsidence (figs. 10 through 12) is not coincidental, then the rate of regional mean dissolution of Permian bedded salt should be similar to the rate of scarp retreat, at least during the late Quaternary.

Surface Erosion Rates

The following discussion of estimates of long-term erosion rates for the Caprock Escarpment presupposes a series of critical assumptions, each of which could strongly affect the magnitude of the estimated rates. For example, effects of climatic cycles are not considered here because the number, duration, and intensity of cyclic climatic changes in the region are unknown. Rainfall and stream and spring discharge probably varied in the past with climatic cycles, thus affecting erosion rates. Furthermore, the original eastward extent of the High Plains and Ogallala Formation is assumed to have been approximately 320 km (200 mi) east of the present Caprock Escarpment on the basis of projections of the High Plains surface (according to Gustavson and others [1981], who reviewed the various published projections of the High Plains surface).

Salt dissolution and subsidence were active during deposition of lower Ogallala sediments (Schultz, 1977), and the extensive deformation of Permian and younger strata in the Rolling Plains indicates that these processes were probably active throughout the late Tertiary and Quaternary. Ogallala sediments that originally overlaid the Rolling Plains were also at least partly water saturated, and therefore spring sapping and seepage erosion occurred along dissected margins of the Ogallala much as they do today. Consequently, processes affecting the Caprock Escarpment during the late Tertiary and Quaternary were probably similar to processes operating today.

Three time periods were examined to analyze the westerly retreat of the Caprock Escarpment: (1) from about 9,500 yr ago, when a Holocene terrace was

deposited along Holmes Creek at the foot of the escarpment, to the present, (2) from about 620,000 yr ago, after deposition of the Seymour Formation, to the present, and (3) from about 3,000,000 to 5,000,000 yr ago, from the end of deposition of the Ogallala Formation, to the present (Gustavson and others, 1981; Simpkins and Baumgardner, 1982). In addition, semi-annual measurements of erosion pins and headcuts in streams draining the escarpment at selected sites record short-term erosion and deposition rates (Simpkins and Gustavson, 1987).

Holmes Creek in Briscoe County, Texas, has headwaters in the Caprock Escarpment and has incised its valley approximately 12.5 m (41 ft) during the last $8,010 \pm 110$ to $9,360 \pm 170$ radiocarbon yr. The 12.5-m-deep incision equals the difference in elevation between the dated horizon (Harrison and Killen, 1978) and the present stream floor. If the longitudinal profile of the stream has not changed substantially over the last 7,900 to 9,500 yr, an incision of 12.5 m (41 ft) would have been accompanied by approximately 1.1 km (0.7 mi) of scarp retreat. This is equivalent to a retreat rate ranging from 0.12 to 0.14 km/1,000 yr (0.08 to 0.09 mi/1,000 yr). Because 12.5 m is the maximum incision that could have occurred within 7,900 to 9,500 yr, the retreat rate is also a maximum estimate.

The Seymour Formation comprises sediments thought to have been derived from the Ogallala Formation at a time when the Caprock Escarpment was just west of the present western limit of the Seymour deposits (Meinzer and Slaughter, 1971). The presence of Lava Creek B Ash (Izett and Wilcox, 1982) in the upper part of the Seymour indicates that most of the silts, sands, and gravels were deposited more than 620,000 yr ago. If the eastern limit of the Ogallala Formation (Caprock Escarpment) was immediately west of the Seymour Formation at the time of its deposition, then the scarp has retreated approximately 114 km (71 mi) since the end of Seymour deposition (Simpkins and Baumgardner, 1982). An escarpment retreat rate of 114 km in 620,000 yr is equivalent to a maximum rate of approximately 0.18 km/1,000 yr (0.11 mi/1,000 yr).

Lava Creek B Ash is also exposed along Duck Creek in Kent County, Texas, approximately 45 km (28.1 mi) southeast of the Caprock Escarpment. Although the context in which the ash was deposited is unknown, deposition was on the Rolling Plains; thus, the Caprock Escarpment lay to the west of the ash bed. In this case, assuming that the escarpment was immediately west of the ash when it was deposited, the maximum scarp retreat rate was approximately 0.07 km/1,000 yr (0.04 mi/1,000 yr).

Several authors have estimated the former easternmost extent of the Ogallala Formation (Harris, 1970; Byrd, 1971; Meinzer and Slaughter, 1971; Thomas, 1972; Gustavson and others, 1980; Osterkamp and Wood, 1984), and on the basis of these projections the Caprock Escarpment seems to have retreated as much as 320 km (200 mi) since deposition of the Ogallala Formation ended. Gustavson and others (1980, 1981)

stated that the end of Ogallala deposition was approximately 3 Ma ago; however, Schultz (1977) and Winkler (1985) suggested that deposition may have ended as early as 5 Ma ago. Clearly, timing of the end of Ogallala deposition is not well constrained, but the 3-Ma age estimated by Gustavson and others (1981) is probably too young. To complicate matters further, the upper eolian part of the Ogallala and the Ogallala caliche caprock in the present area of the High Plains could have been deposited at the same time that the eastern margin of the Ogallala was undergoing erosion. Nevertheless, if we estimate that Ogallala deposition ended 5 Ma ago, we can say that the rate of Caprock Escarpment retreat since then has been approximately 0.06 km/1,000 yr (0.4 mi/1,000 yr).

Measurements of erosion pins and stream headcuts were made at least biannually since 1978 at selected sites along the Caprock Escarpment (Simpkins and Gustavson, 1987). These sites, however, were chosen because they appeared to be actively eroding. Erosion rates were monitored on a variety of slopes, vegetative cover, and substrate textures. Analyses of these data have yielded, for example, mean vertical erosion rates

for slopes of approximately 30° that ranged from 0.4 to 0.6 cm/yr (0.16 to 0.24 inch/yr). These vertical erosion rates probably correspond to a horizontal slope retreat rate of 1 cm/yr, or 0.01 km/1,000 yr (0.4 inch/yr, or 0.006 mi/1,000 yr). Retreat rates of headcuts along stream thalwegs ranged from 0.8 to 1.7 cm/yr (0.3 to 0.7 inch/yr).

Rates of scarp retreat calculated from estimates of the former position of the Caprock Escarpment range from 0.06 to 0.18 km/1,000 yr (0.04 to 0.11 mi/1,000 yr). Retreat rates based on short-term measurements of slope erosion and headcut retreat are about 0.01 to 0.02 km/1,000 yr (0.006 to 0.012 mi/1,000 yr). Subsurface interstratal dissolution rates are minimum rates and average nearly 0.02 km/1,000 yr (0.013 mi/1,000 yr). Even though escarpment retreat rates calculated by these different methods exhibit some variation, these rates differ only by one order of magnitude. This suggests that westward scarp retreat and westward expansion of the dissolution zone throughout the late Cenozoic was about 0.01 to 0.20 km/1,000 yr (0.006 to 0.12 mi/1,000 yr).

Effect of Diminished Spring Discharge on Geomorphic Processes

The discharge of most springs from the base of the Ogallala Formation or from the base of sandstones of the Dockum Group along the Eastern Caprock Escarpment has decreased substantially during the last 50 yr (fig. 4, table 6). From 1900 to 1978, spring discharge decreased as much as 98 to 100 percent, averaging a drop in discharge of 86 percent. Only two springs (Roaring Springs and Wolf Springs) increased discharge. All measurements were made at about the same time of year, and therefore the possibility of discharge variation due to seasonal climatic fluctuations was minimized. Ground-water pumpage has substantially reduced the saturated thickness of the Ogallala aquifer since the beginning of this century, when irrigation began in the Southern High Plains (Knowles and others, 1982). Consequently, decreases in spring discharge probably resulted from ground-water pumpage (Brune, 1981; Gustavson, 1983).

Although diminished discharge is clearly established for springs emitting ground water from the Ogallala aquifer, no comparable data are available for springs emitting ground water from the lower Dockum

Group aquifer. However, because pumping the Ogallala aquifer decreases the vertical head gradient between the Ogallala and lower Dockum and because the Ogallala is the source of recharge to the Dockum (Dutton and Simpkins, 1986), we speculate that leakage and hence recharge to the lower Dockum aquifer have also decreased. Consequently, spring discharge from the Dockum aquifer at the Caprock Escarpment has probably decreased since irrigation was introduced in the Southern High Plains.

Sapping and other geomorphic processes associated with spring discharge along the Caprock Escarpment are demonstrably important in scarp retreat. However, with pumping of large volumes of water from the Ogallala aquifer, spring discharge has decreased to a trickle in most areas. With continued mining of this aquifer, spring discharge may cease and the rate of scarp retreat will be reduced. Partly counterbalancing these effects are land-use practices in the region, including cultivation, overgrazing, and road building, which have probably exacerbated erosion (Machenberg, 1986).

TABLE 6. Spring discharge rates, Eastern Caprock Escarpment, Texas Panhandle (from Brune, 1981). Figure 4 shows distribution of springs along the Eastern Caprock Escarpment (1 liter = 0.26 gal).

County	Spring name	Discharge (L/s)		Discharge (L/s)	
Potter	Cedar Springs	0.79	(1937)	dry	(1978)
	Tecovas Springs	32.00	(1881)	2.50	(1978)
Randall	CCC Springs	0.38	(1937)	0.05	(1978)
Armstrong	Salt Fork Springs	8.80	(1940)	0.65	(1978)
	Baker Springs	0.31	(1940)	seep	(1978)
	Pleasant Springs	9.50	(1940)	1.20	(1978)
	Country Road Springs	0.19	(1940)	dry	(1978)
	Harrell Springs	0.63	(1940)	dry	(1978)
	Dripping Springs	0.95	(1940)	seep	(1978)
	Luttrell Springs	0.44	(1940)	seep	(1978)
	Dry Creek Springs	0.63	(1940)	seep	(1978)
Donley	Dunbar Springs	19.00	(1968)	13.00	(1978)
	Cottonwood Springs	15.00	(1968)	7.50	(1978)
	Luttrell Springs	14.00	(1968)	1.30	(1978)
	Chamberlain Springs	13.00	(1968)	1.60	(1978)
	Eagle Springs	11.00	(1968)	seep	(1978)
	Buck Springs	0.32	(1943)	dry	(1978)
	Parker Springs	0.32	(1932)	seep	(1978)
	Highway Springs	0.13	(1943)	seep	(1978)
	Browder Springs	12.00	(1968)	0.09	(1978)
	Broome Springs	1.60	(1943)	seep	(1943)
	Indian Springs	0.83	(1943)	0.20	(1978)
	Bitter Creek Springs	50.00	(1968)	3.70	(1978)
	West Bitter Creek Springs	10.00	(1967)	0.52	(1978)
	Sandy Springs	3.80	(1968)	dry	(1978)
Swisher	Rogers Springs	0.32	(1943)	seep	(1978)
Briscoe	Deer Springs	19.00	(1946)	1.30	(1978)
	Turkey Springs	25.00	(1946)	2.50	(1978)
	Cedar Springs	16.00	(1946)	1.00	(1978)
	Martin Springs	0.95	(1969)	0.12	(1978)
	Gyp Springs	6.70	(1969)	0.12	(1978)
	Haynes Springs	2.50	(1969)	0.35	(1978)
	Las Lenguas Springs	19.00	(1967)	1.90	(1978)
Floyd	Blue Hole Springs	14.00	(1968)	dry	(1978)
	Bain Springs	6.70	(1938)	dry	(1978)
Motley	Ballard Springs	0.95	(1938)	0.85	(1978)
	Willow Springs	1.50	(1938)	0.95	(1979)
	Mott Camp Springs	0.63	(1938)	dry	(1978)
	Burleson Springs	8.80	(1938)	dry	(1978)
	Roaring Springs	31.00	(1938)	40.00	(1978)
	Wolf Springs	1.90	(1938)	7.10	(1978)

Summary and Conclusions

The Caprock Escarpment developed and is maintained by the interaction of surface and near-surface erosional processes, such as slumping, spring sapping, piping, sheetflood, sheet wash, channel flow, rockfalls, and the subsurface processes of salt dissolution and subsidence. Ground water provides the impetus for slumping, spring sapping, piping, and salt dissolution.

Interpretation of geophysical logs, core, and outcrops indicates that a cumulative thickness of as much as 230 m (750 ft) of bedded Permian salt has dissolved from beneath the Rolling Plains and Caprock Escarpment. Furthermore, high solute loads in local streams indicate that dissolution is an active process and that as much as $15,000,000 \text{ m}^3$ ($525,000,000 \text{ ft}^3$) of salt was carried out of the study area by surface streams between 1969 and 1983. Subsidence resulting from dissolution is locally expressed along the escarpment as clastic dikes, minor folds, extension fractures filled with fibrous gypsum, and a change in the regional southwesterly dip of the Alibates Formation to an easterly or northeasterly dip beneath the escarpment. Dissolution-induced subsidence beneath the Caprock Escarpment may account for as much as 75 m (250 ft) of escarpment relief. Dissolution and subsidence locally extend westward from the Caprock Escarpment and occur locally beneath the Southern High Plains, as evidenced by thinning of Salado and Seven Rivers salts and by deformation of the Alibates Formation in this region. The valleys of Mulberry Creek, Prairie Dog Town Fork of the Red River, Tule Creek, the White River, and Double Mountain Fork of the Brazos River (all reentrants along the escarpment) contain lacustrine sediments in small structural basins that probably formed by salt dissolution and subsidence.

Downward leakage of low-salinity ground water from the High Plains aquifer to underlying Permian salt is partly controlled by fractures and steep head gradients at the Caprock Escarpment. Stream segments and subsidence basins on the Rolling Plains tend to parallel fracture orientations, suggesting that dissolution was enhanced along fractures. Clastic dikes deep within the Ogallala Formation are filled with sediment washed in from the overlying Blackwater Draw Formation, indicating ground-water flow through open fractures.

The interpretation that low-salinity ground water moves downward from the High Plains aquifer to the salt beds is also supported by a numerical model that simulates two-dimensional ground-water flow through strata that underlie the High Plains, Caprock Escarpment, and Rolling Plains (Simpkins and Fogg, 1982). The model illustrates (1) downward flow of fresh, low-salinity ground water from the Ogallala aquifer into the salt dissolution zone at the Caprock Escarpment; (2) eastward movement of the resultant brines through transmissive dolomite/anhydrite beds of the Seven Rivers and San Andres Formations; and (3) discharge of the brines into saline springs at outcrops of those

transmissive units in topographically low areas of the Rolling Plains. Saline springs occur in outcrops of the Seven Rivers and San Andres Formations.

High-intensity convective storms supply most of the rainfall to the High Plains surface. Sheetfloods transport rainwater that falls on the eastern margin of the High Plains to the Caprock Escarpment, and sheet wash and rill wash scour the escarpment surface. Sheetfloods with flow depths of as much as 10 cm (4 inches) have little erosional effect on the High Plains surface. Climate and erosion rates were monitored in a deeply incised tributary of Tierra Blanca Creek, a stream that is developed in the same strata as the upper part of the Caprock Escarpment and is subject to the same weather conditions as the escarpment. As a result of a storm on May 28, 1978, which yielded 7.1 cm (2.8 inches) of rain in 3.2 hr, slopes in the Blackwater Draw and Ogallala Formations, the upper units of the escarpment, were eroded an average of 2.2 cm (0.87 inch) by sheet wash and rill wash. A storm of similar intensity on June 10, 1984, resulted in comparable erosion. Analyses of erosion and weather data collected continuously since 1979 suggest that erosion and transportation of sediment from first-order streams in the Caprock Escarpment occur in a series of incremental steps. The three-step process involves (1) rainfall events of intensities less than approximately 6.0 cm/hr (2.4 inches/hr) that move sediment on slopes and alluvial surfaces of first-order streams, although the sediment is stored locally; (2) intense rainfalls (more than 6.0 cm/hr [2.4 inches/hr]) that result in erosion of hillslopes, erosion and accretion on the floor of first-order streams, and deposition of sediment in the valleys of second-order streams; (3) storms capable of eroding the channels of second-order streams. Storms of step 3 magnitude, however, were not recorded during the study period.

Spring sapping occurs primarily on the floors and slopes of canyons below outcrops of basal sands and gravels of the Ogallala Formation and below fluvial sandstones of the Dockum Group. It undermines resistant overlying sandstones and initiates rockfalls. Mass wasting contributes to escarpment retreat; at least 100 large slumps are recognizable in the Palo Duro Canyon. The lower part of the planes of rotation of many of these features are within or at the upper contact of lacustrine mudstones in the Dockum Group. Smectitic clays in these mudstones probably provided lubrication for the movement of slump blocks. Along the slip planes of these slump blocks, large pipes have developed. Physical disruption of sediments by slumping has accelerated erosion on the escarpment slopes.

The Caprock Escarpment overlies and is roughly parallel to the western edge of the salt dissolution zone, suggesting that the rate of retreat of the Caprock Escarpment and the rate of westerly advance of the salt dissolution zone are similar. Rates of salt dissolution and scarp retreat have been calculated by several

methods and range from 0.01 to 0.20 km/1,000 yr (0.006 to 0.13 mi/1,000 yr). An average dissolution rate was obtained by dividing the annual volume of salt discharged by streams draining the study region by the cross-sectional area of underlying salts. The rate of retreat is approximately 0.2 cm/yr, or 0.02 km/1,000 yr (0.8 inch/yr, or 0.013 mi/1,000 yr)—probably a minimum rate because we did not consider the salt that may leave the study area by means other than stream discharge. The rate of scarp retreat derived from long-term monitoring of hillslope erosion is approximately 0.01 km/1,000 yr (0.006 mi/1,000 yr) under current climatic conditions. Average scarp retreat rates based

on projected former positions of the Caprock Escarpment range from 0.06 to 0.18 km/1,000 yr (0.04 to 0.11 mi/1,000 yr).

Spring discharge in the Caprock Escarpment has decreased substantially in the past 50 yr. Springs that formerly discharged nearly 10 L/s (2.2 gal/s) now discharge barely 1 L/s (0.2 gal/s). Reduction in spring discharge has coincided with and is apparently the result of extensive pumping of the Ogallala aquifer for irrigation water. Reduction of spring discharge is likely to reduce the effectiveness of spring sapping as a process in the erosion of the Caprock Escarpment.

Acknowledgments

This research was funded by the U.S. Department of Energy Salt Repository Project Office under contract no. DE-AC97-83WM46651, T. C. Gustavson and C. W. Kreidler, principal investigators. The conclusions of the authors are not necessarily endorsed or approved by the Department of Energy. Ann D. Hoadley and Julieann Mahler helped compile dissolution-rate data. Special thanks go to Graham Fogg for his help in implementing the numerical model of flow beneath the Caprock Escarpment.

Figures for this report were prepared by Annie Kubert-Kearns under the supervision of Richard L. Dillon. Word processing was by Dottie Johnson and typesetting was by Susan Lloyd under the supervision of Lucille C. Harrell and Susann Doenges. Vance Holliday, Waite Osterkamp, Jay Raney, and Robert W. Baumgardner, Jr., reviewed the report. Technical editing was by Tucker Hentz. Their comments and criticisms are appreciated. Duran Dodson edited and Jamie S. Haynes designed this publication; Lana Dieterich coordinated its production.

References

- Baker, C. L., 1915, Geology and underground waters of the northern Llano Estacado: Austin, University of Texas Bulletin 57, 225 p.
- Bassett, R. L., Bentley, M. E., and Simpkins, W. W., 1981, Regional ground-water flow in the Panhandle of Texas: a conceptual model: in Gustavson, T. C., and others, Geology and geohydrology of the Palo Duro Basin, Texas Panhandle, a report on the progress of nuclear waste isolation feasibility studies (1980): The University of Texas at Austin, Bureau of Economic Geology Geological Circular 81-3, p. 102-107.
- Bath, W. W., 1980, Geomorphic processes at Palo Duro Canyon, Texas Panhandle: The University of Texas at Austin, Master's thesis, 150 p.
- Boyd, S. D., and Murphy, P. J., 1984, Origin of the Salado, Seven Rivers, and San Andres salt margins in Texas and New Mexico: Columbus, OH, report prepared by Stone and Webster Engineering Corporation for U.S. Department of Energy, Office of Nuclear Waste Isolation, Battelle Memorial Institute, ONWI/SUB/84/E512-05000-T27, 41 p.
- Brune, Gunnar, 1981, Springs of Texas, vol. I: Fort Worth, Texas, Branch-Smith, 566 p.
- Budnik, R. T., 1984, Structural geology and tectonic history of the Palo Duro Basin, Texas Panhandle: The University of Texas at Austin, Bureau of Economic Geology, Open-File Report OF-WTWI-1984-55, 33 p.
- Byrd, C. L., 1971, Origin and history of the Uvalde gravel of Central Texas: Baylor University, Baylor Geological Studies Bulletin, no. 20, 43 p.
- Caran, S. C., 1984, Reconstruction of the Late Quaternary paleoclimate of northwestern Texas—progress report, 1984: The University of Texas at Austin, Bureau of Economic Geology, Open-File Report OF-WTWI-1984-53, 11 p.
- Caran, S. C., Baumgardner, R. W., Jr., McGookey, D. A., Gustavson, T. C., and Neck, R. W., 1985, Quaternary stratigraphy of the western Rolling Plains of Texas—preliminary findings: The University of Texas at Austin, Bureau of Economic Geology, Open-File Report OF-WTWI-1985-14, 26 p.
- Collins, E. W., 1983, Joint density of Permian strata at Caprock Canyons State Park, Texas Panhandle, in Gustavson, T. C., and others, Geology and geohydrology of the Palo Duro Basin, Texas Panhandle, a report on the progress of nuclear waste isolation feasibility studies (1982): The University of Texas at Austin, Bureau of Economic Geology Geological Circular 83-4, p. 36-39.
- 1984, Styles of deformation in Permian strata, Texas Panhandle: The University of Texas at Austin, Bureau of Economic Geology Geological Circular 84-4, 32 p.

- Collins, E. W., and Luneau, B. A., 1986, Fracture analyses of the Palo Duro Basin area, Texas Panhandle and eastern New Mexico: The University of Texas at Austin, Bureau of Economic Geology Geological Circular 86-6, 39 p.
- DeConto, R. T., and Murphy, P. J., 1986, Dissolution of the upper Seven Rivers and Salado salt in the interior Palo Duro Basin, Texas: Columbus, OH, report prepared by Stone and Webster Engineering Corporation for U.S. Department of Energy, Office of Nuclear Waste Isolation, Battelle Memorial Institute, ONWI/SUB/86/05000-T45, 177 p.
- Dutton, A. R., 1983, Regional ground-water flow system of the San Andres Formation, West Texas and eastern New Mexico, in Gustavson, T. C., and others, Geology and geohydrology of the Palo Duro Basin, Texas Panhandle, a report on the progress of nuclear waste isolation feasibility studies (1982): The University of Texas at Austin, Bureau of Economic Geology Geological Circular 83-4, p. 97-101.
- 1987, Hydrogeologic and hydrochemical properties of salt-dissolution zones, Palo Duro Basin, Texas Panhandle—preliminary assessment: The University of Texas at Austin, Bureau of Economic Geology Geological Circular 87-2, 32 p.
- Dutton, A. R., and Orr, E. D., 1986, Hydrogeology and hydrochemical facies of the San Andres Formation in eastern New Mexico and the Texas Panhandle: The University of Texas at Austin, Bureau of Economic Geology Report of Investigations No. 157, 58 p.
- Dutton, A. R., and Simpkins, W. W., 1986, Hydrogeochemistry and water resources of the Triassic lower Dockum Group in the Texas Panhandle and eastern New Mexico: The University of Texas at Austin, Bureau of Economic Geology Report of Investigations No. 161, 51 p.
- Dutton, S. P., Finley, R. J., Galloway, W. E., Gustavson, T. C., Handford, C. R., and Presley, M. W., 1979, Geology and geohydrology of the Palo Duro Basin, Texas Panhandle, a report on the progress of nuclear waste isolation feasibility studies (1978): The University of Texas at Austin, Bureau of Economic Geology Geological Circular 79-1, 99 p.
- Eifler, G. K., Jr., 1967, Lubbock sheet: The University of Texas at Austin, Bureau of Economic Geology Geologic Atlas of Texas, scale 1:250,000.
- 1968, Plainview sheet: The University of Texas at Austin, Bureau of Economic Geology Geologic Atlas of Texas, scale 1:250,000.
- 1969, Amarillo sheet: The University of Texas at Austin, Bureau of Economic Geology Geologic Atlas of Texas, scale 1:250,000.
- Evans, G. L., and Meade, G. E., 1944, Quaternary of the Texas High Plains, in Contributions to Geology, 1944: Austin, University of Texas Publication 4401, p. 485-507.
- Fink, B. E., 1963, Ground-water potential of the northern part of the Southern High Plains of Texas: High Plains Underground Water Conservation District No. 1, report no. 163, 76 p.
- Finley, R. J., and Gustavson, T. C., 1980, Climatic controls on erosion in the Rolling Plains along the Caprock Escarpment of the Texas Panhandle: The University of Texas at Austin, Bureau of Economic Geology Geological Circular 80-11, 50 p.
- 1981, Lineament analysis based on Landsat imagery, Texas Panhandle: The University of Texas at Austin, Bureau of Economic Geology Geological Circular 81-5, 37 p.
- 1983, Geomorphic effects of a 10-year storm on a small drainage basin in the Texas Panhandle: Earth Surface Processes and Landforms, v. 8, p. 63-77.
- Fracasso, M. A., and Hovorka, S. D., 1987, Cyclicity in the middle Permian San Andres Formation, Palo Duro Basin, Texas Panhandle: The University of Texas at Austin, Bureau of Economic Geology Report of Investigations No. 156, 48 p.
- Freeze, R. A., and Cherry, J. A., 1979, Groundwater: Englewood Cliffs, New Jersey, Prentice-Hall, 604 p.
- Gable, D. J., and Hatton, T., 1983, Maps of vertical crustal movements in the coterminous United States over the last 10 million years: U.S. Geological Survey, Miscellaneous Investigations Map I-1315.
- Gerster, Georg, 1976, Grand design: New York, Paddington Press, 312 p.
- Goldstein, A. G., 1982, Brittle deformation associated with salt dissolution, Palo Duro Basin, in Gustavson, T. C., and others, Geology and geohydrology of the Palo Duro Basin, Texas Panhandle, a report on the progress of nuclear waste isolation feasibility studies (1981): The University of Texas at Austin, Bureau of Economic Geology Geological Circular 82-7, p. 18-27.
- Goldstein, A. G., and Collins, E. W., 1984, Deformation of Permian strata overlying a zone of salt dissolution and collapse in the Texas Panhandle: Geology, v. 12, p. 314-317.
- Granata, G. E., 1981, Regional sedimentation of the Late Triassic Dockum Group, West Texas and eastern New Mexico: The University of Texas at Austin, Master's thesis, 147 p.
- Gregory, H. E., 1917, Geology of the Navajo country: U.S. Geological Survey Professional Paper 93, 161 p.
- Gustavson, T. C., 1983, Diminished spring discharge: its effect on erosion rates in the Texas Panhandle: in Gustavson, T. C., and others, Geology and geohydrology of the Palo Duro Basin, Texas Panhandle, a report on the progress of nuclear waste isolation feasibility studies (1982): The University of Texas at Austin, Bureau of Economic Geology Geological Circular 83-4, p. 128-132.
- 1986a, Geomorphic development of the Canadian River valley, Texas Panhandle: Geological Society of America Bulletin, v. 97, p. 459-472.

- ed., 1986b, *Geomorphology and Quaternary stratigraphy of the Rolling Plains, Texas Panhandle: The University of Texas at Austin, Bureau of Economic Geology Guidebook 22*, 97 p.
- 1988, Origin of Plio-Pleistocene lake basins, Deaf Smith and Randall Counties, Texas Panhandle (abs): *Geological Society of America Abstracts with Programs*, v. 20, p. 101.
- Gustavson, T. C., and Budnik, R. T., 1985, Structural influences on geomorphic processes and physiographic features, Texas Panhandle: technical issues in the siting of a nuclear waste repository: *Geology*, v. 13, p. 173-176.
- Gustavson, T. C., and Finley, R. J., 1985, Late Cenozoic geomorphic evolution of the Texas Panhandle and northeastern New Mexico—case studies of structural controls on regional drainage development: *The University of Texas at Austin, Bureau of Economic Geology Report of Investigations No. 148*, 42 p.
- Gustavson, T. C., Finley, R. J., and Baumgardner, R. W., Jr., 1981, Retreat of the Caprock Escarpment and denudation of the Rolling Plains in the Texas Panhandle: *Association of Engineering Geologists Bulletin*, v. 18, p. 413-422.
- Gustavson, T. C., Finley, R. J., and McGillis, K. A., 1980, Regional dissolution of Permian salt in the Anadarko, Dalhart, and Palo Duro Basins of the Texas Panhandle: *The University of Texas at Austin, Bureau of Economic Geology Report of Investigations No. 106*, 40 p.
- Gustavson, T. C., and Holliday, V. T., 1985, Depositional architecture of the Quaternary Blackwater Draw and Tertiary Ogallala Formations, Texas Panhandle and eastern New Mexico: *The University of Texas at Austin, Bureau of Economic Geology Open-File Report OF-WTWI-1985-23*, 60 p.
- Gustavson, T. C., Simpkins, W. W., Alhades, A. B., and Hoadley, A. D., 1982, Evaporite dissolution and development of karst features on the Rolling Plains of the Texas Panhandle: *Journal of Earth Surface Processes and Landforms*, v. 7, p. 545-563.
- Gustavson, T. C., and Winkler, D. A., 1988, Depositional facies of the Miocene-Pliocene Ogallala Formation, Texas Panhandle and eastern New Mexico: *Geology*, v. 16, p. 203-206.
- Handford, C. R., and Dutton, S. P., 1980, Pennsylvanian-early Permian depositional systems and shelf margin evolution, Palo Duro Basin, Texas: *American Association of Petroleum Geologists Bulletin*, v. 64, p. 88-106.
- Harris, S. A., 1970, Bends in the South Canadian River: *Shale Shaker*, v. 20, p. 80-84.
- Harrison, B. R., and Killen, K. L., 1978, Lake Theo: a stratified, early man bison butchering and camp site, Briscoe County, Texas, archeological investigations phase II: Canyon, Panhandle-Plains Historical Museum, Special Archeological Report I, 108 p.
- Higgins, C. G., 1982, Drainage systems developed on Earth and Mars: *Geology*, v. 10, p. 147-152.
- 1983, Reply to comments on 'Drainage systems developed on Earth and Mars': *Geology*, v. 11, p. 55-56.
- Hovorka, S. D., Luneau, B. A., and Thomas, S., 1985, Stratigraphy of bedded halite in the Permian San Andres Formation, units 4 and 5, Palo Duro Basin, Texas: *The University of Texas at Austin, Bureau of Economic Geology Open-File Report OF-WTWI-1985-9*, 67 p.
- Izett, G. A., and Wilcox, W. A., 1982, Map showing localities and inferred distributions of Huckleberry Ridge, Mesa Falls, and Lava Creek ash beds (Pearlette family of ash beds) of Pliocene and Pleistocene age in western United States and southern Canada: *U.S. Geological Survey, Miscellaneous Investigations Map I-1325*.
- Johnson, K. S., 1976, Evaluation of Permian salt deposits in the Texas Panhandle and western Oklahoma for underground storage of radioactive wastes: Oak Ridge, Tennessee, Oak Ridge National Laboratories, report to Union Carbide Corporation, 73 p.
- 1981, Dissolution of salt on the east flank of the Permian Basin in the southwestern U.S.A.: *Journal of Hydrology*, v. 54, p. 75-93.
- Kier, R. S., Garner, L. E., and Brown, L. F., Jr., 1977, Land resources of Texas: *The University of Texas at Austin, Bureau of Economic Geology Special Report*, 42 p.
- Knowles, T., Nordstrom, P., and Klemm, W. B., 1982, Evaluating the ground-water resources of the High Plains of Texas: *Texas Department of Water Resources, LP 173*, 2 v.
- Kreitler, C. W., Fisher, R. S., Senger, R. K., Hovorka, S. D., and Dutton, A. R., 1985, Hydrogeology of rocks of low permeability, in *Hydrology of an evaporite aquitard: Permian evaporite strata, Palo Duro Basin, Texas: International Association of Hydrologists, Memoirs*, v. 18, part 1, p. 150-168.
- Linsley, R. K., Jr., Kohler, M. A., and Paulhus, J. L., 1949, *Applied hydrology*: New York, McGraw-Hill, p. 59-125.
- Machel, H. G., 1985, Fibrous gypsum and fibrous anhydrite in veins: *Sedimentology*, v. 32, p. 443-454.
- Machenberg, M. D., 1986, Eolian deflation and deposition, Texas Panhandle, in Gustavson, T. C., ed., *Geomorphology and Quaternary stratigraphy of the Texas Panhandle: The University of Texas at Austin, Bureau of Economic Geology Guidebook 22*, 97 p.
- Machenberg, M. D., DuBar, J. R., Gustavson, T. C., and Holliday, V. T., 1985, A depositional model for post-Ogallala sediments on the Southern High Plains (abs): *Geological Society of America Abstracts with Programs*, v. 17, p. 165.

- Machette, M. N., 1985, Calcic soils of the southwestern United States, in Weide, D. L., ed., *Soils and Quaternary geology of the southwestern United States: Geological Society of America Special Paper 203*, p. 1-22.
- McGillis, K. A., and Presley, M. W., 1981, Tansill, Salado, and Alibates Formations: Upper Permian evaporite/carbonate strata of the Texas Panhandle: The University of Texas at Austin, Bureau of Economic Geology Geological Circular 81-8, 31 p.
- McGookey, D. A., Gustavson, T. C., and Hoadley, A. D., 1988, Regional structural cross sections, mid-Permian to Quaternary strata, Texas Panhandle and eastern New Mexico, distribution of evaporites and areas of evaporite dissolution and collapse: The University of Texas at Austin, Bureau of Economic Geology Cross Sections, 15 plates, 17 p.
- McGowen, J. H., Granata, G. E., and Seni, S. J., 1979, Depositional framework of the lower Dockum Group (Triassic), Texas Panhandle: The University of Texas at Austin, Bureau of Economic Geology Report of Investigations No. 97, 60 p.
- Meinzer, F. J., and Slaughter, B. H., 1971, Upland gravels in Dallas County, Texas, and their bearing on the former extent of the High Plains physiographic province: *Texas Journal of Science*, v. 22, p. 217-222.
- Myers, B. N., 1969, Compilation of results of aquifer tests in Texas: Texas Water Development Board Bulletin, Report No. 98, 532 p.
- Nativ, R., 1988, Hydrogeology and hydrochemistry of the Ogallala aquifer, Southern High Plains, Texas Panhandle and Eastern New Mexico: The University of Texas at Austin, Bureau of Economic Geology Report of Investigations No. 177, 64 p.
- Neuman, S. P., and Narasimhan, T. N., 1977, Mixed explicit-implicit iterative finite-element scheme for diffusion-type problems: I., Theory: *International Journal of Numerical Methods Engineering*, v. 11, p. 309-323.
- Nicholson, J. H., 1960, Geology of the Texas Panhandle, in *Aspects of the geology of Texas*, a symposium: Austin, University of Texas Publication 6017, p. 51-64.
- Orr, E. D., 1983, An application of geostatistics to determine regional ground-water flow in the San Andres Formation, West Texas and eastern New Mexico, in Gustavson, T. C., and others, *Geology and geohydrology of the Palo Duro Basin, Texas Panhandle*, a report on the progress of nuclear waste isolation feasibility studies (1982): The University of Texas at Austin, Bureau of Economic Geology Geological Circular 83-4, p. 102-108.
- Orton, R. B., 1964, *The climate of Texas and adjacent Gulf waters*: Washington, D.C., U.S. Department of Commerce, Weather Bureau, 195 p.
- Osterkamp, W. R., Fenton, M. M., Gustavson, T. C., Hadley, R. F., Holliday, V. T., Morrison, R. B., and Toy, T. J., 1987, Great Plains, in Graf, W. L., ed., *Geomorphic systems of North America: Boulder, Colorado, Geological Society of America Centennial Special Volume 2*, p. 163-209.
- Osterkamp, W. R., and Wood, W. W., 1984, Development and escarpment retreat of the Southern High Plains, in Whetstone, G. A., ed., *Proceedings of the Ogallala Aquifer Symposium II: Texas Tech University, Lubbock*, p. 177-193.
- 1987, Playa-lake basins in the Southern High Plains of Texas and New Mexico: Part I, hydrologic, geomorphic and geologic evidence for their development: *Geological Society of America Bulletin*, v. 99, p. 215-223.
- Peel, R. F., 1941, Denudational landforms in the central Libyan Desert: *Journal of Geomorphology*, v. 4, p. 3-23.
- Presley, M. W., 1979a, Upper Permian evaporites and red beds, in Dutton, S. P., and others, *Geology and geohydrology of the Palo Duro Basin, Texas Panhandle*, a report on the progress of nuclear waste isolation feasibility studies (1978): The University of Texas at Austin, Bureau of Economic Geology Geological Circular 79-1, p. 39-49.
- 1979b, Salt deposits, in Dutton, S. P., and others, *Geology and geohydrology of the Palo Duro Basin, Texas Panhandle*, a report on the progress of nuclear waste isolation feasibility studies (1978): The University of Texas at Austin, Bureau of Economic Geology Geological Circular 79-1, p. 50-56.
- 1980a, Upper Permian salt-bearing stratigraphic units, in Gustavson, T. C., and others, *Geology and geohydrology of the Palo Duro Basin, Texas Panhandle*, a report on the progress of nuclear waste isolation feasibility studies (1979): The University of Texas at Austin, Bureau of Economic Geology Geological Circular 80-7, p. 12-23.
- 1980b, Salt depth and thickness studies, in Gustavson, T. C., and others, *Geology and geohydrology of the Palo Duro Basin*, a report on the progress of nuclear waste isolation feasibility studies (1979): The University of Texas at Austin, Bureau of Economic Geology Geological Circular 80-7, p. 33-40.
- Reeves, C. C., Jr., 1971, Appendix A, in Allen, B. L., and others, *Environmental impact analysis—salt retention structures, upper Brazos River Basin, Texas*: Texas Tech University, Water Resources Center, WRC-71-3, p. A1-A34.
- 1985, Nuclear-waste repository impaired by effects of subsurface salt dissolution (abs): *Geological Society of America Abstracts with Programs*, v. 17, p. 697.
- Reeves, C. C., Jr., and Temple, J. M., 1986, Permian salt dissolution, alkaline lake basins, and nuclear-waste storage, Southern High Plains, Texas and New Mexico: *Geology*, v. 14, p. 939-942.

- Richter, B. C., and Kreitler, C. W., 1986, Geochemistry of salt-spring and shallow subsurface brines in the Rolling Plains of Texas and southwestern Oklahoma: The University of Texas at Austin, Bureau of Economic Geology Report of Investigations No. 155, 47 p.
- Schultz, G. E., 1977, Field conference on late Cenozoic biostratigraphy of the Texas Panhandle and adjacent Oklahoma: West Texas State University, Kilgore Research Center, Department of Geology and Anthropology Special Publication No. 1, 160 p.
- 1986, Biostratigraphy and volcanic ash deposits of the Tule Formation, Briscoe County, Texas, in Gustavson, T. C., ed., *Geomorphology and Quaternary stratigraphy of the Rolling Plains, Texas Panhandle*: The University of Texas at Austin, Bureau of Economic Geology Guidebook 22, p. 82-84.
- Seni, S. J., 1980, Sand-body geometry and depositional systems, Ogallala Formation, Texas: The University of Texas at Austin, Bureau of Economic Geology Report of Investigations No. 105, 36 p.
- Simpkins, W. W., and Baumgardner, R. W., Jr., 1982, Stream incision and scarp retreat rates based on volcanic ash data from the Seymour Formation, in Gustavson, T. C., and others, *Geology and geohydrology of the Palo Duro Basin, Texas Panhandle, a report on the progress of nuclear waste isolation feasibility studies (1981)*: The University of Texas at Austin, Bureau of Economic Geology Geological Circular 82-7, p. 160-163.
- Simpkins, W. W., and Fogg, G. E., 1982, Preliminary modeling of ground-water flow near salt dissolution zones, Texas Panhandle, in Gustavson, T. C., and others, *Geology and geohydrology of the Palo Duro Basin, a report on the progress of nuclear waste isolation feasibility studies (1981)*: The University of Texas at Austin, Bureau of Economic Geology Geological Circular 82-7, p. 130-137.
- Simpkins, W. W., and Gustavson, T. C., 1985, Late Pleistocene and Holocene channel aggradation, Tierra Blanca Creek, Southern High Plains, Texas Panhandle (abs): *Geological Society of America Abstracts with Programs*, v. 17, p. 192.
- 1987, Erosion rates and processes in subhumid and semiarid climates, Texas Panhandle: statistical evaluation of field data: The University of Texas at Austin, Bureau of Economic Geology Report of Investigations No. 162, 54 p.
- Simpkins, W. W., Gustavson, T. C., Alhades, A. B., and Hoadley, A. D., 1981, Impact of evaporite dissolution and collapse on highways and other cultural features in the Texas Panhandle and eastern New Mexico: The University of Texas at Austin, Bureau of Economic Geology Geological Circular 81-4, 23 p.
- Smith, D. A., Bassett, R. L., and Roberts, M. P., 1983, Potentiometric surface of the Wolfcampian aquifer, Palo Duro Basin, in Gustavson, T. C., and others, *Geology and geohydrology of the Palo Duro Basin, a report on the progress of nuclear waste isolation feasibility studies (1982)*: The University of Texas at Austin, Bureau of Economic Geology Geological Circular 83-4, p. 94-96.
- Swenson, F. A., 1974, Rates of salt solution in the Permian Basin: *U.S. Geological Survey Journal of Research*, v. 2, p. 253-257.
- Thomas, R. G., 1972, The geomorphic evolution of the Pecos River system: Baylor University, Baylor Geological Studies Bulletin, no. 22, 31 p.
- U.S. Army Corps of Engineers, 1975, Red River chloride remote-sensing study, final report for NASA SR/T project no. W-13,557: Tulsa District, Tulsa, Oklahoma, Geology Section, Foundation and Materials Branch, 8 p.
- U.S. Department of Agriculture, Soil Conservation Service, 1972, Mansker soil series.
- 1977a, Acuff soil series.
- 1977b, Amarillo soil series.
- 1977c, Pullman soil series.
- U.S. Department of Commerce, 1955, Rainfall intensity-duration-frequency curves for selected stations in the United States, Hawaiian Islands and Puerto Rico: Washington, D.C., U.S. Weather Bureau Technical Paper 25, 53 p.
- 1978a, Local climatological data, annual summary with comparative data, 1978, Lubbock, Texas: Asheville, North Carolina, National Climate Center, 4 p.
- 1978b, Local climatological data, annual summary with comparative data, 1978, Amarillo, Texas: Asheville, North Carolina, National Climate Center, 4 p.
- U.S. Geological Survey, 1969-1983, Water resources for Texas, part II: surface water quality.
- Varnes, D. J., 1958, Landslide types and processes: National Research Council, Highway Research Board, Special Report No. 29, p. 20-47.
- Winkler, D. A., 1984, Biostratigraphy of the Ogallala Group (Miocene), Southern High Plains, Texas (abs): *Geological Society of America Abstracts with Programs*, v. 16, p. 698.
- 1985, Stratigraphy, vertebrate paleontology, and depositional history of the Ogallala Group in Blanco and Yellowhouse Canyons, Northwestern Texas: The University of Texas at Austin, Ph.D. dissertation, 243 p.
- Wood, W. W., and Osterkamp, W. R., 1987, Playa-lake basins in the Southern High Plains of Texas and New Mexico: Part II, a hydrologic model and mass balance arguments for their development: *Geological Society of America Bulletin*, v. 99, p. 224-230.
- Young, A., 1972, Slopes: New York, Longman Group Limited, 288 p.

1861

rec'd with letter
dtd 3/26/93

IMPACT OF TIME AND CLIMATE ON QUATERNARY SOILS
IN THE YUCCA MOUNTAIN AREA
OF THE NEVADA TEST SITE

by

Emily Mahealani Taylor

B.S., University of California, Berkeley, 1980

A thesis submitted to the
Faculty of the Graduate School of the
University of Colorado in partial fulfillment
of the requirements for the degree of
Master of Science
Department of Geological Sciences
1986

102.2

~~4303110411~~

To the GRADUATE SCHOOL OF THE UNIVERSITY OF COLORADO:


Student's Name: Emily Mahealani Taylor


Degree: M. S.

Discipline: Quaternary Geology and Soils

Thesis Title: Impact of Time and Climate on Quaternary Soils in the
Yucca Mountain Area of the Nevada Test Site

The final copy of this thesis has been examined by the undersigned, and we find that both the content and the form meet acceptable presentation standards of scholarly work in the above discipline.


Chairperson


Committee member

May 28 1986
Date 1

Taylor, Emily Mahealani (M.S., Geology)

Impact of time and climate on Quaternary soils in the Yucca

Mountain area of the Nevada Test Site

Thesis directed by Professor Peter W. Birkeland

The influences of time and climate were studied on a Quaternary chronosequence in the Yucca Mountain area of the Nevada Test Site. The soils are formed in alluvium derived from ash-flow tuffs and eolian dust. Both secondary CaCO_3 and opaline SiO_2 appear initially as coatings on the underside of clasts and over time form indurated horizons. The maximum amounts of CaCO_3 , opaline SiO_2 , and usually clay occur in the same horizon. In these horizons, opaline SiO_2 is more abundant than CaCO_3 and clay. There is little change in the soil-clay mineralogy over time. Vesicular A (Av) horizons have not formed on Holocene deposits, but are common on Pleistocene deposits. There is no relationship between the thickness of the Av and the age of the underlying deposit.

Regression statistics suggest that quantified field properties and secondary clay, silt, CaCO_3 , and opaline SiO_2 accumulate at a logarithmic rate. However, owing to the effects of erosion, and eolian additions, these secondary properties may be better expressed by linear rates. It is likely that erosion results in long-term accumulation rates less than the measured accumulation rates. Average accumulation rates are higher for the Holocene soils. This relationship suggests that the translocation of eolian material was not limited by Holocene precipitation.

The modern climate and two climatic models of the last glacial maximum were used to generate soil water balances and to calculate evapotranspiration (ET_p). The Papadakis method was used to calculate ET_p . These calculations suggest that translocation of dissolved and solid material in Holocene soils can be attributed chiefly to high-precipitation storm events.

There are several different trends in $CaCO_3$ accumulation in the Holocene soils, and in older soils that have experienced at least one major climatic change. These trends suggest that changes in temperature and (or) seasonality of the precipitation dominated the climatic change associated with the Holocene-Pleistocene boundary. Comparison of actual Holocene soil $CaCO_3$ profiles with those generated by a computer suggest that this climatic change was gradual.

ACKNOWLEDGMENTS

This work has been funded by the U.S. Geological Survey, Branches of Central and Western Regional Geology, which provided a stipend, office space, field support and lab facilities from the summer of 1983 to the present. The support is from the Tectonics of the Southern Great Basin project and this work began under the encouragement of Michael Carr, our fearless leader, and seen to completion by Ken Fox who took over as project chief in February of 1985.

The lab work was completed only because of the patience of Don Cheney at the Central Regional Geology Soil and Sediment Laboratory, who not only spent a great deal of time on my samples, but also allowed me to spend months in his lab. Some lab work was also completed at the University of Colorado Soils Laboratory and INSTAAR with the help of Rolf Kihl.

The guidance and support from faculty and friends at the University of Colorado made it all possible. A special thanks to Dr. Peter W. Birkeland who made suggestions, read and reread (the one "GOOD!" comment on the final draft was next to a paragraph he had written), and humored me on through the years. His encouragement and faith kept me on track. Dr. Nel Caine's statistical coaching and text review was also very helpful.

My cronies and colleagues at work who criticized my hallway-ramblings were also a great help; they include Will Carr, Jennifer Harden, Michael Machette, Dan Muhs, Steve Personius, Ken Pierce, Marith Reheis, and Dub Swadley. Ralph Shroba's guidance in the field, text reviews, and dietary suggestions were indispensable. Heather Huckins field assistance and Mercury-survival-tips make the long stints in Nevada both productive and enjoyable.

My parents and family who have kept faith can not be forgotten. Finally, thanks to Ross Jacobson who has provided moral support and kindness throughout this entire ordeal.

CONTENTS

CHAPTER

I.	INTRODUCTION AND METHOD OF STUDY	1
	Introduction	1
	Statement of Problem	1
	Objectives	3
	Strategy	4
	Location of Study Area	6
	Methods of Field Work and Soil Description	6
	Locating Study Area	6
	Description and Sampling	7
	Pedogenic Silica	8
	Index of Soil Development	9
	Micromorphology	9
	Statistical Methods	9
II.	ENVIRONMENTAL SETTING, PAST AND PRESENT	11
	Geologic Setting and Chronology	11
	Quaternary Stratigraphy	11
	Ages of Deposits	17
	Geomorphic Setting	17
	Terrace Formation--Tectonic vs Climatic	17
	Ground Water Setting	21
	Modern Climate	22

Paleoclimate in the NTS Region	25
Packrat Midden Evidence	25
Pluvial Lake Evidence	26
Summary of the Glacial Climate Models	27
III. MAJOR PEDOLOGICAL CHANGES WITH TIME	29
Morphology	29
Pedogenic Opaline Silica	29
Carbonate and Opaline Silica	31
Vesicular A Horizons	33
Profile Index Values	34
Accumulations of Carbonate, Clay, Silt, and Opaline Silica	42
Method to Calculate Rates of Accumulation	43
Rates of Accumulation of Carbonate, Clay, Silt, and Opaline Silica	43
Depth Functions of Significant Soil Properties	49
Primary and Secondary Minerals Identified by X-ray Diffraction	56
IV. USING SOIL DATA TO ASSESS PALEOCLIMATE	65
Soil Water Balance and Leaching Index	65
Carbonate Translocation	75
Computer Generated Model for Carbonate Translocation	80
Pedogenic Silica Morphology as a Climatic Indicator ..	83
V. SUMMARY, CONCLUSIONS, AND FUTURE STUDIES	85
REFERENCES	92

APPENDICES

A	Soil Field descriptions for the Yucca Wash and Fortymile Wash Area, Nevada Test Site	104
B	Soil profile index values	112
C	Laboratory Methods--particle size distribution (PSD), bulk density, percent carbonate, gypsum and soluble salts, percent organic carbon and loss on ignition (LOI), pH, silica, clay mineralogy	161
D	Effects on the particle size distribution and clay mineralogy after the removal of opaline silica	165
E	Laboratory procedure for measuring pedogenic opaline silica using a spectrophotometer	170
F	Laboratory Analyses--particle size, bulk density, carbonate, gypsum, soluble salts, organic carbon, oxidizable organic matter, loss on ignition, pH, and silica by weight	179
G	Representative Dates for the Quaternary deposits, NTS ..	192
H	Horizon weights of carbonate, clay, silt, and opaline silica	201
I	Soil parameters used to model calcic soil development ..	200
J	Use of pollen, spores, and opal phytoliths from three different aged deposits as paleoclimatic indicators	193

TABLES

Table

1	Quaternary stratigraphy of the Yucca Mountain area, NTS	12
2	Temperature, precipitation and potential evapotrans- piration data for the Holocene (present) and two models for the last glacial maximum	23
3	General characteristics of pedogenic opaline silica stages	31
4	Comparison of soil profile index values for the study area with those for Las Cruces, New Mexico	42
5	Correlation coefficients (r^2) for carbonate, clay, silt, and opaline silica	46
6	Correlation coefficients (r^2) for linear age, log age, carbonate, clay, and opaline silica for A, B and K, and C horizons and all horizons combined	50
7	Clay minerals identified and their diagnostic features	57
8	X-ray diffraction classification of opaline silica	61
9	Comparison of methods to calculate potential evapotranspiration using Beatty, Nevada weather data	67

FIGURES

Figure

1	Location of study area	2
2	Map of Quaternary deposits, Tertiary bedrock, and trench locations in the study area	5
3	Generalized cross section showing the stratigraphic relationships of Quaternary fluvial deposits along Yucca Wash and Fortymile Wash	18
4	Profiles of terrace deposits along Yucca Wash and Fortymile Wash	20
5	Bivariate regression analyses of significant property profile index values vs time	36
6	Bivariate regression analyses of soil profile index values vs time	38
7	Soil profile index values vs elevation	41
8	Profile sum of horizon weights vs age of carbonate, clay, silt, and opaline silica on soils developed on stratigraphic units Q1c, Q2b, Q2c, and QTa	44
9	Average rates of accumulation of pedogenic carbonate, clay, silt, and opaline silica based on profile weight sums on stratigraphic units Q1c, Q2b, Q2c, and QTa	45
10	Depth plots of pedogenic clay, CaCO_3 , and opaline SiO_2 in soils developed on unit Q1c	51
11	Depth plots of pedogenic clay, CaCO_3 , and opaline SiO_2 in soils developed on unit Q2b	52
12	Depth plots of pedogenic clay, CaCO_3 , and opaline SiO_2 in soils developed on unit Q2c	54
13	Depth plots of pedogenic clay, CaCO_3 , and opaline SiO_2 in soils developed on unit QTa	55
14	Representative XRD traces of tobermorite and mixed layer clays: Untreated, glycolated and heated traces	58

15	Representative XRD trace of Opal-CT	62
16	Relative abundance of clay minerals on soils formed on deposits Q1c, Q2b, Q2c, and QTa	64
17	Soil water budget for Beatty, Nevada, which is assumed to approximate the Holocene climate	69
18	Soil water budget for the glacial maximum climate-- Spaulding model	71
19	Soil water budget for the glacial maximum climate-- Mifflin and Wheat model	73
20	Percent carbonate vs depth for soils formed on deposits Q1c and Q2b	76
21	Percent carbonate vs depth for soils formed on deposits Q2c and QTa	73
22	Modeled carbonate accumulation for 30,000 yrs of glacial climate with either an abrupt or gradual change to the Holocene climate for 10,000 yrs for the low and high ends of the elevation transect	77

CHAPTER I

INTRODUCTION AND METHOD OF STUDY

Introduction

Statement of Problem

A high-level nuclear waste site has been proposed for Yucca Mountain on the Nevada Test Site (NTS) (Fig. 1). This waste is the by-product of commercial enterprises and nuclear weapons production. Estimates vary from 1,000 to 100,000 yrs for the duration that this material remains hazardous (Winograd, 1981). To assure prolonged integrity of any nuclear-waste repository, long-term environmental stability of that site needs to be considered, as well as the impact of future climatic change.

This study addresses the problem of characterizing past climatic variability near the proposed nuclear-waste repository site at Yucca Mountain. Climatic changes are considered to be caused by variation in net global solar-energy input, a consequence of the precession of Earth's orbit and the obliquity and eccentricity of its axial position (Imbrie and Imbrie, 1980). Major global climatic change occurs at regular frequencies of 10,000 to 100,000 yrs (Shackleton and Opdyke, 1973). The Holocene Epoch is the most recent in a long series of relatively brief (7,000-20,000 yrs) interglacials, that punctuate much longer (90,000-150,000 yrs)

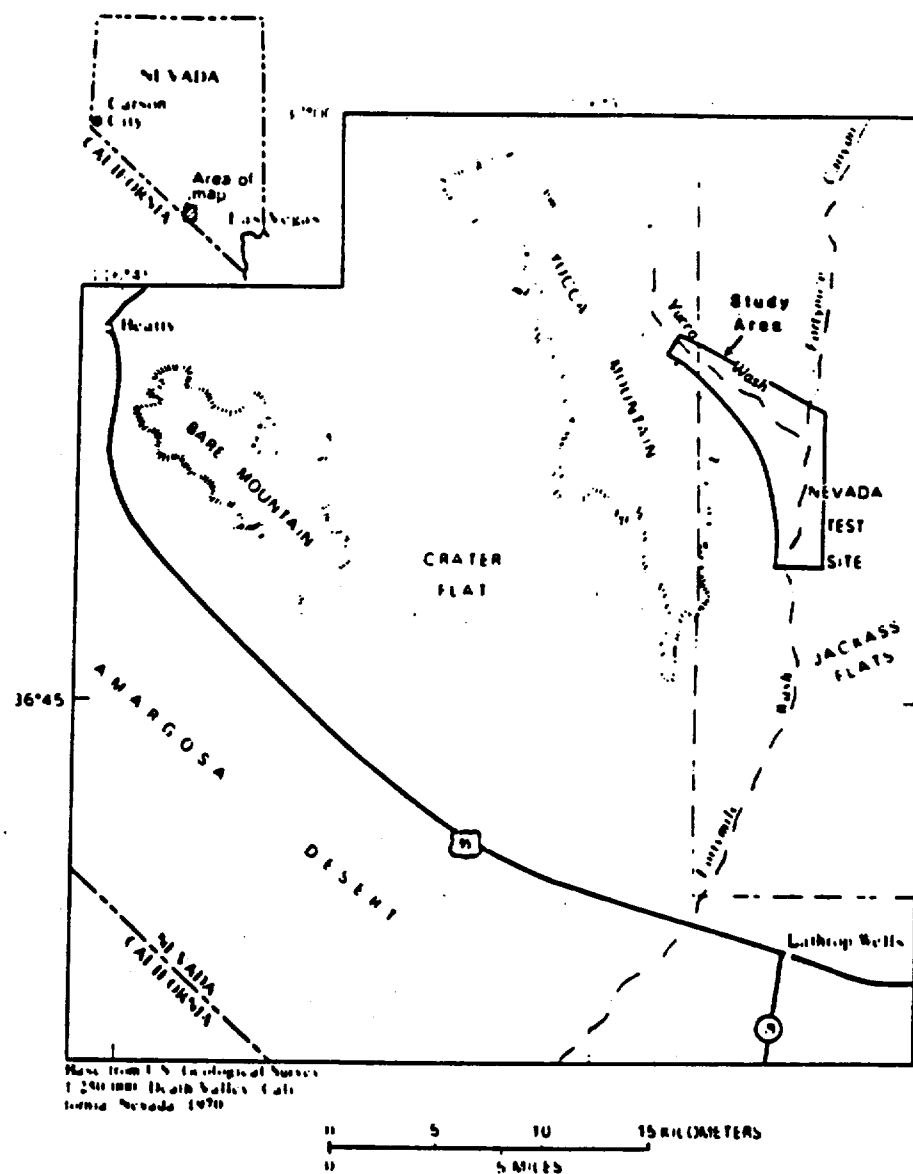


Figure 1. Location of study area.

periods of glaciations. A permanent repository for nuclear waste must be able to withstand the effects of a major climatic change. A climatic change that results in greater effective moisture may cause percolating water to move within the zone of waste material during the time that the material is still hazardous.

Objectives

The objectives of this study are twofold, (1) to document the effects of time and climate on soil development, and (2) to use soil data to characterize long-term, past climatic variability in the study area. Paleoclimatic reconstructions span the last 2 Ma, emphasizing the last 45,000 yrs because the age control and botanical evidence is best understood during this time. This study is part of a larger study of the paleoclimate of the NTS area. For example, other workers are studying past ground water levels and rates of recharge (Winograd, 1981; Winograd and Doty, 1980), regional lake and playa chronologies (L. V. Benson, U.S. Geological Survey, oral communication, 1985), and radiocarbon-dated plant macro and microfossils from ancient packrat middens (Spaulding, 1983, R. S. Thompson, U.S. Geological Survey, oral communication, 1985). One of the assumptions common to all these studies is that past climates approximate the climates that may occur in the next 100,000 yrs.

Strategy

Soil-geomorphic research can provide data useful for interpreting relative and absolute dating of alluvial deposits, stratigraphic correlation, and paleoclimate. To apply pedologic data to this goal, I use the state-factor approach developed by Jenny (1941, 1980) which defines the independent factors of soil formation as climate, biota, parent material, relief, and time. To understand the impact of a single factor on the development of soils, all other factors must either be held constant, or any variation in one of the factors must have little impact on the single factor that is being studied. The assumption then is made that soil development is chiefly dependent on the single varying factor. In this study two factors have varied--climate and time. When all factors are held constant except time, the soil sequence is defined as a chronosequence. When all factors are held constant except climate, the soil sequence is defined as a climosequence. The study area is particularly suitable for soil-paleoclimatic interpretations because the factors can be identified, key ones can be considered constant, and all pedogenic processes occur well above the present or former ground water table.

Five groups of different aged geomorphic deposits were studied along an elevation transect of 400 m of relief, from 1082 to 1483 m (Fig. 2). Present-day annual precipitation nearly doubles along the transect. For any group of deposits of the same approximate age, one can observe or predict the depth relationships of most soil properties. Soil properties that are much deeper than anticipated suggest climatic change. These properties can be

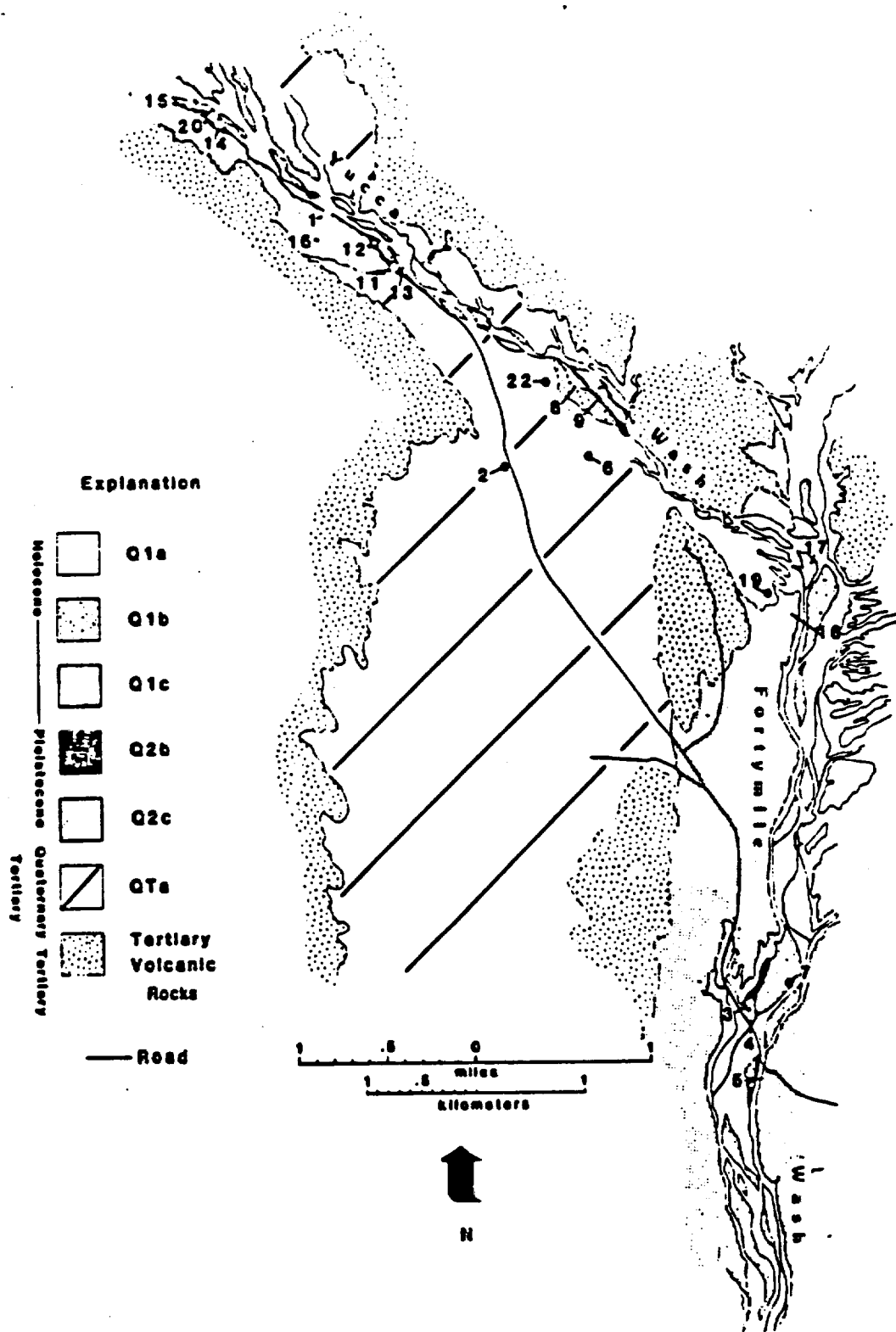


Figure 2. Map of Quaternary deposits, Tertiary bedrock, and trench locations in the study area.

compared to possible climate-models for the glacial maximums. The primary evidence and discussion for the effects of climatic change and time on soil development are based on physical and chemical soil properties.

Location of Study Area

The study area is along Yucca Wash and Fortymile Wash on the east side of Yucca Mountain near the southwest corner of NTS (Fig. 1). This area is in the Basin and Range Province of western North America (Fenneman, 1931), on the southeastern margin of the Great Basin (Morrison, 1965). With respect to the flora, the site is located on the boundary of the Mojave Desert to the south and the Great Basin Desert to the north (Cronquist and others, 1972).

The Quaternary deposits at the upper end of the elevation transect are along Yucca Wash (YW) just northeast of Yucca Mountain. The transect follows Yucca Wash southeastward to its confluence with Fortymile Wash (FW), and proceeds due south to the road crossing across Fortymile Wash. The total transect distance is just over 13 km.

Methods of Field Work and Soil Description

Locating Study Area

The selection of the study area was accomplished with the use of air photos and preliminary surficial geologic maps by D. L. Hoover (U.S. Geological Survey, written communication, 1983). The primary study site was then selected and mapped. Stratigraphic units are defined on the basis of landscape position, surface

morphology, degree of packing and sorting of desert pavement, desert varnish, and soil-profile development.

Description and Sampling

Twenty trenches were excavated by backhoe through the soil into unconsolidated material similar to the parent material. The difference being that in some cases translocated CaCO_3 and opaline SiO_2 are present at depths in the soil profile, and not in the unconsolidated alluvium in the modern washes which is comparable to the parent material (Appendix A). Frequently, buried soils were encountered at depths in the soil exposures. Trenches were located on stable parts of terrace or fan surfaces, with the stability measured by the integrity of the pavement and the preservation of the B horizon.

Soil profiles were described according to methods and terminology outlined by the Soil Survey Staff (1951) and Birkeland (1984). I use the horizon descriptor Cuk for horizons that have all the characteristics of unconsolidated parent material with the exception of translocated CaCO_3 . Soil texture is from laboratory particle-size data after the carbonate and silica cement were removed. Calcic horizon terminology is after Gile and others (1979 and 1981; Bachman and Machette, 1977; Machette, 1985). Greater than 0.20 percent carbonate in the <2 mm fraction is detectable in the field by 10% HCl.

Two to three kg bulk samples, and three to eight peds were collected for each horizon. Bulk samples were sieved and the gravel percent determined on a weight basis in the laboratory.

Measurements were checked with field estimates to make sure that gravel in bouldery deposits was not underestimated. If the present gravel was thought to have been underestimated, the value was corrected with the field observations.

Pedogenic Silica

Silica-cemented horizons or duripans were identified in the field by first soaking air-dried samples in water, followed by soaking in 10% HCl overnight. Cementation and brittleness are preserved when the predominant cementing agent is silica. Duripans in the study area also have a characteristic pinkish-yellow color, 7.5YR 7/4-6 (dry) and 7.5YR 5-6/6 (moist) Munsell colors, and are extremely hard when dry.

Because of the presence of silica, allophane was suspected. Allophane is a noncrystalline-clay weathering product of volcanic glass and associated with duripan formation. A field test (Fieldes and Perrott, 1966) that determines the presence of amorphous allophane by measuring the change in pH with the addition of NaF, was unsuccessful. A simple, laboratory method, independent of pH (Wada and Kakuto, 1985) was not much more successful. Thirty to 50 mg of air-dried soil (<2mm) is placed on a white spot plate, and 0.4 ml of 0.02% toluidine blue solution is added. If the color of the supernatant remains blue after 15 seconds, it suggests the presence of allophane and imogolite. A larger sample, 50-100 mg, is used for coarse-textured soil. The samples frequently remained blue in horizons that contained opaline SiO₂ cement as well as the eolian vesicular A horizons.

Index of Soil Development

Soil field properties were quantified according to Harden (1982), and Harden and Taylor (1983) (Appendix B). The soil development indices were programmed and calculated with the "LOTUS 1-2-3" spreadsheet on an IBM-PC computer (Nelson and Taylor, 1985a and 1985b).

Micromorphology

Oriented samples of soil pedis and gravel were collected. Samples were stained with blue epoxy so that amorphous material could be more easily recognized. Thin sections were cut perpendicular to the soil surface.

Statistical Methods

Statistical techniques used in this study include (1) descriptive statistics that characterize the sample population, (2) bivariate regression and correlation (r^2) analysis of individual properties with time or climate as the dependent variable, and (3) multiple and stepwise regression analyses to test possible predictive models of groups of soil properties with a single soil property as the dependent variable (Till, 1974; Davis, 1973).

The null hypothesis (H_0) for regression analysis is to test whether there is a significant relationship between time or climate, and the independent soil properties. H_0 = no association. When $F_{\text{calculated}} > F_{\text{critical}}$ or $t_{\text{calculated}} > t_{\text{critical}}$, at the 5% significance level, H_0 is rejected and the conclusion is made that there is a significant relationship. Significance is the level of

probability that the described relationship between properties could occur randomly. Thus at 5% there is a 1:20 chance that the relationship is random. The standard error is a measure of the accuracy of prediction. It is an estimate of the standard error of the residuals, or the estimate of the standard error between measured and predicted values of the dependent variable about the regression line. The standard error of B, or the standard deviation regression line. The standard error of B, or the standard deviation due to sampling variability in the slope of the regression, is used to generate the 95% confidence intervals. Residual analysis was used to check multiple regression assumptions. All statistics were done on an IBM-PC computer with the "STATPRO" statistical package.

CHAPTER II

ENVIRONMENTAL SETTING, PAST AND PRESENT

Geologic Setting and Chronology

Yucca Wash originates in an area composed exclusively of Tertiary volcanic rocks (Christiansen and Lipman, 1965; Lipman and McKay, 1965). The alluvium in Yucca Wash is derived from these welded and nonwelded ash-flow tuffs. The alluvium in Fortymile Wash is also derived from similar siliceous volcanic rocks with a small component of basalt. Carbonate and opaline SiO_2 -rich eolian dust have been added to these alluvial deposits over time.

Quaternary Stratigraphy

The Quaternary stratigraphic nomenclature used on NTS (Table 1) was modified from that initially described by Bull (1974; Ku and others, 1979; McFadden, 1982) in the Vidal Junction area, California, about 320 km south of NTS. Deposits at Vidal Junction were differentiated mainly on the basis of soil properties. However, the identification of units at NTS is based primarily on geomorphic features, and to a lesser extent on soil properties (Hoover and others, 1981; Swadley, 1983). The main features include preservation of bar-and-swale topography, elevation above modern washes, packing and sorting of desert pavement, desert varnish, and the presence or absence, and thickness of the vesicular A horizon.

Table 1. Quaternary stratigraphy of the Yucca Mountain area, NTS. Modified from Hoover and others (1981; Szabo and others, 1981; and Swadley and Hoover, 1983); soil properties are those of this study. Textures are for the <2 mm fraction and pertain to all soil horizons. Pleistocene deposits have age estimates based on U-Trend dating. Some of the age estimates may be minimum ages. Holocene deposits on the most part have inferred ages. See Appendix G for information on the origin of assigned ages. Units can be combined (e.g. Q1a/Q1b) in areas where they cannot be differentiated at a given map scale and (or) where a unit is mantled by a thin, patchy unit.

<u>Stratigraphic Units</u>		<u>Key Properties and Diagnostic Criteria</u>
<u>Unit</u>	<u>Estimated</u>	<u>for Recognition</u>
<u>Designation</u>	<u>Age</u>	
<u>Latest Holocene</u>		
Q1a	historic	Fluvial gravel and finer grained over bank deposits on and adjacent to the floors of active washes. No pedogenic alteration. Typically <2 m thick.
<u>Late Holocene</u>		
Q1b	<140 yrs	Fluvial gravel, sheetwash, or debris flows on steep slopes. Fluvial deposits form a terrace 0.5-2 m above active channels; bar-and-swale topography preserved. Thought to date from major episode of arroyo incision considered to have taken place 140 yrs ago (Bryan, 1925). No desert pavement has developed. Soils have a thin A; Cox, Cuk and (or) Cu; stage I CaCO ₃ (commonly contains reworked gravel with stage II CaCO ₃ coats); texture S, LS or SL. Usually <2 m thick.
Q1e		Eolian sand in active modern dunes in areas away from mountain fronts. No pedogenic alteration; texture S or LS. Locally as much as 50 m thick; typically <10 m thick.

Table 1 continued. Quaternary stratigraphy of the Yucca Mountain Area, NTS.

<u>Stratigraphic Units</u>		<u>Key Properties and Diagnostic Criteria</u>
<u>Unit</u>	<u>Estimated</u>	<u>for Recognition</u>
<u>Designation</u>	<u>Age</u>	
Q1s	3.3-7 ka	Slope wash or sand sheets. composed primarily of reworked eolian sand and <25 percent gravel; deposited as much as 10 km from mountain fronts. Commonly dissected near active channels. Soils and pavement are similar to those of unit Q1c, except texture is most commonly S. Usually <2 m thick.
<u>Middle to Early Holocene or Late Pleistocene</u>		
Q1c	~10 ka	Primarily terraces formed in fluvial gravel; may include fans, colluvium, or sheetwash. Fluvial deposits form a terrace 1-2 m above active channels. Lacks bar-and-swale topography. Incipient desert pavement development and little or no varnish development. Soils have an A; 10YR Bw, Bk _j , Bt _j and (or) Bq _j ; stage I-II CaCO ₃ and (or) stage I SiO ₂ ; texture S, LS, or SL. Commonly <2 m thick.
<u>Late Pleistocene</u>		
Q2a	30-47 ka	Mostly sandy slope wash derived in part from eolian sediment. Commonly contains <25 percent gravel. Typically caps older deposits and is locally covered by Holocene deposits. Usually lacks topographic expression. Soils have an Av; Bt and (or) Bk; stage I CaCO ₃ ; texture SL, L, or C. Usually <1.5 m thick.

Table 1 continued. Quaternary stratigraphy of the Yucca Mountain Area, NTS.

<u>Stratigraphic Units</u>		<u>Key Properties and Diagnostic Criteria</u>
<u>Unit</u>	<u>Estimated</u>	<u>for Recognition</u>
<u>Designation</u>	<u>Age</u>	
<u>Middle Pleistocene</u>		
Q2b	145-160 ka	Fluvial gravel that forms strath terraces, or debris flow fans. Fluvial deposits form a terrace 5-12 m above active channels. Typically very poorly sorted with large boulders up to 1 m in diameter; commonly contains fluvial sedimentary features. Desert pavement is well sorted, tightly packed and darkly varnished. Soils have an Av; 10YR to 7.5YR Bw, Bt, Bqm, and (or) Bk; stage I-II CaCO ₃ and (or) stage II-III SiO ₂ ; texture S, LS or SL. Commonly <2 m thick.
Q2c	270-430 ka	Fluvial gravel or debris flows on steep slopes. Fluvial deposits form a terrace 10-21 m above active channels. Desert pavement is well sorted, tightly packed with continuous varnish. Soils have an Av; 7.5YR. Bt, Bqm, B/K and (or) Kqm; stage III-IV CaCO ₃ (K horizon <1 m thick) and (or) stage III SiO ₂ ; texture S to L. Usually <65 m thick.
Q2e	<738 ka	Eolian sand in inactive dunes and sand ramps at and adjacent to hill and mountain fronts. Desert pavement is well sorted, tightly packed, and darkly varnish. Soils have an Av; Bk, Bkq, B/K and (or) K; stage III-IV CaCO ₃ and (or) stage III-IV SiO ₂ ; texture LS, SL, or L. Usually <20 m thick.

Table 1 continued. Quaternary stratigraphy of the Yucca Mountain Area, NTS.

<u>Stratigraphic Units</u>		<u>Key Properties and Diagnostic Criteria</u>
<u>Unit</u>	<u>Estimated</u>	<u>for Recognition</u>
<u>Designation</u>	<u>Age</u>	
Q2s	<738 ka	Slope wash or sand sheets (tabular bodies of sandy slopewash) down slope from sand ramps. Generally lacks desert pavement. Soils have an Av; Bk, Bkq, B/K and (or) K; stage III-IV CaCO_3 and (or) stage III-IV SiO_2 ; texture LS, SL or L. Usually <2 m thick.
<u>Early Pleistocene</u>		
Q1a	1.1-2.0 my	Alluvial fans; usually extremely eroded and overlain by a veneer or mantle of younger deposits. Commonly deposits are adjacent to hills and mountain fronts, 20-30 m above active channels. Lacks depositional form; erosional modification results in ballena or accordant, rounded ridges. Large boulders up to 1 m in diameter may be scattered on the surface. Desert pavement is well-sorted, tightly packed and has continuous dark varnish; commonly contains opaline SiO_2 platelets from the underlying soil. Soils have an A or Av; 7.5YR Bt, Bqm, B/K, Kqm, and (or) Km; stage III-IV CaCO_3 (K horizon >1 m thick) and stage III-IV SiO_2 . Commonly <20 m thick.

The assigned ages for these mapping units are based almost exclusively upon U-trend analyses on soil samples (Rosholt, 1980) (Appendix G).

Several depositional facies are recognized in these deposits. Fluvial deposits are poorly to moderately well sorted and poorly to well bedded; gravel clasts are angular to subrounded. Debris flows are poorly sorted, and poorly stratified to massive. Clasts are matrix supported and are angular to subrounded. Eolian sand and loess are moderately to well sorted, respectively. Sheetwash is moderately well sorted and may have thin bedding.

Features of desert pavement help distinguish some units. Pavement packing tends to change from none to dense with time, sorting increases from poor to well, and varnish changes from none to dull black to shiny purplish-black. Desert pavement features are a useful relative age indicator because they clearly change with time. However, thin layers of eolian and sheetwashed fine-grained deposits tend to blanket most gravelly deposits in the study area, and thus may not preserve the desert pavements.

The expression of fluvial bar-and-swale features become more subdued with time. The obliteration of these features is due primarily to burial by eolian or sheetwash deposits, and (or) to erosion. With time, the surface becomes smoother.

Topographic form of terraces also change in a gross way. Deposits younger than QTa have a good terrace expression. However, erosional modification results in ballenas or accordant, rounded

ridges (Peterson, 1981) that are typical of the QTa unit. These topographic forms represent a distinctive late stage of piedmont dissection.

Ages of Deposits

The ages assigned to the stratigraphic units on NTS and the surrounding area are based primarily on U-trend dating of deposits exposed in trenches excavated to study Quaternary faults (Hoover and others, 1981; Szabo and others, 1981; Swadley and Hoover, 1983) (Appendix G). Other techniques used are the age of assumed channel incision, ^{14}C , and correlation to ash geochronologies. The Quaternary stratigraphy used in the Yucca Mountain area (Table 1) was a product of the above tectonic studies.

Geomorphic Setting

Terrace Formation--Tectonic vs Climatic

The Quaternary landscape in the study area was formed by three major geomorphic processes; (1) fluvial erosion and deposition, (2) eolian erosion and deposition, and (3) hillslope processes. Major influences on these processes are tectonism (basin subsidence and (or) mountain front uplift) and climate. Of most interest here are the fluvial terraces.

The terraces studied are fill terraces (Fig. 3). Although the overall net effect of fluvial activity has been one of downcutting, these were interrupted by periods of aggradation. Subsequent downcutting resulted in fill terraces.

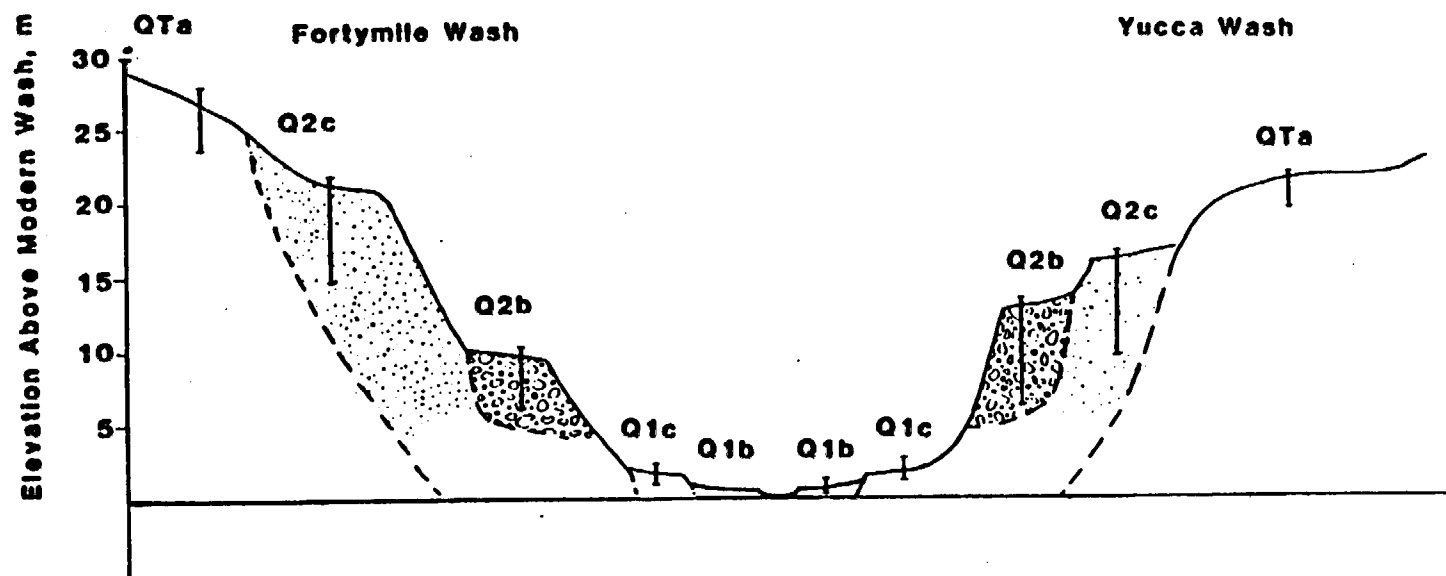


Figure 3. Generalized cross section showing the stratigraphic relationships of Quaternary fluvial deposits along Yucca Wash and Fortymile Wash. Variability in height of terrace surfaces above the modern wash is defined with the vertical bars.

The terraces do not seem to be of tectonic origin. A recent study on the west side of Yucca Mountain suggests that faulting has occurred in the Holocene (J. W. Whitney and R. R. Shroba, U.S. Geological Survey, oral communication, 1985). However there has not been any evidence for faulting of any of the Quaternary fluvial terrace deposits in the study area. In addition, longitudinal profiles of the terraces along Yucca Wash and Fortymile Wash (Fig. 4), although they diverge downstream, do not require tectonism to explain this relationship. Finally, if the terraces have been influenced by tectonic uplifts in the upper reaches of the drainages, cut terraces might be expected rather than fill terraces.

Climatic change may explain the presence of fill terraces in the area. Bull (1979) and Bull and Schick (1979) propose a model for fluvial behavior in arid areas during climatic change. If the climate changes to greater aridity and higher temperatures, the basin characteristics are such that the stream responds by aggrading. As time goes on, sediment availability decreases as erosion exposes bedrock, runoff increases, and erosion of the valley fill takes place. In general, each terrace, therefore could represent a climatic change. In this case, the formation of a terrace could be correlative with the early interglacials.

There have been few paleohydrologic models for the region. that the depositional units in the study area may be correlative. Smith (1984) has proposed one for the last 3.2 my, with most of the data taken from a core in Searles Lake, California. The four most recent climatic regimes are of interest here. Regime I (0 - ~10 ka) was dry. Regime II (~10 - 130 ka) was characterized by both dry and

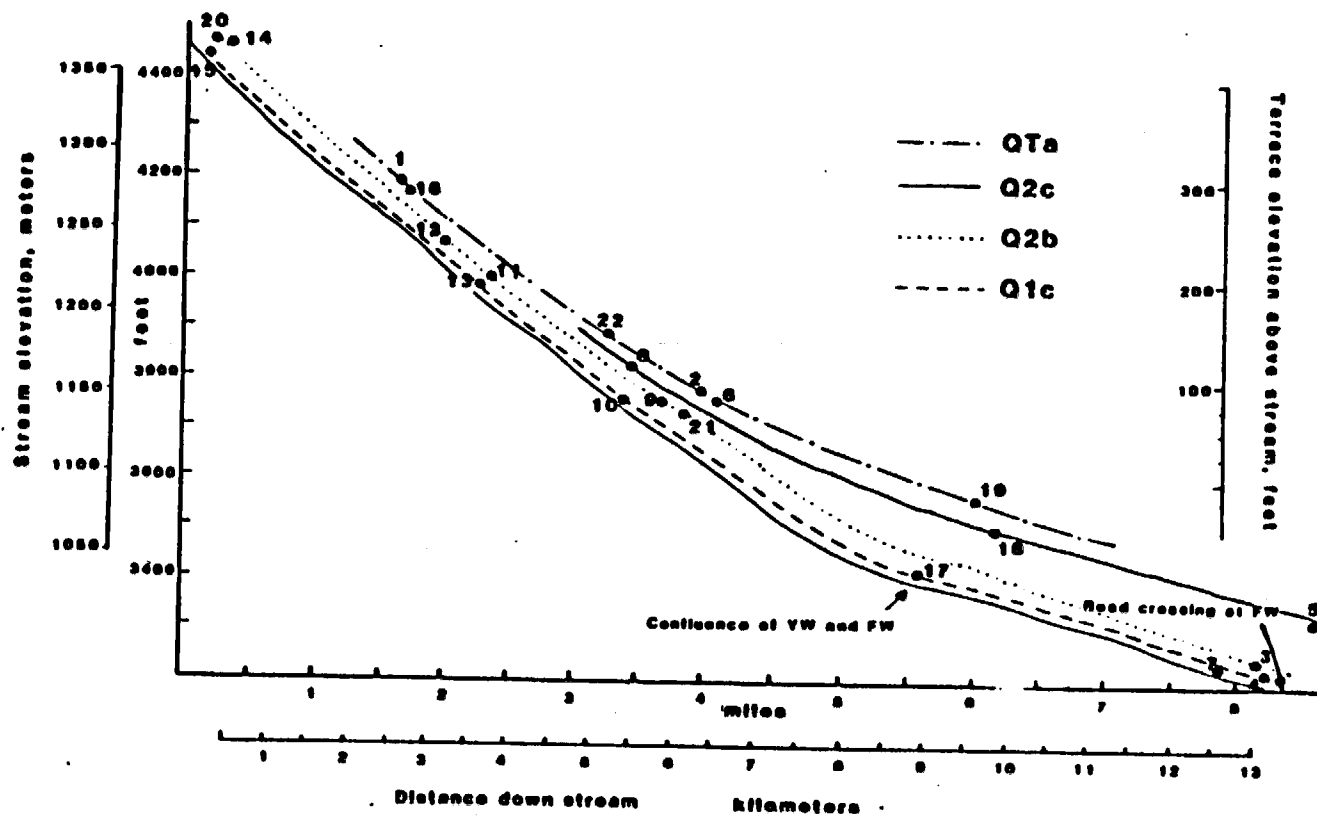


Figure 4. Profiles of terrace deposits along Yucca Wash (YW) and Fortymile Wash (FW). Locations of soil trenches are indicated by dots and numbers.

wet cycles, but long intervals of high lake levels support a relatively wet interval. Regime III (130 - 310 ka) was similar to but drier than Regime II. Finally, Regime IV (310 - 570 ka) was a long dry period.

Correlation can be made of some of the deposits in the area with the climatic model of Smith (1984). Unit Q1c could correlate with the transition from Regime II to I, and that would follow the Bull and Schick (1979) model. Other deposits may correlate to changes from one regime to another. Unit Q2b is a strath terrace deposit inset into the older Q2c. Therefore, deposits of Q2c age place a minimum age on the major time of incision of Fortymile Wash. Unit Q2b could be correlated with the transition from Regime III to II at 130 ka, and likewise the stabilization of unit Q2c would be correlative with the transition from Regime IV to III at 310 ka. These latter correlations are very tentative and do not follow the Bull (1979) model. Obviously the fluvial response to climatic change is not simple, as the threshold model proposed by Schumm (1977) may also explain terrace formation.

Ground Water Setting

Most ground water flow through the NTS area originates in volcanic highlands to the north; these include Pahute Mesa (35 km NW) and Timber Mountain (15 km N). The remainder of the ground water flow enters from the east as underflow in the regional lower carbonate aquifer (Winograd and Thordarson, 1975; Winograd and Doty, 1980). Flow directions beneath the eastern part of NTS are to the south and west from the highlands, until the water surfaces at the

extensive network of active springs at Ash Meadows in the Amargosa Desert (45 km SE). Evidence exists for somewhat greater spring activity during the last glacial maximum. Fossil tufa deposits occur as high as 40 m above present ground water level in this area (Winograd and Doty, 1980). All pedogenic processes in the Yucca Mountain area are well above the ground water table of the area which is from 490 to 610 m below the surface today.

Modern Climate

Southern Nevada is arid to semiarid. Because average annual precipitation in much of this area is less than 150 mm and there is greater than 10% perennial plant cover, it is actually a semiarid desert (Houghton and others, 1975). Beatty, Nevada is only 24 km due west of the study area. It is at the same elevation as the lowest soil-trench elevation in the study transect (1083 m), and is at the same latitude (37°54'N) (Fig. 1). It is used here as an estimate of the climate of the lower end of the study area. The mean annual precipitation (MAP) at Beatty is 117 mm, and the mean annual temperature (MAT) is 15.3°C (Table 2). At the upper end of the transect, which lies 400 m above the lower end, precipitation is assumed to increase by 70% to about 200 mm. This assumption is based on (1) vegetation change, (2) precipitation data from stations in southern and south-central Nevada that are at similar elevations and latitudes, and (3) Quiring's (1983) regression equation relating MAP and elevation on NTS:

$$y = 1.36x - 0.51 \quad \text{Equation (2.1)}$$

where y = MAP in inches and x = elevation in feet.

Table 2: Temperature, precipitation and potential evapotranspiration data for the Holocene (Present) and two models for the last glacial maximum. Precipitation is divided into the low and high ends of the elevation transect, representing a 70% increase.

- 1/ U.S. Department of Commerce Weather Bureau, Beatty, Nevada, elevation 1087 m, latitude $36^{\circ}54'N$.
- 2/ U.S. Department of Commerce Weather Bureau, Pahrump, Nevada, elevation 717 m, latitude $36^{\circ}12'N$.
- 3/ Thornthwaite (1848) and Van Hylckama (1959).
- 4/ Blaney and Criddle (1962) - K coefficient from reach 3, Culler and others, 1982, p. 32.
- 5/ Papadakis (1965) - Mean monthly maximum and minimum temperature used to calculate saturation vapor pressure and dew point according to Linsley and others, (1975, p. 35).

$$\text{Sat Vapor Pressure} = 33.8639 (0.00738 T^{\circ}C + 0.8072)^8 - 0.000019 |1.8 T^{\circ}C + 48| + 0.001316$$
- 6/ Pan evaporation summed for growing season (April-October), with total for entire year in parentheses (Farnsworth and others, 1982, p. 1).

HOLOCENE (PRESENT) CLIMATE

Month	Temperature(°C)			Precipitation (cm)		Pan Evap.	ET _P (cm)		
	Mean Monthly								
	avg. 1/	max	min	low	high	(cm)2/	T 3/	B & C 4/	P 5/
J	4.8	12.4	-2.9	1.80	3.07	5.53	0.71	1.58	5.39
F	6.6	14.6	-1.3	1.78	3.02	7.54	1.17	2.36	6.23
M	9.8	18.7	1.1	1.27	2.16	14.44	2.74	2.83	8.42
A	14.2	23.3	5.0	1.27	2.16	15.14	5.35	4.89	11.18
M	18.4	28.1	8.8	0.84	1.43	26.52	9.06	10.19	15.01
J	23.3	33.5	13.1	0.31	0.52	29.52	13.42	14.72	20.62
J	27.1	37.5	16.7	0.46	0.78	31.64	17.45	16.13	25.61
A	25.9	36.2	15.5	0.51	0.86	27.07	15.17	14.76	23.90
S	22.2	32.5	11.9	0.46	0.78	20.63	10.39	12.17	19.68
O	15.8	25.2	6.4	0.76	1.30	13.34	5.62	8.52	12.62
N	9.7	18.5	0.8	0.91	1.55	6.53	2.22	3.11	8.35
D	5.7	13.5	-2.2	1.32	2.25	5.38	0.91	2.39	5.79
avg or sum									
	15.3	24.5	6.1	11.68	19.86	163.866/	84.21	93.65	162.80
						(203.28)			

CLIMATE DURING GLACIAL MAXIMUM - Spaulding model

J	-2.2	5.5	-2.9	2.44	4.14	4.98	0.00	0.00	2.32
F	-0.4	7.6	-1.3	2.40	4.08	6.79	0.00	0.00	2.76
M	2.8	11.7	1.1	1.72	2.92	13.00	1.28	0.29	4.02
A	7.2	16.3	5.0	1.72	2.92	13.63	3.73	1.10	5.52
M	11.4	21.1	8.8	1.13	1.92	23.87	6.73	3.22	7.70
J	16.3	26.5	13.1	0.15	0.26	26.57	9.92	5.85	10.99
J	20.1	30.5	16.7	0.23	0.39	28.48	12.58	7.23	13.87
A	18.9	29.2	15.5	0.25	0.43	24.36	11.03	6.39	12.88
S	15.2	25.5	11.9	0.23	0.39	18.57	7.71	4.63	10.51
O	8.8	18.2	6.4	1.03	1.75	12.01	4.07	2.24	6.35
N	2.7	11.5	0.8	1.23	2.10	5.88	1.02	0.30	4.00
D	-1.3	6.5	-2.2	1.78	3.31	4.84	0.00	0.00	2.53
avg or sum									
	8.3	17.5	6.1	14.31	24.32	147.47	58.07	31.25	83.45
						(182.96)			

CLIMATE DURING GLACIAL MAXIMUM - Mifflin and Wheat model

J	-0.2	7.5	-2.9	3.03	5.15	4.48	0.00	0.00	3.07
F	1.6	9.6	-1.3	2.99	5.08	6.11	0.40	0.16	3.61
M	4.8	13.7	1.1	2.13	3.63	11.70	1.82	0.50	5.11
A	9.2	18.3	5.0	2.13	3.63	12.27	4.22	1.40	6.92
M	13.4	23.1	8.8	1.41	2.39	21.48	7.33	3.78	9.52
J	18.3	28.5	13.1	0.51	0.87	23.91	10.70	6.56	13.40
J	22.1	32.5	16.7	0.77	1.31	25.63	13.62	7.95	16.82
A	20.9	31.2	15.5	0.85	1.45	21.92	11.93	7.06	15.65
S	17.2	27.5	11.9	0.77	1.31	16.71	8.33	5.24	12.81
O	10.8	20.2	6.4	1.28	2.18	10.81	4.51	2.75	7.91
N	4.7	13.5	0.8	1.54	2.61	5.29	1.47	0.53	5.07
D	0.7	8.5	-2.2	2.22	3.77	4.36	0.15	0.07	3.33
avg or sum									
	10.3	19.5	6.1	19.63	33.37	132.73	64.48	35.96	103.22
						(164.67)			

In addition to the orographic influence on precipitation, two basic storm types exist in the area. The two storm types result in precipitation derived from (1) winter cyclonic activity, and (2) intense summer convection (Houghton and others, 1975). As will be shown later, the seasonality of precipitation will influence some of the soil property vs depth relationships.

No long term temperature data exist for the Yucca Mountain area. D. L. Hoover (U.S. Geological Survey, written communication, 1984) however estimates that there is a 3°C difference in MAT in the 400 m elevation change. He bases this on the relationship that,

$$x = 7.48 - 0.004081y \text{ for MAT} \quad \text{Equation (2.2)}$$

where x = MAT in $^{\circ}\text{F}$ and y = elevation in feet.

Paleoclimate in the NTS Region

A large number of data sources exist to reconstruct the paleoclimate in the American Southwest. There are two sources of paleoclimatic information of particular interest in the study area, packrat middens and inferred climates conducive to the formation of pluvial lakes.

Packrat Midden Evidence

Paleoenvironmental data from analyses of plant microfossils remains in packrat (Neotoma sp.) middens provide perhaps the most detailed information concerning the timing and nature of climatic changes on the NTS during the late Quaternary (Van Devender and Spaulding, 1979; Spaulding, 1983 and 1985). Plants sensitive to frigid temperatures and those restricted to moist habitats are

missing in the plant microfossil record from 45-10 ka (Spaulding, 1985). Juniper and pinyon pine and Joshua tree were present at lower altitudes in the NTS area. These data suggest milder, wetter winters and cooler, drier summers relative to the present during the last glacial maximum (18 ka). Following the last glacial maximum Spaulding (1985) infers a warming trend from 16-10 ka. After 11-10 ka, the conditions like the present prevailed and juniper and pinyon pine woodland are not present. Elements of desert scrub were present by 15 ka at elevations as high as 990 m Spaulding (1982). The vegetation change was transitional, implying a transitional climatic change from late Pleistocene to Holocene.

Based on evidence from packrat middens, climatic conditions in the Yucca Mountain area during the glacial maximum (18 ka), compared to the present climate, probably had (1) a MAT decrease of 6-7°C, (2) drier summers with a temperature decrease of 7-8°C, and (3) winter precipitation up to 70% greater than present. In all the following discussions this climatic change is referred to as the Spaulding climatic model for the glacial maximum (Table 2).

Pluvial Lake Evidence

The pluvial lake chronologies in the southwestern United States suggest that the effective moisture of the late glacial and early Holocene was much greater than the effective moisture in the modern climate. High lake stands are recorded at 14-11 ka in lakes in both glacial and nonglaciaded drainages (Morrison, 1965; Benson, 1978; Lajoie and Robinson, 1982; Wells and others, 1984). The disappearance of juniper and pinyon pine woodland at 11-10 ka is

coincident with the lowering of Lake Mojave from a high stand between 15.5 and 10.5 ka (Wells and others, 1984).

Although the effective moisture was greater, there is little evidence in the northern Mojave Desert for increased annual precipitation during the late Wisconsin (18 ka). Present day playas contained ephemeral lakes or marshes during the full-glacial north of latitude 36° N (Mifflin and Wheat, 1979). Mifflin and Wheat (1979) propose that the MAT was 5°C lower, the MAP 69% greater, and the evaporation 10% less than today. This is referred to in the following discussions as the Mifflin and Wheat glacial maximum climatic model (Table 2).

The reduction of full-glacial summer precipitation in the NTS area, relative to that of today, can be attributed to the dependence of summer precipitation on oceanic air from the Gulf of Mexico. Global cooling weakened these subtropical high-pressure systems and restricted the influence of the oceanic air to very southern regions (Houghton and others, 1975). Summer precipitation also depends upon local convective uplift which is lacking if summer temperature is low.

Summary of the Glacial Climate Models

In the southern Basin and Range and northern Mojave desert regions, the onset of the last major glacial climate began about 45 ka (Spaulding, 1985). The late Wisconsin began about 24 ka, based on dates from Searles Lake (Smith, 1979), and the pollen and lake record from Lake Lahontan (Mehring, 1967; Benson, 1978), and at 18 ka is thought to have been a full glacial in the western United

States (CLIMAP, 1976). The period from 25 to 11 ka was the maximum development of alpine glaciers, intermittent filling of playa lakes, and expansion of upland vegetation. Physical evidence for paleoclimatic and paleoenvironmental reconstructions for the last glacial vary from a 2-3°C temperature decrease and a 100% increase in precipitation, to a 7-11°C temperature decrease and less precipitation than today (Spaulding and others, 1983; Thompson, 1984). At about 11 ka, there was a significant decrease in the pluvial lake levels, and changes in the vegetation, that mark the end of the late Wisconsin in the southwest (Van Devender and Spaulding, 1979). Transitional plant communities persisted until the early Holocene (7.8 ka) (Spaulding and others, 1983).

CHAPTER III

MAJOR PEDOLOGICAL CHANGES WITH TIME

Morphology

Soils that are formed in alluvium, colluvium and eolian sand of Holocene to early Pleistocene or latest Pliocene(?) age near Yucca Mountain are characterized by distinctive trends in the accumulation of secondary clay, CaCO_3 , and opaline SiO_2 that correspond with the ages of the surficial deposits.

Pedogenic Opaline Silica

Cementation by pedogenic opaline SiO_2 is common in the study area. Accumulation of opaline SiO_2 is common in soils containing readily weatherable glass from pyroclastic rock or volcanic ash, such as those in the study area. Eolian influx of readily soluble silica-rich dust is also a likely source. Glass tends to weather rapidly and if it is of mafic composition, rich in bases, weathering can liberate silica at a rapid rate. The glass alters to amorphous SiO_2 or semi-crystalline allophane, imogolite and opaline SiO_2 (Bleeke and Parfitt, 1984).

In general, two terms are used for silica and (or) cemented layers: (1) duripan, specifically for pedogenic accumulations (Soil Survey Staff, 1975), and (2) silcrete for geologic-pedologic occurrences (Summerfield, 1983; Nettleton and Peterson, 1983). Both

terms are applied to an indurated product of surficial and (or) near-surface silicification, formed by the cementation and (or) replacement of bedrock, unconsolidated sediments, or soil. The silicification is produced by low temperature physio-chemical processes. Silcretes are not exclusively the product of pedogenic weathering. A few grade laterally into petrocalcic horizons (Summerfield, 1982 and 1983). Silcrete has an arbitrary lower limit of 85% opaline SiO_2 by weight (Summerfield, 1982 and 1983), so it would be a very unusual pedogenic horizon. Silcretes are not present in the study area. Duripans have no specified limits on the content of opaline SiO_2 , they vary in the degree of cementation by SiO_2 and commonly contain accessory cements, chiefly CaCO_3 .

Because silica accumulation produces a unique morphology that varies with age, stages of development recognized in this study have been defined (Table 3). On the basis of horizon morphology, those with stages III-IV morphology would qualify as duripans of the Soil Conservation Service (Soil Survey Staff, 1975, p. 41).

Table 3. General characteristics of pedogenic opaline silica stages.

Stage I	White, yellow, or pinkish scale-like coatings <2 mm thick on the undersides of gravel clasts. Found in some soils on Q1c deposits, may occur at depths on older deposits.
Stage II	Stalactitic or pendant-like features 2-4 mm long extending downward from a coat on the undersides of gravel clasts. Found in soils on Q2b deposits, may occur at depths on older deposits.
Stage III	Opaline SiO_2 cemented horizon, extremely hard when dry. Peds do not slake in water or a weak solution of HCl. The characteristic 7.5YR hue is probably due to clay particles in the silica cement. Found in soils on Q2b, Q2c and Q1a deposits, and maximum accumulations tend to form in horizons of maximum CaCO_3 accumulation. Frequently in the field stage III appears to be forming above the maximum accumulation of CaCO_3 because the whiteness of the CaCO_3 masks the precipitated opaline SiO_2 .
Stage IV	Stage III morphology along with laminar, indurated opaline SiO_2 platelets, 4-10 mm thick, in the upper part. Maximum CaCO_3 accumulation is below maximum opaline SiO_2 induration. Commonly calcareous ooids are precipitated above platelets. Found in soils on Q2c (infrequently and thin) and Q1a deposits.

Carbonate and Opaline Silica

At the NTS, soils accumulate secondary CaCO_3 and opaline SiO_2 in distinctive trends with increasing ages of the surficial deposits. Soils formed in gravelly alluvium less than 3(?) ka (Q1b) contain little or no secondary CaCO_3 or opaline SiO_2 . Soils formed in gravelly alluvium 3-20(?) ka (Q1c) and sandy colluvium about 30-40 ka (Q2a) commonly have a Bk horizon about 20-50 cm thick that has thin, discontinuous coatings of CaCO_3 (stage I) and (or) opaline SiO_2 scales and pendants on the undersides of stones (stage I-II). Soils formed in gravelly alluvium about 140-160 ka (Q2b) may have a

opaline SiO_2 -cemented Btqm horizon (duripan, stage III) about 50 cm thick that overlies or engulfs a CaCO_3 -enriched Bk/K (stage II-III) horizon about 50-70 cm thick. The secondary opaline SiO_2 in the duripan typically occurs as finely disseminated matrix cement and as coatings and pendants on stones. The secondary CaCO_3 in the underlying Bk/K horizon typically occurs as coatings on stones and as bridges between some of the stones in the Bk-layers, and as coatings and finely disseminated matrix cement in the CaCO_3 -indurated K-lenses. Soils formed in gravelly alluvium about 300-400 ka (Q2c) commonly have a opaline SiO_2 -indurated Kqm horizon (stage III) about 50 cm thick that overlies a Bk/K horizon (stage II-III) about 40-50 cm thick. The oldest alluvium, which is >1 Ma (QTa), has soils with a Kqm horizon more than 100 cm thick. Commonly, the upper part of the Kqm horizon consists of platelets, 0.5-1 cm thick, cemented by laminar opaline SiO_2 (stage IV), and it may be overlain by layers of CaCO_3 ooids as much as 10 cm thick (stage III).

Carbonate is primarily derived from airborne dust and the opaline SiO_2 from in-place weathering of the parent material, although the addition of silica-rich dust may also be a likely source.

The CaCO_3 morphology in the NTS area differs from that described by Gile and others for the Las Cruces area, New Mexico, although both areas have similar climates, soil parent materials, and accumulation rates of modern airborne dust (Gile and others, 1979). In addition, secondary CaCO_3 is less abundant in the NTS area than in deposits of similar age in the Las Cruces area. These differences in the amount of secondary CaCO_3 may result from

differences in the seasonality of precipitation and the amount of secondary opaline SiO_2 . Unlike the Las Cruces area, most precipitation in the NTS area occurs during the cool, winter months at soil moisture temperatures that result in CaCO_3 being more soluble (Table 2). Infiltrating soil moisture tends to translocate CaCO_3 to the base of the wetting zone, where it forms lenses rather than discrete K horizons as in the Las Cruces area. Thin-section studies of soils in the NTS area indicate that opaline SiO_2 has replaced CaCO_3 in some of the older soils. This relationship suggests that opaline SiO_2 accumulation in the NTS soils is favored over that of CaCO_3 .

Vesicular A Horizons

Well developed vesicular A horizons (Av) have not formed on the coarse gravelly Holocene deposits (Qlc) in the Yucca Mountain area. On the Pleistocene deposits the Av 's are typically between 5 and 10 cm thick and there is no relationship between the thickness of the Av horizon and the age of the underlying deposit. Eolian silts and fine sands appear to accumulate only on deposits that have been previously plugged or partly plugged by the addition of fine material into the coarse alluvium. Although McFadden and others (1984) have described the ubiquitous nature of Av 's in the Mojave desert on Holocene deposits and volcanic flows, it appears in this area that due to the coarseness of most of the young deposits, available eolian fines are either translocated deeper into the deposit or lost by wind erosion. It is also possible that the eolian material that forms Av horizons has been less abundant during

the Holocene, although this contradicts many of the current ideas on sediment availability associated with the Holocene-Pleistocene climatic change (Bull, 1979).

Profile Index Values

Field properties of soils (Appendix A) can be quantified by assigning points for developmental increases in soil properties in comparison to those of the parent material (Harden, 1982; Harden and Taylor, 1983) (Appendix B). Ten field properties are quantified and normalized for each horizon, including two properties that reflect CaCO_3 buildup in soils formed in arid environments. The ten properties are rubification (increasing (redder) color hue and (or) chroma), melanization (decreasing (darkening) color value), color paling (decreasing (yellower) color hue and (or) chroma), color lightening (increasing (whitening) color value), total texture (includes texture and wet consistence), clay films, structure, dry consistence, moist consistence, and pH. Unlike the Harden (1982) definition, values for pH were quantified based on the absolute difference in comparison to the parent material. Moist consistence was usually not determined in this study, therefore it was not included in the index calculations.

Soil profile indices were initially calculated two different ways; using all soil properties and (1) rubification and melanization, or (2) color paling and lightening properties. Both ways to calculate the soil profile index include eight properties. I have called the first way to calculate the profile index value rub-mel, and the second pale-light. Rub-mel was developed for a

xeric soil moisture regime, and pale-light for an arid soil moisture regime. According to Harden and Taylor (1983) complete profiles are calculated using either one of the two methods, not combinations for a given profile. Profile indices are calculated using either rubification and melanization, (rub-mel) or color paling and color lightening (pale-light).

Parent material values used to calculate the indices vary with the kind of material. For alluvium they are 10YR 6/2 (dry) and 10YR 4/2 (moist), sand, loose, and non-sticky and non-plastic. In contrast, for the eolian sand and reworked gravels the values are 10YR 6/3 (dry) and 10YR 4/3 (moist), sandy loam, soft, and non-sticky and non-plastic.

Of the ten possible independent properties all were significant with log age at the 5% level, except melanization ($r^2=0.01$) and color paling ($r^2=0.01$) ($N=20$, r^2 critical=0.18) (Fig. 5). The properties most significant in the profile index calculation have the highest r^2 values. They are dry consistence ($r^2=0.48$), color lightening ($r^2=0.45$), rubification ($r^2=0.40$), and structure ($r^2=0.37$), and are referred to as the four best properties (Fig. 5). The profile index values using the four best properties did not improve the relationship between soil development and time over that using all eight properties with the highest r^2 values (Fig. 6).

Significant trends are apparent when profile index values (Appendix B) are plotted as a function of age (Fig. 6). Profile index values have been calculated using rub-mel and pale-light soil properties (Fig. 6). It makes no difference in the index values vs

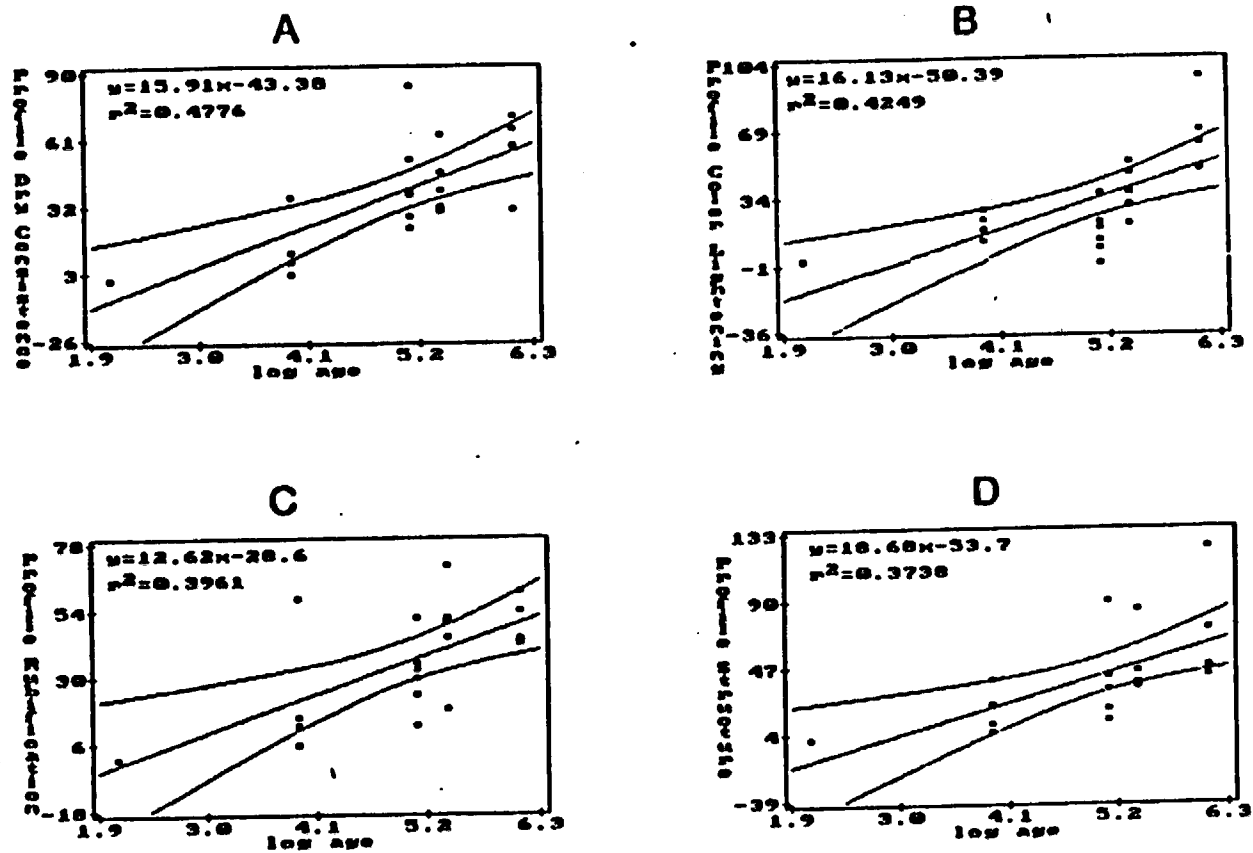


Figure 5. Bivariate regression analyses of significant property profile index values vs time. 95% confidence interval surrounds regression line. (A) dry consistence, (B) color lightening, (C) rubification, (D) structure, (E) texture, (F) clay films.

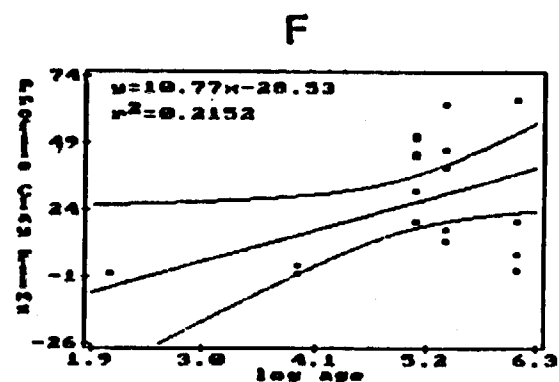
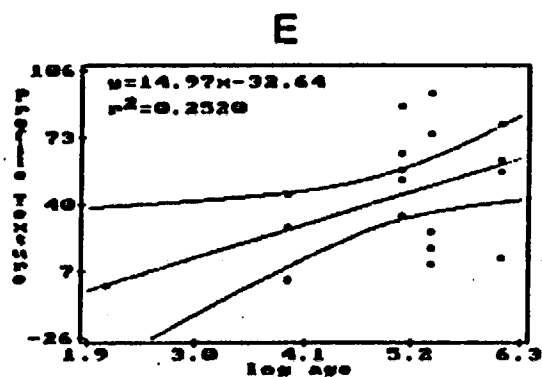


Figure 5 continued. Bivariate regression analyses of significant property profile index values vs time. 95% confidence interval surrounds regression line. (A) dry consistence, (B) color lightening, (C) rubification, (D) structure, (E) texture, (F) clay films.

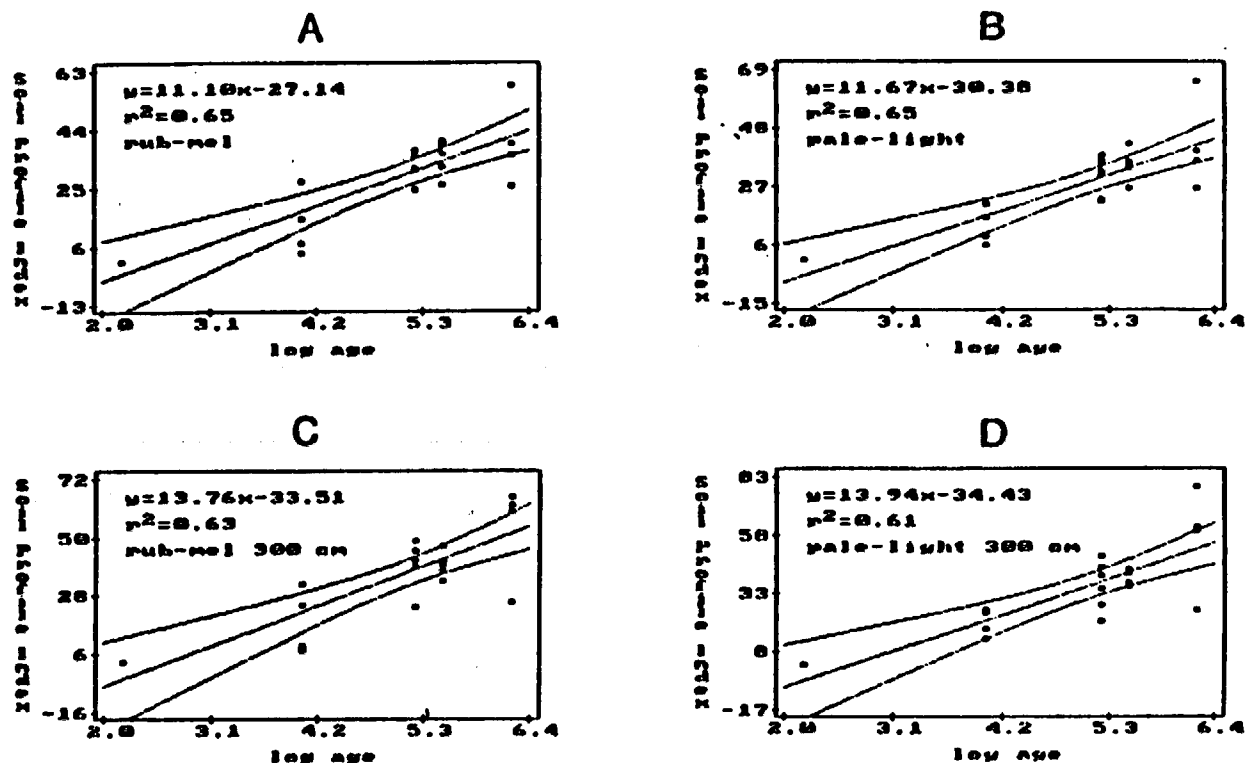


Figure 6. Bivariate regression analyses of soil profile index values vs time. 95% confidence interval limits are above and below the regression line. (A) Rub-mel, all soil properties including rubification and melanization. (B) Pale-light, all soil properties including color lightening and color paling. (C and D) Soil properties for rub-mel and pale-light climatic regime are quantified to an arbitrary maximum depth of 300 cm. (E) Rub-light, all soil properties including rubification and color lightening. (F) Best four properties are dry consistence, color lightening, rubification, and structure.

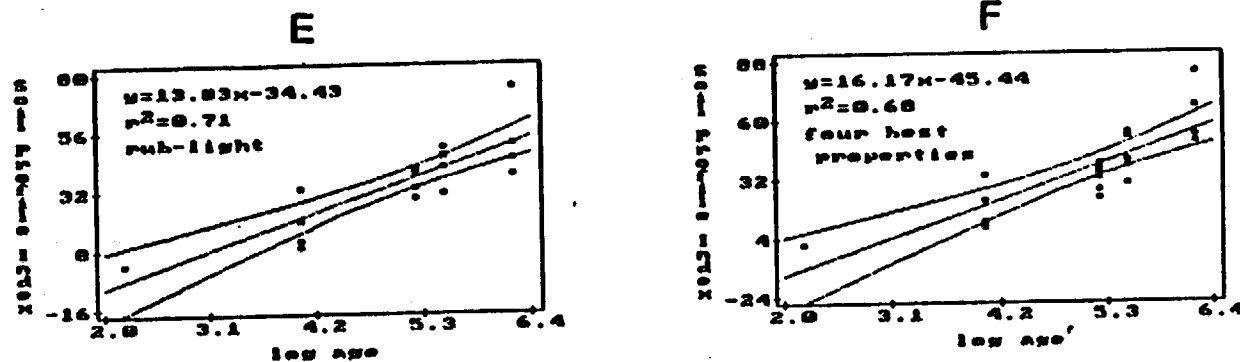


Figure 6 continued. Bivariate regression analyses of soil profile index values vs. time. 95% confidence interval limits are above and below the regression line. (A) Rub-mel, all soil properties including rubification and melanization. (B) Pale-light, all soil properties including color lightening and color paling. (C and D) Soil properties for rub-mel and pale-light climatic regime are quantified to an arbitrary maximum depth of 300 cm. (E) Rub-light, all soil properties including rubification and color lightening. (F) Best four properties are dry consistence, color lightening, rubification, and structure.

time if the rub-mel ($r^2=0.65$) or pale-light ($r^2=0.65$) properties are for the measured profile thickness, or are for an arbitrary depth of 300 cm for the rub-mel ($r^2=0.63$) or pale-light ($r^2=0.61$) properties (Fig. 6).

Because melanization and color paling did not have significant correlations with time, the profile index was calculated using rubification and color lightening. When all soil properties are included with rubification and color lightening the profile index value is called rub-light. The rub-light profile index values vs time increases the r^2 value to 0.71 (Fig. 6).

The increase in the individual profile property values with time (Fig. 5) can be explained by aridic climatic pedogenesis models. Rubification increases both because of the increasing redness of Bt horizons and the accumulation of opaline SiO_2 , as the latter results in colors redder than the parent material. Lightening increase with time because A horizons do not get darker, and CaCO_3 and opaline SiO_2 accumulating horizons are lighter than the parent material. Dry consistence gets harder over time as clay and cementing agents accumulate and indurate horizons. Structure changes from unconsolidated parent material. Texture, wet consistence, structure, and clay films represent pedogenic accumulations of clay.

There may be a subtle influence of local climate on profile index values. Unit Q1c shows little change with elevation, but weak trends are discernable for units Q2b, Q2c, and QTa with the increase in QTa being much greater than that of the younger units when only the four best properties are used (Fig. 7).

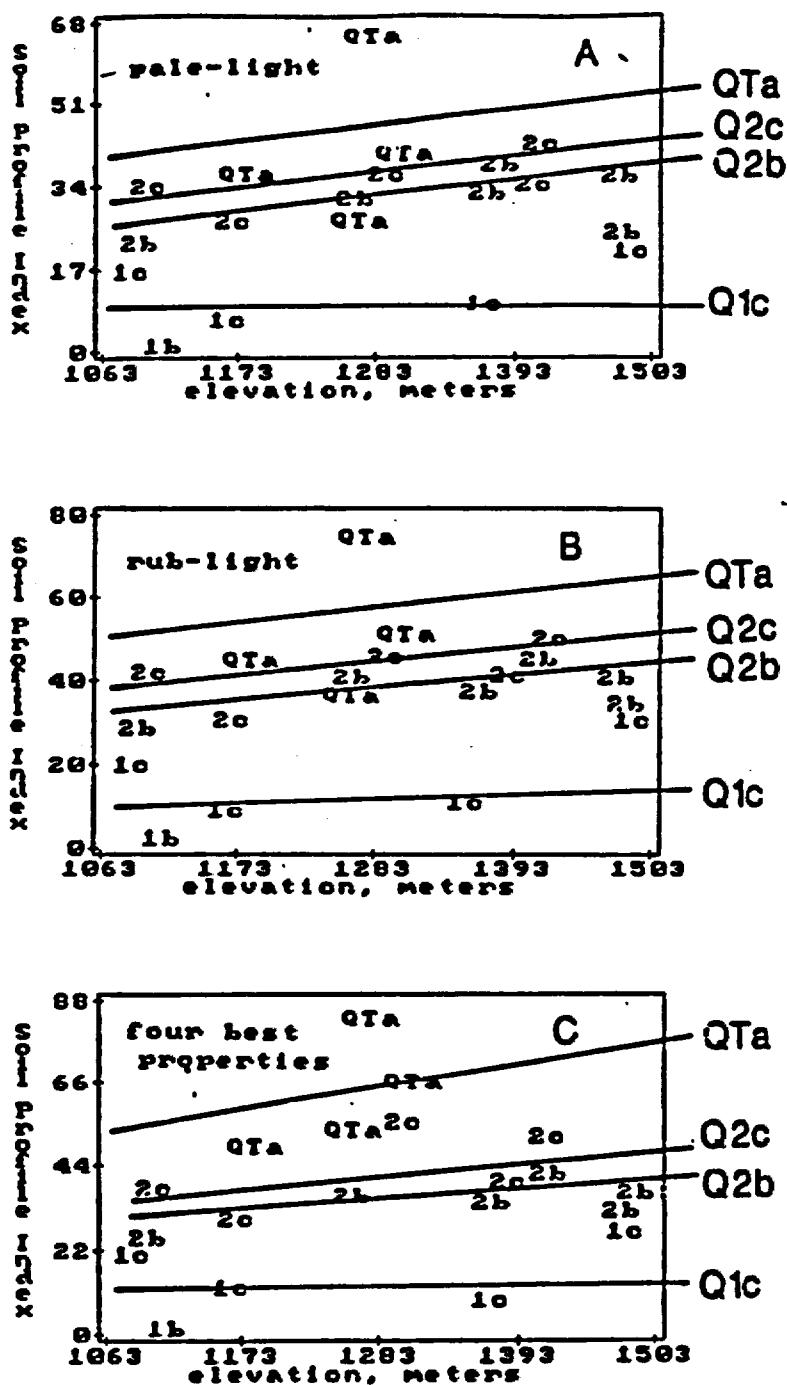


Figure 7. Soil index values vs elevation. The index value plots between the number and letter of each stratigraphic unit. (A) Pale-light field properties including color paling and color lightening. (B) Rub-light properties including rubification and color lightening. (C) Index calculated using four best properties: dry consistence, rubification, color lightening, and structure.

Profile index values for the study area are comparable to index values from the Las Cruces, New Mexico soil chronosequence (Harden and Taylor, 1983) (Table 4). Comparative index values are best when they are based on the four best properties. The older soils in the Las Cruces area have greater values probably because CaCO_3 accumulation is greater for deposits of a given age at Las Cruces than at NTS.

Table 4. Comparison of soil profile index values for the study area and Las Cruces, New Mexico.

AGE		INDEX VALUES				
		This Study	Las Cruces		Four Best Properties	
log Age	Cruces Age	Pale-light ¹	Rub-light ²	Pale-light ¹	This Study ³	Las Cruces ⁴
2.18	150 yrs	--	<5	<5	<5	
4.00	10 ka	4-20 ka	6-21	9-32	5-41	9-33 4-35
5.18	150 ka	120 ka	23-38	29-41	22-26	23-39 24-31
5.48	300 ka	290 ka	26-42	31-49	1-56	30-54 29-95
6.18	1.5 my	>500 ka	27-64	38-74	>43	49-83 >110

¹ all properties including color paling and color lightening

² all properties including rubification and color lightening

³ dry consistence, structure, color lightening, rubification

⁴ dry consistence, structure, color lightening, color paling

Accumulations of Carbonate, Clay, Silt, and Opaline Silica

The influence of age and climate on soils can be evaluated based on trends in the accumulation of pedogenic CaCO_3 , clay, silt, and opaline SiO_2 (Gile and others, 1979 and 1981; McFadden, 1982; Machette, 1985). The amounts of these pedogenic constituents can be determined by deducing the initial amount in the soil parent material from that in the present soil.

Method to Calculate Rates of Accumulation

Trends in soil constituents are best when expressed on a mass basis. Secondary accumulation of all constituents can be computed in gm in a vertical column of 1 cm² area for the <2mm fraction, for each horizon according to equation 3.1.

Equation (3.1)

$$P = ([(\%P)(BD)_{\text{present}} - (\%P)(BD)_{\text{PM}}] \text{thickness})(\%<2\text{mm})$$

where P = pedogenic property, BD = bulk density, and PM = parent material.

The profile sum is calculated by summing the horizon values through the profile (Fig. 8), and rates of accumulation are computed by dividing the estimated age into the average profile sum for a unit (Fig. 9). Predicted profile sums are the average gm/cm²/10³ yr rate for a given unit converted to a yearly number, and multiplied by the soil age (Appendix H). Predicted profile sums are used to check the age assignment for a given unit.

Rates of Accumulation of CaCO₃, Clay, Silt, and Opaline SiO₂

Profile sums suggest that CaCO₃, clay, silt, and opaline SiO₂ accumulated at a logarithmic rate (Fig. 8). All r² values were highest when the log age regression model was used (Table 5). However, these logarithmic rates may be a function of the erosion and soil loss on the older surfaces, and the complete volume of these constituents may not be measured. The long term rates in fact, for properties dependent primarily on eolian additions is probably better expressed as a linear rate.

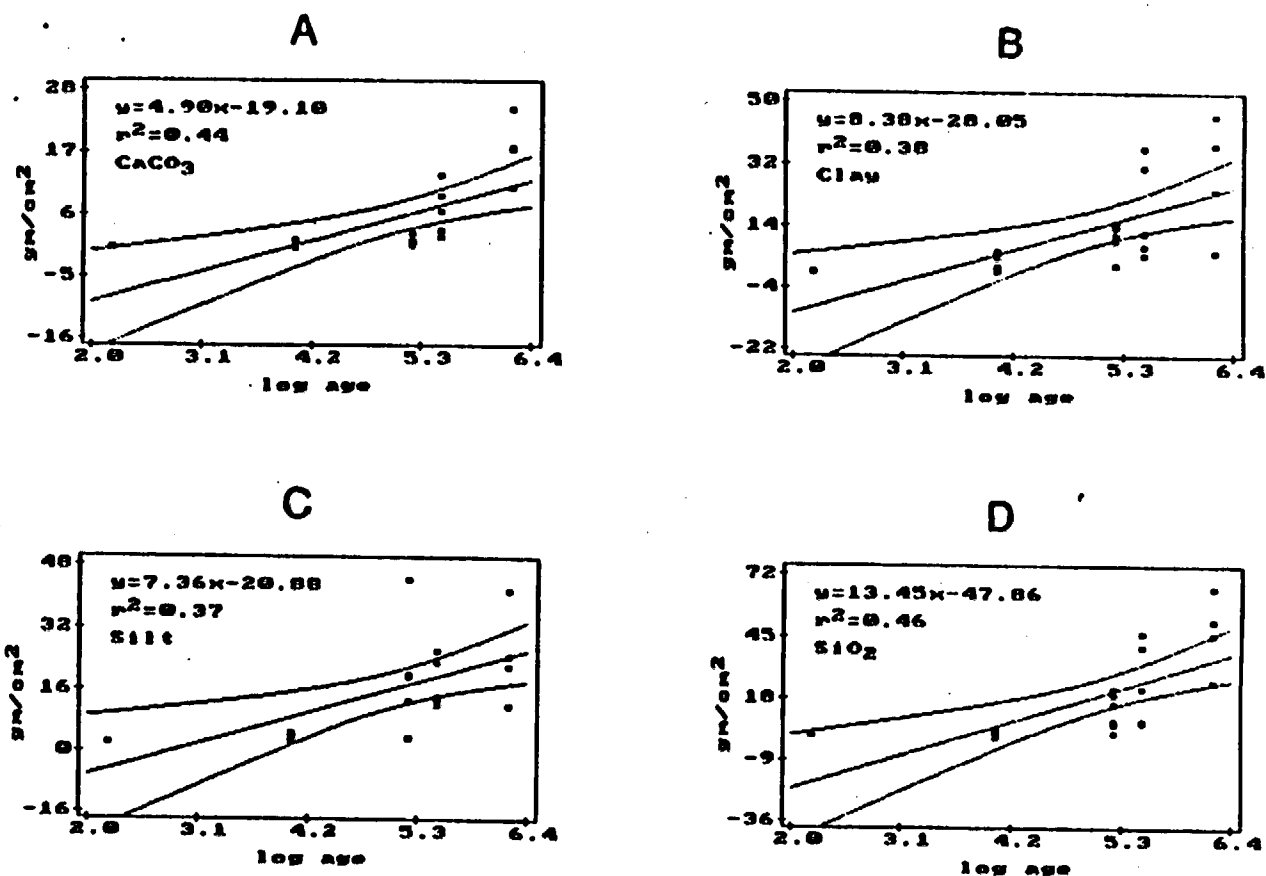


Figure 8. Profile sum of horizon weights vs age for pedogenic CaCO_3 (A), clay (B), silt (C), and opaline SiO_2 (D) on soils developed on stratigraphic units Q1c ($10^{4.0}$), Q2b ($10^{5.18}$), Q2c ($10^{5.48}$), and QTa ($10^{6.182}$).

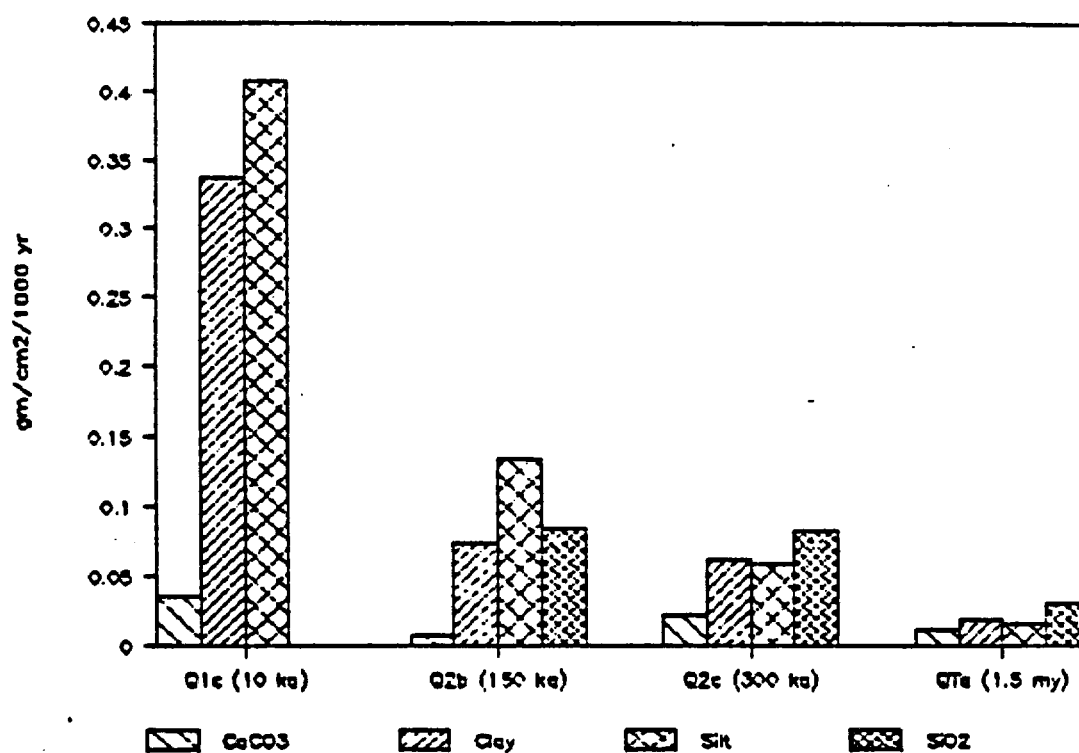


Figure 9. Average rates of accumulation of pedogenic CaCO_3 , clay, silt, and opaline SiO_2 (profile sums divided by age) based on profile weight sums, on soils developed on stratigraphic units Q1c, Q2b, Q2c and QTa.

Table 5. Correlation coefficients (r^2) for CaCO_3 , clay, silt, and opaline SiO_2 profile sums vs. linear age and log age. Critical value for r^2 at a 5% probability level is 0.42, and at 1% is 0.54.

	linear age	log age
CaCO_3	0.39	0.44
Clay	0.12	0.38
Silt	0.02	0.37
SiO_2	0.23	0.46

Holocene soils (Q1c) accumulate CaCO_3 , clay, and silt at a higher average rate than the older soils. For example, CaCO_3 accumulation decreases from an average rate of $0.04 \text{ gm/cm}^2/10^3 \text{ yr}$ during the Holocene to $0.01\text{--}0.03 \text{ gm/cm}^2/10^3 \text{ yr}$ in the older soils (Fig. 9). Clay and silt accumulation rates on the Q1c deposits are considerably higher than on the older deposits. Deposits Q2b and Q2c are the best estimates of long term average rates of accumulation of CaCO_3 , clay, silt, and opaline SiO_2 . The gently rolling topography of Q1a is a result of long term erosion. The low rates for all four properties on Q1a are a result of the erosion which has formed the ballena topography. The loss of soil results in calculated low accumulation rates (Appendix H).

There are several sources for the CaCO_3 , clay, silt, and opaline SiO_2 accumulations in soils. One source is weathering and (or) translocation of a constituent in place. Pedogenic opaline SiO_2 forms this way as may some clays. A second source is atmospheric additions, either as ions in solution (in the case of Ca^{++}) or as solid dust particles (clay, silt, and some CaCO_3) (Gile and others, 1979).

A generalized model for CaCO_3 , clay, silt, and opaline SiO_2 accumulation rates is that the rates vary with climate. During interglacials (7,000-20,000 yrs duration) rates are rapid because increased aridity, decreased vegetation cover, and exposed playa surfaces, all contribute to increased airborne transport. Greater areas are exposed and wind has better access to it, resulting in greater accumulation rates. In contrast increased vegetation and more effective precipitation of glacial climates (100,000-150,000 yrs duration) could result in comparatively slow rates of accumulation. Yet another factor is having sufficient precipitation to move atmospheric materials into the soil. For example, accumulation rates of pedogenic CaCO_3 in the Mojave Desert during the Holocene are characterized by Machette (1985) as climate or precipitation-limited, suggesting that soils may be accumulating material slower now than in the late Pleistocene because of the lack of sufficient precipitation to move material into the soil via soil-water movement. Therefore during glacial climates there is less available eolian material, but greater precipitation to translocate the material, and during interglacial climates insufficient precipitation to translocate the available eolian dust. Accumulation rates could be the same in both climates, or different.

Rates of CaCO_3 accumulation in the study area are extremely low compared to rates calculated by Machette (1985) for the Vidal Junction area, which has a climate similar to that of the study area. The rates also vary with age of stratigraphic unit in the study area (Fig. 9). However, if the Q1c soils actually range in age for 5 to 40 ka, then these reputed Holocene rates may be too

high. If an age of 5,000 yrs is assumed, the rate for CaCO_3 accumulation would be $0.08 \text{ gm/cm}^2/10^3 \text{ yr}$, and if an age of 40,000 yrs is assumed, the rate would decrease to $0.01 \text{ gm/cm}^2/10^3 \text{ yr}$. Both rates fall within the range of long term rates. In either case, the decrease in precipitation associated with the climatic change at the Holocene-Pleistocene boundary was not enough to significantly decrease the already extremely low rate of CaCO_3 influx. In fact, similar rates of carbonate accumulation during the Holocene and pre-Holocene may suggest that the climatic change was the result of decreased temperatures and not precipitation.

Rates of accumulation of clay and silt respond the same way as CaCO_3 to changes in age assessment on the Qlc deposit. If Qlc is estimated to be between 5-40 ka, the rates still remain higher than the long term rates calculated on the older deposits (Fig. 9). For clay the range of accumulations rates is between $0.7-0.09 \text{ gm/cm}^2/10^3 \text{ yr}$, and for silt between $0.8-0.1 \text{ gm/cm}^2/10^3 \text{ yr}$ on the Qlc deposit. The long term rate for clay is $0.08-0.07 \text{ gm/cm}^2/10^3 \text{ yr}$, and for silt $0.13-0.06 \text{ gm/cm}^2/10^3 \text{ yr}$. This suggests that precipitation since the stabilization of Qlc is not a limiting factor, and that clay and silt are not being accumulated slower during the Holocene than during glacial climates. This supports the CaCO_3 accumulation data that the climatic change was not enough to significantly decrease rates of accumulation.

Rates of accumulation of opaline SiO_2 remain relatively constant over time at about $0.08 \text{ gm/cm}^2/10^3 \text{ yr}$. There is little or no opaline SiO_2 to be measured for soils on the Qlc deposits.

Machette (1985) proposes that it is reasonable to use average profile CaCO_3 content of relic soils between about 100,000 and 150,000 yrs old to estimate the ages of still older calcic soils in the same chronosequence. Soils in this age range have experienced a number on glacial-interglacial climatic cycles. Age estimates of soils younger than 100,000 yrs may also be made, but they may be less precise. In this study, no unit consistently best estimated the age.

In the study area a number of different rates for a given property were used to calculate an estimated profile sum (Appendix H). The difference between the estimated sum and the actual profile sum was calculated. The amount of time to account for the difference was then computed. For example, for deposit Q2c the average profile sum is 6.80 gm/cm^2 , but the estimated profile sum is 3.0 gm/cm^2 ($0.01 \text{ gm/cm}^2/10^3 \text{ yr}$, the long term rate, $\times 300,000$ yrs). At a rate of $0.01 \text{ gm/cm}^2/10^3 \text{ yr}$ it would take 380,000 yrs to accumulate the difference ($6.80 - 3.0 = 3.80 \text{ gm/cm}^2$). This discrepancy is either (1) an age error of 100%, (2) accumulation rates are off by one half for that age range, this may be accounted for by erosion on deposits that the long term rates are calculated from or (3) represents additions of about two times the potential CaCO_3 on the Q2c deposits used in this example.

Depth Functions of Significant Soil Properties

Soil properties that commonly exhibit change with time and (or) climate include clay, CaCO_3 , and opaline SiO_2 . Most of these properties are also strongly influenced by vertical position in the

soil profile, as illustrated for some properties of soils in the Yucca Mountain area (Figs. 10-13).

Soils exhibit increases in clay, CaCO_3 , and opaline SiO_2 over time. Pedogenic change can be better examined by converting these properties to horizon weights. Pedogenic clay clearly increases with time, although CaCO_3 and opaline SiO_2 have higher correlation coefficients with the age of the deposit (Table 6). With the exception of soils formed on deposits of Q2c age, clay, CaCO_3 , and opaline SiO_2 maximums occur in the same horizon (Figs. 10-13). On Q2c deposits the maximum occurrence of pedogenic clay is immediately above the maximum occurrence of pedogenic CaCO_3 and opaline SiO_2 . In nearly all soils formed in all deposits, the maximum CaCO_3 and opaline SiO_2 occur in the same horizon, and there is more opaline SiO_2 than CaCO_3 .

Table 6. Correlation coefficients (r^2) for linear age, log age, CaCO_3 , clay, and opaline SiO_2 for A, B and K, and C horizons, and all horizons combined. No significant opaline SiO_2 was measured on A and C horizons. Critical values for r^2 at the 5% probability level are 0.35 for A horizons, 0.18 for B and K horizons combined, 0.37 for C horizons, and 0.14 for all horizons combined.

	A C	B & K all	A C	B & K all	A C	B & K all	A C	B & K all
	linear age		log age		CaCO_3		Clay	
CaCO_3	.55	.49	.43	.42				
	.58	.43	.42	.26				
Clay	.21	.44	.18	.42	.40	.55		
	.11	.37	.49	.34	.30	.58		
Opaline SiO_2	-	.52	-	.47	-	.75	-	.85
	-	-	-	-	-	-	-	-

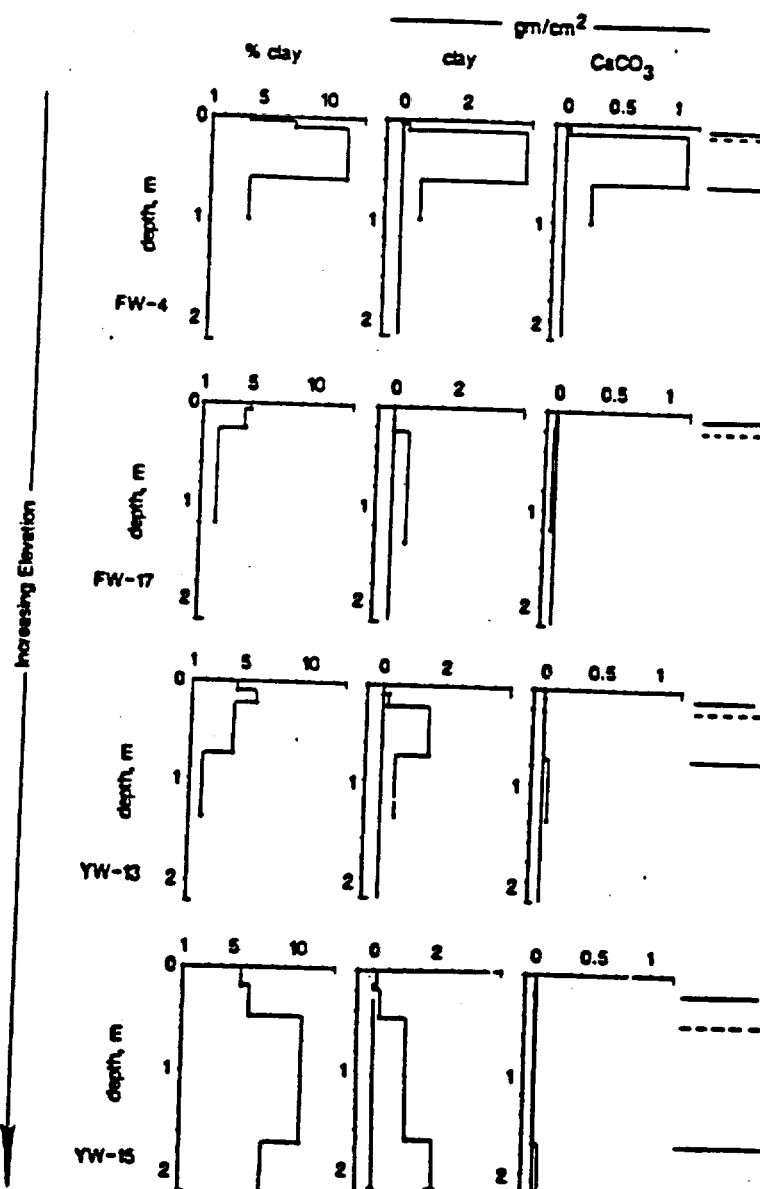


Figure 10. Depth plots of pedogenic clay, CaCO_3 , and opaline SiO_2 in soils developed on unit Q_{1c} . Lines on the far right represent major horizon and depositional boundaries: solid lines are for A-B or K-C horizons, dashed lines are for depositional boundaries.

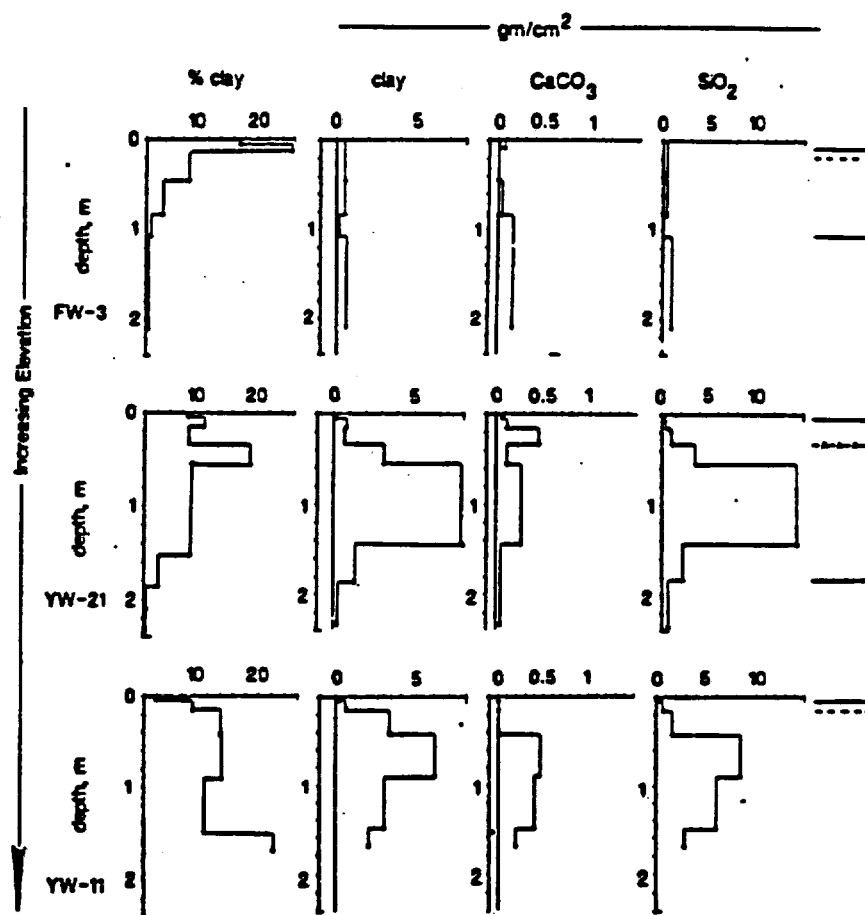


Figure 11. Depth plots of pedogenic clay, CaCO_3 , and opaline SiO_2 in soils developed on unit Q2b. Lines on the far right represent major horizon and depositional boundaries: solid lines are for A-B or K-C horizons, dashed lines are for depositional boundaries, and dashed lines with x's are for buried soils.

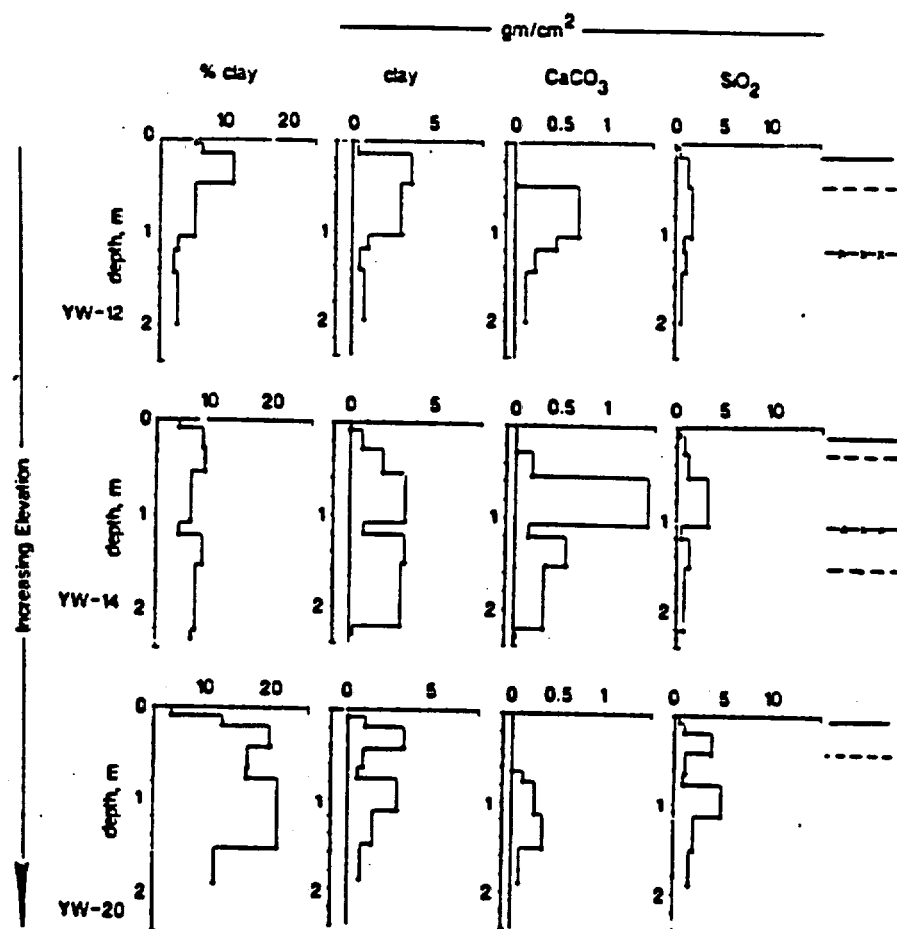


Figure 11 continued. Depth plots of pedogenic clay, CaCO₃, and opaline SiO₂ in soils developed on unit Q2b. Lines on the far right represent major horizon and depositional boundaries: solid lines are for A-B or K-C horizons, dashed lines are for depositional boundaries, and dashed lines with x's are for buried soils.

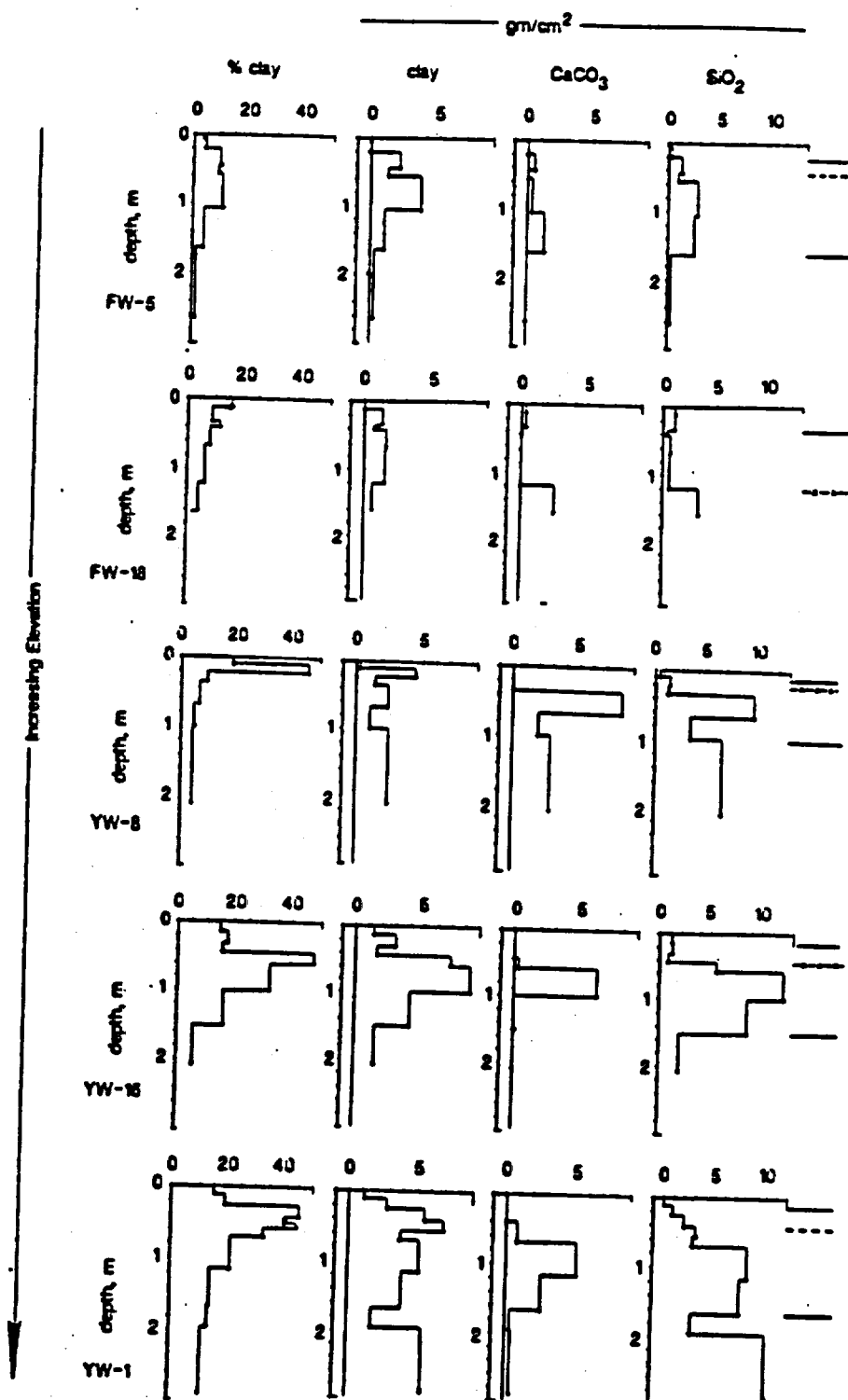


Figure 12. Depth plots of pedogenic clay, CaCO_3 , and opaline SiO_2 in soils developed on unit Q2c. Lines on the far right represent major horizon and depositional boundaries: solid lines are for A-B or K-C horizons, dashed lines are for depositional boundaries, and dashed lines with x's are for buried soils.

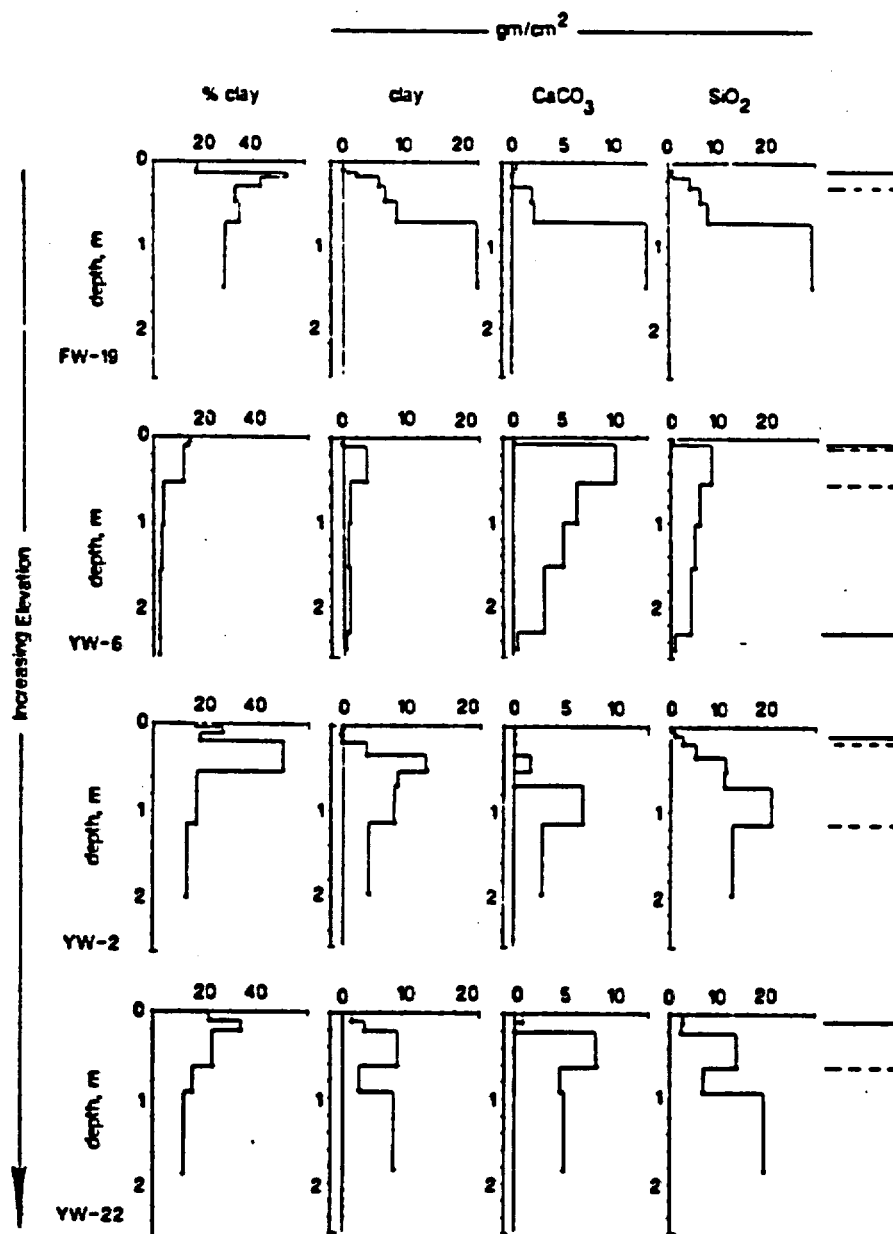


Figure 13. Depth plots of pedogenic clay, CaCO_3 , and opaline SiO_2 in soils developed on unit QTa. Lines on the far right represent major horizon and depositional boundaries: solid lines are for A-B or K-C horizons, dashed lines are for depositional boundaries, and dashed lines with x's are for buried soils.

Primary and Secondary Minerals Identified by X-ray Diffraction

Quartz, feldspars (primarily plagioclase and orthoclase), are the dominant minerals in the parent material sand and silt fraction. These minerals as well as dolomite dominate the clay fraction. Quartz is the dominant peak in most X-ray diffraction (XRD) traces. The following clays were identified in the soils: tobermorite, weathered mica, a mixed layer group of minerals, and kaolinite (Table 7). There is also XRD evidence for amorphous silica.

Tobermorite [$\text{Ca}_5(\text{Si}_6\text{O}_{18}\text{H}_2) \cdot 4\text{H}_2\text{O}$] is a hydrated calcium silicate found in cement, and rarely occurs in nature (Taylor, 1950; Heller and Taylor, 1951). It has a 2:1 layer structure similar to that of vermiculite (Megaw and Kelsey, 1956; Hamid, 1980), with minor variations in structure due to the chemical composition. Tobermorite displays a sharp peak at 11.6\AA when untreated, which shifts to 10.4\AA when glycolated (Fig 14). Although it is always reported to shift to 9.35\AA when heated to 300°C and collapse at 800°C (Taylor, 1959), in these and other soil samples (Reheis, 1984) it is completely destroyed by heat treatment, and when pedogenic opaline SiO_2 is chemically removed (Appendix D). It has cation-exchange and selectivity properties intermediate between those of clay minerals and zeolites (Komarneni and Roy, 1983). Wollastonite is the stable phase resulting from the destruction of tobermorite at 800°C .

Tobermorite is usually found in zones of intense hydrothermal alteration (Heddle, 1880; McConnell, 1954; Harvey and

Table 7. Clay Minerals Identified and their Diagnostic Features

Clay Mineral	Air Dry	TREATMENT				Silica Removed	Probable Source
		I <u>1/</u>	Glycolated	300°C	500°C		
Tobermorite	11.3-11.4 <u>2/</u> (002)	s	10.6	d <u>3/</u>	d	d	parent material and pedogenic
Weathered Mica	10.2-10.3 (001)	m-w, b	nc <u>4/</u>	nc	nc	nc	pedogenic
Mixed Layer	10.5-12.0 (001)	b	nc	nc	peak intensifies (s)	nc	pedogenic
Kaolinite	7.1-7.3 (001)	s-w, b	nc	nc	d	nc	parent material

1/ Intensity of Peak: s, strong or sharp spike; m, moderate spike; w, weak spike; b, broad or spread out.

2/ All values are in Å.

3/ d, peak disappeared

4/ nc, no change in peak intensity or width.

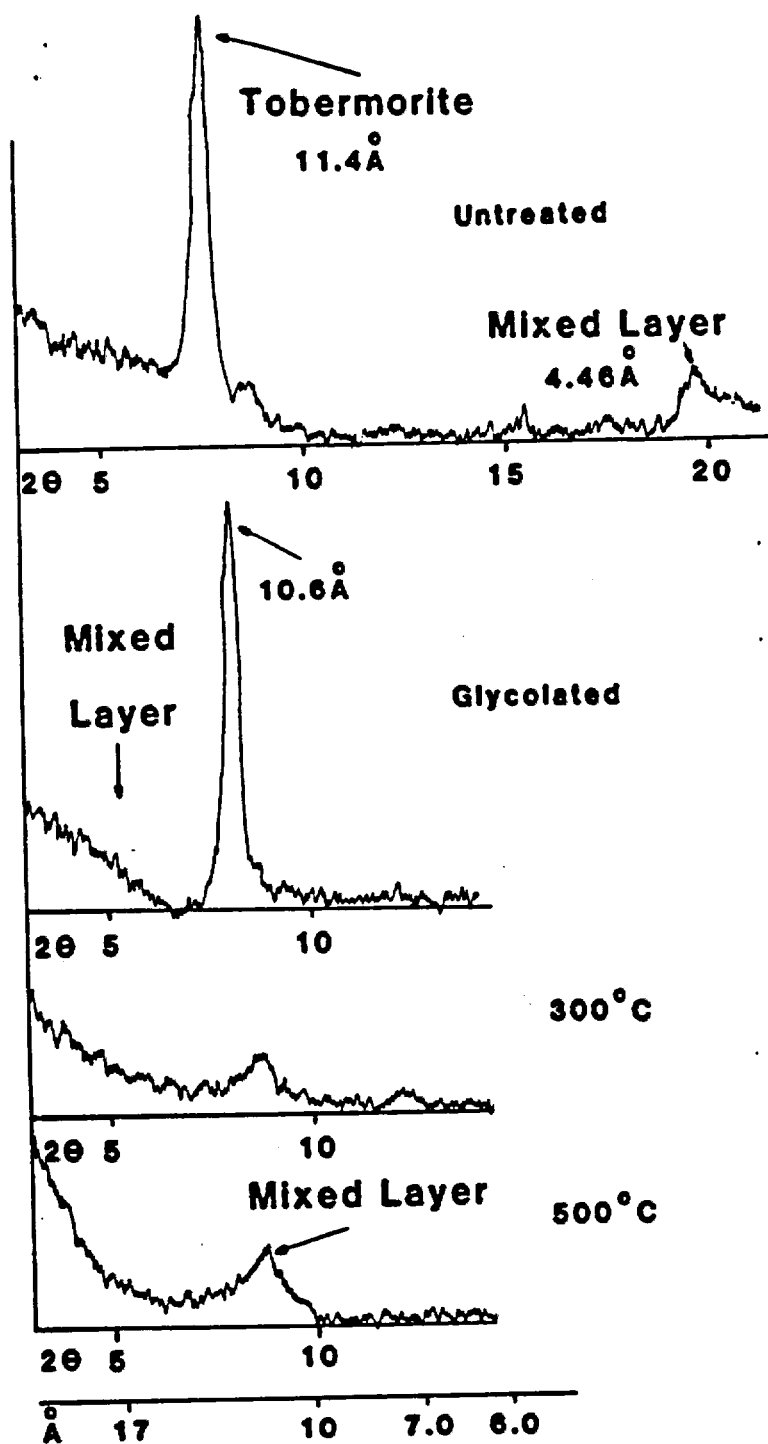


Figure 14. Representative XRD traces of tobermorite and mixed-layer clays: untreated, glycolated, and heated traces.

Beck, 1960; Gross and others, 1967; Webb, 1971; Kusachi and others, 1984). It has also been reported in contact metamorphic limestones (Eakle, 1917). In some cases it is completely replaced by calcite. In all cases tobermorite is of secondary origin. Reheis (1984) reported the presence of tobermorite in Montana soils, that it was pedogenic in origin, and that the amount increased with age.

Tobermorite with an 11\AA primary peak has been synthesized hydrothermally and at low temperatures from many different starting materials such as mixtures of lime or portland cement with either quartz or amorphous silica (Heller and Taylor, 1951; Mitsuda, 1970; Snell, 1975; Mitsuda and Taylor, 1978; Komarneni and Roy, 1983).

It is difficult to know whether the source of the tobermorite is from the parent material (Harvey and Beck, 1960), or formed in place. In the soils studied, tobermorite tends to be most abundant in two places: (1) at the surface where eolian materials are abundant, and (2) at depth in horizons with the greatest amount of secondary opaline SiO_2 and CaCO_3 in older soils developed on deposits Q2c and Q1a. The origin of tobermorite at the surface seems to be from the eolian materials, but that at depth could be pedogenic and formed in place or translocated eolian material.

Weathered mica has a poorly defined broad peak (10.0\AA) and is not effected by glycolation. (Appendix D). Upon heat treatment the peak intensifies.

Mixed-layer illite-montmorillonite clays are recognized by distinct shoulders on diffraction peaks at about 10.5 or 12\AA , suggesting incipient, poorly developed intergrades of layer-lattice clays (Vanden Heuvel, 1966). The intensity and consistency of the

high order (004) $4.5\overset{\circ}{\text{\AA}}$ peak, and low- 2θ angle background levels, reflects random interstratification common in a weathering environment (Jones, 1983). Because of the complete collapse of smectitic layers at 500°C , this treatment produces a sharp, well-defined peak at $10.2\overset{\circ}{\text{\AA}}$ (Figs. 14). These mixed-layer clay minerals are common in volcanic parent materials in southwestern Nevada (Jones, 1983).

Kaolinite ($7.2\overset{\circ}{\text{\AA}}$) in the study area is poorly crystalline, with a low height to width ratio (Appendix D). Because the same peak appears in most samples including unweathered alluvium, it is likely that it is derived from the parent material.

Palygorskite ($10.7\overset{\circ}{\text{\AA}}$ and $5.4\overset{\circ}{\text{\AA}}$) and sepiolite ($12.3\overset{\circ}{\text{\AA}}$ and $2.68\overset{\circ}{\text{\AA}}$) were never identified even though they are abundant in calcic soils in the southwestern U.S. (Vanden Heuvel, 1966; Gardner, 1972; Bachman and Machette, 1977; Hay and Higgins, 1980; Jones, 1983). Most of the above workers attribute the formation of palygorskite and sepiolite to the alteration of detrital mixed-layer illite-montmorillonite. The one speculation that can be made for the absence of these Mg-rich silicate clay minerals is that Ca-rich silicates (tobermorite) may form preferentially in this environment.

Amorphous silica can be identified on the XRD traces (Table 8, Figure 15). Jones and Segnit (1971, 1972) have subdivided opaline SiO_2 (poorly crystalline naturally occurring hydrous silica with $>1\%$ water) into three classes based on XRD and the amount of disorder of crystal stacking. In order of increasing amorphous state they are Opal-C, Opal-CT, and Opal-A. Each is associated with a unique environment of formation (Jones and Segnit, 1971).

Table 8. X-ray Diffraction Classification of Opaline Silica (Jones and Segnit, 1971).

Classification	Temperature of Formation	Environment of Formation	Source in Soil Environment	XRD Peaks (\AA)
Opal-C	high	lava flows.	parent material	4.0, 2.5, and 2.8
Opal-CT (most common)	low	silica associated with secondary clays, biogenic skeletons, volcanic ash, and infrequently gem-quality opal.	primarily pedogenic	4.3, 4.1, 3.9, and 2.5 definition and spacing is variable based on order, water content, and age.
Opal-A	low	gem-quality opal, biogenic skeletons, material and volcanic ash, silica gels, and some silica associated with clays.	parent material and pedogenic	diffuse peak centered at 4.1

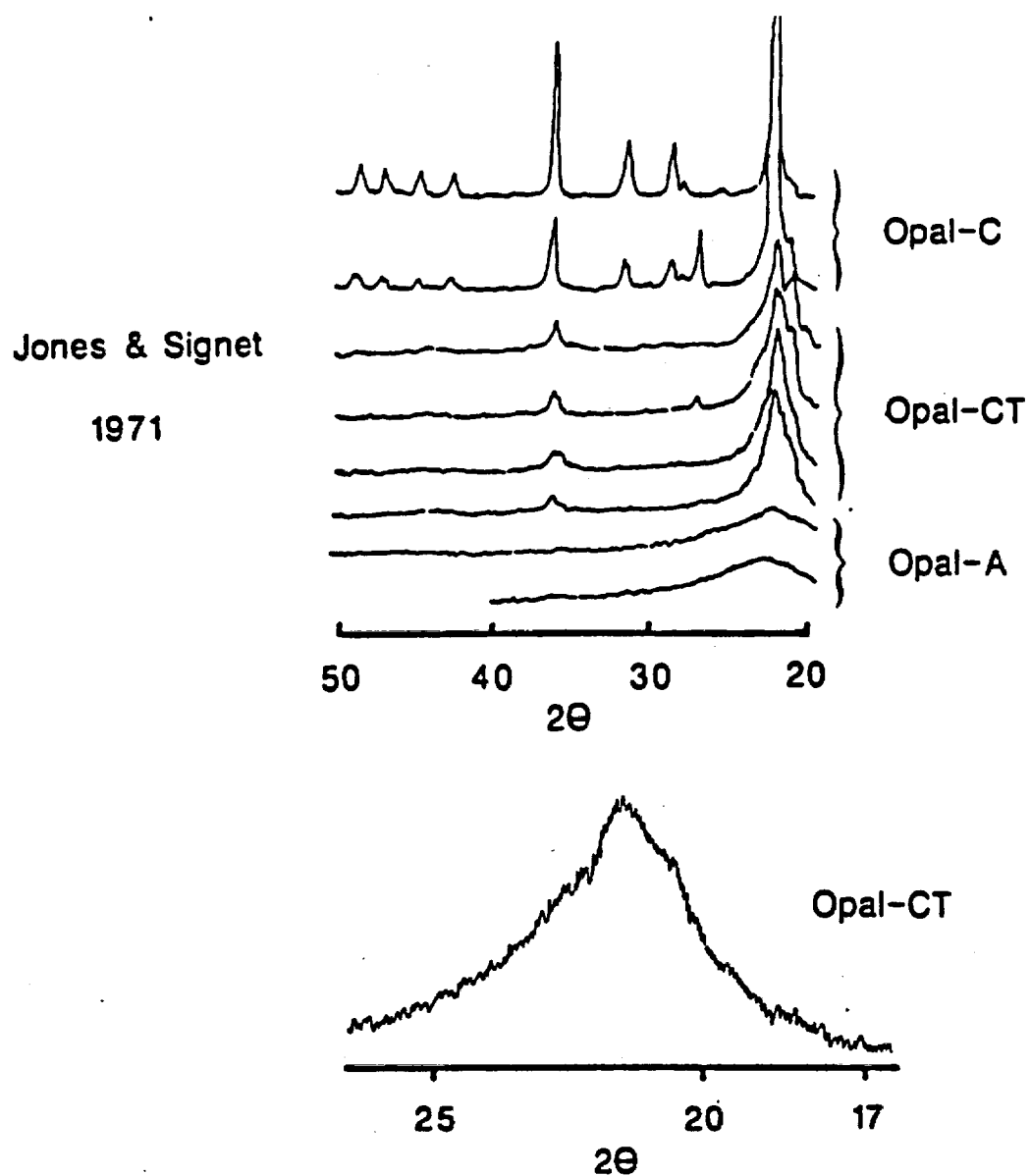
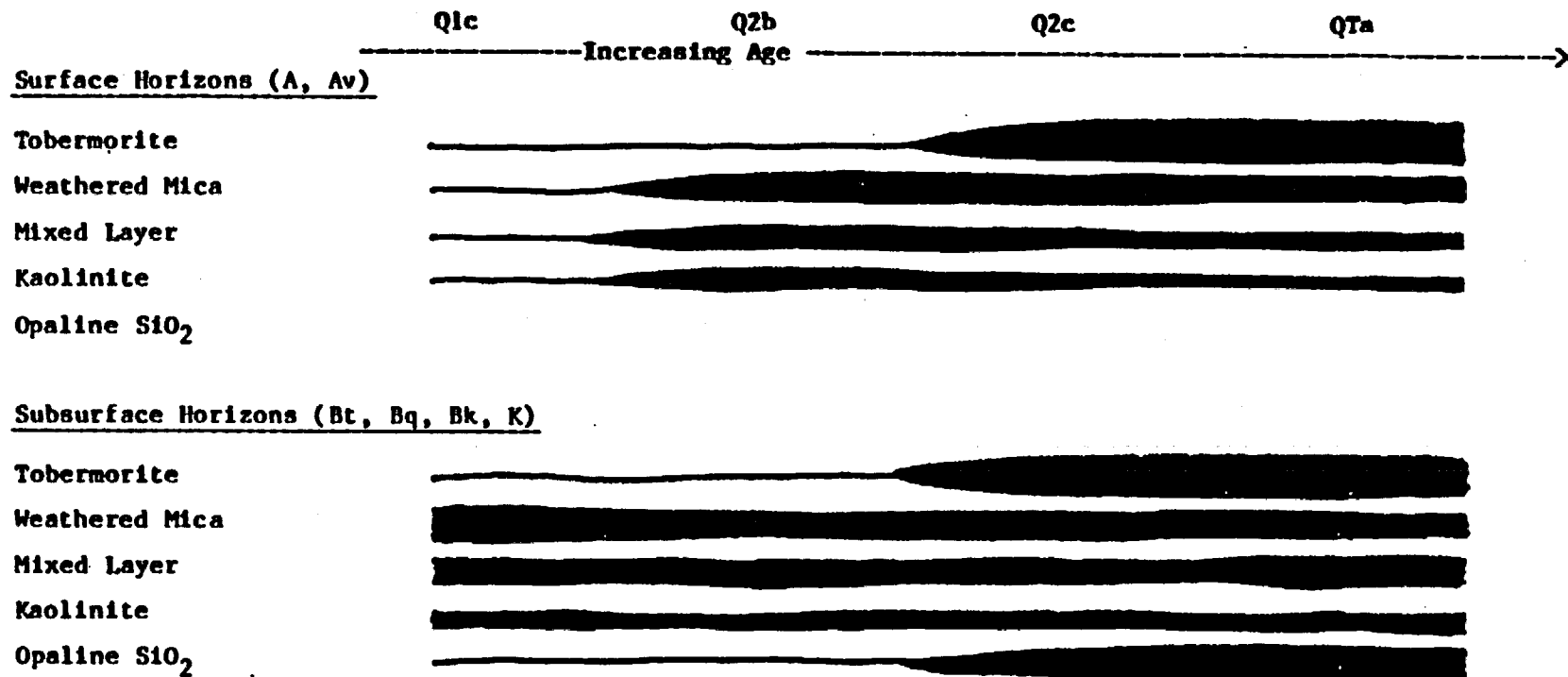


Figure 15. Representative XRD trace of Opal-CT vs the three opal classes of Jones and Signet (1971).

Diffractograms of several of the mixed-layer illite-smectite-dominated soils do have broad, but sharply spiked peaks centered between $4.1-4.3\overset{\circ}{\text{\AA}}$, suggesting the presence of Opal-CT (Figure 15). Peaks are not effected by heat treatment, but are absent after pedogenic silica is removed.

The clay mineralogy and relative abundance is strongly related to the climate, but also changes with the time and with depth in the profile (Birkeland, 1974 and 1984). Time-related changes in clay mineralogy are related to the stability of the various clays in the local soil environment, however Birkeland (1974 and 1984) believed that the clay minerals of soils developed in low-clay parent material change little with time. The uniformity of the clay minerals present in the study area suggest the latter, that there has been little change in either environment or in the mineralogy over time. However, the relative abundances increase with time (Fig. 16).

Figure 16. Relative abundance of clay minerals on the soils formed on deposits Q1c, Q2b, Q2c, and QTa. Width of bars equals approximate abundance.



CHAPTER IV

USING SOIL DATA TO ASSESS PALEOCLIMATE

Soil Water Balance and Leaching Index

The relationship between soils and climate can be approximated by evaluating soil water balance and leaching indices (Arkley, 1963, 1967). If the available water-holding capacity (AWC) of a soil is known, the amount of water that will potentially percolate through each soil horizon or depth increment can be calculated. Sometimes the word recharge is used by pedologists instead of percolation, but to clearly distinguish between the hydrologic application of recharge, I use percolation. Knowing the frequency of wettings per year, and assuming (a) that downward movement of water takes place only when field capacity for that part of the soil has been reached, and (b) that moisture is removed from the soil by evapotranspiration until the permanent wilting point is reached, one can construct curves depicting water movement (Arkley, 1963; Birkeland, 1984). In order to forecast soil water movement it is necessary to know the precipitation (P) and approximate potential evapotranspiration (ET_p). ET_p is the amount of water lost by evaporation and vegetative transpiration as long as sufficient soil moisture is available (Thornthwaite, 1948).

Water balance calculations predict the status of soil moisture on a mean annual basis. Critical to this study are those months when water is stored in various depths in the soil at moisture values above permanent wilting point; this happens when P is greater than ET_p . This water is available for plant growth, weathering reactions, and if the water is moving, it can translocate dissolved or solid material within the soil. In contrast, water is lost from the soil system when $P < ET_p$ until the soil reaches water contents approaching permanent wilting point. One of the key elements to this approach is to get an accurate measurement of ET_p .

Seven methods of calculating ET_p show a wide range of values (Table 9). All are based on empirical formulas. Of the Penman (1956) and Ritchie (1982, Williams, 1984) methods to calculate ET_p , the latter is recommended by the Soil Conservation Service; these were estimated from data in similar climatic regions, because of the lack of necessary data. The methods were selected because they compare favorably with lysimeter measurements in arid regions (Stanhill, 1961; Omar, 1968; McGuinness and Bordne, 1972; Farnsworth and others, 1982).

Pan evaporation data for the growing season only (Apr-Oct) from Pahrump, Nevada, about 30 km south of Yucca Mountain, are used here as a reasonable approximation of ET_p . Pan evaporation data come closest to the lysimeter-derived measurements of 150-200 cm from similar arid regions. Nevada currently has only four stations that measure pan evaporation, and Pahrump (203 cm/yr) is the nearest such station to NTS. Longer term pan evaporation records exist for Boulder City, adjacent to Lake Mead, but because of its proximity to

Table 9. Comparison of methods to calculate potential evapotranspiration using Beatty, Nevada weather information (Table 2).

Method and Calculated Annual ET_p Variables	Limitations
1) <u>Thornthwaite (1948)</u> - 84 cm latitude mean monthly temperature (T) day length factor	Underestimates in an arid environment by as much as 150%.
2) <u>Blaney & Criddle (1962)</u> - 94 cm latitude mean monthly T % daytime hours vegetation consumptive use coefficient	Underestimates in an arid environment, and vegetation factor must estimated for nonirrigated soil.
3) <u>Penman (1956)</u> - ~100 cm mean monthly T mean monthly min T daily solar radiation wind movement (mi/day)	Limited number of solar radiation stations, and a large amount of error in wind movement data due to variability in height of monitoring stations.
4) <u>Ritchie (1972), Williams (1984)</u> - ~100 cm mean monthly maximum and minimum T daily solar radiation and albedo soil cover and biomass indices	Same as Penman, and data are not available for most areas
5) <u>Kohler and others (1955)</u> - 127 cm mean monthly T mean water surface T wind movement (mi/day) pan evaporation	Data are not always available.
6) <u>Pan Evaporation for the growing season only (Apr-Oct)</u> - 164 cm cm of water loss	Data are sparse, may overestimate amount due to the influence of wind, and assumes no ET during cold months.
7) <u>Papadakis (1965)</u> - 163 cm saturation vapor pressure and dew point that can be derived respectively from the mean monthly maximum and minimum T	May overestimate amount

the lake, the pan evaporation values are extremely high compared to lysimeter-derived measurements from areas similar to NTS. The average monthly long term values for pan evaporation from Pahrump was summed for the growing season only, April to October (164 cm), because it is assumed that little or no evapotranspiration occurs during the winter months. The Papadakis method for estimating ET_p is used in this study because it best approximated the pan evaporation data summed for the growing season only from Pahrump.

Water budget plots for several different climatic models for the study area indicate significant soil-moisture differences between glacial and interglacial climates. The data for Beatty (Table 2) is used to approximate the Holocene climate (Fig. 17) and two different models for climates during the last glacial maximum are presented (Figs. 18 and 19). The climatic models for the glacial maximum are (1) Spaulding's (1983 and 1985) with a decrease in MAT of 7°C , an increase MAP of 35%, and a decrease in summer precipitation of 50% and (2), Mifflin and Wheats' (1976) with a decrease in MAT of 5°C , an increase of MAP of 68% and, a decrease in evaporation of 10% (Table 2). These three climatic conditions were evaluated at the low end of the elevation transect, and again at the high end where the modern climate has 70% greater MAP than at the low end of the elevation transect (Quiring, 1983).

When the Papadakis method is used to estimate ET_p , the Holocene climate (Beatty) shows that $ET_p > P$ and no soil water percolation occurs in the soil when monthly climate data are used (Fig. 17). Translocation of dissolved and solid material within the soil can be attributed to periodic high-precipitation storm

Figure 17. Soil water budget for Beatty, Nevada, which is assumed to approximate the Holocene climate. A and B are comparisons of four methods to calculate ET_p including pan evaporation (+), Thornthwaite (Δ), Blaney and Criddle (\diamond), and Papadakis (x) at the lower end (A) and higher end (B) of the elevation transect. C and D are the Papadakis method only at the lower (C) and upper (D) ends of the transect. Temperature is plotted as (\bullet) and precipitation as (\square).

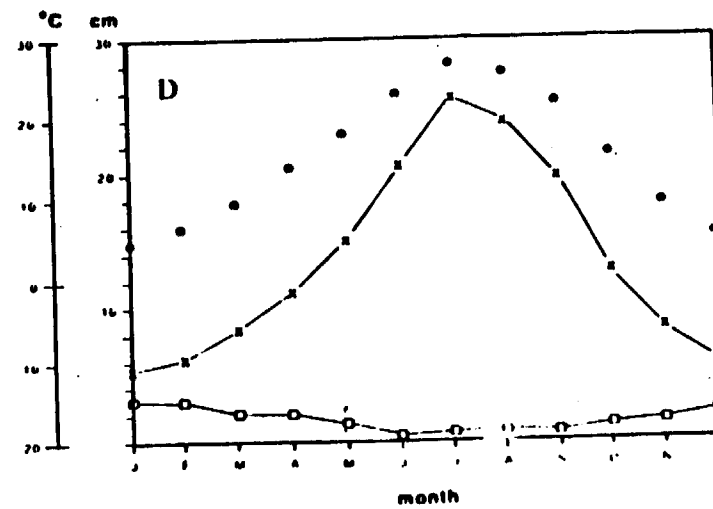
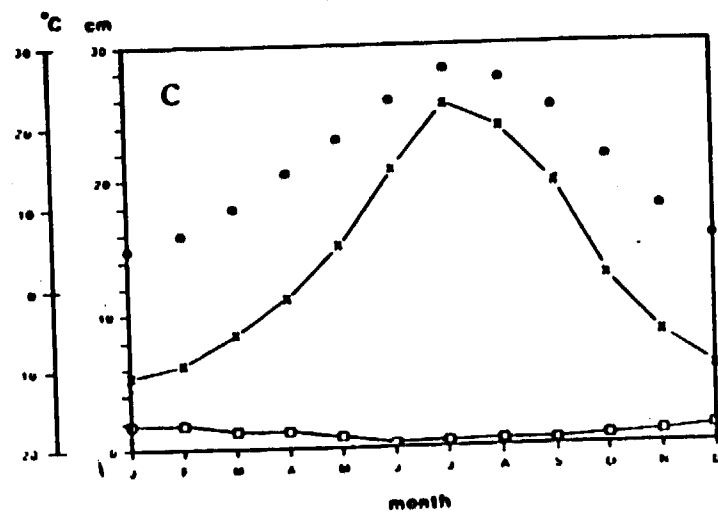
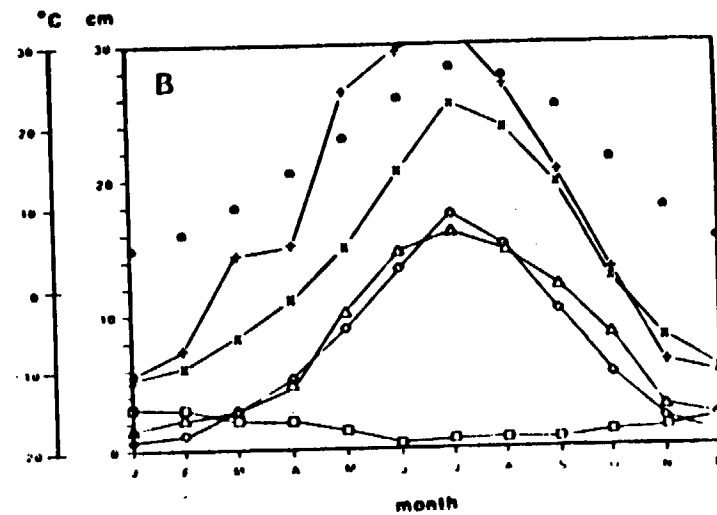
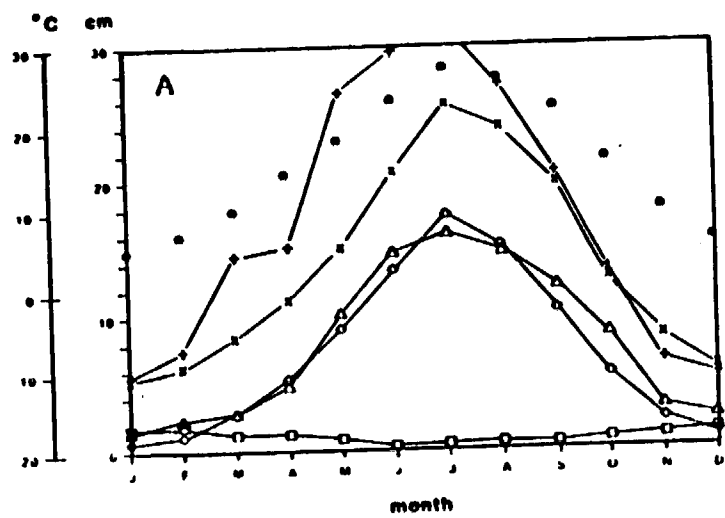


Figure 18. Soil water budget for the glacial maximum climate—Spaulding model. A and B are comparisons of four methods to calculate ET_p including pan evaporation (+), Thornthwaite (Δ), Blaney and Criddle (\diamond), and Papadakis (x) at the lower end (A) and higher end (B) of the elevation transect. C and D are the Papadakis method only at the lower (C) and upper (D) ends of the transect. Temperature is plotted as (\bullet) and precipitation as (\square).

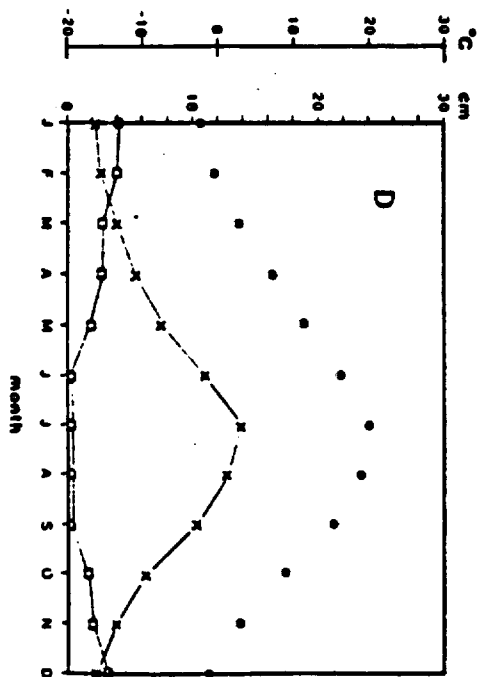
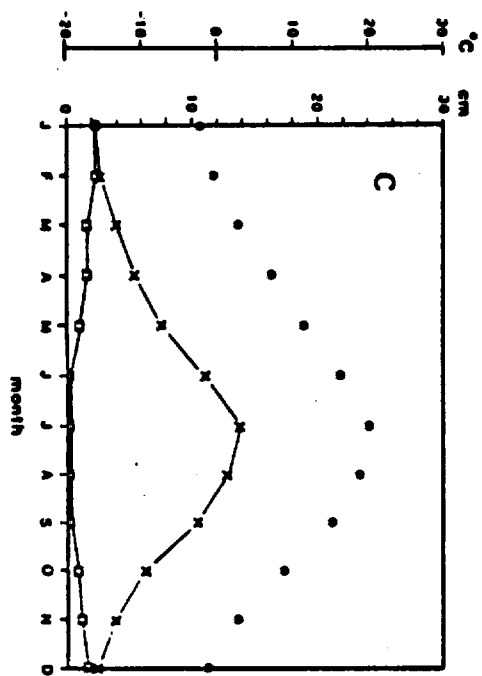
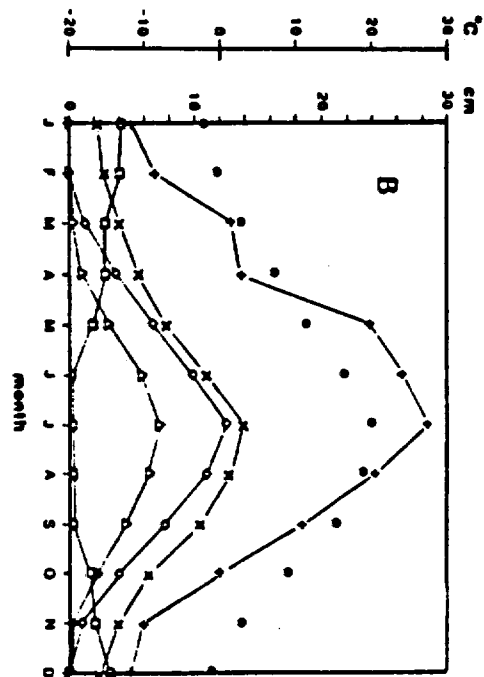
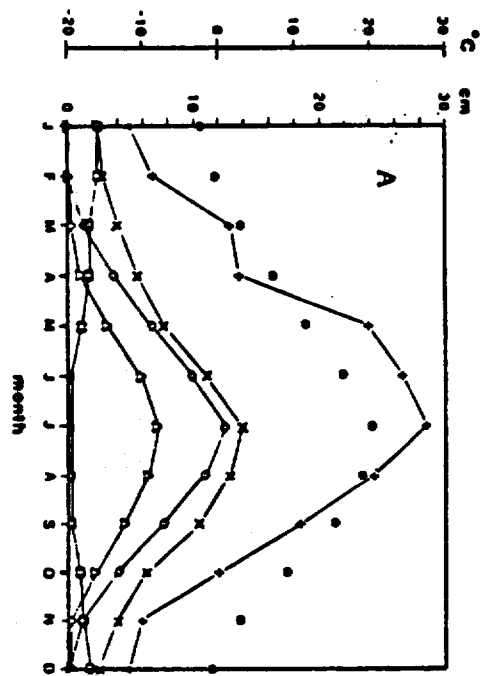
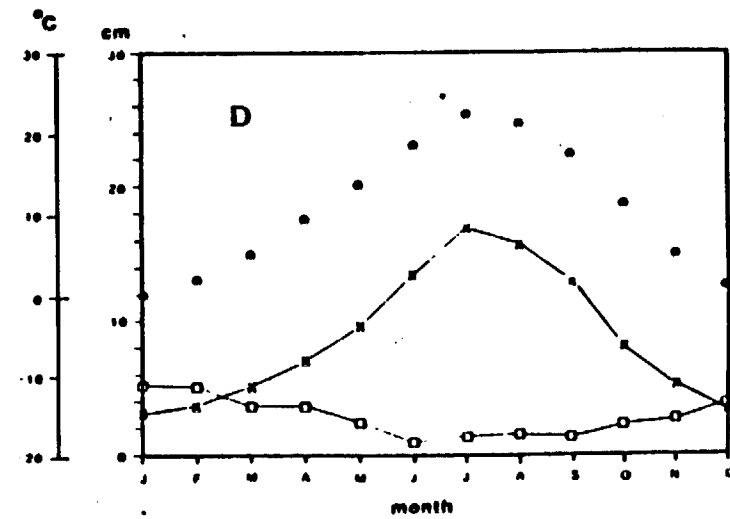
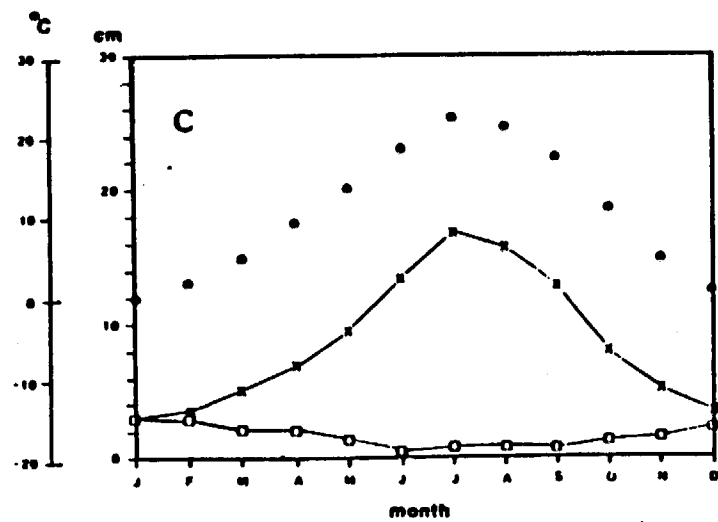
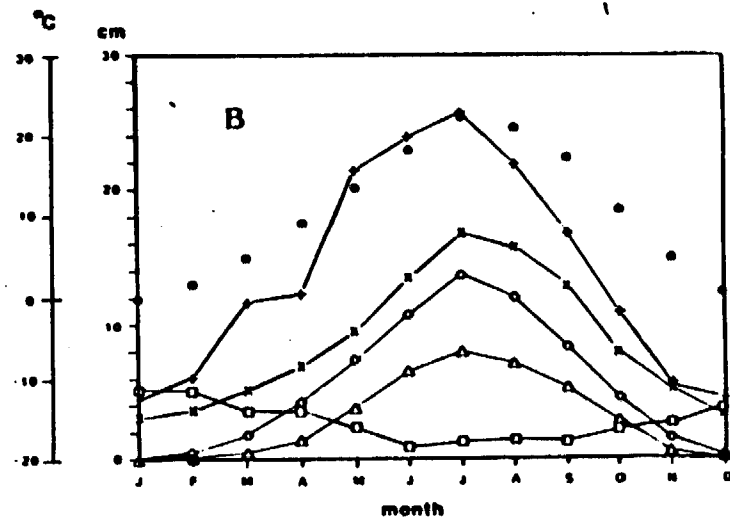
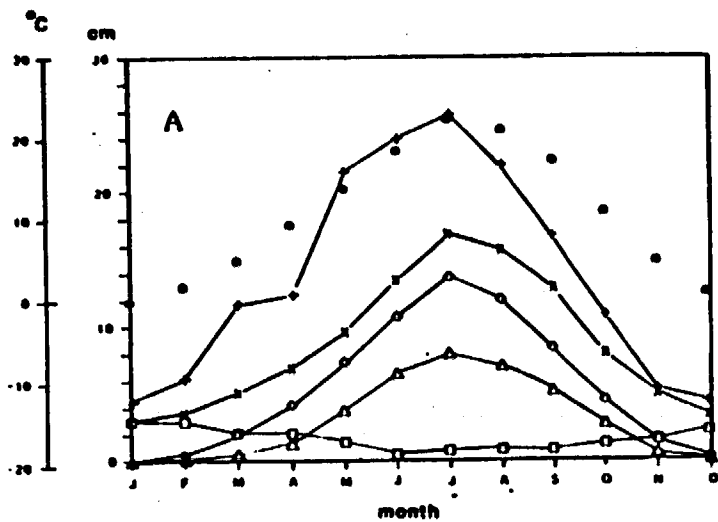


Figure 19. Soil water budget for the glacial maximum climate--Mifflin and Wheat model. A and B are comparisons of four methods to calculate ET_p including pan evaporation (+), Thornthwaite (Δ), Blaney and Criddle (\diamond), and Papadakis (x) at the lower end (A) and higher end (B) of the elevation transect. C and D are the Papadakis method only at the lower (C) and upper (D) ends of the transect. Temperature is plotted as (•) and precipitation as (\square).



events. This is true for both ends of the elevation transect. In contrast, if the Thornthwaite or Blaney-Criddle methods of calculating ET_p had been used, soil water percolation would have been predicted during one or more winter months (Fig. 17).

The two glacial climatic models give very similar water balance plots (Figs. 18 and 19). Soil water balance calculations of the glacial maximum climate using the Papadakis method of calculating ET_p predict that soil water percolation can occur only at the upper end of the elevation transect during January and February (Figs. 18 and 19). It is concluded that translocation could occur during these months in addition to both winter and summer high precipitation storm events. The other models for calculating ET_p predict even longer periods of soil water percolation as well as greater amounts.

Both soil water balance calculations of the glacial maximum predict soil water percolation during the cooler winter months at the upper end of the elevation transect, and not at the lower end. On similar aged deposits there should be a response to the increased available moisture on the dissolved and solid material that is translocated in the soils.

Carbonate Translocation

When moisture is available for translocation, soluble salts and $CaCO_3$ move downward and precipitate at a depth approximated by the wetting front (Arkley, 1963; McFadden and Tinsley, 1985). The percentage of $CaCO_3$ decreases with elevation in the Holocene soils (Q1c, Fig. 20), thus following the suggested difference in leaching

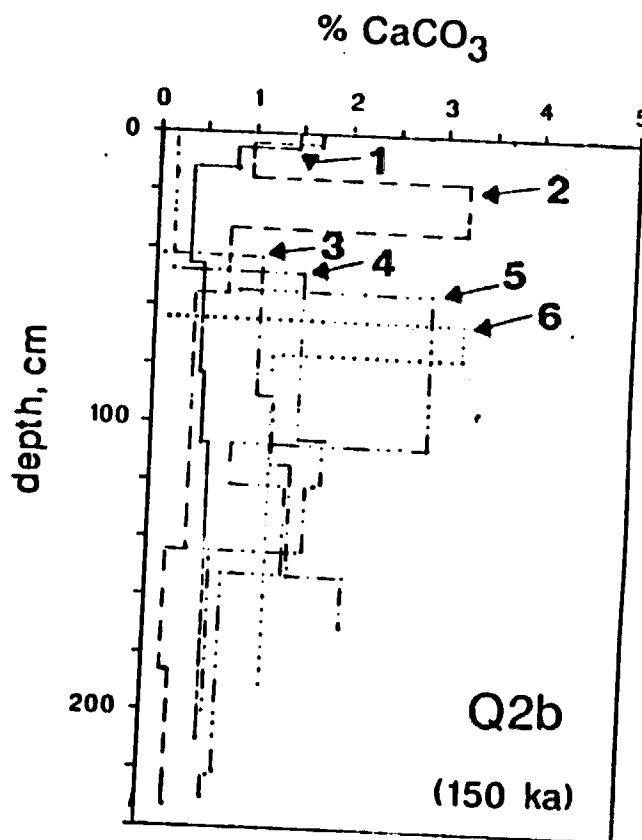
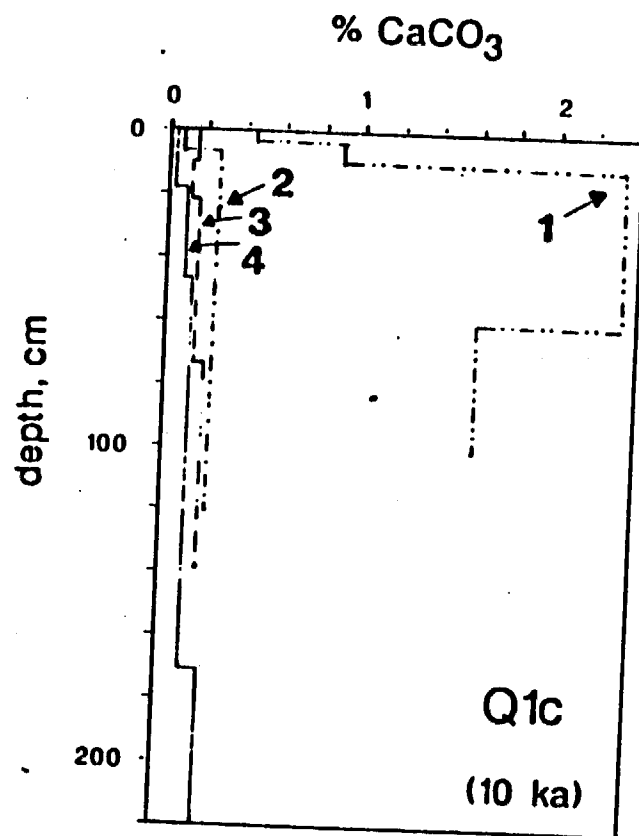


Figure 20. Percent CaCO_3 vs depth for soils formed on deposits Q1c (A) and Q2b (B). Numbers 1 to 6 are in order of lowest to highest soil profile elevation up the transect.

with elevation. The Q1c soil at the lowest elevation in the transect has over 2% CaCO_3 accumulation at 9-60 cm, whereas at greater elevations on the transect, the CaCO_3 accumulation is much less (<0.3%). In addition the depth at which the maximum CaCO_3 occurs in each profile, is deeper with higher elevation. Therefore, with increasing precipitation the CaCO_3 decreases in amount and the depth of maximum accumulation increases. The increase in frequency and amount of precipitation in the modern climate at the upper end of the transect is sufficient to translocate the CaCO_3 , but insufficient at the lower end.

If the climate in the past has been similar to the Holocene, CaCO_3 accumulation should occur at similar depths along the transect in the older soils. Significant variations in the CaCO_3 depths observed in older soils should reflect differences in amounts of effective moisture.

The CaCO_3 in the soils formed on Q2b deposits does not have the predicted response. Generally CaCO_3 increases rather than decreases in amount, and increases to depth of maximum accumulation with increasing elevation (Fig. 20). The CaCO_3 in soils formed on Q2c deposits has a similar response with some reversals, however the two highest soils are nearly at the same elevation (Fig. 21). Although, generally the soils at lower elevations have far less CaCO_3 (1-2%) than the soils at higher elevations (18-23%), and the depth to maximum accumulation increases with elevation. The soils formed on Q1a deposits do not show an obvious trends with increasing elevation (precipitation) (Fig. 21). Irrespective of elevation, detectable CaCO_3 first occurs at a depth of 10 to 30 cm. This could

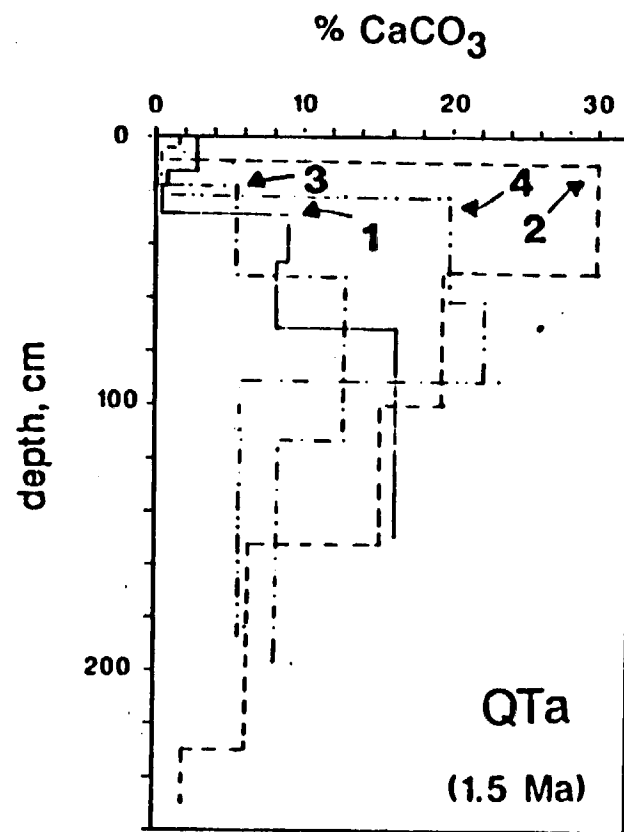
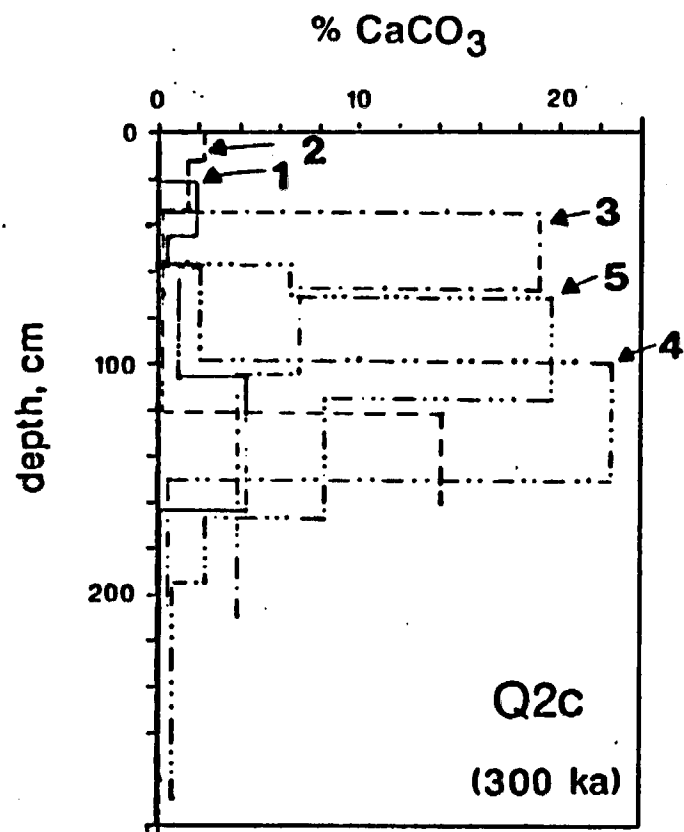


Figure 21. Percent CaCO_3 vs depth for soils formed on deposits Q2c (A) and QTa (B). Numbers 1 to 5 are in order of lowest to highest soil profile elevation up the transect.

be due to the influence of a greater number of climatic changes, and the erosion on the QTa deposits. Soils of extreme age tend to reflect the leaching of occasional wet years.

During the modern climate storm events tend to flush the soil system and translocate any available CaCO_3 (Fig. 20). In comparison, soils that have been exposed to one or more glacial events are "more efficient at accumulating CaCO_3 ". This accumulation effect could be due to two climatic influences. First, based on the soil water budgets during the glacial maximum (Figs. 18 and 19) predictable soil water percolation occurs using monthly climate data at the upper end of the transect. The constant wetting and drying may be more efficient at precipitating CaCO_3 . Secondly, effective precipitation could have actually been less during glacial climatic conditions than during the Holocene, and as a result moisture was not available to translocate soluble CaCO_3 deeper. In the both cases the regional climatic change associated with the Holocene-Pleistocene boundary would not be associated with changes in precipitation, but primarily changes in temperature. Without changing the amount of precipitation during the glacial maximum, CaCO_3 can be translocated deeper by simply increasing the temperature of available moisture and thus the solubility of CaCO_3 . This temperature increase of the available moisture may represent increased precipitation during the warmer summer months.

Some pre-Holocene soil profiles have a bimodal distribution of CaCO_3 (Figs. 20 and 21). The bimodal nature of soil can be explained by climatic change, much the same way McFadden (1982) did. The deeper accumulation represent periods of greater

leaching. In contrast, the shallower accumulation is similar enough to that of the Qlc soils to suggest an origin during the Holocene.

Computer Generated Model for Carbonate Translocation

Computer models can be generated to approximate CaCO_3 distribution in the soils of NTS. Basically they follow those of McFadden and Tinsley (1985). Climate can be related directly to the change in soil moisture throughout the year. The calculation of soil water movement (Arkley 1963, 1967) is based on the concept that the net excess of P over ET_p for those months in which $P > ET_p$ represents the total moisture available to wet the soil, but this is surely a simplification of natural conditions. This value, defined as the leaching index, may be calculated two different ways. In one method the excess of P over ET_p during the months in which $P > ET_p$ is summed. In the other method the average P for the wettest month is used if the maximum P for a given month is greater than the summed difference of $P > ET_p$. For arid and semiarid regions the second method gives a higher leaching index than does the first method. Both the Spaulding and Mifflin and Wheat climatic models along the Fortymile Wash and Yucca Wash transect have a leaching index less than the average January precipitation, and thus the second method is appropriate. The latter value is used in the computer model.

The computer-generated compartment model for CaCO_3 translocation generates "synthetic" distributions showing the translocation of CaCO_3 as a function of soil depth, time, and climate (Mayer and others, 1985). Different scenarios can be simulated, including abrupt or gradual changes in climate. The

variables utilized in the model are the leaching index value, calcic-dust influx, parent material CaCO_3 content, and partial pressure of soil (PCO_2), texture, initial water content, and soil temperature (Appendix I).

Various parameters were used in the model. Fresh alluvium is the parent material. The following parameters were used: a CaCO_3 dust flux of $0.1\text{gm/cm}^2/10^3\text{yrs}$, no parent material carbonate, the PCO_2 at the surface of $10^{-3.5}$, increasing to $10^{-2.5}$ at the maximum rooting depth, and decreasing with depth to $10^{-3.4}$, a sand texture, an initial moisture content of 0.02% with a permanent wilting point of 0.018%, and a soil temperature at the surface of 16.5°C which levels off to 19.3°C at 50 cm. (Appendix I). The calculated precipitation for the two extremes along the transect were used for the Holocene climate, and the glacial maximum climate used is the model proposed by Spaulding (Table 2). The program was run for 30,000 yrs of glacial climate, followed by 10,000 yrs of Holocene climate. Two climatic scenarios were considered for the Pleistocene-Holocene climatic change, abrupt and gradual (Fig. 10).

The abrupt climatic change model predicts a bimodal CaCO_3 distribution, whereas the gradual climatic change model does not (Fig. 22). The CaCO_3 translocation modeled is compared to data from soils on Q2b deposits because they have experienced at least one glacial climate. At the low end of the transect there is a bimodal distribution of CaCO_3 , in contrast at higher elevations the distribution is gradual (Fig. 20). So which climatic model is most closely predicting the expected distribution: the abrupt model for the lower elevations and the trend climatic model for the higher

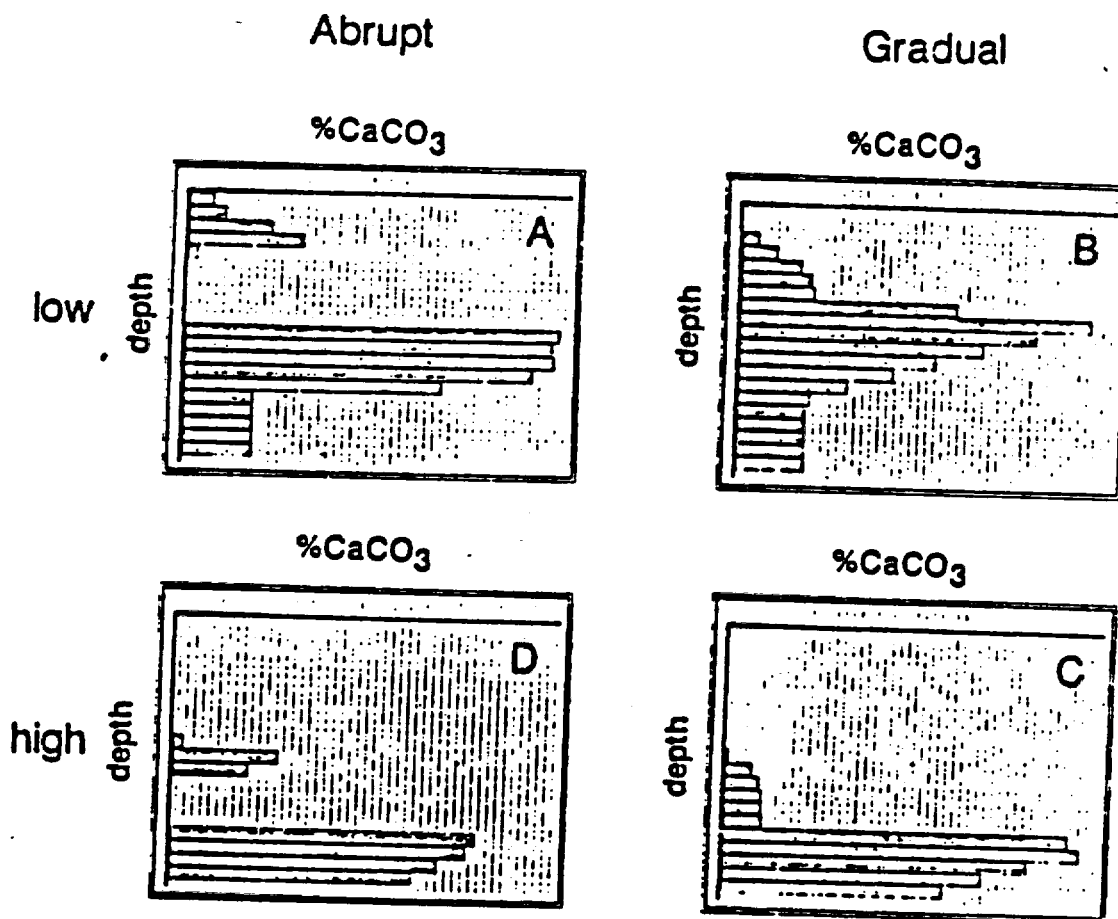


Figure 22. Modeled CaCO_3 accumulation for 30,000 yrs of glacial climate with either an abrupt (A and C) or gradual (B and D) change to the Holocene for 10,000 yrs for the low (A and B) and high (C and D) ends of the elevation transect.

elevations? Based on the CaCO_3 translocation on Q1c (Fig. 8A), CaCO_3 is not being moved out of the soil at lower elevations. The bimodal distribution in the lower soils is considered to be a function of the Holocene climate, and the best long term prediction is that climatic change is gradual, not abrupt.

Pedogenic Silica Morphology as a Climatic Indicator

Duripans are silica-cemented pedogenic horizons which form whenever silica is released by mineral weathering and not subsequently combined with secondary clay minerals or leached from the soil profile.

The chemistry and morphology of duripans are different in areas of arid and subhumid climates (Summerfield, 1983; Chadwick, 1985). In subhumid climates duripans contain Fe and Al as accessory cements along with oriented clays and high concentrations of resistant TiO_2 compared to more soluble cations. They also have prismatic structure. Colloform features and glaeboles dominate the micromorphology of subhumid duripans (Brewer, 1964). The matrix silica is well crystallized quartz rather than opaline silica.

The micromorphology of arid-soil silica concentrations are characterized by length-slow chalcedony in vughs or voids. The secondary fill is microquartz and megaquartz. These void fills are diagnostic of silicification at a high a pH (Folk and Pittman, 1971). Some argue the formation of silica in arid climates is related to the replacement of carbonates (West, 1973; Jacka, 1974; Milner, 1976). Glaeboles of clay are absent or inherited. The primary fabric is floating, and the secondary fabric is grain and

(or) matrix supported (Brewer, 1964). Opaline silica is the primary matrix component. The structure associated with the maximum duripan development is massive to platy.

Silica cemented horizons in the study area have no characteristics associated with duripans formed in subhumid climates. There is a lack of evidence for deep weathering in the profile. CaCO_3 is the accessory cement with little or no secondary clay accumulation. In the absence of effective precipitation or drainage to remove newly dissolved silica, it is precipitated elsewhere within the calcrete horizon, or CaCO_3 preferentially precipitates after opaline silica bonds adjacent soil grains without necessarily plugging intervening pore spaces (Chadwick, 1985). The complimentary solubility relationship with respect to pH between calcite and quartz is a highly alkaline environment ($>\text{pH } 9$). This suggests that localized zones could develop across a pH gradient in which calcite and silica were simultaneously precipitating. This kind of model implies contemporaneous calcrete and duripan development as a function of local variations in pH related to topography and soil-moisture conditions.

CHAPTER V

SUMMARY, CONCLUSIONS, AND FUTURE STUDIES

A high level nuclear waste site has been proposed in the Yucca Mountain area of the Nevada Test Site. A permanent repository for nuclear waste must be able to withstand the effects of a major climatic change. A climatic change that results in greater effective moisture may cause percolating water to move within the zone of waste material during the time that the material is still hazardous. The objectives of this study are to document the effects of time and climate on the soil development and to use soil data to characterize long-term past climatic variability.

Five groups of different-aged deposits were studied along an elevation transect of 400 m, from 1082 to 1483 m (Fig. 2). Present day annual precipitation nearly doubles along the transect from 120 to 200 mm (Table 2).

No definitive evidence exists regarding any climatic or tectonic influences on the formation of the terraces in the study area. The terraces studied are fill terraces (Fig. 3), and are not likely to be of tectonic origin. Although longitudinal profiles of the terraces diverge downstream (Fig. 4), tectonics are not required to explain this relationship. Climatic change may account for the formation of the terraces.

Soils that formed in alluvium and eolian fines of Holocene to early Pleistocene or latest Pliocene (?) age near Yucca Mountain are characterized by distinctive trends in the accumulation of secondary clay, CaCO_3 , and opaline SiO_2 that correspond with the ages of the surficial deposits. Both CaCO_3 and opaline SiO_2 appear initially as coatings on the underside of clasts and over time form cemented and indurated horizons (Table 3). There is no macro- or micromorphological evidence that suggests that the silica cementation occurred under climatic conditions cooler and (or) wetter than those of the present climate. Vesicular A (Av) horizons have not formed on the coarse, gravelly Holocene deposits in the Yucca Mountain area. On the older deposits where Av horizons have formed, there is no relationship between the thickness of the Av horizon and age of the underlying deposit. The Av horizons are consistently between 5 and 10 cm thick.

Quantified field properties, by the Harden method, vs log age of the deposit are all significant at the 5% level except melanization and color paling (Fig. 5). The profile indices also clearly show a relationship with log age of the deposit (Fig. 6). When the four properties with the highest r^2 values vs log age are combined and compared to the same field properties on similar-aged deposits from the Las Cruces, New Mexico area, the index values are very similar in the two areas on similar aged deposits. This suggests that compared to an area with independently-dated deposits the age estimates for the deposits in the Yucca Mountain area, based on field properties, are not unreasonable (Table 4).

The accumulation of secondary CaCO_3 , clay, silt, and opaline SiO_2 is determined on a horizon basis by deducing the initial amount assumed to have been in the soil parent material from that in the present soil horizon. Profile sums of horizon weights of these components suggest that CaCO_3 , clay, silt, and opaline SiO_2 accumulate at a logarithmic rate (Table 5). However, these rates may be primarily a function of the erosion and of secondary material loss from the older soils, and the volumes determined for these constituents may only be minimum values. The long term rates for properties dependent primarily on eolian additions is probably better expressed by linear rate.

Holocene aged soils (Q1c) have accumulated CaCO_3 , clay, silt, and opaline SiO_2 at a higher average rate than the older soils (Fig. 9). Accumulation rates are dependent upon the availability of eolian material on the soil surface and sufficient precipitation to move the material into the soil. Increased rates of accumulation of CaCO_3 , clay, silt, and opaline SiO_2 during the Holocene can be attributed to several possible climatic scenarios associated with the Holocene-Pleistocene climate change. The accumulation rates suggest that precipitation since the stabilization of Q1c has not been a limiting factor, and that climatic change was not sufficient to significantly decrease rates of accumulation. This suggests that the climatic change was the result of decreases in temperature rather than precipitation.

No one long term rate of accumulation approximates the actual profile sum for CaCO_3 , clay, silt, or opaline SiO_2 for a given aged deposit. The predicted profile sums using rates from

deposits that are known to have experienced at least one cycle of climatic change tend to underestimate the actual profile sums.

These discrepancies in estimating the actual age are either (1) age errors on the deposits, (2) long term accumulation rates are off for that age range, this may be accounted for by erosion on the deposits that the long term rates are calculated from, or (3) represent much greater additions of CaCO_3 , clay, silt, or opaline SiO_2 than the potential rates of accumulation predicts.

Soil properties that commonly exhibit changes with time and (or) climate include clay, CaCO_3 , and opaline SiO_2 . Most of these properties are strongly influenced by vertical position in the soil profile. With the exception of soils formed on deposits of Q2c age, clay, CaCO_3 , and opaline SiO_2 maximums occur in the same horizon. On Q2c deposits the maximum amount of pedogenic clay is in a zone immediately above the zone with the maximum amount of pedogenic CaCO_3 and opaline SiO_2 . In nearly all of the soils in this study, the maximum amounts of CaCO_3 and opaline SiO_2 occur in the same horizon, and in these horizons opaline SiO_2 is more abundant than CaCO_3 .

The mineralogy and relative abundance of soil-clay minerals are strongly related to the climate, but they also changes with the time and with depth in the profile. The pedogenic clays in the Yucca Mountain soils have developed in very low-clay parent materials. There has been little change in the soil-clay mineralogy over time, in spite of climatic changes that have occurred since the stabilization of these deposits and initiation of soil development (Fig. 16).

The relationship between soils and climate can be approximated by evaluating soil water balance and leaching indices. Two climatic models of the glacial climate, one based on packrat midden evidence and a second on pluvial lake chronologies, were used along with modern climate data from Beatty, Nevada to calculate the soil water balance (Figs. 17-19). The Papadakis method of calculating potential evapotranspiration was used in this study (Table 9). The Holocene soil water balance calculations suggest that no soil water will percolate to depths using climatic data on a mean monthly basis. Translocation of dissolved and solid material within the soil can be attributed to periodic high-precipitation storm events. Both models of the glacial-maximum climate predict that at the high end of the elevation transect soil water percolation will occur during the cooler winter months, as well as during high-precipitation storm events.

When moisture is available for translocation, soluble salts and CaCO_3 move downward in solution and precipitate at depths approximated by the estimated depth of the wetting front. Depth plots of percent CaCO_3 for soils formed in Q1c-aged deposits suggest that near the upper end of the transect the modern-climatic soil moisture conditions are sufficient to translocate the available CaCO_3 (Fig. 20). Carbonate accumulates near the surface on the Q1c-aged deposits at the low end of the elevation transect, but appears to be translocated to greater depths, below the base of the soil, at higher elevations where precipitation is greater.

With increasing elevation, soils on the Q2b deposits that have experienced at least one climatic change have different CaCO_3

depth plots than the Q1c deposits (Fig. 20). Generally with increasing elevation and precipitation in the Q2b soils, CaCO_3 increases rather than decreases in amount, and increases in amount to the depth of maximum CaCO_3 accumulation with increasing elevation and precipitation (Fig. 20). The older soils tend to reflect the effects of leaching during occasional wetter years much more than do the younger soils. As a result, the older soils do not show trends in the accumulation of CaCO_3 with elevation (Fig. 21).

The different trends in accumulation in CaCO_3 on the Q1c and Q2b soils could be due primarily to two climatic influences: (1) additional moisture during a glacial maximum as determined from the water balance calculations, and (2) the likely changes in the effective precipitation during a glacial maximum. With only modest increases in the precipitation, the depth to which CaCO_3 would be translocated and deposited in a soil would be greatly increased. Without change in precipitation, CaCO_3 can be translocated deeper by merely decreasing the temperature of the soil water and thus increasing the solubility of CaCO_3 . This temperature increase of available moisture may represent increased precipitation during the warmer summer months during a glacial maximum.

A computer model was used to generate an approximate vertical CaCO_3 distribution in the soils in the Yucca Mountain area. Parameters used to generate the model describe the physical characteristics of the deposit, CaCO_3 influx rates, and climate. The model was run using the Spaulding (1985) glacial-maximum climate model for 30,000 yrs followed by 10,000 yrs of the modern climate (Fig. 22). This climatic change was generated both abruptly and

gradually. By comparing the computer-generated model to field data for the depths and distributions of CaCO_3 , the model-generated data suggest that the climatic change at the Holocene-Pleistocene boundary was gradual.

Several future studies of the soils in the Yucca Mountain area have been planned in order to expand and clarify the findings of this study. They include the following: (1) soil thin-section analyses and total chemistry in order to help determine the genesis of the silica-cemented horizons; (2) a relative dating study of the degree of preservation of bar-and-swale topography, degree of rounding and size of surface boulders, and degree of sorting and packing of desert pavements; (3) evapotranspiration measurements with weighing lysimeters and evaporative pans with the Water Resources Division of the U.S. Geological Survey; (4) stable oxygen and carbon isotopes in the pedogenic silica and opal phytoliths for paleoclimatic indicators; (5) the relative abundance and distribution of tobermorite (?) and its relationship to mixed layer clays, palygorskite and sepiolite; (6) a more refined and complete stratigraphy for the surficial deposits in the NTS area.

REFERENCES

- Allison, L. E., 1965, Organic carbon, in Black, C. A., ed., Methods of Soil Analysis, Part 2: American Society of Agronomy, Monograph series No. 9, p. 1367-1378.
- Arkley, R. J., 1963, Calculation of carbonate movement in soil from climatic data: Soil Science, v. 96, no. 4, p. 239-248.
- 1967, Climates of some great soil groups of the western United States: Soil Science, v. 103, no. 6, p. 389-400.
- Bachman, G. O., and Machette, M. N., 1977, Calcic soils and calcretes in the southwestern United States: U.S. Geological Survey Open-File Report 77-794, 163 p.
- Benson, L. V., 1978, Fluctuation in the level of pluvial Lake Lahontan during the last 40,000 years: Quaternary Research, v. 9, p. 300-318.
- Birkeland, P. W., 1974, Pedology, Weathering, and Geomorphological Research: New York, Oxford University Press, 285 p.
- 1984, Soils and Geomorphology: New York, Oxford University Press, 372 p.
- Blaney, H. F., and Criddle, W. D., 1962, Determining consumption use and irrigation water requirements: U.S. Department of Agriculture Technical Bulletin No. 1275, 55 p.
- Bleeke, P., and Parfitt, R. L., 1984, Volcanic ash and its clay mineralogy at Cape Hoskins, New Britain, Papu New Guinea: Geoderma, v. 11, p. 123-135.
- Brewer, Roy, 1964, Fabric and mineral analysis of soils: John Wiley and Sons, New York.
- Bryan, Kirk, 1925, Date of channel trenching in the arid Southwest: Science, v. 62, no. 1607, p. 338-344.
- Bull, W. B., 1974, Geomorphic tectonic analysis of the Vidal region, in Information concerning site characteristics, Vidal Nuclear Generating Station: Southern California Edison Company, 1975, appendix 2.5 B, amendment 1.

- 1979, Threshold of critical power in streams: Geological Society of America Bulletin, Part 1, v. 90, p. 453-464.
- Bull, W. B., and Schick, A. P., 1979, Impact of climatic change on an arid watershed Nahal Yael, southern Israel: Quaternary Research, v. 11, p. 153-171.
- Busacca, A. J., Aniku, J. R., and Singer, M. J., 1984, Dispersion of soils by an ultrasonic method that eliminates probe contact: Soil Science Society of America Journal, v. 48, no. 5, p. 1125-1129.
- Chadwick, O. A., 1985, Incipient silica cementation in central Nevada alluvial soils influenced by tephra: Tucson, University of Arizona PhD. dissertation 176 p.
- Chleborad, A. F., Powers, P. S., and Farrow, R. A., 1975, A technique for measuring bulk volume of rock material: Bulletin of the Association of Engineering Geology, v. 12, no. 4, p. 317-322.
- Christiansen, R. L., and Lipman, P. W., 1965, Geologic map of the Topopah Spring NW quadrangle: U.S. Geological Survey Geologic Quadrangle Map GQ-444, scale 1:24,000.
- CLIMAP Project Members (Climate: Long-range Investigation Mapping and Prediction), 1976, The surface of the Ice-Age Earth: Science, v. 191, no. 4232, p. 1131-1137.
- Cronquist, Arthur, Holmgren, A. H., Holmgren, N. H., and Revel, J. L., 1972, Intermountain flora, Volume 1: New York Botanical Garden, New York, Hafner, 270 p.
- Culler, R. C., Hanson, R. L., Myrich, R. M., Turner, R. M., and Kipple, F. D., 1982, Evaporation before and after clearing phreatophytes, Gila River flood plain, Graham County Arizona: U.S. Geological Survey Professional Paper 655-P.
- Davis, J. C., 1973, Statistics and data analysis in geology: New York, John Wiley and Sons, 550 p.
- Day, P. R., 1965, Particle fractionation and particle-size analysis, in Black C. A., ed., Methods of Soil Analysis, Part 2: American Society of Agronomy, Monograph No. 9, p. 545-567.
- Dreimanis, Aleksis, 1962, Quantitative determination of calcite and dolomite by using Chittick apparatus: Journal of Sedimentary Petrology, v. 32, no. 3, p. 520-529.
- Eakle, A. S., 1917, Minerals associated with crystalline limestones at Crestmore, Riverside County, California: California University, Department of Geology Bulletin 10, p. 327-360.

- Elgawhary, S. M., and Lindsay, W. L., 1972, Solubility of silica in soils: Soil Science Society of America Proceedings, v. 36, p. 439-442.
- Farnsworth, R. K., Thompson, E. S., and Peck, E. L., 1982, Evaporation atlas for the contiguous 48 United States: NOAA Technical Report NWS 33, Office of Hydrology, National Weather Service.
- Fenneman, N. M., 1931, Physiography of the western United States: New York, McGraw-Hill, 534 p.
- Fieldes, M., and Perrott, K. W., 1966, The nature of allophane in soils, Part 3 - Rapid field and laboratory test for allophane: New Zealand Journal of Science, v. 9, p. 623-629.
- Folk, R. L., and Pittman, J. S., 1971, Length-slow chalcedony: A new testament for vanished evaporites: Journal of Sedimentary Petrology, v. 41, no. 4, p. 1045-1058.
- Gardner, L. R., 1972, Origin of Mormon Mesa Caliche, Clark County, Nevada: Bulletin of the Geological Society of America, v. 83, p. 143-156.
- Gile, L. H., Peterson, F. F., Grossman, R. B., 1979, The desert project soil monograph: Soil Conservation Service, U.S. Department of Agriculture, 984 p.
- Gile, L. H., Hawley, J. W., and Grossman, R. B., 1981, Soils and geomorphology in the Basin and Range area of Southern New Mexico - Guidebook to the Desert Project: New Mexico Bureau of Mines and Mineral resources, Memoir 39, 222 p.
- Gross, S., Manzor, E., Sass, E., and Zak, I., 1967, The mottled zone complex of Nahal Ayalon (Central Israel): Israel Journal of Earth-Sciences, v. 16, p., 84-96.
- Hallmark, C. T., Wilding, L. P., and Smeck, N. E., 1982, Silicon, in Page, A. L., Miller, R. H., and Keeney, D. R., eds., Methods of Soil Analysis, Part 2: American Society of Agronomy, Monograph No. 9, (2nd edition), p. 263-273.
- Hamid, S. A., 1980, The crystal structure of 11\AA tobermorite: Zeitschrift fur Kristallographie, v. 154, p. 189-198.
- Harden, J. W., 1982, A Quantitative index of soil development from field descriptions, Example from a chronosequence in central California: Geoderma, v. 28, p. 1-28.
- Harden, J. W., and Taylor, E. M., 1983, A quantitative comparison of soil development in four climatic regimes: Quaternary Research, v. 20, p. 342-359.

- Harvey, R. D., and Beck, C. W., 1960, Hydrothermal regularly interstratified chlorite-vermiculite and tobermorite in alteration zones at Goldfield Nevada: Proceedings of the Ninth National Conference on Clays and Clay Minerals, Clays and Clay Minerals, v. 9, p. 343-354.
- Hay, R. L., and Wiggins, Brian, 1980, Pellets, ooids, sepiolite and silica in three calcretes of southwestern United States: Sedimentology, v. 27, p. 559-576.
- Heddle, M. F., 1880, Preliminary notice of substances which may prove to be new minerals: The Mineralogical Magazine and Journal, v. 4, no. 17, p. 117-121.
- Heller, L., and Taylor, H. F. W., 1951, Hydrated calcium silicates, Part II: Journal of the Chemical Society of London, p. 2397.
- Hoover, D. L., Swadley, W. C., and Gordon, A. J., 1981, Correlation characteristics of surficial deposits with a description of surficial stratigraphy in the Nevada Test Site region: U.S. Geological Survey Open-File Report 81-512, 27 p.
- Houghton, J. G., Sakamoto, C. M., and Gifford, R. O., 1975, Nevada's weather and climate: Nevada Bureau of Mines Special Publication 2, 78 p.
- Imbrie, John, and Imbrie, J. Z., 1980, Modeling the climatic response to orbital variations: Science, v. 207, p. 943-953.
- Jacka, A. D., 1974, Replacement of fossils by length-slow chalcedony and associated dolomitization: Journal of Sedimentary Petrology, v. 44, no. 2, p. 421-427.
- Jackson, M. L., 1969, Soil Chemical Analysis - Advanced Course, 2nd edition, 10th printing: Published by the author, Madison, Wisconsin, 53705, p. 59-61, 524-528.
- Jenny, Hans, 1941, Factors of Soil Formation: New York, McGraw-Hill, 281 p.
- 1980, The soil resource, origin and behavior: New York, Springer-Verlag, 377 p.
- Jones, B. F., 1983, Occurrence of clay minerals in surficial deposits of southwestern Nevada: Sciences Geologiques Memoire 72, Strasbourg, p. 81-92.
- Jones, J. B., and Segnit, E. R., 1971, The nature of opal, nomenclature and constituent phases: Journal of the Geological Society of Australia, v. 18, pt. 1, p. 57-68.

- 1972, Genesis of cristobalite and tridymite at low temperatures: *Journal of the Geological Society of Australia*, v. 18, pt. 4, p. 419-422.
- Kohler, M. A., Nordenson, T. J., and Fox, W. E., 1955, Evaporation from pans and lakes: U.S. Weather Bureau Research Paper 38, 21 p.
- Komarneni, Shidhar, and Roy, D. M., 1983, Tobermorite: A new family of cation exchangers: *Science*, v. 221, p. 647-648.
- Ku, Teh-Lung, Bull, W. B., Freeman, S. T., Knauss, K. G., 1979, Th^{230} - U^{238} dating of pedogenic carbonates in gravelly desert soils of Vidal Valley, southeastern California: *Geological Society of America Bulletin*, p. 1063-1073.
- Kusachi, Isao, Henmi, Chiyoko, and Henmi, Kitinosuke, 1984, An oyelite-bearing vein at Fuka, the town of Bitchu, Okayama Prefecture: *Journal of the Japanese Association of Mineralogist, Petrologist and Economic Geologist*, v. 79, no. 7, p. 267-275.
- Lajoie K. R., and Robinson, S. W., 1982, Late Quaternary glacio-lacustrine chronology of Mono Basin, California: *Geological Society of America Abstracts with Programs*, v. 14, p. 179.
- Lindsley, R. K., Jr., Kohler, M. A., and Paulhaus, J. L. H., 1975, *Hydrology for Engineers* (2nd ed.): New York, McGraw-Hill, p. 34-36.
- Lipman, P. W., and McKay, E. J., 1965, Geologic map of the Topopah Spring SW quadrangle: U.S. Geological Survey Geologic Quadrangle Map GQ-439, scale 1:24,000.
- Machette, M. N., 1985, Calcic soils of the Southwestern United States, in Weide, D. L., ed., *Quaternary soils and geomorphology of the Southwestern United States*: *Geological Society of America Special Paper* 203, p. 1-21.
- Mayer, Larry, McFadden, L. D., Harden, J. W., Taylor, E. M., Reheis, M. C., and Arkley, R. J., 1985, Computer simulation of calcic soil development for paleoclimatic reconstructions using an interactive forward method structured on the computer model: *Geological Society of America Abstracts with Program*, v. 17, no. 7, p. 656.
- McConnell, J. D. C., 1954, The hydrated calcium silicates riversideite, tobermorite, and plombierite: *Mineralogical Magazine*, v. 30, p. 293-305.
- McFadden, L. D., 1982, The impacts of temporal and spatial climatic change on alluvial soil genesis in southern California: Tucson, University of Arizona PhD. dissertation, 430 p.

- McFadden, L. D., Wells, S. G., Dohrenwend, J. C., and Turrin, B. D., 1984, Cumlic soils formed in eolian parent materials on flows of the Cima Volcanic Field, Mojave Desert, California, in Dohrenwend, J. C. ed., *Surficial geology of the eastern Mojave Desert, California: Geological Society of America, 97th Annual Meeting, Field Trip 14 Guidebook*, p. 69-87.
- McFadden, L. D., and Tinsley, J. C., 1985, Rate and depth of pedogenic-carbonate accumulation in soils: Formation and testing of a compartment model: in Weide, D. L., ed., *Quaternary soils and geomorphology of the Southwestern United States: Geological Society of America Special Paper 203*, p. 23-42.
- McGuinness, J. L., and Bordne, E. F., 1972, A comparison of lysimeter-derived potential evapotranspiration with computed values: U.S. Department of Agriculture Technical Bulletin No. 1452, 71 p.
- Megaw, H. D., and Kelsey, C. H., 1956, The crystal structure of the tobermorite: *Nature*, v. 177, p. 390-393.
- Mehring, P. J., 1967, Pollen analysis of the Tule Springs site, Nevada, in Wormington, H. M., and Ellis, D., eds., *Pleistocene studies in southern Nevada: Nevada State Museum Anthropological Papers*, v. 13, p. 129-200.
- Mifflin, M. D., and Wheat, M. M., 1976, Pluvial lakes and estimated pluvial climates of Nevada: *Nevada Bureau of Mines and Geology Bulletin No. 94*, 57 p.
- Milner, Sam, 1976, Carbonate petrology and syndepositional facies of the lower San Andreas Formation (Middle Permian), Lincoln County, New Mexico: *Journal of Sedimentary Petrology*, v. 46., no. 3, p. 463-482.
- Mitsuda, Takeshi, 1970, Synthesis of tobermorite from zeolite: *Mineralogical Journal*, v. 6, no. 3, p. 143-158.
- Mitsuda, Takeshi, and Taylor, H. F. W., 1978, Normal and anomalous tobermorite: *Mineralogical Magazine*, v. 42, p. 229-235.
- Morrison, R. B., 1965, Quaternary geology of the Great Basin, in Wright, H. E., and Frey, D. G., eds., *The Quaternary of the United States: Princeton, N. J., Princeton University Press*, p. 265-285.

- Nelson, A. R., and Taylor, E. M., 1985 a, Automated calculation of soil profile development indices using a microcomputer and integrated spreadsheet: Geological Society of America Abstracts with Program, v. 17, no. 4, p. 258.
- 1985 b, LOTUS 1-2-3 template to calculate soil development indices: Computer Oriented Geological Society, Denver, Colorado public domain diskette no. 5.
- Nettleton, W. D., and Peterson, F. F., 1983, Aridisols, in Wilding, L. P., and others, eds., Pedogenesis and soil taxonomy, II The soil orders: Amsterdam, Elsevier.
- Omar, M. H., 1968, Potential evapotranspiration in a warm arid climate, in Agroclimatological Methods: Proceedings of the Reading Symposium, Natural Resources Research Publication 7, Paris, UNESCO, p. 347-353.
- Papadakis, Jaun, 1965, Potential Evapotranspiration: Buenos Aries, Argentina, 54 p.
- Penman, H. L., 1956, Estimating Evaporation: American Geophysical Union Transactions, v. 37, no. 1, p. 43-50.
- Peterson, F. F., 1981, Landforms of the Basin and Range Province, defined for soil survey: Nevada Agricultural Experimental Station, Technical Bulletin 28, 52 p.
- Quiring, R. F., 1983, Precipitation climatology of the Nevada Test Site: U.S. Department of Commerce, NOAA-U.S. Weather Bureau, WSN50 351-88, 37 p.
- Quinlivan, W. D., and Byers, Jr., F. M., 1977, Chemical data and variation diagrams of igneous rocks from the Timber Mountain-Oasis Valley caldera complex, southern Nevada: U.S. Geological Survey Open-File Report 77-724, 9 p.
- Reheis, M. C., 1984, Chronologic and climatic control on soil development, northern Bighorn Basin, Wyoming and Montana: Boulder, University of Colorado PhD. dissertation, 346 p.
- Ritchie, J. T., 1982, A model for predicting evaporation from a row crop with incomplete cover: Water Resources Research, v. 8, no. 5, p. 1204-1213.
- Romney, E. M., Hale, V. Q., Wallace, A., Lunt, O. R., Childress, J. D., Haaz, H., Alexander, G. V., Kinnear, J. E., and Ackerman, T. L., 1973, Some characteristics of soil and perennial vegetation in the northern Mojave Desert area of the Nevada Test Site: Los Angeles, University of California, Laboratory of Nuclear Medicine and Radiation Biology, 339 p.

- Rosholt, J. N., 1980, Uranium-trend dating of Quaternary sediments: U.S. Geological Survey Open-File Report 80-1087, 74 p.
- Salter, P. J., and Williams, J. B., 1965, The influence of texture on the moisture characteristics of soils, II. Available-water capacity and moisture release characteristics: Journal of Soil Science, v. 16, no. 2, p. 310-316.
- Schumm, S. A., 1977, The fluvial system: New York, John Wiley and Sons, 338 p.
- Shackleton, N. J., and Opdyke, N. D., 1973, Oxygen isotope and paleomagnetic stratigraphy of equatorial Pacific core V28-238--Oxygen isotope temperatures and ice volumes on a 10^5 year and 10^6 year scale: Quaternary Research, v. 3, p. 39-55.
- Smith, G. I., 1979, Subsurface stratigraphy and geochemistry of late Quaternary evaporites, Searles Lake, California: U.S. Geological Survey Professional Paper 1043, 130 p.
- 1984, Paleohydrologic regimes in the southwestern Great Basin, 0-3.2 my ago, compared with other long term records of "global" climate: Quaternary Research, v. 22, p. 1-17.
- Snell, D. S., 1975, Review of synthesis of properties of tobermorite C-S-H(I), and C-S-H Gel: Journal of the American Ceramic Society, v. 58, no. 7-8, p. 292-295.
- Soil Survey Staff, 1951, Soil survey manual: U.S. Department of Agriculture Handbook No. 18.
- 1975, Soil taxonomy, A basic system of soil classification for making and interpreting soil surveys: U.S. Department of Agriculture Handbook No. 436, 754 p.
- Spaulding, W. G., 1982, Processes and rates of vegetation change in the arid southwest: Program and Abstracts, Seventh Biennial Conference, American Quaternary Association, p. 22-24.
- 1983, Vegetation and climates of the last 45,000 years in the vicinity of the Nevada Test Site, south-central Nevada: U.S. Geological Survey Open-File Report 83-535, 199 p.
- 1985, Vegetation and climates of the last 45,000 years in the vicinity of the Nevada Test Site, south-central Nevada: U.S. Geological Professional Paper 1329, 83 p.

- Spaulding, W. G., Leopold, E. P., and Van Devender, T. R., 1983, Late Wisconsin paleoecology of the American southwest, in Porter, S. C., and Wright, H. E., Jr., eds., The late Pleistocene of the United States: Minneapolis, University of Minnesota Press, p. 259-289.
- Stanhill, G., 1961, A comparison of methods of calculating potential evapotranspiration from climatic data: Israel Journal of Agricultural Research, v. 11, no. 3-4, p. 159-171.
- Summerfield, M. A., 1982, Distribution, nature and genesis of silcrete in arid and semiarid southern Africa, in Yaalon, D. H., ed., Aridic Soils and Geomorphic Processes: Catena, Supplement 1, p. 37-65.
- 1983, Silcrete as a paleoclimatic indicator: Evidence from southern Africa: Paleogeography, paleoclimatology, and paleoecology, v. 41, p. 65-79.
- Swadley, W C, 1983, Map showing surficial geology of the Lathrop Wells quadrangle, Nye County, Nevada: U.S. Geological Survey Miscellaneous Investigations Map I-1361, scale 1:48,000.
- Swadley, W C, and Hoover, D. L., 1983, Geology of faults exposed in trenches in Crater Flat, Nye County, Nevada: U.S. Geological Survey Open-File Report 83-608, 15 p.
- Szabo, B. J., Carr, W. J., and Gottschall, W. C., 1981, Uranium-thorium dating of Quaternary carbonate accumulation in the Nevada Test Site region, southern Nevada: U.S. Geological Survey Open-File Report 81-119, 35 p.
- Taylor, H. F. W., 1950, Hydrated calcium silicates, Part I, Compound formation at ordinary temperatures: Journal of the Chemical Society of London, p. 3682-3690.
- 1959, The dehydration of tobermorite: Proceedings of the Sixth National Conference on Clays and Clay Minerals, Clays and Clay Minerals, v. 6, p. 101-109.
- Thompson, R. S., 1984, Late Pleistocene and Holocene environs in the Great Basin: Tucson, University of Arizona PhD. dissertation, 256 p.
- Thorntwaite, C. W., 1948, An approach toward a rational classification of climate: Geographical Review, v. 38, p. 55-94.
- Till, Roger, 1974, Statistical methods for the earth scientist: New York, John Wiley and Sons, 154 p.

- Torrent, J., Nettleton, W. D., and Borst, G., 1980, Genesis of a Typic Durixeralf of Southern California: Soil Science Society of America Journal, v. 44, p. 575-582.
- Twiss, P. C., 1983, Dust deposition and opal phytoliths in the Great Plains: Transactions of the Nebraska Academy of Science XI, p. 73-82.
- Twiss, P. C., Suess, Erwin, Smith, Ron, 1969, Morphological classification of grass phytoliths: Soil Science Society of America Proceedings, v. 33, p. 109-115.
- U.S. Department of Commerce, Weather Bureau, Climatic Summary of the United States, Supplement of 1951 through 1960, 1961 through 1970, and 1971 through 1980, Nevada.
- Van Devender, T. R., and Spaulding, W. G., 1979, The development of vegetation and climate in the southwestern United States: Science, v. 204, p. 701-710.
- Vanden Heuvel, R. C., 1966, The occurrence of sepiolite and attapulgite in the calcareous zone of a soil near Las Cruces, New Mexico: Proceeding of the Thirteenth National Conference of Clays and Clay Mineralists, Clays and Clay Minerals, v. 13, p. 193-207.
- Van Hylckama, T. E. A., 1959, A nomogram to determine monthly potential evapotranspiration: Monthly Weather Review, v. 87, p. 107-110.
- Wada, Koji, and Kakuto, Yasuko, 1985, A spot test with toluidine blue for allophane and imogolite: Soil Society of America Journal, v. 49, p. 276-278.
- Webb, A. B. St. J., 1971, Tobermorite from Castle Hill near Kilbirnie, Ayrshire: Mineralogical Magazine, v. 38, p. 253.
- Wells, S. G., McFadden, L. D., Dohrenwend, J. C., Bullard, T. F., Feilberg, B. F., Ford, R. L., Grimm, J. P., Miller, J. R., Orbock, S. M., and Pickle, J. D., 1984, Late Quaternary geomorphic history of the Silver Lake area, eastern Mojave Desert, California, An example of the influence of climatic change on desert piedmonts, in Dohrenwend, J. C. ed., Surficial geology of the eastern Mojave Desert, California: Geological Society of America, 97th Annual Meeting, Field Trip 14 Guidebook, p. 69-87.
- West, Ian, 1973, Vanishing evaporites - Significance of strontium minerals: Journal of Sedimentary Petrology, v. 43, p. 278-279.

- Williams, J. R., ed., 1984, EPIC, The erosion-productivity impact calculator, Volume 1, Model documentation: U.S. Department of Agriculture, Agricultural Research Service, p. 21-24.
- Winograd, I. J., 1981, Radioactive waste disposal in thick unsaturated zones: Science, v. 212, no. 4502, p. 1457-1464.
- Winograd, I. J., and Thordarson, William, 1975, Hydrologic and hydrogeochemical framework, south-central Great Basin, Nevada-California, with special reference to the Nevada Test Site: U.S. Geological Professional Paper 712-C, 126 p.
- Winograd, I. J., and Doty, G. C., 1980, Paleohydrology of the southern Great Basin with special reference to water table fluctuations beneath the Nevada Test Site during the late(?) Pleistocene: U.S. Geological Survey Open-File report 80-569, 97 p.
- Yuan, T. L., and Breland, H. L., 1969, Evaluation of atomic absorption methods for determinations of aluminum, iron, and silicon in clay and soil extracts: Soil Science Society of America Proceedings, v. 33, p. 868-872.

APPENDICES

Appendix A. Soil field descriptions for the Yucca Wash and
Fortymile Wash area, Nevada Test Site.

501

Map Ref. elev (m) (in Datum)	Sample number	Depth cm	Lower boundary	Color	Texture	Structure	Consistence	Clay	Percent Material
			dry	moist	LS	gravel	dry Moist Wet	Filler	
Q1c over TW-21									
Q2c	Avh	4	no	10YR6/3	SL 19	3 co. abh	no. pe	2 m. pe	collen. shootwash and gravel
	Bljh	15	no	10YR6/3	SL 17	2 c. pl. abh	no. pe	3 m. br	
	Bh	33	41	10YR6.5/3	SL 47	06	no. pe	0	channel gravel
	20Yqhb1	55	41	10YR5.5/3	SL 54	2 m. abh	no. pe	1 m. gr	channel gravel
Q2c over TW-21	20Yqhb1	144	no	10YR6/4	SL 59	0	no. pe	1 m. gr	channel gravel
	30Yqhb2	186	no	7.5YR-10YR 7/4	LS 48	0	no. pe	1 m. gr	channel gravel
	Ab/	30Yqhb2	233+	7/4	LS 79	06	no. pe	0	fluvial gravel
	Ab/	30Yqhb2	233+	7/4	LS 79	06	no. pe	0	fluvial gravel
Q2b over TW-11									
Q2b (7.3)	Av	4	no	10YR6/3	LS 40	3 m. pl	no. pe	0	shootwash & collen
	Bc1	15	no	10YR6/3	SL 37	2 m. abh	no. pe	0	shootwash & collen
	20Yqhb2	42	no	10YR6/4	SL 39	2 m. abh	no. pe	0	shootwash & collen
	20Yqhb2	90	no	10YR6.5/4	SL 48	0.1 m. place	no. pe	1 m. gr	channel gravel
Ab/	20Yqhb2	130	no	10YR6/2	SL 73	2 m. abh	no. pe	1 m. br	channel gravel
	20Yqhb2	170+	no	10YR6/2	SL 73	2 m. abh	no. pe	1 m. br	channel gravel
	Ab/	30Yqhb2	233+	7/4	LS 79	06	no. pe	0	fluvial gravel
	Ab/	30Yqhb2	233+	7/4	LS 79	06	no. pe	0	fluvial gravel
Q1c over TW-12									
Q2b (6.1)	Av1	4	no	10YR6/3	SL 35	1-2 m. pl	no. pe	0	shootwash & collen
	Av2	14	no	10YR6/3	SL 23	1-2 m. pl	no. pe	0	shootwash & collen
	Bc1	47	no	10YR6.5/3	SL 26	2 m. abh	no. pe	0	shootwash & collen
	20Yqhb2	165	no	10YR6.5/3	SL 36	2 m. abh	no. pe	0	channel gravel
Ab/	20Yqhb2	120	no	10YR6/4	LS 10	06	no. pe	0	channel gravel
	20Yqhb2	130	no	10YR6/4	LS 10	06	no. pe	0	channel gravel
	Ab/	30Yqhb2	233+	7/4	LS 79	06	no. pe	0	fluvial gravel
	Ab/	30Yqhb2	233+	7/4	LS 79	06	no. pe	0	fluvial gravel
Q1c over TW-14									
Q2b (12.2)	Av	4	no	10YR6/3	SL 32	2 m. pl	no. pe	0	collen & shootwash
	Bc1	20	no	10YR6/3	SL 26	1 m. abh	no. pe	0	collen & shootwash
	20Yqhb2	107	no	10YR6.5/3	SL 42	06	no. pe	0	collen & shootwash
	20Yqhb2	121	no	10YR6.5/3	SL 19	2 m. abh	no. pe	0	collen & shootwash
Ab/	20Yqhb2	152	no	10YR6/3	SL 30	06	no. pe	0	collen & shootwash
	20Yqhb2	221	no	10YR6/3	SL 30	06	no. pe	0	collen & shootwash
	Ab/	30Yqhb2	233+	7/4	LS 79	06	no. pe	0	fluvial gravel
	Ab/	30Yqhb2	233+	7/4	LS 79	06	no. pe	0	fluvial gravel

Map Sheet, Sample elev (m) number (m > stream)	Sample number	Horizon	Soil depth cm	Lower boundary dry	Color	Texture 1/ moist	Structure	pH	Consistence Dry Moist Wet	CaCO ₃	Clay Plum	SiO ₂	Parent Material
Q2b(1)	YU-20	Av	0	ca	10YR6/3	SL	30	1 m-co abh	6.90 sh	0	0	0	sheetwash & collan
1373		Bc1	19	ca	10YR6/3	SL	24	3 co-vc abh	6.90 sh	0	0	0	sheetwash & collan
(10.3)		Bc2	42	gw	10YR6/4	L	39	2 m-co abh	6.75 sh fr	0	3 m pe 0	0	sheetwash & collan
		2Bq	64	gw	7.5YR5/4	SL	84	1-2 m abh	7.10 sh	0	0	1	sheetwash & collan
		2Bq1	76	ab	7.5YR5/4	SL	84	1-2 m abh	7.00 sh	0	2 m br 1	1	fluvial gravel
		2Bq2-1	116		7.5YR5/4	SL	84	m-co	7.05 sh	0	1 m gr 1-11	1-11	fluvial gravel
		2Bq2-2	132		7.5YR6/4	SL	68	m-co	7.05 sh	0	2 m br 11	11	bedded fluvial
		2Bq2-3	190		7.5YR6/4	SL	89		8.00	1. disc	0	1-11	gravel
									8.00				
Q1c over	PM-3	A	5	an	7.5YR7/3	S	25	1 vt pl	7.55 sh	0	0	0	sheetwash
Q2c		AB	20	aw	10YR6/3	S	9	2 vt-f abh	7.30 sh	0	0	0	sheetwash
1021		Bc1	45	aw-b	10-7.5YR7/2	SL	14	1 m-abh	7.45 sh	0	1 m gr 1	1	sheetwash
(13.4)		2Bc1b	56	an-d	7.5YR5.5/4	SL	10	3 m abh	7.55 sh	0	2 m-h 1	1	fluvial gravel
		2Bc1qb1	106	cw	7.5YR6/4	SL	60	m	7.50 sh	0	2 m br 11	11	fluvial gravel
		2Bc1b	166	aw	7.5YR7/4	S	71	m, 2° 2m abh	7.60 sh (co) 0.00	0	3 m br 10	10	fluvial gravel
		2Cqa	263+		10YR6/1	S	72	og	7.50 sh	0	0	0	fluvial gravel
									7.50 sh	0	0	0	fluvial gravel
Q2c over	PM-10	Av1	11	aw	10YR7/3	L	13	3 co abh	8.10 sh	0	0	0	sheetwash & collan
Q2a		Ab	37	ca	10YR7/3	SL	24	2° 1 co-vc pl	8.00 sh	0	0	0	sheetwash & collan
1005		Bc1j	40	cw	10YR6/4	SL	30	2 m-co pl	7.55 sh	0	2 m pe 0	0	sheetwash & collan
(21.3)		2Bc1j1	66	cw	7.5-10YR6/4	SL	53	1 co pl	7.55 sh	0	2 m pe 1-11	1-11	fluvial gravel
		2Bc1j2	120	aw	10YR6/3	LS	72	2° 3 vc abh	7.25 sh	0	2 m br 11	11	fluvial gravel
		3Bb	160+	--	white d/ 10YR6/4	S	76	m	7.20 sh	0	0	0	fluvial gravel
									7.20 sh	0	0	0	fluvial gravel
Q2a over	YU-0	Av	11	cu	10YR6/3	L	13	3 co abh	7.60 sh fr	0	3 m pe 0	0	collan & sheetwash
Q2c		Bc1	21	cu	7.5YR6/4	C	13	2 f fr	7.30 sh	0	3 m br 0	0	collan & reworked gravel
1190		2Bc2b	35	cu	7.5YR7/6	SL	27	3 m-co abh	7.45 sh	0	0	0	fluvial gravel
(18.0)		2Bc1b	68	aw	7.5YR7/6	LS	18	2 co-vc abh	7.90 sh	0	3 m br 11	11	fluvial gravel
		2Bc1	100	cl	10YR6/2	S	52	3 vc pl in place	8.15 sh	0	0	0	fluvial gravel
		2Cub1	210+	--	(CaCO ₃) 10YR7/3	S	67	1 f pl	8.15 sh	0	0	0	fluvial gravel
									8.15 sh	0	0	0	fluvial gravel

Map Unit, Sample elev (m) (m > stream)	Sample number	Horizon	Soil depth cm	Lower boundary	Color moist	Texture 1/2	Structure	pH	Consistence Dry Moist Wet	CaCO ₃	Clay Pline	SiO ₂	Parent Material
Q7a	YU-6	Ash	6	cm	10YR4/3	L 24	3 vco ash	7.70	fr	o dia	0	0	collan & sheetwash
1170	37	Bk	10	cm	7.5YR5/6	SL 14	2 m ash	7.60	fr	o dia	2 m pl	0	collan & sheetwash
(19.0)	40/	28cm	52	cm	7.5YR5/2	white (CaCO ₃)	3 vco pl	7.75	o, p	IV	0	IV	fluvial gravel
	34cm		101	cm	7.5YR7/3	white (CaCO ₃)	59		o, p	III	0	II	fluvial gravel
	36cm		153	cm	10YR6/3	S 67	ss	7.60	ss	lenses of III	0	II	fluvial gravel
	304cm		230	cm	10YR4/3	S 63	ss	7.60	ss	I	0	II	fluvial gravel
	304cm		250+	cm	10YR4/3	S 61	ss	7.70	ss	I	0	II	fluvial gravel
Q7a	YU-20	Ash	3	cm	10YR7/3	L 6	3 co ash	7.95	oh	ov	0	0	collan & sheetwash
1100	21	Bk	10	cm	10YR7/4	L 9	1 m ash-ss	7.95	ss	o	0	0	collan & sheetwash
(21.1)	23/ 40/	201cm	19	cm	10YR5.5/3	L 12	2 v ash-ss	7.60	ss	o	0	0	collan & sheetwash
	201cm		34	cm	10YR7/6	L- 23	3 co pl	7.50	oh	1-2 mm lenses & br	2 m gr, III	0	fluvial gravel
	201cm		70+	cm	7.5YR6/4	7.5YR4/4			ss	II on pl top	0	III	fluvial gravel
	201cm		70+	cm	7.5YR5.5/6	7.5YR4/4	L- 33	2 co pl	ss	lenses & m pl	0	III	fluvial gravel
	201cm		70+	cm	7.5YR5.5/6	7.5YR4/4	L- 33	2 co pl	ss	lenses & m pl	0	III	fluvial gravel
Q7a	YU-28	Spall	4	cm	10YR7/3	L 6	3 co ash	7.95	oh	ov	0	0	collan & sheetwash
1100	29/ 40/	28cm	19	cm	10YR7/4	L 9	1 m ash-ss	7.95	ss	o	0	0	collan & sheetwash
(21.1)	28cm		52	cm	10YR5.5/3	L 12	2 v ash-ss	7.60	ss	o	0	0	collan & sheetwash
	28cm		116	cm	10YR7/6	L- 23	3 co pl	7.50	oh	1-2 mm lenses & br	2 m gr, III	0	fluvial gravel
	28cm		197+	cm	7.5YR6/4	7.5YR4/4			ss	II on pl top	0	III	fluvial gravel
	28cm		197+	cm	7.5YR5.5/6	7.5YR4/4	L- 33	2 co pl	ss	lenses & m pl	0	III	fluvial gravel
Q7a	YU-22	Ash	10	cm	10YR7/3	L 6	3 co ash	7.95	oh	ov	0	0	collan & sheetwash
1100	23/ 40/	28cm	19	cm	10YR7/4	L 9	1 m ash-ss	7.95	ss	o	0	0	collan & sheetwash
(19.2)	28cm		52	cm	10YR5.5/3	L 12	2 v ash-ss	7.60	ss	o	0	0	collan & sheetwash
	28cm		116	cm	10YR7/6	L- 23	3 co pl	7.50	oh	1-2 mm lenses & br	2 m gr, III	0	fluvial gravel
	28cm		197+	cm	7.5YR6/4	7.5YR4/4			ss	II on pl top	0	III	fluvial gravel
	28cm		197+	cm	7.5YR5.5/6	7.5YR4/4	L- 33	2 co pl	ss	lenses & m pl	0	III	fluvial gravel
Q7a	YU-22	Ash	10	cm	10YR7/3	L 6	3 co ash	7.95	oh	ov	0	0	collan & sheetwash
1100	23/ 40/	28cm	19	cm	10YR7/4	L 9	1 m ash-ss	7.95	ss	o	0	0	collan & sheetwash
(19.2)	28cm		52	cm	10YR5.5/3	L 12	2 v ash-ss	7.60	ss	o	0	0	collan & sheetwash
	28cm		116	cm	10YR7/6	L- 23	3 co pl	7.50	oh	1-2 mm lenses & br	2 m gr, III	0	fluvial gravel
	28cm		197+	cm	7.5YR6/4	7.5YR4/4			ss	II on pl top	0	III	fluvial gravel
	28cm		197+	cm	7.5YR5.5/6	7.5YR4/4	L- 33	2 co pl	ss	lenses & m pl	0	III	fluvial gravel
Q7a	YU-22	Ash	10	cm	10YR7/3	L 6	3 co ash	7.95	oh	ov	0	0	collan & sheetwash
1100	23/ 40/	28cm	19	cm	10YR7/4	L 9	1 m ash-ss	7.95	ss	o	0	0	collan & sheetwash
(19.2)	28cm		52	cm	10YR5.5/3	L 12	2 v ash-ss	7.60	ss	o	0	0	collan & sheetwash
	28cm		116	cm	10YR7/6	L- 23	3 co pl	7.50	oh	1-2 mm lenses & br	2 m gr, III	0	fluvial gravel
	28cm		197+	cm	7.5YR6/4	7.5YR4/4			ss	II on pl top	0	III	fluvial gravel
	28cm		197+	cm	7.5YR5.5/6	7.5YR4/4	L- 33	2 co pl	ss	lenses & m pl	0	III	fluvial gravel
Q7a	YU-22	Ash	10	cm	10YR7/3	L 6	3 co ash	7.95	oh	ov	0	0	collan & sheetwash
1100	23/ 40/	28cm	19	cm	10YR7/4	L 9	1 m ash-ss	7.95	ss	o	0	0	collan & sheetwash
(19.2)	28cm		52	cm	10YR5.5/3	L 12	2 v ash-ss	7.60	ss	o	0	0	collan & sheetwash
	28cm		116	cm	10YR7/6	L- 23	3 co pl	7.50	oh	1-2 mm lenses & br	2 m gr, III	0	fluvial gravel
	28cm		197+	cm	7.5YR6/4	7.5YR4/4			ss	II on pl top	0	III	fluvial gravel
	28cm		197+	cm	7.5YR5.5/6	7.5YR4/4	L- 33	2 co pl	ss	lenses & m pl	0	III	fluvial gravel
Q7a	YU-22	Ash	10	cm	10YR7/3	L 6	3 co ash	7.95	oh	ov	0	0	collan & sheetwash
1100	23/ 40/	28cm	19	cm	10YR7/4	L 9	1 m ash-ss	7.95	ss	o	0	0	collan & sheetwash
(19.2)	28cm		52	cm	10YR5.5/3	L 12	2 v ash-ss	7.60	ss	o	0	0	collan & sheetwash
	28cm		116	cm	10YR7/6	L- 23	3 co pl	7.50	oh	1-2 mm lenses & br	2 m gr, III	0	fluvial gravel
	28cm		197+	cm	7.5YR6/4	7.5YR4/4			ss	II on pl top	0	III	fluvial gravel
	28cm		197+	cm	7.5YR5.5/6	7.5YR4/4	L- 33	2 co pl	ss	lenses & m pl	0	III	fluvial gravel
Q7a	YU-22	Ash	10	cm	10YR7/3	L 6	3 co ash	7.95	oh	ov	0	0	collan & sheetwash
1100	23/ 40/	28cm	19	cm	10YR7/4	L 9	1 m ash-ss	7.95	ss	o	0	0	collan & sheetwash
(19.2)	28cm		52	cm	10YR5.5/3	L 12	2 v ash-ss	7.60	ss	o	0	0	collan & sheetwash
	28cm		116	cm	10YR7/6	L- 23	3 co pl	7.50	oh	1-2 mm lenses & br	2 m gr, III	0	fluvial gravel
	28cm		197+	cm	7.5YR6/4	7.5YR4/4			ss	II on pl top	0	III	fluvial gravel
	28cm		197+	cm	7.5YR5.5/6	7.5YR4/4	L- 33	2 co pl	ss	lenses & m pl	0	III	fluvial gravel
Q7a	YU-22	Ash	10	cm	10YR7/3	L 6	3 co ash	7.95	oh	ov	0	0	collan & sheetwash
1100	23/ 40/	28cm	19	cm	10YR7/4	L 9	1 m ash-ss	7.95	ss	o	0	0	collan & sheetwash
(19.2)	28cm		52	cm	10YR5.5/3	L 12	2 v ash-ss	7.60	ss	o	0	0	collan & sheetwash
	28cm		116	cm	10YR7/6	L- 23	3 co pl	7.50	oh	1-2 mm lenses & br	2 m gr, III	0	fluvial gravel
	28cm		197+	cm	7.5YR6/4	7.5YR4/4			ss	II on pl top	0	III	fluvial gravel
	28cm		197+	cm	7.5YR5.5/6	7.5YR4/4	L- 33	2 co pl	ss	lenses & m pl	0	III	fluvial gravel
Q7a	YU-22	Ash	10	cm	10YR7/3	L 6	3 co ash	7.95	oh	ov	0	0	collan & sheetwash
1100	23/ 40/	28cm	19	cm	10YR7/4	L 9	1 m ash-ss	7.95	ss	o	0	0	collan & sheetwash
(19.2)	28cm		52	cm	10YR5.5/3	L 12	2 v ash-ss	7.60	ss	o	0	0	collan & sheetwash
	28cm		116	cm	10YR7/6	L- 23	3 co pl	7.50	oh	1-2 mm lenses & br	2 m gr, III	0	fluvial gravel
	28cm		197+	cm	7.5YR6/4	7.5YR4/4			ss	II on pl top	0	III	fluvial gravel
	28cm		197+	cm	7.5YR5.5/6	7.5YR4/4	L- 33	2 co pl	ss	lenses & m pl	0	III	fluvial gravel
Q7a	YU-22	Ash	10	cm	10YR7/3	L 6	3 co ash	7.95	oh	ov	0	0	collan & sheetwash
1100	23/ 40/	28cm	19	cm	10YR7/4	L 9	1 m ash-ss	7.95	ss	o	0	0	collan & sheetwash
(19.2)	28cm		52	cm	10YR5.5/3	L 12	2 v ash-ss	7.60	ss	o	0	0	collan & sheetwash
	28cm		116	cm	10YR7/6	L- 23	3 co pl	7.50	oh	1-2 mm lenses & br	2 m gr, III	0	fluvial gravel
	28cm		197+	cm	7.5YR6/4	7.5YR4/4			ss	II on pl top	0	III	fluvial gravel
	28cm		197+	cm	7.5YR5.5/6	7.5YR4/4	L- 33	2 co pl	ss	lenses & m pl	0	III	fluvial gravel
Q7a	YU-22	Ash	10	cm	10YR7/3	L 6	3 co ash	7.95	oh	ov	0	0	collan & sheetwash
1100	23/ 40/	28cm	19	cm	10YR7/4	L 9	1 m ash-ss	7.95	ss	o	0	0	collan & sheetwash
(19.2)	28cm		52	cm	10YR5.5/3	L 12	2 v ash-ss	7.60	ss	o	0	0	collan & sheetwash
	28cm		116	cm	10YR7/6	L- 23	3 co pl	7.50	oh	1-2 mm lenses & br	2 m gr, III	0	fluvial gravel
	28cm		197+	cm	7.5YR6/4	7.5YR4/4			ss	II on pl top	0	III	fluvial gravel
	28cm		197+	cm	7.5YR5.5/6	7.5YR4/4	L- 33	2 co pl	ss	lenses & m pl	0	III	fluvial gravel
Q7a	YU-22	Ash	10	cm	10YR7/3	L 6	3 co ash	7.95	oh	ov	0	0	collan & sheetwash
1100	23/ 40/	28cm	19	cm	10YR7/4	L 9	1 m ash-ss	7.95	ss	o	0	0	collan & sheetwash
(19.2)	28cm		52	cm	10YR5.5/3	L 12	2 v ash-ss	7.60	ss	o	0	0	collan & sheetwash
	28cm		116	cm	10YR7/6	L- 23	3 co pl	7.50	oh	1-2 mm lenses & br	2 m gr, III	0	fluvial gravel
	28cm		197+	cm	7.5YR6/4	7.5YR4/4			ss	II on pl top	0	III	fluvial gravel
	28cm		197+	cm	7.5YR5.5/6	7.5YR4/4	L- 33	2 co pl	ss	lenses & m pl	0	III	fluvial gravel
Q7a	YU-22	Ash	10	cm	10YR7/3	L 6	3 co ash	7.95	oh	ov	0	0	collan & sheetwash
1100	23/ 40/	28cm	19	cm	10YR7/4	L 9	1 m ash-ss	7.95	ss	o	0	0	collan & sheetwash
(19.2)	28cm		52	cm	10YR5.5/3	L 12	2 v ash-ss	7.60	ss	o	0	0	collan & sheetwash
	28cm		116	cm	10YR7/6	L- 23	3 co pl	7.50	oh	1-2 mm lenses & br	2 m gr, III	0	fluvial gravel
	28cm		197+	cm	7.5YR6/4	7.5YR4/4			ss	II on pl top	0	III	fluvial gravel
	28cm		197+	cm	7.5YR5.5/6	7.5YR4/4	L- 33	2 co pl	ss	lenses & m pl	0	III	fluvial gravel
Q7a	YU-22	Ash	10	cm	10YR7/3	L 6	3 co ash	7.95	oh	ov	0	0	collan & sheetwash
1100	23/ 40/	28cm	19	cm	10YR7/4	L 9	1 m ash-ss	7.95	ss	o	0	0	collan & sheetwash
(19.2)	28cm		52	cm	10YR5.5/3	L 12	2 v ash-ss	7.60	ss	o	0	0	collan & sheetwash
	28cm		116	cm	10YR7/6	L- 23	3 co pl	7.50	oh	1-2 mm lenses & br	2 m gr, III	0	fluvial gravel
	28cm		197+	cm	7.5YR6/4	7.5YR4/4			ss	II on pl top	0	III	fluvial gravel
	28cm		197+	cm	7.5YR5.5/6	7.5YR4/4	L- 33	2 co pl	ss	lenses & m pl	0	III	fluvial gravel
Q7a	YU-22	Ash	10	cm	10YR7/3	L 6	3 co ash	7.95	oh	ov	0	0	collan & sheetwash
1100	23/ 40/	28cm	19	cm	10YR7/4	L 9	1 m ash-ss	7.95	ss	o	0	0	collan & sheetwash
(19.2)	28cm		52	cm	10YR5.5/3	L 12	2 v ash-ss	7.60	ss	o	0	0	collan & sheetwash
	28cm		116	cm	10YR7/6	L- 23	3 co pl	7.50	oh	1-2 mm lenses & br	2 m gr, III	0	fluvial gravel
	28cm		197+	cm	7.5YR6/4	7.5YR4/4			ss	II on pl top	0	III	fluvial gravel
	28cm		197+	cm	7.5YR5.5/6	7.5YR4/4	L- 33	2 co pl	ss	lenses & m pl	0	III	fluvial gravel
Q7a	YU-22	Ash	10	cm	10YR7/3	L 6	3 co ash	7.95	oh	ov	0	0	collan & sheetwash
1100	23/ 40/	28cm	19	cm	10YR7/4	L 9	1 m ash-ss	7.95	ss	o	0	0	collan & sheetwash
(19.2)	28cm		52	cm	10YR5.5/3	L 12	2 v ash-ss	7.60	ss	o	0	0	collan & sheetwash
	28cm	</											

Key to Appendix A *

Horizon Boundary

Distinctness

va very abrupt
a abrupt
c clear
g gradual
d diffuse

Topography

s smooth
w wavy
i irregular
b broken

Soil Texture

co coarse
f fine
vf very fine

S sand
LS loamy sand
SL sandy loam
L loam
SiL silt loam
Si silt

SCL sandy clay loam
CL clay loam
SiCL silty clay loam
SC sandy clay
C clay
SiC silty clay

Soil Structure

Grade

m massive
sg single grained
1 weak
2 moderate
3 strong

Size

vf very fine (v thin)
f fine (thin)
m medium
co coarse (thick)
vco very coarse
(v thick)

Type

gr granular
pl platey
pr prismatic
cpr columnar
abk angular blocky
sbk subangular
blocky

If two structures - listed as primary and secondary (2°)

Soil Consistence

Dry

lo loose
so soft
sh slightly hard
h hard
vh very hard
eh ex hard

Moist

lo loose
vfr very friable
friable
fi firm
vfi very firm
efi extremely firm

Wet

so,po non-sticky or plastic
ss,ps slightly sticky or plastic
s,p sticky or plastic
vs,vp very sticky or plastic

Clay Films

Frequency

vf very few
1 few
2 common
3 many

Thickness

n thin
mk moderately thick
k thick

Morphology

pf ped face coating
br bridging grains
po pore linings
gr gravel coats

CaCO₃

Effervescence on matrix

0 - none in matrix.
diss - disseminated; discontinuous.
e - slightly, bubbles are readily observed.
es - strongly, bubbles form a low foam.
ev - violently, thick foam "jumps" up.

Key to Appendix A (continued)

- * For more information, see Soil Survey Staff 1951 and 1975
- 1/ Texture is based on lab analyses
- 2/ Sampled for phytolith and pollen analyses
- 3/ Sampled for U-trend dating
- 4a/ Soil ped thin section
- 4b/ Rock thin section
- 5/ Sampled for ^{36}Cl analyses
- 6/ White carbonate is whiter than 10YR8/0

Appendix B. Soil Profile Index Values

SOIL PROFILE INDEX VALUES

Sample	Horizon	Depth (cm)	RUBIFICATION (maximum=190)			X thickness	Profile Weighted	
			Color M1	Color M2	Normalized property		property	mean
FMA-1			0.00	0.00	0.00	0.00		
FMA-2			0.00	0.00	0.00	0.00		
FMA-3			0.00	0.00	0.00	0.00		
FMA-4			0.00	0.00	0.00	0.00		
YMA-1			0.00	0.00	0.00	0.00		
YMA-2			0.00	0.00	0.00	0.00		
7.01 A		0 15	0.00	0.00	0.00	0.00	0.87	0.01
7.02 Bw		2 18	10.00	0.00	0.05	0.87		
7.03 20cm		18 100	0.00	0.00	0.00	0.00		
4.01 A		0 3	20.00	0.00	0.11	0.32	15.47	0.15
4.02 Bx1		3 9	25.00	0.00	0.13	0.79		
4.03 28cm		9 60	30.00	0.00	0.16	2.05		
4.04 20cm		60 100	30.00	0.00	0.16	6.32		
17.01 A		0 6	20.00	0.00	0.11	0.62	12.63	0.11
17.02 Bw		6 24	20.00	0.00	0.11	1.69		
17.03 20cm		24 120	20.00	0.00	0.11	10.11		
13.01 A		0 9	0.00	0.00	0.00	0.00	5.47	0.04
13.02 Bw		9 21	0.00	0.00	0.00	0.00		
13.03 28cm		21 73	20.00	0.00	0.11	5.47		
13.04 20cm		73 138	0.00	0.00	0.00	0.00		
15.01 A		0 18	0.00	0.00	0.00	0.00	57.89	0.26
15.02 Bw		18 46	20.00	0.00	0.11	2.95		
15.03 28cm		46 170	60.00	0.00	0.32	39.16		
15.05 20cm		170 220	60.00	0.00	0.32	15.79		
3.01 Av		0 5	0.00	0.00	0.00	0.00	34.45	0.16
3.02 mvpj		5 12	5.00	0.00	0.03	0.18		
3.03 28cm		12 45	60.00	0.00	0.32	10.42		
3.04 28tjql1		45 83	60.00	70.00	0.39	15.00		
3.05 28tjql2		83 107	70.00	0.00	0.37	8.64		
3.06 20cm		107 210	0.00	0.00	0.00	0.00		
21.01 Av		0 4	0.00	0.00	0.00	0.00	32.11	0.14
21.02 Bw		4 15	0.00	0.00	0.00	0.00		
21.03 Bx		15 33	0.00	0.00	0.00	0.00		
21.04 28tjqlb1		33 55	20.00	0.00	0.11	2.32		
21.05 28tjqlb1		55 144	40.00	0.00	0.21	18.74		
21.06 38cm b2		144 186	50.00	0.00	0.26	11.05		
21.07 30cm		186 233	99.00	0.00	0.00	0.00		

SOIL PROFILE INDEX VALUES

Sample	Horizon	Depth (cm)	RUBIFICATION (maximum=190)				X thickness property	Profile Weighted	
			Color M1	Color M2	Normalized property			property	mean
11.01	Av	0 4	0.00	0.00	0.00	0.00	29.58	0.17	
11.02	A	4 15	0.00	0.00	0.00	0.00			
11.03	2Btj	15 42	40.00	0.00	0.21	5.68			
11.04	2Btqm	42 96	40.00	20.00	0.16	7.58			
11.05	2Bxc	96 150	40.00	0.00	0.21	12.67			
11.06	3Cqab	150 170	20.00	50.00	0.18	3.88			
12.01	Av1	0 4	0.00	0.00	0.00	0.00	12.16	0.06	
12.02	Av2	4 14	0.00	0.00	0.00	0.00			
12.03	Bt	14 47	0.00	0.00	0.00	0.00			
12.04	2Bx1	47 105	10.00	20.00	0.08	4.58			
12.05	2Bx2	105 120	40.00	0.00	0.21	3.14			
12.06	2Btqab	120 144	60.00	10.00	0.18	4.42			
12.07	Bqab	144 200	999.00	0.00	0.00	0.00			
14.01	A	0 8	0.00	0.00	0.00	0.00	23.53	0.10	
14.02	Bw	8 28	0.00	0.00	0.00	0.00			
14.03	2Bx	28 54	20.00	0.00	0.11	2.74			
14.04	2Btjxc	54 107	20.00	0.00	0.11	5.58			
14.05	3Bxjc	107 121	25.00	0.00	0.13	1.84			
14.06	3Bqab1b	121 152	20.00	0.00	0.11	3.26			
14.07	4Bqab2c	152 221	20.00	0.00	0.11	7.26			
14.08	4Bxjc	221 230	60.00	0.00	0.32	2.84			
20.01	Av1	0 8	10.00	0.00	0.05	0.42	51.08	0.27	
20.02	Av2	8 19	5.00	0.00	0.03	0.29			
20.03	Bw	19 42	30.00	0.00	0.16	3.63			
20.04	2Btjq	42 64	60.00	0.00	0.32	6.95			
20.05	2Btjq-1	64 76	60.00	0.00	0.32	3.79			
20.06	2Btjqk2-1	76 114	60.00	0.00	0.32	12.00			
20.07	2Btjqk2-2	114 152	60.00	0.00	0.32	12.00			
20.08	2Btjqk2-3	152 190	60.00	0.00	0.32	12.00			
5.01	A	0 5	20.00	0.00	0.11	0.53	44.03	0.17	
5.02	Bw	5 20	0.00	0.00	0.00	0.00			
5.03	Bx	20 45	5.00	0.00	0.03	0.66			
5.04	2Btb	45 56	60.00	0.00	0.32	3.47			
5.05	2Btqab	56 106	80.00	0.00	0.42	21.05			
5.06	2Btqb	106 164	80.00	40.00	0.32	18.32			
5.07	2Cqn	164 263	0.00	0.00	0.00	0.00			

SOIL PROFILE INDEX VALUES

		RUBIFICATION (maximum=190) ----->						
Sample	Horizon	Depth (cm)	Color #1	Color #2	Normalized property	X thickness	Profile Weighted property	mean
18.01	Av	0 11	0.00	0.00	0.00	0.00	18.21	0.11
18.02	A	11 33	0.00	0.00	0.00	0.00		
18.03	Bt	33 40	20.00	0.00	0.11	0.74		
18.04	2Btqk	40 66	55.00	0.00	0.29	7.53		
18.05	2Btq	66 120	40.00	30.00	0.18	9.95		
18.06	2Bt	120 180	999.00	0.00	0.00	0.00		
8.01	Av	0 9	0.00	0.00	0.00	0.00	50.85	0.24
8.02	Bt1	9 21	70.00	0.00	0.37	4.42		
8.03	2Bt2	21 35	100.00	0.00	0.53	7.37		
8.04	2Bqk	35 68	110.00	0.00	0.58	19.11		
8.05	2B	68 100	50.00	0.00	0.26	8.42		
8.06	2Ck	100 210	20.00	0.00	0.11	11.58		
16.01	Av	0 13	0.00	0.00	0.00	0.00	70.00	5.83
16.02	Bw	13 30	20.00	0.00	0.11	1.79		
16.03	Bt	30 43	30.00	0.00	0.16	2.05		
16.04	2Btqk	43 58	90.00	0.00	0.47	7.11		
16.05	2Bq	58 100	70.00	0.00	0.37	15.47		
16.06	2Bqa (nc)	100 150	60.00	0.00	0.32	15.79		
16.07	2Bqa	100 150	60.00	0.00	0.32	15.79		
16.08	2Ckq	150 207	40.00	0.00	0.21	12.00		
1.01	A	0 10	0.00	0.00	0.00	0.00	49.28	0.17
1.02	Bt	10 25	0.00	0.00	0.00	0.00		
1.03	2Btqb1	25 42	40.00	0.00	0.21	3.58		
1.04	2Btqb2	42 56	60.00	0.00	0.32	4.42		
1.08	3Bqab1	56 70	0.00	0.00	0.00	0.00		
1.09	4Bqab2	70 115	999.00	0.00	0.00	0.00		
1.10	5B	115 167	50.00	0.00	0.26	13.88		
1.11	5Cn	167 195	60.00	0.00	0.32	8.84		
1.12	5Cn	195 290	60.00	15.00	0.20	18.75		
19.01	Av1	0 4	0.00	0.00	0.00	0.00	43.37	0.00
	Av2	4 9	0.00	0.00	0.00	0.00		
19.03	Bk	9 13	40.00	0.00	0.21	0.84		
19.04	Bw	13 17	40.00	0.00	0.21	0.84		
19.05	Btqa	17 29	70.00	0.00	0.37	4.42		
19.06	2Btqa	29 47	20.00	80.00	0.26	4.74		
19.07	2Bqa1	47 72	60.00	0.00	0.32	7.89		
19.08	2Bqa2	72 150	60.00	0.00	0.32	24.63		

SOIL PROFILE INDEX VALUES

Sample	Horizon	Depth (cm)	RUBIFICATION (maximum=190)			X thickness	Profile Weighted	
			Color #1	Color #2	Normalized property		property	mean
6.01	Av	0 6	0.00	0.00	0.00	0.00	53.42	0.00
6.02	Bt	6 10	80.00	0.00	0.42	1.62		
6.03	2tq*	10 52	100.00	10.00	0.29	12.16		
6.04	3tq*	52 101	80.00	0.00	0.42	20.63		
6.05	3tq	101 153	10.00	0.00	0.05	2.74		
6.06	3Ckq	153 230	40.00	0.00	0.21	16.21		
6.07	3Ctq*	230 300	999.00	0.00	0.90	0.00		
2.01	Av	0 3	0.00	0.00	0.00	0.00	41.87	0.21
2.02	A	3 10	10.00	0.00	0.05	0.37		
2.03	By	10 19	10.00	0.00	0.05	0.47		
2.04	2Btqey	19 34	30.00	80.00	0.29	4.34		
2.05	2Btqey	34 70	80.00	0.00	0.42	15.16		
2.07	4tq*	19 52	100.00	60.00	0.42	13.89		
2.08	kq	52 114	10.00	0.00	0.05	3.26		
2.09	2*	114 197	10.00	0.00	0.05	4.37		
22.01	Av	0 10	0.00	0.00	0.00	0.00	60.42	0.33
22.02	Bw	10 21	80.00	0.00	0.42	4.63		
22.03	k	21 62	60.00	0.00	0.42	17.26		
22.04	k*	62 92	60.00	0.00	0.32	9.47		
22.05	Bkq*	92 184	60.00	0.00	0.32	29.05		

SOIL PROFILE INDEX VALUES

Sample	Horizon	Depth (cm)	MELANIZATION (maximum=85)				Profile Weighted property mean
			Color #1	Color #2	Normalized property	X thickness	
FNA-1			0.00	0.00	0.00	0.00	
FNA-2			0.00	0.00	0.00	0.00	
FNA-3			0.00	0.00	0.00	0.00	
FNA-4			0.00	0.00	0.00	0.00	
YMA-1			0.00	0.00	0.00	0.00	
YMA-2			0.00	0.00	0.00	0.00	
7.01 A		0 1.5	0.00	0.00	0.00	0.00	1.94 0.02
7.02 Cox		2 18	10.00	0.00	0.12	1.94	
7.03 2Ckx		18 100	0.00	0.00	0.00	0.00	
4.01 A		0 3	0.00	0.00	0.00	0.00	0.00 0.00
4.02 Bk1		3 9	0.00	0.00	0.00	0.00	
4.03 2Bk2		9 60	0.00	0.00	0.00	0.00	
4.04 2Ckn		60 100	0.00	0.00	0.00	0.00	
17.01 A		0 6	0.00	0.00	0.00	0.00	0.00 0.00
17.02 Bw		6 24	0.00	0.00	0.00	0.00	
17.03 2Ckn		24 120	0.00	0.00	0.00	0.00	
13.01 A		0 9	20.00	0.00	0.24	2.12	2.12 0.02
13.02 Bw		9 21	0.00	0.00	0.00	0.00	
13.03 2Bqj		21 73	0.00	0.00	0.00	0.00	
13.04 2Ckqn		73 136	0.00	0.00	0.00	0.00	
15.01 A		0 18	10.00	0.00	0.12	2.12	3.76 0.02
15.02 Bw		18 46	5.00	0.00	0.06	1.65	
15.03 2Bqt		46 170	0.00	0.00	0.00	0.00	
15.05 2Ckn		170 220	0.00	0.00	0.00	0.00	
3.01 Av		0 5	0.00	0.00	0.00	0.00	0.00 0.00
3.02 Avrj		5 12	0.00	0.00	0.00	0.00	
3.03 2Btkj		12 45	0.00	0.00	0.00	0.00	
3.04 2Btjqk1		45 83	0.00	-10.00	0.00	0.00	
3.05 2Btjqk2		83 107	0.00	0.00	0.00	0.00	
3.06 2Ckqn		107 210	0.00	0.00	0.00	0.00	
21.01 Av		0 4	0.00	0.00	0.00	0.00	2.59 0.01
21.02 Bw		4 15	0.00	0.00	0.00	0.00	
21.03 Bt		15 33	0.00	0.00	0.00	0.00	
21.04 2Btjqkbl		33 55	10.00	0.00	0.12	2.59	
21.05 2Btjqkbl		55 144	0.00	0.00	0.00	0.00	
21.06 3Bqrb2		144 186	0.00	0.00	0.00	0.00	
21.07 3Ckqn		186 233	0.00	0.00	0.00	0.00	

SOIL PROFILE INDEX VALUES

			MELANIZATION (maximum=85) -----)						
Sample	Horizon	Depth (cm)	Color 81	Color 82	Normalized property	Thickness	Profile property	Weighted mean	
11.01	Av	0 4	0.00	0.00	0.00	0.00	0.00	0.00	
11.02	A	4 15	0.00	0.00	0.00	0.00			
11.03	2Btj	15 42	0.00	0.00	0.00	0.00			
11.04	2Btqak	42 90	0.00	0.00	0.00	0.00			
11.05	2Btq	90 150	0.00	0.00	0.00	0.00			
11.06	3Kqab	150 170	0.00	0.00	0.00	0.00			
12.01	Av1	0 4	5.00	0.00	0.00	0.24	0.24	0.00	
12.02	Av2	4 14	0.00	0.00	0.00	0.00			
12.03	Bt	14 47	0.00	0.00	0.00	0.00			
12.04	2Bt1	47 105	0.00	0.00	0.00	0.00			
12.05	2Bt2	105 120	0.00	0.00	0.00	0.00			
12.06	2Btqak	120 144	0.00	0.00	0.00	0.00			
12.07	5qab	144 200	0.00	0.00	0.00	0.00			
14.01	A	0 8	0.00	0.00	0.00	0.00	0.00	0.00	
14.02	Bw	8 28	0.00	0.00	0.00	0.00			
14.03	2Bk	28 54	0.00	0.00	0.00	0.00			
14.04	2Btjk	54 107	0.00	0.00	0.00	0.00			
14.05	3Btjb	107 121	0.00	0.00	0.00	0.00			
14.06	3Bqai1b	121 152	0.00	0.00	0.00	0.00			
14.07	4Bqak2a	152 221	0.00	0.00	0.00	0.00			
14.08	4Btjb	221 230	0.00	0.00	0.00	0.00			
20.01	A-1	0 8	10.00	0.00	0.12	0.94	4.94	0.03	
20.02	Av2	8 19	0.00	0.00	0.00	0.00			
20.03	Bw	19 42	0.00	0.00	0.00	0.00			
20.04	2Btjq	42 64	10.00	0.00	0.12	2.59			
20.05	2Btjqk1	64 76	10.00	0.00	0.12	1.41			
20.06	2Btjqk2-1	76 114	0.00	0.00	0.00	0.00			
20.07	2Btjqk2-2	114 152	0.00	0.00	0.00	0.00			
20.08	2Btjqk2-3	152 190	0.00	0.00	0.00	0.00			
5.01	A	0 5	0.00	0.00	0.00	0.00	2.41	0.01	
5.02	Bw	5 20	10.00	0.00	0.12	1.76			
5.03	Bk	20 45	0.00	0.00	0.00	0.00			
5.04	2Btb	45 56	5.00	0.00	0.00	0.05			
5.05	2Btqab	56 106	0.00	0.00	0.00	0.00			
5.06	2Ktqb	106 164	0.00	0.00	0.00	0.00			
5.07	2Cqn	164 263	0.00	0.00	0.00	0.00			

SOIL PROFILE INDEX VALUES

			MELANIZATION (maximum=85) ----->					
Sample	Horizon	Depth (cm)	Color M1	Color M2	Normalized property	X thickness	Profile property	Weighted mean
18.01	Av	0 11	0.00	0.00	0.00	0.00	0.00	0.00
18.02	A	11 33	0.00	0.00	0.00	0.00		
18.03	Bt	33 40	0.00	0.00	0.00	0.00		
18.04	2Btq1	40 66	0.00	0.00	0.00	0.00		
18.05	2Btq2	66 120	0.00	0.00	0.00	0.00		
18.06	3Bk	120 160	0.00	0.00	0.00	0.00		
8.01	Av	0 9	0.00	0.00	0.00	0.00	2.52	0.01
8.02	Bt1	9 21	20.00	0.00	0.24	2.82		
8.03	2Bt2	21 35	0.00	0.00	0.00	0.00		
8.04	2Bq2	35 68	0.00	0.00	0.00	0.00		
8.05	2r	68 100	0.00	0.00	0.00	0.00		
8.05	2Ck	100 210	0.00	0.00	0.00	0.00		
16.01	Av	0 13	20.00	0.00	0.24	3.06	5.59	0.47
16.02	Bw	13 30	5.00	0.00	0.06	1.00		
16.03	Bt	30 43	10.00	0.00	0.12	1.53		
16.04	2Btq1	43 58	0.00	0.00	0.00	0.00		
16.05	2Bq	58 100	0.00	0.00	0.00	0.00		
16.06	2Bqa (inc)	100 150	0.00	0.00	0.00	0.00		
16.07	2Bqa	100 150	0.00	0.00	0.00	0.00		
16.08	2Cvqa	150 207	0.00	0.00	0.00	0.00		
1.01	A	0 10	0.00	0.00	0.00	0.00	4.53	0.02
1.02	Bt	10 25	5.00	0.00	0.06	0.88		
1.03	2Btqb1	25 42	10.00	0.00	0.12	2.00		
1.04	2Btqb2	42 56	10.00	0.00	0.12	1.65		
1.08	3Bqab1	56 70	0.00	0.00	0.00	0.00		
1.09	4Bqab2	70 115	0.00	0.00	0.00	0.00		
1.10	5Bk	115 167	0.00	0.00	0.00	0.00		
1.11	5Cnk	167 195	0.00	0.00	0.00	0.00		
1.12	5Cn	195 290	0.00	0.00	0.00	0.00		
19.01	Av1	0 4	5.00	0.00	0.06	0.24	0.24	0.00
	Av2	4 9	0.00	0.00	0.00	0.00		
19.03	Bk	9 13	0.00	0.00	0.00	0.00		
19.04	Bw	13 17	0.00	0.00	0.00	0.00		
19.05	Btqa	17 29	0.00	0.00	0.00	0.00		
19.06	2Btqa	29 47	0.00	0.00	0.00	0.00		
19.07	2Bqa1	47 72	0.00	0.00	0.00	0.00		
19.08	2Bqa2	72 150	0.00	0.00	0.00	0.00		

SOIL PROFILE INDEX VALUES

Sample	Horizon	Depth (cm)	MELANIZATION (maximum=85)				Profile Weighted mean
			Color 01	Color 02	Normalized property	X thickness	
6.01	Av	0 6	10.00	0.00	0.12	0.71	0.71
6.02	Bt	6 10	0.00	0.00	0.00	0.00	0.00
6.03	2kq	10 52	0.00	-40.00	0.00	0.00	0.00
6.04	3kq	52 101	0.00	0.00	0.00	0.00	0.00
6.05	3p	101 153	0.00	0.00	0.00	0.00	0.00
6.06	3kq	153 230	0.00	0.00	0.00	0.00	0.00
6.07	3kq	230 300	0.00	0.00	0.00	0.00	0.00
2.01	Av	0 3	0.00	0.00	0.00	0.00	5.68
2.02	A	3 10	5.00	0.00	0.00	0.41	0.03
2.03	Bv	10 19	15.00	0.00	0.18	1.59	
2.04	2Bq	19 34	10.00	0.00	0.12	1.76	
2.05	2Bq	34 70	5.00	0.00	0.00	2.12	
2.07	kq	19 52	0.00	0.00	0.00	0.00	
2.08	p	52 114	0.00	0.00	0.00	0.00	
2.09	2k	114 157	0.00	0.00	0.00	0.00	
22.01	Av	0 10	0.00	0.00	0.00	0.00	0.65
22.02	Bw	10 21	5.00	0.00	0.00	0.65	0.00
22.03	E	21 62	0.00	0.00	0.00	0.00	
22.04	ka	62 92	0.00	0.00	0.00	0.00	
22.05	Bxq	92 164	0.00	0.00	0.00	0.00	

SOIL PROFILE INDEX VALUES

Sample	Horizon	Depth in	COLOR-PALING (maximum=60)		Normalized property thickness	X Profile Weighted property mean		
			Color M	Color P				
FNA-1			0.00	0.00	0.00	0.00		
FNA-2			0.00	0.00	0.00	0.00		
FNA-3			0.00	0.00	0.00	0.00		
FNA-4			0.00	0.00	0.00	0.00		
YNA-1			0.00	0.00	0.00	0.00		
YNA-2			0.00	0.00	0.00	0.00		
7.01 A		0 1.5	0.00	0.00	0.00	0.00	0.00	0.00
7.02 Eex		2 16	0.00	0.00	0.00	0.00		
7.03 2Cex		16 100	0.00	0.00	0.00	0.00		
4.01 A		0 3	0.00	0.00	0.00	0.00	0.00	0.00
4.02 Bk1		3 9	0.00	0.00	0.00	0.00		
4.03 2Bk2		9 60	0.00	0.00	0.00	0.00		
4.04 2Ckn		60 100	0.00	0.00	0.00	0.00		
17.01 A		0 6	0.00	0.00	0.00	0.00	0.00	0.00
17.02 Bw		6 24	0.00	0.00	0.00	0.00		
17.03 2Ckn		24 120	0.00	0.00	0.00	0.00		
13.01 A		0 9	0.00	0.00	0.00	0.00	10.83	0.00
13.02 Bw		9 21	0.00	0.00	0.00	0.00		
13.03 2Bq1		21 73	0.00	0.00	0.00	0.00		
13.04 2Ckqn		73 138	10.00	0.00	0.17	10.83		
15.01 A		0 16	0.00	0.00	0.00	0.00	0.00	0.00
15.02 Bw		16 46	0.00	0.00	0.00	0.00		
15.03 2Bq1		46 170	0.00	0.00	0.00	0.00		
15.05 2Ckn		170 220	0.00	0.00	0.00	0.00		
3.01 A		0 5	5.00	0.00	0.08	0.42	0.42	0.00
3.02 A+Aj		5 12	0.00	0.00	0.00	0.00		
3.03 2Btk1		12 45	0.00	0.00	0.00	0.00		
3.04 2Btjqkbl		45 83	0.00	0.00	0.00	0.00		
3.05 2Btjqkbl		83 107	0.00	0.00	0.00	0.00		
3.06 2Ckqn		107 210	0.00	0.00	0.00	0.00		
21.01 Av		0 4	0.00	0.00	0.00	0.00	0.00	0.00
21.02 Bw		4 15	0.00	0.00	0.00	0.00		
21.03 Bk		15 33	0.00	0.00	0.00	0.00		
21.04 2Btjqkbl		33 55	0.00	0.00	0.00	0.00		
21.05 2Btjqkbl		55 144	0.00	0.00	0.00	0.00		
21.06 3Bqkbl2		144 186	0.00	0.00	0.00	0.00		
21.07 3Ckqn		186 233	999.00	0.00	0.00	0.00		

SOIL PROFILE INDEX VALUES

Sample	Horizon	Depth (cm)	COLOR-PALINS (maximum=60)				Profile Weighted mean
			Color 81	Color 82	Normalized property	Thickness property	
11.01 A	0 4	0.00	0.00	0.00	0.00	0.00	0.00
11.02 A	4 15	0.00	0.00	0.00	0.00	0.00	0.00
11.03 2Et	15 42	0.00	0.00	0.00	0.00	0.00	0.00
11.04 2Etqb	42 90	0.00	0.00	0.00	0.00	0.00	0.00
11.05 2Etq	90 150	0.00	0.00	0.00	0.00	0.00	0.00
11.06 3kqab	150 170	0.00	0.00	0.00	0.00	0.00	0.00
12.01 Av1	0 4	0.00	0.00	0.00	0.00	0.00	0.00
12.02 Av2	4 14	0.00	0.00	0.00	0.00	0.00	0.00
12.03 Et	14 47	0.00	0.00	0.00	0.00	0.00	0.00
12.04 2Et1	47 105	0.00	0.00	0.00	0.00	0.00	0.00
12.05 2Et2	105 120	0.00	0.00	0.00	0.00	0.00	0.00
12.06 2Etqab	120 144	0.00	0.00	0.00	0.00	0.00	0.00
12.07 2Etq	144 200	999.00	0.00	0.00	0.00	0.00	0.00
14.01 A	0 8	0.00	0.00	0.00	0.00	0.00	0.00
14.02 Bw	8 28	0.00	0.00	0.00	0.00	0.00	0.00
14.03 2B	28 54	0.00	0.00	0.00	0.00	0.00	0.00
14.04 2Btjq	54 107	0.00	0.00	0.00	0.00	0.00	0.00
14.05 3Btjb	107 121	0.00	0.00	0.00	0.00	0.00	0.00
14.06 3Bqab	121 152	0.00	0.00	0.00	0.00	0.00	0.00
14.07 4Bqab	152 221	0.00	0.00	0.00	0.00	0.00	0.00
14.08 4Btjb	221 230	0.00	0.00	0.00	0.00	0.00	0.00
20.01 Av1	0 8	0.00	0.00	0.00	0.00	0.00	0.00
20.02 Av2	8 19	0.00	0.00	0.00	0.00	0.00	0.00
20.03 Bw	19 42	0.00	0.00	0.00	0.00	0.00	0.00
20.04 2Btjq	42 64	0.00	0.00	0.00	0.00	0.00	0.00
20.05 2Btjq-1	64 76	0.00	0.00	0.00	0.00	0.00	0.00
20.06 2Btjq2-1	76 114	0.00	0.00	0.00	0.00	0.00	0.00
20.07 2Btjq2-2	114 152	0.00	0.00	0.00	0.00	0.00	0.00
20.08 2Btjq2-3	152 190	0.00	0.00	0.00	0.00	0.00	0.00
5.01 A	0 5	0.00	0.00	0.00	0.00	0.00	0.00
5.02 Bw	5 20	0.00	0.00	0.00	0.00	0.00	0.00
5.03 Bx	20 45	10.00	0.00	0.17	4.17	0.00	0.00
5.04 2Et	45 56	0.00	0.00	0.00	0.00	0.00	0.00
5.05 2Etqab	56 106	0.00	0.00	0.00	0.00	0.00	0.00
5.06 2Etqb	106 164	0.00	0.00	0.00	0.00	0.00	0.00
5.07 2Cqn	164 267	10.00	0.00	0.17	16.50	0.00	0.00

SDIC PROFILE INDEX VALUES

			COLOR-FALING (maximum=60)						
Sample	Horizon	Depth (cm)	Color #1	Color #2	Normalized property	X thickness	Profile property	Weighted mean	
18.01	Av	0 11	0.00	0.00	0.00	0.00	0.00	0.00	
18.02	A	11 33	0.00	0.00	0.00	0.00			
18.03	Bt	33 40	0.00	0.00	0.00	0.00			
18.04	2Btq ₁	40 66	0.00	0.00	0.00	0.00			
18.05	2Btq ₂	66 120	0.00	0.00	0.00	0.00			
18.06	3Fc	120 160	999.00	0.00	0.00	0.00			
8.01	Av	0 9	0.00	0.00	0.00	0.00	0.00	0.00	
8.02	Bt1	9 21	0.00	0.00	0.00	0.00			
8.03	2Bt2	21 35	0.00	0.00	0.00	0.00			
8.04	2kq ₁	35 68	0.00	0.00	0.00	0.00			
8.05	2k	68 100	0.00	0.00	0.00	0.00			
8.05	2Sk	100 210	0.00	0.00	0.00	0.00			
16.01	Av	0 13	0.00	0.00	0.00	0.00	0.00	0.00	
16.02	Bw	13 30	0.00	0.00	0.00	0.00			
16.03	Bt	30 43	0.00	0.00	0.00	0.00			
16.04	2Btq ₁	43 58	0.00	0.00	0.00	0.00			
16.05	2k ₁	58 100	0.00	0.00	0.00	0.00			
16.06	2Bq ₁ (incl)	100 150	0.00	0.00	0.00	0.00			
16.07	2Bq ₂	100 150	0.00	0.00	0.00	0.00			
16.08	2Ckq ₁	150 207	0.00	0.00	0.00	0.00			
1.01	A	0 10	10.00	0.00	0.17	1.67	36.33	0.13	
1.02	Bt	10 25	0.00	0.00	0.00	0.00			
1.03	2Btqb1	25 42	0.00	0.00	0.00	0.00			
1.04	2Btqb2	42 56	0.00	0.00	0.00	0.00			
1.08	3kqab1	56 70	0.00	0.00	0.00	0.00			
1.09	4kqab2	70 115	999.00	0.00	0.00	0.00			
1.10	5Sk	115 167	40.00	0.00	0.67	34.67			
1.11	5Cnk	167 195	0.00	0.00	0.00	0.00			
1.12	5Cn	195 290	0.00	0.00	0.00	0.00			
19.01	Av1	0 4	10.00	0.00	0.17	0.67	1.50	0.00	
	Av2	4 9	10.00	0.00	0.17	0.83			
19.03	Bk	9 13	0.00	0.00	0.00	0.00			
19.04	Bw	13 17	0.00	0.00	0.00	0.00			
19.05	Btq ₁	17 29	0.00	0.00	0.00	0.00			
19.06	2kq ₁	29 47	0.00	0.00	0.00	0.00			
19.07	2kq ₂	47 72	0.00	0.00	0.00	0.00			
19.08	2kq ₃	72 150	0.00	0.00	0.00	0.00			

Sample	Horizon	Depth (cm)	COLOR-PALING (maximum=50)				X Profile thickness	Weighted property mean
			Color #1	Color #2	Normalized property			
6.01	Av	0 6	0.00	0.00	0.00	0.00	0.00	0.00
6.02	Et	6 10	0.00	0.00	0.00	0.00		
6.03	2tqa	10 52	0.00	0.00	0.00	0.00		
6.04	3tqg	52 101	0.00	0.00	0.00	0.00		
6.05	3tq	101 153	0.00	0.00	0.00	0.00		
6.06	30kg	153 230	0.00	0.00	0.00	0.00		
6.07	30tqg	230 300	999.00	0.00	0.00	0.00		
2.01	Av	0 3	0.00	0.00	0.00	0.00	0.00	0.00
2.02	A	3 10	0.00	0.00	0.00	0.00		
2.03	Bv	10 19	0.00	0.00	0.00	0.00		
2.04	28qg+y	19 34	0.00	0.00	0.00	0.00		
2.05	28tqg+y	34 70	0.00	0.00	0.00	0.00		
2.07	ktqa	19 52	0.00	0.00	0.00	0.00		
2.08	kg	52 114	0.00	0.00	0.00	0.00		
2.09	2t	114 157	0.00	0.00	0.00	0.00		
22.01	4.	0 10	0.00	0.00	0.00	0.00	0.00	0.00
22.02	Bw	10 21	0.00	0.00	0.00	0.00		
22.03	t	21 62	0.00	0.00	0.00	0.00		
22.04	sa	62 92	0.00	0.00	0.00	0.00		
22.05	8tqg	92 124	0.00	0.00	0.00	0.00		

SOIL PROFILE INDEX VALUES

Sample	Horizon	Depth (cm)	COLOR-LIGHTENING (maximum=90)				Profile property	Weighted mean pp
			Color #1	Color #2	Normalized property	X thickness		
FNA-1			0.00	0.00	0.00	0.00		
FNA-2			0.00	0.00	0.00	0.00		
FNA-3			0.00	0.00	0.00	0.00		
FNA-4			0.00	0.00	0.00	0.00		
YNA-1			0.00	0.00	0.00	0.00		
YNA-2			0.00	0.00	0.00	0.00		
7.01 A		0 1.5	10.00	0.00	0.13	0.19	1.22	0.01
7.02 Cov		2 18	5.00	0.00	0.06	1.02		
7.03 2Ctex		18 100	0.00	0.00	0.00	0.00		
4.01 A		0 3	0.00	0.00	0.00	0.00	21.75	0.22
4.02 Bk1		3 9	20.00	0.00	0.25	1.50		
4.03 2Bx2		9 60	20.00	0.00	0.25	12.75		
4.04 2Ckn		60 100	15.00	0.00	0.19	7.50		
17.01 A		0 6	0.00	0.00	0.00	0.00	27.38	0.27
17.02 Bw		6 24	15.00	0.00	0.19	3.38		
17.03 2Ckn		24 120	20.00	0.00	0.25	24.00		
13.01 A		0 9	0.00	0.00	0.00	0.00	11.36	0.08
13.02 Bw		9 21	0.00	0.00	0.00	0.00		
13.03 2Eqj		21 73	5.00	0.00	0.06	3.25		
13.04 2Ckqn		73 136	10.00	0.00	0.13	8.13		
15.01 A		0 18	0.00	0.00	0.00	0.00	17.13	0.08
15.02 Bw		18 46	0.00	0.00	0.00	0.00		
15.03 2Bqk		46 170	5.00	0.00	0.06	7.75		
15.05 2Ckn		170 220	15.00	0.00	0.19	9.38		
3.01 Av		0 5	10.00	0.00	0.13	0.63	17.00	0.09
3.02 Avk1		5 12	10.00	0.00	0.13	0.88		
3.03 2Btrj		12 45	0.00	0.00	0.00	0.00		
3.04 2Btjqk1		45 83	20.00	0.00	0.25	9.50		
3.05 2Btjqk2		83 107	20.00	0.00	0.25	6.00		
3.06 2Ckqn		107 210	0.00	0.00	0.00	0.00		
21.01 Av		0 4	10.00	0.00	0.13	0.50	6.88	0.03
21.02 Bw		4 15	0.00	0.00	0.00	0.00		
21.03 Bk		15 33	5.00	0.00	0.06	1.13		
21.04 2Btjqk1		33 55	0.00	0.00	0.00	0.00		
21.05 2Btjqk1		55 144	0.00	0.00	0.00	0.00		
21.06 3Bqk1		144 186	10.00	0.00	0.13	5.25		
21.07 3Ckqn		186 233	999.00	0.00	0.00	0.00		

SOIL PROFILE INDEX VALUES

Sample	Horizon	Depth (cm)	COLOR-LIGHTENING (maximum=50)				X property thickness	Profile property	Weighted mean
			Color #1	Color #2	Normalized	property			
11.01 Av	0	4	0.00	0.00	0.00	0.00	32.00	0.21	
11.02 A	4	15	0.00	0.00	0.00	0.00			
11.03 2Btj	15	42	0.00	0.00	0.00	0.00			
11.04 2Btqk1	42	90	5.00	40.00	0.28	13.50			
11.05 2Btq	90	150	20.00	0.00	0.25	15.00			
11.06 3Bqgk2	150	170	40.00	20.00	0.38	7.50			
12.01 Av1	0	4	0.00	0.00	0.00	0.00	20.44	0.10	
12.02 Av2	4	14	0.00	0.00	0.00	0.00			
12.03 Et	14	47	5.00	0.00	0.06	2.06			
12.04 2Bx1	47	105	15.00	0.00	0.19	10.88			
12.05 2Bx2	105	120	0.00	0.00	0.00	0.00			
12.06 2Btqk1b	120	144	0.00	50.00	0.31	7.50			
12.07 3Bqk3	144	200	99.00	0.00	0.00	0.00			
14.01 A	0	8	10.00	0.00	0.13	1.00	10.94	0.05	
14.02 Bw	8	22	0.00	0.00	0.00	0.00			
14.03 2Bt	22	54	0.00	0.00	0.00	0.00			
14.04 2Btjq	54	107	15.00	0.00	0.19	9.94			
14.05 3Bxjc	107	121	0.00	0.00	0.00	0.00			
14.06 3Bqk1a	121	152	0.00	0.00	0.00	0.00			
14.07 4Bqk2a	152	221	0.00	0.00	0.00	0.00			
14.08 4Btjc	221	230	0.00	0.00	0.00	0.00			
20.01 Av1	0	8	0.00	0.00	0.00	0.00	0.00	0.00	
20.02 A.2	8	19	0.00	0.00	0.00	0.00			
20.03 Bw	19	42	0.00	0.00	0.00	0.00			
20.04 2Btjq	42	64	0.00	0.00	0.00	0.00			
20.05 2Btjqk1	64	76	0.00	0.00	0.00	0.00			
20.06 2Btjqk2-1	76	114	0.00	0.00	0.00	0.00			
20.07 2Btjqk2-2	114	152	0.00	0.00	0.00	0.00			
20.08 2Btjqk2-3	152	190	0.00	0.00	0.00	0.00			
5.01 A	0	5	10.00	0.00	0.13	0.63	35.38	0.17	
5.02 Bw	5	20	0.00	0.00	0.00	0.00			
5.03 Bt	20	45	10.00	0.00	0.13	3.13			
5.04 2Btb	45	52	0.00	0.00	0.00	0.00			
5.05 2Btqk1b	52	106	10.00	0.00	0.13	6.25			
5.06 2Btqb	106	164	20.00	50.00	0.44	25.38			
5.07 2Cqn	164	263	0.00	0.00	0.00	0.00			

SOIL PROFILE INDEX VALUES

			COLOR-LIGHTENING (maximum=80) -----						
Sample	Horizon	Depth (cm)	Color #1	Color #2	Normalized property	Thickness X	Profile property	Weighted mean pp	
18.01	Av	0 11	15.00	0.00	0.19	2.06	19.69	0.12	
18.02	A	11 33	15.00	0.00	0.19	4.13			
18.03	Bt	33 40	0.00	0.00	0.00	0.00			
18.04	2Btqb1	40 66	0.00	0.00	0.00	0.00			
18.05	2Btq	66 120	20.00	0.00	0.25	13.50			
18.06	2C	120 160	999.00	0.00	0.00	0.00			
8.01	A	0 9	0.00	0.00	0.00	0.00	51.67	0.25	
8.02	Bt1	9 21	0.00	0.00	0.00	0.00			
8.03	2Bt2	21 35	20.00	0.00	0.25	3.50			
8.04	2Bqa	35 68	30.00	0.00	0.38	12.38			
8.05	2k	68 100	55.00	0.00	0.69	22.00			
8.05	2C	100 210	10.00	0.00	0.13	13.75			
16.01	Av	0 13	0.00	0.00	0.00	0.00	30.00	2.50	
16.02	Bw	13 30	0.00	0.00	0.00	0.00			
16.03	Bt	30 43	0.00	0.00	0.00	0.00			
16.04	2Btqb	43 58	20.00	0.00	0.25	3.75			
16.05	2Bq	58 101	50.00	0.00	0.63	26.25			
16.06	2Bqa (incl)	100 150	0.00	0.00	0.00	0.00			
16.07	2Bqa	100 150	0.00	0.00	0.00	0.00			
16.08	2Cqqa	150 207	0.00	0.00	0.00	0.00			
1.01	A	0 10	0.00	0.00	0.00	0.00	46.00	0.10	
1.02	Bt	10 25	0.00	0.00	0.00	0.00			
1.03	2Btqb1	25 42	0.00	0.00	0.00	0.00			
1.04	2Btqb2	42 56	0.00	0.00	0.00	0.00			
1.08	3Bqab1	56 70	50.00	0.00	0.63	8.75			
1.09	4Bqab2	70 115	999.00	0.00	0.00	0.00			
1.10	5Bk	115 167	10.00	0.00	0.13	6.50			
1.11	5Cn	167 195	20.00	0.00	0.25	7.00			
1.12	5Cn	195 290	20.00	0.00	0.25	23.75			
19.01	Av1	0 4	10.00	0.00	0.13	0.50	47.63	0.00	
	Av2	4 9	10.00	0.00	0.13	0.63			
19.03	Bk	9 13	20.00	0.00	0.25	1.00			
19.04	Bw	13 17	5.00	0.00	0.06	0.25			
19.05	Btqa	17 29	15.00	0.00	0.19	2.25			
19.06	2Btqa	29 47	50.00	20.00	0.44	7.88			
19.07	2Bqa1	47 72	50.00	0.00	0.63	15.63			
19.08	2Bqa2	72 150	20.00	0.00	0.25	19.50			

SOIL PROFILE INDEX VALUES

Sample	Horizon	Depth (cm)	COLOR-LIGHTENING (maximum=50)				Profile property	Weighted mean pp
			Color #1	Color #2	Normalized property	X thickness		
6.01	Av	0 6	0.00	0.00	0.00	0.00	61.50	0.00
6.02	Bt	6 10	10.00	0.00	0.13	0.50		
6.03	2kqa	10 52	30.00	20.00	0.31	13.13		
6.04	3kq	52 101	20.00	0.00	0.25	12.25		
6.05	3kq	101 153	40.00	0.00	0.50	20.00		
6.06	3Ckq	153 230	10.00	0.00	0.13	9.63		
6.07	3Ckq*	230 300	999.00	0.00	0.00	0.00		
2.01	Av	0 3	10.00	0.00	0.13	0.38	96.25	0.49
2.02	A	3 10	10.00	0.00	0.13	0.68		
2.03	By	10 19	0.00	0.00	0.00	0.00		
2.04	2Bqely	19 34	10.00	0.00	0.13	1.88		
2.05	2Btqny	34 70	0.00	0.00	0.00	0.00		
2.07	ktqa	19 52	50.00	50.00	0.63	20.63		
2.08	kq	52 114	40.00	0.00	0.50	31.00		
2.09	2t	114 197	40.00	0.00	0.50	41.50		
22.01	Av	0 10	20.00	0.00	0.25	2.50	68.00	0.37
22.02	Bw	10 21	0.00	0.00	0.00	0.00		
22.03	k	21 62	50.00	0.00	0.63	25.63		
22.04	k*	62 92	45.00	0.00	0.56	16.88		
22.05	Bkqa	92 124	20.00	0.00	0.25	23.00		

		Total texture (maximum=90) ----->				
Sample	Horizon	Depth (cm)	Normalized property	X thickness	Profile Weighted property	mean pp
<hr/>						
FM-1			0.00	0.00		
FM-2			0.11	0.00		
FM-3			0.00	0.00		
FM-4			0.00	0.00		
<hr/>						
YM-1			0.00	0.00		
YM-2			0.00	0.00		
<hr/>						
7.01	A	0 1.5	0.00	0.00	0.00	0.00
7.02	Cox	2 18	0.00	0.00		
7.03	2Ckox	18 100	0.00	0.00		
<hr/>						
4.01	A	0 3	0.17	0.50	28.94	0.29
4.02	Bk1	3 9	0.22	1.33		
4.03	2Bk2	9 60	0.44	22.67		
4.04	2Ckn	60 100	0.11	4.44		
<hr/>						
17.01	A	0 6	0.22	1.33	3.33	0.03
17.02	Bw	6 24	0.11	2.00		
17.03	2Ckn	24 120	0.00	0.00		
<hr/>						
13.01	A	0 9	0.11	1.00	2.33	0.02
13.02	Bw	9 21	0.11	1.33		
13.03	2Bqj	21 73	0.00	0.00		
13.04	2Ckqn	73 138	0.00	0.00		
<hr/>						
15.01	A	0 18	0.22	4.00	44.89	0.20
15.02	Bw	18 46	0.28	7.78		
15.03	2Bqk	46 170	0.22	27.56		
15.05	2Ckn	170 220	0.11	5.56		
<hr/>						
3.01	Av	0 5	0.56	2.78	34.44	0.16
3.02	Avkj	5 12	0.78	5.44		
3.03	2Btkj	12 45	0.67	22.00		
3.04	2Btjqnk1	45 83	0.11	4.22		
3.05	2Btjqnk2	83 107	0.00	0.00		
3.06	2Ckqn	107 210	0.00	0.00		
<hr/>						
21.01	Av	0 4	0.56	2.22	52.28	0.22
21.02	Bw	4 15	0.44	4.89		
21.03	Bt	15 33	0.33	6.00		
21.04	2Btjqtkb1	33 55	0.44	9.78		
21.05	2Btjqtkb1	55 144	0.28	24.72		
21.06	3Bqtkb2	144 186	0.11	4.67		
21.07	3Ckqn	186 253	0.00	0.00		

Sample	Horizon	Depth (cm)	Total texture (maximum=90) -----			
			Normalized property	X thickness	Profile Weighted property	Weighted mean ps
11.01	Av	0 4	0.37	1.33	64.89	0.38
11.02	A	4 15	0.44	4.89		
11.03	2Btj	15 42	0.44	12.00		
11.04	2Btqab	42 90	0.56	26.67		
11.05	2Btq	90 150	0.22	13.33		
11.06	3Bqab	150 170	0.33	6.67		
12.01	Av1	0 4	0.33	1.33	56.67	0.28
12.02	Av2	4 14	0.33	3.33		
12.03	Bt	14 47	0.56	12.33		
12.04	2Bv1	47 105	0.44	25.78		
12.05	2Bv2	105 120	0.11	1.67		
12.06	2Btqab	120 144	0.09	0.00		
12.07	Bqab	144 200	0.11	6.22		
14.01	A	0 8	0.33	2.67	82.22	0.38
14.02	Bw	8 28	0.39	7.76		
14.03	2Bt	28 54	0.44	11.56		
14.04	2Btjq	54 107	0.44	23.56		
14.05	2Btjb	107 121	0.22	3.11		
14.06	3Bqab1b	121 152	0.22	6.89		
14.07	4Bqab2b	152 221	0.44	30.67		
14.08	4Btjb	221 230	0.22	2.00		
20.01	Av1	0 8	0.11	0.89	51.89	0.27
20.02	Av2	8 19	0.22	2.44		
20.03	Bw	19 42	0.33	7.67		
20.04	2Btjq	42 64	0.33	7.33		
20.05	2Btjqb1	64 76	0.33	4.00		
20.06	2Btjqb2-1	76 114	0.22	8.44		
20.07	2Btjqb2-2	114 152	0.33	12.67		
20.08	2Btjqb2-3	152 190	0.22	8.44		
5.01	A	0 5	-0.22	-1.11	10.33	0.04
5.02	Bw	5 20	-0.22	-3.33		
5.03	Bt	20 45	0.00	0.00		
5.04	2Btb	45 56	0.33	3.67		
5.05	2Btqab	56 106	0.22	11.11		
5.06	2Btqb	106 164	0.00	0.00		
5.07	2Cqn	164 263	0.00	0.00		

Sample	Horizon	Depth		Total texture (maximum=90)		Profile Weighted	mean pp
		(cm)	Normalized property	Normalized property	Thickness		
18.01	Av	0	11	0.33	3.67	18.22	0.11
18.02	A	11	33	0.06	1.22		
18.03	Bt	33	40	0.22	1.56		
18.04	2Btq1	40	66	0.22	5.78		
18.05	2Btq2	66	120	0.11	6.00		
18.06	Ctb	120	160	0.00	0.00		
8.01	Av	0	9	0.44	4.00	26.33	0.17
8.02	Bt1	9	21	1.00	12.00		
8.03	2Bt2	21	35	0.22	3.11		
8.04	2Btq	35	68	0.11	3.67		
8.05	2Bt	68	100	0.11	3.56		
8.06	2Ct	100	210	0.00	0.00		
16.01	Av	0	13	0.33	4.33	74.89	6.24
16.02	Bw	13	30	0.33	5.67		
16.03	Bt	30	43	0.33	4.33		
16.04	2Btq1	43	58	0.80	13.33		
16.05	2Btq	58	100	0.44	18.67		
16.06	2Btq2 (inc)	100	150	0.22	11.11		
16.07	2Btq2	100	150	0.22	11.11		
16.08	2Ct	150	207	0.11	6.33		
1.01	A	0	10	0.22	2.22	95.11	0.33
1.02	Bt	10	25	0.22	3.33		
1.03	2Btq1	25	42	1.00	17.00		
1.04	2Btq2	42	56	1.00	14.00		
1.05	3Btq1	56	70	0.33	4.67		
1.06	4Btq2	70	115	0.33	15.00		
1.10	5Bt	115	167	0.22	11.56		
1.11	5Ct	167	195	0.22	6.22		
1.12	5Ct	195	290	0.22	21.11		
19.01	Av1	0	4	0.33	1.33	61.89	0.60
	Av2	4	9	0.44	2.22		
19.03	Bt	9	13	0.33	1.33		
19.04	Bw	13	17	0.33	1.33		
19.05	Btq	17	29	0.56	6.67		
19.06	2Btq	29	47	0.33	6.00		
19.07	2Btq1	47	72	0.33	8.33		
19.08	2Btq2	72	150	0.44	34.67		

Total texture (maximum=90) -----						
Sample	Horizon	Depth (cm)	Normalized property	X thickness	Profile Weighted property	Weighted gear cc
6.01	Av	0 6	0.33	2.00	13.56	0.00
6.02	Bt	6 10	0.56	2.22		
6.03	2tqs	10 52	0.22	9.33		
6.04	3tq	52 101	0.00	0.00		
6.05	3tq	101 153	0.00	0.00		
6.06	3Etq	153 230	0.00	0.00		
6.07	3Etq+	230 330	0.00	0.00		
2.01	Av	0 3	0.44	1.33	79.83	0.41
2.02	A	3 10	0.44	3.11		
2.03	Bv	10 19	0.56	5.00		
2.04	2Bqvy	19 34	0.39	5.67		
2.05	2Btqvy	34 70	0.39	14.00		
2.07	Ktqa	19 52	0.56	18.33		
2.08	Kq	52 114	0.22	13.78		
2.09	2k	114 197	0.22	18.44		
22.01	Av	0 10	0.56	5.56	56.11	0.30
22.02	Bw	10 21	0.89	9.78		
22.03	r	21 62	0.33	13.67		
22.04	ka	62 92	0.22	6.67		
22.05	Btqa	92 184	0.22	20.44		

STRUCTURE (maximum=20)						
Sample	Horizon	Depth (cm)	Normalized property	X thickness	Profile Weighted property	Weighted mean
<hr/>						
FWA-1			0.00	0.00		
FWA-2			0.00	0.00		
FWA-3			0.00	0.00		
FWA-4			0.00	0.00		
YMA-1			0.00	0.00		
YMA-2			0.00	0.00		
7.01 A		0 15	0.25	0.38	0.78	0.00
7.02 Ccn		2 18	0.00	0.00		
7.03 2Ckn		18 100	0.00	0.00		
4.01 A		0 3	0.50	1.50	38.50	0.39
4.02 Bk1		3 9	0.50	3.00		
4.03 2Bk2		9 60	0.67	34.00		
4.04 2Ckn		60 100	0.00	0.00		
17.01 A		0 6	0.42	2.50	5.50	0.05
17.02 Bw		6 24	0.17	3.00		
17.03 2Ckn		24 120	0.00	0.00		
13.01 A		0 9	0.67	6.00	10.00	0.07
13.02 Bw		9 21	0.33	4.00		
13.03 2Bq		21 73	0.00	0.00		
13.04 2Ckqn		73 138	0.00	0.00		
15.01 A		0 18	0.50	9.00	23.00	0.10
15.02 Bw		18 46	0.50	14.00		
15.03 2Bqk		46 170	0.00	0.00		
15.05 2Ckn		170 220	0.00	0.00		
3.01 Av		0 5	0.67	3.33	12.33	0.06
3.02 Avk1		5 12	0.50	3.50		
3.03 2Btkj		12 45	0.17	5.50		
3.04 2Btjcnk1		45 83	0.00	0.00		
3.05 2Btjcnk2		83 107	0.00	0.00		
3.06 2Ckqn		107 210	0.00	0.00		
21.01 Av		0 4	0.67	2.67	20.08	0.09
21.02 Bw		4 15	0.50	6.42		
21.03 Br		15 33	0.00	0.00		
21.04 2Btjcnk1		33 55	0.50	11.00		
21.05 2Btjcnk2		55 144	0.00	0.00		
21.06 3Bqnb2		144 186	0.00	0.00		
21.07 3Ckqn		186 233	0.00	0.00		

STRUCTURE (maximum=60)						
Sample	Horizon	Depth 'cm'	Normalized property	X thickness	Profile Weighted property	Weighted mean
11.01	Av	0 4	0.83	3.33	32.50	0.19
11.02	A	4 15	0.33	3.67		
11.03	2Pt	15 42	0.50	13.50		
11.04	2Btqm	42 90	0.25	12.00		
11.05	2Btq	90 150	0.00	0.00		
11.06	3Bqmb	150 170	0.00	0.00		
12.01	Av1	0 4	0.33	1.33	88.67	0.44
12.02	Av2	4 14	0.58	5.83		
12.03	Bt	14 47	0.67	22.00		
12.04	2Bv1	47 105	0.75	43.50		
12.05	2Bv2	105 120	0.00	0.00		
12.06	2Btqmb	120 144	0.67	16.00		
12.07	Bqmb	144 200	0.00	0.00		
14.01	A	0 8	0.42	3.33	40.33	0.18
14.02	Bw	8 28	0.33	6.67		
14.03	2Bv	28 54	0.50	13.00		
14.04	2Btjkq	54 107	0.00	0.00		
14.05	3Btjb	107 121	0.50	7.00		
14.06	3Bqmb	121 152	0.33	10.33		
14.07	4Bqmb	152 221	0.00	0.00		
14.08	4Btjb	221 230	0.00	0.00		
20.01	Av1	0 8	0.33	2.67	32.83	0.17
20.02	Av2	8 19	0.67	7.33		
20.03	Bw	19 42	0.50	11.50		
20.04	2Btjq	42 64	0.33	7.33		
20.05	2Btjqr1	64 76	0.33	4.00		
20.06	2Btjqk2-1	76 114	0.00	0.00		
20.07	2Btjqk2-2	114 152	0.00	0.00		
20.08	2Btjqk2-3	152 190	0.00	0.00		
5.01	A	0 5	0.42	2.08	33.06	0.13
5.02	Bw	5 20	0.33	5.00		
5.03	Bi	20 45	0.17	4.17		
5.04	2Pt	45 56	0.67	7.33		
5.05	2Btqmb	56 106	0.00	0.00		
5.06	2Btqb	106 164	0.25	14.50		
5.07	2Cqn	164 263	0.00	0.00		

STRUCTURE (maximum=60)						
Sample	Horizon	Depth (cm)	Normalized property	k thickness	Profile Weighted property	mean
18.01	Av	0 11	0.79	8.71	34.46	0.22
18.02	A	11 33	0.00	0.00		
18.03	Bt	33 40	0.58	4.08		
18.04	2Btqb1	40 66	0.83	21.67		
18.05	2Btqb	66 120	0.00	0.00		
18.06	3Kb	120 160	0.00	0.00		
8.01	Av	0 9	0.67	6.00	85.25	0.40
8.02	Bt1	9 21	0.92	11.00		
8.03	2Bt2	21 35	0.67	9.33		
8.04	2Kqa	35 68	0.92	30.25		
8.05	2K	68 100	0.83	26.67		
8.05	2Ca	100 210	0.00	0.00		
16.01	Av	0 13	0.33	4.33	43.50	3.63
16.02	Bw	13 30	0.33	3.67		
16.03	Bt	30 43	0.75	9.75		
16.04	2Btqr	43 58	0.75	11.25		
16.05	2Kq	58 100	0.00	0.00		
16.06	2Bqa (nc)	100 150	0.25	12.50		
16.07	2Bqa	100 150	0.00	0.00		
16.08	2Ckqr	150 267	0.00	0.00		
1.01	A	0 10	0.33	3.33	36.92	0.13
1.02	Bt	10 25	0.58	8.75		
1.03	2Btqb1	25 42	0.50	8.50		
1.04	2Btqb2	42 56	0.50	7.00		
1.08	3Kqb1	56 70	0.67	9.33		
1.09	4Kqb2	70 115	0.00	0.00		
1.10	5Bv	115 167	0.00	0.00		
1.11	5Cnk	167 195	0.00	0.00		
1.12	5Cn	195 290	0.00	0.00		
19.01	Av1	0 4	0.67	2.67	46.92	0.00
	Av2	4 9	0.67	3.33		
19.03	Bk	9 13	0.33	1.33		
19.04	Bw	13 17	0.58	2.33		
19.05	Btqa	17 29	0.83	10.00		
19.06	2Ktqa	29 47	1.17	21.00		
19.07	2kqa1	47 72	0.25	6.25		
19.08	2Kqa2	72 150	0.00	0.00		

STRUCTURE (max=1000=60)						
Sample Horizon	Depth (cm)	Normalized property	X thickness	Profile	Weighted property	mean
6.01 Av	0 6	0.67	4.00	41.00	0.00	
6.02 Bt	6 10	0.50	2.00			
6.03 2tqa	10 52	0.83	35.00			
6.04 3tq	52 101	0.00	0.00			
6.05 3tq	101 153	0.00	0.00			
6.06 3tq	153 230	0.00	0.00			
6.07 3tq+	230 300	0.00	0.00			
2.01 Av	0 3	0.67	2.00	123.17	0.63	
2.02 h	3 10	0.33	2.33			
2.03 By	10 19	0.50	4.50			
2.04 2Bqay	19 34	0.83	12.50			
2.05 2Bqay	34 70	0.92	33.00			
2.07 ktqa	19 52	0.83	27.50			
2.08 tq	52 114	0.67	41.33			
2.09 2k	114 157	0.00	0.00			
22.01 Av	0 10	0.75	7.50	71.00	0.35	
22.02 En	10 21	0.50	5.50			
22.03 k	21 62	0.67	27.33			
22.04 ka	62 92	0.00	0.00			
22.05 Brqa	92 184	0.33	30.67			

Sample	Horizon	Depth (cm)	DRY CONSISTENCE (maximum=100)-----			
			Normalized property	X thickness	Profile property	Weighted mean pp

FNA-1			0.00	0.00		
FNA-2			0.00	0.00		
FNA-3			0.00	0.00		
FNA-4			0.00	0.00		
YNA-1			0.00	0.00		
YNA-2			0.00	0.00		
7.01 A		0 15	0.10	0.15	0.15	0.00
7.02 Cox		2 18	0.00	0.00		
7.03 2Ckox		18 100	0.00	0.00		
4.01 A		0 3	0.10	0.30	11.70	0.12
4.02 Bk1		3 9	0.20	1.20		
4.03 2Bk2		9 60	0.20	10.20		
4.04 2Ckn		60 100	0.00	0.00		
17.01 A		0 6	0.10	0.60	2.40	0.02
17.02 Bw		6 24	0.10	1.80		
17.03 2Ckn		24 120	0.00	0.00		
13.01 A		0 9	0.10	0.90	7.30	0.05
13.02 Bw		9 21	0.10	1.20		
13.03 2Bqj		21 73	0.10	5.20		
13.04 2Ckqn		73 138	0.00	0.00		
15.01 A		0 18	0.10	1.80	35.80	0.16
15.02 Bw		18 46	0.15	4.20		
15.03 2Bqk		46 170	0.20	24.80		
15.05 2Ckn		170 220	0.10	5.00		
3.01 Av		0 5	0.15	0.75	27.35	0.13
3.02 Avkj		5 12	0.20	1.40		
3.03 2Btrj		12 45	0.20	6.60		
3.04 2Btjqak1		45 83	0.30	11.40		
3.05 2Btjqak2		83 107	0.30	7.20		
3.06 2Ckqn		107 210	0.00	0.00		
21.01 Av		0 4	0.15	0.60	83.75	0.36
21.02 Bw		4 15	0.20	2.20		
21.03 Bk		15 33	0.10	1.80		
21.04 2Btjqakb1		33 55	0.30	6.60		
21.05 2Btjqakb1		55 144	0.50	44.50		
21.06 3Bqakb2		144 186	0.50	21.00		
21.07 3Ckqn		186 233	0.15	7.65		

			DRY CONSISTENCE (maximum=100)-----			
Sample	Horizon	Depth (cm)	Normalized property	X thickness	Profile property	Weighted mean pp
11.01	Av	0 4	0.10	0.40	37.60	0.22
11.02	A	4 15	0.10	1.10		
11.03	2Btj	15 42	0.30	8.10		
11.04	2Btan	42 90	0.50	24.00		
11.05	2Bkq	90 150	0.00	0.00		
11.06	3Kqab	150 170	0.20	4.00		
12.01	Av1	0 4	0.10	0.40	36.00	0.18
12.02	Av2	4 14	0.10	1.00		
12.03	Bt	14 47	0.20	6.60		
12.04	2Bk1	47 105	0.25	14.50		
12.05	2Bk2	105 120	0.10	1.50		
12.06	2Btqab	120 144	0.50	12.00		
12.07	Bqkb	144 200	0.00	0.00		
14.01	A	0 8	0.10	0.80	52.00	0.25
14.02	Bw	8 28	0.10	2.00		
14.03	2Bk	28 54	0.10	2.60		
14.04	2Btjkq	54 107	0.00	0.00		
14.05	3Bkjb	107 121	0.25	3.50		
14.06	3Bqak1b	121 152	0.50	15.50		
14.07	4Bqak2b	152 221	0.40	27.60		
14.08	4Bkjb	221 230	0.00	0.00		
20.01	Av1	0 8	0.10	0.80	22.40	0.12
20.02	Av2	8 19	0.10	1.10		
20.03	Bw	19 42	0.10	2.30		
20.04	2Btjq	42 64	0.20	4.40		
20.05	2Btjqk1	64 76	0.20	2.40		
20.06	2Btjqk2-1	76 114	0.10	3.80		
20.07	2Btjqk2-2	114 152	0.10	3.80		
20.08	2Btjqk2-3	152 190	0.10	3.80		
5.01	A	0 5	0.00	0.00	38.15	0.15
5.02	Bw	5 20	0.05	0.75		
5.03	Bk	20 45	0.10	2.50		
5.04	2Btb	45 56	0.30	3.30		
5.05	2Btqakb	56 100	0.40	20.00		
5.06	2Ktqb	100 164	0.20	11.60		
5.07	2Cqn	164 203	0.00	0.00		

			DRY CONSISTENCE (maximum=100)-----			
Sample	Horizon	Depth (cm)	Normalized property	X thickness	Profile property	Weighted mean pp
18.01	Av	0 11	0.10	1.10	45.80	0.29
18.02	A	11 33	0.00	0.00		
18.03	Bt	33 40	0.10	0.70		
18.04	2Btql	40 66	0.30	7.80		
18.05	2Btq	66 120	0.30	16.20		
18.06	3Bb	120 160	0.50	20.00		
8.01	Av	0 9	0.10	0.90	29.30	0.14
8.02	Bt1	9 21	0.00	0.00		
8.03	2Bt2	21 35	0.40	5.60		
8.04	2kqa	35 68	0.40	13.20		
8.05	2k	68 100	0.30	9.60		
8.06	2Ck	100 210	0.00	0.00		
16.01	Av	0 13	0.00	0.00	62.20	5.18
16.02	Bw	13 30	0.00	0.00		
16.03	Bt	30 43	0.00	0.00		
16.04	2Btq1	43 58	0.20	3.00		
16.05	2kq	58 100	0.50	21.00		
16.06	2Bqa (nc)	100 150	0.35	17.50		
16.07	2Bqa	100 150	0.30	15.00		
16.08	2Ckqa	150 207	0.10	5.70		
1.01	A	0 10	0.00	0.00	31.20	0.11
1.02	Bt	10 25	0.00	0.00		
1.03	2Btqb1	25 42	0.20	3.40		
1.04	2Btqb2	42 56	0.20	2.80		
1.05	3kqab1	56 70	0.50	7.00		
1.06	4kqab2	70 115	0.40	18.00		
1.10	5Bt	115 167	0.00	0.00		
1.11	5Cka	167 195	0.00	0.00		
1.12	5Cn	195 290	0.00	0.00		
19.01	Av1	0 4	0.00	0.00	57.20	0.00
	Av2	4 9	0.20	1.00		
19.03	Bt	9 13	0.00	0.00		
19.04	Bw	13 17	0.00	0.00		
19.05	Btqa	17 29	0.50	6.00		
19.06	2kta	29 47	0.50	9.00		
19.07	2kqa1	47 72	0.40	10.00		
19.08	2kqa2	72 150	0.40	31.20		

Sassie	Horizon	Depth (cm)	DRY CONSISTENCE (maximum=100)-----			
			Normalized property	x thickness	Profile	Weighted property mean pp
6.01	Av	0 6	999.00	0.00	29.70	0.00
6.02	Bt	6 10	999.00	0.00		
6.03	2kqs	10 52	999.00	0.00		
6.04	3kq	52 101	0.50	24.50		
6.05	3kq	101 153	0.10	5.20		
6.06	3Ckq	153 230	0.00	0.00		
6.07	3Ckq+	230 300	0.00	0.00		
2.01	Av	0 3	0.10	0.30	70.30	0.36
2.02	A	3 10	0.00	0.00		
2.03	B _y	10 19	0.00	0.00		
2.04	2Bqxy	19 34	0.40	6.00		
2.05	2Btqxy	34 70	0.40	14.40		
2.07	ktqz	19 52	0.50	16.50		
2.08	Fq	52 114	0.40	24.80		
2.09	2k	114 197	0.10	6.30		
22.01	Av	0 10	0.05	0.50	64.70	0.35
22.02	Bw	10 21	0.10	1.10		
22.03	A	21 62	0.50	20.50		
22.04	ka	62 92	0.50	15.00		
22.05	Btqz	92 184	0.30	27.60		

		MOIST CONSISTENCE (maximum=100) ----->				
Sample	Horizon	Depth (cm)	Normalized property	X thickness	Profile Weighted property	Weighted mean pp
<hr/>						
FNA-1			999.00	0.00		
FNA-2			999.00	0.00		
FNA-3			999.00	0.00		
FNA-4			999.00	0.00		
YNA-1			999.00	0.00		
YNA-2			999.00	0.00		
7.01	A	0 1.5	999.00	0.00	0.00	0.00
7.02	Cox	2 18	999.00	0.00		
7.03	2Ckox	18 100	999.00	0.00		
4.01	A	0 3	999.00	0.00	0.00	0.00
4.02	Ek1	3 9	999.00	0.00		
4.03	2Ek2	9 60	999.00	0.00		
4.04	2Ckn	60 100	999.00	0.00		
17.01	A	0 6	999.00	0.00	0.00	0.00
17.02	Bw	6 24	999.00	0.00		
17.03	2Ckn	24 120	999.00	0.00		
13.01	A	0 9	999.00	0.00	0.00	0.00
13.02	Bw	9 21	999.00	0.00		
13.03	2Bqj	21 73	999.00	0.00		
13.04	2Ckqn	73 138	999.00	0.00		
15.01	A	0 18	999.00	0.00	0.00	0.00
15.02	Bw	18 46	999.00	0.00		
15.03	2Bqk	46 170	999.00	0.00		
15.05	2Ckn	170 220	999.00	0.00		
3.01	Av	0 5	999.00	0.00	0.00	0.00
3.02	Avvj	5 12	999.00	0.00		
3.03	2Btj	12 45	999.00	0.00		
3.04	2Btjqak1	45 83	999.00	0.00		
3.05	2Btjqak2	83 107	999.00	0.00		
3.06	2Ckqn	107 210	999.00	0.00		
21.01	Av	0 4	999.00	0.00	0.00	0.00
21.02	Bw	4 15	999.00	0.00		
21.03	Bk	15 33	999.00	0.00		
21.04	2Btjqkjb1	33 55	999.00	0.00		
21.05	2Btjqakb1	55 144	999.00	0.00		
21.06	3Bqakb2	144 186	999.00	0.00		
21.07	3Ckqn	186 233	999.00	0.00		

			MOIST CONSISTENCE (maximum=100: -----)			
Sample	Horizon	Depth (cm)	Normalized property	X thickness	Profile Weighted property	near pp
11.01	Av	0 4	999.00	0.00	0.00	0.00
11.02	A	4 15	999.00	0.00		
11.03	2Btj	15 42	999.00	0.00		
11.04	2Btqak	42 90	999.00	0.00		
11.05	2Bxq	90 150	999.00	0.00		
11.06	3Kqmb	150 170	999.00	0.00		
12.01	Av1	0 4	999.00	0.00	0.00	0.00
12.02	Av2	4 14	999.00	0.00		
12.03	Bt	14 47	999.00	0.00		
12.04	2Bx1	47 105	999.00	0.00		
12.05	2Bx2	105 120	999.00	0.00		
12.06	2Btqakb	120 144	999.00	0.00		
12.07	Bq-b	144 200	999.00	0.00		
14.01	A	0 8	999.00	0.00	0.00	0.00
14.02	2w	8 28	999.00	0.00		
14.03	2Bv	28 54	999.00	0.00		
14.04	2Btjrq	54 107	999.00	0.00		
14.05	2Btjb	107 121	999.00	0.00		
14.06	2Bqak1b	121 152	999.00	0.00		
14.07	4Bqa-2b	152 221	999.00	0.00		
14.08	4Btjb	221 230	999.00	0.00		
20.01	Av1	0 8	999.00	0.00	0.00	0.00
20.02	Av2	8 19	999.00	0.00		
20.03	Bw	19 42	999.00	0.00		
20.04	2Btjq	42 64	999.00	0.00		
20.05	2Btjqk1	64 76	999.00	0.00		
20.06	2Btjqk2-1	76 114	999.00	0.00		
20.07	2Btjqk2-2	114 152	999.00	0.00		
20.08	2Btjqk2-3	152 190	999.00	0.00		
5.01	A	0 5	999.00	0.00	0.00	0.00
5.02	Bw	5 20	999.00	0.00		
5.03	Bk	20 45	999.00	0.00		
5.04	2Btb	45 56	999.00	0.00		
5.05	2Btqmb	56 106	999.00	0.00		
5.06	2Ktqb	106 164	999.00	0.00		
5.07	2Cqn	164 263	999.00	0.00		

		MOIST CONSISTENCE (maximum=100) ----->				
Sample	Horizon	Depth (cm)	Normalized property	X thickness	Profile Weighted property	Weighted mean pp
18.01	Av	0 11	999.00	0.00	0.00	0.00
18.02	A	11 33	999.00	0.00		
18.03	Bt	33 40	999.00	0.00		
18.04	2Btq ₁	40 66	999.00	0.00		
18.05	2Btq ₂	66 120	999.00	0.00		
18.06	3Bt	120 160	999.00	0.00		
8.01	Av	0 9	999.00	0.00	0.00	0.00
8.02	Bt1	9 21	999.00	0.00		
8.03	2Bt2	21 35	999.00	0.00		
8.04	2kqa	35 68	999.00	0.00		
8.05	2k	68 100	999.00	0.00		
8.06	2Cl	100 210	999.00	0.00		
16.01	Av	0 13	999.00	0.00	0.00	0.00
16.02	Bw	13 30	999.00	0.00		
16.03	Bt	30 43	999.00	0.00		
16.04	2Btq ₁	43 58	999.00	0.00		
16.05	2kq	58 100	999.00	0.00		
16.06	2Bqa (incl)	100 150	999.00	0.00		
16.07	2Bqa	100 150	999.00	0.00		
16.08	2Clqn	150 207	999.00	0.00		
1.01	A	0 10	999.00	0.00	11.80	0.04
1.02	Bt	10 25	999.00	0.00		
1.03	2Btqb1	25 42	999.00	0.00		
1.04	2Btqb2	42 56	999.00	0.00		
1.05	3kqmb1	56 70	0.20	2.80		
1.06	4kqmb2	70 115	0.20	9.00		
1.10	5Ex	115 167	0.00	0.00		
1.11	5Cnk	167 195	0.00	0.00		
1.12	5Cn	195 290	0.00	0.00		
19.01	Av1	0 4	999.00	0.00	0.00	0.00
	Av2	4 9	999.00	0.00		
19.03	Bk	9 13	999.00	0.00		
19.04	Bw	13 17	999.00	0.00		
19.05	Btqa	17 29	999.00	0.00		
19.06	2Btqa	29 47	999.00	0.00		
19.07	2kqa1	47 72	999.00	0.00		
19.08	2kqa2	72 150	999.00	0.00		

		MOIST CONSISTENCE (maximum=100) ----->				
Sample	Horizon	Depth (cm)	Normalized property	X thickness	Profile Weighted property	Weighted mean pp
6.01	Av	0 6	0.20	1.20	2.00	0.00
6.02	Bt	6 10	0.20	0.80		
6.03	2Kqa	10 52	999.00	0.00		
6.04	3Kqa	52 101	999.00	0.00		
6.05	3Kq	101 153	999.00	0.00		
6.06	3Cq	153 230	999.00	0.00		
6.07	3Cq+	230 300	999.00	0.00		
2.01	Av	0 3	999.00	0.00	0.00	0.00
2.02	A	3 10	999.00	0.00		
2.03	By	10 19	999.00	0.00		
2.04	2Bqak	19 34	999.00	0.00		
2.05	2Btaky	34 70	999.00	0.00		
2.07	ktqa	19 52	999.00	0.00		
2.09	kq	52 114	999.00	0.00		
2.09	2t	114 197	999.00	0.00		
22.01	Av	0 10	999.00	0.00	0.00	0.00
22.02	Bw	10 21	999.00	0.00		
22.03	t	21 62	999.00	0.00		
22.04	ka	62 92	999.00	0.00		
22.05	Bxqa	92 184	999.00	0.00		

Sample	Horizon	Depth (cm)	pH (maximum=7.5) ----->		Profile Weighted property mean	
			Normalized property	X thickness		
FNA-1			0.04	0.00		
FNA-2			0.06	0.00		
FNA-3			0.05	0.00		
FNA-4			0.21	0.00		
YNA-1			0.06	0.00		
YNA-2			0.19	0.00		
7.01	A	0 1.5	0.06	0.09	5.30	0.05
7.02	Cox	2 18	0.05	0.75		
7.03	2Ckn	18 100	0.05	4.45		
4.01	A	0 3	0.19	0.57	8.69	0.09
4.02	Bk1	3 9	0.17	1.05		
4.03	2Bk2	9 60	0.19	5.25		
4.04	2Ckn	60 100	0.05	1.83		
17.01	A	0 6	0.13	0.79	4.83	0.04
17.02	Ew	6 24	0.01	0.21		
17.03	2Ckn	24 120	0.04	3.84		
13.01	A	0 9	0.33	2.96	20.94	0.15
13.02	Ew	9 21	0.25	2.95		
13.03	2Bqj	21 73	0.16	8.32		
13.04	2Ckn	73 138	0.10	6.69		
15.01	A	0 16	0.22	3.91	23.66	0.11
15.02	Bw	16 46	0.19	5.28		
15.03	2Bqj	46 170	0.12	14.53		
15.05	2Ckn	170 220	0.00	0.14		
3.01	4v	0 5	0.06	0.30	11.99	0.06
3.02	Ava1	5 12	0.09	0.62		
3.03	2Btkj	12 45	0.09	2.92		
3.04	2Btjqk1	45 83	0.10	3.91		
3.05	2Btjqk2	83 107	0.10	2.47		
3.06	2Ckqn	107 210	0.02	1.77		
21.01	Av	0 4	0.01	0.05	26.75	0.11
21.02	Bw	4 15	0.13	1.45		
21.03	Bk	15 33	0.15	2.62		
21.04	2Btjqk1b1	33 55	0.13	2.89		
21.05	2Btjqk1b1	55 144	0.04	3.56		
21.06	3Bqk1b2	144 186	0.17	7.32		
21.07	3Ckqn	186 233	0.19	6.86		

Sample	Horizon	Depth (cm)	pH (maximum=3.5) ----->			
			Normalized property	X thickness	Profile property	Weighted mean
11.01	Av	0 4	0.27	1.10	11.73	0.07
11.02	A	4 15	0.22	2.35		
11.03	2Btj	15 42	0.26	7.02		
11.04	2Btqav	42 90	0.02	0.62		
11.05	2Btq	90 150	0.00	0.17		
11.06	2Btqab	150 170	0.01	0.23		
12.01	Av1	0 4	0.22	0.87	10.31	0.05
12.02	Av2	4 14	0.05	0.45		
12.03	Bt	14 47	0.13	4.34		
12.04	2Bt1	47 105	0.05	2.65		
12.05	2Bt2	105 120	0.01	0.17		
12.06	2Btqab	120 144	0.00	0.07		
12.07	Bqab	144 200	0.03	1.76		
14.01	A	0 8	0.23	1.85	11.92	0.05
14.02	Bw	8 25	0.23	4.63		
14.03	2Bk	25 54	0.05	1.17		
14.04	2Btjka	54 107	0.03	1.36		
14.05	3Btjb	107 121	0.03	0.36		
14.06	3Btjkb	121 152	0.01	0.25		
14.07	4Btjca	152 221	0.01	0.75		
14.08	4Btjb	221 230	0.15	1.35		
20.01	Av1	0 8	0.30	2.42	19.36	0.10
20.02	Av2	8 19	0.30	3.33		
20.03	Bw	19 42	0.35	7.95		
20.04	2Btjq	42 64	0.19	4.15		
20.05	2Btjqk1	64 76	0.05	0.55		
20.06	2Btjqk2-1	76 114	0.00	0.11		
20.07	2Btjqk2-2	114 152	0.01	0.43		
20.08	2Btjqk2-3	152 190	0.01	0.43		
5.01	A	0 5	0.12	0.59	33.07	0.13
5.02	Aw	5 20	0.19	2.83		
5.03	Bt	20 45	0.15	3.64		
5.04	2Btb	45 56	0.12	1.29		
5.05	2Btqab	56 106	0.13	6.57		
5.06	2Btqb	106 164	0.09	5.14		
5.07	2Cqn	164 263	0.13	13.01		

Sample	Horizon	Depth (cm)	pH (maximum=3.5) -----			
			Normalized property	λ thickness	Profile weighted property	mean
18.01	Av	0 11	0.64	0.44	19.20	0.12
18.02	A	11 33	0.01	0.25		
18.03	Bt	33 40	0.12	0.82		
18.04	2Btq1	40 66	0.26	5.27		
18.05	2Btq	66 120	0.22	11.73		
18.06	3Bt	120 160	0.02	0.69		
8.01	Av	0 9	0.16	1.44	14.65	0.07
8.02	Bt1	9 21	0.19	2.26		
8.03	2Bt2	21 35	0.15	2.04		
8.04	2kq	35 68	0.02	0.57		
8.05	2k	68 100	0.05	1.74		
8.06	2Ck	100 210	0.06	6.60		
16.01	Av	0 13	0.26	3.38	14.81	1.23
16.02	Aw	13 30	0.12	1.99		
16.03	Bt	30 43	0.10	1.34		
16.04	2Btq1	43 58	0.07	1.11		
16.05	2kq	58 100	0.02	0.72		
16.06	2Bq (nc)	100 150	0.02	4.43		
16.07	2Bq	100 150	0.02	0.86		
16.08	2Bq	150 207	0.02	0.98		
1.01	A	0 10	0.20	2.03	34.69	0.12
1.02	Bt	10 25	0.22	3.26		
1.03	2Btq1	25 42	0.19	3.21		
1.04	2Btq2	42 56	0.16	2.24		
1.05	3kq1	56 70	0.05	0.76		
1.09	4kq1	70 115	0.13	5.66		
1.10	5Bk	115 167	0.04	2.08		
1.11	5Ck	167 195	0.13	3.52		
1.12	5Ck	195 290	0.13	11.94		
19.01	Av1	0 4	0.14	0.56	17.97	0.00
	Av2	4 9	0.14	0.70		
19.02	Bt	9 13	0.05	0.22		
19.04	Aw	13 17	0.05	0.18		
19.05	Btq	17 29	0.07	0.89		
19.06	2kq	29 47	0.19	3.39		
19.07	2kq1	47 72	0.16	4.00		
19.08	2kq2	72 150	0.10	8.02		

Sample	Horizon	Depth (cm)	pH (mean: mean=3.5) ----->			
			Normalized property	x thickness	Profile Weighted property	Weighted mean
6.01	Av	0 6	0.07	0.45	24.05	0.05
6.02	Et	6 10	0.10	0.41		
6.03	2tqr	10 52	0.08	2.52		
6.04	3tqr	52 101	0.05	2.24		
6.05	3tq	101 153	0.10	5.35		
6.06	3Ctq	153 230	0.10	7.92		
6.07	3Ctqr	230 390	0.07	5.20		
22.01	Av	0 3	0.09	0.01	20.75	0.10
22.02	A	3 10	0.09	0.02		
22.03	By	10 19	0.10	0.92		
22.04	2Btqay	19 34	0.13	1.97		
22.05	2Btqay	34 70	0.13	4.73		
22.07	4tqr	19 52	0.07	2.28		
22.08	4q	52 114	0.01	0.71		
22.09	2r	114 157	0.12	5.72		
22.01	Av	0 10	0.15	1.54	13.18	0.07
22.02	Aw	10 21	0.01	0.13		
22.03	B	21 62	0.02	0.70		
22.04	rs	62 92	0.09	2.06		
22.05	Brqr	92 164	0.09	6.15		

br, bridge; po, pore; pf, ped face; cl, clast

CLAY FILM INDEX

Sample	Horizon	Depth cm	br				po				pf				cl				Normal prop	X thick	Profile weigh	
			01	02	01	02	01	02	01	02	01	02	01	02	01	02	01	02			prop	mean
Fm4-1			0	0	0	0	0	0	0	0	0	0	0	0	0	0	0	0	0.00	0.00		
Fm4-2			0	0	0	0	0	0	0	0	0	0	0	0	0	0	0	0	0.00	0.00		
Fm4-3			0	0	0	0	0	0	0	0	0	0	0	0	0	0	0	0	0.00	0.00		
Fm4-4			0	0	0	0	0	0	0	0	0	0	0	0	0	0	0	0	0.00	0.00		
Ym4-1			0	0	0	0	0	0	0	0	0	0	0	0	0	0	0	0	0.00	0.00		
Ym4-2			0	0	0	0	0	0	0	0	0	0	0	0	0	0	0	0	0.00	0.00		
7.01 A		0 1.5	0	0	0	0	0	0	0	0	0	0	0	0	0	0	0	0	0.00	0.00	0.00	0.00
7.02 Cox		2 16	0	0	0	0	0	0	0	0	0	0	0	0	0	0	0	0	0.00	0.00		
7.03 2Cox		18 100	0	0	0	0	0	0	0	0	0	0	0	0	0	0	0	0	0.00	0.00		
4.01 A		0 3	0	0	0	0	0	0	0	0	0	0	0	0	0	0	0	0	0.00	0.00	3.23	0.00
4.02 Bx1		3 9 70	0	0	0	0	0	0	0	0	0	0	0	0	0	0	0	0	0.54	3.23		
4.03 2Bx2		9 60	0	0	0	0	0	0	0	0	0	0	0	0	0	0	0	0	0.00	0.00		
4.04 2Ckn		60 100	0	0	0	0	0	0	0	0	0	0	0	0	0	0	0	0	0.00	0.00		
17.01 A		0 6	0	0	0	0	0	0	0	0	0	0	0	0	0	0	0	0	0.00	0.00	0.00	0.00
17.02 Bw		6 24	0	0	0	0	0	0	0	0	0	0	0	0	0	0	0	0	0.00	0.00		
17.03 2Crr		24 120	0	0	0	0	0	0	0	0	0	0	0	0	0	0	0	0	0.00	0.00		
13.01 A		0 9	0	0	0	0	0	0	0	0	0	0	0	0	0	0	0	0	0.00	0.00	0.00	0.00
13.02 Bw		9 21	0	0	0	0	0	0	0	0	0	0	0	0	0	0	0	0	0.00	0.00		
13.03 2Bqj		21 73	0	0	0	0	0	0	0	0	0	0	0	0	0	0	0	0	0.00	0.00		
13.04 2Ckqn		73 136	0	0	0	0	0	0	0	0	0	0	0	0	0	0	0	0	0.00	0.00		
15.01 A		0 18	0	0	0	0	0	0	0	0	0	0	0	0	0	0	0	0	0.00	0.00	0.00	0.00
15.02 Bw		18 46	0	0	0	0	0	0	0	0	0	0	0	0	0	0	0	0	0.00	0.00		
15.03 2Bqk		46 170	0	0	0	0	0	0	0	0	0	0	0	0	0	0	0	0	0.00	0.00		
15.05 2Ckn		170 220	0	0	0	0	0	0	0	0	0	0	0	0	0	0	0	0	0.00	0.00		
3.01 Av		0 5	0	0	0	0	0	0	0	0	0	0	0	0	0	0	0	0	0.00	0.00	50.54	0.24
3.02 Avkj		5 12	0	0	0	50	60	0	0	0	0	0	0	0	0	0	0	0	0.46	3.23		
3.03 2Btkj		12 45	0	70	60	0	0	0	0	0	0	0	0	0	0	0	0	0	0.69	22.85		
3.04 2Btjqkx1		45 83	0	0	0	0	0	0	0	60	0	0	0	0	0	0	0	0	0.46	17.54		
3.05 2Btjqkx2		83 107	0	0	0	0	0	0	0	45	0	0	0	0	0	0	0	0	0.29	6.92		
3.06 2Ckqn		107 210	0	0	0	0	0	0	0	0	0	0	0	0	0	0	0	0	0.00	0.00		
21.01 Av		0 4	0	0	50	0	0	0	0	0	0	0	0	0	0	0	0	0	0.35	1.38	20.00	0.05
21.02 Bw		4 15	60	0	0	0	0	0	0	0	0	0	0	0	0	0	0	0	0.62	6.77		
21.03 Bk		15 33	0	0	0	0	0	0	0	0	0	0	0	0	0	0	0	0	0.00	0.00		
21.04 2Btjqkx1		33 55	70	0	0	0	0	0	0	0	0	0	0	0	0	0	0	0	0.54	11.65		
21.05 2Btjqkx1		55 144	0	0	0	0	0	0	0	0	0	0	0	0	0	0	0	0	0.00	0.00		
21.06 3Bqkx2		144 186	0	0	0	0	0	0	0	0	0	0	0	0	0	0	0	0	0.00	0.00		
21.07 3Ckqn		186 233	0	0	0	0	0	0	0	0	0	0	0	0	0	0	0	0	0.00	0.00		

br, bridge; po, pore; pf, ped face; cl, clast

CLAY FILM INDEX-----

Sample	Horizon	Depth (cm)	br				po				pf				cl				Normal prop	X thick	Profile weight	
			01	02	01	02	01	02	01	02	01	02	01	02	01	02	01	02			prop	mean
11.01	Av	0	4	0	0	0	0	0	0	0	0	0	0	0	0	0	0	0	0.00	0.00	44.31	0.20
11.02	A	4	15	0	0	0	0	0	0	0	0	0	0	0	0	0	0	0	0.00	0.00		
11.03	2Btj	15	42	0	0	0	0	0	0	0	0	0	0	0	0	0	0	0	0.00	0.00		
11.04	2Btqk1	42	90	50	0	0	50	0	0	0	0	0	0	0	0	0	0	0	0.54	25.85		
11.05	2Bq	90	150	50	0	0	0	0	0	0	0	0	0	0	0	0	0	0	0.31	18.40		
11.06	2Bqk2	150	170	0	0	0	0	0	0	0	0	0	0	0	0	0	0	0	0.00	0.00		
12.01	Av1	0	4	0	0	0	0	0	0	0	0	0	0	0	0	0	0	0	0.00	0.00	52.23	0.20
12.02	A-2	4	14	0	0	0	0	0	0	0	0	0	0	0	0	0	0	0	0.00	0.00		
12.03	Bt	14	47	0	0	0	0	0	0	0	0	0	0	0	0	0	0	0	0.00	0.00		
12.04	2B-1	47	105	0	60	50	0	0	0	0	0	0	0	0	0	0	0	0	0.54	31.23		
12.05	2B-2	105	120	0	60	50	0	0	0	0	0	0	0	0	0	0	0	0	0.54	8.05		
12.06	2Btqk2	120	144	0	0	0	0	60	0	0	50	0	0	0	0	0	0	0	0.54	12.92		
12.07	Bqk2	144	200	0	0	0	0	0	0	0	0	0	0	0	0	0	0	0	0.00	0.00		
14.01	A	0	8	0	0	0	0	0	0	0	0	0	0	0	0	0	0	0	0.00	0.00	45.42	0.20
14.02	Bw	8	28	0	0	0	0	0	0	0	0	0	0	0	0	0	0	0	0.00	0.00		
14.03	2Bv	28	54	0	0	0	0	0	0	0	0	0	0	0	0	0	0	0	0.00	0.00		
14.04	2Btjq	54	107	0	0	0	0	0	0	0	0	0	0	0	0	0	0	0	0.00	0.00		
14.05	2Btjb	107	121	0	0	0	0	0	0	50	0	0	0	0	0	0	0	0	0.35	4.85		
14.06	2Bqk2	121	152	0	0	0	0	50	0	0	0	0	0	0	0	0	0	0	0.31	9.54		
14.07	4Bqk2b	152	221	0	0	0	0	50	0	0	40	0	0	0	0	0	0	0	0.38	20.54		
14.08	4Bk2b	221	230	0	0	0	0	70	0	0	0	0	0	0	0	0	0	0	0.50	4.50		
20.01	Av1	0	8	0	0	0	0	0	0	0	0	0	0	0	0	0	0	0	0.00	0.00	31.31	0.16
20.02	Av2	8	19	0	0	70	0	0	0	0	0	0	0	0	0	0	0	0	0.54	5.92		
20.03	Bw	19	42	0	0	0	0	0	0	0	0	0	0	0	0	0	0	0	0.00	0.00		
20.04	2Btjq	42	64	60	0	0	0	0	0	0	0	0	0	0	0	0	0	0	0.42	9.31		
20.05	2Btjqk1	64	76	0	0	0	0	0	0	0	0	0	0	0	0	0	0	0	0.00	0.00		
20.06	2Btjqk2-1	76	114	60	0	0	0	0	0	0	0	0	0	0	0	0	0	0	0.42	16.08		
20.07	2Btjqk2-2	114	152	0	0	0	0	0	0	0	0	0	0	0	0	0	0	0	0.00	0.00		
20.08	2Btjqk2-3	152	190	0	0	0	0	0	0	0	0	0	0	0	0	0	0	0	0.00	0.00		
5.01	A	0	5	0	0	0	0	0	0	0	0	0	0	0	0	0	0	0	0.00	0.00	63.42	0.24
5.02	Bw	5	20	0	0	0	0	0	0	0	0	0	0	0	0	0	0	0	0.00	0.00		
5.03	Bx	20	45	0	0	0	0	0	0	0	0	0	0	0	0	0	0	0	0.00	0.00		
5.04	2Btb	45	56	0	0	0	65	75	0	0	0	0	0	0	0	0	0	0	0.65	7.19		
5.05	2Btqk2	56	106	70	0	0	0	0	0	0	0	0	0	0	0	0	0	0	0.50	25.00		
5.06	2Ktqb	106	164	70	0	0	0	0	0	0	0	0	0	0	0	0	0	0	0.54	31.23		
5.07	2Cqn	164	263	0	0	0	0	0	0	0	0	0	0	0	0	0	0	0	0.00	0.00		

br, bridge; po, pore; pf, ped face; cl, clast

CLAY FILM INDEX

Sample	Horizon	Depth (cm)	br				po				pf				cl				Normal prop	X thick	Profile Weigh	
			01	02	01	02	01	02	01	02	01	02	01	02	01	02	01	02			prop	mean
18.01	Av	0	11	0	0	0	0	0	0	0	0	0	0	0	0	0	0	0	0.00	0.00	39.58	0.25
18.02	A	11	33	0	0	0	0	0	0	0	0	0	0	0	0	0	0	0	0.00	0.00		
18.03	Bt	33	40	0	0	0	0	0	0	0	0	0	0	0	0	0	0	0	0.42	2.96		
18.04	2Btqb1	40	66	0	0	7	0	0	0	0	0	0	0	0	0	0	0	0	0.77	20.00		
18.05	2Btqb	66	120	0	0	0	0	5	0	0	0	0	0	0	0	0	0	0	0.31	16.62		
18.06	3Bt	120	160	0	0	0	0	0	0	0	0	0	0	0	0	0	0	0	0.00	0.00		
8.01	Av	0	9	0	70	80	0	0	0	0	0	0	0	0	0	0	0	0	0.77	6.92	40.02	0.22
8.02	Bt1	9	21	0	0	0	0	100	0	0	0	0	0	0	0	0	0	0	0.81	9.69		
8.03	2Bt2	21	35	0	0	0	0	90	0	0	0	0	0	0	0	0	0	0	0.65	9.55		
8.04	2Btqb	35	65	60	0	0	0	0	0	0	0	0	0	0	0	0	0	0	0.62	20.31		
8.05	2B	65	100	0	0	0	0	0	0	0	0	0	0	0	0	0	0	0	0.00	0.00		
8.06	3B	100	210	0	0	0	0	0	0	0	0	0	0	0	0	0	0	0	0.00	0.00		
10.01	Av	0	13	0	0	0	40	0	0	0	0	0	0	0	0	0	0	0	0.23	3.00	12.23	1.02
10.02	Bw	13	30	0	0	0	0	0	0	0	0	0	0	0	0	0	0	0	0.00	0.00		
10.03	Bt	30	45	0	0	0	0	0	0	0	0	0	0	0	0	0	0	0	0.00	0.00		
10.04	2Btqb	45	58	0	0	0	0	80	0	0	0	0	0	0	0	0	0	0	0.62	9.23		
10.05	2Bq	58	100	0	0	0	0	0	0	0	0	0	0	0	0	0	0	0	0.00	0.00		
10.06	2Bq (incl)	100	150	0	0	0	0	0	0	0	0	0	0	0	0	0	0	0	0.00	0.00		
10.07	2Bq	100	150	0	0	0	0	0	0	0	0	0	0	0	0	0	0	0	0.00	0.00		
10.08	2Bq	150	207	0	0	0	0	0	0	0	0	0	0	0	0	0	0	0	0.00	0.00		
1.01	A	0	10	0	0	0	0	0	0	0	0	0	0	0	0	0	0	0	0.00	0.00	10.56	0.00
1.02	Bt	10	25	0	0	0	0	0	0	0	0	0	0	0	0	0	0	0	0.00	0.00		
1.03	2Btqb1	25	42	0	0	0	0	70	0	0	0	0	0	0	0	0	0	0	0.50	6.50		
1.04	2Btqb2	42	56	0	0	0	0	80	0	0	0	0	0	0	0	0	0	0	0.58	6.08		
1.05	3Bqb1	56	70	0	0	0	0	0	0	0	0	0	0	0	0	0	0	0	0.00	0.00		
1.06	4Bqb2	70	115	0	0	0	0	0	0	0	0	0	0	0	0	0	0	0	0.00	0.00		
1.10	SBt	115	167	0	0	0	0	0	0	0	0	0	0	0	0	0	0	0	0.00	0.00		
1.11	5Cbt	167	195	0	0	0	0	0	0	0	0	0	0	0	0	0	0	0	0.00	0.00		
1.12	5Cn	195	290	0	0	0	0	0	0	0	0	0	0	0	0	0	0	0	0.00	0.00		
19.01	Av1	0	4	0	0	0	0	0	0	0	0	0	0	0	0	0	0	0	0.00	0.00	19.73	0.00
	Av2	4	9	0	0	40	0	0	0	0	0	0	0	0	0	0	0	0	0.23	1.15		
19.03	Et	9	13	0	0	0	0	0	0	0	0	0	0	0	0	0	0	0	0.00	0.00		
19.04	Bw	13	17	0	0	0	0	0	0	0	0	0	0	0	0	0	0	0	0.00	0.00		
19.05	Btqb	17	29	70	0	0	0	0	0	0	0	0	0	0	0	0	0	0	0.54	6.46		
19.06	2Btqb	29	47	0	0	0	0	85	0	0	0	0	0	0	0	0	0	0	0.67	12.12		
19.07	2Bqb1	47	72	0	0	0	0	0	0	0	0	0	0	0	0	0	0	0	0.00	0.00		
19.08	2Bqb2	72	150	0	0	0	0	0	0	0	0	0	0	0	0	0	0	0	0.00	0.00		

br, bridge; po, pore; pf, ped face; cl, clast

CLAY FILM INDEX-----

Sample	Horizon	Depth (cm)	br		po		pf		cl		Normal prop	X thick	Profile Weigh	
			61	62	61	62	61	62	61	62			prop	mean
6.01	A-	0	6	0	0	0	0	0	0	0	0.00	0.00	1.29	0.00
6.02	Bt	6	10	0	0	0	63	0	0	0	0.42	1.25		
6.03	21qf	10	52	0	0	0	0	0	0	0	0.00	0.00		
6.04	21qf	52	101	0	0	0	0	0	0	0	0.00	0.00		
6.05	21q	101	153	0	0	0	0	0	0	0	0.00	0.00		
6.06	30q	153	230	0	0	0	0	0	0	0	0.00	0.00		
6.07	30q*	230	300	0	0	0	0	0	0	0	0.00	0.00		
2.01	Av	0	3	0	0	0	0	0	0	0	0.00	0.00	65.46	0.33
2.02	A	3	10	0	0	0	0	0	0	0	0.00	0.00		
2.03	Bv	10	19	0	0	0	0	0	0	0	0.00	0.00		
2.04	28qf-v	19	34	0	60	0	0	0	0	0	0.42	6.25		
2.05	28qf-v	34	70	0	0	0	60	0	0	0	0.65	23.54		
2.07	4tqf	19	52	0	0	0	0	70	0	0	0.50	16.50		
2.08	4q	52	114	0	50	0	0	0	0	0	0.31	19.08		
2.09	2t	114	197	0	0	0	0	0	0	0	0.00	0.00		
22.01	Av	0	10	0	0	40	0	0	0	0	0.23	2.31	7.61	0.04
22.02	Ew	10	21	70	0	0	0	0	0	0	0.50	5.50		
22.03	K	21	62	0	0	0	0	0	0	0	0.00	0.00		
22.04	1t	62	92	0	0	0	0	0	0	0	0.00	0.00		
22.05	Brq	92	164	0	0	0	0	0	0	0	0.00	0.00		

INDEX VALUE - RUBIFICATION & MELANIZATION ---						
Horizon Index						
Sample	Horizon	Depth (cm)	(Sum normalized prop/4 prop)	Horizon thickness	Profile Index	Weighted Mean
<hr/>						
FWA-1			0.04	0.01	0.00	
FWA-2			0.17	0.02	0.00	
FWA-3			0.05	0.01	0.00	
FWA-4			0.21	0.03	0.00	
YWA-1			0.06	0.01	0.00	
YWA-2			0.19	0.03	0.00	
7.01 A		0 1.5	0.41	0.06	0.09	1.23 0.01
7.02 Eox		2 18	0.22	0.03	0.51	
7.03 2Ckex		18 106	0.05	0.01	0.64	
4.01 A		0 3	1.06	0.15	0.45	15.22 0.15
4.02 Bb1		3 9	1.77	0.25	1.51	
4.03 2Bx2		9 60	1.57	0.22	11.45	
4.04 2Ckx		60 100	0.31	0.04	1.80	
17.01 A		0 6	0.98	0.14	0.24	4.10 0.03
17.02 Bw		6 24	0.49	0.07	1.27	
17.03 2Ckx		24 120	0.15	0.02	1.99	
13.01 A		0 9	1.44	0.21	1.86	6.85 0.05
13.02 Bw		9 21	0.75	0.11	1.35	
13.03 2Bq2		21 73	0.37	0.05	2.71	
13.04 2Ckqn		73 138	0.10	0.01	0.96	
15.01 A		0 18	1.16	0.17	2.98	27.03 0.12
15.02 Bw		18 46	1.28	0.18	5.12	
15.03 2Bqk		46 170	0.86	0.12	15.15	
15.05 2Ckx		170 220	0.53	0.06	3.78	
3.01 Av		0 5	1.43	0.20	1.02	24.44 0.12
3.02 mvpj		5 12	2.05	0.29	2.05	
3.03 2Btkj		12 45	2.13	0.30	10.04	
3.04 2Btjqnb1		45 83	1.37	0.20	7.44	
3.05 2Btjqnb2		83 107	1.96	0.15	3.63	
3.06 2Ckqn		107 210	0.62	0.09	0.25	
21.01 Av		0 4	1.73	0.25	0.99	34.85 0.15
21.02 Bw		4 15	1.97	0.26	3.10	
21.03 Bk		15 33	0.58	0.08	1.49	
21.04 2Btjqrb1		33 55	2.14	0.31	6.72	
21.05 2Btjqnb1		55 144	1.03	0.15	13.07	
21.06 3Bqnb2		144 186	1.05	0.15	6.29	
21.07 3Ckqn		186 233	0.34	0.07	3.18	

INDEX VALUE - RUBIFICATION & MELANIZATION --->							
Sample		Horizon		Depth (cm)		Horizon Index (Sum normalized prop/% prop)	
						x horizon thickness	
						Profile Index	
						Weighted Mean	
11.01	Av	0	4	1.54	0.22	0.86	31.51
11.02	A	4	15	1.09	0.16	1.72	0.19
11.03	2Etj	15	42	1.71	0.24	6.61	
11.04	2Etqai	42	90	2.02	0.29	12.84	
11.05	2Etq	90	150	0.74	0.11	6.37	
11.06	3Etqab	150	170	0.73	0.10	2.06	
12.01	Av1	0	4	1.04	0.15	0.60	37.07
12.02	Av2	4	14	1.06	0.15	1.52	0.15
12.03	Bt	14	47	1.55	0.22	7.32	
12.04	2Et1	47	105	2.11	0.30	17.45	
12.05	2Et2	105	120	0.97	0.14	2.08	
12.06	2Etqab	120	144	1.89	0.27	6.49	
12.07	Bqab	144	200	0.14	0.02	1.60	
14.01	A	0	8	1.06	0.15	1.24	37.35
14.02	Bw	8	28	1.05	0.15	3.01	0.16
14.03	2Et	28	54	1.20	0.17	4.44	
14.04	2Etjq	54	107	0.58	0.08	4.36	
14.05	3Etjb	107	121	1.48	0.21	2.95	
14.06	3Etqab	121	152	1.48	0.21	6.55	
14.07	4Etqab	152	221	1.35	0.19	10.27	
14.08	4Etjb	221	230	1.19	0.17	1.53	
20.01	Av1	0	8	1.02	0.15	1.16	30.55
20.02	Av2	8	19	1.86	0.27	2.92	0.16
20.03	Bw	19	42	1.44	0.21	4.72	
20.04	2Etjq	42	64	1.91	0.27	6.01	
20.05	2Etjq1	64	76	1.35	0.19	2.31	
20.06	2Etjqk2-1	76	114	1.06	0.15	5.78	
20.07	2Etjqk2-2	114	152	0.76	0.11	4.13	
20.08	2Etjqk2-3	152	190	0.65	0.09	3.53	
5.01	A	0	5	0.42	0.06	0.30	32.07
5.02	Bw	5	20	0.47	0.07	1.00	0.12
5.03	Bt	20	45	0.44	0.06	1.57	
5.04	2Et	45	56	2.45	0.35	3.64	
5.05	2Etqab	56	106	1.67	0.24	11.95	
5.06	2Etqb	106	164	1.39	0.20	11.54	
5.07	2Cq	164	263	0.13	0.02	1.86	

INDEX VALUE - RUBIFICATION & MELANIZATION ---->

Sample	Horizon	Depth (cm)	Horizon Index (Sum normalized prop'd prop)		1 horizon thickness	Profile Index	Weighted Mean
18.01	Av	0 11	1.27	0.18	1.59	26.25	0.16
18.02	A	11 33	0.07	0.01	0.21		
18.03	Bt	33 40	1.55	0.22	1.55		
18.04	2Btqa	40 65	2.62	0.37	9.72		
18.05	2Btqa	65 120	1.12	0.16	6.64		
18.06	3Ab	120 160	0.52	0.10	4.14		
8.01	Av	0 9	2.14	0.31	2.75	36.27	0.17
8.02	Bt1	9 21	3.52	0.50	6.03		
8.03	2Bt2	21 35	2.65	0.36	5.31		
8.04	2Bqa	35 68	2.64	0.38	12.44		
8.05	2r	68 100	1.56	0.22	7.14		
8.06	2D	100 210	0.17	0.02	2.60		
16.01	Av	0 13	1.39	0.20	2.59	40.46	3.37
16.02	Bw	13 30	0.95	0.14	2.30		
16.03	Bt	30 43	1.46	0.21	2.71		
16.04	2Btqa	43 58	3.00	0.47	6.43		
16.05	2r	58 100	1.32	0.19	7.92		
16.06	2Bqa (nc)	100 150	1.23	0.18	8.76		
16.07	2Bqa	100 150	0.86	0.12	6.11	38.97	0.13
16.08	2Ckqa	150 207	0.44	0.06	3.57		
1.01	A	0 10	0.76	0.11	1.06		
1.02	Bt	10 25	1.08	0.15	2.32		
1.03	2Btqb1	25 42	2.72	0.39	6.60		
1.04	2Btqb2	42 56	2.87	0.41	5.74		
1.05	3kqb1	56 70	1.75	0.22	3.07	35.33	0.00
1.09	4kqb2	70 115	1.06	0.18	7.94		
1.10	5Bk	115 167	0.53	0.07	3.41		
1.11	5Cnk	167 195	0.66	0.08	2.32		
1.12	5Cn	195 250	0.55	0.07	6.42		
19.01	Av1	0 4	1.20	0.17	0.69	35.33	0.00
	Av2	4 9	1.68	0.24	1.20		
19.02	Bv	9 13	0.53	0.13	0.53		
19.04	Bw	13 17	1.17	0.17	0.67		
19.05	Btqa	17 29	2.87	0.41	4.92		
19.06	2Btqa	29 47	3.12	0.45	8.04		
19.07	2Kqa1	47 72	1.46	0.21	5.21		
19.08	2Kqa2	72 150	1.26	0.16	14.07		

INDEX VALUE - RUEIFICATION & MELANIZATION --->								
Horizon Index								
Sample	Horizon	Depth (cm)	(Sum normalized prop/8 prop)	X horizon thickness	Profile Index	Weighted Mean		

6.01 A		0 0	1.39	0.20	1.19	25.44	0.00	
6.02 B		6 10	2.20	0.31	1.26			
6.03 2+qm		10 52	1.41	0.23	9.64			
6.04 3kmq		52 101	0.97	0.14	6.77			
6.05 3mq		101 153	0.26	0.04	1.90			
6.06 3Dmq		153 230	0.31	0.04	3.45			
6.07 3Dmq+		230 300	0.07	0.01	1.04			
2.01 Av		0 3	1.21	0.17	0.52	58.12	0.30	
2.02 A		3 10	0.89	0.13	0.89			
2.03 Bv		10 19	1.39	0.20	1.78			
2.04 2Bqey		19 34	2.58	0.37	5.54			
2.05 2Btqy		34 70	2.97	0.42	15.22			
2.07 Atqm		19 52	2.88	0.41	13.57			
2.08 +q		52 114	1.65	0.24	14.71			
2.09 2r		114 197	0.49	0.07	5.63			
22.01 A		0 10	1.74	0.25	2.49	35.12	0.21	
22.02 B		10 21	2.46	0.35	3.90			
22.03 K		21 62	1.94	0.28	11.35			
22.04 K		62 92	1.13	0.16	4.63			
22.05 Bxqm		92 184	1.26	0.18	16.56			

INDEX VALUE - COLOR PALING & COLOR LIGHTENING						
Sample	Horizon	Depth (cm)	Horizon Index (Sum normalized prop/8 prop)		A horizon thickness	Profile Index
						Weighted Mean
FNA-1			0.04	0.01	0.00	
FNA-2			0.17	0.02	0.00	
FNA-3			0.05	0.01	0.00	
FNA-4			0.21	0.03	0.00	
YNA-1			0.06	0.01	0.00	
YNA-2			0.19	0.03	0.00	
7.01 A		0 1.5	0.54	0.08	0.11	1.01 0.01
7.02 Cor		2 18	0.11	0.02	0.26	
7.03 2Cko-		18 100	0.05	0.01	0.64	
4.01 A		0 3	0.92	0.14	0.41	12.12 0.16
4.02 Bx1		3 9	1.58	0.27	1.62	
4.03 2Bx2		9 60	1.00	0.24	12.12	
4.04 2Ckn		60 100	0.34	0.05	1.97	
17.01 A		0 6	0.87	0.12	0.75	6.21 0.05
17.02 Bw		6 24	0.59	0.08	1.48	
17.03 2Ckn		24 120	0.25	0.04	3.98	
13.01 A		0 9	1.21	0.17	1.55	8.97 0.06
13.02 Bw		9 21	0.79	0.11	1.35	
13.03 2Bq1		21 73	0.32	0.05	2.40	
13.04 2Ckn		73 138	0.39	0.06	3.06	
15.01 A		0 18	1.04	0.15	2.67	20.67 0.09
15.02 Bw		18 46	1.12	0.16	4.47	
15.03 2Bq1		46 170	0.60	0.09	10.66	
15.05 2Ckn		170 220	0.40	0.06	2.87	
3.01 Av		0 5	1.64	0.23	1.17	22.01 0.10
3.02 Axb1		5 12	2.15	0.31	2.15	
3.03 2Bxb1		12 45	1.81	0.26	8.55	
3.04 2Btjqxb1		45 83	1.23	0.16	6.65	
3.05 2Btjqxb2		83 167	0.94	0.13	3.23	
3.06 2Ckqn		167 210	0.02	0.00	0.25	
21.01 Av		0 4	1.85	0.26	1.06	30.87 0.13
21.02 Bw		4 15	1.97	0.28	3.10	
21.03 Bk		15 33	0.64	0.09	1.65	
21.04 2Btjqxb1		33 55	1.91	0.27	8.02	
21.05 2Btjqxb1		55 144	0.82	0.12	10.40	
21.06 3Bqxb2		144 186	0.91	0.13	5.46	
21.07 3Ckqn		186 233	0.34	0.07	3.18	

INDEX VALUE - COLOR PALING & COLOR LIGHTENING							
Horizon Index							
Sample	Horizon	Depth (cm)	(Sun normalized prop/# prop)		X horizon thickness	Profile Index	Weighted Mean
11.01	Av	0 4	1.54	0.22	0.68	32.47	0.19
11.02	A	4 15	1.09	0.16	1.72		
11.03	2Btj	15 42	1.50	0.21	5.80		
11.04	2Btqk1	42 90	2.14	0.31	14.69		
11.05	2Bkq	90 150	0.78	0.11	6.71		
11.06	3kqk1b	150 170	0.92	0.13	2.67		
12.01	Av1	0 4	0.98	0.14	0.55	38.22	0.19
12.02	Av2	4 14	1.06	0.15	1.52		
12.03	Bt	14 47	1.62	0.23	7.62		
12.04	2Bv1	47 105	2.22	0.32	18.36		
12.05	2Bv2	105 120	0.76	0.11	1.63		
12.06	2Btqk1b	120 144	2.02	0.29	6.53		
12.07	Bqk1b	144 200	0.14	0.03	1.60		
14.01	A	0 8	1.21	0.17	1.38	35.55	0.15
14.02	Bw	8 26	1.05	0.15	3.01		
14.03	2Bv	26 54	1.09	0.16	4.05		
14.04	2Btj1q	54 107	0.65	0.09	4.98		
14.05	3Bv1b	107 121	1.54	0.19	2.69		
14.06	3Bqk1b	121 152	1.37	0.20	6.09		
14.07	4Bqk1b	152 221	1.24	0.16	12.23		
14.08	4Bv1b	221 230	0.89	0.13	1.13		
20.01	Av1	0 8	0.85	0.12	0.97	22.54	0.12
20.02	Av2	8 19	1.83	0.26	2.88		
20.03	Bw	19 42	1.26	0.16	4.20		
20.04	2Btj1q	42 64	1.46	0.21	4.65		
20.05	2Btj1q1	64 76	0.91	0.13	1.56		
20.06	2Btj1q2-1	76 114	0.75	0.11	4.06		
20.07	2Btj1q2-2	114 152	0.44	0.06	2.41		
20.08	2Btj1q2-3	152 190	0.33	0.05	1.81		
5.01	A	0 5	0.44	0.06	0.31	33.44	0.13
5.02	Bw	5 20	0.35	0.05	0.75		
5.03	Bv	20 45	0.70	0.10	2.51		
5.04	2Btb	45 56	2.07	0.30	3.25		
5.05	2Btqk1b	56 106	1.36	0.20	9.65		
5.06	2ktq1b	106 164	1.51	0.22	12.55		
5.07	2Cqn	164 263	0.30	0.04	4.22		

INDEX VALUE - COLOR PALING & COLOR LIGHTENING							
Horizon Index							
Sample	Horizon	Depth (cm)	(Sum normalized prop./# prop)		X horizon thickness	Profile Index	Weighted Mean
18.01 Av		0 11	1.45	0.21	2.25	26.46	0.17
18.02 A		11 37	0.25	0.04	0.50		
18.03 Bt		33 40	1.45	0.21	1.45		
18.04 2Btqb1		40 66	2.33	0.33	6.65		
18.05 2Btqb		66 120	1.19	0.17	9.15		
18.06 2Bt		120 160	0.52	0.10	4.14		
8.01 Av		0 9	2.14	0.71	2.75	35.97	0.17
8.02 Bt1		9 21	2.91	0.42	4.99		
8.03 2Bt2		21 35	2.35	0.34	4.75		
8.04 2kqb		35 66	2.44	0.35	11.48		
8.05 2k		66 100	1.99	0.28	5.08		
8.06 20k		100 210	0.19	0.03	2.91		
16.01 Av		0 13	1.16	0.17	2.15	33.95	2.83
16.02 Bw		13 30	0.78	0.11	1.90		
16.03 Bt		30 43	1.19	0.17	2.20		
16.04 2Btqb		43 56	2.78	0.40	5.95		
16.05 2kq		56 100	1.59	0.23	9.52		
16.06 2Bqb (inc)		100 150	0.91	0.13	6.51		
16.07 2Bqa		100 150	0.54	0.06	3.85	42.34	0.15
16.08 2Bxqb		150 207	0.23	0.03	1.66		
1.01 A		0 10	0.93	0.13	1.32		
1.02 Bt		10 25	1.02	0.15	2.19		
1.03 2Btqb1		25 42	2.39	0.34	5.80		
1.04 2Btqb2		42 56	2.44	0.35	4.67		
1.06 3kqab1		56 70	2.38	0.30	4.16	36.12	0.09
1.09 4kqab2		70 115	1.06	0.18	7.94		
1.10 5Bx		115 167	1.05	0.13	6.85		
1.11 5Cnx		167 195	0.60	0.07	2.09		
1.12 5Cn		195 290	0.60	0.07	7.10		
19.01 A-1		0 4	1.43	0.20	0.62	36.12	0.09
A-2		4 9	1.97	0.28	1.41		
19.02 Br		9 13	0.97	0.14	0.55		
19.04 Bw		13 17	1.02	0.15	0.59		
19.05 Btqa		17 29	2.69	0.38	4.61		
19.06 2Btqa		29 47	3.30	0.47	8.46		
19.07 2kqa1		47 72	1.77	0.25	6.32	13.34	
19.08 2Bqa2		72 150	1.20	0.17			

INDEX VALUE - COLOR PALING & COLOR LIGHTENING							
Sample	Horizon	Depth (cm)	Horizon Index		1 horizon thickness	Profile Index	Weighted Mean
			(Sun normalized prop's prop)	(Sun normalized prop's prop)			
6.01 Av		0 6	1.27	0.18	1.00	26.52	0.00
6.02 Bc		6 10	1.91	0.27	1.09		
6.03 2tqr		10 52	1.47	0.24	10.00		
6.04 3knc		52 101	0.80	0.11	5.57		
6.05 3tq		101 153	0.70	0.10	5.22		
6.06 30kq		153 230	0.23	0.03	2.51		
6.07 30tqr		230 300	0.07	0.01	1.64		
2.01 Av		0 3	1.34	0.19	0.57	65.05	0.33
2.02 A		3 10	0.91	0.12	0.91		
2.03 Bv		10 15	1.15	0.17	1.46		
2.04 2Bqay		15 34	2.30	0.33	4.93		
2.05 2Btqay		34 70	2.45	0.36	12.61		
2.07 4tqr		15 52	3.08	0.44	14.53		
2.08 4q		52 114	2.11	0.30	18.67		
2.09 2k		114 197	0.94	0.12	11.14		
22.01 Av		0 10	1.65	0.25	2.84	40.11	0.22
22.02 Bw		10 21	2.00	0.29	3.14		
22.03 K		21 62	2.14	0.31	12.55		
22.04 K		62 92	1.37	0.20	5.65		
22.05 8vqs		92 164	1.15	0.17	15.69		

Appendix C. Laboratory Methods--particle size distribution (PSD), bulk density, percent carbonate, gypsum and soluble salts, percent organic carbon and loss on ignition (LOI), pH, silica, and clay mineralogy.

Particle Size Distribution (PSD)

Percent gravel (>2 mm) was measured on a weight basis by sieving the bulk sample in the laboratory. Measurements were checked with field estimates to make sure that gravel in bouldery deposits was not underestimated. If percent gravel was thought to have been underestimated, the value was corrected with field observations.

Carbonate, organic matter and then silica were removed before particle size analyses (Day, 1965). Carbonate was removed with 1N NaOAc or 10% HCl, and organic matter with either dilute H₂O₂ or "Clorox" bleach. Samples were heated in a water bath to just below boiling until the reaction was complete and subsequently rinsed before the next pretreatment. Pedogenic silica was removed by heating the sample in a 5% Na₂CO₃ solution to just below boiling. One hundred ml of solution was used for each 25 gm sample. Each sample was treated for about one hour, then rinsed. Treatment was repeated three times. However, samples from horizons that were well-cemented were treated up to 12 hours before being rinsed. PSD size fractions were measured in phi units, but will be reported in USDA size classes (Table 1). Sand, silt, and clay boundaries are equal in both methods; the major discrepancy is in the silt size fraction.

Table 1: Particle Sizes in
Phi units and USDA Size Classes

mm	<u>Measured</u>	Phi unit	<u>Reported</u>
	US Std sieve mesh number		USDA Size Classes
2.0			
1.0	18	0	very coarse sand (2.0-1.0 mm)
0.5	35	1	coarse sand (1.0-0.5 mm)
0.25	60	2	medium sand (0.5-0.25 mm)
0.125	120	3	fine sand (0.25-0.10 mm)
0.053	270	4.25	very fine sand (0.10-0.05 mm)
<0.031	pipet	5	co + med silt (0.05-0.02 mm)
<0.0156	"	6	fi + vfi silt (0.02-0.002 mm)
<0.00195	"	9	co + med clay (0.002-0.0005 mm)
<0.00049	"	11	fine clay (<0.0005 mm)

2.0-0.053	0-4.25	total sand (2.0-0.5 mm)
0.053-0.00195	5-6	total silt (0.05-0.002 mm)
<0.00195	9-11	total clay (<0.002 mm)

Bulk Density

Three to eight bulk density (BD) measurements were made on paraffin-coated ped samples from each horizon (Chleborad and others, 1975). After the density was measured, each ped was opened to assure that gravel was not present. In horizons where large percentages of gravel were unavoidable in the ped samples, measured bulk density was adjusted to account for the bulk density of the gravel. Equation (1.1) was used for gravelly ped samples to estimate the bulk density of the <2 mm fraction. The assumption is made that the known percent gravel measured from the bulk sample, not the ped sample, has a bulk density of 2.6 gm/cm³

$$BD_{<2mm} = \frac{(gm < 2 mm)}{(cm^3 \text{ total volume}) - ((gm > 2 mm) / (2.6 gm/cm^3))} \quad \text{Equation (1.1)}$$

The excavation method and Equation (1.1) were used to determine the bulk density of the fresh alluvium samples for Fortymile Wash and Yucca Wash alluvium. A shallow hole in the surface of the fresh alluvium was lined with a plastic bag, then filled with water to determine the volume. The weight of the > and <2 mm fractions were measured in the laboratory. Bulk density means and standard deviations were calculated for each horizon. When the standard deviation exceeded 0.1 gm/cm^3 , the outlying density values were omitted.

Percent Carbonate, Gypsum and Soluble Salts

Pedogenic carbonate was measured on a Chittick apparatus (Dreimanis, 1962). Gypsum and soluble salts were measured in solution by electro-conductivity (Marith Reheis, U.S. Geological Survey, written communication, 1984).

Percent Organic Carbon and Loss on Ignition (LOI)

Organic carbon was measured using the Walkley-Black titration procedure (Allison, 1965). Loss on ignition (LOI) was calculated by the difference in weight loss at heat treatments of 105°C for 4 hours (soil moisture factor) and 540°C for 1 hour.

pH

pH was measured in a ratio of 1:1 soil:water slurry. After 1 hour of equilibration, samples were stirred with the electrode, allowed to stand for 1 minute, and then the pH was read.

Silica

The weight loss after the removal of carbonate, organic matter and silica cement is used to estimate the percent extractable pedogenic silica (Appendix C). The known percent of carbonate and organic matter are used to calculate the weight loss of these materials, and the remaining weight loss assumed to approximate the percent silica. Although this estimate is referred to as a percentage, it is at best an index or trend that correlates to field observations in relative amounts of pedogenic silica.

Clay Mineralogy

X-ray diffraction traces (CuK alpha radiation) were run on oriented samples of the clay and silt fractions on a "MINIFLEX" diffractometer. Samples were run air-dried, glycolated, and heated to 300°C and 500°C each for one hour. Tiles were placed face down on a glycol-saturated towel, instead of saturating in a desiccator.

Appendix D. Effects on the particle size distribution and clay mineralogy after the removal of opaline silica.

All of the particle size fractions were effected by the removal of silica. Particle size distribution for YW-16 was compared before and after silica removal (Table 1). The surface soil at YW-16 is late Pleistocene to early Holocene and due to the lack of silica cement, responded very differently to treatment than did the underlying buried mid-Pleistocene soil. Percentages of sand and clay increase or are virtually unchanged in the younger soil, whereas the percentage of silt decreases. This is probably due to

- (1) dissolving silica-cemented aggregates in the silt fraction, and
- (2) total or partial dissolving of silt particles high in silica.

The latter could be the major cause as much of the ash and phytoliths are silt size. In contrast, the same treatment of samples of the buried soil results in major losses in the sand fraction and corresponding gains in the clay-size fraction (Table 1, Fig. 1). This seems to be due to the dissolution of the silica cement.

There are problems related to the above assumption that only the dissolution of pedogenic silica influences the PSD results. X-ray diffraction proves that some clays, notably tobermorite, are destroyed (Fig. 2). However this alone may not noticeably effect the abundance of clay-size fraction unless the mineral is abundant and is dissolved.

Synthetic Nepheline (Nepheline (syn)) were produced in the laboratory after samples were dispersed with sodium hexametaphosphate and (or) treated with sodium hydroxide to remove pedogenic silica cement. Nepheline has not been recognized in any of the rocks in the study area (Quinlivan and Byers, 1977).

Table 1. Comparison of sand, silt and clay before (1) and after (2) silica removal on soil profile YW-16. +'s represent a relative gain in the size fraction after the removal of opaline SiO_2 , and -'s a relative loss.

<u>Horizon</u>		<u>% sand</u>	<u>% silt</u>	<u>% clay</u>	<u>texture</u>
Av	(1)	59.60	28.90	11.60	SL
	(2)	68.88	16.39	14.73	SL
		+9.28	-12.51	+3.13	
Bt1	(1)	48.37	40.30	11.30	L
	(2)	66.15	16.57	17.28	SL
		+17.78	-23.73	+5.98	
Bt2	(1)	57.00	26.30	16.60	SL+
	(2)	62.77	21.73	15.50	SL+
		+5.77	-4.57	-1.10	
2Btqkb	(1)	63.48	32.30	4.08	SL
	(2)	31.01	21.54	47.45	C
		-32.47	-10.76	+43.37	
2Kqb	(1)	80.30	14.50	5.20	LS
	(2)	42.93	24.88	32.18	CL
		-37.37	+10.38	+26.98	
2Bqmkb-1	(1)	82.74	16.00	1.10	LS
	(2)	69.16	14.68	16.17	SL
		-13.56	-1.32	+15.07	
2Bqmkb-2	(1)	74.60	22.90	2.60	LS
	(2)	56.24	24.11	19.65	SL+
		-18.36	+1.21	+17.05	
2Ckqnb	(1)	87.00	11.30	1.51	S
	(2)	82.16	12.31	5.53	LS
		-4.84	+1.01	+4.02	

Table 1 continued.

depth	% v co s			% co s		
	before	after	% change	before	after	% change
13	7.9	3.3	-4.6	6.0	3.8	-2.2
30	3.5	3.0	-0.5	4.3	3.1	-1.2
43	5.2	3.1	-2.1	5.2	3.0	-2.2
58 *	18.9	4.1	-14.8	14.8	4.4	-10.4
100 *	24.4	7.1	-17.3	18.8	5.2	-13.6
150 (1)*	20.2	9.8	-10.4	17.3	10.4	-6.9
150 (2)*	14.6	6.8	-7.8	14.8	5.0	-9.8
207+ *	40.5	18.0	-22.5	26.6	20.0	-6.6

depth	% med s			% fi s		
	before	after	% change	before	after	% change
13	6.4	7.4	1.0	37.8	31.0	-6.8
30	4.9	6.8	1.9	35.6	28.8	-6.8
43	6.4	6.2	-0.2	39.3	26.5	-12.8
58 *	10.4	4.3	-6.1	19.3	9.0	-10.3
100 *	13.0	6.0	-7.0	19.7	12.3	-7.4
150 (1)*	13.8	11.8	-2.0	31.4	20.2	-11.2
150 (2)*	13.9	7.9	-6.0	30.1	17.9	-12.2
207+ *	9.0	17.2	8.2	10.4	15.6	5.2

depth	% v fi s		
	before	after	% change
13	1.5	23.4	21.9
20	0.1	24.4	24.3
43	0.9	24.0	23.1
58 *	0.1	9.1	9.0
100 *	4.4	12.4	8.0
150 (1)*	0.0	17.0	17.0
150 (2)*	1.2	18.6	17.4
207+ *	0.5	11.3	10.8

* Field recognizable silica accumulations

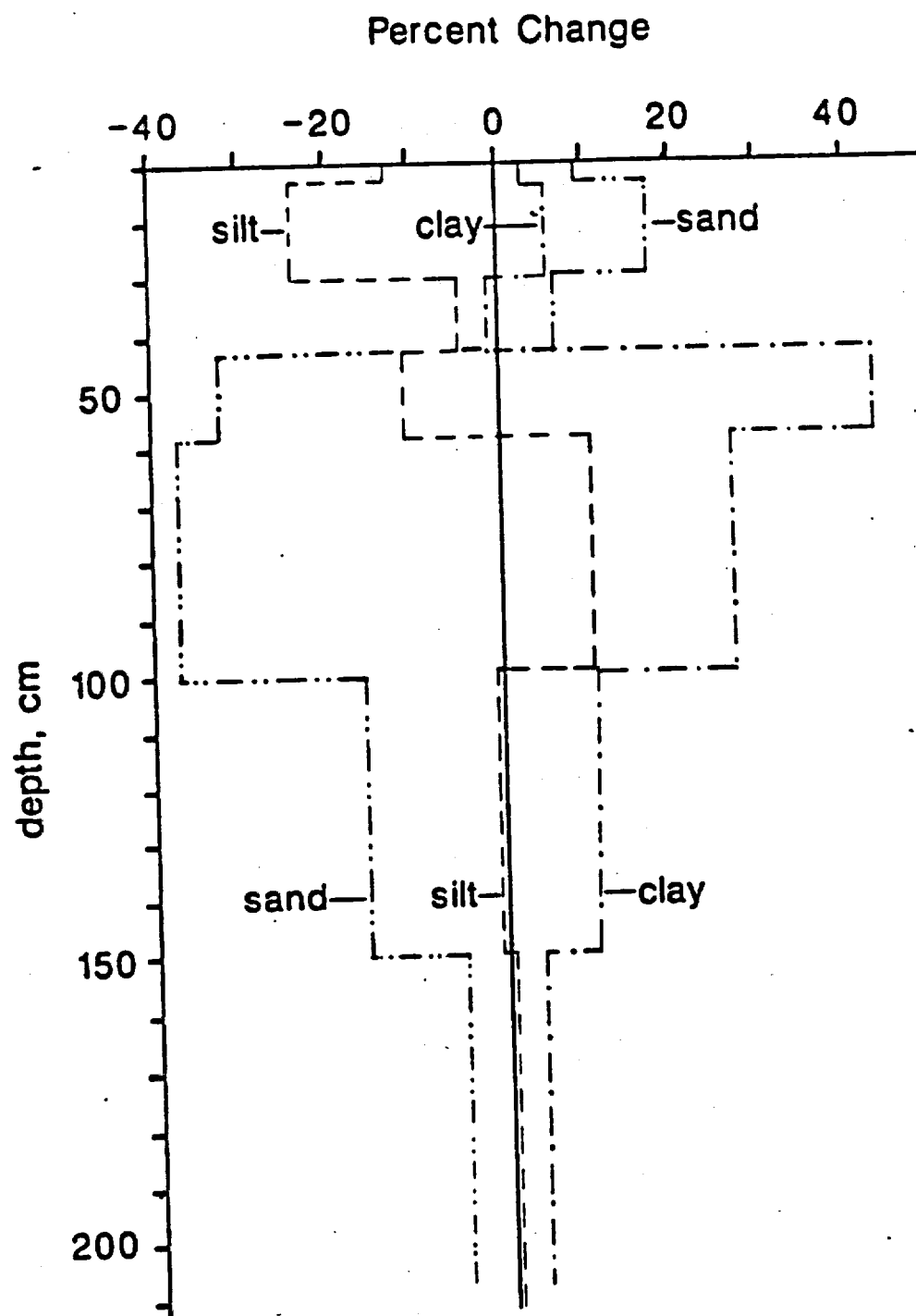


Figure 1. Percent change in particle size classes due to the removal of pedogenic silica cement in profile YW-16. Total % sand, % silt, and % clay are plotted vs depth.

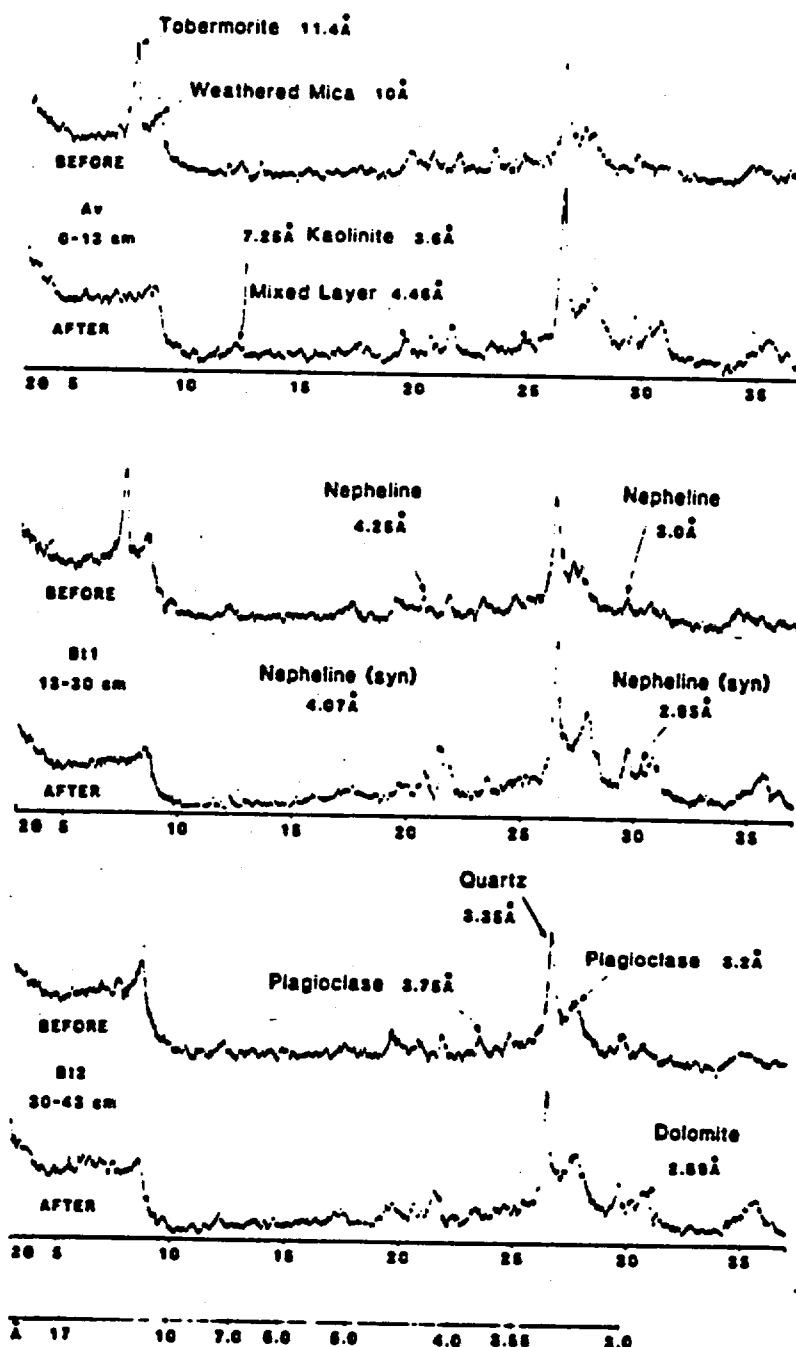


Figure 2. An example of clay mineralogy alteration owing to the removal of pedogenic silica. Traces are for profile YW-16 before and after the removal of pedogenic silica. The three horizons in a depth sequence all have approximately 15% clay, with a net gain or loss of +5 to -1% after treatment (Table 1). Tobermorite is the only clay mineral destroyed by the treatment.

Appendix E. Laboratory procedure for measuring pedogenic opaline silica using a spectrophotometer.

Introduction

There is little agreement on the best method to extract and measure pedogenic silica (Jackson, 1969; Yuan and Breland, 1969; Elgawhary and Lindsay, 1972; Torrent and others, 1980; Hallmark and others, 1982). A summary of the literature and subsequent laboratory tests produced an extraction and colorimetric determination to most accurately measure pedogenic silica

This procedure is based on the reaction of dissolved silica and ammonium molybdate in an acid medium (pH 1.0-2.0) to form the yellow silicomolybdate complex which is subsequently reduced by sodium sulfite to form blue molybdosilicate (Mo-blue). Because phosphate produces a similar molybdate complex that absorbs in the same wavelength range, oxalic acid is added to suppress phosphate interference.

All reactions when possible should be carried out in Ni, stainless steel, or plastic (polypropylene or nalgene) containers to avoid Si contamination from glass. Where plastic is specifically stated, either of the other two container types can be used. Glassware is used for dilutions, prolonged contact (>2 hours) with glass is not recommended.

Summary of Procedure

- 1) Grind, oven-dry, then weigh 1.0 gm soil sample for Si extraction.
- 2) Disperse by sonication

- 3) Remove both cementing agents CaCO_3 and iron-oxides, and organic matter.
- 4) Mix all the necessary reagents and working standard.
- 5) Extract soil silica.
- 6) Pipet working standard and sample aliquots into volumetric flasks.
- 7) Add reagents.
- 8) Run samples on spectrophotometer - consider time to warm up spectrophotometer if necessary.

Soil Sample Preparation

- 1) Sieve soil and crush to desired size. The size should vary with the largest particle size of your sample. A suggested size would be slightly larger than the dominant size fraction in fine-grained deposits (e.g., medium sand for a loess parent material), and ground finer in coarse-grained deposits. Only 1.0 gm of sample is required for the procedure.
- 2) Oven dry sample for one hour at 105°C , then lightly crush in an agate mortar to break up aggregates.
- 3) Weigh 1.0 gm of sample.
- 4) Wash sample with distilled water into a plastic centrifuge tube or bottle, filling to half the volume. Disperse by sonication (Busacca and others, 1984) for 10 minutes. Choose the sonicator setting that produces the most cavitation bubbles within the sample. To find that setting, simulate the sonication step with water only and same container so you can see the bubble action. Starting from the zero setting, as you

turn the dial, the number of bubbles is the setting to use for you samples. It is important to stir the sample while it is being sonicated, otherwise the grains just pack together at the bottom of the container and do not get the full benefit of the treatment. Since conventional stirrers do not fit inside the centrifuge tubes, Sharon Feldman (Dept. of Agronomy and Soils, Washington State University, Pullman, written communication, 1984) suggests blowing air into the sample. This is simply done with tygon tubing connected to the lab bench air valve. Blow in just enough air to keep the soil in suspension. Once the sonicator is on, it does not take much air to keep the soil in suspension.

- 5) Remove carbonate then organic matter with the same procedures used in grain size analysis, but do not remove the sample from the plastic tube. It is not necessary to remove organic matter from soils that contain very little of it (e.g., arid environment soils with <1% organic matter). If appreciable amounts of free iron oxides are present, they should also be removed by the dithionite method (Jackson, 1969).
- 6) Wash samples with distilled water. Centrifuge for a half an hour at a setting between 2500 and 3000 rpm, or until the supernatant is clear. Repeat if necessary. The time may vary for individual samples.

Reagents

6 N HCl - Dilute 50 ml concentrated HCl (37% or 12.1 N) to 100 ml.

Ammonium molybdate solution - Dissolve 100 gm ammonium paramolybdate tetrahydrate (ammonium molybdate) $[(\text{NH}_4)_6\text{Mo}_7\text{O}_{24} \cdot 4\text{H}_2\text{O}]$ in 600 ml H_2O , warm and stir to obtain complete dissolution. When cool, transfer to a volumetric flask, adjust pH to 7-8 with concentrated NaOH and dilute to 1.0 liter. 2 ml/sample is used.

Oxalic acid solution - Dissolve 100 gm oxalic acid ($\text{C}_2\text{H}_2\text{O}_2 \cdot \text{H}_2\text{O}$) and dilute to 1.0 liter. 2 ml/sample is used.

Reducing Agent - Dissolve 0.5 gm 1-amino-2-naphthol-4-sulfonic acid and 1 gm anhydrous sodium sulfite (Na_2SO_3) in 50 ml water. Dissolve 30 gm sodium bisulfite (NaHSO_3) in 150 ml water. Mix the two solutions in a plastic bottle and allow the reagent to sit for a few hours in the refrigerator. The supersaturated solution should form a precipitate that must be filtered before use. If the precipitate is not allowed to form before using, it will form a white precipitate in your colored samples. If this happens throw the samples out and start again with a reducing agent that has formed a precipitate and has been filtered. Refrigerate this reagent when not in use; it is unstable and should be made fresh every week. Total volume 200 ml. 2 ml/sample is used.

Silica Extraction

- 1) Amorphous soil silica is extracted with 0.5 N KOH or 0.5 N NaOH. Sharon Feldman (Dept. of Agronomy and Soils, Washington State University, Pullman, written communication, 1984) prefers to use KOH because it is less damaging to the silicate clay minerals. See Jackson (1969, Sec. 11-27) for quantitative measure of the kaolinite and halloysite peaks following NaOH extraction of Si. Dissolve 2.3 gm reagent grade KOH pellets, or 2.0 gm NaOH pellets, in 100 ml of H₂O in a plastic container, or dilute stock KOH or NaOH solutions to 0.5 N.
- 2) Soil:solution ratio is 1:50 (1 gm/50 ml or 0.5 gm/25 ml).
Perform the entire extraction procedure under a fume hood.
- 3) Prepare a boiling water bath. It is important that the temperature remain stable. Heat the 0.5 N KOH (or NaOH) solution to 100°C.
- 4) Place the room temperature sample in a plastic container, in the bath, and add the correct amount of heated 0.5 N KOH (or NaOH). Allow reaction to continue for exactly 2.5 minutes (Torrent and others, 1980).
- 5) Remove from hot bath, and cool rapidly in an ice water bath.
Remove and centrifuge the sample for 10 minutes at 1600 rpm, then immediately decant the 50 ml of supernatant into a 100 ml volumetric flask.
- 6) Add 10 ml room temperature 0.25 N KOH (or NaOH) per 1.0 gm sample to centrifuge tube. Mix well. Centrifuge and decant into the 100 ml volumetric flask containing the original 50 ml of extract. This completes the removal of amorphous Si.

- 7) Dilute to volume with distilled H_2O .

Standard Silica Solution

Stock Solution (use 1 or 2)

- 1) Clean pure quartz crystal in concentrated HCl for one hour, then rinse. Grind quartz to pass through a 100 mesh sieve. Heat quartz to redness in a crucible for a brief period to dry. Cool and store in an air tight vial. Add 0.1070 gm ground quartz to a Ni crucible containing 2.0 gm solid NaOH. Cover crucible and heat to a dull red for at least 10 minutes. After melt is cooled, dissolve in 50 ml of water and allow to sit overnight. The next day acidify with 1 N H_2SO_4 to a pH of 1.5. Transfer to a 1.0 liter volumetric flask and dilute to volume. Resulting stock solution is 50 mg Si/l (ug/ml or ppm). Store in a plastic bottle.
- 2) Use atomic absorption silicon standard available through American Scientific Products (1984-85 Cat # S7385-14, \$13.91), 500 ml of 1000 mg Si/l.

Working Stock

- 1) Dilute 20 ml of the 50 mg Si/l standard stock (1) to 200 ml for a final concentration of 5 mg Si/l.
- 2) Dilute 1 ml of the 1000 mg Si/l standard stock (2) to 200 ml.
 $(1000 \text{ ug Si/ml})(1 \text{ ml}/200 \text{ ml}) = (5 \text{ ug Si/ml}) = 5 \text{ mg Si/l}.$

Procedure

- 1) Add 1.0 ml 6 N HCl to a 50 ml volumetric flask and bring to volume with distilled H₂O.

Standard Curve Development

- 2) Pipette 1, 5, 10, 15, 20, (30, 40, 50) ml of the working stock into the 50 ml volumetric flasks. Use distilled water for your zero standard. When they are brought to volume (see instructions below), these standards will contain 0, 0.1, 0.5, 1.0, 1.5, 2.0, (3.0, 4.0, 5.0) mg Si/l. Label them.

Sample Color Development

- 3) Add a 1 ml aliquot of sample solution, from the silica extraction, to the volumetric flasks.

This next section applies to all standards and samples. Best results are obtained if the same period of time is allowed for color development in the standards and samples. Be careful to label everything.

- 4) Wash sides of flasks down carefully and dilute to 30 ml.
- 5) Add 2.0 ml ammonium molybdate solution
- 6) Swirl to mix and allow to react for 20 minutes. Yellowish color develops if Si is present.
- 7) Add 2.0 ml oxalic acid solution. Mix and let stand 10 minutes to complex any phosphates which may be present. Do not allow to stand much more than 10 minutes or low Si results will be obtained.

- 8) Add 2.0 ml reducing solution and take to volume with distilled water.
- 9) Wait 20 minutes for complete reaction. It will be blue if Si is present. NOTE: If a sample solution develops to a darker blue than the highest standard (2.0 or 5.0 mg Si/l), either 1) make a higher standard >2.0 mg Si/l, 2) redo it with a smaller sample aliquot, or 3) dilute the original (unknown) Si extract and use a 1.0 ml or larger aliquot.
- 10) Mix the solutions well. Measure the absorbance with a red phototube at 625 um. Adjust the sensitivity multiplier to position 2. The first cuvette should always contain the 0 standard. Measure standards at least three times.
- 11) If you have to redo any number of samples make up a new set of standards. They should be stable over the one half to one hour it take to do the initial reading, but no longer.

Comments

- 1) Aging of reagents changes the standard curve. Always run standard solutions with samples as a check.
- 2) Variation in sample temperature shows little colorimetric effect. Permissible range is 18-29°C (65-85°F)

Calculations

Determine the mg of Si in each sample from a regression on the absorbences of the standards:

- 1) Calculate the linear regression for the standards where

$$x = \text{mg Si/l of standard}$$

$$y = \text{absorbance reading}$$

The correlation (r^2 between x and y should approximate 1.0.

- 2) Take the calculated linear regression and solve for the curve value.

$$\text{absorbance} = b(\text{curve value}) + a$$

$$\text{curve value} = (\text{absorbance} - a)/b$$

- 3) Use this equation to determine the curve value of the Si in mg Si/l.

$$4) \quad \% \text{ Si} = \frac{\left(\frac{\text{mg Si}}{\text{ml}} \right) \left(\frac{\text{ml Mo-blue soln}}{\text{ml sample aliquot}} \right) (\text{ml diluted extract})}{\text{gm oven-dried soil}} \quad 1000$$

(1000 combines conversion of mg Si to gm Si and conversion to %)

If you 1) use 50 ml volumetric flasks for Mo-blue solution, 2)

dilute 50 ml Si extract to 100 ml, 3) use a 1 ml sample aliquot

for Mo blue determination, and 4) use 1.0 gm soil, the

calculation is:

$$\% \text{ Si} = \frac{\left(\frac{\text{mg Si}}{1} \right) \left(\frac{50 \text{ ml}}{1.0 \text{ ml}} \right) (100 \text{ ml})}{1.0 \text{ gm}} \quad 1000$$

Appendix F. Laboratory Analyses--particle size, bulk density, carbonate, gypsum, soluble salts, organic carbon, oxidizable organic matter, loss on ignition, pH, and silica by weight. Starred (*) bulk density values are estimations.

Surface Profile	Elevation ft	Soil No	Horizon	Depth cm (gravel top base %)	vc	co	med	fi	vf	catm (10vfi)	silt (10vfi)	clay (10vfi)
01a		FMA-1 FMA-2 FMA-3 FMA-4		51	12.76	14.23	27.16	26.76	13.44	3.50	0.94	0.51
				0	0.57	2.29	9.97	24.56	37.29	11.31	1.91	0.96
				41	19.47	33.75	31.80	10.11	3.41	0.60	0.26	0.17
				60	25.17	30.57	28.05	10.46	2.59	1.61	1.15	0.33
01a		VMA-1 VMA-2		67	29.44	40.69	22.67	5.52	0.82	0.25	0.17	0.08
				58	17.08	24.09	31.02	13.97	5.13	0.43	0.51	0.21
01b	3380	7.01 A 7.02 C 7.03 2Lup		18	7.24	12.70	23.60	28.50	21.33	4.23	0.69	0.57
				12	6.79	9.57	19.58	31.09	24.00	5.50	1.02	1.16
				63	20.86	26.91	25.69	14.81	7.14	2.12	1.12	0.45
01c	3500	4.01 A 4.02 MJK 4.03 2Lup 4.04 2Lup		19	2.33	3.49	7.79	32.62	40.32	6.65	2.72	1.66
				3	1.60	2.25	9.16	34.62	33.32	5.07	5.58	4.79
				7	3.39	4.76	8.89	22.27	32.11	11.97	5.00	6.97
				60	8.56	8.27	12.82	21.91	20.47	10.45	3.43	1.63
01c	3540	17.01 A 17.02 Bw 17.03 2Lup		40	9.12	8.60	10.77	17.98	25.60	21.05	4.00	1.91
				6	9.32	10.16	13.26	18.04	24.61	15.65	2.66	1.67
				24	19.59	27.06	20.85	15.11	10.13	3.75	1.25	0.60
01c	4155	13.01 A 13.02 Bw 13.03 2Lup 13.04 2Lup		53	12.77	14.30	15.95	18.23	20.40	9.84	3.94	1.79
				9	8.27	10.29	15.74	21.44	24.82	9.71	3.75	2.56
				21	17.01	19.53	18.47	16.65	15.90	5.45	2.73	1.53
				73	15.85	25.78	21.06	16.39	15.28	5.31	1.60	1.03
01c	4520	15.01 A 15.02 Bw 15.03 2Lup 15.04 2Lup 15.05 2Lup		55	19.73	16.07	10.51	15.17	18.88	10.99	5.07	2.32
				18	22.55	17.57	10.94	12.28	16.54	8.85	5.03	2.43
				46	13.49	15.64	11.51	14.43	17.91	10.02	8.62	5.26
				74	18.21	19.25	15.96	14.76	12.17	6.74	5.22	7.67
				85	9.62	9.35	9.14	13.43	12.81	13.94	11.82	6.71
				63	18.40	20.51	18.40	15.03	12.50	4.01	3.32	3.65
02b	3320	3.01 Avf 3.02 B1 3.03 2M1 3.04 2Lup 3.05 2Lup 3.06 2Lup		10	1.63	1.84	3.93	14.80	19.90	15.85	24.99	12.52
				5	3.42	2.84	4.00	11.05	13.79	14.40	24.04	10.17
				12	23.41	19.77	14.66	10.42	8.71	6.28	7.78	5.14
				45	19.98	26.20	23.25	10.24	5.97	4.29	5.29	2.03
				107	27.52	36.79	22.76	5.31	2.03	1.14	1.60	0.91
				107	26.63	35.68	23.52	6.36	2.93	0.80	1.48	0.81
01c and 02b over 02c	3050	21.01 Avf 21.02 B1 21.03 B 21.04 2Lup 21.05 2Lup 21.06 2Lup 21.07 2Lup		19	2.15	3.89	6.76	18.18	21.27	16.81	22.12	6.27
				4	2.51	4.87	10.27	10.27	20.62	15.02	19.04	7.95
				15	7.83	7.72	9.49	19.20	22.56	11.67	12.04	6.29
				47	6.56	9.27	12.73	10.11	15.57	6.01	10.01	8.72
				54	17.47	16.41	16.10	10.01	3.26	7.26	4.62	7.14
				59	14.28	17.47	10.82	19.20	14.49	4.77	6.71	1.54
				48	10.98	27.44	24.67	15.60	7.70	1.47	1.70	0.60

Surface Profile	Elevation ft	Soil No	Horizon	Depth cm (Gravel) top base	VCL	CO	SMD med	FI	VFI	(Silt coarse)	(Clay coarse)				
Q2b YM-11	4180		11.01 Av	0	4	40	0.45	8.87	7.94	22.99	31.91	10.45	5.57	1.22	2.61
			11.02 Bt1	4	15	27	7.20	9.31	9.31	22.75	23.97	8.94	9.29	5.54	4.11
			11.03 Bt2	15	42	39	6.45	8.10	8.58	20.51	23.07	9.26	9.90	8.10	5.94
			11.04 Bt3	42	90	48	4.23	5.78	9.08	21.27	22.89	12.18	10.29	6.51	7.77
			11.05 Bt4	90	150	75	13.28	10.31	12.24	20.82	18.11	7.10	6.52	7.11	7.11
			11.06 Bt5	150	170	75	15.47	15.47	15.75	13.35	8.38	4.11	7.26	6.29	15.54
Q1c over Q2b YM-12	4210		12.01 Av1	0	4	25	6.15	7.28	7.49	21.51	28.25	12.29	8.56	4.19	3.26
			12.02 Av2	4	14	25	4.76	6.02	7.28	20.78	30.41	12.19	9.97	5.36	7.14
			12.03 Bt1	14	47	26	5.34	6.85	8.17	19.50	23.80	11.32	11.80	8.77	4.42
			12.04 Bt2	47	100	56	12.75	12.03	12.21	18.99	17.39	10.11	8.19	4.01	2.31
			12.05 Bt3	105	120	10	18.24	18.60	16.45	15.67	12.10	7.43	6.72	2.12	2.65
			12.06 Bt4	120	144	66	24.97	21.02	19.59	14.77	8.39	3.70	1.45	2.74	2.74
Q1c over Q2b YM-14	4490		13.07 Bt1	144	200	80	26.29	21.02	14.61	13.39	10.10	4.98	4.82	1.90	2.76
			14.01 A	0	8	32	4.31	3.85	5.00	17.75	33.73	21.44	8.45	2.97	2.50
			14.02 Bt1	8	28	24	3.00	3.28	4.34	16.68	26.36	17.92	9.06	5.07	4.17
			14.03 Bt2	28	54	25	4.25	5.02	5.86	15.97	29.90	19.10	10.26	5.30	4.24
			14.04 Bt3	54	107	42	6.07	6.68	8.32	18.28	26.65	16.62	9.98	5.51	2.82
			14.05 Bt4	107	121	19	10.22	9.16	11.29	21.29	23.27	11.76	7.40	2.66	2.62
Q2b YM-20	4505		14.06 Bt5	121	152	20	6.55	6.04	7.00	17.77	25.79	13.89	13.71	4.80	4.42
			14.07 Bt6	152	221	63	12.45	11.80	12.15	18.65	18.75	8.61	9.46	3.88	4.22
			14.08 Bt7	221	230	80	12.81	13.37	11.80	16.96	17.98	7.70	7.87	5.29	2.97
			20.01 Av	0	8	36	5.42	5.15	5.36	21.56	34.72	15.06	8.07	1.97	2.65
			20.02 Bt1	8	19	24	3.06	4.57	5.48	18.59	26.28	13.97	15.87	7.98	4.72
			20.03 Bt2	19	42	29	5.12	4.76	5.41	13.09	19.54	16.08	15.87	9.65	10.42
Q1c over Q2c FM-5	3350		20.04 Bt3	42	64	84	12.74	11.64	15.34	15.83	7.49	6.87	6.45	10.15	
			20.05 Bt4	64	16	84	16.41	12.74	9.57	13.00	12.07	8.02	6.69	6.24	10.22
			20.06 Bt5	76	114	68	18.77	18.45	12.23	10.29	5.68	7.65	5.68	5.40	4.42
			20.07 Bt6	114	152	89	7.30	9.75	9.40	13.82	16.35	11.14	10.90	7.58	12.22
			20.08 Bt7	152	190	89	15.10	13.94	12.52	17.74	15.07	6.97	6.32	4.14	7.41
			20.09 Bt8	190	230	89	15.10	13.94	12.52	17.74	15.07	6.97	6.32	4.14	7.41
Q2c FM-18	3560		20.01 A	0	5	25	4.62	8.11	15.62	33.65	26.24	5.20	2.60	1.38	2.15
			20.02 Bt1	5	20	9	1.85	6.40	14.68	37.84	26.21	4.87	2.96	1.67	2.47
			20.03 Bt2	20	45	14	2.13	6.82	19.50	26.94	16.57	8.14	8.84	6.07	2.55
			20.04 Bt3	45	56	18	3.80	6.52	16.19	23.69	17.97	11.60	11.52	5.17	4.00
			20.05 Bt4	56	106	60	11.21	12.28	13.63	17.13	15.73	8.55	10.52	5.09	5.67
			20.06 Bt5	106	164	71	24.28	24.70	24.49	11.13	5.19	2.86	3.40	1.07	2.62
Q1c over Q2c FM-18	3560		20.07 Bt6	164	263	72	21.96	24.29	28.27	10.25	2.51	0.29	0.19	1.06	
			20.08 Bt7	263	300	72	21.96	24.29	28.27	10.25	2.51	0.29	0.19	1.06	
			20.09 Bt8	300	340	72	21.96	24.29	28.27	10.25	2.51	0.29	0.19	1.06	
			20.10 Bt9	340	380	72	21.96	24.29	28.27	10.25	2.51	0.29	0.19	1.06	
			20.11 Bt10	380	420	72	21.96	24.29	28.27	10.25	2.51	0.29	0.19	1.06	
			20.12 Bt11	420	460	72	21.96	24.29	28.27	10.25	2.51	0.29	0.19	1.06	

Surface	Profile	Elevation ft	Soil No	Horizon	Depth cm		Gravel %	vco	SAND			SILT			CLAY	
					top	base			co	med	fi	vfi	co+m	fi+vfi	co+med	fi
OTA	YM-2W	3870	2.01	Avk	0	3	6	2.20	2.55	4.89	16.20	17.63	23.00	17.25	10.57	5.75
			2.02	At	3	10	9	1.95	2.87	5.50	16.60	19.96	19.56	20.27	8.95	4.75
			2.03	Bty	10	19	12	2.16	2.02	4.11	14.83	19.07	20.26	19.57	9.79	8.19
			2.04	2Btqey	19	34	23	2.54	3.08	4.75	17.20	21.35	15.60	16.75	9.17	9.49
			2.05	2Btqey	34	70	33	4.06	4.40	6.45	16.65	18.88	14.17	14.62	10.28	10.51
OTA	YM-2E	3870	2.06	Btl	4	19	13	1.90	2.56	3.59	12.90	14.21	11.14	16.33	15.54	22.02
			2.07	2Btqm	19	52	39	2.45	2.88	3.87	7.37	6.02	6.07	21.26	16.09	34.01
			2.08	2Btqm	52	114	48	6.00	9.92	11.92	20.93	17.43	6.76	10.42	7.04	9.57
			2.09	3Bq	114	197	76	9.05	9.13	11.23	16.26	20.36	10.75	10.19	5.66	7.36
OTA	YM-22	3965	22.01	Avl	0	10	5	1.19	2.80	5.37	16.01	16.64	12.69	17.92	17.92	8.66
			22.02	Btl	10	21	20	4.14	5.63	5.69	15.02	14.40	9.40	11.90	16.70	17.12
			22.03	1qm	21	62	42	6.72	7.72	8.00	18.94	14.54	6.76	14.00	12.07	10.85
			22.04	2Bmq	62	92	54	11.34	13.68	13.46	16.09	13.31	6.42	10.62	6.92	8.15
			22.05	2Bmq	92	184	52	12.46	13.06	12.38	18.44	16.29	6.59	8.41	5.68	5.68

Surface Profile	Elevation ft	No	Horizon	Depth cm Gravel top base	vc	med	vl	SILT com	ELAY covered				
02a over VM-8 02c	3970	8.01 Av	0	9	1.67	3.19	19.99	16.71	14.77	21.44	12.30	6.15	
		8.02 R41	9	21	1.82	2.73	9.89	7.27	5.60	23.29	25.81	19.86	
		8.03 2Ht 2b	21	35	9.89	14.60	12.32	18.06	15.16	7.49	11.32	5.29	3.88
		8.04 2Ht 2b	35	68	23.00	20.63	16.78	13.66	9.09	4.14	6.21	2.82	3.88
		8.05 2Ht	68	100	20.76	19.23	18.11	16.10	8.16	3.59	4.34	2.64	2.64
		8.06 2Ht b	100	210	13.67	14.58	18.76	24.31	17.10	4.26	3.24	1.36	2.73
02a over VM-16 02c	4200	16.01 Av	0	13	3.27	3.82	21.03	23.39	7.18	9.21	9.02	5.71	
		16.02 R41	13	30	2.98	3.08	28.82	24.43	6.88	9.70	10.58	6.70	
		16.03 R42	30	43	3.06	3.01	26.40	24.00	6.41	15.32	8.73	6.77	
		16.04 2Ht 2b	43	58	4.12	4.44	9.04	9.12	5.18	16.36	18.54	28.91	
		16.05 2Ht	58	100	7.07	5.21	12.30	12.30	7.30	17.54	12.61	19.54	
		16.06 2Ht 2b (incl)	100	150	9.80	10.18	11.70	20.18	17.01	5.72	8.95	7.21	8.95
		16.07 2Ht 2b	150	150	6.79	5.02	7.93	17.89	18.60	19.73	12.40	8.93	10.72
		16.08 2Ht 2b	150	207	18.02	20.02	17.22	15.59	11.31	5.17	7.14	3.21	3.23
01c/02c VM-1W	4210	1.01 A	0	10	3.86	4.57	19.51	20.76	11.72	11.54	7.82	7.26	
		1.02 Bc	10	25	2.40	3.40	18.52	23.97	13.13	14.77	10.94	8.02	
		1.03 2Ht 2b 11b	25	42	3.27	4.52	9.76	11.20	7.24	12.49	12.48	29.63	
		1.04 2Ht 2b 12b	42	56	4.16	5.04	9.94	11.15	6.80	12.93	14.74	29.68	
		1.05 2Ht	56	70	5.47	7.50	9.80	10.80	5.68	12.02	13.50	25.81	
		1.06 2Ht 11b	70	115	13.19	13.19	12.66	12.66	10.31	5.12	12.20	7.42	13.56
01c/02c VM-1E	4210	1.07 2Ht 2b 11b	115	167	15.41	18.37	16.89	13.36	9.95	4.99	7.59	8.67	
		1.10 5Ht b	167	195	15.21	15.54	14.80	13.65	11.56	6.79	10.04	4.79	8.22
		1.11 5Ht 11b	195	290	19.74	23.64	20.61	9.64	4.74	2.39	6.60	4.21	6.45
		1.12 5Ht 12b	290										
		1.06 2Ht 11b	50	50	3.89	4.28	5.12	13.61	14.25	6.75	12.65	14.22	26.04
		1.07 2Ht 2b 11b	50	56	4.57	5.20	4.92	9.76	9.83	5.46	14.23	13.05	22.98
01a	3585	1.08 2Ht 2b 11b	56	70	9.95	8.81	10.02	9.95	5.28	15.38	11.28	21.79	
		1.09 4Ht 2b	70	115	13.19	13.19	12.66	12.66	10.31	5.12	12.20	7.42	13.56
		1.10 5Ht b	115	167	15.41	18.37	16.89	13.36	9.95	4.99	7.59	8.67	
		1.11 5Ht 11b	167	195	15.21	15.54	14.80	13.65	11.56	6.79	10.04	4.79	8.22
		1.12 5Ht 12b	195	290	19.74	23.64	20.61	9.64	4.74	2.39	6.60	4.21	6.45
		1.06 2Ht 11b	50	50	3.89	4.28	5.12	13.61	14.25	6.75	12.65	14.22	26.04
01a	3585	1.07 2Ht 2b 11b	50	56	4.57	5.20	4.92	9.76	9.83	5.46	14.23	13.05	22.98
		1.08 2Ht 2b 11b	56	70	9.95	8.81	10.02	9.95	5.28	15.38	11.28	21.79	
		1.09 4Ht 2b	70	115	13.19	13.19	12.66	12.66	10.31	5.12	12.20	7.42	13.56
		1.10 5Ht b	115	167	15.41	18.37	16.89	13.36	9.95	4.99	7.59	8.67	
		1.11 5Ht 11b	167	195	15.21	15.54	14.80	13.65	11.56	6.79	10.04	4.79	8.22
		1.12 5Ht 12b	195	290	19.74	23.64	20.61	9.64	4.74	2.39	6.60	4.21	6.45
01a	3585	19.01 Av 1	0	9	0.65	1.56	16.47	16.95	15.81	29.26	12.72	4.73	
		19.03 B4	9	13	2.73	3.20	14.12	28.23	14.33	7.62	12.76	12.94	4.08
		19.04 R41	13	17	0.82	1.29	6.67	13.54	7.14	3.68	17.74	22.50	29.10
		19.05 R4t 2b 11	17	29	0.79	1.57	9.79	21.15	10.00	3.02	10.38	16.65	26.06
		19.06 2Ht 2b 11	29	47	4.05	5.77	9.15	16.72	16.87	7.09	12.48	12.48	18.94
		19.07 2Ht 2b 11	47	72	3.60	2.67	9.25	18.22	13.20	6.76	13.02	14.52	19.34
01a	3840	19.08 2Ht 2b 11	72	150	3.71	4.31	19.70	17.59	2.07	11.59	10.06	12.52	
		6.01 Av 1	0	6	2.08	2.91	6.46	21.71	17.39	16.42	18.23	10.01	4.01
		6.02 R41	6	10	4.05	4.11	6.72	14.16	14.84	15.64	19.02	11.20	10.45
		6.03 2Ht 2b	10	52	14.20	14.20	15.99	15.99	7.07	9.25	6.06	5.89	
		6.04 2Ht 2b	52	101	24.01	18.65	10.17	16.59	10.42	4.23	7.97	1.31	2.47
		6.05 2Ht 2b	101	152	23.02	18.65	10.07	10.77	2.47	3.68	0.90	2.21	
01a	3840	6.06 2Ht 2b	152	230	20.13	22.59	20.99	17.11	11.11	3.31	0.01	1.62	
		6.07 2Ht 2b	230	290	23.77	21.08	19.11	11.17	7.22	3.76	1.80	0.60	1.60

Surface Profile	Elevation ft	Soil No	Horizon	Depth, cm top base	% Total by Summation			Density (gd)	CaUOS (Gypsum)		(Soluble Salts)	
					sand	silt	clay	gm/cc	%	micro/cm	%	micro/cm
D1a					94.57	4.52	1.11	1.75	0.43			
					84.78	13.22	2.00	1.71	0.31			
					90.55	0.85	0.60	1.40	0.34			
					95.65	2.76	1.61	0.32	0.31			
D1a					99.16	0.42	0.42	1.75	0.15			
					98.30	0.94	0.77	1.35	0.16			
D1b					93.37	4.97	1.71	0.35	0.40			
					90.83	6.53	2.64	0.33	0.19			
					95.42	3.34	1.34	0.35	0.72			
D1c					86.55	9.37	4.08	1.45	0.44	0.00000	0.00000	0.00000
					81.75	10.64	7.60	1.36	0.90	0.00002	0.00002	0.00002
					71.42	16.97	11.61	1.48	2.34	0.00003	0.00003	0.00003
					82.03	13.80	4.08	0.42	1.59	0.00004	0.00004	0.00004
D1c					70.07	25.06	4.87	0.35	0.07			
					76.19	19.32	4.14	1.50	0.27			
					92.73	5.00	2.27	0.42	0.24			
D1c					81.75	13.78	4.47	1.42	0.14			
					80.57	13.46	5.96	0.42	0.12			
					87.56	8.18	4.26	1.41	0.15			
					93.15	4.91	1.94	1.81	0.22			
D1c					78.36	16.06	5.58	0.40	0.02			
					79.88	13.80	6.25	0.40	0.09			
					70.48	10.64	10.38	0.40	0.13			
					80.46	11.96	7.58	0.42	0.21			
					61.35	25.77	12.88	0.40	0.20			
					85.35	7.33	7.33	0.60	0.24			
					42.10	40.84	17.06	1.62	1.49	0.00002	0.00002	0.00002
D2b					35.11	59.29	25.60	1.72	0.85	0.00001	0.00001	0.00001
					76.96	14.16	8.87	0.80	0.34	0.00001	0.00001	0.00001
					85.71	9.58	4.72	1.94	0.54	0.00001	0.00001	0.00001
					94.40	2.74	2.85	2.00	0.57	0.00001	0.00001	0.00001
					95.34	2.27	2.27	0.60	0.70	0.00002	0.00002	0.00002
					55.23	28.92	8.85	1.37	1.73			
					59.58	24.11	11.51	1.59	1.03			
D1c and D2b over D2c					67.17	23.71	9.12	1.52	0.52			
					64.23	16.82	18.95	1.71	0.79			
					77.23	10.92	11.76	1.95	0.48			
					104.20	11.40	4.24	1.79	0.24			
					84.57	3.16	3.16	0.60	0.26			
					21.01	40.84	17.06	1.62	1.49	0.00002	0.00002	0.00002
					21.02	40.84	17.06	1.62	1.49	0.00002	0.00002	0.00002

Surface Profile	Elevation ft	Soil No	Horizon	Depth cm top base	% Total by Summation			Density (gd)	CaCO ₃ %	Gypsum %	(Soluble Salts) EC	Z
02b	4180	11.01	Av	0	4	80.15	16.02	3.83	1.57	0.23		Z
		11.02	Bt1	4	15	75.12	18.23	9.65	1.59	0.18		
		11.03	2Bt2	15	42	66.71	19.25	14.04	1.54	0.20		
		11.04	2Bt2q	42	90	67.25	22.47	14.28	1.61	1.14		
		11.05	2Bt2	90	150	74.75	12.71	11.53	1.67	1.55		
		11.06	2Bt2b	150	170	66.26	11.37	20.35	1.62	2.12		
01c over 02b	4210	12.01	Av1	0	4	70.68	21.85	7.47	1.56	0.07		
		12.02	Av2	4	14	69.24	22.16	8.50	1.40	0.20		
		12.03	2Bt1	14	47	63.64	22.12	12.23	1.64	0.19		
		12.04	2Bt1	47	105	74.38	18.20	7.22	1.65	1.61		
		12.05	2Bt2	105	120	81.06	14.16	4.78	1.69	1.86		
		12.06	2Bt2b	120	144	88.72	7.08	4.18	1.77	1.68		
		12.07	2Bt2b	144	200	85.51	9.81	4.68	1.75	0.73		
01c over 02b (?)	4090	14.01	A	0	8	64.64	29.10	5.48	1.26	0.20		
		14.02	Bt1	8	28	67.77	26.99	9.24	1.26	0.19		
		14.03	2Bt1	28	54	61.10	29.15	9.55	1.29	0.92		
		14.04	2Bt2	54	107	65.99	26.61	7.29	1.65	2.98		
		14.05	2Bt2b	107	121	70.34	19.16	5.50	1.62	0.91		
		14.06	2Bt2b	121	152	62.14	27.60	9.26	1.83	1.53		
		14.07	4Bt2b	152	221	72.82	18.07	8.11	1.67	0.67		
		14.08	4Bt2b	221	220	76.91	15.56	7.52	1.75	0.74		
02b (?)	4545	20.01	Av	0	8	72.21	23.13	4.66	1.51	0.06		
		20.02	Bt1	8	19	58.18	29.22	12.70	1.53	0.09		
		20.03	Bt2	19	42	47.96	31.95	20.09	1.56	0.10		
		20.04	2Bt1	42	64	69.00	14.36	16.64	1.65	0.19		
		20.05	2Bt2	64	76	66.79	16.72	16.49	1.96	2.21		
		20.06	2Bt2-1	76	114	71.54	13.32	12.08	1.72	1.22		
		20.07	2Bt2-2	114	152	56.63	22.04	21.22	1.72	4.77		
		20.08	2Bt2-3	152	190	75.16	12.29	11.55	1.72	1.30		
01c over 02c	3750	5.01	A	0	5	88.53	7.80	3.67	1.51	0.29	0.00001	0.00
		5.02	AB	5	20	87.07	8.82	4.11	1.44	0.13	0.00005	0.00
		5.03	Bt1	20	40	72.97	16.98	10.05	1.64	1.94	0.00001	0.00
		5.04	2Bt1b	40	56	64.16	22.67	9.17	1.66	0.39	0.00005	0.00
		5.05	2Bt2b	56	106	69.98	19.10	10.92	1.78	1.18	0.00001	0.00
		5.06	2Bt2b	106	164	89.89	6.27	7.94	1.86	4.51	0.00001	0.00
		5.07	2Bt2b	164	165	98.07	0.67	1.25	1.80	0.19	0.00005	0.00
02c over 01a	3760	18.01	Av1	0	11	79.27	45.10	15.63	1.72	2.34		
		18.02	AB	11	32	64.13	27.24	8.52	1.69	1.61		
		18.03	Bt1	32	40	62.90	29.58	11.52	1.81	0.19		
		18.04	2Bt2-1	40	66	70.22	16.85	7.92	1.79	0.22		
		18.05	2Bt2-2	66	120	85.97	7.87	6.16	1.80	0.17		
		18.06	2Bt2b	120	160	89.01	5.97	4.22	1.82	14.42		

Surface Profile	Elevation, ft	Soil No	Horizon	Depth, cm	% Total by Summation			Density (ind)	CaCl ₂	Gypsum		(Soluble Salts)	
02a over VM-8	3920				top	base	cm	gm/cc	%	mm/cm	%	mm/cm	%
02c		8.01 Av		0	9	45.32	36.21	18.44	1.65	0.00			
		8.02 H01		9	31	28.44	28.88	42.67	1.52	0.07			
		8.03 2H02b		21	35	72.07	18.81	9.12	1.64	0.11			
		8.04 2H02b		35	48	83.24	10.26	6.40	1.56	19.41			
		8.05 2H02b		68	100	87.25	7.92	4.72	1.70	7.52			
		8.06 2H02b		100	110	88.42	7.49	4.09	1.72	4.09			
02a over VM-16	4300												
02c		16.01 Av		0	13	68.88	16.39	14.72	1.26	0.00	0.00001	0.01	0.00012
		16.02 H01		13	30	64.15	16.57	17.28	1.49	0.05	0.00000	0.00	0.00007
		16.03 H02		20	47	62.77	21.72	15.50	1.48	0.07	0.00001	0.01	0.00005
		16.04 2H02b		43	58	21.01	21.54	47.45	1.76	2.18	0.00010	0.05	0.00012
		16.05 2H02b		58	100	42.92	24.68	22.18	1.40	22.92	0.00001	0.01	0.00014
		16.06 2H02b (mc)		100	150	69.16	14.68	16.17	1.70	0.19	0.00001	0.01	0.00016
		16.07 2H02b		100	150	56.24	24.11	19.65	1.70	1.01	0.00000	0.00	0.00015
		16.08 2H02b		150	207	82.16	12.31	5.52	1.84	0.07	0.00002	0.02	0.00001
01c/02c VM-1W	4210												
		1.01 A		0	10	61.66	23.26	15.07	1.47	0.06			
		1.02 H01		10	25	52.13	27.90	18.97	1.52	0.14			
		1.03 2H02b 11b		25	42	22.66	21.22	45.11	1.40	0.22			
		1.04 2H02b 11b		42	56	26.06	19.73	44.22	1.62	0.24			
		1.05 2H02b		56	70	41.99	18.70	39.30	1.72	0.40			
01c/02c VM-1E	4310												
		1.06 2H02b		50	41.14	18.60	40.26	1.47	0.25				
		1.07 2H02b		50	56	24.28	19.69	46.02	1.49	1.52			
		1.08 2H02b		56	70	46.16	20.77	32.07	1.64	6.79			
		1.09 4H02b		70	115	61.61	17.40	20.99	1.48	20.02			
		1.10 5H02b		115	167	72.98	12.58	13.45	1.71	9.54			
		1.11 5H02b		167	195	70.26	16.42	13.01	1.75	2.51			
		1.12 5H02b		195	290	80.26	8.98	10.66	1.75	0.92			
01a FM-19	3585												
		19.01 Av01		0	9	41.49	41.07	17.45	1.61	3.30			
		19.02 H01		9	13	62.61	20.38	17.01	1.75	2.96			
		19.04 H01		13	17	29.46	17.46	53.08	1.24	1.12			
		19.05 1H02b		17	29	42.20	12.99	42.71	1.42	0.27			
		19.06 2H02b		29	47	46.57	20.77	22.67	1.59	8.99			
		19.07 2H02b		47	72	46.14	19.79	34.07	1.59	8.36			
		19.08 2H02b		72	150	52.85	18.16	27.98	1.72	16.22			
01a VM-6	2840												
		6.01 Av01		0	6	50.33	24.65	14.82	1.46	1.97	0.00002	0.01	0.00010
		6.02 H01		6	10	43.47	24.66	21.86	1.21	0.92	0.00002	0.01	0.00010
		6.03 2H02b		10	52	71.74	16.22	11.92	1.20	30.22	0.00004	0.02	0.00015
		6.04 2H02b		52	101	87.01	8.22	2.97	1.60	19.28	0.00006	0.02	0.00009
		6.05 2H02b		101	153	90.69	6.15	2.15	1.84	12.17	0.00001	0.43	0.00002
		6.06 2H02b		153	220	92.02	2.54	2.42	1.72	6.18	0.00024	0.12	0.00020
		6.07 2H02b		220	250	93.12	4.37	2.20	1.77	2.01	0.00024	0.29	0.00025

Surface	Profile	Elevation ft	Soil No	Horizon	Depth cm top base	% Total by Summation			Density (gd) gm/cc	CaCO ₃ %	(Gypsum)		(Soluble Salts)	
						sand	silt	clay			EC mho/cm	%	EC mho/cm	%
01a	VN-2W	3870	2.01	Avl	0	3	43.44	40.24	16.32	1.53	1.72			
			2.02	Al	3	10	46.67	39.63	13.70	1.52	0.51			
			2.03	Bty	10	19	42.19	39.02	17.98	1.30	0.21			
			2.04	2Btqmy	19	34	48.92	32.32	18.76	1.80	0.29			
			2.05	2Btqmy	34	70	50.41	28.79	20.80	1.79	0.11			
01a	VN-2E	3870	2.06	Btl	4	19	35.17	27.47	37.36	1.31	1.19			
			2.07	2Btqm	19	52	22.57	27.33	50.10	1.36	5.64			
			2.08	2Bqm	52	114	66.31	17.18	16.61	1.63	12.90			
			2.09	3Bq	114	197	66.04	20.94	13.02	1.73	7.96			
01a	VN-22	3965	22.01	Avl	0	10	42.81	30.61	26.58	1.58	5.26			
			22.02	Btl	10	21	44.88	21.30	33.82	1.77	0.88			
			22.03	Aqm	21	62	56.31	20.76	22.93	1.66	20.10			
			22.04	2Bmq	62	92	67.88	17.05	15.07	1.42	22.36			
			22.05	2Bqm	92	164	73.63	15.00	11.37	11.75	6.10			

Surface Profile	Elevation ft	Soil No	Horizon	Depth cm top base	Carbon % org	XL01 UM	P mg %	pH	Fe-d %	Fe-o %	Iron %	Feo/edi %	SiO2 % by wt
D1a		FWA-1 FWA-2 FWA-3 FWA-4			0.05 0.17 0.05 0.07	0.08 0.26 0.05 0.11	0.44 0.31 0.31 0.44	8.10 7.75 8.15 8.70					1.80 3.11 1.27 2.09
D1a		VMA-1 VMA-2			0.01 0.02	0.02 0.03	0.32 0.30	7.75 7.30					0.49 1.06
D1b	3780	FW-7	7.01 A 7.02 C 7.03 C1C2	0 2 18	0.18 0.09 0.10	0.71 0.16 0.17	0.30 0.32 0.35	7.75 7.80 8.15					2.02 2.58 2.14
D1c	3290	FW-4	4.01 A 4.02 B1 4.03 B1 4.04 C1C2	0 3 9 60	0.09 0.25 0.11 0.07	0.16 0.42 0.20 0.12	0.46 0.42 0.48 0.46	7.30 7.55 7.60 7.80					2.70 2.95 6.26 4.60
D1c	7540	FW-17	17.01 A 17.02 B 17.03 C1C2	0 6 24	0.35 0.18 0.19	0.61 0.21 0.15	0.24 0.40 0.36	7.50 8.00 8.10					4.37 2.78 1.12
D1c	4155	VM-13	13.01 A 13.02 B 13.03 B1 13.04 C1C2	0 9 21 72	0.61 0.32 0.12 0.06	1.05 0.43 0.20 0.10	0.48 0.47 0.35 0.25	6.80 7.10 7.40 7.60	0.48 0.51 0.45 0.42	0.023 0.021 0.019 0.017	0.05 0.04 0.04 0.04		6.16 2.80 2.68 2.18
D1c	4520	VM-15	15.01 A 15.02 B 15.03 B1 15.04 B1 15.05 C1C2	0 18 46 46 108	0.56 0.39 0.21 0.14 0.29	0.96 0.68 0.26 0.25 0.31	0.71 0.55 0.75 0.40 0.76	7.30 7.30 7.55 7.75 7.95					4.48 2.76 3.49 3.08 4.54 1.85
D2b	3320	FW-3	3.01 A 3.02 B1 3.03 B1 3.04 B1 3.05 C1C2	0 5 12 45 83	0.08 0.07 0.11 0.07 0.04	0.14 0.13 0.19 0.12 0.07	0.47 0.67 0.45 0.37 0.35	7.75 7.65 7.65 7.60 7.90					6.61 6.27 2.90 2.75 1.32 2.59
D1c and D2b over D2c	3850	VM-21	21.01 A 21.02 B1 21.03 B1 21.04 B1 21.05 B1 21.06 B1 21.07 C1C2	0 4 15 33 55 144 106	0.11 0.13 0.22 0.07 0.05 0.06 0.03	0.19 0.22 0.30 0.11 0.05 0.10 0.05	0.32 0.40 0.29 0.36 0.34 0.34 0.22	8.10 7.50 7.45 7.50 8.10 7.35 7.30					6.08 5.74 7.69 20.65 20.19 2.61 2.61

Surface Profile	Elevation ft	Soil No	Horizon	Depth cm top base	Carbon % org	XLOI	P % mg %	pH	Fe-d %	Iron % Fe ₂ O ₃ /Fed	SiO ₂ % by wt
02b	4180	11.01 Av		0	0.20	0.24	0.26	7.00			5.05
		11.02 Bt1		4	0.12	0.21	0.41	7.20			5.24
		11.03 2Bt2		15	0.19	0.33	0.57	7.05			6.46
		11.04 2Btqpk		42	0.07	0.12	0.76	7.90			18.70
		11.05 2Bt q		90	0.18	0.31	0.86	7.95			21.34
		11.06 2Btqb		150	0.07	0.13	0.75	8.00			29.38
01c over VM-12	4210	12.01 Av1		0	0.58	0.99	0.73	7.20	0.61	0.040	6.43
02b		12.02 Av2		4	0.27	0.46	0.46	7.50	0.65	0.042	4.36
		12.03 2Bt		14	0.20	0.35	0.48	7.50	0.64	0.039	5.41
		12.04 2Bt1		47	0.23	0.59	0.41	7.80	0.54	0.023	5.69
		12.05 2Bt2		105	0.25	0.40	0.47	8.00	0.51	0.025	3.36
		12.06 2Btqpk		120	0.14	0.24	0.57	7.95	0.46	0.020	7.80
		12.07 2Btqb		144	0.11	0.19	0.42	7.65	0.47	0.027	5.27
01c over VM-14	4490	14.01 A		0	0.29	0.50	0.38	7.15			5.29
02b(?)		14.02 Bt		8	0.22	0.37	0.45	7.15			4.32
		14.03 2Bt		28	0.26	0.45	0.59	7.80			5.25
		14.04 2Bt q		54	0.22	0.38	0.48	8.05			6.51
		14.05 3Bt qb		107	0.14	0.25	0.45	8.05			2.57
		14.06 3Btqpk 1b		171	0.11	0.18	0.46	8.00			2.25
		14.07 4Btqpk 2b		152	0.11	0.19	0.53	8.00			1.85
		14.08 4Bt qb		221	0.10	0.18	0.44	8.50			1.82
02b(?) VM-20	4505	20.01 Av		0	0.17	0.29	0.28	6.90			5.57
		20.02 Bt1		8	0.16	0.38	0.36	6.90			7.82
		20.03 Bt2		19	0.18	0.31	0.41	6.75			17.19
		20.04 2Bt q		42	0.25	0.44	0.49	7.30			19.12
		20.05 2Bt q 1		64	0.27	0.47	0.44	7.80			24.86
		20.06 2Btq 2-1		76	0.07	0.13	0.31	7.95			22.91
		20.07 2Btq 2-2		114	0.24	0.59	0.56	8.00			27.45
		20.08 2Btq 2-3		152	0.06	0.10	0.25	8.00			20.42
01c over FM-5	3350	5.01 A		0	0.20	0.74	0.41	7.55			1.31
02c		5.02 AB		5	0.13	0.22	0.35	7.30			1.67
		5.03 Bt1		20	0.13	0.22	0.33	7.45			3.74
		5.04 2Bt1b		45	0.09	0.16	0.42	7.25			6.52
		5.05 2Btqpk b		56	0.05	0.09	0.46	7.50			7.71
		5.06 2Bt q		100	0.08	0.14	0.42	7.65			7.91
		5.07 2Bt q		164	0.02	0.03	0.22	7.50			0.55
02c over FM-18	3560	18.01 Av1		0	0.09	0.16	0.50	8.10			7.14
01a		18.02 Av		11	0.10	0.18	0.36	8.00			7.96
		18.03 Bt1		22	0.10	0.13	0.38	7.55			4.53
		18.04 2Bt q 1		40	0.08	0.12	0.45	7.25			5.74
		18.05 2Bt q 12		66	0.06	0.11	0.48	7.10			2.27
		18.06 2Bt b		120	0.17	0.39	0.64	7.90			19.21

Surface Profile	Elevation ft	Soil No	Horizon	Depth cm	Grain % over	Grain % and	MLL	P % eq	W % 110/20	Iron Fe-O %	Pen/Fed %	MLL %
02a over VM-8	3850	8.01 Av		0	0.14	0.14	0.47	20.9	7.40	0.55	0.038	0.07
02c		8.02 B1		9	0.16	0.16	0.41	17.7	7.20	0.58	0.027	0.06
		8.03 2H1a		21	0.16	0.16	0.91	11.3	7.05	0.50	0.026	0.07
		8.04 2H2a		35	0.27	0.27	1.20	9.0	7.00	0.51	0.028	0.05
		8.05 2H3a		40	0.10	0.10	0.92	21.2	7.00	0.57	0.048	0.03
		8.06 2H4a		100	0.14	0.14	0.59	4.8	7.05	0.57	0.020	0.05
		8.07 2H5a		100	0.07	0.07	0.31	4.0	7.00	0.54	0.019	0.05
		8.08 2H6a		100	0.02	0.02	0.21	6.9	7.00	0.42	0.024	0.06
		8.09 2H7a		100	0.25	0.25	0.41	7.25	7.00	0.76	0.073	0.10
		8.10 2H8a		10	0.21	0.21	0.60	7.20	7.00	0.46	0.163	0.17
		8.11 2H9a		25	0.30	0.30	0.85	7.20	7.00	0.74	0.037	0.05
		8.12 2H10a		42	0.27	0.27	1.14	7.40	7.00	0.60	0.025	0.05
		8.13 2H11a		54	0.24	0.24	1.11	7.40	7.00	0.77	0.020	0.04
		8.14 2H12a		54	0.19	0.19	0.48	7.00	7.00	0.66	0.024	0.05
		8.15 2H13a		54	0.11	0.11	1.54	6.10	6.10	0.59	0.024	0.04
		8.16 2H14a		54	0.18	0.18	1.93	6.15	6.15	0.47	0.017	0.04
		8.17 2H15a		70	0.17	0.17	2.19	6.40	6.40	0.27	0.049	0.03
		8.18 2H16a		115	0.10	0.10	1.24	6.10	6.10	0.37	0.014	0.04
		8.19 2H17a		167	0.02	0.02	0.85	6.40	6.40	0.60	0.017	0.03
		8.20 2H18a		195	0.01	0.01	0.43	6.40	6.40	0.55	0.016	0.03
		8.21 2H19a		195	0.09	0.09	0.46	6.45	6.45			
		8.22 2H20a		9	0.07	0.07	0.79	6.15	6.15			
		8.23 2H21a		13	0.07	0.07	1.04	7.00	7.00			
		8.24 2H22a		17	0.09	0.09	0.68	7.20	7.20			
		8.25 2H23a		29	0.20	0.20	0.94	7.30	7.30			
		8.26 2H24a		47	0.17	0.17	0.67	7.40	7.40			
		8.27 2H25a		72	0.15	0.15	0.60	7.60	7.60			
		8.28 2H26a		72	0.10	0.10	0.49	7.70	7.70			
		8.29 2H27a		6	0.08	0.08	1.70	7.60	7.60			
		8.30 2H28a		10	0.42	0.42	0.64	7.75	7.75			
		8.31 2H29a		52	0.13	0.13	0.37	7.80	7.80			
		8.32 2H30a		101	0.16	0.16	0.25	7.80	7.80			
		8.33 2H31a		123	0.14	0.14	0.25	7.80	7.80			
		8.34 2H32a		220	0.02	0.02	0.26	7.80	7.80			
		8.35 2H33a		220	0.02	0.02	0.26	7.80	7.80			
		8.36 2H34a		220	0.02	0.02	0.26	7.80	7.80			
		8.37 2H35a		220	0.02	0.02	0.26	7.80	7.80			
		8.38 2H36a		220	0.02	0.02	0.26	7.80	7.80			
		8.39 2H37a		220	0.02	0.02	0.26	7.80	7.80			
		8.40 2H38a		220	0.02	0.02	0.26	7.80	7.80			
		8.41 2H39a		220	0.02	0.02	0.26	7.80	7.80			
		8.42 2H40a		220	0.02	0.02	0.26	7.80	7.80			
		8.43 2H41a		220	0.02	0.02	0.26	7.80	7.80			
		8.44 2H42a		220	0.02	0.02	0.26	7.80	7.80			
		8.45 2H43a		220	0.02	0.02	0.26	7.80	7.80			
		8.46 2H44a		220	0.02	0.02	0.26	7.80	7.80			
		8.47 2H45a		220	0.02	0.02	0.26	7.80	7.80			
		8.48 2H46a		220	0.02	0.02	0.26	7.80	7.80			
		8.49 2H47a		220	0.02	0.02	0.26	7.80	7.80			
		8.50 2H48a		220	0.02	0.02	0.26	7.80	7.80			
		8.51 2H49a		220	0.02	0.02	0.26	7.80	7.80			
		8.52 2H50a		220	0.02	0.02	0.26	7.80	7.80			
		8.53 2H51a		220	0.02	0.02	0.26	7.80	7.80			
		8.54 2H52a		220	0.02	0.02	0.26	7.80	7.80			
		8.55 2H53a		220	0.02	0.02	0.26	7.80	7.80			
		8.56 2H54a		220	0.02	0.02	0.26	7.80	7.80			
		8.57 2H55a		220	0.02	0.02	0.26	7.80	7.80			
		8.58 2H56a		220	0.02	0.02	0.26	7.80	7.80			
		8.59 2H57a		220	0.02	0.02	0.26	7.80	7.80			
		8.60 2H58a		220	0.02	0.02	0.26	7.80	7.80			
		8.61 2H59a		220	0.02	0.02	0.26	7.80	7.80			
		8.62 2H60a		220	0.02	0.02	0.26	7.80	7.80			
		8.63 2H61a		220	0.02	0.02	0.26	7.80	7.80			
		8.64 2H62a		220	0.02	0.02	0.26	7.80	7.80			
		8.65 2H63a		220	0.02	0.02	0.26	7.80	7.80			
		8.66 2H64a		220	0.02	0.02	0.26	7.80	7.80			
		8.67 2H65a		220	0.02	0.02	0.26	7.80	7.80			
		8.68 2H66a		220	0.02	0.02	0.26	7.80	7.80			
		8.69 2H67a		220	0.02	0.02	0.26	7.80	7.80			
		8.70 2H68a		220	0.02	0.02	0.26	7.80	7.80			
		8.71 2H69a		220	0.02	0.02	0.26	7.80	7.80			
		8.72 2H70a		220	0.02	0.02	0.26	7.80	7.80			
		8.73 2H71a		220	0.02	0.02	0.26	7.80	7.80			
		8.74 2H72a		220	0.02	0.02	0.26	7.80	7.80			
		8.75 2H73a		220	0.02	0.02	0.26	7.80	7.80			
		8.76 2H74a		220	0.02	0.02	0.26	7.80	7.80			
		8.77 2H75a		220	0.02	0.02	0.26	7.80	7.80			
		8.78 2H76a		220	0.02	0.02	0.26	7.80	7.80			
		8.79 2H77a		220	0.02	0.02	0.26	7.80	7.80			
		8.80 2H78a		220	0.02	0.02	0.26	7.80	7.80			
		8.81 2H79a		220	0.02	0.02	0.26	7.80	7.80			
		8.82 2H80a		220	0.02	0.02	0.26	7.80	7.80			
		8.83 2H81a		220	0.02	0.02	0.26	7.80	7.80			
		8.84 2H82a		220	0.02	0.02	0.26	7.80	7.80			
		8.85 2H83a		220	0.02	0.02	0.26	7.80	7.80			
		8.86 2H84a		220	0.02	0.02	0.26	7.80	7.80			
		8.87 2H85a		220	0.02	0.02	0.26	7.80	7.80			
		8.88 2H86a		220	0.02	0.02	0.26	7.80	7.80			
		8.89 2H87a		220	0.02	0.02	0.26	7.80	7.80			
		8.90 2H88a		220	0.02	0.02	0.26	7.80	7.80			
		8.91 2H89a		220	0.02	0.02	0.26	7.80	7.80			
		8.92 2H90a		220	0.02	0.02	0.26	7.80	7.80			
		8.93 2H91a		220	0.02	0.02	0.26	7.80	7.80			
		8.94 2H92a		220	0.02	0.02	0.26	7.80	7.80			
		8.95 2H93a		220	0.02	0.02	0.26	7.80	7.80			
		8.96 2H94a		220	0.02	0.02	0.26	7.80	7.80			
		8.97 2H95a		220	0.02	0.02	0.26	7.80	7.80			
		8.98 2H96a		220	0.02	0.02	0.26	7.80	7.80			
		8.99 2H97a		220	0.02	0.02	0.26	7.80	7.80			
		9.00 2H98a		220	0.02	0.02	0.26	7.80	7.80			
		9.01 2H99a		220	0.02	0.02	0.26	7.80	7.80			
		9.02 2H100a		220	0.02	0.02	0.26	7.80	7.80			
		9.03 2H101a		220	0.02	0.02	0.26	7.80	7.80			
		9.04 2H102a		220	0.02	0.02	0.26	7.80	7.80			
		9.05 2H103a		220	0.02	0.02	0.26	7.80	7.80			
		9.06 2H104a		220	0.02	0.02	0.26	7.80	7.80			
		9.07 2H105a		220	0.02	0.02	0.26	7.80	7.80			
		9.08 2H106a		220	0.02	0.02	0.26	7.80	7.80			
		9.09 2H107a		220	0.02	0.02	0.26	7.80	7.80			
		9.10 2H108a		220	0.02	0.02	0.26	7.80	7.80			
		9.11 2H109a		220	0.02	0.02	0.26	7.80	7.80			
		9.12 2H110a		220	0.02	0.02	0.26	7.80	7.80			
		9.13 2H111a		220	0.02	0.02	0.26	7.80	7.80			
		9.14 2H112a		220	0.02	0.02	0.26	7.80	7.80			
		9.15 2H113a		220	0.02	0.02	0.26	7.80	7.80			
		9.16 2H114a		220	0.02	0.02	0.26	7.80	7.80			
		9.17 2H115a		220	0.02	0.02	0.26	7.80	7.80			
		9.18 2H116a		220	0.02	0.02	0.26	7.80	7.80			
		9.19 2H117a		220	0.02	0.02	0.26	7.80	7.80			
		9.20 2H118a		220	0.02	0.02	0.26	7.80	7.80			
		9.21 2H119a		220	0.02	0.02	0.26	7.80	7.80			
		9.22 2										

Surface Profile	Elevation ft	Soil No	Horizon	Depth cm top base	Carbon % org	Carbon % oxid	2LOI	P mg %	pH	Fe-d %	Iron Fe-o %	Feo/Fed %	SiO2 % by wt
01a	2870	2.01 Avl		0	3	0.04	0.08	0.58	7.95				9.09
		2.02 At		3	10	0.04	0.07	0.52	7.95				9.19
		2.03 Bty		10	19	0.04	0.07	0.29	7.60				25.06
		2.04 2Btqny		19	34	0.07	0.13	0.32	7.50				25.12
		2.05 2Btqny		34	70	0.04	0.07	0.33	7.50				26.26
01a	2870	2.06 Btl		4	19	0.26	0.44	0.50	0.20				31.39
		2.07 2Btq		19	52	0.26	0.45	0.66	8.20				42.20
		2.08 2Bq		52	114	0.10	0.18	0.72	8.00				39.95
		2.09 2Bq		114	197	0.07	0.12	0.36	7.55				37.81
01a	2965	22.01 6v1		0	10	0.17	0.30	0.73	0.50				18.50
		22.02 Btl		10	21	0.24	0.41	0.87	8.00				19.28
		22.03 1 qn		21	62	0.22	0.37	1.05	7.90				25.01
		22.04 2Bq		62	92	0.13	0.23	0.96	7.65				25.73
		22.05 2Bq		92	184	0.08	0.13	0.67	7.65				25.47

Appendix G. Representative Dates for the Quaternary deposits, NTS

Stratigraphic Unit Material Dated	Age ¹ (ka)	Method	Location
Q1b	140 years		channel trenching correlation (Bryan, 1925)
Q1c Charcoal in fluvial gravel	8.3±0.075	¹⁴ C	Amargosa River, Beatty NV
Q2a Slopewash	40±10	U-trend	Crater Flat Trench 3, NTS
Slopewash	41±10	U-trend	Yucca Mountain Trench 13, NTS
Fluvial gravel	47±10	U-trend	Yucca Mountain Trench 2, NTS
Q2b Fluvial gravel	145±25	U-trend	Yucca Mountain Trench 3, NTS
Fluvial gravel	160±18	U-trend	Gravel Pit, Shoshone CA
Colluvium	160±90	U-trend	Yucca Mountain Trench 13, NTS
Q2s Fluvial sand	160±90	U-trend	Jackass Flat ETS Trench, NTS
Q2c Fluvial gravel	270±30	U-trend	Crater Flat Trench 3, NTS
(younger) "	270±30	U-trend	Jackass Divide Trench, NTS
Fluvial gravel	310±30	U-trend	Rock Valley Trench 1, NTS
Q2c Fluvial gravel	430±40	U-trend	Jackass Divide Trench, NTS
(older) "	430±60	U-trend	Crater Flat S Trench, Beatty
Q2e Bishop Ash	738±3	Geochemical correlation	Jackass Flat and Amargosa Desert, NV
QTa Basalt Ash	1.11±0.3	Geochemical	Yucca Mountain Trench 8,
(older than)	my	correlation	NTS, and Crater Flat Trench 1, Beatty NV
Ash	2.1±0.4	Fission	Carson Slough, Amargosa
(younger than)	my	track	Desert

¹ Analyzed by:

¹⁴C: S. W. Robinson, U.S. Geological Survey, Menlo Park, CA.
 U-trend: J. N. Rosholt, U.S. Geological Survey, Denver, CO.
 Geochemical correlation on Bishop Ash:
 G. A. Izett, U.S. Geological Survey, Reston, VA.
 Geochemical correlation on Basalt Ash:
 D. Vaniiman, Los Alamos National Laboratory, Los Alamos, NM.
 Fission track on Zircon:
 C. W. Naeser, U.S. Geological Survey, Menlo Park, CA.

Appendix J. Use of pollen, spores, and opal phytoliths from three different aged deposits as paleoclimatic indicators.

Three soil horizons from different aged deposits (Table 1) were submitted to the University of Kansas Palynology Laboratory to evaluate the potential for stratigraphic and paleoenvironmental use of Quaternary pollen, spores and opal phytoliths. Samples were selected at depth in an attempt to look at pollen and phytoliths deposited with the unit and out of the range of modern infiltration. The analyses were performed by Glen Fredlund, Wakefield Dort, Jr., and William C. Johnson, and completed in January of 1985.

Table 1. Samples analyzed For pollen, spores and opal phytoliths

Sample No.	Unit	Age	Profile No.	Horizon	depth
1	Q1c	10 ka	FW-4	2Btk	9-60 cm
2	Q2a	40 ka	YW-1W	2Btqkjl b	25-42 cm
3	Q2b	150 ka	FW-3	2Btk	12-45 cm

Pollen

The pollen count in the soil horizons was low compared to similar aged lake sediments, but not insignificantly so. The major problems in interpretation are associated with redeposition of older pollen and post-depositional translocation from the surface. An additional problem is the predicted slow response of vegetation in arid environments to climatic change (Thompson, 1984). Evidence from the comparison of packrat midden microfossils and pollen data suggest that pollen is a much more continuous record of vegetation change, but does not offer the very local taxonomically precise discontinuous records of packrat middens (Thompson, 1984).

Taking these limitations of pollen data interpretation into consideration, the three samples do suggest some interesting preliminary results. Consistently Sample 2 biotically represents a wetter and (or) cooler environment than Samples 1 and 3.

Very little aboreal pollen (AP) including pine (P) which indicates a wetter or cooler climate, were present in the three samples (Fig. 1). The greatest amount is found in Sample 2, and where no other AP is found in Samples 1 and 3, a small amount is present in Sample 2.

Nonaboreal pollen (NAP) taxa dominates the three pollen assemblages (Fig. 1). All of the species identified are currently present in the study area. Therefore at best these data can be used to interpret wetter and (or) cooler climatic conditions, than indicators of aridity. Of major interest, is the fact that in most cases or subdivisions of the NAP, Samples 1 and 3 are similar and Sample 2 has more or less than the other like samples.

The final subdivision of pollen is either deteriorated or mechanically damaged. There is significantly a greater amount in Sample 1 (~10 ka) which could be associated with the increased eolian activity due to decreased vegetative cover associated with the Holocene climate.

In summary, the 40 ka Sample 2 is probably correlative to the onset of cooler and (or) wetter glacial climatic conditions in the NTS area. Samples 1 and 3 represent warmer and (or) drier interglacials.

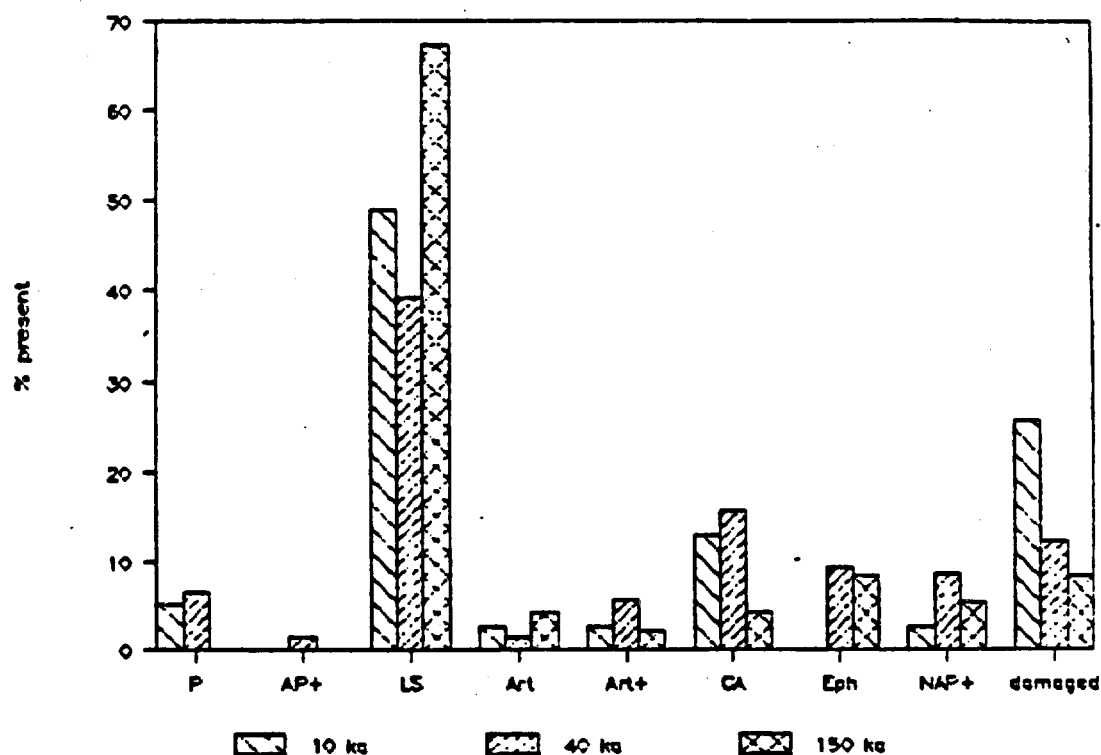


Figure 1. Relative frequency of pollen in three different aged soil horizons. Sample 1 is 10 ka, Sample 2 is 40 ka and Sample 3 is 150 ka. (P) Pinus sp. or Pine; (AP+) other aboreal pollen primarily Juniperus sp. and Quercus sp.; (LS) low spined Asteraceae or ragweed; (Art) Artemisia sp. or sage; (Art+) other Artemisia sp.; (CA) Chenopodiaceae-Amaranthaceae or Cheno-Am primarily Atriplex sp. or saltbush; (Eph) Ephedra sp. or Mormon tea; (NAP+) other nonaboreal pollen including grasses; (damaged) deteriorated, mechanically damaged or indeterminate pollen.

Opal phytoliths, aquatic organisms and ash.

Other information on paleoclimate could come from the examination of opal phytoliths and aquatic organisms in the same samples used for pollen analyses. Heavy-liquid fractionation permits recovery of other light silicates along with opal phytoliths. Opal phytoliths are formed by the precipitation of silica in and among the living cells of plants. These silicate bodies maintain their morphological consonance after the death and decay of the plant. A simple morphological classification of these bodies is the grass family (Poaceae) and non-grass families (Twiss and others, 1969; Twiss, 1983) (Fig. 2). Aquatic organisms recovered include diatoms, sponge spicules and chrysomonad cysts. Volcanic ash shards were also retrieved.

There is no significant difference in the percent of grass and non-grass phytoliths present with age of the sample (Fig. 2). The major difference between samples occurs in the aquatic organisms and ash. Aquatic organisms do not necessarily represent a local wet environment because they are easily wind-transported great distances from dry playas. Ash can be derived both from the eolian component and in situ weathering of the parent material. The greater amount of aquatic organisms and ash in Sample 2 could be interpreted as (1) a drier climate increasing the possibility that playa sediments are susceptible to eolian transport, or (2) a wetter climate capable of translocating aquatic organisms and ash into the soil profile. I favor the latter of the two mechanisms.

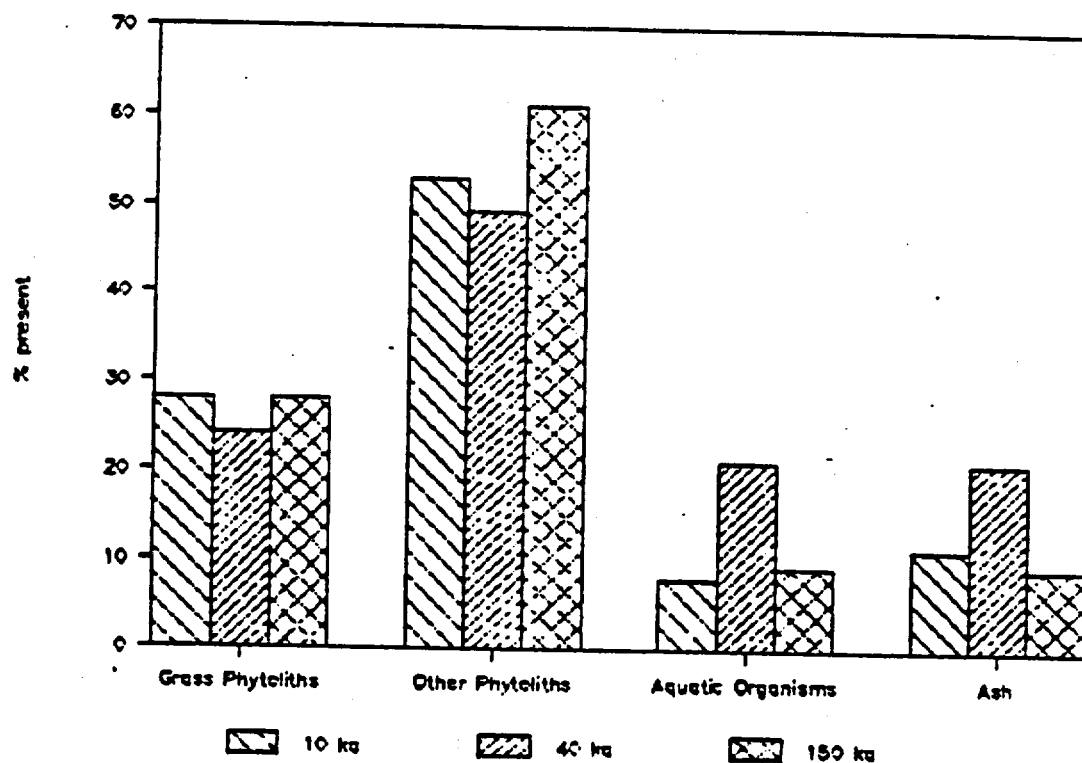


Figure 2. Relative frequency of opal phytoliths, aquatic organisms and volcanic ash in three different aged soil horizons. Sample 1 is 10 ka, Sample 2 is 40 ka and Sample 3 is 150 ka. Grass Phytoliths - total Poaceae family phytoliths; Other Phytoliths - irregular, aberrant and unique phytoliths; Aquatic Organisms including diatoms, sponge spicules and chrysomonad cysts; Ash - "light" volcanic glass shards.

Grass Phytoliths

In order to look at the paleoclimate in more detail the grass phytoliths were subdivided to the tribe level (Fig. 3). Each tribe exhibits a unique adaptive propensity reflecting the regional climate. Festuceae grasses are associated with cooler sagebrush steppes like the Snake River Plateau today, Chlorideae are short-grasses and associated with warmer and more arid regions like the American Southwest today, and Paniceae is associated with the native tall-grasses of the true prairie vegetation in the Eastern Great Plains today. Phytoliths in the elongate category have no subfamily implications and occur in other monocots as well as grasses (Fig. 3).

The data indicate that grass phytoliths from Sample 2 are from a slightly wetter and (or) cooler climate than that of the other two samples. The presence of greater amounts of Festuceae suggests that during the formation of these phytoliths the climate was more temperate, like that in northern Nevada today. Samples 1 and 3 are more alike and indicate drier and (or) warmer conditions than that of during the deposition of Sample 2 (Fig. 3).

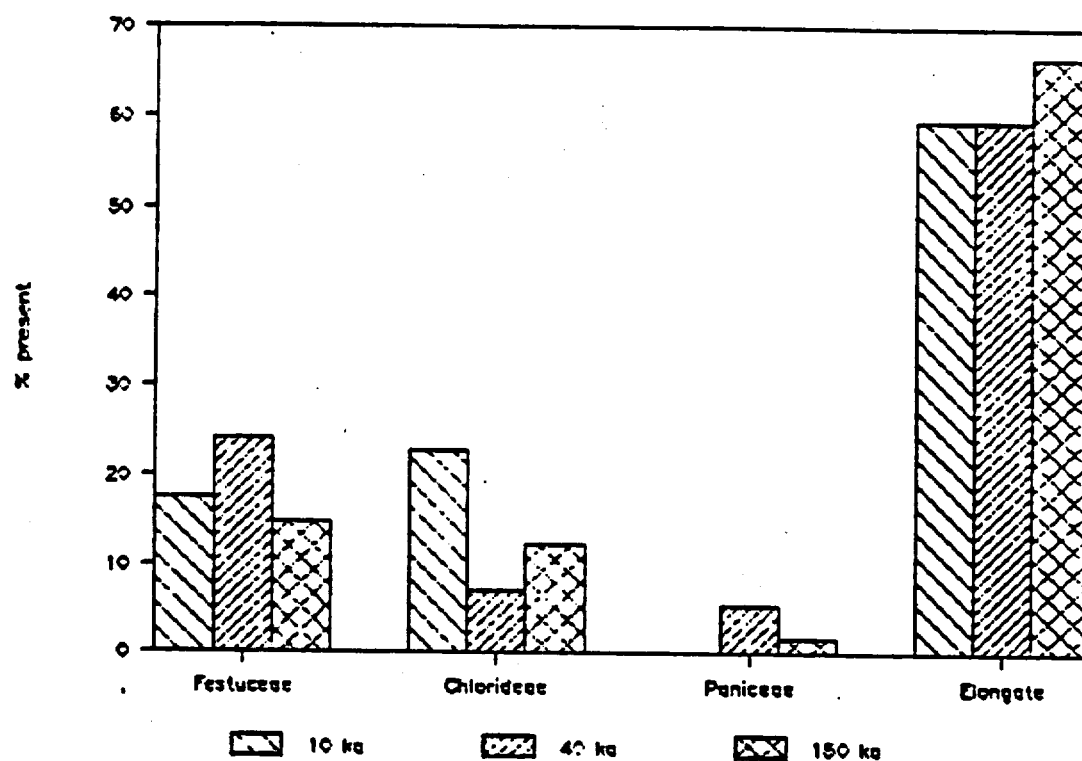


Figure 3. Relative frequency of grass (Poaceae) phytoliths in three different aged soil horizons. Sample 1 is 10 ka, Sample 2 is 40 ka and Sample 3 is 150 ka.

Appendix I: Soil parameters used to model calcic soil development. Parameters define a fresh alluvial sample with a sand texture and minimum vegetation. The maximum rooting depth is between 40 and 60 cm.

Twenty compartments each 10 cm thick. Particulate carbonate equals $0.1 \text{ gm/cm}^2/10^3 \text{ yr}$. Climatic data are in Table 3.

Compartment	Moisture Content			Parent	Soil		
	AWC <u>1/</u>	Present	Permanent	Material	PCO_2 <u>2/</u>	Temperature <u>3/</u>	ET
			Wilting Point	CaCO_3	$10^{-\text{exp}}$	$^{\circ}\text{C}$	<u>4/</u> Index
1	0.049	0.02	0.018	0.27	3.50	16.5	0.25
2	0.049	0.02	0.018	0.27	3.20	17.9	0.20
3	0.049	0.02	0.018	0.27	3.00	18.8	0.15
4	0.049	0.02	0.018	0.27	2.70	19.0	0.10
5	0.049	0.02	0.018	0.27	2.50	19.3	0.10
6	0.049	0.02	0.018	0.27	2.50	19.3	0.10
7	0.049	0.02	0.018	0.27	2.55	19.3	0.05
8	0.049	0.02	0.018	0.27	2.60	19.3	0.05
9	0.049	0.02	0.018	0.27	2.63	19.3	0
10	0.049	0.02	0.018	0.27	2.66	19.3	0
11	0.049	0.02	0.018	0.27	2.68	19.3	0
12	0.049	0.02	0.018	0.27	2.70	19.3	0
13	0.049	0.02	0.018	0.27	2.75	19.3	0
14	0.049	0.02	0.018	0.27	2.80	19.3	0
15	0.049	0.02	0.018	0.27	2.90	19.3	0
16	0.049	0.02	0.018	0.27	3.00	19.3	0
17	0.049	0.02	0.018	0.27	3.10	19.3	0
18	0.049	0.02	0.018	0.27	3.20	19.3	0
19	0.049	0.02	0.018	0.27	3.30	19.3	0
20	0.049	0.02	0.018	0.27	3.40	19.3	0

1/ Calculated for sand from Salter and Williams (1965).

2/ Atmospheric PCO_2 at surface, decreasing until the maximum rooting depth between 40 and 60 cm, and again gradually increasing with depth.

3/ Actual soil temperature values from Rock Valley, NTS, averaged from 3/67 to 12/72 (Romney and others, 1973).

4/ Estimated percent of total evapotranspiration occurring in each compartment.

Appendix H. Horizon weights of carbonate, clay, silt, and opaline silica.

Soil no	linear age	thickness	bulk density	% Carbonate		rate of acc	Unit	AVERAGE FROM THE SUM OF THE				
				lab	in			0.01 rate	0.01 rate	0.02 rate	0.04 rate	Act prof
		% gravel				prof sum per 11 yr	avg	Estimated profile sum avg				sum avg
11.01	150000	4	1.57	0.23	0.15	0.00						
11.02	150000	11	1.59	0.18	0.15	0.01						
11.03	150000	27	1.54	0.20	0.15	0.02						
11.04	150000	48	1.81	1.14	0.15	0.46						
11.05	150000	60	1.07	1.50	0.15	0.40						
11.06	150000	20	1.82	2.13	0.15	0.20						
12.01	150000	4	1.56	0.07	0.15	-0.00						
12.02	150000	10	1.40	0.20	0.15	0.01						
12.03	150000	22	1.64	0.19	0.15	0.02						
12.04	150000	58	1.05	1.61	0.15	0.70						
12.05	150000	15	1.89	1.86	0.15	0.45						
12.06	150000	24	1.77	1.64	0.15	0.22						
12.07	150000	56	1.75	0.73	0.15	0.12						
14.01	150000	8	1.36	0.20	0.15	0.00						
14.02	150000	20	1.26	0.19	0.15	0.01						
14.03	150000	26	1.39	0.92	0.15	0.10						
14.04	150000	23	1.62	2.56	0.15	1.44						
14.05	150000	14	1.62	0.91	0.15	0.14						
14.06	150000	31	1.83	1.52	0.15	0.26						
14.07	150000	69	1.67	0.87	0.15	0.20						
14.08	150000	9	1.75	0.74	0.15	0.02						
20.01	150000	8	1.51	0.06	0.15	-0.01						
20.02	150000	11	1.53	0.09	0.15	-0.01						
20.03	150000	22	1.56	0.10	0.15	-0.01						
20.04	150000	22	1.65	0.19	0.15	0.00						
20.05	150000	12	1.96	2.31	0.15	0.12						
20.06	150000	28	1.72	1.22	0.15	0.25						
20.07	150000	38	1.72	4.77	0.15	0.24						
20.08	150000	38	1.72	1.30	0.15	0.00						
5.01	200000	5	1.51	0.29	0.25	-0.00						
5.02	200000	15	1.44	0.13	0.25	-0.04						
5.03	200000	25	1.64	1.94	0.25	0.58						
5.04	200000	11	1.66	0.29	0.25	0.02						
5.05	200000	50	1.78	1.10	0.25	0.22						
5.06	200000	58	1.06	4.51	0.25	1.21						
5.07	200000	99	1.60	0.19	0.25	-0.04						
18.01	200000	11	1.72	2.24	0.25	0.24						
18.02	200000	22	1.69	1.61	0.25	0.38						
18.03	200000	7	1.81	0.19	0.25	-0.01						
18.04	200000	26	1.79	0.22	0.25	-0.01						
18.05	200000	54	1.60	0.17	0.25	-0.02						
18.06	200000	40	1.32	14.42	0.25	2.47						

AVERAGE FROM ILE SUM USING													
Soil no	linear age	thickness % (wavel	bulk Density	Z Carbonate lab	qm/cm ²	prof sum per 11 yr	rate of acc	Unit Avg	0.7 rate 0.1 rate 0.1 rate 0.1 rate 0.1 rate				
									0.01	0.04	0.12	0.14	0.16
estimated profile sum avg													
B.01	300000	9	1.65	0.00	0.15	-0.02							
B.02	300000	12	1.52	0.07	0.15	-0.01							
B.03	300000	14	1.64	0.11	0.15	-0.00							
B.04	300000	22	1.56	19.41	0.15	8.16							
B.05	300000	22	1.70	7.53	0.15	1.92							
B.06	300000	110	1.75	4.08	0.15	2.86	12.91	0.04					
16.01	300000	13	1.26	0.00	0.15	-0.02							
16.02	300000	17	1.49	0.05	0.15	-0.02							
16.03	300000	15	1.48	0.07	0.15	-0.01							
16.04	300000	15	1.76	2.18	0.15	0.21							
16.05	300000	42	1.48	22.93	0.15	6.10							
16.06	300000	50	1.40	9.19	0.15	0.03							
16.07	300000	50	1.70	1.01	0.15	0.11							
16.08	300000	57	1.04	0.07	0.15	-0.01	6.49	0.02					
1.01	300000	10	1.47	0.06	0.15	-0.01							
1.02	300000	15	1.52	0.14	0.15	0.00							
1.03	300000	17	1.40	0.22	0.15	0.01							
1.04	300000	14	1.62	0.24	0.15	0.02							
1.06	300000	14	1.64	6.79	0.15	0.77							
1.09	300000	45	1.48	20.05	0.15	5.11							
1.10	300000	52	1.71	8.58	0.15	2.57							
1.11	300000	28	1.75	2.51	0.15	0.35							
1.12	300000	45	1.75	0.92	0.15	0.45	9.27	0.03					
19.01	1500000	9	1.61	3.30	0.15	0.44							
19.03	1500000	4	1.75	2.96	0.15	0.17							
19.04	1500000	4	1.24	1.92	0.15	0.05							
19.05	1500000	12	1.43	0.27	0.15	0.02							
19.06	1500000	18	1.59	8.99	0.15	1.90							
19.07	1500000	25	1.59	8.26	0.15	2.15							
19.08	1500000	78	1.72	16.32	0.15	13.00	17.72	0.01					
6.01	1500000	6	1.46	1.97	0.15	0.12							
6.02	1500000	4	1.31	0.95	0.15	0.04							
6.03	1500000	42	1.50	20.32	0.15	9.89							
6.04	1500000	49	1.60	19.58	0.15	6.26							
6.05	1500000	52	1.84	15.27	0.15	4.04							
6.06	1500000	77	1.73	6.18	0.15	2.96							
6.07	1500000	20	1.77	2.01	0.15	0.39	24.49	0.02					
2.01	1500000	3	1.53	1.72	0.15	0.07							
2.02	1500000	7	1.52	0.51	0.15	0.04							
2.03	1500000	9	1.70	0.21	0.15	0.01							
2.04	1500000	15	1.00	0.29	0.15	0.04							
2.05	1500000	26	1.79	0.11	0.15	-0.00							
2.06	1500000	33	1.56	5.64	0.15	1.50							
2.07	1500000	42	1.63	12.90	0.15	6.69							
2.08	1500000	62	1.63	12.90	0.15	6.69							
2.09	1500000	83	1.73	7.96	0.15	2.66	11.00	0.01					

Soil no	linear age	thickness % Gravel	Bulk Density	% Carbonate		qa/cm ²	prof sum	rate of acc per 11 yr	Unit Avg	AVERAGE PROFILE SUM USING								
				lab	IM					U2b rate	U1c rate	U1c rate	U1c rate					
										0.01	0.04	101a	0.02	201a				
										Estimated profile sum avg								
										Act prof sum avg								
22.01	1500000	10	5	1.58	5.26	0.15	0.77											
22.02	1500000	11	20	1.57	0.88	0.15	0.09											
22.03	1500000	41	42	1.66	20.10	0.15	7.96											
22.04	1500000	30	54	1.42	22.36	0.15	4.37											
22.05	1500000	92	52	1.75	6.18	0.15	4.68	17.82	0.01	(DTa) 0.01	(DTa) 12.60	(DTa) 52.06	(DTa) 16.53	(DTa) 17.76				

Soil no	CLAY lab	FM	gm/LC	prof sum per 10 yr	rate of arc	Unit Avg	AVERAGE PROFILL SUM USING			
							Uc rate	Uic rate	Uic rate	Uic rate
							0.07	0.34	0.17	201a Act prof
							Estimated profile	sum avg	sum avg	sum avg
FMA-1	1.11	1.00	0.00							
FMA-2	2.00	1.00	0.00							
FMA-3	0.60	1.00	0.00							
FMA-4	1.61	1.00	0.00	0.00	0.00					
YMA-1	0.42	1.00	0.00							
YMA-2	0.77	1.00	0.00	0.00	0.00	(aluv)	0.00	Alluvium	0.00	(aluv)
7.01	1.71	1.00	0.01							
7.02	2.64	1.00	0.21							
7.03	1.54	1.00	0.14	0.46	3.09	(01b)	(01b)	(01b)	(01b)	(01b)
4.01	4.08	5.00	-0.02				0.01	0.05	0.02	0.46
4.02	7.60	5.00	0.20							
4.03	11.61	5.00	3.87							
4.04	4.08	1.00	0.59	4.64	0.46					
17.01	4.87	5.00	-0.01							
17.02	4.50	5.00	0.00							
17.03	5.27	1.00	0.46	0.45	0.05					
13.01	4.47	5.00	-0.02							
13.02	5.96	5.00	0.14							
13.03	4.26	1.00	1.51							
13.04	1.94	1.00	0.46	3.09	0.21					
15.01	5.58	5.00	0.09							
15.02	6.25	5.00	0.21							
15.03	10.78	5.00	2.57							
15.06	7.58	5.00	0.65							
15.04	12.88	5.00	1.07							
15.05	7.33	1.00	1.91	6.29	0.63	(01c)	(01c)	(01c)	(01c)	(01c)
3.01	17.06	20.00	0.02				0.74	3.37	1.68	3.37
3.02	25.60	20.00	0.80							
3.03	8.87	5.00	0.53							
3.04	4.72	1.00	0.57							
3.05	3.85	1.00	0.10							
3.06	2.39	1.00	0.62	2.73	0.02					
21.01	6.05	5.00	0.17							
21.02	11.31	5.00	0.82							
21.03	9.12	5.00	0.60							
21.04	10.95	1.00	2.13							
21.05	11.76	1.00	7.89							
21.06	4.24	1.00	1.77							
21.07	3.52	1.00	0.27	14.33	0.10					

Soil no	CLAY lab	PM	gm/cm ²	prof	sum per 11 yr	rate of acc	limit	AVERAGE PROFILE SUM USING			
								02b rate	01c rate	01d rate	01e rate
								0.07	0.34	0.17	0.17
								Estimated profile	sum avg	sum avg	sum avg
11.01	3.82	5.00	-0.02								
11.02	9.65	5.00	0.64								
11.03	14.04	1.00	2.24								
11.04	14.28	1.00	6.08								
11.05	11.52	1.00	3.03								
11.06	22.25	1.00	2.09		15.22	0.10					
12.01	7.47	5.00	0.13								
12.02	8.50	5.00	0.39								
12.03	12.23	5.00	3.64								
12.04	7.32	1.00	3.09								
12.05	4.78	1.00	1.04								
12.06	4.18	1.00	0.49								
12.07	4.68	1.00	0.77		9.54	0.06					
14.01	5.48	5.00	0.04								
14.02	9.24	5.00	0.75								
14.03	9.55	1.00	2.00								
14.04	7.39	1.00	3.32								
14.05	5.50	1.00	0.86								
14.06	9.26	1.00	3.26								
14.07	8.11	1.00	3.08								
14.08	7.52	1.00	0.21		13.60	0.09					
20.01	4.66	5.00	0.01								
20.02	12.70	5.00	1.06								
20.03	20.09	5.00	3.42								
20.04	16.64	1.00	0.94								
20.05	16.49	1.00	0.59								
20.06	15.06	1.00	3.00								
20.07	21.33	1.00	1.50								
20.08	11.55	1.00	0.76		11.31	0.08	0.07	11.12	50.52	25.26	11.12
5.01	3.67	5.00	-0.05								
5.02	4.11	5.00	-0.11								
5.03	10.05	5.00	2.09								
5.04	9.17	1.00	1.26								
5.05	10.92	1.00	3.62								
5.06	3.94	1.00	0.99								
5.07	1.25	1.00	0.26		8.05	0.03					
18.01	15.63	20.00	-0.01								
18.02	8.57	5.00	1.29								
18.03	11.52	5.00	0.69								
18.04	7.92	1.00	1.57								
18.05	6.16	1.00	1.47								
18.06	4.22	1.00	0.61		5.63	0.02					

Soil no	LAV lab	FM	qm/cm2	prof sum per 11. yr	rate of acc	Unit Avg	AVERAGE PROFILE SUM USING			
							0.07 rate	0.14 rate	0.17 rate	0.20 rate
							Estimated profile sum avg	Estimated profile sum avg	Estimated profile sum avg	Estimated profile sum avg
8.01	18.46	20.00	0.27							
8.02	45.67	20.00	4.43							
8.03	9.13	1.00	1.29							
8.04	6.40	1.00	2.34							
8.05	4.72	1.00	1.02							
8.06	4.09	1.00	2.40	11.85	0.04					
16.01	14.73	5.00	1.31							
16.02	17.28	5.00	2.89							
16.03	15.50	5.00	1.58							
16.04	47.45	1.00	6.92							
16.05	32.18	1.00	8.37							
16.06	16.17	1.00	5.60							
16.07	19.65	1.00	2.42							
16.08	5.53	1.00	1.47	50.77	0.10					
1.01	15.07	5.00	1.13							
1.02	18.97	5.00	2.84							
1.03	45.11	1.00	5.56							
1.04	44.22	1.00	6.91							
1.08	33.07	1.00	3.73							
1.09	20.99	1.00	5.16							
1.10	13.45	1.00	2.84							
1.11	13.01	1.00	1.78							
1.12	10.66	1.00	5.50	36.45	0.12					
19.01	17.42	20.00	0.10							
19.02	17.01	5.00	0.80							
19.04	52.08	5.00	7.28							
19.05	42.71	5.00	5.78							
19.06	32.67	1.00	6.81							
19.07	34.07	1.00	8.67							
19.08	27.58	1.00	21.60	46.25	0.03					
6.01	14.82	20.00	-0.35							
6.02	21.86	20.00	0.06							
6.03	11.95	1.00	3.62							
6.04	3.97	1.00	1.00							
6.05	3.15	1.00	0.77							
6.06	2.42	1.00	0.80							
6.07	2.28	1.00	0.22	6.33	0.00					
2.01	16.32	20.00	-0.06							
2.02	12.70	20.00	-0.79							
2.03	17.98	20.00	-0.29							
2.04	10.76	1.00	3.72							
2.05	20.80	1.00	0.66							
2.07	20.10	1.00	17.41							
2.08	16.61	1.00	0.27							
2.09	13.02	1.00	4.15	77.48	0.07					
							0.06	0.04	0.03	0.01
							25.24	101.04	50.52	18.55

Soil no	CLAY		rate of acc	rate of yr	AVERAGE PROFILE SUM USING		Act prof sum avg
	lab	FM	gm/cm2	prof sum	0.07 Estimated profile sum avg	0.24 0.17 20% sum avg	
22.01	26.58	20.00	1.41				
22.02	22.82	5.00	3.50				
22.03	22.92	1.00	8.81				
22.04	15.07	1.00	2.75				
22.05	11.27	1.00	9.17	24.65	111.22	545.22	257.61
					(Total)	(Total)	(Total)
					0.02	0.02	28.67

Soil no	SIL1					Rate of acc	AVERAGE FROM ILE SUM USING					
	lab	PM	qm/cm2	prof	sum per il y		Unit avg	Urb rate Dlc rate Dlc rate At prof				
								0.13	0.41	0.20	sum avg	
												Estimated profile sum avg

FMA-1	4.52	1.00	0.00									
FMA-2	13.22	1.00	0.00									
FMA-3	0.65	1.00	0.00									
FMA-4	2.76	1.00	0.00		0.00	0.00						
YMA-1	0.42	1.00	0.00									
YMA-2	0.54	1.00	0.00		0.00	0.00						
7.01	4.92	1.00	0.07									
7.02	6.53	1.00	1.07									
7.03	3.24	1.00	0.91		2.04	13.63	(01b)	(01b)	(01b)	(01b)		
4.01	9.37	15.00	-0.16									
4.02	10.64	15.00	-0.22									
4.03	16.97	15.00	1.83									
4.04	12.88	1.00	2.45		2.80	0.28						
17.01	25.06	15.00	0.49									
17.02	19.22	15.00	0.95									
17.03	5.00	1.00	1.40		2.84	0.28						
12.01	12.78	15.00	-0.03									
12.02	13.46	15.00	-0.09									
12.03	8.18	1.00	3.24									
12.04	4.41	1.00	1.54		4.71	0.47						
15.01	16.06	15.00	0.18									
15.02	13.88	15.00	-0.09									
15.03	18.64	15.00	2.92									
15.06	11.96	15.00	-0.22									
15.04	25.77	15.00	1.50									
15.05	7.35	1.00	1.91		5.00	0.50	(01c)	(01c)	(01c)	(01c)		
3.01	40.84	40.00	0.34				0.41	1.24	2.04	4.09		
3.02	29.29	40.00	0.64									
3.03	14.16	15.00	0.30									
3.04	9.58	1.00	1.25									
3.05	2.74	1.00	0.17									
3.06	2.27	1.00	0.58		3.49	0.02						
21.01	38.92	15.00	1.07									
21.02	24.11	15.00	2.48									
21.03	23.71	15.00	1.50									
21.04	16.82	1.00	2.76									
21.05	10.92	1.00	7.29									
21.06	11.40	1.00	4.21									
21.07	2.16	1.00	0.43		19.75	0.17						

Soil no	SILT lab	rate of acc			unit Avg	AVAILABLE 1948 ILE SUM USING			
		gm/cm ²	prof	sum per ft		Urb rate 0.13	Dic rate 0.41	Est profile sum avg	Act prof sum avg
		FW							
11.01	16.02	15.00							
11.02	18.23	15.00	0.12						
11.03	19.25	15.00	0.70						
11.04	22.47	1.00	4.67						
11.05	17.71	1.00	9.77						
11.06	11.77	1.00	3.64						
		1.00	1.02	19.92	0.12				
12.01	21.85	15.00							
12.02	20.16	15.00	0.36						
12.03	23.12	15.00	0.81						
12.04	18.20	1.00	4.30						
12.05	14.16	1.00	0.25						
12.06	7.00	1.00	5.42						
12.07	9.81	1.00	0.91						
		1.00	1.79	19.83	0.12				
14.01	29.89	15.00	1.10						
14.02	26.99	15.00	2.10						
14.03	29.35	1.00	6.62						
14.04	26.61	1.00	12.01						
14.05	19.16	1.00	3.36						
14.06	27.60	1.00	10.59						
14.07	18.07	1.00	7.28						
14.08	15.56	1.00	0.46	44.52	0.20				
20.01	23.12	15.00	0.72						
20.02	29.22	15.00	2.04						
20.03	31.95	15.00	4.15						
20.04	14.26	1.00	0.80						
20.05	16.72	1.00	0.60						
20.06	13.33	1.00	2.62						
20.07	22.04	1.00	1.55						
20.08	17.29	1.00	0.89	13.38	0.09	(0.20)	61.31	(0.20)	(0.20)
5.01	7.80	15.00	-0.32						
5.02	8.82	15.00	-1.02						
5.03	16.48	15.00	1.63						
5.04	22.67	1.00	3.29						
5.05	19.10	1.00	6.55						
5.06	6.27	1.00	1.71						
5.07	0.67	1.00	-0.04	11.70	0.04				
18.01	45.10	40.00	2.25						
18.02	27.34	15.00	4.37						
18.03	25.58	15.00	1.28						
18.04	16.65	1.00	3.52						
18.05	7.87	1.00	1.94						
18.06	5.97	1.00	0.92	14.29	0.09				

Soil no	SILT		TH	qa/cu	prof sum	rate of acc per ft	unit avg	AVERAGE PROFILE SUM USING				net prof sum avg
	lab	%						0.1% rate	0.1% rate	0.1% rate	0.1% rate	
8.01	26.21	40.00	0.46									
8.02	28.88	40.00	-1.06									
8.03	18.81	1.00	3.01									
8.04	10.36	1.00	4.02									
8.05	7.93	1.00	1.05									
8.06	7.49	1.00	4.16	13.15	0.04							
16.01	16.39	15.00	0.05									
16.02	16.57	15.00	0.67									
16.03	21.73	15.00	1.16									
16.04	21.54	1.00	3.08									
16.05	24.88	1.00	6.42									
16.06	14.68	1.00	5.24									
16.07	24.11	1.00	3.90									
16.08	12.31	1.00	3.54	23.16	0.08							
1.01	23.26	15.00	1.03									
1.02	27.90	15.00	2.85									
1.03	21.23	1.00	2.55									
1.04	19.73	1.00	3.01									
1.08	20.77	1.00	2.20									
1.09	17.40	1.00	4.24									
1.10	12.58	1.00	3.58									
1.11	16.43	1.00	2.27									
1.12	8.98	1.00	4.57	26.40	0.09	0.06	0.06	0.06	0.06	0.06	0.06	0.06
19.01	41.07	40.00	1.02									
19.02	20.38	15.00	0.54									
19.04	17.46	15.00	0.05									
19.05	13.99	15.00	-0.02									
19.06	20.77	1.00	4.26									
19.07	19.79	1.00	4.94									
19.08	18.16	1.00	13.93	24.75	0.02							
6.01	24.65	40.00	-0.16									
6.02	24.66	40.00	-0.20									
6.03	16.32	1.00	5.05									
6.04	8.22	1.00	2.37									
6.05	6.15	1.00	1.73									
6.06	5.84	1.00	2.32									
6.07	4.57	1.00	0.79	11.81	0.01							
2.01	40.24	40.00	0.22									
2.02	29.63	40.00	0.41									
2.03	29.83	40.00	-0.19									
2.04	32.32	1.00	6.52									
2.05	28.79	1.00	1.11									
2.07	27.32	1.00	7.19									
2.08	17.18	1.00	8.57									
2.09	20.94	1.00	6.84	41.68	0.02							

Soil no	SILT		gm/cm2	rate of Acc prof sum per 11' y	Unit Avg	AVERAGE PROFILE SUM USING					Act prof sum avg
	lab	FM				02b rate 0.13	01c rate 0.41	01a 101a	01c rate 0.20	01a 201a	
Estimated profile sum avg											
22.01	20.61	40.00	-0.55								
22.02	21.30	15.00	0.79								
22.03	20.76	1.00	7.94								
22.04	17.05	1.00	5.14								
22.05	15.00	1.00	10.97	22.30	0.01	(01a) 0.02	(01a) 201.49	(01a) 613.13	(01a) 306.56	(01a) 25.14	

Soil no	est 2.500" lab	FM	qa/cm2	prof sum per 10 yr	rate of acc	Unit avg	AVERAGE PROFILE SUM USING					Alt prof sum avg
							Urb rate	Uic rate	Uic rate	Uic rate	Estimated profile sum avg	
FMA-1	1.00	0.00	0.00									
FMA-2	3.11	0.00	0.00									
FMA-3	1.27	0.00	0.00									
FMA-4	2.09	0.00	0.00	0.00	0.00							
YMA-1	0.49	0.00	0.00									
YMA-2	1.06	0.00	0.00	0.00	0.00	(aluv)	0.00	Alluvium	0.00	0.00	(aluv)	0.00
7.01	2.02	0.00	0.03									
7.02	2.48	0.00	0.50									
7.03	2.14	0.00	0.87	1.40	9.26	(01b)	0.01	(01b)	0.05	0.02	(01b)	1.40
4.01	2.70	0.00	0.09									
4.02	2.95	0.00	0.22									
4.03	6.26	0.00	2.43									
4.04	4.60	0.00	0.07	4.62	0.46							
17.01	4.37	0.00	0.21									
17.02	2.78	0.00	0.45									
17.03	1.15	0.00	0.39	1.06	0.11							
12.01	6.16	0.00	0.37									
12.02	3.88	0.00	0.44									
12.03	2.68	0.00	1.18									
13.04	2.18	0.00	0.83	2.83	0.28							
15.01	4.48	0.00	0.51									
15.02	2.76	0.00	0.41									
15.03	2.49	0.00	1.42									
15.04	2.08	0.00	0.70									
15.05	4.56	0.00	0.61									
15.06	1.85	0.00	0.54	4.19	0.42	(01c)	0.04	(01c)	0.17	1.59	(01c)	3.17
2.01	6.61	0.00	0.48									
2.02	6.27	0.00	0.51									
2.03	3.90	0.00	0.41									
2.04	2.75	0.00	0.39									
2.05	1.32	0.00	0.11									
2.06	2.59	0.00	0.90	2.40	0.02							
21.01	6.08	0.00	0.27									
21.02	2.74	0.00	0.72									
21.03	2.69	0.00	1.11									
21.04	20.62	0.00	3.56									
21.05	20.19	0.00	14.39									
21.06	5.61	0.00	2.20									
21.07	3.63	0.00	0.47	22.77	0.15							

Soil no	lab	est % SiO ₂		rate of acc	Unit	ANALOG PROFILE SIM USING			
		ft	gm/cm ²			Urb rate	Uic rate	Uic rate	At prof
				prof sum	per ft yr	Estimated	profile sum	avg	sum avg
11.01	5.05	0.00	0.19						
11.02	5.24	0.00	0.67						
11.03	6.46	0.00	1.64						
11.04	18.70	0.00	8.40						
11.05	21.39	0.00	6.00						
11.06	29.20	0.00	2.86	19.76	0.13				
12.01	6.43	0.00	0.26						
12.02	4.56	0.00	0.48						
12.03	3.41	0.00	1.26						
12.04	3.69	0.00	1.72						
12.05	3.76	0.00	0.86						
12.06	7.80	0.00	1.12						
12.07	2.27	0.00	0.62	6.45	0.04				
14.01	3.29	0.00	0.24						
14.02	4.22	0.00	0.83						
14.03	3.25	0.00	1.22						
14.04	6.51	0.00	3.29						
14.05	2.57	0.00	0.47						
14.06	3.23	0.00	1.28						
14.07	1.85	0.00	0.78						
14.08	1.82	0.00	0.06	8.16	0.05				
20.01	5.57	0.00	0.41						
20.02	7.62	0.00	1.00						
20.03	17.19	0.00	3.76						
20.04	19.12	0.00	1.12						
20.05	24.06	0.00	0.93						
20.06	22.91	0.00	4.81						
20.07	27.45	0.00	2.00						
20.08	22.42	0.00	1.29	15.63	0.10	(0.20)	(0.20)	(0.20)	(0.20)
5.01	1.21	0.00	0.07						
5.02	1.67	0.00	0.23						
5.03	3.74	0.00	1.22						
5.04	6.52	0.00	0.98						
5.05	7.71	0.00	2.75						
5.06	7.91	0.00	2.44						
5.07	0.26	0.00	0.28	8.17	0.03				
18.01	7.14	0.00	1.18						
18.02	2.96	0.00	1.12						
18.03	4.53	0.00	0.40						
18.04	2.74	0.00	0.72						
18.05	2.27	0.00	0.62						
18.06	19.21	0.00	2.27	7.42	0.02				

Soil no	est % SiO ₂ lab	pH	qm/cm ²	prof sum per ft yr	rate of scr	Unit Avg	AVERAGE PROFILE SIM USING					Act prof sum avg
							0.4 rate	0.4 rate	0.4 rate	0.4 rate	0.4 rate	
							0.08	0.32	0.16	0.16	0.16	
							Estimated profile sum avg					

8.01	3.78	0.00	0.44									
8.02	8.93	0.00	1.42									
8.03	7.79	0.00	1.24									
8.04	22.70	0.00	9.60									
8.05	13.22	0.00	3.45									
8.06	9.05	0.00	6.54	22.69	0.08							
16.01	8.28	0.00	1.16									
16.02	5.78	0.00	1.22									
16.03	5.68	0.00	0.82									
16.04	37.47	0.00	5.55									
16.05	45.65	0.00	12.22									
16.06	32.74	0.00	12.56									
16.07	42.22	0.00	5.57									
16.08	6.77	0.00	1.92	40.81	0.14							
1.01	9.47	0.00	1.02									
1.02	8.84	0.00	1.72									
1.03	22.68	0.00	2.98									
1.04	26.10	0.00	4.19									
1.05	22.18	0.00	3.82									
1.06	26.25	0.00	9.31									
1.10	28.20	0.00	8.56									
1.11	25.97	0.00	3.77									
1.12	20.10	0.00	11.18	46.58	0.16	(0.2c) 0.08	(0.2c) 27.21	(0.2c) 90.18	(0.2c) 47.59	(0.2c) 25.13		
19.01	7.86	0.00	1.09									
19.02	5.92	0.00	0.26									
19.04	26.80	0.00	1.28									
19.05	29.92	0.00	4.55									
19.06	31.15	0.00	6.67									
19.07	31.49	0.00	8.22									
19.08	26.59	0.00	29.24	51.51	0.02							
6.01	7.65	0.00	0.51									
6.02	8.57	0.00	0.39									
6.03	25.61	0.00	8.29									
6.04	19.01	0.00	6.11									
6.05	16.39	0.00	5.25									
6.06	8.68	0.00	4.22									
6.07	4.74	0.00	0.96	25.83	0.02							
2.01	9.09	0.00	0.39									
2.02	9.19	0.00	0.09									
2.03	25.06	0.00	2.54									
2.04	25.12	0.00	5.19									
2.05	26.28	0.00	11.14									
2.07	42.20	0.00	11.52									
2.08	29.95	0.00	20.93									
2.09	27.01	0.00	12.05	65.70	0.04							

Soil no	est % SiO2		rate of			Unit Avg	AVERAGE FICOFILL SUM USING				Act prof sum avg
	lab	FM	gm/cm2	prof sum	acc per ft. yr		UCb rate	01c rate	01c rate		
							0.08	0.32 101a	0.16 201a		
							Estimated profile sum avg				
22.01	18.50	0.00	2.76								
22.02	19.38	0.00	2.35								
22.03	35.01	0.00	13.95								
22.04	35.73	0.00	6.96			(01a)	(01a)	(01a)	(01a)	(01a)	
22.05	25.47	0.00	19.63	45.65	0.03	0.03	126.03	475.90	237.95	47.17	